



8-2013

Development of a Computational Methodology for Evaluating In Vivo Vertebral Mechanics in Subjects Having Various Conditions of the Lumbar Spine

Christopher Brian Carr
ccarr@utk.edu

Follow this and additional works at: https://trace.tennessee.edu/utk_graddiss



Part of the [Biomechanics and Biotransport Commons](#)

Recommended Citation

Carr, Christopher Brian, "Development of a Computational Methodology for Evaluating In Vivo Vertebral Mechanics in Subjects Having Various Conditions of the Lumbar Spine. " PhD diss., University of Tennessee, 2013.
https://trace.tennessee.edu/utk_graddiss/2405

This Dissertation is brought to you for free and open access by the Graduate School at TRACE: Tennessee Research and Creative Exchange. It has been accepted for inclusion in Doctoral Dissertations by an authorized administrator of TRACE: Tennessee Research and Creative Exchange. For more information, please contact trace@utk.edu.

To the Graduate Council:

I am submitting herewith a dissertation written by Christopher Brian Carr entitled "Development of a Computational Methodology for Evaluating In Vivo Vertebral Mechanics in Subjects Having Various Conditions of the Lumbar Spine." I have examined the final electronic copy of this dissertation for form and content and recommend that it be accepted in partial fulfillment of the requirements for the degree of Doctor of Philosophy, with a major in Biomedical Engineering.

Richard D. Komistek, Major Professor

We have read this dissertation and recommend its acceptance:

Mohamed R. Mahfouz, William Hamel, Aly Fathy, Adrija Sharma

Accepted for the Council:

Carolyn R. Hodges

Vice Provost and Dean of the Graduate School

(Original signatures are on file with official student records.)

**Development of a Computational Methodology
for Evaluating In Vivo Vertebral Mechanics in
Subjects Having Various Clinical Conditions
of the Lumbar Spine**

A Dissertation
Presented for the
Doctor of Philosophy
Degree
The University of Tennessee, Knoxville

Christopher Brian Carr
August 2013

To my grandparents,

Ben and Edna

Worth and Mildred

Acknowledgements

I would like to first acknowledge and thank my major professor, Dr. Richard Komistek for affording me the opportunity to study under his guidance and reach limits well beyond what I thought possible. He always led with encouragement and a sense of enthusiasm that inspired everyone around him. He has tremendous vision and insight with a determination that few possess. His approach in both his professional life and his personal life has been an inspiration that continues to challenge me to grow not only intellectually, but also personally and spiritually.

I would like to also thank Dr. Mohamed Mahfouz, Dr. William Hamel and Dr. Aly Fathy for their guidance and support during my research. To Dr. Adrija Sharma, I owe many thanks as well for his invaluable advice for helping progress my research when I seemed to hit a snag. His personal approach and strive for excellence was always a positive motivation. I would like to also thank Dr. Joseph Cheng and Christy Hagewood for sharing their clinical expertise and allowing me the opportunity to work with many wonderful patients. Special thanks is also extended to Rebecca Robertson for her kindness and willingness to always be of assistance to help make things a little easier along the way.

To all my fellow lab mates at the Center for Musculoskeletal Research, thank you for your help and support. Your friendship and generosity will always be a warm reminder of my time at the University of Tennessee. I would like to specifically thank Joe Mitchell for helping collect all data and the many trips to Nashville. We had a lot of good times....it's been a long ride! To Sumesh Zingde, Dr. John Mueller, Dr. Filip Lezsko, Brad Meccia, and Thibaut DeBock, thanks for your friendship and for always being a part of the team that banded together to accomplish many goals. Thank you, Dr. Gary To for always being available to go grab lunch and

for all great stories. To the new guys Michael LeCour, Ian Zeller and Trevor Grieco, thank you for all your assistance. Best of luck to you all!

I would like to also thank my two sisters, their husbands, my aunt and uncles, my in-laws as well as my friends that have always lended support along the way. To my parents, Jim and Debbie, who sacrificed and instilled in me the values and integrity that have helped me to get to this point. Thank you for your many words of encouragement and for the love that you gave so freely. Lastly, to my wife, Nikki, thank you for always believing in me and encouraging me to be at my best. Your undying love and support always inspired me and because of your willingness to forego some of your dreams, I was able to pursue mine.

Abstract

Treating and evaluating the causes of low back pain (LBP) is difficult and not fully understood. However, assessing the *in vivo* motions and loading characteristics in the lumbar spine may provide important data for progressing the diagnosis and treatment of pathologies linked with LBP.

This dissertation describes the development of a comprehensive approach for collecting both the kinematics and kinetics of the lumbar vertebrae under *in vivo* conditions. Forty-four subjects representing healthy, symptomatic, pathological, and surgically implanted (pre- and post-operative) conditions of the lumbar spine were evaluated using dynamic fluoroscopy and 3D-to-2D image registration to assess the motions of the five lumbar vertebrae while patients performed an active flexion-extension, lateral flexion, and axial rotation of the spine. 3D kinematics were extracted describing the relative in-plane and coupled out-of-plane motions of the intervertebral joints. A computational methodology was then utilized for the development of a multi-body, inverse mathematical model based on principles from Kane's dynamics. The kinematics, as well as patient-specific bone geometries, recreated from CT, and ground reaction forces, collected using force plates, served as inputs to the model. Vertebral bones were defined as rigid bodies, while massless frames represented non-specific bone geometries for the lower body, torso and abdominal wall. Soft tissue attachment sites were selected on the vertebral bones allowing for ligaments to be defined for constraint and modeled as linear springs. Relevant muscle groups were also included and solved for using the pseudo-inverse algorithm, which enabled for decoupling of the derived resultant torques and ultimately defined the kinetic trajectory for the muscles.

These methodologies allowed for the theoretical modeling of the entire lumbar region and prediction of joint reaction contact forces, ligament constraint forces, and applied musculotendon forces. Results from the model were validated for the prescribed motions using experimental loading data measured directly using telemetrized vertebral implants and intervertebral disc pressure sensors. A comparative analysis of the predicted forces from the model with experimentally collected data showed good agreement in the force profiles and an average combined error around 6.9%. This demonstrated the use of this methodology for *in vivo* analyses of the lumbar spine.

Table of Contents

Chapter 1 Introduction	1
Chapter 2 Background	4
2.1 Anatomy of the Lumbar Spine	4
2.1.1 The Lumbar Vertebra	4
2.1.2 The Intervertebral Disc	9
2.1.3 Ligaments of the Lumbar Spine	11
2.1.4 Muscles of the Lumbar Spine	13
2.2 Clinical Relevance	16
Chapter 3 Review of Related Literature	19
3.1 Kinematics in the Lumbar Spine	19
3.2 Kinetics in the Lumbar Spine	23
3.3 Lumbar Intervertebral Disc Pressures	28
3.4 Finite Element Modeling of the Lumbar Spine	30
Chapter 4 Research Aims and Fundamental Contributions	32
4.1 Research Aims	32
4.2 Fundamental Contributions	35
4.3 Research Motivation	37
Chapter 5 Materials and Methods	38
5.1 Research Study Design	38
5.1.1 Patient Selection	39
5.1.2 Description of Participants	40
5.1.3 Activity Description	42
5.2 Reconstruction of Patient-Specific Lumbar Vertebrae	44
5.3 3D-to-2D Image Registration Technique	46
5.3.1 3D-to-2D Image Registration Error Analysis	48
5.4 Determination of In Vivo Lumbar Kinematics	49
5.5 Development of the 3D Mathematical Model	50

5.5.1 Model Inputs	52
5.5.2 Model Description	54
5.6 Methodology for Mathematical Model Validation	69
Chapter 6 Results	71
6.1 Determination of 3D In Vivo Lumbar Kinematics	71
6.1.1 Flexion-Extension Activity	72
6.1.2 Lateral Flexion Activity	77
6.1.3 Axial Rotation Activity	81
6.2 Derivation of 3D In Vivo Lumbar Kinetics	86
6.2.1 Flexion-Extension Activity	87
6.2.2 Lateral Flexion Activity	96
6.2.3 Axial Rotation Activity	104
6.3 Validation of the Mathematical Model	114
6.3.1 Telemetry vs Theoretically Derived Forces	114
6.3.2 Intervertebral Disc Pressure vs Theoretically Derived Forces	117
Chapter 7 Discussion	122
7.1 Kinematics Analysis	123
7.2 Kinetics Analysis	127
Chapter 8 Limitations and Future Work	139
Bibliography	144
Appendix Detailed Analysis of Patients' Results	155
Vita	398

List of Tables

6.1 Average absolute intersegmental coupled rotations (degrees) in the coronal and transverse planes, along with their combined percentage of the overall main FE rotation at each level during movement between maximum flexion and maximum extension..... 76

6.2 Average intersegmental translations (mm) along the AP, SI, and LR directions while moving between maximum flexion and maximum extension..... 76

6.3 Average absolute intersegmental coupled rotations (degrees) in the transverse and sagittal planes, along with their combined percentage of the overall main LB rotation at each level during movement between left laterally flexed position and right laterally flexed position.79

6.4 Average intersegmental translations (mm) along the AP, SI, and LR directions while moving between left laterally flexed position and right laterally flexed position. 82

6.5 Average absolute intersegmental coupled rotations (degrees) in the coronal and sagittal planes, along with the combined percentage of the overall main AR rotation at each level during movement between left axially rotated position and right axially rotated postition. 84

6.6 Average intersegmental translations (mm) along the AP, SI, and LR directions while moving between left axially rotated position and right axially rotated position. 85

6.7 Average intersegmental compressive forces relative to body weight during FE activity for all lumbar spine conditions at each increment captured during the motion. 89

6.8 Average intersegmental compressive forces relative to body weight during LF activity for all lumbar spine conditions at each increment captured during the motion. 98

6.9 Average intersegmental compressive forces relative to body weight during AR activity for all lumbar spine conditions at each increment captured during the motion. 106

List of Figures

2.1	Anatomy of the complete lumbar spine with ligaments [http://www.backpain-guide.com]....	5
2.2	Anatomy of the typical lumbar vertebra (http://www.backpain-guide.com).	6
2.3	Viscoelasticity enables for greater stiffness and strength characteristics when rapidloading occurs. This helps protects the tissue from injury during trauma [9].	12
2.4	Load-displacement curve of spinal ligaments [116].	13
2.5	Muscles of the lumbar spine (http://www.chiropracticposters.com).	15
5.1	Process of using CT scan image dicoms to recreate 3D patient-specific bone models.	45
5.2	In vivo fluoroscopy at specified increments during flexion-extension (top) with subsequent 3D-to-2D registration of the bone models (bottom).	47
5.3	Schematic of the mathematical model showing a sagittal view of the lumbar region. The points of contact were defined on each vertebral body at the inferior and superior endplates at each FSU.	56
5.4	The ALL (shown in orange) attached at the mid-height of the anterior aspect of each vertebral body and was divided into a left, medial, and right bundle.	59
5.5	The PLL (shown in orange) attached at the mid-height of the posterior aspect of each vertebral body and was divided into a left and right bundle.	60
5.6	The LF (shown in orange) attached along the antero-superior and antero-inferior border of the laminae at each level and was divided into a left and right bundle.	60
5.7	The ISL (shown in orange) attached along the inferior and superior apex of the spinous process at each level and was divided into an anterior, medial, and posterior bundle.	61
5.8	The SSL (shown in orange) attached at the mid-height of the posterior aspect of the spinous process at each level and was defined as a single bundle.	61
5.9	The PM (shown in red) is a bi-lateral muscle group attaching at each level on the superior-lateral surface and on the anterior face of the transverse process. It wraps around the anterior pelvis and inserts on the femur near the lesser trochanter.	63
5.10	The multifidus (shown in red) is a bi-lateral muscle group attaching at each level on the posterior surface of the laminae and inferiorly and laterally on the spinous process. It exists in layers spanning multiple levels and inserts at the mammillary processes and along the sacrum.	64
5.11	The QLL (shown in red) is a bi-lateral muscle group attaching at L1 through L4 on the lateral aspect of the transverse process. It inserts posteriorly along the iliac crest on the pelvis.	64

5.12	The EO (shown in red) is a bi-lateral muscle group attaching along the anterior ribcage from the 7 th rib down to the 10 th rib. They insert into the superior abdominal wall and help generate intra-abdominal pressure.....	65
5.13	The IO (shown in red) is a bi-lateral muscle group. Some fibers attach along the lateral ribcage from the 9 th rib down to the 11 th rib and insert along the iliac crest of the pelvis. Additional fibers attach along the lateral abdominal wall and insert on the more anterior aspects of the iliac crest on the pelvis. These also help generate intra-abdominal pressure.	65
5.14	The RA (shown in red) is a bi-lateral muscle group attaching on the anterior ribcage from the sternum and spreading laterally down from the 5 th rib through the 7 th rib. These muscles span the abdominal wall insert at the pubic bone on the inferior-anterior pelvis. These muscles also help generate intra-abdominal pressure.....	66
6.1	Average intersegmental rotations while performing FE between the maximum flexion and maximum extension in patients having a native (left) or surgically implanted (right) lumbar spine. Degen (NS) = degenerative without need for surgery; Degen (SR) = degenerative with surgery required.....	74
6.2	Average intersegmental rotations while performing LF between the left- and right-sided laterally flexed positions in patients having a native (left) or surgically implanted (right) lumbar spine. Degen (NS) = degenerative without need for surgery; Degen (SR) = degenerative with surgery required	79
6.3	Average intersegmental rotations while performing AR between left and right axially rotated positions in patients having a native (left) or surgically implanted (right) lumbar spine. Degen (NS) = degenerative without need for surgery; Degen (SR) = degenerative with surgery required.....	84
6.4	Illustration of the defined coordinate axes at each level of the spine where N1> was directed along the AP direction, N2> along the SI direction, and N3> along the lateral LR direction.	87
6.5	Average compressive force profiles normalized with respect to body weight during FE for both native and surgically implanted lumbar spines with comparisons pre- and post-operatively.	90
6.6	Average AP forces at each intervertebral level for all native and surgically implanted lumbar spine conditions while performing FE.	94
6.7	Average LR forces at each intervertebral level for all native and surgically implanted lumbar spine conditions while performing FE.	96
6.8	Average profiles for the theoretical muscle forces normalized with respect to muscle predicted to generate the largest force during FE for both native and surgically implanted lumbar spines with comparisons pre- and post-operatively.	97
6.9	Average compressive force profiles normalized with respect to body weight during LF for both native and surgically implanted lumbar spines with comparisons pre- and post-operatively.	100

6.10	Average AP forces at each intervertebral level for all native and surgically implanted lumbar spine conditions while performing LF.	103
6.11	Average lateral right and left forces at each intervertebral level for all native and surgically implanted lumbar spine conditions while performing LF.	103
6.12	Average profiles for the theoretical muscle forces normalized with respect to the muscle predicted to generate the largest force during AR for both native and surgically implanted lumbar spines with comparisons pre- and post-operatively.	105
6.13	Average compressive force profiles normalized with respect to body weight during AR for both native and surgically implanted lumbar spines with comparisons pre- and post-operatively.	108
6.14	Average AP forces at each intervertebral level for all native and surgically implanted lumbar spine conditions while performing AR.	111
6.15	Average lateral LR forces at each intervertebral level for all native and surgically implanted lumbar spine conditions while performing AR.	112
6.16	Average profiles for the theoretical muscle forces normalized with respect to the muscle predicted to generate the largest force during AR for both native and surgically implanted lumbar spines with comparisons pre- and post-operatively.	113
6.17	Comparison of the theoretically derived forces, averaged across various lumbar spine conditions at L1L2, with force data directly measured using a telemeterized vertebral body replacement between T12 and L2 while moving between maximum flexion and upright, neutral position.	115
6.18	Comparison of the theoretically derived forces for three sample patients at L1L2 with force data directly measured using a telemeterized vertebral body replacement between T12 and L2 while moving between maximum flexion and upright, neutral position.	115
6.19	Comparison of the theoretically derived forces, averaged across various lumbar spine conditions at L1L2, with force data directly measured using a telemeterized vertebral body replacement between T12 and L2 while performing LF to the right side.	116
6.20	Comparison of theoretically derived forces for three sample patients at L1L2 with force data measured using a telemeterized vertebral body replacement between T12 and L2 while performing LF to the right-side.	116
6.21	Comparison of theoretically derived forces averaged across various lumbar spine conditions at L4L5 with data reported in the literature, measuring <i>in vivo</i> loads using pressure sensors placed in the L4L5 intervertebral disc while performing FE.	118
6.22	Comparison of theoretically derived forces averaged across various lumbar spine conditions at L4L5 with data reported in the literature, measuring <i>in vivo</i> loads using pressure sensors placed in the L4L5 intervertebral disc while performing left-to right LF.	118

6.23	Comparison of theoretically derived forces averaged across various lumbar spine condition at L4L5 with data reported in the literature, measuring <i>in vivo</i> loads using pressure sensors placed in the L4L5 intervertebral disc while performing left-to right AR.	119
6.24	Comparison of theoretically derived forces for three sample patients at L4L5 with data reported in the literature, measuring <i>in vivo</i> loads using pressure sensors placed in the L4L5 intervertebral disc while performing FE.....	119
6. 25	Comparison of theoretically derived forces for three sample patients at L4L5 with data reported in the literature measuring <i>in vivo</i> loads using pressure sensors placed in the L4L5 intervertebral disc while performing left-to-right LF.....	120
6.26	Comparison of theoretically derived force data for three sample patients at L4L5 with data reported in the literature, measuring <i>in vivo</i> loads using pressure sensors placed in the L4L5 intervertebral disc while performing left-to-right AR.	120
A.1	Patient 1H relative rotations (left) and translations (right) at each vertebral level during flexion-extension.	156
A.2	Patient 1H intervertebral contact forces normalized with respect to body weight during flexion-extension. 1-dir=Ant(+)/Post(-), 2-dir=Sup(+)/Inf(-), 3-dir=Rt(+)/Lt(-).....	156
A.3	Patient 1H segmental ligament forces normalized with respect to body weight during flexion-extension.	157
A.4	Patient 1H bilateral muscle forces normalized with respect to body weight during flexion-extension.....	157
A.5	Patient 1H relative rotations (left) and translations (right) at each vertebral level during lateral flexion.....	157
A.6	Patient 1H intervertebral contact forces normalized with respect to body weight during right-to-left lateral flexion. 1-dir=Ant(+)/Post(-), 2-dir=Sup(+)/Inf(-), 3-dir=Rt(+)/Lt(-).....	158
A.7	Patient 1H segmental ligament forces normalized with respect to body weight during left-to-right lateral flexion.	158
A.8	Patient 1H bilateral muscle forces normalized with respect to body weight during left-to-right lateral flexion.	158
A.9	Patient 1H relative rotations (left) and translations (right) at each vertebral level during axial rotation.....	159
A.10	Patient 1H intervertebral contact forces normalized with respect to body weight during left-to-right axial rotation. 1-dir=Ant(+)/Post(-), 2-dir=Sup(+)/Inf(-), 3-dir=Rt(+)/Lt(-).....	159
A.11	Patient 1H segmental ligament forces normalized with respect to body weight during left-to-right axial rotation.	159
A.12	Patient 1H bilateral muscle forces normalized to body weight during left-to-right axial rotation.....	160

A.13 Patient 2H relative rotations (left) and translations (right) at each vertebral level during flexion-extension.	161
A.14 Patient 2H intervertebral contact forces normalized with respect to body weight during flexion-extension. 1-dir=Ant(+)/Post(-), 2-dir=Sup(+)/Inf(-), 3-dir=Rt(+)/Lt(-).	161
A.15 Patient 2H segmental ligament forces normalized with respect to body weight during flexion-extension.	162
A.16 Patient 2H bilateral muscle forces normalized with respect to body weight during flexion-extension.	162
A.17 Patient 2H relative rotations (left) and translations (right) at each vertebral level during left-to-right lateral flexion.	162
A.18 Patient 2H intervertebral contact forces normalized with respect to body weight during right-to-left lateral flexion. 1-dir=Ant(+)/Post(-), 2-dir=Sup(+)/Inf(-), 3-dir=Rt(+)/Lt(-).	163
A.19 Patient 2H segmental ligament forces normalized with respect to body weight during left-to-right lateral flexion.	163
A.20 Patient 2H bilateral muscle forces normalized with respect to body weight during left-to-right lateral flexion.	163
A.21 Patient 2H relative rotations (left) and translations (right) at each vertebral level during left-to-right axial rotation.	164
A.22 Patient 2H intervertebral contact forces normalized with respect to body weight during left-to-right axial rotation. 1-dir=Ant(+)/Post(-), 2-dir=Sup(+)/Inf(-), 3-dir=Rt(+)/Lt(-).	164
A.23 Patient 2H segmental ligament forces normalized with respect to body weight during left-to-right axial rotation.	164
A.24 Patient 2H bilateral muscle forces normalized to body weight during left-to-right axial rotation.	165
A.25 Patient 3H relative rotations (left) and translations (right) at each vertebral level during flexion-extension.	166
A.26 Patient 3H intervertebral contact forces normalized with respect to body weight during flexion-extension. 1-dir=Ant(+)/Post(-), 2-dir=Sup(+)/Inf(-), 3-dir=Rt(+)/Lt(-).	166
A.27 Patient 3H segmental ligament forces normalized with respect to body weight during flexion-extension.	167
A.28 Patient 3H bilateral muscle forces normalized with respect to body weight during flexion-extension.	167
A.29 Patient 3H relative rotations (left) and translations (right) at each vertebral level during left-to-right lateral flexion.	167

A.30	Patient 3H intervertebral contact forces normalized with respect to body weight during right-to-left lateral flexion. 1-dir=Ant(+)/Post(-), 2-dir=Sup(+)/Inf(-), 3-dir=Rt(+)/Lt(-).	168
A.31	Patient 3H segmental ligament forces normalized with respect to body weight during left-to-right lateral flexion.	168
A.32	Patient 3H bilateral muscle forces normalized with respect to body weight during left-to-right lateral flexion.	168
A.33	Patient 3H relative rotations (left) and translations (right) at each vertebral level during left-to-right axial rotation.	169
A.34	Patient 3H intervertebral contact forces normalized with respect to body weight during left-to-right axial rotation. 1-dir=Ant(+)/Post(-), 2-dir=Sup(+)/Inf(-), 3-dir=Rt(+)/Lt(-).	169
A.35	Patient 3H segmental ligament forces normalized with respect to body weight during left-to-right axial rotation.	169
A.36	Patient 3H bilateral muscle forces normalized to body weight during left-to-right axial rotation.	170
A.37	Patient 4H relative rotations (left) and translations (right) at each vertebral level during flexion-extension.	171
A.38	Patient 4H intervertebral contact forces normalized with respect to body weight during flexion-extension. 1-dir=Ant(+)/Post(-), 2-dir=Sup(+)/Inf(-), 3-dir=Rt(+)/Lt(-).	171
A.39	Patient 4H segmental ligament forces normalized with respect to body weight during flexion-extension.	172
A.40	Patient 1H bilateral muscle forces normalized with respect to body weight during flexion-extension.	172
A.41	Patient 4H relative rotations (left) and translations (right) at each vertebral level during left-to-right lateral flexion.	172
A.42	Patient 4H intervertebral contact forces normalized with respect to body weight during right-to-left lateral flexion. 1-dir=Ant(+)/Post(-), 2-dir=Sup(+)/Inf(-), 3-dir=Rt(+)/Lt(-).	173
A.43	Patient 4H segmental ligament forces normalized with respect to body weight during left-to-right lateral flexion.	173
A.44	Patient 4H bilateral muscle forces normalized with respect to body weight during left-to-right lateral flexion.	173
A.45	Patient 4H relative rotations (left) and translations (right) at each vertebral level during left-to-right axial rotation.	174
A.46	Patient 4H intervertebral contact forces normalized with respect to body weight during left-to-right axial rotation. 1-dir=Ant(+)/Post(-), 2-dir=Sup(+)/Inf(-), 3-dir=Rt(+)/Lt(-).	174

A.47 Patient 4H bilateral muscle forces normalized to body weight during left-to-right axial rotation.....	174
A.48 Patient 4H bi-lateral muscle forces normalized to patient's body weight (BW) during left-to-right axial rotation.....	175
A.49 Patient 5H relative rotations (left) and translations (right) at each vertebral level during flexion-extension.	176
A.50 Patient 5H intervertebral contact forces normalized with respect to body weight during flexion-extension. 1-dir=Ant(+)/Post(-), 2-dir=Sup(+)/Inf(-), 3-dir=Rt(+)/Lt(-).....	176
A.51 Patient 5H segmental ligament forces normalized with respect to body weight during flexion-extension.	177
A.52 Patient 5H bilateral muscle forces normalized with respect to body weight during flexion-extension.....	177
A.53 Patient 5H relative rotations (left) and translations (right) at each vertebral level during left-to-right lateral flexion.	177
A.54 Patient 5H intervertebral contact forces normalized with respect to body weight during right-to-left lateral flexion. 1-dir=Ant(+)/Post(-), 2-dir=Sup(+)/Inf(-), 3-dir=Rt(+)/Lt(-). 178	
A.55 Patient 2H segmental ligament forces normalized with respect to body weight during left-to-right lateral flexion.....	178
A.56 Patient 5H bilateral muscle forces normalized with respect to body weight during left-to-right lateral flexion.	178
A.57 Patient 5H relative rotations (left) and translations (right) at each vertebral level during left-to-right axial rotation.	179
A.58 Patient 5H intervertebral contact forces normalized with respect to body weight during left-to-right axial rotation. 1-dir=Ant(+)/Post(-), 2-dir=Sup(+)/Inf(-), 3-dir=Rt(+)/Lt(-).....	179
A.59 Patient 5H segmental ligament forces normalized with respect to body weight during left-to-right axial rotation.....	179
A.60 Patient 5H bilateral muscle forces normalized to body weight during left-to-right axial rotation.....	180
A.61 Patient 6H relative rotations (left) and translations (right) at each vertebral level during flexion-extension.	181
A.62 Patient 6H intervertebral contact forces normalized with respect to body weight during flexion-extension. 1-dir=Ant(+)/Post(-), 2-dir=Sup(+)/Inf(-), 3-dir=Rt(+)/Lt(-).....	181
A.63 Patient 6H segmental ligament forces normalized with respect to body weight during flexion-extension.	182

A.64 Patient 6H bilateral muscle forces normalized with respect to body weight during flexion-extension.....	182
A.65 Patient 6H relative rotations (left) and translations (right) at each vertebral level during left-to-right lateral flexion.	182
A.66 Patient 6H intervertebral contact forces normalized with respect to body weight during right-to-left lateral flexion. 1-dir=Ant(+)/Post(-), 2-dir=Sup(+)/Inf(-), 3-dir=Rt(+)/Lt(-). 183	
A.67 Patient 6H segmental ligament forces normalized with respect to body weight during left-to-right lateral flexion.	183
A.68 Patient 6H bilateral muscle forces normalized with respect to body weight during left-to-right lateral flexion.	183
A.69 Patient 6H relative rotations (left) and translations (right) at each vertebral level during left-to-right axial rotation.	184
A.70 Patient 6H intervertebral contact forces normalized with respect to body weight during left-to-right axial rotation. 1-dir=Ant(+)/Post(-), 2-dir=Sup(+)/Inf(-), 3-dir=Rt(+)/Lt(-).....	184
A.71 Patient 6H segmental ligament forces normalized with respect to body weight during left-to-right axial rotation.....	184
A.72 Patient 6H bilateral muscle forces normalized to body weight during left-to-right axial rotation.....	185
A.73 Patient 7H relative rotations (left) and translations (right) at each vertebral level during flexion-extension.	186
A.74 Patient 7H intervertebral contact forces normalized with respect to body weight during flexion-extension. 1-dir=Ant(+)/Post(-), 2-dir=Sup(+)/Inf(-), 3-dir=Rt(+)/Lt(-).....	186
A.75 Patient 7H segmental ligament forces normalized with respect to body weight during flexion-extension.	187
A.76 Patient 7H bilateral muscle forces normalized with respect to body weight during flexion-extension.....	187
A.77 Patient 7H relative rotations (left) and translations (right) at each vertebral level during left-to-right lateral flexion.	187
A.78 Patient 7H intervertebral contact forces normalized with respect to body weight during right-to-left lateral flexion. 1-dir=Ant(+)/Post(-), 2-dir=Sup(+)/Inf(-), 3-dir=Rt(+)/Lt(-). 188	
A.79 Patient 7H segmental ligament forces normalized with respect to body weight during left-to-right lateral flexion.....	188
A.80 Patient 7H bilateral muscle forces normalized with respect to body weight during left-to-right lateral flexion.	188

A.81 Patient 7H relative rotations (left) and translations (right) at each vertebral level during left-to-right axial rotation.	189
A.82 Patient 7H intervertebral contact forces normalized with respect to body weight during left-to-right axial rotation. 1-dir=Ant(+)/Post(-), 2-dir=Sup(+)/Inf(-), 3-dir=Rt(+)/Lt(-).....	189
A.83 Patient 7H segmental ligament forces normalized with respect to body weight during left-to-right axial rotation.	189
A.84 Patient 7H bilateral muscle forces normalized to body weight during left-to-right axial rotation.	190
A.85 Patient 8H relative rotations (left) and translations (right) at each vertebral level during flexion-extension.	191
A.86 Patient 8H intervertebral contact forces normalized with respect to body weight during flexion-extension. 1-dir=Ant(+)/Post(-), 2-dir=Sup(+)/Inf(-), 3-dir=Rt(+)/Lt(-).....	191
A.87 Patient 8H segmental ligament forces normalized with respect to body weight during flexion-extension.	192
A.88 Patient 8H bilateral muscle forces normalized with respect to body weight during flexion-extension.	192
A.89 Patient 8H relative rotations (left) and translations (right) at each vertebral level during left-to-right lateral flexion.	192
A.90 Patient 8H intervertebral contact forces normalized with respect to body weight during right-to-left lateral flexion. 1-dir=Ant(+)/Post(-), 2-dir=Sup(+)/Inf(-), 3-dir=Rt(+)/Lt(-).	193
A.91 Patient 8H segmental ligament forces normalized with respect to body weight during left-to-right lateral flexion.	193
A.92 Patient 8H bilateral muscle forces normalized with respect to body weight during left-to-right lateral flexion.	193
A.93 Patient 8H relative rotations (left) and translations (right) at each vertebral level during left-to-right axial rotation.	194
A.94 Patient 8H intervertebral contact forces normalized with respect to body weight during left-to-right axial rotation. 1-dir=Ant(+)/Post(-), 2-dir=Sup(+)/Inf(-), 3-dir=Rt(+)/Lt(-).....	194
A.95 Patient 8H segmental ligament forces normalized with respect to body weight during left-to-right axial rotation.	194
A.96 Patient 8H bilateral muscle forces normalized to body weight during left-to-right axial rotation.	195
A.97 Patient 9H relative rotations (left) and translations (right) at each vertebral level during flexion-extension.	196

A.98 Patient 9H intervertebral contact forces normalized with respect to body weight during flexion-extension. 1-dir=Ant(+)/Post(-), 2-dir=Sup(+)/Inf(-), 3-dir=Rt(+)/Lt(-).....	196
A.99 Patient 9H segmental ligament forces normalized with respect to body weight during flexion-extension.	197
A.100 Patient 9H bilateral muscle forces normalized with respect to body weight during flexion-extension.....	197
A.101 Patient 9H relative rotations (left) and translations (right) at each vertebral level during left-to-right lateral flexion.	197
A.102 Patient 9H intervertebral contact forces normalized with respect to body weight during right-to-left lateral flexion. 1-dir=Ant(+)/Post(-), 2-dir=Sup(+)/Inf(-), 3-dir=Rt(+)/Lt(-).	198
A.103 Patient 9H segmental ligament forces normalized with respect to body weight during left-to-right lateral flexion.....	198
A.104 Patient 9H bilateral muscle forces normalized with respect to body weight during left-to-right lateral flexion.	198
A.105 Patient 9H relative rotations (left) and translations (right) at each vertebral level during left-to-right axial rotation.	199
A.106 Patient 9H intervertebral contact forces normalized with respect to body weight during left-to-right axial rotation. 1-dir=Ant(+)/Post(-), 2-dir=Sup(+)/Inf(-), 3-dir=Rt(+)/Lt(-)..	199
A.107 Patient 9H segmental ligament forces normalized with respect to body weight during left-to-right axial rotation.....	199
A.108 Patient 9H bilateral muscle forces normalized to body weight during left-to-right axial rotation.....	200
A.109 Patient 10H relative rotations (left) and translations (right) at each vertebral level during flexion-extension.	201
A.110 Patient 10H intervertebral contact forces normalized with respect to body weight during flexion-extension. 1-dir=Ant(+)/Post(-), 2-dir=Sup(+)/Inf(-), 3-dir=Rt(+)/Lt(-).....	201
A.111 Patient 10H segmental ligament forces normalized with respect to body weight during flexion-extension.	202
A.112 Patient 10H bilateral muscle forces normalized with respect to body weight during flexion-extension.	202
A.113 Patient 10H relative rotations (left) and translations (right) at each vertebral level during left-to-right lateral flexion.	202
A.114 Patient 10H intervertebral contact forces normalized with respect to body weight during left-to-right lateral flexion. 1-dir=Ant(+)/Post(-), 2-dir=Sup(+)/Inf(-), 3-dir=Rt(+)/Lt(-).	203

A.115 Patient 10H segmental ligament forces normalized with respect to body weight during left-to-right lateral flexion.	203
A.116 Patient 10H bilateral muscle forces normalized with respect to body weight during left-to-right lateral flexion	203
A.117 Patient 10H relative rotations (left) and translations (right) at each vertebral level during left-to-right axial rotation.	204
A.118 Patient 1H intervertebral contact forces normalized with respect to body weight during left-to-right axial rotation. 1-dir=Ant(+)/Post(-), 2-dir=Sup(+)/Inf(-), 3-dir=Rt(+)/Lt(-)..	204
A.119 Patient 10H segmental ligament forces normalized with respect to body weight during left-to-right axial rotation.	204
A.120 Patient 10H bilateral muscle forces normalized to body weight during left-to-right axial rotation.....	205
A.121 Patient 1LBP relative rotations (left) and translations (right) at each vertebral level during flexion-extension.	206
A.122 Patient 1LBP intervertebral contact forces normalized with respect to body weight during flexion-extension. 1-dir=Ant(+)/Post(-), 2-dir=Sup(+)/Inf(-), 3-dir=Rt(+)/Lt(-).....	206
A.123 Patient 1LBP segmental ligament forces normalized with respect to body weight during flexion-extension.	207
A.124 Patient 1LBP bilateral muscle forces normalized with respect to body weight during flexion-extension.	207
A.125 Patient 1LBP relative rotations (left) and translations (right) at each vertebral level during left-to-right lateral flexion.	207
A.126 Patient 1LBP intervertebral contact forces normalized with respect to body weight during left-to-right lateral flexion. 1-dir=Ant(+)/Post(-), 2-dir=Sup(+)/Inf(-), 3-dir=Rt(+)/Lt(-).	208
A.127 Patient 1LBP segmental ligament forces normalized with respect to body weight during left-to-right lateral flexion.	208
A.128 Patient 1LBP bilateral muscle forces normalized to body weight during left-to-right lateral flexion.....	208
A.129 Patient 1LBP relative rotations (left) and translations (right) at each vertebral level during left-to-right axial rotation.	209
A.130 Patient 1LBP intervertebral contact forces normalized with respect to body weight during left-to-right axial rotation. 1-dir=Ant(+)/Post(-), 2-dir=Sup(+)/Inf(-), 3-dir=Rt(+)/Lt(-)..	209
A.131 Patient 1LBP segmental ligament forces normalized with respect to body weight during left-to-right axial rotation.	209

A.132 Patient 1LBP bilateral muscle forces normalized with respect to body weight during left-to-right axial rotation.	210
A.133 Patient 2LBP relative rotations (left) and translations (right) at each vertebral level during flexion-extension.	211
A.134 Patient 2LBP intervertebral contact forces normalized with respect to body weight during flexion-extension. 1-dir=Ant(+)/Post(-), 2-dir=Sup(+)/Inf(-), 3-dir=Rt(+)/Lt(-).	211
A.135 Patient 2LBP segmental ligament forces normalized with respect to body weight during flexion-extension.	212
A.136 Patient 2LBP bilateral muscle forces normalized with respect to body weight during flexion-extension.	212
A.137 Patient 2LBP relative rotations (left) and translations (right) at each vertebral level during left-to-right lateral flexion.	212
A.138 Patient 2LBP intervertebral contact forces normalized with respect to body weight during left-to-right lateral flexion. 1-dir=Ant(+)/Post(-), 2-dir=Sup(+)/Inf(-), 3-dir=Rt(+)/Lt(-).	213
A.139 Patient 2LBP segmental ligament forces normalized with respect to body weight during left-to-right lateral flexion.	213
A.140 Patient 2LBP bilateral muscle forces normalized to body weight during left-to-right lateral flexion.	213
A.141 Patient 2LBP relative rotations (left) and translations (right) at each vertebral level during left-to-right axial rotation.	214
A.142 Patient 2LBP intervertebral contact forces normalized with respect to body weight during left-to-right axial rotation. 1-dir=Ant(+)/Post(-), 2-dir=Sup(+)/Inf(-), 3-dir=Rt(+)/Lt(-).	214
A.143 Patient 2LBP segmental ligament forces normalized with respect to body weight during left-to-right axial rotation.	214
A.144 Patient 2LBP bilateral muscle forces normalized with respect to body weight during left-to-right axial rotation.	215
A.145 Patient 3LBP relative rotations (left) and translations (right) at each vertebral level during flexion-extension.	216
A.146 Patient 3LBP intervertebral contact forces normalized with respect to body weight during flexion-extension. 1-dir=Ant(+)/Post(-), 2-dir=Sup(+)/Inf(-), 3-dir=Rt(+)/Lt(-).	216
A.147 Patient 3LBP segmental ligament forces normalized with respect to body weight during flexion-extension.	217
A.148 Patient 3LBP bilateral muscle forces normalized with respect to body weight during flexion-extension.	217

A.149 Patient 3LBP relative rotations (left) and translations (right) at each vertebral level during left-to-right lateral flexion.	217
A.150 Patient 3LBP intervertebral contact forces normalized with respect to body weight during left-to-right lateral flexion. 1-dir=Ant(+)/Post(-), 2-dir=Sup(+)/Inf(-), 3-dir=Rt(+)/Lt(-).	218
A.151 Patient 3LBP segmental ligament forces normalized with respect to body weight during left-to-right lateral flexion.	218
A.152 Patient 3LBP bilateral muscle forces normalized to body weight during left-to-right lateral flexion.	218
A.153 Patient 3LBP relative rotations (left) and translations (right) at each vertebral level during left-to-right axial rotation.	219
A.154 Patient 3LBP intervertebral contact forces normalized with respect to body weight during left-to-right axial rotation. 1-dir=Ant(+)/Post(-), 2-dir=Sup(+)/Inf(-), 3-dir=Rt(+)/Lt(-).	219
A.155 Patient 3LBP segmental ligament forces normalized with respect to body weight during left-to-right axial rotation.	219
A.156 Patient 3LBP bilateral muscle forces normalized with respect to body weight during left-to-right axial rotation.	220
A.157 Patient 4LBP relative rotations (left) and translations (right) at each vertebral level during flexion-extension.	221
A.158 Patient 4LBP intervertebral contact forces normalized with respect to body weight during flexion-extension. 1-dir=Ant(+)/Post(-), 2-dir=Sup(+)/Inf(-), 3-dir=Rt(+)/Lt(-).	221
A.159 Patient 4LBP segmental ligament forces normalized with respect to body weight during flexion-extension.	222
A.160 Patient 4LBP bilateral muscle forces normalized with respect to body weight during flexion-extension.	222
A.161 Patient 4LBP relative rotations (left) and translations (right) at each vertebral level during left-to-right lateral flexion.	222
A.162 Patient 4LBP intervertebral contact forces normalized with respect to body weight during left-to-right lateral flexion. 1-dir=Ant(+)/Post(-), 2-dir=Sup(+)/Inf(-), 3-dir=Rt(+)/Lt(-).	223
A.163 Patient 4LBP segmental ligament forces normalized with respect to body weight during left-to-right lateral flexion.	223
A.164 Patient 4LBP bilateral muscle forces normalized to body weight during left-to-right lateral flexion.	223
A.165 Patient 4LBP relative rotations (left) and translations (right) at each vertebral level during left-to-right axial rotation.	224

A.166	Patient 4LBP intervertebral contact forces normalized with respect to body weight during left-to-right axial rotation. 1-dir=Ant(+)/Post(-), 2-dir=Sup(+)/Inf(-), 3-dir=Rt(+)/Lt(-)..	224
A.167	Patient 4LBP segmental ligament forces normalized with respect to body weight during left-to-right axial rotation.	224
A.168	Patient 4LBP bilateral muscle forces normalized with respect to body weight during left-to-right axial rotation.	225
A.169	Patient 5LBP relative rotations (left) and translations (right) at each vertebral level during flexion-extension.	226
A.170	Patient 5LBP intervertebral contact forces normalized with respect to body weight during flexion-extension. 1-dir=Ant(+)/Post(-), 2-dir=Sup(+)/Inf(-), 3-dir=Rt(+)/Lt(-).	226
A.171	Patient 5LBP segmental ligament forces normalized with respect to body weight during flexion-extension.	227
A.172	Patient 5LBP bilateral muscle forces normalized with respect to body weight during flexion-extension.	227
A.173	Patient 5LBP relative rotations (left) and translations (right) at each vertebral level during left-to-right lateral flexion.	227
A.174	Patient 5LBP intervertebral contact forces normalized with respect to body weight during left-to-right lateral flexion. 1-dir=Ant(+)/Post(-), 2-dir=Sup(+)/Inf(-), 3-dir=Rt(+)/Lt(-).	228
A.175	Patient 5LBP segmental ligament forces normalized with respect to body weight during left-to-right lateral flexion.	228
A.176	Patient 5LBP bilateral muscle forces normalized to body weight during left-to-right lateral flexion.	228
A.177	Patient 5LBP relative rotations (left) and translations (right) at each vertebral level during left-to-right axial rotation.	229
A.178	Patient 5LBP intervertebral contact forces normalized with respect to body weight during left-to-right axial rotation. 1-dir=Ant(+)/Post(-), 2-dir=Sup(+)/Inf(-), 3-dir=Rt(+)/Lt(-)..	229
A.179	Patient 5LBP segmental ligament forces normalized with respect to body weight during left-to-right axial rotation.	229
A.180	Patient 5LBP bilateral muscle forces normalized with respect to body weight during left-to-right axial rotation.	230
A.181	Patient 6LBP relative rotations (left) and translations (right) at each vertebral level during flexion-extension.	231
A.182	Patient 6LBP intervertebral contact forces normalized with respect to body weight during flexion-extension. 1-dir=Ant(+)/Post(-), 2-dir=Sup(+)/Inf(-), 3-dir=Rt(+)/Lt(-).	231

A.183 Patient 6LBP segmental ligament forces normalized with respect to body weight during flexion-extension.	232
A.184 Patient 6LBP bilateral muscle forces normalized with respect to body weight during flexion-extension.	232
A.185 Patient 6LBP relative rotations (left) and translations (right) at each vertebral level during left-to-right lateral flexion.	232
A.186 Patient 6LBP intervertebral contact forces normalized with respect to body weight during left-to-right lateral flexion. 1-dir=Ant(+)/Post(-), 2-dir=Sup(+)/Inf(-), 3-dir=Rt(+)/Lt(-). 233	
A.187 Patient 6LBP segmental ligament forces normalized with respect to body weight during left-to-right lateral flexion.	233
A.188 Patient 6LBP bilateral muscle forces normalized to body weight during left-to-right lateral flexion.	233
A.189 Patient 6LBP relative rotations (left) and translations (right) at each vertebral level during left-to-right axial rotation.	234
A.190 Patient 6LBP intervertebral contact forces normalized with respect to body weight during left-to-right axial rotation. 1-dir=Ant(+)/Post(-), 2-dir=Sup(+)/Inf(-), 3-dir=Rt(+)/Lt(-).. 234	
A.191 Patient 6LBP segmental ligament forces normalized with respect to body weight during left-to-right axial rotation.	234
A.192 Patient 6LBP bilateral muscle forces normalized with respect to body weight during left-to-right axial rotation.	235
A.193 Patient 7LBP relative rotations (left) and translations (right) at each vertebral level during flexion-extension.	236
A.194 Patient 7LBP intervertebral contact forces normalized with respect to body weight during flexion-extension. 1-dir=Ant(+)/Post(-), 2-dir=Sup(+)/Inf(-), 3-dir=Rt(+)/Lt(-).	236
A.195 Patient 7LBP segmental ligament forces normalized with respect to body weight during flexion-extension.	237
A.196 Patient 7LBP bilateral muscle forces normalized with respect to body weight during flexion-extension.	237
A.197 Patient 7LBP relative rotations (left) and translations (right) at each vertebral level during left-to-right lateral flexion.	237
A.198 Patient 7LBP intervertebral contact forces normalized with respect to body weight during left-to-right lateral flexion. 1-dir=Ant(+)/Post(-), 2-dir=Sup(+)/Inf(-), 3-dir=Rt(+)/Lt(-). 238	
A.199 Patient 7LBP segmental ligament forces normalized with respect to body weight during left-to-right lateral flexion.	238

A.200 Patient 7LBP bilateral muscle forces normalized to body weight during left-to-right lateral flexion.	238
A.201 Patient 7LBP relative rotations (left) and translations (right) at each vertebral level during left-to-right axial rotation.	239
A.202 Patient 7LBP intervertebral contact forces normalized with respect to body weight during left-to-right axial rotation. 1-dir=Ant(+)/Post(-), 2-dir=Sup(+)/Inf(-), 3-dir=Rt(+)/Lt(-)..	239
A.203 Patient 7LBP segmental ligament forces normalized with respect to body weight during left-to-right axial rotation.	239
A.204 Patient 7LBP bilateral muscle forces normalized with respect to body weight during left-to-right axial rotation.	240
A.205 Patient 8LBP relative rotations (left) and translations (right) at each vertebral level during flexion-extension.	241
A.206 Patient 8LBP intervertebral contact forces normalized with respect to body weight during flexion-extension. 1-dir=Ant(+)/Post(-), 2-dir=Sup(+)/Inf(-), 3-dir=Rt(+)/Lt(-).	241
A.207 Patient 8LBP segmental ligament forces normalized with respect to body weight during flexion-extension.	242
A.208 Patient 8LBP bilateral muscle forces normalized with respect to body weight during flexion-extension.	242
A.209 Patient 8LBP relative rotations (left) and translations (right) at each vertebral level during left-to-right lateral flexion.	242
A.210 Patient 8LBP intervertebral contact forces normalized with respect to body weight during left-to-right lateral flexion. 1-dir=Ant(+)/Post(-), 2-dir=Sup(+)/Inf(-), 3-dir=Rt(+)/Lt(-).	243
A.211 Patient 8LBP segmental ligament forces normalized with respect to body weight during left-to-right lateral flexion.	243
A.212 Patient 8LBP bilateral muscle forces normalized to body weight during left-to-right lateral flexion.	243
A.213 Patient 8LBP relative rotations (left) and translations (right) at each vertebral level during left-to-right axial rotation.	244
A.214 Patient 8LBP intervertebral contact forces normalized with respect to body weight during left-to-right axial rotation. 1-dir=Ant(+)/Post(-), 2-dir=Sup(+)/Inf(-), 3-dir=Rt(+)/Lt(-)..	244
A.215 Patient 8LBP segmental ligament forces normalized with respect to body weight during left-to-right axial rotation.	244
A.216 Patient 8LBP bilateral muscle forces normalized with respect to body weight during left-to-right axial rotation.	245

A.217 Patient 9LBP relative rotations (left) and translations (right) at each vertebral level during flexion-extension.	246
A.218 Patient 9LBP intervertebral contact forces normalized with respect to body weight during flexion-extension. 1-dir=Ant(+)/Post(-), 2-dir=Sup(+)/Inf(-), 3-dir=Rt(+)/Lt(-).	246
A.219 Patient 9LBP segmental ligament forces normalized with respect to body weight during flexion-extension.	247
A.220 Patient 9LBP bilateral muscle forces normalized with respect to body weight during flexion-extension.	247
A.221 Patient 9LBP relative rotations (left) and translations (right) at each vertebral level during left-to-right lateral flexion.	247
A.222 Patient 9LBP intervertebral contact forces normalized with respect to body weight during left-to-right lateral flexion. 1-dir=Ant(+)/Post(-), 2-dir=Sup(+)/Inf(-), 3-dir=Rt(+)/Lt(-).	248
A.223 Patient 9LBP segmental ligament forces normalized with respect to body weight during left-to-right lateral flexion.	248
A.224 Patient 9LBP bilateral muscle forces normalized to body weight during left-to-right lateral flexion.	248
A.225 Patient 9LBP relative rotations (left) and translations (right) at each vertebral level during left-to-right axial rotation.	249
A.226 Patient 9LBP intervertebral contact forces normalized with respect to body weight during left-to-right axial rotation. 1-dir=Ant(+)/Post(-), 2-dir=Sup(+)/Inf(-), 3-dir=Rt(+)/Lt(-). ..	249
A.227 Patient 9LBP segmental ligament forces normalized with respect to body weight during left-to-right axial rotation.	249
A.228 Patient 9LBP bilateral muscle forces normalized with respect to body weight during left-to-right axial rotation.	250
A.229 Patient 10LBP relative rotations (left) and translations (right) at each vertebral level during flexion-extension.	251
A.230 Patient 10LBP intervertebral contact forces normalized with respect to body weight during flexion-extension. 1-dir=Ant(+)/Post(-), 2-dir=Sup(+)/Inf(-), 3-dir=Rt(+)/Lt(-). ..	251
A.231 Patient 10LBP segmental ligament forces normalized with respect to body weight during flexion-extension.	252
A.232 Patient 10LBP bilateral muscle forces normalized with respect to body weight during flexion-extension.	252
A.233 Patient 10LBP relative rotations (left) and translations (right) at each vertebral level during left-to-right lateral flexion.	252

A.234 Patient 10LBP intervertebral contact forces normalized with respect to body weight during left-to-right lateral flexion. 1-dir=Ant(+)/Post(-), 2-dir=Sup(+)/Inf(-), 3-dir=Rt(+)/Lt(-).	253
A.235 Patient 10LBP segmental ligament forces normalized with respect to body weight during left-to-right lateral flexion.	253
A.236 Patient 10LBP bilateral muscle forces normalized to body weight during left-to-right lateral flexion.	253
A.237 Patient 10LBP relative rotations (left) and translations (right) at each vertebral level during left-to-right axial rotation.	254
A.238 Patient 10LBP intervertebral contact forces normalized with respect to body weight during left-to-right axial rotation. 1-dir=Ant(+)/Post(-), 2-dir=Sup(+)/Inf(-), 3-dir=Rt(+)/Lt(-).	254
A.239 Patient 10LBP segmental ligament forces normalized with respect to body weight during left-to-right axial rotation.	254
A.240 Patient 10LBP bilateral muscle forces normalized with respect to body weight during left-to-right axial rotation.	255
A.241 Patient 1D relative rotations (left) and translations (right) at each vertebral level during flexion-extension.	256
A.242 Patient 1D intervertebral contact forces normalized with respect to body weight during flexion-extension. 1-dir=Ant(+)/Post(-), 2-dir=Sup(+)/Inf(-), 3-dir=Rt(+)/Lt(-).	256
A.243 Patient 1D segmental ligament forces normalized with respect to body weight during flexion-extension.	257
A.244 Patient 1D bilateral muscle forces normalized with respect to body weight during flexion-extension.	257
A.245 Patient 1D relative rotations (left) and translations (right) at each vertebral level during left-to-right lateral flexion.	257
A.246 Patient 1D intervertebral contact forces normalized with respect to body weight during left-to-right lateral flexion. 1-dir=Ant(+)/Post(-), 2-dir=Sup(+)/Inf(-), 3-dir=Rt(+)/Lt(-).	258
A.247 Patient 1D segmental ligament forces normalized with respect to body weight during left-to-right lateral flexion.	258
A.248 Patient 1D bilateral muscle forces normalized with respect to body weight during left-to-right lateral flexion.	258
A.249 Patient 1D relative rotations (left) and translations (right) at each vertebral level during left-to-right axial rotation.	259
A.250 Patient 1D intervertebral contact forces normalized with respect to body weight during left-to-right axial rotation. 1-dir=Ant(+)/Post(-), 2-dir=Sup(+)/Inf(-), 3-dir=Rt(+)/Lt(-).	259

A.251 Patient 1D segmental ligament forces normalized with respect to body weight during left-to-right axial rotation.	259
A.252 Patient 1D bilateral muscle forces normalized with respect to body weight during left-to-right axial rotation.	260
A.253 Patient 2D relative rotations (left) and translations (right) at each vertebral level during flexion-extension.	261
A.254 Patient 2D intervertebral contact forces normalized with respect to body weight during flexion-extension. 1-dir=Ant(+)/Post(-), 2-dir=Sup(+)/Inf(-), 3-dir=Rt(+)/Lt(-).	261
A.255 Patient 2D segmental ligament forces normalized with respect to body weight during flexion-extension.	262
A.256 Patient 2D bilateral muscle forces normalized with respect to body weight during flexion-extension.	262
A.257 Patient 2D relative rotations (left) and translations (right) at each vertebral level during left-to-right lateral flexion.	262
A.258 Patient 2D intervertebral contact forces normalized with respect to body weight during left-to-right lateral flexion. 1-dir=Ant(+)/Post(-), 2-dir=Sup(+)/Inf(-), 3-dir=Rt(+)/Lt(-).	263
A.259 Patient 2D segmental ligament forces normalized with respect to body weight during left-to-right lateral flexion.	263
A.260 Patient 2D bilateral muscle forces normalized with respect to body weight during left-to-right lateral flexion.	263
A.261 Patient 2D relative rotations (left) and translations (right) at each vertebral level during left-to-right axial rotation.	264
A.262 Patient 2D intervertebral contact forces normalized with respect to body weight during left-to-right axial rotation. 1-dir=Ant(+)/Post(-), 2-dir=Sup(+)/Inf(-), 3-dir=Rt(+)/Lt(-).	264
A.263 Patient 2D segmental ligament forces normalized with respect to body weight during left-to-right axial rotation.	264
A.264 Patient 2D bilateral muscle forces normalized with respect to body weight during left-to-right axial rotation.	265
A.265 Patient 3D relative rotations (left) and translations (right) at each vertebral level during flexion-extension.	266
A.266 Patient 3D intervertebral contact forces normalized with respect to body weight during flexion-extension. 1-dir=Ant(+)/Post(-), 2-dir=Sup(+)/Inf(-), 3-dir=Rt(+)/Lt(-).	266
A.267 Patient 3D segmental ligament forces normalized with respect to body weight during flexion-extension.	267

A.268 Patient 3D bilateral muscle forces normalized with respect to body weight during flexion-extension.....	267
A.269 Patient 3D relative rotations (left) and translations (right) at each vertebral level during left-to-right lateral flexion.	267
A.270 Patient 3D intervertebral contact forces normalized with respect to body weight during left-to-right lateral flexion. 1-dir=Ant(+)/Post(-), 2-dir=Sup(+)/Inf(-), 3-dir=Rt(+)/Lt(-). ..	268
A.271 Patient 3D segmental ligament forces normalized with respect to body weight during left-to-right lateral flexion.	268
A.272 Patient 3D bilateral muscle forces normalized with respect to body weight during left-to-right lateral flexion.	268
A.273 Patient 3D relative rotations (left) and translations (right) at each vertebral level during left-to-right axial rotation.	269
A.274 Patient 3D intervertebral contact forces normalized with respect to body weight during left-to-right axial rotation. 1-dir=Ant(+)/Post(-), 2-dir=Sup(+)/Inf(-), 3-dir=Rt(+)/Lt(-)..	269
A.275 Patient 3D segmental ligament forces normalized with respect to body weight during left-to-right axial rotation.	269
A.276 Patient 3D bilateral muscle forces normalized with respect to body weight during left-to-right axial rotation.	270
A.277 Patient 4D relative rotations (left) and translations (right) at each vertebral level during flexion-extension.	271
A.278 Patient 4D intervertebral contact forces normalized with respect to body weight during flexion-extension. 1-dir=Ant(+)/Post(-), 2-dir=Sup(+)/Inf(-), 3-dir=Rt(+)/Lt(-).	271
A.279 Patient 4D segmental ligament forces normalized with respect to body weight during flexion-extension.	272
A.280 Patient 4D bilateral muscle forces normalized with respect to body weight during flexion-extension.	272
A.281 Patient 4D relative rotations (left) and translations (right) at each vertebral level during left-to-right lateral flexion.	272
A.282 Patient 4D intervertebral contact forces normalized with respect to body weight during left-to-right lateral flexion. 1-dir=Ant(+)/Post(-), 2-dir=Sup(+)/Inf(-), 3-dir=Rt(+)/Lt(-). ..	273
A.283 Patient 4D segmental ligament forces normalized with respect to body weight during left-to-right lateral flexion.	273
A.284 Patient 4D bilateral muscle forces normalized with respect to body weight during left-to-right lateral flexion.	273

A.285 Patient 4D relative rotations (left) and translations (right) at each vertebral level during left-to-right axial rotation.	274
A.286 Patient 4D intervertebral contact forces normalized with respect to body weight during left-to-right axial rotation. 1-dir=Ant(+)/Post(-), 2-dir=Sup(+)/Inf(-), 3-dir=Rt(+)/Lt(-)..	274
A.287 Patient 4D segmental ligament forces normalized with respect to body weight during left-to-right axial rotation.	274
A.288 Patient 4D bilateral muscle forces normalized with respect to body weight during left-to-right axial rotation.	275
A.289 Patient 5D relative rotations (left) and translations (right) at each vertebral level during flexion-extension.	276
A.290 Patient 5D intervertebral contact forces normalized with respect to body weight during flexion-extension. 1-dir=Ant(+)/Post(-), 2-dir=Sup(+)/Inf(-), 3-dir=Rt(+)/Lt(-).....	276
A.291 Patient 5D segmental ligament forces normalized with respect to body weight during flexion-extension.	277
A.292 Patient 5D bilateral muscle forces normalized with respect to body weight during flexion-extension.	277
A.293 Patient 5D relative rotations (left) and translations (right) at each vertebral level during left-to-right lateral flexion.	277
A.294 Patient 5D intervertebral contact forces normalized with respect to body weight during left-to-right lateral flexion. 1-dir=Ant(+)/Post(-), 2-dir=Sup(+)/Inf(-), 3-dir=Rt(+)/Lt(-).	278
A.295 Patient 5D segmental ligament forces normalized with respect to body weight during left-to-right lateral flexion.	278
A.296 Patient 5D bilateral muscle forces normalized with respect to body weight during left-to-right lateral flexion.	278
A.297 Patient 5D relative rotations (left) and translations (right) at each vertebral level during left-to-right axial rotation.	279
A.298 Patient 5D intervertebral contact forces normalized with respect to body weight during left-to-right axial rotation. 1-dir=Ant(+)/Post(-), 2-dir=Sup(+)/Inf(-), 3-dir=Rt(+)/Lt(-)..	279
A.299 Patient 5D segmental ligament forces normalized with respect to body weight during left-to-right axial rotation.	279
A.300 Patient 5D bilateral muscle forces normalized with respect to body weight during left-to-right axial rotation.	280
A.301. Patient 6D relative rotations (left) and translations (right) at each vertebral level during flexion-extension.	281

A.302 Patient 6D intervertebral contact forces normalized with respect to body weight during flexion-extension. 1-dir=Ant(+)/Post(-), 2-dir=Sup(+)/Inf(-), 3-dir=Rt(+)/Lt(-).....	281
A.303 Patient 6D segmental ligament forces normalized with respect to body weight during flexion-extension.	282
A.304 Patient 6D bilateral muscle forces normalized with respect to body weight during flexion-extension.....	282
A.305 Patient 6D relative rotations (left) and translations (right) at each vertebral level during left-to-right lateral flexion.	282
A.306 Patient 6D intervertebral contact forces normalized with respect to body weight during left-to-right lateral flexion. 1-dir=Ant(+)/Post(-), 2-dir=Sup(+)/Inf(-), 3-dir=Rt(+)/Lt(-).	283
A.307 Patient 6D segmental ligament forces normalized with respect to body weight during left-to-right lateral flexion.....	283
A.308 Patient 6D bilateral muscle forces normalized with respect to body weight during left-to-right lateral flexion.	283
A.309 Patient 6D relative rotations (left) and translations (right) at each vertebral level during left-to-right axial rotation.	284
A.310 Patient 6D intervertebral contact forces normalized with respect to body weight during left-to-right axial rotation. 1-dir=Ant(+)/Post(-), 2-dir=Sup(+)/Inf(-), 3-dir=Rt(+)/Lt(-).	284
A.311 Patient 6D segmental ligament forces normalized with respect to body weight during left-to-right axial rotation.....	284
A.312 Patient 6D bilateral muscle forces normalized with respect to body weight during left-to-right axial rotation.	285
A.313 Patient 7D relative rotations (left) and translations (right) at each vertebral level during flexion-extension.	286
A.314 Patient 7D intervertebral contact forces normalized with respect to body weight during flexion-extension. 1-dir=Ant(+)/Post(-), 2-dir=Sup(+)/Inf(-), 3-dir=Rt(+)/Lt(-).....	286
A.315 Patient 7D segmental ligament forces normalized with respect to body weight during flexion-extension.	287
A.316 Patient 7D bilateral muscle forces normalized with respect to body weight during flexion-extension.....	287
A.317 Patient 7D relative rotations (left) and translations (right) at each vertebral level during left-to-right lateral flexion.	287
A.318 Patient 7D intervertebral contact forces normalized with respect to body weight during left-to-right lateral flexion. 1-dir=Ant(+)/Post(-), 2-dir=Sup(+)/Inf(-), 3-dir=Rt(+)/Lt(-).	288

A.319 Patient 7D segmental ligament forces normalized with respect to body weight during left-to-right lateral flexion.....	288
A.320 Patient 7D bilateral muscle forces normalized with respect to body weight during left-to-right lateral flexion.	288
A.321 Patient 7D relative rotations (left) and translations (right) at each vertebral level during left-to-right axial rotation.	289
A.322 Patient 7D intervertebral contact forces normalized with respect to body weight during left-to-right axial rotation. 1-dir=Ant(+)/Post(-), 2-dir=Sup(+)/Inf(-), 3-dir=Rt(+)/Lt(-)..	289
A.323 Patient 7D segmental ligament forces normalized with respect to body weight during left-to-right axial rotation.	289
A.324 Patient 7D bilateral muscle forces normalized with respect to body weight during left-to-right axial rotation.	290
A.325 Patient 8D relative rotations (left) and translations (right) at each vertebral level during flexion-extension.	291
A.326 Patient 8D intervertebral contact forces normalized with respect to body weight during flexion-extension. 1-dir=Ant(+)/Post(-), 2-dir=Sup(+)/Inf(-), 3-dir=Rt(+)/Lt(-).....	291
A.327 Patient 8D segmental ligament forces normalized with respect to body weight during flexion-extension.	292
A.328 Patient 8D bilateral muscle forces normalized with respect to body weight during flexion-extension.....	292
A.329 Patient 8D relative rotations (left) and translations (right) at each vertebral level during left-to-right lateral flexion.	292
A.330 Patient 8D intervertebral contact forces normalized with respect to body weight during left-to-right lateral flexion. 1-dir=Ant(+)/Post(-), 2-dir=Sup(+)/Inf(-), 3-dir=Rt(+)/Lt(-). 293	
A.331 Patient 8D segmental ligament forces normalized with respect to body weight during left-to-right lateral flexion.....	293
A.332 Patient 8D bilateral muscle forces normalized with respect to body weight during left-to-right lateral flexion.	293
A.333 Patient 8D relative rotations (left) and translations (right) at each vertebral level during left-to-right axial rotation.	294
A.334 Patient 8D intervertebral contact forces normalized with respect to body weight during left-to-right axial rotation. 1-dir=Ant(+)/Post(-), 2-dir=Sup(+)/Inf(-), 3-dir=Rt(+)/Lt(-)..	294
A.335 Patient 8D segmental ligament forces normalized with respect to body weight during left-to-right axial rotation.....	294

A.336 Patient 8D bilateral muscle forces normalized with respect to body weight during left-to-right axial rotation.	295
A.337 Patient 9D relative rotations (left) and translations (right) at each vertebral level during flexion-extension.	296
A.338 Patient 9D intervertebral contact forces normalized with respect to body weight during flexion-extension. 1-dir=Ant(+)/Post(-), 2-dir=Sup(+)/Inf(-), 3-dir=Rt(+)/Lt(-).	296
A.339 Patient 9D segmental ligament forces normalized with respect to body weight during flexion-extension.	297
A.340 Patient 9D bilateral muscle forces normalized with respect to body weight during flexion-extension.	297
A.341 Patient 9D relative rotations (left) and translations (right) at each vertebral level during left-to-right lateral flexion.	297
A.342 Patient 9D intervertebral contact forces normalized with respect to body weight during left-to-right lateral flexion. 1-dir=Ant(+)/Post(-), 2-dir=Sup(+)/Inf(-), 3-dir=Rt(+)/Lt(-).	298
A.343 Patient 9D segmental ligament forces normalized with respect to body weight during left-to-right lateral flexion.	298
A.344 Patient 9D bilateral muscle forces normalized with respect to body weight during left-to-right lateral flexion.	298
A.345 Patient 9D relative rotations (left) and translations (right) at each vertebral level during left-to-right axial rotation.	299
A.346 Patient 9D intervertebral contact forces normalized with respect to body weight during left-to-right axial rotation. 1-dir=Ant(+)/Post(-), 2-dir=Sup(+)/Inf(-), 3-dir=Rt(+)/Lt(-).	299
A.347 Patient 9D segmental ligament forces normalized with respect to body weight during left-to-right axial rotation.	299
A.348 Patient 9D bilateral muscle forces normalized with respect to body weight during left-to-right axial rotation.	300
A.349 Patient 10D relative rotations (left) and translations (right) at each vertebral level during flexion-extension.	301
A.350 Patient 10D intervertebral contact forces normalized with respect to body weight during flexion-extension. 1-dir=Ant(+)/Post(-), 2-dir=Sup(+)/Inf(-), 3-dir=Rt(+)/Lt(-).	301
A.351 Patient 10D segmental ligament forces normalized with respect to body weight during flexion-extension.	302
A.352 Patient 10D bilateral muscle forces normalized with respect to body weight during flexion-extension.	302

A.353 Patient 10D relative rotations (left) and translations (right) at each vertebral level during left-to-right lateral flexion.	302
A.354 Patient 10D intervertebral contact forces normalized with respect to body weight during left-to-right lateral flexion. 1-dir=Ant(+)/Post(-), 2-dir=Sup(+)/Inf(-), 3-dir=Rt(+)/Lt(-).	303
A.355 Patient 10D segmental ligament forces normalized with respect to body weight during left-to-right lateral flexion.	303
A.356 Patient 10D bilateral muscle forces normalized with respect to body weight during left-to-right lateral flexion.	303
A.357 Patient 10D relative rotations (left) and translations (right) at each vertebral level during left-to-right axial rotation.	304
A.358 Patient 10D intervertebral contact forces normalized with respect to body weight during left-to-right axial rotation. 1-dir=Ant(+)/Post(-), 2-dir=Sup(+)/Inf(-), 3-dir=Rt(+)/Lt(-)..	304
A.359 Patient 10D segmental ligament forces normalized with respect to body weight during left-to-right axial rotation.	304
A.360 Patient 10D bilateral muscle forces normalized with respect to body weight during left-to-right axial rotation.	305
A.361 Patient 1F pre-operative (top row) and post-operative (bottom row) relative rotations (left) and translations (right) at each vertebral level during flexion-extension.	306
A.362 Patient 1F pre- (top row) and post-operative (bottom row) intervertebral contact forces normalized with respect to body weight during flexion-extension.1-dir=Ant(+)/Post (-),2-dir=Sup(+)/Inf(-),3-dir=Rt(+)/Lt(-).	307
A.363 Patient 1F pre- (top row) and post-operative (bottom row) segmental ligament forces normalized with respect to body weight during flexion-extension.	307
A.364 Patient 1F pre- (top row) and post-operative (bottom row) bilateral muscle forces normalized with respect to body weight during flexion-extension.	308
A.365 Patient 1F pre-operative (top row) and post-operative (bottom row) relative rotations (left) and translations (right) at each vertebral level during left-to-right lateral flexion.	308
A.366 Patient 1F pre- (top row) and post-operative (bottom row) intervertebral contact forces normalized with respect to body weight during right-to-left lateral flexion. 1-dir=Ant(+)/Post(-), 2-dir=Sup (+)/Inf(-), 3-dir=Rt(+)/Lt(-).	309
A.367 Patient 1F pre- (top row) and post-operative (bottom row) segmental ligament forces normalized with respect to body weight during left-to-right lateral flexion.	309
A.368 Patient 1F pre- (top row) and post-operative (bottom row) bilateral muscle forces normalized with respect to body weight during left-to-right lateral flexion.	310
A.369 Patient 1F pre-operative (top row) and post-operative (bottom row) relative rotations (left) and translations (right) at each vertebral level during left-to-right axial rotation.	310

A.370 Patient 1F pre- (top row) and post-operative (bottom row) normalized with respect to body weight during left-to-right axial rotation. 1-dir=Ant(+)/Post(-), 2-dir=Sup(+)/Inf(-), 3-dir=Rt(+)/Lt(-).	311
A.371 Patient 1F pre- (top row) and post-operative (bottom row) segmental ligament forces normalized with respect to body weight during left-to-right axial rotation.	311
A.372 Patient 1F pre- (top row) and post-operative (bottom row) bilateral muscle forces normalized with respect to body weight during left-to-right axial rotation.	312
A.373 Patient 2F pre-operative (top row) and post-operative (bottom row) relative rotations (left) and translations (right) at each vertebral level during flexion-extension.	313
A.374 Patient 2F pre- (top row) and post-operative (bottom row) segmental ligament forces normalized with respect to body weight during flexion-extension.	314
A.375 Patient 2F pre- (top row) and post-operative (bottom row) segmental ligament forces normalized with respect to body weight during flexion-extension.	314
A.376 Patient 2F pre- (top row) and post-operative (bottom row) bilateral muscle forces normalized with respect to body weight during flexion-extension.	315
A.377 Patient 2F pre-operative (top row) and post-operative (bottom row) relative rotations (left) and translations (right) at each vertebral level during left-to-right lateral flexion.	315
A.378 Patient 2F pre- (top row) and post-operative (bottom row) intervertebral contact forces normalized with respect to body weight during right-to-left lateral flexion. 1-dir=Ant(+)/Post(-), 2-dir=Sup (+)/Inf(-), 3-dir=Rt(+)/Lt(-).	316
A.379 Patient 2F pre- (top row) and post-operative (bottom row) segmental ligament forces normalized with respect to body weight during left-to-right lateral flexion.	316
A.380 Patient 2F pre- (top row) and post-operative (bottom row) bilateral muscle forces normalized with respect to body weight during left-to-right lateral flexion.	317
A.381 Patient 2F pre-operative (top row) and post-operative (bottom row) relative rotations (left) and translations (right) at each vertebral level during left-to-right axial rotation.	317
A.382 Patient 2F pre- (top row) and post-operative (bottom row) intervertebral contact forces normalized with respect to body weight during left-to-right axial rotation. 1-dir=Ant(+)/Post(-), 2-dir=Sup(+)/Inf(-), 3-dir=Rt(+)/Lt(-).	318
A.383 Patient 2F pre- (top row) and post-operative (bottom row) segmental ligament forces normalized with respect to body weight during left-to-right axial rotation.	318
A.384 Patient 2F pre- (top row) and post-operative (bottom row) bilateral muscle forces normalized with respect to body weight during left-to-right axial rotation.	319
A.385 Patient 3F pre-operative (top row) and post-operative (bottom row) relative rotations (left) and translations (right) at each vertebral level during flexion-extension.	320

A.386 Patient 3F pre- (top row) and post-operative (bottom row) segmental ligament forces normalized with respect to body weight during flexion-extension.	321
A.387 Patient 3F pre- (top row) and post-operative (bottom row) segmental ligament forces normalized with respect to body weight during flexion-extension.	321
A.388 Patient 3F pre- (top row) and post-operative (bottom row) bilateral muscle forces normalized with respect to body weight during flexion-extension.	322
A.389 Patient 3F pre-operative (top row) and post-operative (bottom row) relative rotations (left) and translations (right) at each vertebral level during left-to-right lateral flexion.	322
A.390 Patient 3F pre- (top row) and post-operative (bottom row) intervertebral contact forces normalized with respect to body weight during right-to-left lateral flexion. 1-dir=Ant(+)/Post(-), 2-dir=Sup (+)/Inf(-), 3-dir=Rt(+)/Lt(-).	323
A.391 Patient 3F pre- (top row) and post-operative (bottom row) segmental ligament forces normalized with respect to body weight during left-to-right lateral flexion.	323
A.392 Patient 3F pre- (top row) and post-operative (bottom row) bilateral muscle forces normalized with respect to body weight during left-to-right lateral flexion.	324
A.393 Patient 3F pre-operative (top row) and post-operative (bottom row) relative rotations (left) and translations (right) at each vertebral level during left-to-right axial rotation.	324
A.394 Patient 3F pre- (top row) and post-operative (bottom row) intervertebral contact forces normalized with respect to body weight during left-to-right axial rotation. 1-dir=Ant(+)/Post(-), 2-dir=Sup(+)/Inf(-), 3-dir=Rt(+)/Lt(-).	325
A.395 Patient 3F pre- (top row) and post-operative (bottom row) segmental ligament forces normalized with respect to body weight during left-to-right axial rotation.	325
A.396 Patient 3F pre- (top row) and post-operative (bottom row) bilateral muscle forces normalized with respect to body weight during left-to-right axial rotation.	326
A.397 Patient 4F pre-operative (top row) and post-operative (bottom row) relative rotations (left) and translations (right) at each vertebral level during flexion-extension.	327
A.398 Patient 4F pre- (top row) and post-operative (bottom row) segmental ligament forces normalized with respect to body weight during flexion-extension.	328
A.399 Patient 4F pre- (top row) and post-operative (bottom row) segmental ligament forces normalized with respect to body weight during flexion-extension.	328
A.400 Patient 4F pre- (top row) and post-operative (bottom row) bilateral muscle forces normalized with respect to body weight during flexion-extension.	329
A.401 Patient 4F pre-operative (top row) and post-operative (bottom row) relative rotations (left) and translations (right) at each vertebral level during left-to-right lateral flexion.	329

A.402 Patient 4F pre- (top row) and post-operative (bottom row) intervertebral contact forces normalized with respect to body weight during right-to-left lateral flexion. 1-dir=Ant(+)/Post(-), 2-dir=Sup (+)/Inf(-), 3-dir=Rt(+)/Lt(-).	330
A.403 Patient 4F pre- (top row) and post-operative (bottom row) segmental ligament forces normalized with respect to body weight during left-to-right lateral flexion.	330
A.404 Patient 4F pre- (top row) and post-operative (bottom row) bilateral muscle forces normalized with respect to body weight during left-to-right lateral flexion.	331
A.405 Patient 4F pre-operative (top row) and post-operative (bottom row) relative rotations (left) and translations (right) at each vertebral level during left-to-right axial rotation.	331
A.406 Patient 4F pre- (top row) and post-operative (bottom row) intervertebral contact forces normalized with respect to body weight during left-to-right axial rotation. 1-dir=Ant(+)/Post(-), 2-dir=Sup(+)/Inf(-), 3-dir=Rt(+)/Lt(-).	332
A.407 Patient 4F pre- (top row) and post-operative (bottom row) segmental ligament forces normalized with respect to body weight during left-to-right axial rotation.	332
A.408 Patient 4F pre- (top row) and post-operative (bottom row) bilateral muscle forces normalized with respect to body weight during left-to-right axial rotation.	333
A.409 Patient 5F pre-operative (top row) and post-operative (bottom row) relative rotations (left) and translations (right) at each vertebral level during flexion-extension.	334
A.410 Patient 5F pre- (top row) and post-operative (bottom row) segmental ligament forces normalized with respect to body weight during flexion-extension.	335
A.411 Patient 5F pre- (top row) and post-operative (bottom row) segmental ligament forces normalized with respect to body weight during flexion-extension.	335
A.412 Patient 5F pre- (top row) and post-operative (bottom row) bilateral muscle forces normalized with respect to body weight during flexion-extension.	336
A.413 Patient 5F pre-operative (top row) and post-operative (bottom row) relative rotations (left) and translations (right) at each vertebral level during left-to-right lateral flexion.	336
A.414. Patient 5F pre- (top row) and post-operative (bottom row) intervertebral contact forces normalized with respect to body weight during right-to-left lateral flexion. 1-dir=Ant(+)/Post(-), 2-dir=Sup (+)/Inf(-), 3-dir=Rt(+)/Lt(-).	337
A.415 Patient 5F pre- (top row) and post-operative (bottom row) segmental ligament forces normalized with respect to body weight during left-to-right lateral flexion.	337
A.416 Patient 5F pre- (top row) and post-operative (bottom row) bilateral muscle forces normalized with respect to body weight during left-to-right lateral flexion.	338
A.417 Patient 5F pre-operative (top row) and post-operative (bottom row) relative rotations (left) and translations (right) at each vertebral level during left-to-right axial rotation.	338

A.418	Patient 5F pre- (top row) and post-operative (bottom row) intervertebral contact forces normalized with respect to body weight during left-to-right axial rotation. 1-dir=Ant(+)/Post(-), 2-dir=Sup(+)/Inf(-), 3-dir=Rt(+)/Lt(-).	339
A.419	Patient 5F pre- (top row) and post-operative (bottom row) segmental ligament forces normalized with respect to body weight during left-to-right axial rotation.	339
A.420	Patient 5F pre- (top row) and post-operative (bottom row) bilateral muscle forces normalized with respect to body weight during left-to-right axial rotation.	340
A.421	Patient 6F pre-operative (top row) and post-operative (bottom row) relative rotations (left) and translations (right) at each vertebral level during flexion-extension.	341
A.422	Patient 6F pre- (top row) and post-operative (bottom row) segmental ligament forces normalized with respect to body weight during flexion-extension.	342
A.423	Patient 6F pre- (top row) and post-operative (bottom row) segmental ligament forces normalized with respect to body weight during flexion-extension.	342
A.424	Patient 6F pre- (top row) and post-operative (bottom row) bilateral muscle forces normalized with respect to body weight during flexion-extension.	343
A.425	Patient 6F pre-operative (top row) and post-operative (bottom row) relative rotations (left) and translations (right) at each vertebral level during left-to-right lateral flexion.	343
A.426	Patient 6F pre- (top row) and post-operative (bottom row) intervertebral contact forces normalized with respect to body weight during right-to-left lateral flexion. 1-dir=Ant(+)/Post(-), 2-dir=Sup (+)/Inf(-), 3-dir=Rt(+)/Lt(-).	344
A.427	Patient 6F pre- (top row) and post-operative (bottom row) segmental ligament forces normalized with respect to body weight during left-to-right lateral flexion.	344
A.428	Patient 6F pre- (top row) and post-operative (bottom row) bilateral muscle forces normalized with respect to body weight during left-to-right lateral flexion.	345
A.429	Patient 6F pre-operative (top row) and post-operative (bottom row) relative rotations (left) and translations (right) at each vertebral level during left-to-right axial rotation.	345
A.430	Patient 6F pre- (top row) and post-operative (bottom row) intervertebral contact forces normalized with respect to body weight during left-to-right axial rotation. 1-dir=Ant(+)/Post(-), 2-dir=Sup(+)/Inf(-), 3-dir=Rt(+)/Lt(-).	346
A.431	Patient 6F pre- (top row) and post-operative (bottom row) segmental ligament forces normalized with respect to body weight during left-to-right axial rotation.	346
A.432	Patient 6F pre- (top row) and post-operative (bottom row) bilateral muscle forces normalized with respect to body weight during left-to-right axial rotation.	347
A.433	Patient 7F pre-operative (top row) and post-operative (bottom row) relative rotations (left) and translations (right) at each vertebral level during flexion-extension.	348

A.434 Patient 7F pre- (top row) and post-operative (bottom row) segmental ligament forces normalized with respect to body weight during flexion-extension.	349
A.435 Patient 7F pre- (top row) and post-operative (bottom row) segmental ligament forces normalized with respect to body weight during flexion-extension.	349
A.436 Patient 7F pre- (top row) and post-operative (bottom row) bilateral muscle forces normalized with respect to body weight during flexion-extension.	350
A.437 Patient 7F pre-operative (top row) and post-operative (bottom row) relative rotations (left) and translations (right) at each vertebral level during left-to-right lateral flexion.	350
A.438 Patient 7F pre- (top row) and post-operative (bottom row) intervertebral contact forces normalized with respect to body weight during right-to-left lateral flexion. 1-dir=Ant(+)/Post(-), 2-dir=Sup (+)/Inf(-), 3-dir=Rt(+)/Lt(-).	351
A.439 Patient 7F pre- (top row) and post-operative (bottom row) segmental ligament forces normalized with respect to body weight during left-to-right lateral flexion.	351
A.440 Patient 7F pre- (top row) and post-operative (bottom row) bilateral muscle forces normalized with respect to body weight during left-to-right lateral flexion.	352
A.441 Patient 7F pre-operative (top row) and post-operative (bottom row) relative rotations (left) and translations (right) at each vertebral level during left-to-right axial rotation.	352
A.442 Patient 7F pre- (top row) and post-operative (bottom row) intervertebral contact forces normalized with respect to body weight during left-to-right axial rotation. 1-dir=Ant(+)/Post(-), 2-dir=Sup(+)/Inf(-), 3-dir=Rt(+)/Lt(-).	353
A.443 Patient 7F pre- (top row) and post-operative (bottom row) segmental ligament forces normalized with respect to body weight during left-to-right axial rotation.	353
A.444 Patient 7F pre- (top row) and post-operative (bottom row) bilateral muscle forces normalized with respect to body weight during left-to-right axial rotation.	354
A.445 Patient 8F pre-operative (top row) and post-operative (bottom row) relative rotations (left) and translations (right) at each vertebral level during flexion-extension.	355
A.446 Patient 8F pre- (top row) and post-operative (bottom row) segmental ligament forces normalized with respect to body weight during flexion-extension.	356
A.447 Patient 8F pre- (top row) and post-operative (bottom row) segmental ligament forces normalized with respect to body weight during flexion-extension.	356
A.448 Patient 8F pre- (top row) and post-operative (bottom row) bilateral muscle forces normalized with respect to body weight during flexion-extension.	357
A.449 Patient 8F pre-operative (top row) and post-operative (bottom row) relative rotations (left) and translations (right) at each vertebral level during left-to-right lateral flexion.	357

A.450 Patient 8F pre- (top row) and post-operative (bottom row) intervertebral contact forces normalized with respect to body weight during right-to-left lateral flexion. 1-dir=Ant(+)/Post(-), 2-dir=Sup (+)/Inf(-), 3-dir=Rt(+)/Lt(-).	358
A.451 Patient 8F pre- (top row) and post-operative (bottom row) segmental ligament forces normalized with respect to body weight during left-to-right lateral flexion.	358
A.452 Patient 8F pre- (top row) and post-operative (bottom row) bilateral muscle forces normalized with respect to body weight during left-to-right lateral flexion.	359
A.453 Patient 8F pre-operative (top row) and post-operative (bottom row) relative rotations (left) and translations (right) at each vertebral level during left-to-right axial rotation.	359
A.454 Patient 8F pre- (top row) and post-operative (bottom row) intervertebral contact forces normalized with respect to body weight during left-to-right axial rotation. 1-dir=Ant(+)/Post(-), 2-dir=Sup(+)/Inf(-), 3-dir=Rt(+)/Lt(-).	360
A.455 Patient 8F pre- (top row) and post-operative (bottom row) segmental ligament forces normalized with respect to body weight during left-to-right axial rotation.	360
A.456 Patient 8F pre- (top row) and post-operative (bottom row) bilateral muscle forces normalized with respect to body weight during left-to-right axial rotation.	361
A.457 Patient 9F pre-operative (top row) and post-operative (bottom row) relative rotations (left) and translations (right) at each vertebral level during flexion-extension.	362
A.458 Patient 9F pre- (top row) and post-operative (bottom row) segmental ligament forces normalized with respect to body weight during flexion-extension.	363
A.459 Patient 9F pre- (top row) and post-operative (bottom row) segmental ligament forces normalized with respect to body weight during flexion-extension.	363
A.460 Patient 9F pre- (top row) and post-operative (bottom row) bilateral muscle forces normalized with respect to body weight during flexion-extension.	364
A.461 Patient 9F pre-operative (top row) and post-operative (bottom row) relative rotations (left) and translations (right) at each vertebral level during left-to-right lateral flexion.	364
A.462 Patient 9F pre- (top row) and post-operative (bottom row) intervertebral contact forces normalized with respect to body weight during right-to-left lateral flexion. 1-dir=Ant(+)/Post(-), 2-dir=Sup (+)/Inf(-), 3-dir=Rt(+)/Lt(-).	365
A.463 Patient 9F pre- (top row) and post-operative (bottom row) segmental ligament forces normalized with respect to body weight during left-to-right lateral flexion.	365
A.464 Patient 9F pre- (top row) and post-operative (bottom row) bilateral muscle forces normalized with respect to body weight during left-to-right lateral flexion.	366
A.465 Patient 9F pre-operative (top row) and post-operative (bottom row) relative rotations (left) and translations (right) at each vertebral level during left-to-right axial rotation.	366

A.466 Patient 9F pre- (top row) and post-operative (bottom row) intervertebral contact forces normalized with respect to body weight during left-to-right axial rotation. 1-dir=Ant(+)/Post(-), 2-dir=Sup(+)/Inf(-), 3-dir=Rt(+)/Lt(-).	367
A.467 Patient 9F pre- (top row) and post-operative (bottom row) segmental ligament forces normalized with respect to body weight during left-to-right axial rotation.	367
A.468 Patient 9F pre- (top row) and post-operative (bottom row) bilateral muscle forces normalized with respect to body weight during left-to-right axial rotation.	368
A.469 Patient 10F pre-operative relative rotations (left) and translations (right) at each vertebral level during flexion-extension.	369
A.470 Patient 10F pre-operative intervertebral contact forces normalized with respect to body weight during flexion-extension. 1-dir=Ant (+)/Post(-), 2-dir=Sup(+)/Inf(-), 3-dir=Rt (+)/Lt(-).....	369
A.471 Patient 10F pre-operative segmental ligament forces normalized with respect to body weight during flexion-extension.....	370
A.472 Patient 10F pre-operative bilateral muscle forces normalized with respect to body weight during flexion-extension.....	370
A.473 Patient 10F pre-operative relative rotations (left) and translations (right) at each vertebral level during left-to-right lateral flexion.	370
A.474 Patient 10F pre-operative intervertebral contact forces normalized with respect to body weight during right-to-left lateral flexion. 1-dir= Ant (+)/Post (-), 2-dir=Sup (+)/Inf(-),3-dir=Rt(+)/Lt(-).	371
A.475 Patient 10F pre-operative segmental ligament forces normalized with respect to body weight during left-to-right lateral flexion.....	371
A.476 Patient 10F pre-operative bilateral muscle forces normalized with respect to body weight during left-to-right lateral flexion.....	371
A.477 Patient 10F pre-operative relative rotations (left) and translations (right) at each vertebral level during left-to-right axial rotation.	372
A.478 Patient 10F pre-operative intervertebral contact forces normalized with respect to body weight (BW) during left-to-right axial rotation. 1-dir= Ant(+)/Post(-), 2-dir=Sup(+)/Inf(-),3-dir=Rt(+)/Lt(-).	372
A.479 Patient 10F pre-operative segmental ligament forces normalized with respect to body weight during left-to-right axial rotation.....	372
A.480 Patient 10F pre-operative bilateral muscle forces normalized with respect to body weight during left-to-right axial rotation.....	373
A.481 Patient 1HDS pre-operative (top row) and post-operative (bottom row) relative rotations (left) and translations (right) at each vertebral level during flexion-extension.	374

A.482 Patient 1HDS pre- (top row) and post-operative (bottom row) intervertebral contact forces normalized with respect to body weight during flexion-extension. 1-dir=Ant (+)/Post(-), 2-dir=Sup(+)/Inf(-), 3-dir=Rt (+)/Lt(-).	375
A.483 Patient 1HDS pre- (top row) and post-operative (bottom row) segmental ligament forces normalized with respect to body weight during flexion-extension.	375
A.484 Patient 1HDS pre- (top row) and post-operative (bottom row) bilateral muscle forces normalized with respect to body weight during flexion-extension.	376
A.485 Patient 1HDS pre-operative (top row) and post-operative (bottom row) relative rotations (left) and translations (right) at each vertebral level during left-to-right lateral flexion. ...	376
A.486 Patient 1HDS pre- (top row) and post-operative (bottom row) intervertebral contact forces normalized with respect to body weight during right-to-left lateral flexion. 1-dir= Ant (+)/Post (-), 2-dir=Sup (+)/Inf(-),3-dir=Rt(+)/Lt(-).	377
A.487 Patient 1HDS pre- (top row) and post-operative (bottom row) segmental ligament forces normalized with respect to body weight during left-to-right lateral flexion.	377
A.488 Patient 1HDS pre- (top row) and post-operative (bottom row) bilateral muscle forces normalized with respect to body weight during left-to-right lateral flexion.	378
A.489 Patient 1HDS pre-operative (top row) and post-operative (bottom row) relative rotations (left) and translations (right) at each vertebral level during left-to-right axial rotation.	378
A.490 Patient 1HDS pre- (top row) and post-operative (bottom row) intervertebral contact forces normalized with respect to body weight during left-to-right axial rotation. 1-dir= Ant(+)/Post(-), 2-dir=Sup(+)/Inf(-),3-dir=Rt(+)/Lt(-).	379
A.491 Patient 1HDS pre- (top row) and post-operative (bottom row) segmental ligament forces normalized with respect to body weight during left-to-right axial rotation.	379
A.492 Patient 1HDS pre- (top row) and post-operative (bottom row) bilateral muscle forces normalized to body weight during left-to-right axial rotation.	380
A.493 Patient 2HDS pre-operative (top row) and post-operative (bottom row) relative rotations (left) and translations (right) at each vertebral level during flexion-extension.	381
A.494 Patient 2HDS pre- (top row) and post-operative (bottom row) intervertebral contact forces normalized with respect to body weight during flexion-extension. 1-dir=Ant (+)/Post(-), 2-dir=Sup(+)/Inf(-), 3-dir=Rt (+)/Lt(-).	382
A.495 Patient 2HDS pre- (top row) and post-operative (bottom row) segmental ligament forces normalized with respect to body weight during flexion-extension.	382
A.496. Patient 2HDS pre- (top row) and post-operative (bottom row) bilateral muscle forces normalized with respect to body weight during flexion-extension.	383
A.497 Patient 2HDS pre-operative (top row) and post-operative (bottom row) relative rotations (left) and translations (right) at each vertebral level during left-to-right lateral flexion. ...	383

A.498 Patient 2HDS pre- (top row) and post-operative (bottom row) intervertebral contact forces normalized with respect to body weight during right-to-left lateral flexion. 1-dir= Ant (+)/Post (-), 2-dir=Sup (+)/Inf(-),3-dir=Rt(+)/Lt(-).	384
A.499 Patient 2DS pre- (top row) and post-operative (bottom row) segmental ligament forces normalized with respect to body weight during left-to-right lateral flexion.	384
A.500 Patient 2HDS pre- (top row) and post-operative (bottom row) bilateral muscle forces normalized with respect to body weight during left-to-right lateral flexion.	385
A.501 Patient 2HDS pre-operative (top row) and post-operative (bottom row) relative rotations (left) and translations (right) at each vertebral level during left-to-right axial rotation.	385
A.502 Patient 2HDS pre- (top row) and post-operative (bottom row) intervertebral contact forces normalized with respect to body weight during left-to-right axial rotation. 1-dir= Ant(+)/Post(-), 2-dir=Sup(+)/Inf(-),3-dir=Rt(+)/Lt(-).	386
A.503 Patient 2HDS pre- (top row) and post-operative (bottom row) segmental ligament forces normalized with respect body weight during left-to-right axial rotation.	386
A.504 Patient 2HDS pre- (top row) and post-operative (bottom row) bilateral muscle forces normalized to body weight during left-to-right axial rotation.	387
A.505 Patient 1LADR post-operative relative rotations (left) and translations (right) at each vertebral level during flexion-extension.	388
A.506 Patient 1LADR post-operative intervertebral contact forces normalized with respect to body weight during flexion-extension. 1-dir=Ant (+)/Post(-), 2-dir=Sup(+)/Inf(-), 3-dir=Rt (+)/Lt(-).	388
A.507. Patient 1LADR post-operative segmental ligament forces normalized with respect to body weight during flexion-extension.	389
A.508 Patient 1LADR post-operative bilateral muscle forces normalized with respect to body weight during flexion-extension.	389
A.509 Patient 1LADR post-operative relative rotations (left) and translations (right) at each vertebral level during left-to-right lateral flexion.	389
A.510 Patient 1LADR post-operative intervertebral contact forces normalized with respect to body weight during right-to-left lateral flexion. 1-dir= Ant (+)/Post (-), 2-dir=Sup (+)/Inf(-),3-dir=Rt(+)/Lt(-).	390
A.511 Patient 1LADR post-operative segmental ligament forces normalized with respect to body weight during left-to-right lateral flexion.	390
A.512 Patient 1LADR post-operative bilateral muscle forces normalized with respect to body weight during left-to-right lateral flexion.	390
A.513 Patient 1LADR post-operative relative rotations (left) and translations (right) at each vertebral level during left-to-right axial rotation.	391

A.514. Patient 1LADR post-operative intervertebral contact forces normalized with respect to body weight during left-to-right axial rotation. 1-dir= Ant(+)/Post(-), 2-dir=Sup(+)/Inf(-), 3-dir=Rt(+)/Lt(-).	391
A.515 Patient 1LADR post-operative segmental ligament forces normalized with respect to body weight during left-to-right axial rotation.	392
A.516 Patient 1LADR post-operative bilateral muscle forces normalized to body weight during left-to-right axial rotation.	392
A.517 Patient 2LADR post-operative relative rotations (left) and translations (right) at each vertebral level during flexion-extension.....	393
A.518 Patient 2LADR post-operative intervertebral contact forces normalized with respect to body weight during flexion-extension. 1-dir=Ant (+)/Post(-), 2-dir=Sup(+)/Inf(-), 3-dir=Rt (+)/Lt(-).....	393
A.519 Patient 2LADR post-operative segmental ligament forces normalized with respect to body weight during flexion-extension.....	394
A.520 Patient 2LADR post-operative bilateral muscle forces normalized with respect to body weight during flexion-extension.....	394
A.521 Patient 2LADR post-operative relative rotations (left) and translations (right) at each vertebral level during left-to-right lateral flexion.....	394
A.522 Patient 2LADR post-operative intervertebral contact forces normalized with respect to body weight during right-to-left lateral flexion. 1-dir= Ant (+)/Post (-), 2-dir=Sup (+)/Inf(-), 3-dir=Rt(+)/Lt(-).	395
A.523 Patient 2LADR post-operative segmental ligament forces normalized with respect to body weight during left-to-right lateral flexion.....	395
A.524 Patient 2LADR post-operative bilateral muscle forces normalized with respect to body weight during left-to-right lateral flexion.....	395
A.525 Patient 2LADR post-operative relative rotations (left) and translations (right) at each vertebral level during left-to-right axial rotation.....	396
A.526 Patient 2LADR post-operative intervertebral contact forces normalized with respect to body weight during left-to-right axial rotation. 1-dir= Ant(+)/Post(-), 2-dir=Sup(+)/Inf(-), 3-dir=Rt(+)/Lt(-).	396
A.527 Patient 2LADR post-operative segmental ligament forces normalized with respect to body weight during left-to-right axial rotation.....	397
A.528 Patient 2LADR post-operative bilateral muscle forces normalized to body weight during left-to-right axial rotation.	397

Chapter 1

Introduction

The human vertebral spine is a multi-faceted anatomical structure which forms a complex arrangement of articulating joints that serve as the main load bearing structure for the musculoskeletal system. In general, the spine's upright orientation, appropriate curvature and intricate soft tissue structures enable for large gross motions such as flexing and extending, bending, and rotation, while at the same time providing the necessary framework at the segmental levels for performing more refined motions utilized during specific maneuvers. At the most caudal portion of the spine is the lumbar region, consisting of five vertebrae. These structures provide protection for the delicate neural elements passing down the trunk and branching out to the rest of the body. In addition, the large, rigid vertebrae making up the lumbar spine, coupled with the viscoelastic nature of the spinous ligaments and intervertebral discs as well as the stabilizing properties imparted by the vast network of overlapping musculature, provides unique advantages for transferring the upper body loads down through the pelvis and into the legs. Together, these structures work to help reduce impact magnitudes while increasing impact times, thereby contributing to the ability of the lumbar spine to endure tremendous loads.

Under normal daily regimes, mechanical loadings resulting from upper body weight, muscle contributions, and the lifting and holding of objects are manageable. However, when the lumbar spine is exposed to traumatic loads, which occur suddenly and with large force magnitudes, or abnormal loads occurring in less than optimal locations, the load bearing capacities in the discs,

zygapophyseal or facet joints, and soft tissue structures may begin to fail. Further amplifying these loading scenarios are the inevitable effects of aging, which set forth a cascade of events that trigger uniform changes in the lumbar spine. The transformation of these tissues can affect the biomechanical properties, morphologies, and dynamic characteristics of the entire lumbar spine and ultimately can hamper its ability to perform and maintain mechanical stability.

Often times, the degree at which the lumbar spine is able to fulfill its role in the body is related to the sensation of pain and the perceived origin of that pain. When pain arises in the region of the lumbar spine, it is generally classified as low back pain (LBP). And while the genesis of this pain is sometimes not well understood, its impact on the population continues to be widespread. In fact, it is estimated that 80% of adults will experience an episode of LBP at some point during their lives [89]. Researchers and clinicians have traced possible sources of LBP to muscles and ligaments surrounding the spine, the zygapophyseal joints, and the intervertebral discs [10], with manifestation of this pain type often considered to be debilitating. However, no matter whether pain is thought of as a biological response to tissue injury or as the result of excessive kinetic energy introduced into the biological system and perturbed by mechanical stimulus, a broader understanding of the anatomical structures and mechanics of the lumbar spine is fundamental for the expansion of *in vivo* biomechanical studies.

Few research studies have addressed *in vivo* three-dimensional (3D) dynamics (kinematics and kinetics) of the entire lumbar spine and compared the data between healthy, symptomatic, pathologic, and pre-and post-operative subjects. Therefore, the objective of this research study was to determine and analyze the 3D *in vivo* mechanics of various lumbar spine conditions. This

research study could provide important information for surgeons and researchers by aiding in the diagnosis, treatment and rehabilitation of problems associated with pain in the lower back region.

Chapter 2

Background

2.1 Anatomy of the Lumbar Spine

This research study investigated the kinematic and kinetic characteristics of the lumbar vertebrae and surrounding soft tissue structures for many types of clinically defined lumbar spine conditions. Having a fundamental knowledge of the lumbar anatomy was vital for providing an understanding of the functional roles of each structure and for the development of a mathematical model that accurately represented the anatomical conditions in the lumbar system.

2.1.1 The Lumbar Vertebra

The lumbar vertebral column consists of L1 through L5 vertebrae, stacked one on top another (Figures 2.1 and 2.2). In the healthy spine, they are aligned straight in the coronal plane. However, in the sagittal plane, the healthy spine displays a curvature referred to as lordotic in nature, meaning the vertebrae are oriented in the sagittal plane with a convexity to the front or anterior side of the body. The angle of this lordosis varies, especially between men and women. Average lordosis angles are reported to be around 43° in men, while women tend to exhibit significantly greater angles near 50° [117].

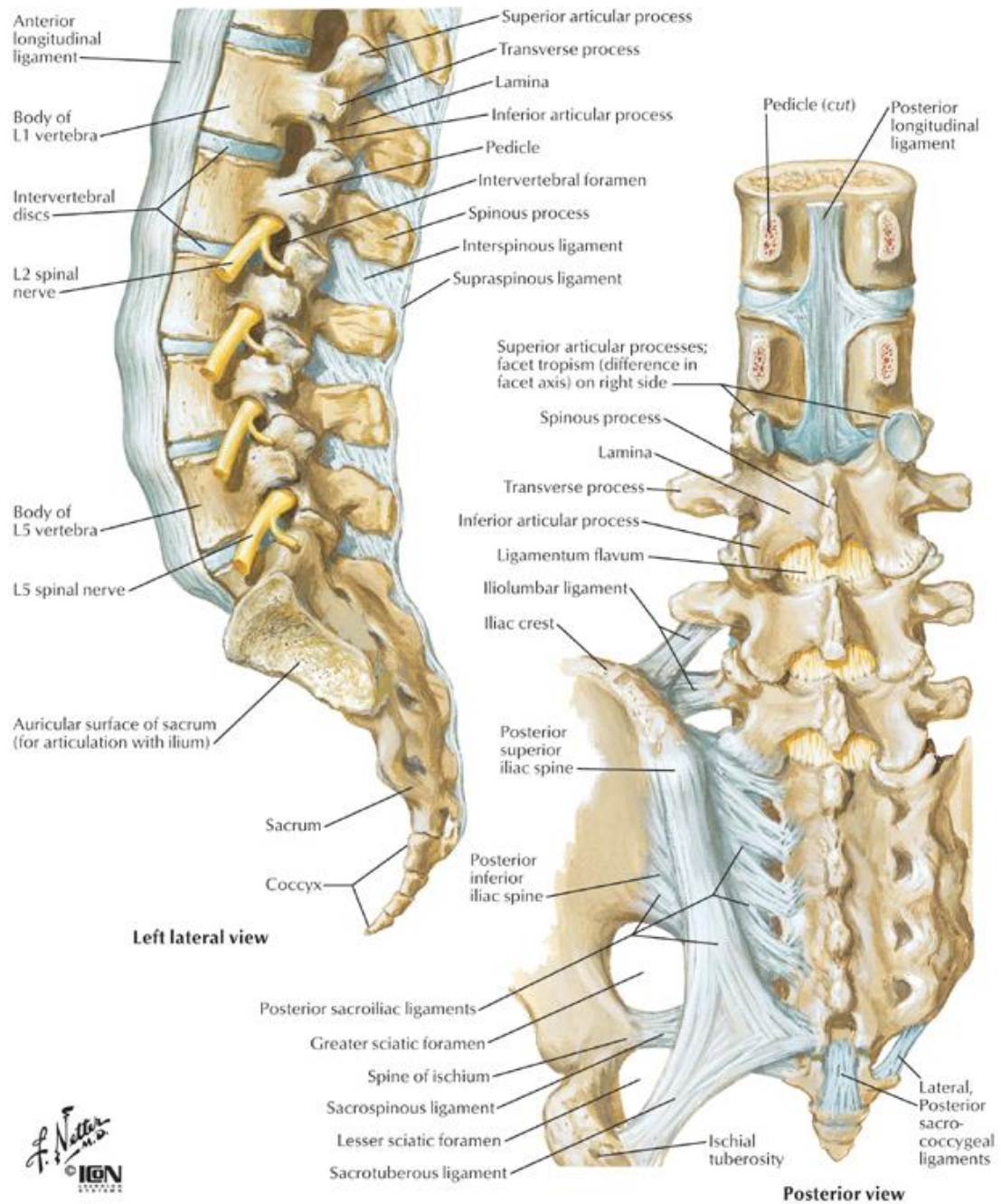


Figure 2.1 Anatomy of the complete lumbar spine with ligaments [<http://www.backpain-guide.com>].

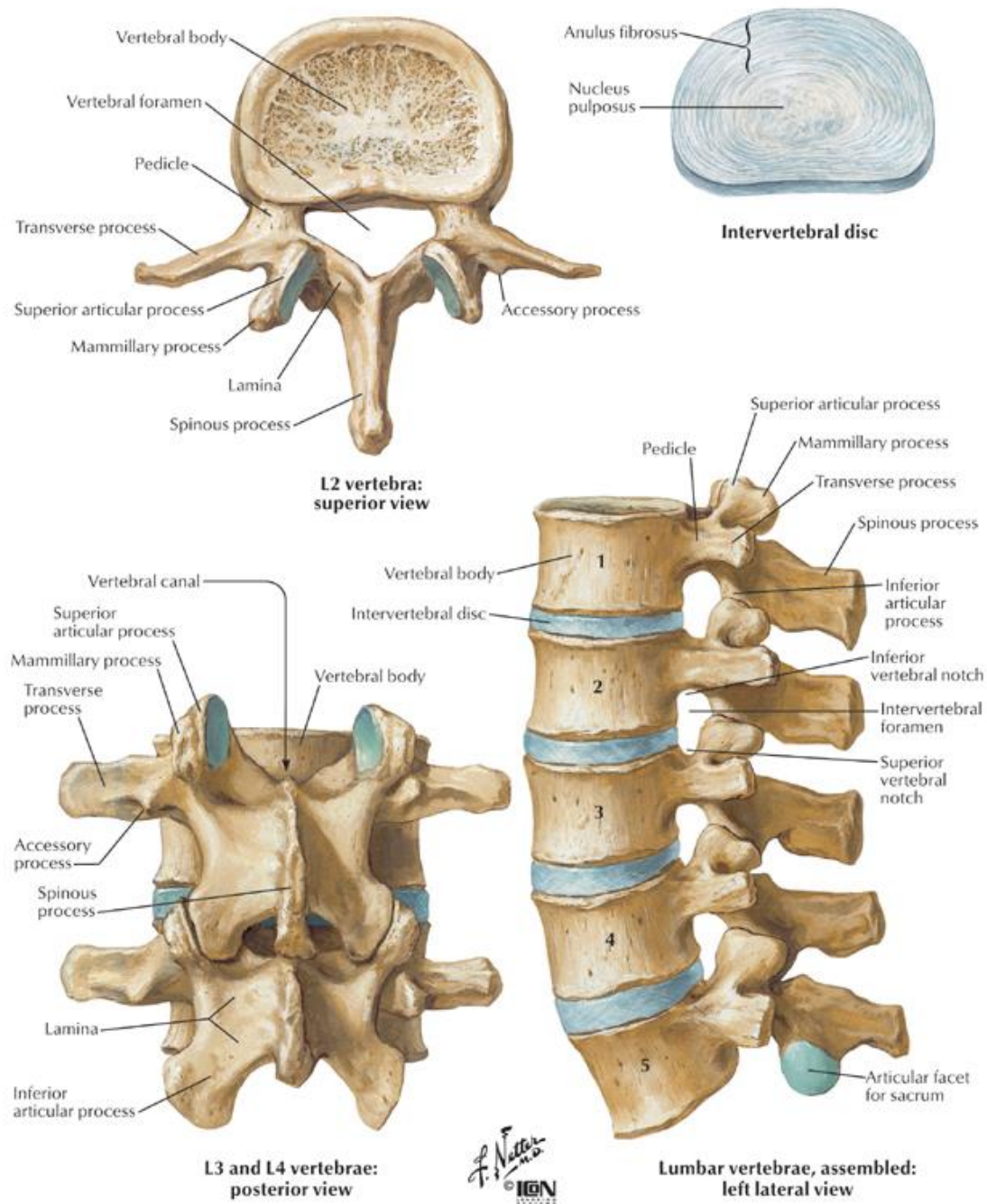


Figure 2.2 Anatomy of the typical lumbar vertebra [<http://www.backpain-guide.com>].

Each lumbar vertebra has common structural components which serve specific functional roles. In general, the vertebra as a whole exhibits a very irregular shape; however its anatomy can be divided into three functional components when viewed from the sagittal plane. The vertebral body makes up the anterior portion of the vertebra. Structurally, it is a thin shell of dense, hard cortical bone encompassing a matrix of trabecular, cancellous bone. From the sagittal and coronal plane views, the vertebral body is shaped like an hourglass, having a thinner central portion and wider towards the superior and inferior ends. When viewed from the top, it is kidney-shaped, larger dimensionally along the transverse axis versus that seen along the anterior-posterior direction. The vertebral body has a relatively flat superior and inferior surface, with a slightly raised perimeter forming what is known as the ring apophysis. These shape and structural features of the vertebral body are designed to maintain stability and provide support for longitudinally applied loads. Ranges for the loads borne by the anterior vertebral body have been estimated to be between 70-82% of the total load passing through the vertebra [54, 61]. On both the superior and inferior vertebral body surface lie the vertebral endplates, which serve to interface the intervertebral disc structure with the bony vertebra.

Structurally, the vertebral body of the lumbar vertebra is well-suited to fulfill its role. The hard outer shell combined with the latticed, cancellous bone making up the inner portion is ideal for supporting various loading conditions. These characteristics minimize weight, while providing rigidity. The hollow spaces in the cancellous bone also enable for blood flow within the vertebral body. The blood supplies nutrients to the bone and is thought to also assist in transmitting and absorbing loads [109].

The medial portion of the vertebra begins with the formation of two prominences extending posteriorly from the lateral margin of the dorsal surface of the vertebral body. These short, bony column-like processes are known as the pedicles. The pedicles serve to bridge the anterior vertebral body with the posterior elements. Their unique structure and design enables for optimal transmission of both tensile and bending forces. Extending out from each pedicle medially are flat sheets of bone which go on to form the laminae. Once the laminae come together, the vertebral foramen, which encompasses the spinal cord as it extends down through the posterior spine, is formed.

While the anterior and medial segments of the vertebra are important for supporting and transmitting loads, the posterior portion is well-suited for constraining large out-of-plane rotations and providing structural prominences which receive musculotendinous forces that act on the vertebra. Various pieces of bone extend out from the laminae in all directions. Of these bony processes, two project superiorly and two inferiorly. The superior processes interact with the inferior processes of the vertebra above, while the inferior processes interact with superior processes of the vertebra below. The interactions of these bony prominences form the zygapophyseal joints. The processes making up these joints are large, more centrally located, and oriented almost parallel to the sagittal plane. This allows for considerable flexion and extension, while limiting the amount of lateral flexion and axial torsion between vertebral levels. As a whole, these joints mainly assist in constraining motion and help in stabilizing the spine, yet may also provide some contributions for load bearing during certain postures as previously noted by Lorenz *et al.* [54]. Like many other joints in the body, the facets are susceptible to degenerative or pathological changes. These deviations from normal can lead to an individual experiencing

pain and/or aberrant motions between adjacent facets, thereby contributing to clinical pathologies related to stenosis, spondylolisthesis, or instability of the spinal unit.

Additional prominences extend laterally from the junction of the pedicle and the laminae. These consist of flattened, rectangular bones extending from both sides to form the two transverse processes. At the junction of the two laminae, the spinous process also begins to form as it extends posteriorly as a slender vane of bone. Both the transverse and spinous processes serve as areas for attachment of ligamentous and tendonous tissue. The outward extension of these bony processes away from the center of the vertebra also enables for the forces generated in the connecting soft tissues to be enhanced due to the lever or moment arm effect. This mechanical phenomenon enables for smaller forces to have a greater and ideally, a more efficient influence on the control mechanisms in the spine.

2.1.2 The Intervertebral Disc

Lying between each of the vertebral bodies is a strong, deformable soft tissue structure known as the intervertebral disc. Each intervertebral disc is made up of two components. The inner portion is a semi-fluid, jelly-like material called the nucleus pulposus. Surrounding the nucleus is a radial-like structure called the annulus fibrosus. The annulus consists of collagen fibers oriented concentrically in sheet-like layers known as lamellae. Within each layer, the collagen fibers lie parallel to one another, passing from the vertebra above to the vertebra below. Previously, the vertebral endplates were mentioned to act as an interface between the disc and the vertebra; however, it is largely considered to be a part of the intervertebral disc. The vertebral endplates form a cartilaginous layer covering the superior and inferior portions of the nucleus pulposus, as

well as the inner lamellae making up the annulus. Attachment of the collagen fibers within the annulus fibrosus to the vertebral endplates enables for a strong connection. In the areas where the vertebral endplate is deficient, the collagen fibers making up the annulus insert directly into the bone of the vertebral body.

The intervertebral discs are a crucial element in the lumbar spine. Each component of the intervertebral disc imparts various mechanisms which can either work in unison with other structures or independently to serve the overall function of the disc. During movement, the discs contribute to the flexibility, motion characteristics, and transfer of loads between the vertebral bodies by completing what is referred to as the functional spinal unit (FSU). These are comprised of two adjacent vertebrae, the intervertebral disc lying between them, the articulating zygapophyseal joint capsules and the intervertebral soft tissues. Each spinal unit facilitates varying degrees of motion about all three rotational and translational axes. Movement may be somewhat limited at the local spinal unit; however, larger global motion can be achieved with the contributions from several FSUs.

The role of the intervertebral disc is not only to allow for motion between two vertebral levels, but also to absorb and distribute force and pressure. Under axial loading conditions and bending motions, the nucleus pulposus primarily acts to sustain and transmit pressure omnidirectionally while also providing support for the lamellae of the annulus fibrosus. The annulus, on the other hand, works to restrain movements and help stabilize the joint. The tensile properties inherent in the collagen fibers resist the expanding nucleus pulposus under weight-bearing loads and help to redirect the forces into the adjacent vertebral bodies. The unique biological structure of the intervertebral disc helps to serve as a series of shock absorbers along

the lumbar spine, thereby reducing the impact between the sacrum and upper body. This profoundly enhances the mechanical properties of the lumbar spine.

In spite of the remarkable ability of the intervertebral disc to tolerate various loading conditions, microscopic and macroscopic injuries can occur leaving the disc damaged. Avascularity of the disc, disruptions in nutrient flow, and chemical changes can begin to impact the rate and effective healing strategies of the intervertebral tissue. As a result, numerous pathologies and conditions can develop leading to low back pain and other related problems.

2.1.3 Ligaments of the Lumbar Spine

In general, ligaments in the low back are similar to other ligamentous structures in the body. They consist of tough, fibrous bands comprised of collagen and elastin tissue enmeshed in a hydrated gel. In the spine, the ligaments function to connect one vertebral body to another and help control motion. All ligaments are viscoelastic and exhibit protective strategies to prevent injury (Figure 2.3). However, each ligament type exhibits its own mechanical behavior based on relative amounts of collagen and elastin fibers along with how the fibers are oriented in the constitutive matrix. Since the vertebrae and intervertebral discs cannot maintain stability of the spinal structure independently, the ligaments serve to guide and constrain overall motion at each level of the spine.

Collectively, the passive ligament structures and active muscle fibers in the lumbar region act as equilibratory components to control the various physiologic motions, while at the same time working to prevent excessive movements which may place the spinal cord or other

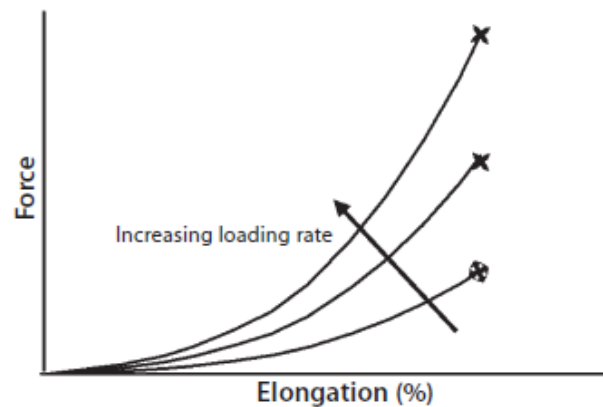


Figure 2.3 Viscoelasticity enables for greater stiffness and strength characteristics when rapid loading occurs. This helps protect the tissue from injury during trauma [9].

soft tissue structures at risk for injury. The primary collagenous structure of a ligament limits its capabilities of only resisting tension when stretched beyond its resting slack length. However, when ligaments are subjected to compressive forces, buckling occurs.

In the lumbar region, seven different types of ligaments are defined between L1 to L5. They are the anterior longitudinal ligament (ALL), the posterior longitudinal ligament (PLL), the ligamentum flavum (LF), the intertransverse ligament, the interspinous ligament (ISL), the supraspinous ligament (SSL), and the capsular ligament.

Slack lengths, cross-sectional areas, attachment coordinates, and material characteristics are all used to help model ligamentous constraint forces inherent in the lumbar spine. Most parameters are quantified using cadaveric experiments, computed tomography (CT), magnetic resonance imaging (MRI), and fluoroscopic radiological techniques, of which can be visualized through the use of a load-displacement curve (Figure 2.4). This curve, by convention, is divided into three regions: the neutral zone, the elastic zone, and the plastic zone. The neutral zone is the range of displacements near the neutral position due to a small force or torque. The elastic zone

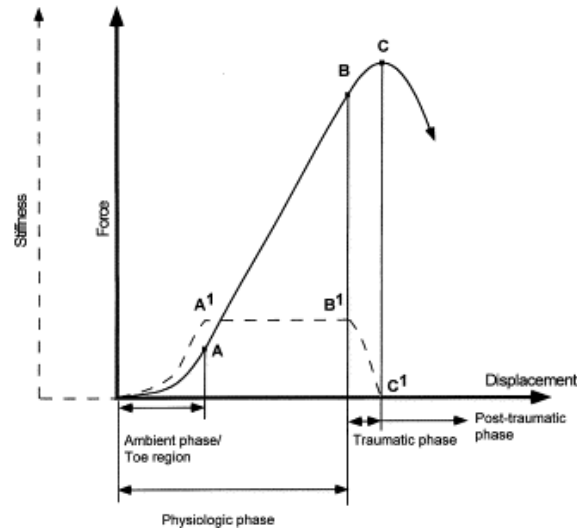


Figure 2.4 Load-displacement curve of spinal ligaments [116].

is the range between the neutral zone and the plastic zone. The plastic zone is the range from the elastic zone up, along the curve until failure. Together, the neutral zone and the elastic zone constitute the normal physiological range, while ligament strain occurring in the plastic zone may result in possible trauma or injury to the ligament.

2.1.4 Muscles of the Lumbar Spine

Generally speaking, muscles are soft tissue structures attached to bones through tendons and serve as actuators for controlling and producing motion. Muscles are also responsible for helping to carry loads. In the low back region, a number of larger and smaller muscles work in unison to actively govern spinal motion through antagonist and protagonist muscle fibers, thus driving the movements of the vertebrae. The back musculature also functions both actively and passively to stabilize the spine by providing support during both static and dynamic activities. The tendons which serve as the interface between the bone and muscle boundaries have a parallel collagenous

tissue fiber structure providing viscoelastic properties that are strong enough to sustain high tensile forces produced by contraction of muscle. However, these muscle properties also allow for flexibility enabling wrapping of the tissues around the diverse vertebral bone geometries. This wrapping re-iterates that simply connecting a straight line between a muscle's origin and insertion may not necessarily be the best way to represent a muscle or muscle fascicle. The angulation change that occurs as muscles wrap around various structures may influence not only the direction of the force produced by a muscle but also generate moment arms that enhance the effectiveness of the muscle. Tendonous tissue connecting muscle to bones is also likely to aid in muscle force generation by providing constant tension along the entire soft tissue structure. This enables for effective force generation without necessarily changing the length of the muscle fibers.

Muscles surrounding the lumbar spine are shown in Figure 2.5 and can be categorized using differing methodologies. In regards to this research study, muscles of the low back have been classified according to their role in controlling the motions inherent in the lumbar spine. The four main functional subgroups are flexors, extensors, lateral flexors, and rotators. However, some muscles perform multiple functional roles based on whether unilateral or bilateral contraction occurs. Therefore, the major forward flexors have been classified as being either extrinsic or intrinsic in their function. The extrinsic muscles are the rectus abdominis (RA), external abdominal obliques (EO), internal abdominal obliques (IO), and the transversus abdominis. The only primary intrinsic muscle in the lumbar region is the psoas major (PM). Conversely, lumbar muscles working to provide extensory action are the erector spinae,

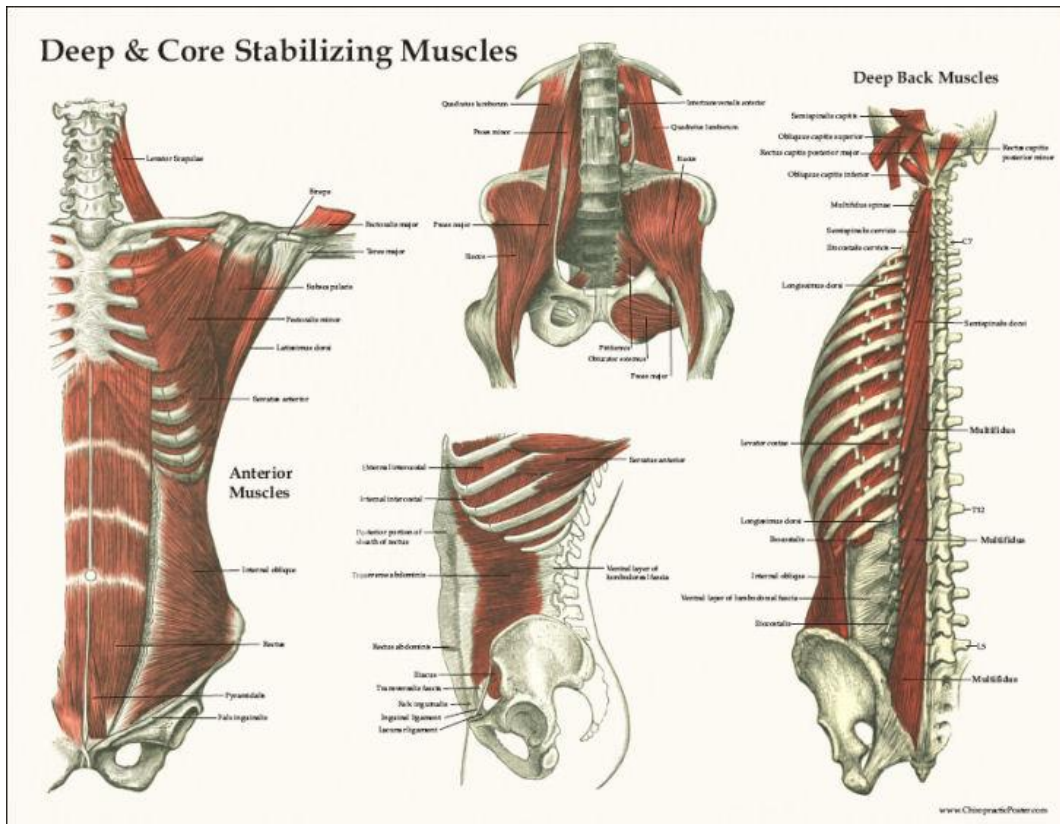


Figure 2.5 Muscles of the lumbar spine [<http://www.chiropracticposters.com>].

semispinalis, multifidi (MUL), and rotatores lumborum. Lateral flexion, normally a combination of side bending and rotation, is brought about by unilateral contraction of the oblique and transversus abdominal muscles and quadratus lumborum (QL).

Although tendons, which interface the bone and muscle attachment sites, have load-displacement curves similar to ligaments, it is not correct to simply derive forces produced in the muscle by multiplying the length change with the derived stiffness. Under active situations, Knudson *et al.* [41] found muscles to generate maximum forces at 120-130% of their original length. Conversely, these same muscles were not capable of producing force when the fibers have shortened to 50% of their original length. In addition, during passive situations, muscles

produce forces with respect to their extended length due to the tensile properties inherent in the muscle fibers. Therefore, muscular tissues were shown to be appropriately modeled using spring-damping systems with three mechanical characteristics used to define their parameters: force-velocity relationship, force-length relationship, and force-time relationship.

Muscles are also capable of sustaining static stability with and without external load, when performing tasks. However, when large muscle groups are recruited to perform overall gross motions, secondary effects on neighboring vertebrae may arise and cause inadvertent movement. In order to balance and protect against these unsolicited motions, additional muscles need to be called upon for control and smoothness of motion. Contrary to conventional wisdom, muscles thought to be silent during a prescribed motion, can possibly be active and serve as antagonist muscles controlling motion. Electromyography can be a useful tool for evaluating these types of muscle activation patterns. However, evaluating muscle dynamics often utilizes surface electromyography, and in the lower back region difficulties may exist related to capturing specific muscles due to the various sizes, depths and overlapping nature of the back musculature.

2.2 Clinical Relevance

Back pain and conditions known to contribute to the symptomatic observation of this syndrome in the overall population have been well documented. As recent as 2007, the reported incidence of adults having problems limited to the back region was nearly 12% of the US population [98]. Within that same group, more than 70% of people reported receiving some type of treatment for their condition, with an annual cost of over \$30 billion. The following year, LBP continued its widespread prevalence and ranked just behind the common cold for number of visits to the

physician's office. Maybe even more astounding, though, was the number of emergency room visits for patients complaining specifically of LBP, which averaged 9,400 per day [67].

Despite the increasing evidence for back pain being one of the most common epidemics in the U.S, its origins continue to remain elusive. Estimates predict that only about 15% of the reported cases of LBP has any type of identifiable etiology, with the remaining 85% simply regarded as non-specific in nature [21]. Regardless, most individuals suggest that pain is a manifestation of some type of injury to the structures of the spine. However, more recent studies report only about one-third of the presenting cases link the incidence of LBP with a specific injury or event [8, 81]. As a result, the current concepts are being challenged, suggesting that further investigation is needed to assess the complexity of the conditions associated with LBP [89].

Many of the treatments aimed at maintaining and rebuilding the function of the pathologic lumbar spine have a profound significance for patients experiencing LBP. In past decades, arthrodesis, also known as spinal fusion, has been the method of choice for treating LBP patients who do not benefit from more conservative approaches. Although the success of arthrodesis, clinically, is defined as the solid fusion of the vertebrae, satisfaction rates related to patient outcomes hover around 68% with an overall range between 16% and 95% [104]. However, varying criteria has previously been used to define successful patient outcomes, making the measurement process difficult and likely contributing to this wide range. A more recent study reporting on patients having circumferential fusion utilized criteria defined by the North American Spine Society and documented overall satisfaction rates near 62% [97]. This same

study, however also reported a significant correlation between patient outcome and surgical diagnosis.

Despite these varying results, data from Medicare documented the rate of arthrodesis had increased 307% between 1996 and 2004. At present, these trends are still evident with more than 3.0 million spinal procedures being performed annually around the world. In 2010, the global spine market was valued at \$5.5 billion by Global Industry Analysts. However, this same group projected the spinal surgery market to reach \$9.3 billion by the year 2017, driven largely by changing patient demographics, rising incidences of LBP, and the introduction of advanced technologies. In addition, although spinal fusion is projected to continue to dominate the spinal surgery market, data reporting on the loss of motion at the affected level as well as the incidence of adjacent segment deterioration [48, 93, 94] may lead to the emergence of alternative treatment options. The adoption of these newer motion preserving technologies, including dynamic stabilization and lumbar disc replacement, offer patients the prospect of engaging in more active lifestyles as a result of the idealized decreased loss of motion. In addition, these technologies have also been suggested to lead to improved clinical outcomes [29, 69] and increased spinal mobility [14, 71], thereby possibly reducing the incidence of adjacent segment deterioration.

Chapter 3

Review of Related Literature

3.1 Kinematics in the Lumbar Spine

The lumbar spine, under normal conditions exhibits motion about all six degrees-of-freedom. Each vertebral body is capable of three rotational motions: flexion-extension (FE) in the sagittal plane, lateral flexion (LF) in the coronal plane, and axial rotation (AR) in the transverse plane. In addition, three translational movements are permitted along the anterior-posterior (AP), superior-inferior (SI), and transverse left-right (LR) directions.

The characteristics of lumbar spinal motion in healthy, symptomatic, pathological and surgically implanted patients have been analyzed previously using various techniques and can be divided into two major categories: *in vitro* and *in vivo*. Studies conducted *in vitro* utilize cadaver specimens and can investigate either a single FSU or the entire lumbar spine specimen. Conversely, *in vivo* studies report on experiments performed directly on live human subjects. Most often, the activities under investigation are dynamic movements requiring the patient to perform an action up to maximum physiological range without the application of any external loads. Less frequently reported are passive studies which use external forces or torques applied directly to the joint in order to position the spine in a desired posture.

A number of different methodologies have been implemented to evaluate the rotational and translational magnitudes, as well as kinematic patterns describing relative vertebral motion in the lumbar spine during many types of functional activities. Many of these studies have focused on

measuring maximal physiological global range-of-motion (ROM) or segmental motion at each FSU. Examples of these types of analyses have been conducted *in vitro* using cadaveric spines [3, 13, 115], while others have utilized non-invasive skin markers [92, 110] and various external fixation devices [49, 58, 105, 106] to measure *in vivo* kinematics in the lumbar spine. Other kinematic tools for measuring *in vivo* motion in the spine include invasive bone pins [88, 99], radiostereometric analysis [7, 76], MRI [26, 46], and single- and dual-plane fluoroscopy techniques [45, 47, 50, 52, 77].

Traditional methods for evaluating movement in the lower back have focused on overall end ROM of the entire lumbar spine in the primary motion plane for a specified activity. However, these measurements can be influenced by factors such as age and gender and exhibit considerable variation among patients [11, 102, 106]. As a result, the evaluation of in-plane motion only, generally, has not been a differentiable characteristic between healthy subjects and those subjects experiencing pain and/or degeneration in the low back [55, 107]. More recently, some research studies have suggested a possible relationship between patients having LBP or degenerative conditions in the lumbar region and various degrees of restricted, excessive, or poorly-controlled lumbar motion [1, 70, 72]. However, others continue to maintain that no distinct correlation exists between mobility in the lumbar spine and clinical symptoms [11, 103].

One study, in particular, conducted by Johnson et al. [39] utilized *in vivo*, 3D motion analyses coupled with derived coefficients of motion to classify patients according to diagnosed clinical conditions. Forty subjects, distributed among four classification groups ranging from healthy to degenerative and requiring surgery, were evaluated under fluoroscopy and 3D kinematics were determined. Using both statistical and Bayesian classification techniques,

Johnson and colleagues were able to effectively differentiate among patient groups having differing pathologies. The most accurate classification scheme resulted in 95% sensitivity and specificity using only the derived motion coefficients, along with a single variable of motion. This study suggested that clinical pathologies of the lumbar spine may be linked with the vertebral motion characteristics measured during a prescribed activity.

Other research investigating centrodome patterns [31, 109], asymmetrical motion patterns [33], and intervertebral motion patterns [70] have also reported on the lumbar kinematics and indicate that motion pathways during a prescribed activity may be sensitive to certain pathologies in the spine. Normally, these motions have been analyzed using a more classic approach which attempted to quantify abnormal motion in the lumbar spine through the use of two-dimensional (2D) functional radiographs taken in the sagittal plane. However, the lumbar spine is a complex structure involving a number of motion segments and intervertebral joints and therefore, can be expected to exhibit complex 3D coupled movements. Several studies support this assumption and suggest that out-of-plane motions may be more responsive to detecting pathologies in the low back region [56, 73, 74].

White and Panjabi [109] have extensively studied the characteristics of the lumbar spine. The mean rotational kinematics were documented in healthy subjects while performing FE, one-sided LF, and one-sided AR. During the FE activity, overall intersegmental ROM at L1L2, L2L3, L3L4, and L4L5 were found to be 12.0°, 14.0°, 15.0°, and 16.0°, respectively. In a similar fashion from L1 to L5 at each vertebral level, one-sided LF ROM averaged 6.0°, 6.0°, 8.0°, and 6.0°, respectively. For one-sided AR, rotational magnitudes were substantially less at each level, averaging 2.0° at each level between L1 and L4 and 1.0° at L4L5 level.

Few studies have analyzed the 3D, *in vivo* motions among varying conditions of the lumbar spine; however, Li *et al.* [50] documented both in-plane and out-of-plane rotational magnitudes for subjects performing FE of the trunk. In their study, healthy subjects were evaluated for overall rotational magnitudes at L2L3, L3L4, and L4L5 between 45° of flexion and maximal extension with a reported average out-of-plane ROM between 2.0° and 2.3° of LF and 1.7° and 2.9° of AR at each level. Lund *et al.* [56] also analyzed 3D motion patterns in 34 chronic LBP patients and compared their results to healthy subjects reported in previous literature. Lund's work was conducted using optoelectronic camera markers attached to percutaneous transpedicular screws, which were fixated to each of the vertebrae. These markers were tracked while patients performed FE, bilateral LF, and bilateral AR. Differences were observed in the FE ratio, the LF asymmetry, and the coupled AR-LF ratio, which suggested that the motion characteristics of symptomatic patients may differ from those seen in healthy subjects. Pearcy *et al.* [77] also performed a 3D kinematic analysis on two different groups of 10 healthy, male subjects, each time analyzing primary AR and LF of the spine. Intersegmental rotations during AR were reported around 2° at L1L2, L2L3, and L5S1, with slightly higher mobility observed at L3L4 and L4L5. During LF, the rotational contribution at each lumbar level was approximately 10° at the superior L1L2, L2L3, and L3L4 levels. However, at the inferior levels, significant differences were found, measuring around 6° at L4L5 and 3° at L5S1.

The motion characteristics observed in the native spine may be influenced by a number of factors, one of which is related to instability at one or more vertebral levels. This was suggested by White *et al.* [109] who had conducted an *in vitro* study investigating the kinematics of the

spine. Other studies have also analyzed the instance of disc degeneration in patients using functional radiographs and suggest a possible link with segmental instability [24, 25].

Kinematics analyses have also been reported when the normal architecture of the lumbar spine has been altered as a result of fusion [28, 96], disc arthroplasty [6, 119], or dynamic stabilization [67, 68, 75]. A recent clinical study investigating the cervical spine evaluated whether or not increased motion occurred at proximal levels adjacent to fusion and disc arthroplasty [111]. Results revealed an increase in motion at levels adjacent to fusion but not in levels proximal to total disc arthroplasty. In the lumbar spine, similar results were reported from a cadaveric biomechanical study [18]. In that study, total disc replacements maintained kinematic parameters, while fusions experienced increased shared ROM at the proximal adjacent level. A similar study design was later conducted by Auerbach *et al.* [6] using an *in vivo* experimental set-up. In that study, the motion profiles for patients having either a normal, circumferential fusion, or total disc replacement were evaluated. It was reported that fusion patients experienced steeper motion gradients at proximal adjacent levels compared to total disc replacement subjects. In addition, between L3 and S1, the total ROM accounted for at the L4L5 segment proximal to the L5S1 operative level was 59% in single-level fusions, 38% in total disc replacement subjects and 29% in healthy subjects.

3.2 Kinetics in the Lumbar Spine

Many complex loading conditions are thought to exist in the lumbar spine. This is the result of numerous research studies which have been performed through the years in an effort to investigate these kinetic profiles. However, in spite of the considerable amount of published data

reporting on the forces, stresses, and moments acting in the spine, very few studies have been able to experimentally measure *in vivo* data describing relevant loading scenarios. Of these, telemetry has been at the forefront.

One of the first uses of telemetry in the spine was described by Waugh [108] and Hirsh and Waugh [37] in the 1960s. In these studies, Harrington distraction rods, which were originally used to treat conditions related to scoliosis, were modified to measure axial forces during distraction or decompression of the spine. This technology was eventually extended for use as a telemeterized internal spinal fixation device capable of collecting three force components and three moments acting on the fixation device [82]. In that study, ten patients were implanted at various levels with the described telemeterized implant and evaluated for different body positions and activities pre- and post-operatively in patients having anterior interbody fusion. Researchers reported the presence of mainly compression forces and flexion bending moments, along with an increase in implant loading shortly after anterior fusion. These loading levels tended to remain high in many of the patients even after solid bony fusion had occurred.

Subsequent studies by the same group of researchers assessed spinal loads in a different patient cohort having a newly developed telemetrized vertebral body replacement (VBR) implanted at various levels while performing a variety of activities [83, 84, 86, 87]. In 2008, Rohlmann *et al.* reported data from the evaluation of three patients within the first month [87] and two patients within the first six-months following surgery [83], whom of which performed a number of activities including but not limited to unsupported standing, walking, flexion, lateral bending, and axial torsion of the upper body. Spine loads were generally reported as a percentage of the force measured at the upright, standing position. The overall resultant forces were mainly

dominated by the measured compressive force magnitudes and varied from patient to patient and between evaluations. The average flexion resultant force for subjects was 233% of the standing force and was greatest around 35° of flexion, which was just after beginning the return movement from forward flexion to erect standing. On the contrary, during lateral bending motion the average maximum force for patients was decreased to around 136% of standing, while during axial torsion only minor force increases were observed over standing. Other measured *in vivo* data during walking along a level surface resulted in implant forces ranging between 127% and 150% of the standing value, while ascending and descending stairs increased spinal loads with ranges from 169% to 217% and from 159% to 206%, respectively.

Although the use of telemetry in the lumbar spine provides valuable insight into *in vivo* loading conditions, its use is limited due to the small number of subjects available for data collection. Expanding to larger patient populations would be costly and restrictive due to lack of implementation across different types of spinal arthrodesis and motion preserving type technologies. The use of telemetry is also only warranted for measuring kinetics in surgically implanted spinal joints.

An alternative method to direct, *in vivo* measurements pertains to the use of multi-body mathematical modeling techniques which have been utilized as alternative theoretical approaches for calculating *in vivo* joint forces. The basic principles and concepts for modeling have previously been implemented in the knee and hip joints with reliable accuracy [42,43] and extended to other joints including the spine [52].

One of the challenges, though, in using mathematical modeling for the human body is dealing with the possible indeterminacies within the system. In the spine, with the large number

of muscles and interactive joint forces, the system can easily become indeterminate, thereby creating a situation where it is impossible to solve for all the forces directly. To deal with this problem, two modeling strategies can be implemented. One strategy is to utilize a reduction technique which minimizes the number of unknown forces in the system based on various assumptions which may include neglecting or grouping of some muscles and/or using *a priori* relations between the unknowns. The second approach is to implement an optimization technique which deals with the large number of unknowns by minimization of the most physiologically suitable objective cost function.

De Zee *et al.* [22] recently used an optimization technique as part of the development of a generic musculo-skeletal model of the lumbar spine. The model investigated the compressive axial load on L5S1 using a min-max optimization criterion proposed by Rasmussen *et al.* [80] and incorporated 154 muscle fascicles across 7 different muscle groups. The model produced a maximum extension moment of 238 Nm around L5S1 with a predicted compressive force of 4520 N and a shear force of 639 N. Stokes *et al.* [100] also conducted a study in which mathematical modeling was used to predict the compressive force at the L5S1 level in response to a maximum bending effort made in the neutral standing posture. In their research, a generic, 3D lumbar spine model was developed with the intervertebral joint represented using either linear beam elements with published stiffness values or as a simple ball-and-socket joint. In total, 132 spinal muscles were included in the model. The resulting compressive and shear forces were predicted to be 1359 N and 458N, respectively, in response to an extension effort of 63 Nm. During forward flexion, a maximal flexion effort generated 23 Nm with a 770 N compressive force and 482 N shear force.

Other mathematical modeling techniques have been conducted which attempt to incorporate the biological sensitivity of muscle recruitment and co-contraction patterns into the model [27]. Models of this type are referred to as EMG-assisted models and utilize the measured electrical activity data of selected muscles to assist in the portioning of the total moment of forces acting about a joint. These can then be subdivided into the individual contributions made by the many anatomical structures capable of producing forces and moments. Furthermore, hybrid type methods have also been used incorporating both the optimization and EMG methodologies, thereby reported to minimize the variations in gains while still satisfying the moment equations of equilibrium in multiple planes [15,30]. These models were capable of assessing both the spinal loads and muscle forces during various activities.

Regardless of the type of methodology used, the forces borne by the lumbar segments can vary depending upon the type of activity performed, as well as the amount of external load being input into the system. Many of the previously reported models have estimated forces to reach into the thousands of Newtons [15, 16, 27] For example, El-rich *et al* [27] predicted compressive forces of about 2000 N in lower lumbar levels when a weight of 380 N was held in front of the body. On the other hand, Cholewicki *et al.* [15] reported compressive forces in the lumbar spine at the L4L5 level greater than 4000 N while performing forward flexion, extension and lateral bending of the trunk. Even during an extreme power lifting activity, compressive forces have been evaluated in the lumbar spine were estimated around 18000 N [16].

Results from these varying mathematical modeling techniques demonstrate considerable ambiguity in the predicted magnitudes, re-iterating a lack of consensus for the most physiologically suitable mathematical modeling approach. As such, even with the large

compressive loads the lumbar spine is likely equipped to handle under *in vivo* conditions, questions still remain concerning the loading magnitudes and tolerances that can be sustained before conditions related to low back pain begin to surface.

3.3 Lumbar Intervertebral Disc Pressures

As previously mentioned, few methods are available for directly measuring *in vivo* loading conditions in the lumbar spine. In fact, aside from telemetry, the measurement of the intervertebral disc pressures is the only other known method for directly evaluating the *in vivo* loading environment in the low back. The technique of placing pressure sensors in the intervertebral disc was first introduced in the 1960s and has since been used by several researchers as a method for documenting *in vivo* stresses in the lumbar intervertebral disc [19, 62, 63, 91, 112]. In 1964, Nachemson and Morris [62] reported the first uses for the collection of *in vivo* data pertaining to the measurement of pressures within the disc. In their studies, a pressure-sensitive polyethylene tipped needle was inserted into the nucleus pulposus of a normal disc at either the L3L4 or L4L5 level in 16 test subjects. Many of the subjects had undergone fusion at one more levels, but all were symptomatic for LBP. Intradiscal pressures were assessed while patients positioned themselves during sitting, standing, and reclining. In general, intradiscal pressures were 30% less during standing and 50% less when reclining compared to the sitting position. Tensile forces were also found to exist along the posterior portion of the annulus, thereby lending support to the occurrence of ruptures which are generally found to be more prominent in this region of the disc. Later, Wilke et al. [112] conducted a similar study on a single patient having a healthy spine. However, this time the pressure probe was inserted at L4L5

and the data was collected while the subject performed a wide array of dynamic activities. Of these, FE, LF, and AR were analyzed and demonstrated unique patterns for each of the prescribed activities. The patient's intervertebral disc cross-sectional area at L4L5 level was also found using MRI and reported.

Other studies have also been conducted investigating the use of pressure sensors. Sato *et al.* [91] performed an *in vivo* examination of patients having degenerative disc pathologies, and found that pressures decreased compared to healthy, which was suggested to possibly be a result of the disc's inability to retain appropriate fluid levels. Furthermore, research by Cunningham *et al.* [19] performed a cadaveric study analyzing the pressure changes in intervertebral discs at levels proximal to a destabilized or instrumented level, as well as at operative levels. Results of documented pressures at proximal levels increased as much as 45% in response to destabilization and instrumentation, while intradiscal pressures at operative levels were 41-55% lower compared to the intact spine.

Similar to telemetry, pressure sensors offer a rare glimpse into the *in vivo* loading conditions in the spine, yet widespread implantation of this technique is not yet warranted. Due to the invasive nature of placing sensors into a patient's intervertebral disc, there are possible long-term consequences that have yet to be explored. Also, the reliance of pressure sensors on appropriate fluid levels in the nucleus may limit its use in pathological patients, as hydration in degenerative discs has been shown to decrease [5, 101], which may artificially lower the intradiscal pressure readings.

3.4 Finite Element Modeling of the Lumbar Spine

The lumbar spine has also been modeled over a number of different scenarios using finite element techniques. These type of models often assist in the simulation of spinal biomechanics including both kinematics and kinetics, along with various mechanisms of injury and the effect of surgical treatment methods [65, 119]. Finite element models of the healthy lumbar spine have also been modeling to simulate defects and/or clinical symptoms to investigate mechanical influences on the spine [44, 65, 85, 90]. Of these models, spondylolisthesis [90], herniated discs [65], and muscle dysfunction [44] simulations have been conducted, with results having suggested that the force distributions in the lumbar spine change with varying symptoms and pathologies. In total, the resulting data from the use of finite element has greatly enhanced the comprehension of the degenerative cascades in the lumbar spine and the impact these mechanisms may have on the pathological and adjacent levels.

Finite element modeling has also enabled for the assessment of surgical treatments on the biomechanical response of the lumbar spine. Traditional spinal surgeries such as fusion [51], along with newer treatments such as lumbar artificial disc replacement (LADR) [23] and dynamic stabilization [118] have been simulated using finite element models. Detailed comparisons of the results pre- and post-operatively have enhanced the understanding for better surgical strategies and help explain potential complications.

However, despite the many advantages and uses of finite element modeling, its drawbacks may serve as major detriments for its widespread use. Many of the finite element models require external loads be applied to the spine to calculate the kinematic responses, internal forces and moments of the various spinal structures. These inputs are critically important for the simulation

of accurate loading conditions. However, determination of these physiological loadings is not widely available. In addition, finite element analyses require considerable amounts of time, in terms of both setting up the model and running the model. Substantial amounts of computational power are also often required to run the simulations. When multiple simulations are required with completely new geometries and boundary conditions, the setup procedure typically must be repeated. This limits the suitability of finite element modeling to analyze large patient cohorts across a number of different pathological conditions.

Chapter 4

Research Aims and Fundamental Contributions

4.1 Research Aims

Accurately describing the physiologic motions and loads of the lumbar spinal vertebrae is important to the continued growth in understanding the complex etiologies of LBP and associated spinal degeneration. Development of this knowledge can also be a tremendous asset for helping guide therapeutic strategies and improve surgical treatments that may impact the overall mechanics of the spine.

In spite of the considerable amounts of data previously obtained through *in vitro* and *in vivo* studies, few reports have accurately described the 3D, *in vivo* kinematic and kinetic magnitudes and patterns of the entire lumbar spine system. Additionally, the correlation of these dynamic characteristics with various pathologic and implanted conditions in the lumbar region is lacking. As a consequence, the progression of LBP attributed to various conditions in the lumbar spine requires a more in-depth analysis and understanding of the lower back region. This push for enhancing the knowledge base in the lumbar spine is critical for advancement in the field of spinal orthopaedics.

Nearly half a century ago, Nachemson [64] recognized the growing need for addressing problems in the low back. He called on orthopaedic surgeons to focus not only on treating just the symptoms of lumbar pain but also to explore the etiologies associated with LBP. Since this time, the prevalence of LBP and its complex etiologies have proven to be formidable opponents

for orthopaedists and researchers alike. As a result, clinicians today still face the difficult task of trying to decide upon the most effective treatments which attempt to address both the symptoms and the causes of LBP.

Many of the treatment methodologies available for patients experiencing the debilitating effects of LBP range from conservative therapies to more invasive type surgical techniques which attempt to relieve the symptoms associated with degraded, diseased or degenerative type conditions of the lumbar spine. For those individuals facing the possibility of surgery, many undergo fusion or spinal fixation at one or more vertebral levels to address the presenting clinical symptoms. Other surgical treatments, such as LADR and hybrid dynamic stabilization (HDS) have also become available. However, limited research has been conducted to verify these new treatments as viable alternatives to fusion. And although the technique of rigid fixation of the spine has long been considered the gold standard and the most preferred treatment for severe spinal conditions, its functional role and impact on the overall structure of the spine continues to be debated.

The reported success rates across all types of fusion range from 65% up to 93% [6]. However, patient satisfaction rates, which are different from fusion success rates, have been reported to be around 62% for circumferential fusion and have strong correlations with patient diagnoses describing type, severity, and anatomical location of the lumbar pathology as well as the patient's perception of a successful treatment. Ideally, a patient's expectation for successfully treating low back conditions should be cessation of pain, restoration or maintenance of range of motion, and longevity of the performed treatment. This suggests that diagnoses and treatments

should be designed with the best understanding of the factors relating LBP to both the physiological and mechanical origins.

The natural biological progression and complex mechanisms associated with LBP are likely to progress with aging and injury; however, biomechanical influences can also play a critical role in contributing to the genesis of pain [2, 109]. Mechanically speaking, LBP can be thought of as a function of the kinematics and kinetics borne in the lumbar spine, and many contributing factors can influence the manifestation of this pain. Even with this knowledge, voids exist where the kinematics and kinetics are still not well understood for the various conditions describing healthy, symptomatic, pathologic, and surgically altered lumbar spines. Therefore, the objective of this dissertation was to develop and utilize an advanced methodology for determining the mechanics at each lumbar vertebral level, which could then be implemented for evaluating various conditions of the lumbar spine. This includes determining and analyzing the intervertebral kinematics with stratification according to clinically diagnosed condition and also further investigating the mechanics of the lumbar spine using a computationally efficient, multi-body mathematical model. This model could then be used to determine the *in vivo* bearing surface forces and muscle forces throughout the lumbar spine system.

In total, this dissertation describes the initial process derived for the comprehensive analysis of the lumbar vertebral mechanics in 44 subjects having either a healthy, healthy with LBP, degenerative (non-surgical), fused, HDS, or LADR condition of lumbar spine. This study included findings for the intersegmental kinematics during FE, LF, and AR of the spine, along with the development of a mathematical model used to determine the vertebral joint forces at each lumbar level during the prescribed activities.

4.2 Fundamental Contributions

The current research study contributes to the scientific and clinical community with the comprehensive analysis of the vertebral joint mechanics at all lumbar levels with simultaneous determination of the *in vivo* 3D kinematics, joint reaction contact forces, ligament forces, and muscle forces. This data was evaluated for a number of patients having various conditions of the lumbar spine.

The present work will provide important fundamental bases for better understanding the motions and loading conditions present within the lumbar spine as well as the influences on its function. To this end, the following contributions have been made to the field of orthopedics:

1. Determination of 3D lumbar vertebral joint kinematics under *in vivo*, dynamic conditions of healthy, symptomatic, pathological and pre- and post-operative lumbar spines within the context of a single study.
2. Development of a new methodology for analyzing the vertebral kinematics using the overall path of rotation to describe the motions at each intervertebral segment.
3. Creation of a new patient-specific, multi-body mathematical model of the lumbar spinal region with inclusion of the pelvis and legs, which is capable of predicting intervertebral joint forces and contributing muscle and ligament forces at each level of the lumbar spine.
4. Use of patient-specific ground reaction forces corresponding to the performance of the prescribed activities and serving as input into the mathematical model.

5. Utilization of a pseudo-inverse method for decoupling torques solved for in the lumbar system, which enabled for the calculation of multiple muscle forces acting in the lumbar spine.
6. Correlation of the derived 3D kinematics with the predicted kinetics at each level throughout the entire lumbar system for the activities of FE, LF, and AR.

The proposed methodology utilizes a comprehensive approach that combines inverse modeling techniques and pseudo-inverse algorithms to determine the bearing surface forces and the muscle forces within each fascicle. Kinematic data derived in this research will serve as the main input to this multi-body model, leading to the determination of 3D, *in vivo* forces. Utilization of patient-specific data including bone geometries, kinematics, and soft tissue attachment sites, lend to the development of system capable of calculating force profiles and magnitudes in individuals having various clinical conditions, which to the best of the author's knowledge has not been done across multiple patient groups when modeling *in vivo*, weight-bearing conditions in the lumbar spine. Evaluation of the kinematics and kinetics for the complete lumbar spine in patients having healthy, symptomatic, pathological, and implanted (pre- and post-operative) conditions offer tremendous insight into helping further define the mechanical etiologies of pain in the low back region. As a whole, the methodologies outlined in this research may help in defining parameters that can be used for the diagnosis of conditions in the low back as well as possibly assessing potential risk for future development of low back problems.

4.3 Research Motivation

There are numerous studies investigating the kinematics and kinetics of the intervertebral joints making up the lumbar spine. However, data related to similar studies that specifically address the comparison of all these characteristics within a large cohort of pathologically different subjects and utilizing patient-specific inputs into a newly derived multi-body, mathematical model is limited in some areas (kinematics), and nearly non-existent in others (force prediction). Therefore, this research has been conducted to bridge the gap between the current data available on the mechanics of the lumbar spine with areas where data is lacking, hopefully enhancing the understanding of the complex etiologies influencing LBP and related pathologies.

Chapter 5

Materials and Methods

5.1 Research Study Design

The biomechanics of the vertebral joints in the lumbar spine were studied in subjects having both implanted and non-implanted conditions of the lower back region. All subjects were asked to perform a series of active lower back maneuvers while under fluoroscopic surveillance to assess the dynamic characteristics of the vertebrae and surrounding structures. In addition, CT and MRI modalities were conducted to enable for bony tissue reconstruction, accurate determination of soft tissue attachment sites, and to allow for accurate clinical diagnoses of each subject's lumbar spine. Through the use of both imaging and clinically reported data, a single, fellowship-trained neurological surgeon (Dr. Joseph S. Cheng, Vanderbilt University Medical Center, Nashville, TN, USA), evaluated and categorized each subject into one of six pre-defined classification groups: healthy, healthy with LBP, degenerative (non-surgical), fusion, HDS, or LADR.

Each subject was asked to perform prescribed activities using their natural, dynamic motion pathways without use of any supportive devices. The activities evaluated were FE, LF, and AR. A C-Arm type fluoroscopic unit (General Electric, Salt Lake City, UT) was utilized to capture motion of L1 through L5 vertebrae. The 2D fluoroscopic images were stored on videotape for subsequent re-digitization and analysis using a frame grabber. While performing the prescribed activities, the patients placed each of their feet on one of two AMTI (Advanced Mechanical Technology, Inc., Watertown, MA) force plates. This enabled for the synchronous collection of

ground reaction force (GRF) data with the recorded fluoroscopy video. 3D kinematics of each functional spinal unit were determined using a 3D-to-2D registration algorithm. These motions later served as input into a mathematical model designed to output patient-specific, *in vivo* joint contact forces at each vertebral joint level and the surrounding soft tissue structures.

All study protocols were approved by Institutional Review Boards (IRB# 7393) at both the University of Tennessee (Knoxville, TN) and Vanderbilt University Medical Center (Nashville, TN). In addition, prior to collection of data, each study participant read and signed an informed consent form as well as Health Insurance Portability and Accountability Act confidentiality and privacy statements.

5.1.1 Patient Selection

For the purpose of this study, subjects were selected and classified into one of six groups by a single surgeon using three available subject pools. These included the patient pool at Vanderbilt Neurosurgery Clinic, Nashville, TN; and the staff and student populations at both Vanderbilt University (Nashville, TN) and the University of Tennessee (Knoxville, TN). Following a satisfactory evaluation of a sufficient number of potential enrollees meeting the study criteria for participation, individuals having expressed interest were invited to participate in the study by Dr. Joseph S. Cheng. Subjects were contacted using telephone and email notification. Detailed information regarding the study objectives, potential benefits and any risks were thoroughly explained to each interested subject. Each subject was informed that participation was entirely voluntary and the option of withdrawal was open at any time.

All relative data including age, gender, height, body weight, diagnosis, and other parameters concerning a patient's condition were recorded. The age of the subjects was limited to range between 18-85 years and their weight had to be less than 275 lbs in order to ensure experimental results represented the population demographics and maintained a safe experimental environment which minimized radiation exposure.

5.1.2 Description of Participants

Forty-four subjects were selected for participation in this study and classified into one of six groups specifically designed to provide stratification among various characteristics describing each subject's lumbar spine condition. The healthy group included 10 subjects determined to have a normal lumbar spine for their age with no reported pain or limitation in daily activities. An equal distribution of five males and five females were selected with a mean age of 39 ± 13.2 years of age. The LBP group consisted of 10 subjects (five males, five females) with a mean age of 46 ± 9.9 years. Subjects in this group were healthy without radiological evidence of degeneration or deficiencies in the lumbar spine but were noted to be symptomatic for acute LBP. At the time of evaluation, eight of ten subjects within this group were experiencing mild pain in the low back region, while the two remaining subjects reported having at least one episode of acute low back pain within the six months prior to assessment. The degenerative (non-surgical) group included 10 subjects (six male, four female) averaging 39 ± 9.3 years of age. Subjects experienced LBP prior to and during the evaluation and were also clinically classified as having degenerative defects in the lumbar region. Radiological evidence of degenerative pathologies was observed in all subjects within this category and associated with one or more of

the following conditions: Schmorl's Nodes, disc bulging both with and without canal or foraminal stenosis, disc osteophyte complexes, decreased height and fluid signal loss in the intervertebral disc, or posterior facet hypertrophy. Evidence of these defects was considered mild to moderate and was not severe enough to warrant surgery. Six of the subjects in the degenerative, non-surgical group were diagnosed with pathological changes at a single vertebral level, while the remaining four were identified to have degenerative pathologies at multiple levels. Patients were also selected as part of a fusion group and stratified according to the level of instrumented fusion. In total, 10 subjects (six male, four female) were enrolled having a mean age of 48 ± 10.3 years. Fusion subjects required rigid fixation at one or more levels and were analyzed pre-operatively (classified as a subset of the degenerative (surgery required) group) and at least six months post-operatively. Five of the subjects underwent fusion at L4L5 level, three at L5S1 level, one at L4 through S1 levels, and one at L3 through L5 levels. One patient within the L4L5 fusion category opted to withdraw from the study following surgery due to complaints of severe pain and did not want to further exacerbate these symptoms.

While the previous lumbar spine classification groups each had 10 subjects initially enrolled, the remaining two groups were much smaller in the number of enrollees. During the planning stages of this research, six primary classification groups were defined with the goal of including an equal distribution of ten subjects for each lumbar spine condition. However, over the course of enrolling subjects to fill each group, the number of surgeries using HDS and LADR had sharply declined in the United States, thereby hampering enrollment efforts within these categories. As a result, the HDS group included only two subjects (two male; zero female). The mean age of subjects having hybrid dynamic stabilization was 38 ± 4.9 years of age. Patients in

this group were implanted with the Isobar® TTL Dynamic Compression Rod (Scient'x Groupe S.A., Guyancourt, France) at L4L5 level as an adjunct to posterior instrumented fusion at L5S1. Patients were evaluated pre-operatively and classified as a subset of the degenerative (surgery required) group and at least six months post-operatively. In the final lumbar classification group, patients were enrolled who had previously undergone LADR. The average age for this group was 49 ± 9.9 years at the time of evaluation. LADR subjects were implanted with the Charité® (Depuy Spine, a Johnson & Johnson company, Raynham, Ma) artificial disc replacement at the L5S1 level. However, as a result of the limited availability of patients for this category, potential enrollees from a group of patients implanted by an alternative surgeon in the Nashville area approximately 10 years prior were contacted for participation in the current study. In total, only two patients (0 male; 2 female) were available for enrollment and evaluations were conducted at 120 months post-surgery.

5.1.3 Activity Description

All subjects performed three activities while under fluoroscopic observation. These activities included FE from maximum flexion to maximum extension, LF from left to right, and AR from left to right. Prior to beginning the testing protocols, subjects were provided with proper lead shielding for the thyroid region and were positioned next to the image intensifier so as to capture the motion of the entire lumbar spine between L1 and L5 in either the sagittal or coronal plane. For each activity sequence, subjects were verbally instructed and visually demonstrated the correct way for performing the prescribed motions. Subjects were encouraged to ask any questions they may have and were given ample time to practice and become accustomed to

performing each of the activities prior to turning on the fluoroscopy unit. Subjects were asked to try and complete all activities with minimal movement of the pelvic region and to his/her comfortable ROM and speed, emphasizing a smooth, consistent motion.

During each of the activities the participant always started at the upright, neutral standing position and portions of the activity were extracted for analyses. For FE of the lumbar spine, the subject began by rotating the trunk within the sagittal viewing plane until reaching the maximum flexed position. Following a slight pause, the subject began the return path back towards the upright, standing position. Without stopping the motion, the patient continued through the neutral position into extension. Once reaching the fully extended position, the patient paused once more and then proceeded to return to the neutral, upright standing position. Following the performance of this FE activity, the fluoroscopy machine was repositioned to allow for motion capture within the coronal plane. Both LF and AR motions were evaluated using this setup. LF of the lumbar spine was performed by rotating the trunk in the coronal plane. Beginning at neutral, the subject began moving to the left until reaching a full, laterally flexed position. Following a brief pause, the patient began rotating the spine back towards the upright, standing position and continued without pause to a right, full laterally flexed position. Again, the patient paused and began the return path back to the neutral, upright standing position. During AR of the spine, subjects rotated his/her lumbar spine within the transverse plane to a full, left axially rotated position. Following a short pause, the subject proceeded to rotate back towards neutral. The subject continued through neutral continuing to rotate until reaching a full, right axially rotated position. The patient, again, paused briefly and then returned to the neutral, upright standing position.

The fluoroscopy machine recorded *in vivo* motions of the lumbar vertebrae for no more than two trials per activity, and completion of all three activities occurred with a fluoroscopic “on-time” of less than two minutes. Participants were instructed to rest between each activity in order to allow for adequate time for the muscles and ligaments in and around the lumbar spine to relax. All patient evaluations utilized video fluoroscopy. At least one evaluation was conducted for patients having a native lumbar spine and not requiring surgery, while a follow-up evaluation was conducted at least six months later to evaluate the effect of fusion and HDS in patients. Since patients in the LADR group were not available prior to surgery, individuals in this group only underwent a single evaluation using fluoroscopy.

5.2 Reconstruction of Patient-Specific Lumbar Vertebrae

The 3D, computer aided design (CAD) models of L1, L2, L3, L4, and L5 were recreated for each patient using segmentation techniques shown below in Figure 5.1. All patients underwent CT scans of their low back region and the resulting images were obtained for processing. This process allowed for the reconstruction of volumetric data at the interpolated slices in the transverse plane. Using the commercially available AMIRA software (TGS Inc., San Diego, CA), the segmentation process was initiated. A semi-automated technique, which applied a thresholding filter, isolated the vertebral bones from surrounding soft tissues. Some manual segmentation was required around the zygapophyseal joints between adjacent levels. The resulting data were then used to create patient-specific, 3D polygonal surface models of each lumbar vertebra.

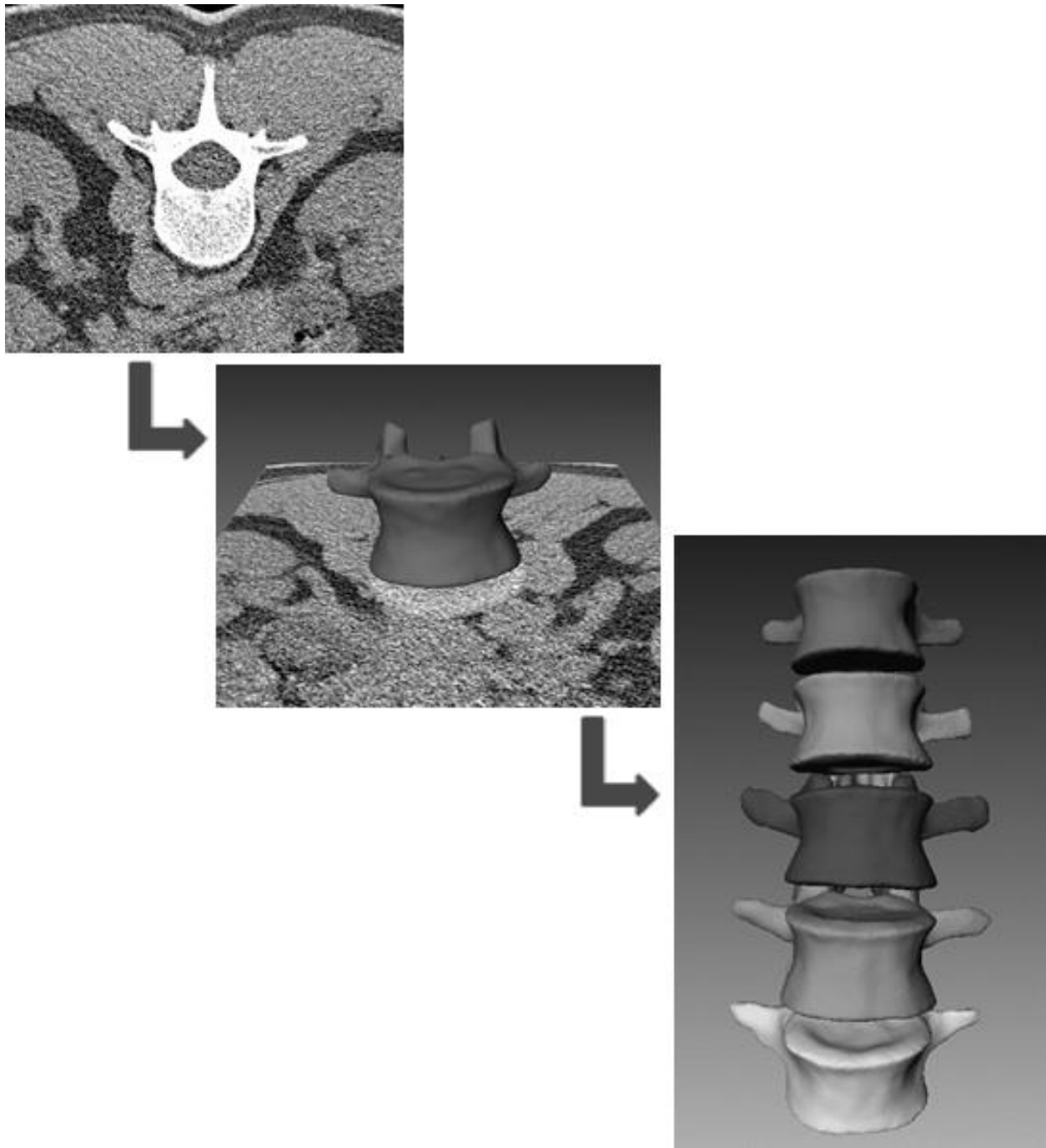


Figure 5.1 Process of using CT scan image dicoms to recreate 3D patient-specific bone models.

5.3 3D-to-2D Image Registration Technique

A 3D analysis of the fluoroscopic image series was achieved by fitting the projection of the recreated 3D vertebral CAD models to the 2D fluoroscopy images. Using a previously published 3D-to-2D intensity-based image registration method described by Mahfouz *et al.* [57], both in-plane and coupled out-of-plane motions at each level of the lumbar spine (L1 through L5) were recovered. This 3D model fitting approach allowed for the relative pose of each vertebra to be determined from a single-perspective fluoroscopic image by manipulating representative CAD models in 3D space. A 3D scene of the fluoroscopic unit was created using a client based server application on the Windows (Redmond, WA) platform using the Open Inventor Toolkit (Mountainview, CA) library. The scene consisted of a light source (x-ray), an image plane on which to project the fluoroscopic image (image intensifier), an area to manipulate a 3D model (subject area), and a camera to view the entire scene.

Individual fluoroscopic frames were captured at specified increments for each activity as follows:

1. FE: maximum flexion (MxF), mid-flexion (MdF), neutral (N), and maximum extension (MxE).
2. LF: maximum left lateral flexion (MxLt), neutral (N), and maximum right lateral flexion (MxRt).
3. AR: maximum left axial rotation (MxLt), neutral (N), and maximum right axial rotation (MxRt).

The specified fluoroscopic frames were then digitized and projected onto the image plane with the corresponding bone and implant models added to the scene. Initially, the models were positioned so that the silhouettes of each vertebral bone best matched the analogous representative edges visualized in the fluoroscopic image. A final fit was achieved using a global optimization algorithm which minimized the image similarity error between the 3D model and the corresponding component in the 2D image (Figure 5.2). The 3D positions of each vertebra at the captured fluoroscopy increment were calculated using the aforementioned model fitting application. For each evaluation, analyses were conducted to derive the relative transformations at each level of the lumbar spine. Determination of the transformation matrices for each vertebral model enabled for the calculation of 3D motions and allowed for kinematic observations to be made at pre-operative (degenerative (surgery required) and post-operative stages for the implanted subjects (fusion, HDS, LADR) and comparisons of these trends with those found to occur in native, non-implanted healthy, LBP and degenerative (non-surgical and surgical) lumbar spine subjects.



Figure 5.2 In vivo fluoroscopy at specified increments during flexion-extension (top) with subsequent 3D-to-2D registration of the bone models (bottom).

5.3.1 3D-to-2D Image Registration Error Analysis

An error analysis of the 3D-to-2D image registration process used throughout this research had previously been conducted on the knee [20, 57] and in the spine [52] using fresh cadaver specimens.

For the knee, discrete points were placed on the femoral and tibial components. Using an OptoTrack system (Northern Digital Inc., Waterloo, Canada), these points were digitized and the femur was defined relative to the tibia, in the tibial reference frame. Each orientation of the femur, relative to the tibia was fluoroscoped and using the 3D model-fitting software package [57], the relative orientation of the femur with respect to the tibia was predicted and compared to the known orientation derived using the OptoTrack system. The results from this error analysis and accuracy tests revealed average errors in the 1-direction, 2-direction, and 3-direction translations were -0.023, -0.086, and 1.054 mm, (standard deviations were 0.473, 0.449, and 3.031 mm), respectively. Likewise, average errors in rotations about the 1-axis, 2-axis, and 3-axis were -0.068, 0.001, 0.253 degrees (standard deviations were 0.942, 0.771, and 0.841 degrees), respectively. These numbers represented the errors in the model fitting process plus the errors associated with the independent measurement system (i.e. the upper bound). In addition, since the knee joint was imaged in the sagittal plane, the relative translational motion of the implants in the 3-direction was minimal.

Similarly, for the spine error analysis, a fresh cadaveric spine was obtained and FE, LF, and AR motions were represented using a Spine Simulator. Utilizing a Micron Tracker system, three markers were attached at each vertebral level and absolute 3D translations and orientation data were tracked during the prescribed motions. Synchronously, fluoroscopic surveillance was

conducted during the motion. Using the 3D model fitting software package described previously by Mahfouz *et al.* [57], the relative orientation of each vertebra with respect to the adjacent level was determined and compared to the known orientation measured using the Micron Tracker system. The results from this error analysis and accuracy tests revealed average errors in the 1-direction, 2-direction, and 3-direction translations of 0.61, 0.67, and 0.57 mm, respectively (standard deviations were 0.61, 0.55, and 0.43 mm, respectively). Likewise, the average errors in rotations about the 1-axis, 2-axis, and 3-axis were 0.44, 0.43, 0.56 degrees (standard deviations were 0.39, 0.47, and 0.42 degrees), respectively. Again, these numbers were found to represent the errors in the model fitting process plus the errors associated with the independent measurement system.

5.4 Determination of In Vivo Lumbar Kinematics

Once the 3D-to-2D registration technique had been completed, the 3D orientations of each of the vertebrae were imported into a custom, in-house software package, known as Kinetic Analysis of Rigid Body Systems (KARBS). This software was built using the MATLAB (The Mathworks Inc., Natick, MA) development package and enabled for further determination of kinematic parameters. Transformation matrices describing the 3D translations and rotations of each vertebral body at the captured increments were imported into KARBS, and the 3D vertebral CAD models were designated to each matrix contained in the metafiles. Positions of the vertebrae at increments lying between the captured increments were interpolated using KARBS. Through the creation of directory files and subsequent files specific to KARBS, the 3D kinematics were extracted.

The rotational magnitudes reported in this dissertation were calculated using software specifically written to extract relative motion at each vertebral level with respect to the most caudal vertebra. Traditional methods were used to calculate rotational ROM about the main motion planes throughout each of the prescribed activities. This technique calculated the difference between the two increments, representing the minimum and maximum rotational magnitudes observed during the entire activity. The rotational paths were also investigated and better represented the couple motions at each functional spinal unit. These values were derived at each level by tracking the cephalad vertebrae as it articulated upon the more caudal vertebrae. At each designated increment, the absolute rotation about each axis was derived. The absolute difference between each subsequent increment was then calculated and a summation of the absolute magnitudes over the entire flexion plus extension activity was performed. As a result, the motion paths could then be quantified at each level among the different spine types.

5.5 Development of the 3D Mathematical Model

With the methods available for assessing *in vivo* loading conditions being limited, the ability to accurately model and analyze a system dynamically can be a tremendous asset for aiding the study and progression of knowledge in the area of biomechanics. The human body, and all its complexities, exhibits many of the same core characteristics inherent in other mechanical systems. As a result, mathematical models represented by a set of well-defined equations, describing motion and inertial parameters, can often serve as useful tools in replicating the physical laws which govern a particular system. For the purpose of this research, the traditional laws developed by Isaac Newton have been implemented. However, the ideologies and

techniques from Dr. Thomas Kane have also been applied to not only simplify the modeling algorithms, but also to enhance the usefulness of the model by generalizing the equations of motion.

In order to predict the *in vivo* forces at each level of the lumbar spine during the FE, LF, and AR activities, a 3D, multi-body, inverse dynamics computational model was developed. Using the principal of rigid body dynamics described by Dr. Kane, the motion and external loads were known and input into the model, thereby allowing for the system's internal forces and torques to be solved [40]. Generally, reduction modeling techniques are implemented when using inverse modeling in order to keep the system determinant. By assuming that certain muscles do not contribute to the system during an activity and assuming grouped muscles accurately represent individual muscles, the redundancies in the model can be minimized. This maintains an equal number of unknowns and available number of equations of motion, thus keeping all the parameters solvable. However, the model presented in this dissertation circumvents these redundancies by incorporating the pseudo-inverse method [114] into the solver. Prior to running the solver, the inverse model was developed in the symbolic manipulator AutolevTM (Online Dynamics Inc, Sunnyvale, CA), which is based on Kane's dynamics [40]. This method is extremely efficient and well suited for multi-body systems having large degrees of freedom. Each rigid body in the system can have as many as six kinetic terms solved for in the model.

In addition to finding the resulting joint reaction forces, this research also investigated the individual muscle forces acting in the lumbar region which contribute to the overall internal forces calculated at each level. Decomposition of the output resultant torques, calculated from the inverse model, enabled for determination of the appropriate forces in the individual muscles

to balance out the system. Since these soft tissue forces could not be solved for directly because the number of muscles included in the model was far greater than the number of available equations of motion, the previously mentioned pseudo-inverse algorithm was utilized and included in the model. Using the resultant torques calculated during the inverse modeling portion of the multi-body model, a matching criterion was implemented to recruit defined muscles in an efficient way which derived the muscle forces required to produce the desired resultant torque being matched.

5.5.1 Model Inputs

Motion parameters derived from the 3D-to-2D registration process provided three rotational and three translational values for each vertebra. These values described how the geometrical center of each vertebral model was positioned relative to the global origin at the selected motion increment. The captured increments were selected sequentially along the motion path relative to time and represented a defined position during the prescribed activity. To prepare the data for use in the model, the kinematic parameters were made smooth and continuous using spline interpolation. The representative polynomial equations of the vertebral motions, with respect to time, were required to be of the third order or higher. This ensured that the accelerations derived by the double differentiation of the positional motion were also continuous. The most appropriate spline of order greater than three was selected following the fit of the original kinematic data based on the least sum of squares error.

GRF data were also collected and input into the mathematical model. The inclusion of the GRF data provided a methodology for introducing accurate patient-specific, external force

loadings acting on the multi-body system, all while accounting for the time-dependent changes in the force over the course of the activity. This data collection process was initiated following the patient placing the left and right foot in the center of one of two force plates positioned side-by-side on the floor. Raw force plate data was compiled for both the left and right foot in the form of voltage magnitudes with respect to time. Subsequent post-processing of the force plate voltage data was then required using each force plate's sensitivity matrix, resulting in the calculation of three reaction forces and three reaction moments acting at each foot. Since the reaction moments were found to be relatively small, it was verified that the center of pressure of both feet where the measured forces were acting corresponded well with the coordinate axis system defined on the force plate. The resulting time-dependent GRF were then smoothed using a shape-preserving piecewise-cubic hermite interpolation. This produced one vertical and two shear forces at each foot.

The predictive, multi-body computational model described in this dissertation also relied on the use of patient-specific vertebral bone geometries. This specificity enabled for the most accurate representation of the rigid bodies and accompanying bony prominences. This was important for defining precise locations for the soft tissue origin and insertion sites. While some of the ligaments and muscles in the lumbar region were fairly small and inserted over reduced attachment areas, others were quite large and required more expansive areas for attachment. As a result, modeling the ligaments and muscles as single lines could have oversimplified the system and prevented the most accurate representation of the soft tissue structures under *in vivo* conditions. In many cases, single line elements would have also significantly over or under predicted the active torques present in the system, thereby leading to inaccuracies in the

predicted muscle forces. Hence, most of the ligaments and all of the muscles in the present mathematical model have been partitioned into multiple strands. The ligaments were sectioned parallel to their longitudinal length, thereby creating two to three bundles representing a single ligament. Similarly, the muscles were also divided into multiple fascicles inserting at various sites that represented the lines of action for the muscle. In both cases, defining multiple strands to represent the soft tissue structure in the model allowed for a more refined analysis of tissues and enabled for the diverse mechanical function of each ligament and muscle to be modeled more appropriately.

Additional inclusions to the multi-body model consisted of rigid generic bones symbolizing the structures of the lower body (left and right legs, pelvis and sacrum) and the upper body (T12-C1 spine, ribs, arms and head), as well as a geometric shape representing the abdominal wall. Incorporating these non-specific geometries into the model enabled for the inclusion of secondary soft tissue structures, which did not attach directly to the vertebral bones but were thought to play a functional role in the mechanics of the lumbar spine. *In vivo* conditions are believed to utilize some of these secondary soft tissues, to not only stabilize the lower back, but also to assist in dynamic maneuvers of the lumbar region.

5.5.2 Model Description

The primary purpose of the proposed multi-body, computational model was to accurately predict the *in vivo* force patterns at each lumbar vertebral level across various conditions of the spine. However, although the lumbar spine was the main system being modeled in this dissertation, the previously mentioned lower and upper bodies along with the abdominal wall have been included

to enable for soft tissue attachment sites as well as providing a location where the external GRF could be introduced. Since the GRF data are the only externally applied loads input into the system, it was important to apply the loads at a reasonable anatomic location. While the lumbar vertebrae from L1 to L5 were modeled as rigid bodies, specific to each patient with a prescribed mass and inertia, the lower and upper bodies, as well as the abdomen wall were defined as singular structures and treated as massless frames. Using this methodology, the entire dynamic system, starting at the foot-ground interaction up through the entire lumbar spine, could be modeled.

Initially, the free body diagram of the mathematical model was developed in the sagittal plane (Figure 5.3). The feet were assumed to always be in contact with the ground (force plate)

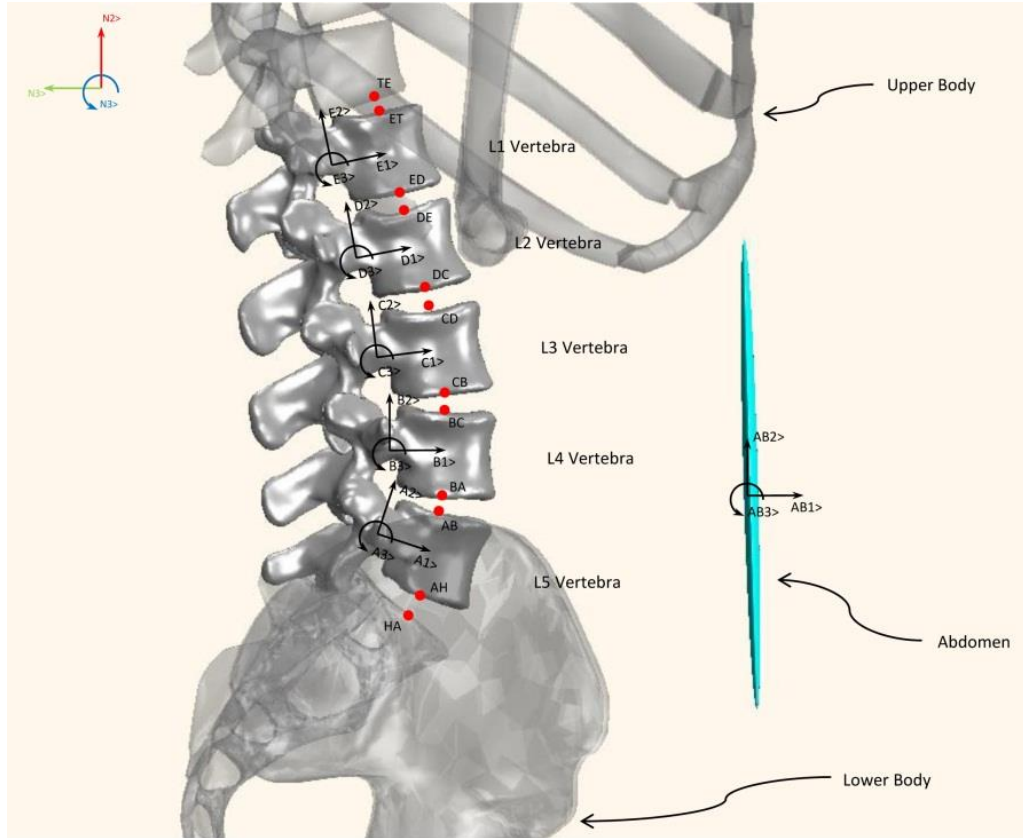


Figure 5.3 Schematic of the mathematical model showing a sagittal view of the lumbar region. The points of contact were defined on each vertebral body at the inferior and superior endplates at each FSU.

while performing the three prescribed activities. The origin of the Newtonian reference frame was placed at the mid-point between the two feet, along the transverse coordinate axis and parallel to the force plate surface. On each body and frame defined in the model, the origin of the local coordinate system was defined at the geometrical center. The corresponding unit vectors were oriented along the AP, SI, and LR directions and corresponded to the unit vectors in the 1-, 2-, and 3-directions, respectively.

Inertial properties of each of the vertebral bodies about the major FE axis were assigned using previously published literature [78]. However, since motions in the coronal and transverse

planes were generally considered small in the lumbar spine compared to the amount of motion in the sagittal plane, inertial properties of the vertebrae along these less prominent motion axes were assumed to be zero. In addition, the mass of the lower torso and abdominal region lying between L5S1 and T12L1 joints was distributed throughout the vertebrae levels according to Pearsall *et al.* [78].

The lower body, L5, L4, L3, L2, L1, upper body, and abdomen wall were all defined in the multi-body, computational model. While the kinematic parameters of the rigid vertebral bodies, inclusive of L1 through L5, were expressed using the derived polynomial equations, the motions of the lower body frame, upper body frame, and abdominal wall frame were unknown. Therefore, a simple alternative was to constrain the motions of these frames so that their movement relative to an adjacent vertebra was zero. Hence, for both the lower and upper bodies, the specified kinematics were the same as those derived for L5 and L1, respectively, thereby resulting in no movement at the L5S1 and T12L1 junctions. Similarly, the abdominal wall motion was represented using the same kinematics as those determined for L4.

Points were also defined representing the contact point between two adjacent bodies. These points were selected at the center of the vertebral endplate on the inferior and superior vertebral surfaces, as well as the proximal sacrum surface and the inferior T12 vertebral surface. These points served as the location where the three interactive contact forces and resultant torques were solved for in the model.

Ligaments were included in the model to act as tensile constraint elements that apply forces at the joint level to aid in stabilizing the lumbar spine structure. The contributions of the ligaments in the model were dependent upon the low back posture and the associated positions of

the vertebrae throughout the activity motion. For example, at the maximum flexion position, the ALL which spans superiorly and inferiorly along the anterior portion of the lumbar spine, ideally, would not be in tension. As a result, it carries minimal or no load, and therefore does not provide restraint during the movement. Conversely; the posterior ligaments in the spine, positioned along the dorsal portion of the vertebral body and spanning attachment sites on various processes would be under tension. Therefore, loading of these ligaments would occur and serve as constraint to the vertebral motion, thereby helping to maintain stability during flexion. Similarly, during extension, the anteriorly positioned ligaments would carry load, thereby constraining motion and stabilizing the lumbar spinal segments. According to classic dynamics, the ligament force farthest from the center of rotation of the vertebra carries the largest lever arm, and ideally, is the most efficient at influencing the motion at a lumbar segment. At the neutral position, the majority of the ligaments should provide only a minimal amount of tension, as the ligament lengths are assumed to be close to their slack lengths. However, some small amounts of force are hypothesized to be a necessary characteristic of the healthy, native lumbar spine as a way to maintain structural stability.

Ligament forces were calculated using position vector data derived based on the location of the origin and insertion attachment sites. Any wrapping of the ligaments around bony surfaces were also accounted for in the calculated lengths. The ligaments included in the current model were the ALL, PLL, LF, ISL, and SSL and have been shown in Figures 5.4 - 5.8, respectively. Because of the larger ligament widths in the spine, many of the ligaments were divided into a number of bundles depending upon the size of the ligament. In total, 55 ligament bundles were represented in the present model. The attachment sites for each ligament bundle have been

incorporated using single points. In addition, since the ligament properties used in the present model mirror those from a study conducted by Pintar et al. [79], similar guidelines for choosing the approximate locations of the ligament attachment sites were used. However, since this model included patient-specific geometries, final anatomic positions of the ligament attachments varied slightly from patient to patient.

In the study by Pintar et al. [79], the mean force-deformation curves of all the lumbar ligaments were plotted, but only the slope of the most linear part of these curves was numerically reported. Therefore, the ligaments in this current study have been modeled as linear spring elements, although other researchers have suggested that ligaments respond to loading in a more non-linear fashion. The reasoning for using a linear modeling function for ligaments in the current model was based on the activities chosen for the patients to perform. Since FE, LF, and AR are among many of the movements experienced over the course of normal daily routines, the

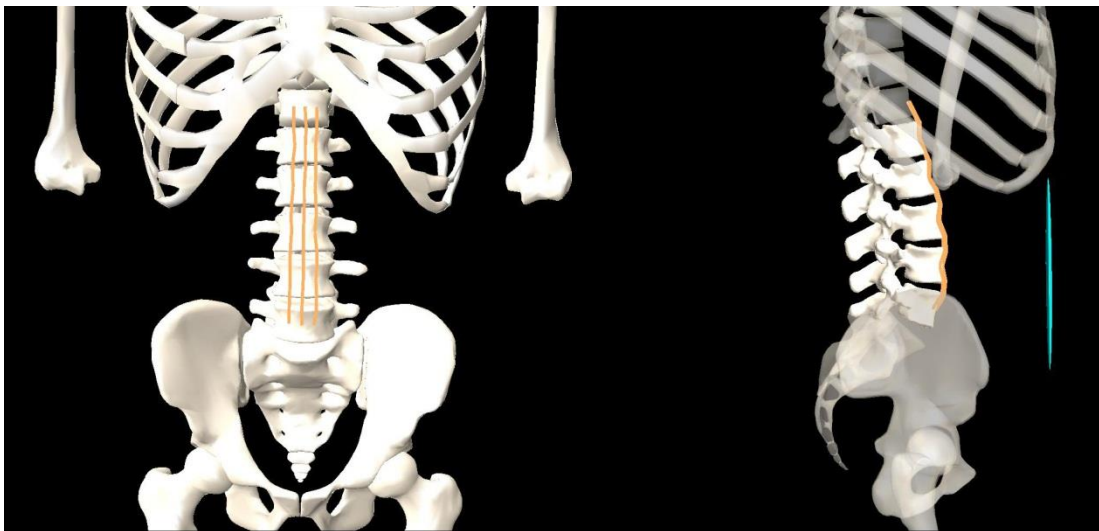


Figure 5.4 The ALL (shown in orange) attached at the mid-height of the anterior aspect of each vertebral body and was divided into a left, medial, and right bundle.

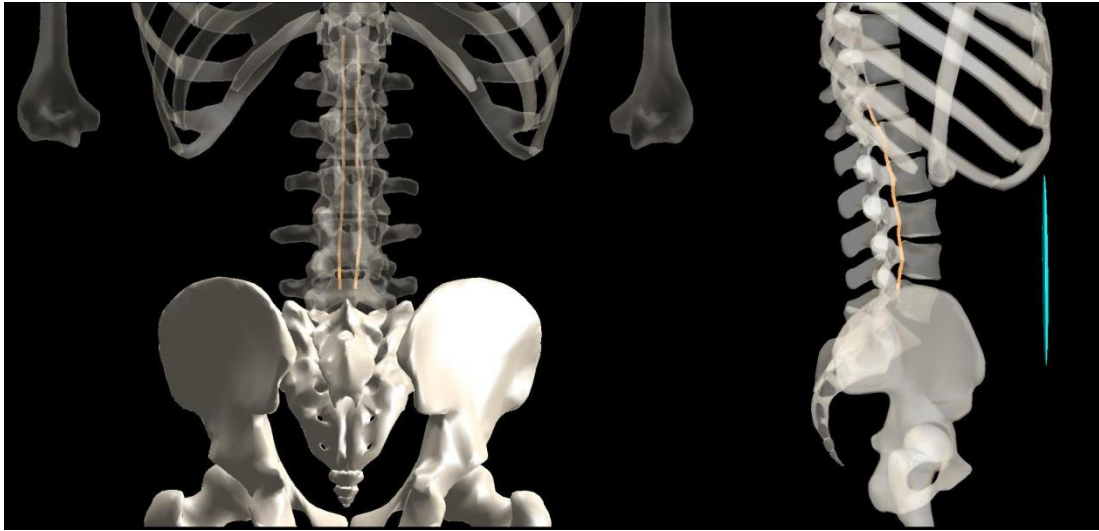


Figure 5.5 The PLL (shown in orange) attached at the mid-height of the posterior aspect of each vertebral body and was divided into a left and right bundle.

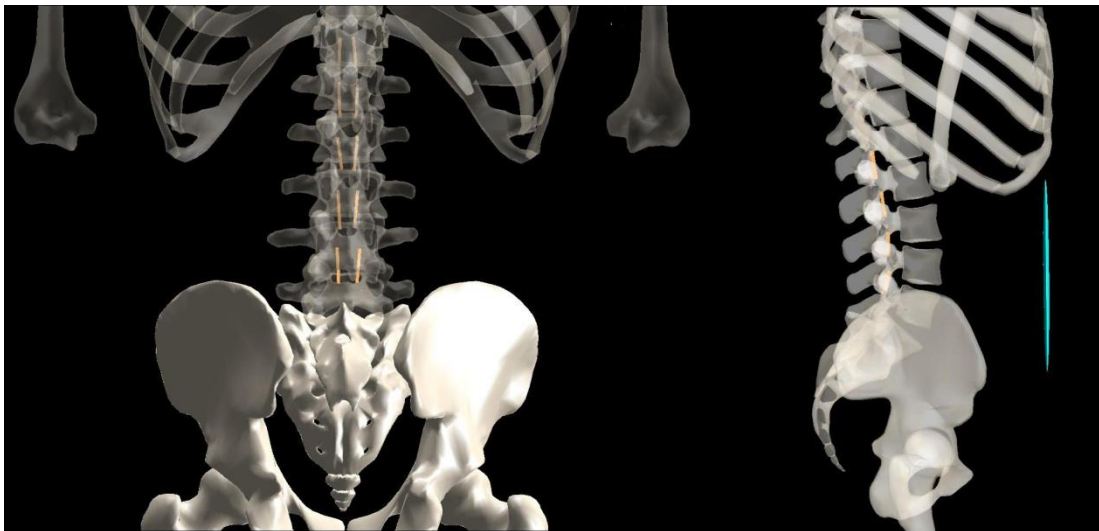


Figure 5.6 The LF (shown in orange) attached along the antero-superior and antero-inferior border of the laminae at each level and was divided into a left and right bundle.

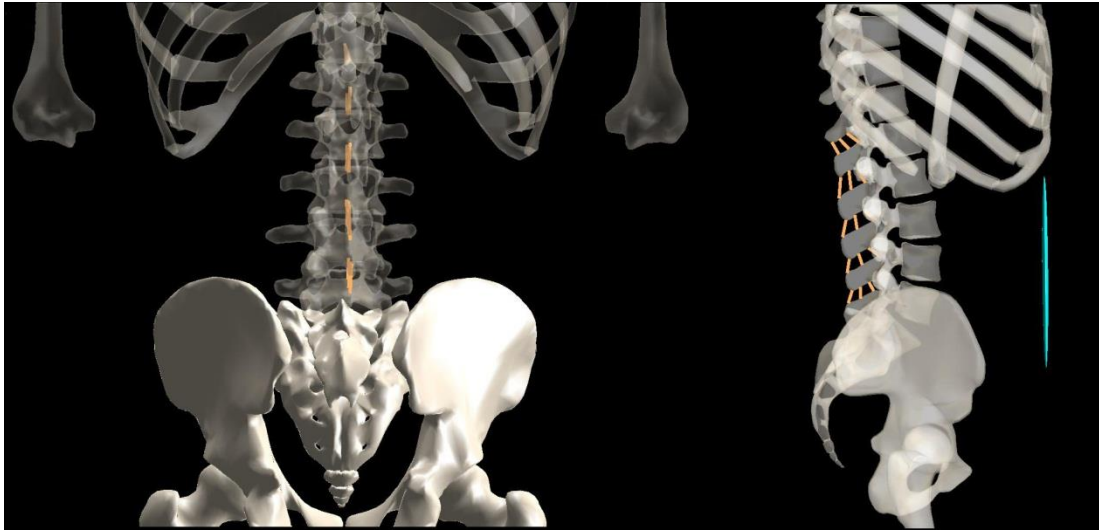


Figure 5.7 The ISL (shown in orange) attached along the inferior and superior apex of the spinous process at each level and was divided into an anterior, medial, and posterior bundle.

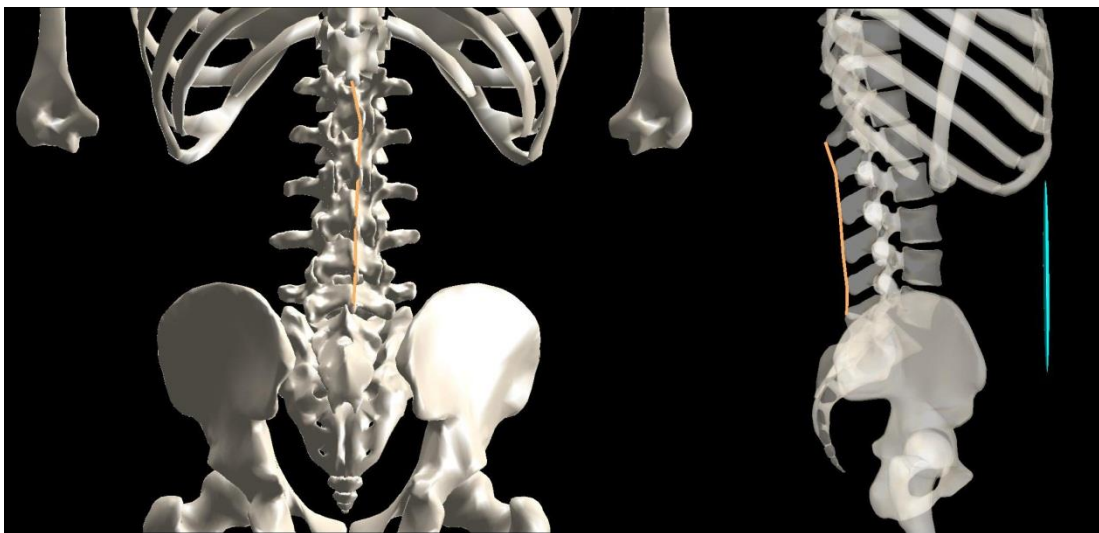


Figure 5.8 The SSL (shown in orange) attached at the mid-height of the posterior aspect of the spinous process at each level and was defined as a single bundle.

ligament forces modeled here were expected to remain in their physiologic, primarily linear phase. Therefore, the ligament force calculated at each increment of an activity was derived using a modification of Hooke's law:

$$F = \frac{\Delta L}{L} EA$$

where F represented the force in the ligament, E was Young's modulus for a particular ligament, A was the average cross-sectional area of the ligament, L was the defined slack length measured at the neutral, upright standing posture, and ΔL was the deformation in the ligament represented by the change from the incrementally measured length to the resting slack length. It is also worth noting that since ligaments can only apply a restrictive, tensile force, in cases where ΔL was found to be less than or equal to zero, the force in the ligament was automatically assigned a value of zero.

The complex musculature of the lumbar spine aids the ligamentous structures in maintaining stability, while also providing the means for performing a number of daily tasks. In the current model, all of the muscles spanning the length of the spine were not able to be included; however, the major muscles thought to contribute to the prescribed motions in the spine were added. Thus, this model incorporated the PM, MUL, QL, EO, IO, and the RA muscles and have been depicted in Figures 5.9 - 5.14, respectively. Again, each muscle fascicle attachment site was modeled as a point. Approximate sites for fascicle origin and insertion were obtained from previous literature [22, 35] and then the most anatomically correct attachment site was selected on the patient-specific, bony geometry. As in the case of the ligaments, muscles were also divided into multiple fascicles with individual attachment sites connected to represent the lines of action for each particular muscle. An algorithm was utilized to allow for each muscle fascicle to wrap around bony structures. In total, 98 fascicles, over six main muscle groups, were included in the mathematical model. This allowed for a more refined analysis of the muscular structures and enabled for the diverse mechanical function of each muscle to be modeled more appropriately.

In combination, the inclusion of patient-specific *in vivo* 3D kinematics, bone geometries, body segment properties, and muscle/ligament lines of action enabled for the development of an efficient and robust dynamic, computational methodology. As a result, when performing the inverse modeling step, joint reaction forces and torques were able to be derived. However, in order to predict the individual muscle forces, the resultant torques had to be decomposed into forces applied by the individual muscle fascicles. Solving for these forces directly was not possible because the number of unknowns was larger than the number of available equations of

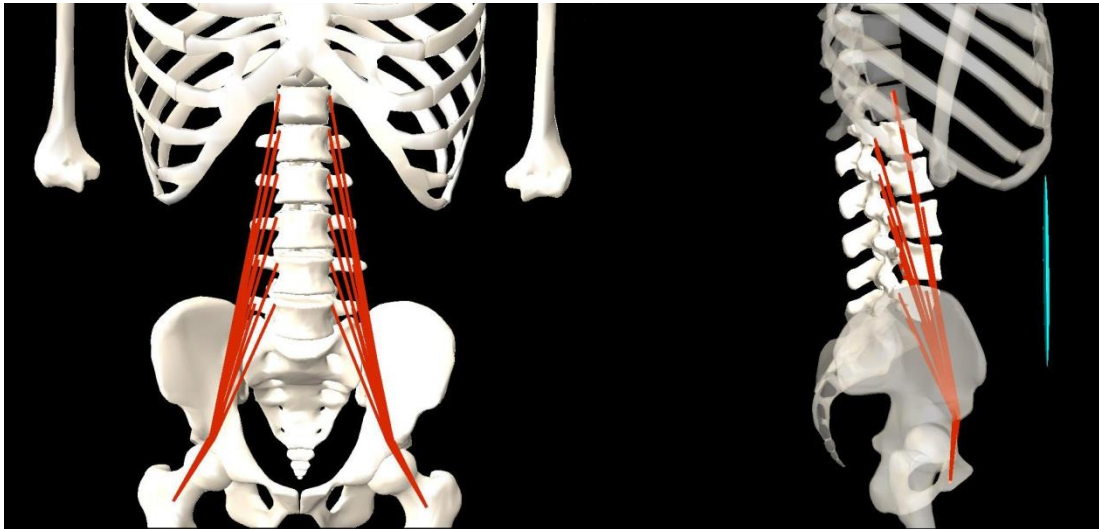


Figure 5.9 The PM (shown in red) is a bi-lateral muscle group attaching at each level on the superior-lateral surface and on the anterior face of the transverse process. It wraps around the anterior pelvis and inserts on the femur near the lesser trochanter.

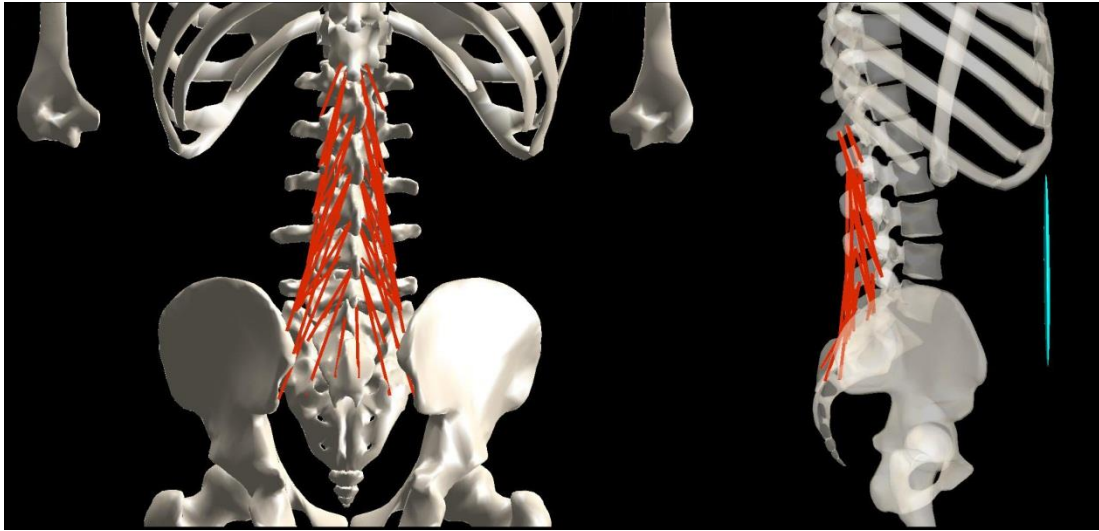


Figure 5.10 The multifidus (shown in red) is a bi-lateral muscle group attaching at each level on the posterior surface of the laminae and inferiorly and laterally on the spinous process. It exists in layers spanning multiple levels and inserts at the mammillary processes and along the sacrum.

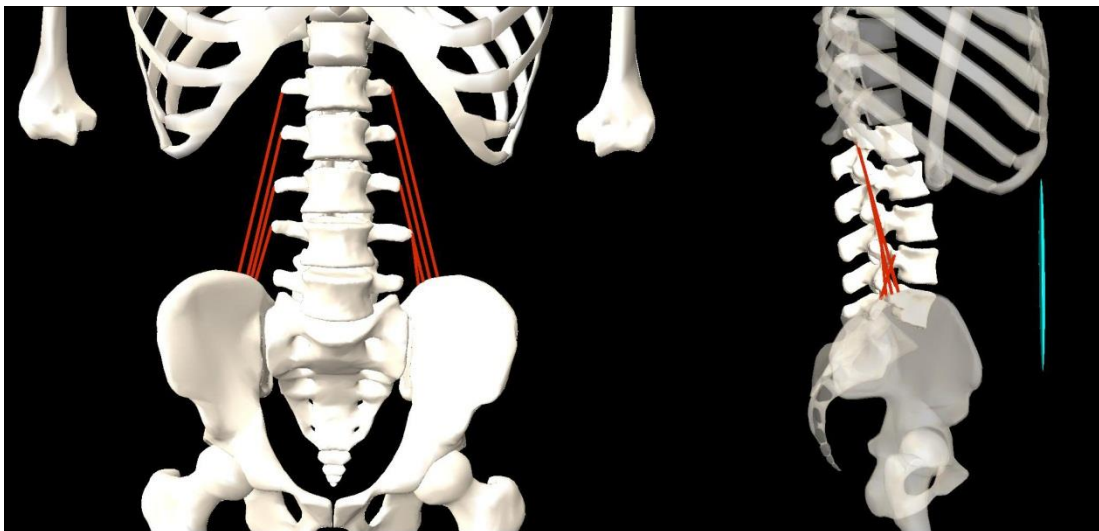


Figure 5.11 The QLL (shown in red) is a bi-lateral muscle group attaching at L1 through L4 on the lateral aspect of the transverse process. It inserts posteriorly along the iliac crest on the pelvis.

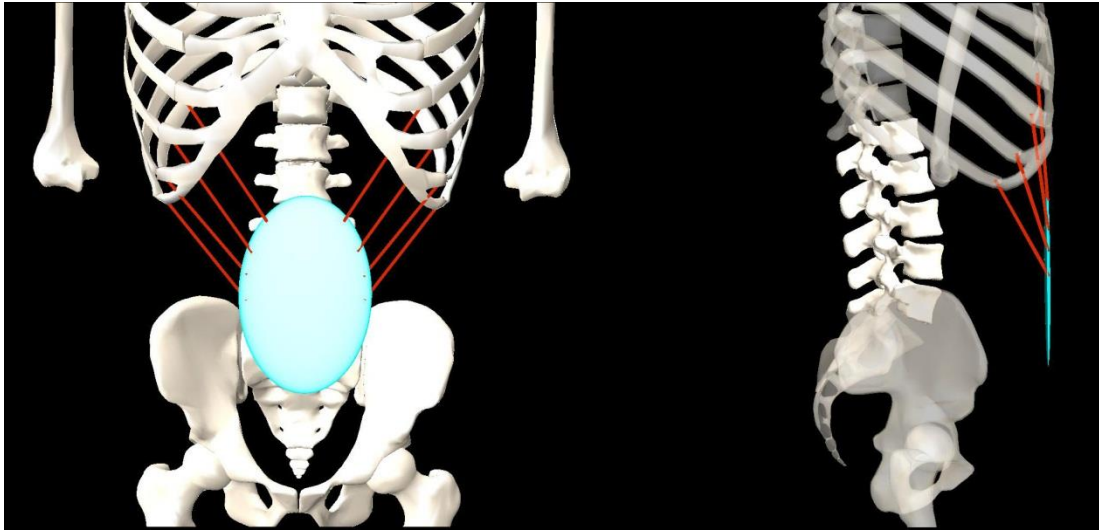


Figure 5.12 The EO (shown in red) is a bi-lateral muscle group attaching along the anterior ribcage from the 7th rib down to the 10th rib. They insert into the superior abdominal wall and help generate intra-abdominal pressure.

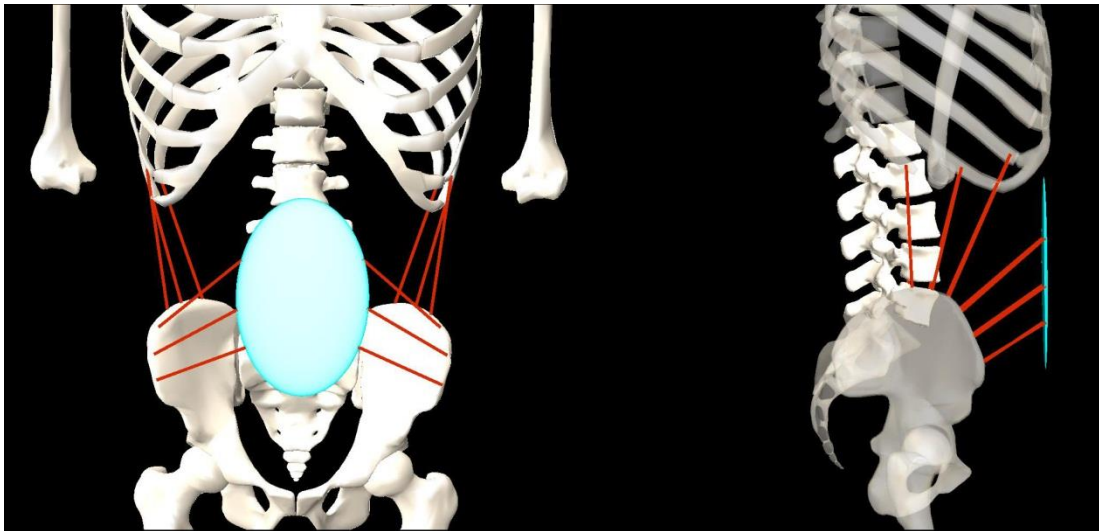


Figure 5.13 The IO (shown in red) is a bi-lateral muscle group. Some fibers attach along the lateral ribcage from the 9th rib down to the 11th rib and insert along the iliac crest of the pelvis. Additional fibers attach along the lateral abdominal wall and insert on the more anterior aspects of the iliac crest on the pelvis. These also help generate intra-abdominal pressure.

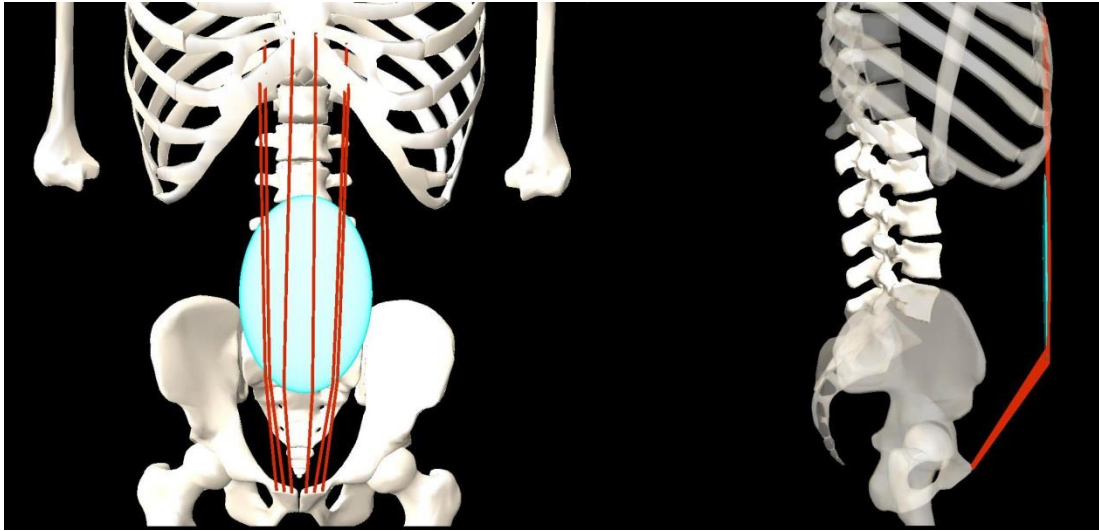


Figure 5.14 The RA (shown in red) is a bi-lateral muscle group attaching on the anterior ribcage from the sternum and spreading laterally down from the 5th rib through the 7th rib. These muscles span the abdominal wall insert at the pubic bone on the inferior-anterior pelvis. These muscles also help generate intra-abdominal pressure.

motion. To circumvent this problem, the pseudo-inverse method described by Yamaguchi [114] and Yamaguchi *et al.* [113] was implemented as part of the algorithm used to solve the dynamic system.

The pseudo-inverse method had not previously been used in the spine to solve the redundancy problem. However, the techniques and methodologies have proven to be a very efficient process for performing dynamics optimization of movement, without many of the undesirable features such as parameter optimization and gradient searching [113]. As a result, the pseudo-inverse algorithm neatly eludes many of the problems associated with other methods used to obtain solutions to biomechanical force distribution problems. The one obstacle hindering the initial use of this process was that typically, the pseudo-inverse method required the desired motion trajectory be predefined. However, for this particular research study, a slightly modified approach was implemented. Since the resultant torques acting on the vertebral

bones were calculated using the inverse dynamics portion of the computational model, it was thought the pseudo-inverse method could serve as a tool to assist in the direct decomposition of the derived torques. Essentially, the torques represented the outcome of the muscle fascicle forces defined in the model, working as attenuators for generating a preferred motion. In other words, instead of prescribing the desired motion trajectory, the resultant torques derived from the inverse modeling routine of the mathematical model were used, instead, to define the desired kinetic trajectory.

In the multi-body, computational model presented here, the redundancy occurs as a result of the 98 muscle fascicle forces that need to be solved for using only 12 pre-defined torque equations. However, since every muscle fascicle's line of action lies in 3D space, the contraction of each muscle fascicle induced a torque acting in all three degrees-of-freedom. To facilitate this process, it was necessary to first calculate the torque resulting from an application of a unit force acting along the line of action for every muscle fascicle. The resulting unit torques were then stored in a matrix A , which was referred to as the Unit Response Matrix. In the general case, this builds an $n \times m$ matrix, where n is the number of degrees of freedom, and m is the number of muscles. However, when used for musculoskeletal systems m is usually much larger than n . Once the unit response matrix was formed, the problem could be written as:

$$Ax = b$$

where A was the Unit Response Matrix, x was the column vector of the n unknown muscle forces (to be solved for), and b was the column vector of the m desired torques (derived from the inverse dynamics portion of the model).

However, this equation could not be solved by simply inverting the A matrix and pre-multiplying by b because A was not a square matrix. Therefore, the solution was achieved by using the right pseudo-inverse A^+ of matrix A .

$$Ax = (AA^+)b = b$$

$$x = A^+b$$

where A^+ was given by:

$$A^+ = A^T(AA^T)^{-1}$$

The solution x obtained by the pseudo-inverse method yielded the optimal solution having minimum error $|\varepsilon| = \|Ax - b\|$, and minimum vector length [111].

Therefore, the solution:

$$x = [\sigma_1 \sigma_2 \sigma_3 \dots \sigma_m]^T$$

will have a minimum magnitude:

$$\min(|x|) = \sqrt{\sigma_1^2 + \sigma_2^2 + \sigma_3^2 + \dots + \sigma_m^2} = \sqrt{\sum_{j=1}^m \sigma_j^2}$$

This result was equivalent to minimizing the Crowninshield-Brand criterion (cost) function for the exponent parameter $p = 2$:

$$C = \sqrt[p]{\sum_{j=1}^m \left(\frac{f_j}{PCSA_j} \right)^p}$$

Thus, the pseudo-inverse method was able to yield an optimal solution without running any optimization algorithm. Although Crowninshield and Brand found that when $p = 3$, results were yielded that were most consistent with other data available in the literature, they also reported that there was no difference in the number of active muscles and only slight differences in the muscle forces for $p=2, 3, 4$.

5.6 Methodology for Mathematical Model Validation

An important and often omitted factor with the development of mathematical models is the validation of the derived results. Under ideal situations, experimental tests should be conducted that enable for direct validation of the theoretical results with measured data; however, for the current research such options were not available. Nevertheless, comparative analyses can be conducted, instead, using previously reported data which have utilized technologies capable of directly measuring *in vivo* loading conditions at specified levels of the lumbar spine during commonly prescribed activities.

One of the technologies used to validate the results derived from the use of this model was presented in research previously discussed and conducted by Rohlmann *et al.* [83]. In that study, a telemeterized implant was positioned between T12 and L2 in a space created from the removal of parts of the L1 vertebral body and adjacent intervertebral discs. Implantation of this device was secondary to the placement of posterior spinal fixation rods as way to help stabilize the spine. Overall force magnitudes were measured relative to the subadjacent L2 vertebra while performing a number of commonly prescribed activities. Since the kinetic data was generally reported as a percentage of the force measured at the upright, standing position, the validation

analysis utilized the same methodology. In addition, although two subjects participated in the telemetry study measuring *in vivo* joint loads at the vertebral body, some data was not available for a complete analysis of both subjects. Therefore, only data from one of the subjects was used for comparison.

In addition to telemetry, a second technology, also previously discussed, had been reported on by Wilke *et al.* [112]. In their study, direct measurements of the loading conditions in the lumbar spine were collected using a pressure transducer inserted into the center of the nucleus pulposus in the L4L5 intervertebral disc. Maximum intervertebral disc pressures for multiple activities were reported on, along with pressure profiles derived during dynamic FE, LF, and AR. These pressure profiles, as well as the cross-sectional area of the patient's intervertebral disc and other pertinent patient data, were used to convert to equivalent force values in Newtons. Secondary calculations were then performed to represent the data as a percentage of the force in the disc at the upright, standing position.

Following collection of the data from the previously described studies, the forces at L1L2 and L4L5 were normalized relative to position during the prescribed activity and comparative analyses were conducted to evaluate the predictive capabilities of the multi-body, mathematical model described in the current research. The theoretically derived forces were found for each patient and analyzed. Average force profiles were also calculated for each lumbar spine condition. The average and maximum errors were then calculated.

Chapter 6

Results

6.1 Determination of 3D In Vivo Lumbar Kinematics

3D, *in vivo* kinematics were determined in the lumbar spine while patients performed FE, LF, and AR. These activities were selected to evaluate the three primary motions performed by a human. Each of these activities utilized a specific rotation as the dominant motion. These motions were assessed to evaluate the global and segmental ROM in the lumbar spine. Other vertebral motions, which occurred during these chosen activities, other than main motion, were defined as coupled rotations. This means that, during FE, the primary motion was in the sagittal plane with coupled rotations occurring in the coronal and transverse planes. Likewise, during LF and AR, the main rotations were in the coronal and transverse planes, respectively. Coupled rotations for LF were in the transverse and sagittal planes, whereas during AR, coupled rotations were defined in the coronal and sagittal planes. Overall FE ROM was the combined rotation while moving between maximum flexion and maximum extension. Similarly, LF and AR ROMs were defined between the maximum left position and the maximum right position within the plane for which the primary motion took place. In addition, vertebral segmental translations were described relative to the subadjacent vertebra during the main rotation of interest. Translations have been represented along each of the anatomical planes and referenced as motion in the AP, SI, and LR directions.

The results presented in the following sections describe the average kinematics for the various spine groups. To see a detailed analysis of each patient's rotational and translational kinematics, please see Appendix.

6.1.1 Flexion-Extension Activity

The global ROM for the entire lumbar spine was evaluated by calculating the relative angles of the lumbar vertebrae between L1 and L5. Determination of the motion between these spinal units enabled for analysis of only the lumbar vertebrae and their contribution in flexing and extending the lower back. Any influence on motion from the thoracic and sacral regions was not included in this analysis.

The resulting average global ROM for the native lumbar spine in healthy, LBP, and non-surgical degenerative subjects was 43.0°, 40.5°, and 44.4°, respectively. In patients having severe degeneration and instability at one or more levels, which was to require surgery to stabilize the dysfunctional lumbar segment, the average ROM decreased significantly to 28.2° ($p = 0.01$). Subsequent analysis was performed post-operatively following subjects having either a stand-alone fusion or HDS of the pathological segments. In patients having instrumented fusion at L5S1, the global FE ROM was 26.3°, an increase of 2.8% compared to pre-operative ROM. Conversely, when fusion was performed at L4L5 level, L4 through S1 levels, or L3 through L5 levels global ROM decreased to 22.9°, 28.1°, and 9.7°, respectively. Compared to pre-operative ROMs, these rotational magnitudes translated into a 35.9% loss of global motion with fusion at L4L5, a 26.2% loss with fusion at L4 through S1, and a 57.0% loss with fusion at L3 through L5. However, patients having HDS with rigid fixation at L5S1 and dynamic stabilization at L4L5,

achieved an average of 26.5° , resulting in a 36.1% increase over pre-operative ROM. Additionally, patients implanted with LADR were not available pre-operatively but post-operatively were found to experience an average global ROM of 23.6° .

The rotational magnitudes of each lumbar vertebral segment and their contribution towards the global ROM varied considerably between patient groups having a native lumbar spine (healthy, LBP, and degenerative) and patient groups having instrumentation surgically implanted (fusion, HDS, and LADR). Figure 6.1 illustrates the differences in the average intersegmental ROMs achieved by patients having variable conditions of the lumbar spine. Since the levels for vertebral fusion varied among patients in the fusion group, calculation of the average vertebral rotations at each level was not the most suitable technique for quantifying the overall kinematics. Therefore, intersegmental comparisons analyzing the effect of fusion on ROM at adjacent FSUs, one- and two- levels superior to the level of fusion were conducted. Pre-operatively, the average percent contributions of the affected pathological level, first superior level, and second superior level toward the overall ROM were 21%, 26%, and 22%, respectively. Following instrumented fusion at the pathologic level, the first superior level to fusion contributed, on average, 28% of the global ROM, while the contribution at the second superior level increased to nearly 32% of the overall ROM. This observed increase at the second superior level was contrary to the overall ROM decrease observed post-operatively in the majority of fused spines, excluding those having L5S1 fusion, and may be a compensatory response for the loss of motion at the more inferiorly fused level.

In general, healthy patients experienced the greatest amount of rotation and largest percent contribution toward global ROM at L4L5. Moving more superiorly from L5 to L1, the

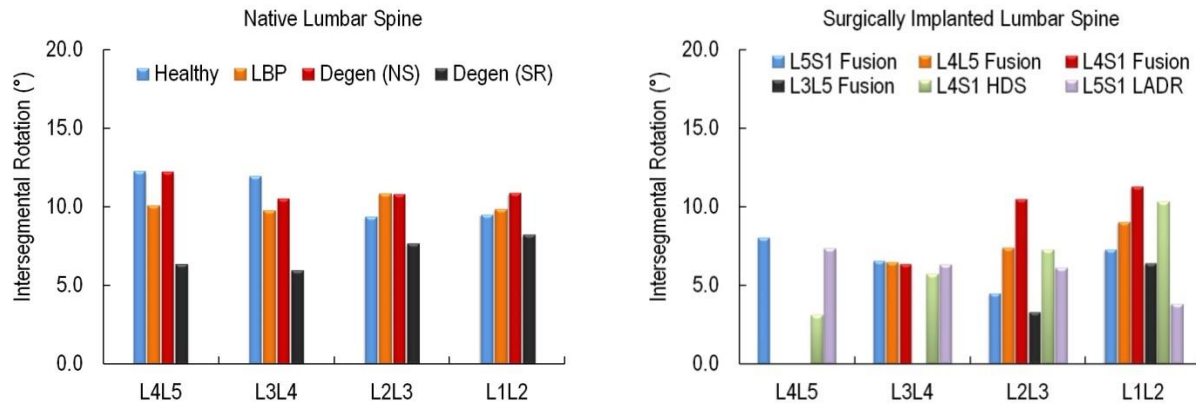


Figure 6.1 Average intersegmental rotations while performing FE between the maximum flexion and maximum extension in patients having a native (left) or surgically implanted (right) lumbar spine. Degen (NS) = degenerative without need for surgery; Degen (SR) = degenerative with surgery required.

average rotational magnitudes and associated percentage of segmental ROM decreased. Likewise, in the LBP and non-surgical degenerative groups, similar trends were found with only slight variations. In contrast, the severely degenerative spines requiring surgery began to experience an increasing trend of segmental percent contribution toward overall ROM while moving from L5 to L1. Post-operatively, in both fusion and HDS groups, a redistribution of the intersegmental rotations continued with greater contributions toward the global ROM originating from the more superior lumbar levels. Alternatively, the LADR group, which averaged considerably less ROM at all levels compared to the healthy group, managed to achieve a more representative pattern of segmental motion distribution similar to that observed in patients having a healthy lumbar spine.

Analysis of the average coupled rotations pertaining to LF and AR were less than one degree at all vertebral levels in healthy patients. The combined coupled rotations represented less than 17% of the intersegmental FE rotation at each level. However, all other patient groups were

found to experience increasingly greater amounts of coupled motion during FE, regardless of vertebral level (Table 6.1). As a result of the observed increases in coupled rotational magnitudes combined with specific instances of decreasing ROM in the fused spines, the percentages of coupled LF and AR rotation relative to amount of FE rotation were considerably greater, on average.

Translational magnitudes were also assessed at each functional spinal unit and calculated by tracking the directional movement of the superior vertebra relative to the subadjacent vertebra. Results suggested that regardless of symptom, pathology, or surgically implanted instrumentation, significant differences did not exist in the translational magnitudes calculated across the various patient groups (Table 6.2). However, comparison of the LBP group with data from the healthy group revealed greater amounts of translation, on average, in the LR direction. In addition, although LR translation was generally smaller relative to the amount of AP and SI translation, magnitudes in the pre-operative fusion group at L4L5 were considerably greater, comparatively. This translational dissimilarity was eliminated post-operatively due to many of the patients undergoing fusion at the L4L5 level. Post-operative evaluations also revealed translational magnitudes at the levels adjacent to fusion were similar to pre-operative measurements. However, a disparity was found at the second superior level with respect to the fusion where translational magnitudes increased more than 2mm in the AP direction. Similarly, in the HDS group at L1L2, substantial increases were observed in both the AP and SI directions. Conversely, patients having LADR tended to experience the least amount of overall translational motion in both the AP and SI directions, but achieved comparative amounts of LR translation relative to the healthy group.

Table 6.1 Average absolute intersegmental coupled rotations (degrees) in the coronal and transverse planes, along with their combined percentage of the overall main FE rotation at each level during movement between maximum flexion and maximum extension.

		L4L5			L3L4			L2L3			L1L2		
		LF	AR	% FE	LF	AR	% FE	LF	AR	% FE	LF	AR	% FE
Healthy		0.9	0.6	12%	0.6	0.5	9%	0.9	0.7	17%	0.7	0.8	16%
LBP		1.8	1.5	32%	1.7	1.4	33%	2.4	1.7	39%	2.4	2.3	48%
Degenerative (NS)		2.8	2.2	41%	2.2	2.6	45%	3.1	4.0	66%	3.9	2.8	61%
Degenerative (SR)		3.4	4.2	120%	2.8	3.4	105%	2.9	2.2	67%	2.2	2.6	59%
Fusion	L5S1	1.4	2.1	44%	2.6	1.4	61%	1.8	1.3	68%	2.5	2.9	74%
	L4L5	--	--	--	2.5	2.6	79%	1.7	3.3	67%	4.1	3.9	88%
	L4S1	--	--	--	5.4	4.2	152%	2.3	1.6	37%	3.4	5.1	75%
	L3L5	--	--	--	--	--	--	4.6	2.0	198%	3.1	1.0	65%
HDS	L4S1	0.9	1.2	68%	1.1	0.6	29%	0.9	0.7	22%	0.4	1.1	15%
LADR	L5S1	0.7	1.2	25%	1.1	0.5	25%	1.2	0.8	32%	1.0	0.6	43%

Table 6.2 Average intersegmental translations (mm) along the AP, SI, and LR directions while moving between maximum flexion and maximum extension.

		L4L5			L3L4			L2L3			L1L2		
		AP	SI	LR	AP	SI	LR	AP	SI	LR	AP	SI	LR
Healthy		3.7	4.9	0.5	4.5	5.0	0.6	3.9	4.2	0.7	3.8	3.6	0.7
LBP		3.7	3.7	1.2	4.0	3.8	0.6	3.7	3.8	0.9	3.5	3.0	1.0
Degenerative (NS)		4.5	4.9	1.6	4.0	4.3	1.5	4.1	4.6	1.5	3.6	3.8	1.6
Degenerative (SR)		2.6	2.9	2.8	2.8	2.9	1.0	3.2	3.7	1.4	3.3	3.4	1.2
Fusion	L5S1	4.2	2.1	1.2	4.5	2.2	1.4	2.8	1.5	1.4	3.0	2.1	2.1
	L4L5	--	--	--	2.5	3.2	1.7	4.2	3.9	1.8	3.0	3.3	1.9
	L4S1	--	--	--	7.2	2.5	1.4	6.1	5.0	1.3	8.7	3.0	3.1
	L3L5	--	--	--	--	--	--	3.6	3.4	1.2	6.5	1.7	1.3
HDS	L4S1	1.9	1.3	1.2	2.1	2.6	0.6	3.7	2.3	0.8	4.1	4.0	0.6
LADR	L5S1	3.6	3.3	0.6	2.2	2.5	0.4	2.4	2.9	0.5	2.0	2.4	0.4

6.1.2 Lateral Flexion Activity

During the activity of left to right bending of the lumbar spine, subjects were evaluated, primarily in the coronal plane. Since one-sided ROM was variable from patient to patient and from group to group, the overall range of LF while moving between the left and right sides was assessed. This allowed for the entire motion pathway to be evaluated, thereby eliminating the occurrence of any motion asymmetries that may have occurred between left- and right-sided flexion.

The resulting average LF global ROM for the native lumbar spine was 39.7° in healthy patients, 33.4° for patients experiencing LBP, and 39.2° in patients with non-surgical degeneration of the lumbar spine. Severely degenerative patients which were requiring surgery at dysfunctional segments achieved 28.3° LF ROM, which was significantly less than the global ROM achieved in healthy subjects ($p = 0.04$). Of those severely degenerative subjects which were later fused at L5S1, all experienced an increase over pre-operative ROM and averaged 35.6° of lateral flexion, which translated to a 32.7% increase. However, in patients fused at L4L5, L4 through S1, and L3 through L5 average global ROM decreased to 28.8°, 28.9°, and 17.9°, respectively. This resulted in an effective loss in LF ROM of 5.7% with fusion at L4L5 level, 11.6% with fusion at L4 through S1 levels, and 35.6% with fusion at L3 through L5 levels. Conversely, patients having HDS achieved 36.9° of global LF ROM post-operatively, representing a 51.1% increase over pre-operative ROM. In patients having LADR, the average amount of overall LF ROM was 29.4°.

At each intervertebral level, the amount of lateral rotation and percent contribution towards the global LF ROM was mainly uniform in patients having a healthy lumbar spine. On the

contrary, patients symptomatic with LBP, degeneration, or instrumented with rigid (fusion) or semi-rigid (HDS) constructs experienced progressively more uneven distribution of intersegmental LF rotations (Figure 6.2). In general, these patient groups were found to have a decreased ROM at the most inferior level of L4L5, thereby generating various amounts of increased rotational percent contributions toward the overall ROM at the more superior levels compared to the healthy group. This trend was especially evident in the fusion patients when evaluating the ROM at adjacent vertebral segments superior to the level of fusion. Pre-operatively, the average percent contribution toward overall lateral ROM was 15.7% at the affected pathological level, 27.0% at the first superior level, and 25.3% at the second superior level. Post-operatively at the first superior level, the fused spines achieved similar magnitudes as those observed prior to surgery. However, at the second level superior to fusion, the average intersegmental ROM increased from 7.4° pre-operatively to 11.4° post-operatively, which translated into 38.2% of the overall LF ROM. Likewise, patients having HDS experienced larger average intersegmental LF rotation at the most superior lumbar levels both pre- and post-operatively. However, contrary to the fused spines, patients having HDS achieved an average increase in overall ROM. In contrast to the HDS group, the LADR patients experienced, on average, less overall ROM during LF, but as noted during the FE activity, the distribution of the in-plane intersegmental rotations were more comparable with those observed in the healthy group.

During LF of the lumbar spine, coupled motion patterns were observed in all patient groups, and despite the dissimilarities among the lumbar spine conditions for each of the groups, similar coupled rotational magnitudes were achieved at each intervertebral level (Table 6.3).

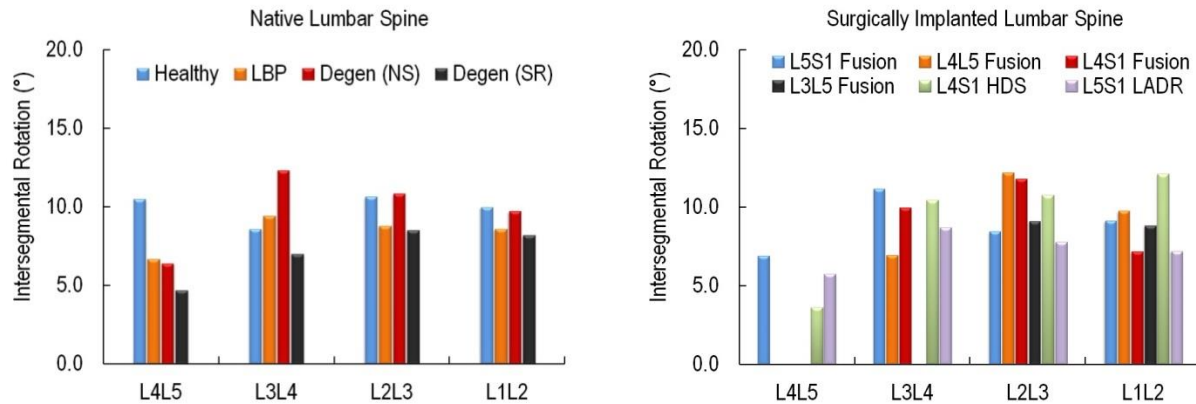


Figure 6.2 Average intersegmental rotations while performing LF between the left- and right-sided laterally flexed positions in patients having a native (left) or surgically implanted (right) lumbar spine. Degen (NS) = degenerative without need for surgery; Degen (SR) = degenerative with surgery required

Table 6.3 Average absolute intersegmental coupled rotations (degrees) in the transverse and sagittal planes, along with their combined percentage of the overall main LB rotation at each level during movement between left laterally flexed position and right laterally flexed position.

		L4L5			L3L4			L2L3			L1L2		
		AR	FE	% LF	AR	FE	% LF	AR	FE	% LF	AR	FE	% LF
Healthy		3.5	3.4	66%	3.4	3.0	74%	2.7	4.4	67%	3.6	2.9	65%
LBP		2.3	2.4	71%	3.2	5.1	88%	8.8	3.3	74%	4.2	5.2	109%
Degenerative (NS)		2.7	4.6	115%	2.5	3.9	52%	2.5	3.8	59%	5.2	3.9	95%
Degenerative (SR)		3.7	3.6	155%	2.2	4.5	97%	3.9	3.3	84%	4.4	3.3	95%
Fusion	L5S1	1.3	2.7	57%	1.8	3.6	48%	5.3	4.6	116%	2.4	2.7	56%
	L4L5	--	--	--	3.8	4.2	115%	2.0	2.6	38%	5.3	2.6	81%
	L4S1	--	--	--	10.6	7.2	180%	2.9	7.6	89%	9.1	4.6	191%
	L3L5	--	--	--	--	--	--	4.0	4.9	98%	2.1	1.0	36%
HDS	L4S1	1.1	1.3	67%	4.2	5.7	94%	2.8	2.8	52%	5.7	4.5	84%
LADR	L5S1	2.8	3.3	107%	2.5	3.6	70%	0.6	2.4	38%	3.8	1.7	76%

However, the coupled AR and FE motions analyzed as a percentage of the main LF motion revealed differences among the various spine groups. In patients having a healthy spine, the combined coupled AR and FE rotations as a percentage of LF were between 65% and 75%. This was attributed to the consistent coupled rotational magnitudes and relatively uniform distribution of LF motion at each level. However, as previously observed in findings from this research, the progressive change in the lumbar spine conditions away from the healthy, native structure, tended to produce more aberrant motions during LF. This phenomenon, together with the decreased amounts of segmental LF ROM in many of the patients implanted with instrumented fixation constructs, resulted in the combined coupled AR and FE rotations as a percentage of LF to become rather large.

A more generalized analysis investigated the average amount of coupled rotation and segmental LF rotation across all levels. These calculations revealed healthy patients experienced, on average, 3.3° (33.3%) coupled AR rotation and 3.4° (34.6%) coupled FE rotation, with an average of 9.9° LF at each intervertebral level between L5 and L1. For comparison, the coupled rotations in the remaining patient groups were also calculated. Thus, the average amount of coupled AR rotation at all levels in the LBP and non-surgical degenerative groups was 3.2° (38.6%) and 3.3° (33.1%), respectively. On average, both groups experienced 4.0° (47.6% in LBP and 40.7% in degenerative) of coupled FE rotation with 8.4° LF in the LBP group and 9.8° LF in the degenerative group at each level. The largest percentage of coupled rotational motion to LF rotation was found in the severely degenerative group requiring surgery. Patients in this group averaged 3.6° (50.2%) coupled AR rotation and 3.7° (51.9%) coupled FE rotation with 7.1° LF at each level. Post-operatively, the amount of coupled AR and FE rotation in all fused

subjects at the superior levels adjacent to fusion decreased to 2.9° (30.6%) and 3.7° (39.0%), respectively, with 9.5° LF at the superior levels. Patients undergoing HDS were found to have decreased amounts of average coupled rotation at each level pre-operatively. Post-operatively, subjects averaged more coupled motion in terms of magnitude, but since overall LF ROM also increased at each level the coupled AR and FE rotations as a percentage of LF rotation were similar. Finally, the LADR group exhibited 2.4° (33.0%) coupled AR rotation and 2.7° (37.1%) coupled FE motion with 7.3° LF, on average, at each level.

The intersegmental translations during LF were also similar among all lumbar spine conditions in each of the three directions (Table 6.4). In general, translations in the AP and SI directions were less than 2.5 mm, while the largest translational magnitudes were found along the transverse plane in the LR direction. The most common levels for increased translation during LF were at the more superior L2L3 and L1L2 levels in the degenerative and HDS. Average translations at these levels were approximately 1-2 mm greater in the aforementioned groups than those observed in the healthy group. The remaining AP and SI translational magnitudes exhibited mild variability, without any significant differences.

6.1.3 Axial Rotation Activity

Overall rotational magnitudes were primarily calculated in the transverse plane between the adjacent vertebrae beginning at L5 and progressing up through L1 for each patient while moving between the maximal left and right axially rotated positions. Comparatively, the amount of rotation achieved while performing the AR activity was substantially less than the rotational magnitudes achieved during flexion-extension and lateral flexion of the lower spine. Therefore,

Table 6.4 Average intersegmental translations (mm) along the AP, SI, and LR directions while moving between left laterally flexed position and right laterally flexed position.

	L4L5			L3L4			L2L3			L1L2			
	AP	SI	LR	AP	SI	LR	AP	SI	LR	AP	SI	LR	
Healthy	1.6	2.0	2.6	1.5	1.2	2.6	1.6	2.5	3.2	1.7	1.4	3.1	
LBP	1.8	1.5	1.2	1.9	2.1	2.0	1.6	1.9	2.8	2.0	2.1	2.6	
Degenerative (NS)	2.1	2.2	1.6	1.6	2.0	3.4	1.9	1.5	3.8	2.2	2.0	4.1	
Degenerative (SR)	1.9	1.9	1.5	1.8	2.4	2.2	2.0	2.3	3.0	1.6	1.7	2.8	
Fusion	L5S1	2.0	0.8	2.1	1.9	1.1	2.5	1.4	1.8	3.1	1.7	0.8	2.9
	L4L5	--	--	--	1.3	2.5	2.7	1.7	1.4	3.9	1.9	1.3	3.7
	L4S1	--	--	--	2.0	4.5	3.1	2.1	5.1	4.2	1.4	3.2	4.5
	L3L5	--	--	--	--	--	--	1.6	2.3	3.2	1.9	2.7	3.9
HDS	L4S1	1.3	0.8	0.7	1.1	2.9	3.3	1.4	0.9	3.5	2.6	1.1	5.3
LADR	L5S1	1.0	1.7	1.4	1.7	1.4	2.8	0.7	2.0	2.9	1.4	1.7	2.7

the average global AR ROM calculated for the native lumbar spine in healthy, LBP and non-surgical degenerative groups was 13.5°, 11.5°, and 11.9°, respectively. In degenerative patients requiring surgery at pathologic levels in the lumbar spine, the average global AR ROM was 12.1°. Post-operatively, subjects from the degenerative surgical group and having fusion at L5S1 averaged 12.1° global AR ROM, which represented an increase of 6% over pre-operative ROM. In patients where fusion was performed at L4L5 level, L4 through S1 levels, or L3 through L5 levels average global AR ROM decreased to 8.4°, 6.9°, and 10.8°, respectively. Compared to pre-operative ROMs for these same patients, the resulting rotational magnitudes represented a 38.6% loss in global AR motion when fused at L4L5, a 37.0% loss when fused at L4 through S1, and a 9.0% loss when fused at L3 through L5. Similarly, patients having HDS achieved an average of 9.9° of global AR, resulting in an 8% decrease compared to pre-operative ROM. Similar to the other post-operative groups, LADR patients managed an average of 9.0° of AR

ROM post-operatively. All surgical groups achieved lesser amounts of global AR motion compared to the healthy group.

Intersegmental rotations were similar across all spine conditions, with average rotations at each level generally found to be less than four degrees for the entire left-to-right AR activity. Additionally, the inferior L4L5 and L3L4 levels typically achieved slightly less AR ROM compared to the more superior L2L3 and L1L2 levels (Figure 6.3). Despite these average trends which occurred across most lumbar spine conditions, patients having fusion at L3 through L5, were found have increased motion at both superior levels, L2L3 and L1L2, adjacent to the multi-level fusion.

Similar to the previously reported motions during the lateral flexion activity, the main AR rotation during axial torsion of the lumbar spine was found to have accompanying coupled LF and FE motions (Table 6.5). However, with the smaller magnitudes and variability among patients, no significant differences were found between groups. Further analyses, however, did reveal decreased amounts of coupled motion, on average, in healthy patients compared to the LBP, degenerative (non-surgical and surgical), and fusion groups. Combination of the average coupled LF and FE rotations at all levels for each group also revealed that healthy, HDS and LADR lumbar spines experienced similar amounts of total coupled motion. Conversely, both non-surgical and surgical degenerative patients tended to exhibit larger amounts of coupled motion during AR, with post-operative fusion and LBP patients following close behind. Despite these generalized trends, no specific intervertebral level was found to be prone to experience greater amounts of coupled rotations.

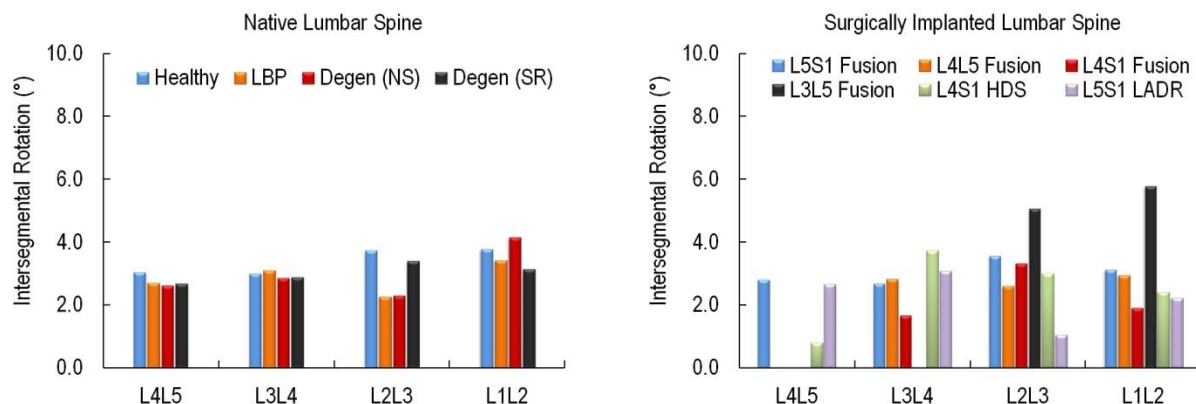


Figure 6.3 Average intersegmental rotations while performing AR between left and right axially rotated positions in patients having a native (left) or surgically implanted (right) lumbar spine. Degen (NS) = degenerative without need for surgery; Degen (SR) = degenerative with surgery required

Table 6.5 Average absolute intersegmental coupled rotations (degrees) in the coronal and sagittal planes, along with the combined percentage of the overall main AR rotation at each level during movement between left axially rotated position and right axially rotated position.

		L4L5			L3L4			L2L3			L1L2			
		LF	FE	%AR	AR	FE	%AR	AR	FE	%AR	AR	FE	%AR	
Healthy		1.5	3.1	150%	2.8	2.5	170%	1.9	3.3	140%	2.4	3.8	122%	
LBP		1.7	5.4	261%	2.6	2.9	179%	3.8	3.9	337%	3.4	3.0	187%	
Degenerative (NS)		2.0	4.3	240%	3.2	6.6	341%	3.2	3.2	278%	3.6	3.5	163%	
Degenerative (SR)		1.7	4.6	237%	2.9	4.3	253%	3.8	3.3	210%	3.6	3.5	225%	
Fusion	L5S1	2.8	2.5	191%	5.3	3.0	312%	3.2	2.5	159%	3.7	3.4	225%	
	L4L5	--	--	--	4.2	2.1	224%	3.5	4.1	292%	4.4	1.4	198%	
	L4S1	--	--	--	1.5	0.7	131%	4.7	6.5	335%	4.7	3.4	428%	
	L3L5	--	--	--	--	--	--	5.6	1.5	141%	4.4	2.8	124%	
HDS		L4S1	0.9	2.2	395%	1.4	4.1	149%	3.1	1.6	155%	4.2	1.9	255%
LADR		L5S1	2.2	4.6	251%	1.7	1.8	111%	1.6	1.9	328%	3.2	1.8	222%

The average intersegmental translations along the AP, SI, and LR directions were determined at each level between L5 and L1 (Table 6.6). In direct correspondence with the smaller AR rotational magnitudes in the lumbar spine, the overall translations were also decreased. This trend was observed at all levels and across all groups with no significant differences found. However, though not considered significantly different, larger average translational magnitudes were experienced in spinal fusion patients at the second superior level to instrumented fixation. This was most apparent in patients having multiple levels fused in the lumbar spine. The largest average translation was observed in the SI direction at the second superior level in patients having fusion at L4 through S1. Large translations in the AP direction were also observed when the spine was fused at L3 through L5 levels. The majority of the remaining translations averaged less than 3.0 mm.

Table 6.6 Average intersegmental translations (mm) along the AP, SI, and LR directions while moving between left axially rotated position and right axially rotated position.

		L4L5			L3L4			L2L3			L1L2		
		AP	SI	LR	AP	SI	LR	AP	SI	LR	AP	SI	LR
Healthy		1.9	1.6	1.0	1.6	1.0	1.1	2.1	1.6	1.4	1.7	1.6	1.2
LBP		1.6	2.7	1.0	1.4	1.5	1.1	2.3	2.2	0.9	1.9	1.8	1.4
Degenerative (NS)		1.9	2.6	1.7	2.7	2.5	1.7	1.5	2.4	1.3	1.8	1.9	1.2
Degenerative (SR)		2.1	1.9	1.6	1.7	2.2	1.3	1.8	2.3	1.0	2.5	1.6	1.5
Fusion	L5S1	1.4	1.1	1.3	1.4	1.3	1.3	2.2	1.9	0.9	3.0	1.3	1.7
	L4L5	--	--	--	1.1	1.4	1.7	1.6	2.2	1.2	1.2	1.0	1.1
	L4S1	--	--	--	1.3	1.4	1.0	3.5	6.9	0.7	1.2	2.6	0.8
	L3L5	--	--	--	--	--	--	1.3	2.6	2.0	5.1	1.6	1.8
HDS	L4S1	0.9	0.8	0.7	1.1	1.7	1.1	1.4	1.1	0.6	2.1	0.7	1.6
LADR	L5S1	2.6	1.9	0.5	1.3	1.2	0.4	2.1	1.5	0.9	1.7	1.3	1.1

6.2 Derivation of 3D In Vivo Lumbar Kinetics

A novel, 3D mathematical model, which included patient-specific kinematic and geometric data along with important ligament and muscle tissues was developed using combined principles from Kane's dynamics [40] and pseudo-inverse modeling [111, 112]. This model allowed for the prediction of interactive joint contact and soft tissue forces in the lumbar spine. The contact forces at each level of the lumbar spine were derived in the $N1>$, $N2>$, and $N3>$ directions (Figure 6.4). These were representative of the AP forces, compressive or SI forces, and lateral LR forces, respectively. Both the force patterns and magnitudes were determined in all subjects while performing FE, LF, and AR. The contributions of the ligament constraint forces and active muscle forces have been included in the overall calculation of the resultant forces at each segment. In addition, the forces generated within each individual ligament and bilateral muscle was also derived to better evaluate the role soft tissues have during the prescribed motion.

The forces calculated in the model represented the total force magnitude acting at a vertebral level along one of the three main directions. Since all activities were performed while the patient was standing, each lumbar spinal unit was assumed to always have been subjected to varying amounts of upper body weight and soft tissue forces working to stabilize and actively move the lower spine. Therefore, even though certain areas likely experienced localized tension during the motion sequence, the overall force at each vertebral level in the SI direction was always compressive in nature.

The results presented in the following sections describe the average kinetics for the various spine groups. To see a detailed analysis of each patient's joint contact forces and soft tissue forces, please see Appendix.

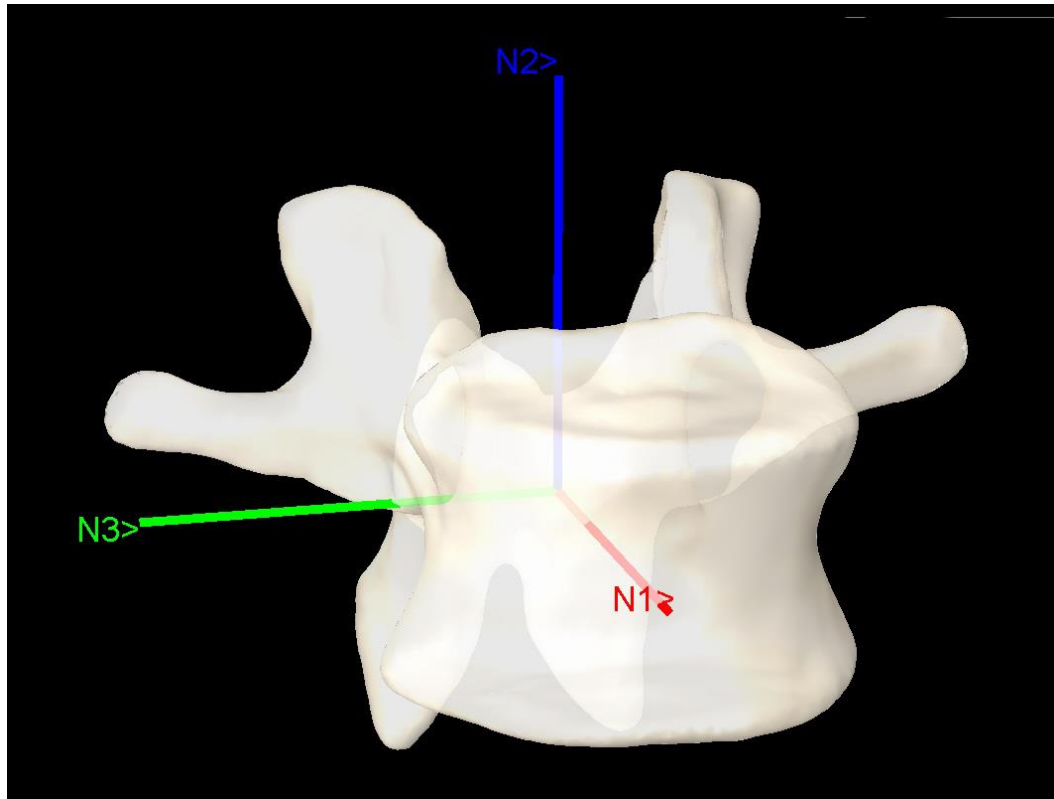


Figure 6.4 Illustration of the defined coordinate axes at each level of the spine where N1> was directed along the AP direction, N2> along the SI direction, and N3> along the lateral LR direction.

6.2.1 Flexion-Extension Activity

The greatest force magnitudes were observed in the SI direction, which represented the compressive forces acting in the lumbar spine. Over the course of the motion between maximum and maximum extension, the greatest compressive force was generally calculated at the maximally flexed position, while the minimum force was at or near the neutral, upright standing position. As patients continued into extension of their lower back, average compressive forces tended to increase slightly over magnitudes observed at neutral. These trends are illustrated in

Table 6.7, which lists the average force magnitudes across the native and surgically implanted lumbar spine conditions.

Although the above generalized trends loosely describe the force profiles derived for all lumbar spine conditions, variations in both magnitude and pattern across subject groups and between pre- and post-operative evaluations were evident (Figure 6.5).

For the native lumbar spine in healthy and LBP patients, the average maximum compressive force was 2.47 times body weight (\times BW) and 2.33 \times BW, respectively, with maximum forces occurring at the L4L5 level. However, in patients having degeneration without the need for surgery, the average maximum compressive force increased to 3.08 \times BW at L4L5 level. It is believed that instabilities in these mild-to-moderately degenerative lumbar spines enabled for larger overall ROM and coupled rotation compared to healthy and LBP groups, and thereby contributed to greater compressive force magnitudes. Conversely, in patients where degeneration was more progressed and surgery was required to stabilize the dysfunctional lumbar segments, global and segmental ROM decreased, possibly as a result of motion induced pain, which was progressively evident in patients of this type. The resulting motion limitations in this group contributed to a smaller average maximum compressive force of 1.83 \times BW. However, in congruence with the overall aforementioned trends, among all conditions of the native spine, average maximum compressive magnitudes were greatest at L4L5 and progressively decreased moving superiorly along the lumbar spine.

In contrast, subsequent post-operative analysis following either a stand-alone fusion or HDS of the pathological segments revealed variable results. These findings were contrary to the observed decrease in ROM for patients having fusion of the vertebral segments and may indicate

Table 6.7 Average intersegmental compressive forces relative to body weight during FE activity for all lumbar spine conditions at each increment captured during the motion.

Lumbar Spine Condition		L4L5				L3L4				L2L3				L1L2			
		MxF	MdF	N	MxE	MxF	MdF	N	MxE	MxF	MdF	N	MxE	MxF	MdF	N	MxE
Healthy		2.47	1.60	0.66	0.79	2.30	1.51	0.65	0.75	2.04	1.42	0.64	0.77	1.89	1.42	0.70	0.88
LBP		2.33	1.49	0.67	0.72	2.21	1.41	0.69	0.77	2.04	1.31	0.66	0.77	1.95	1.36	0.70	0.87
Degenerative (NS)		3.08	2.08	0.69	0.86	2.78	1.93	0.69	0.87	2.56	1.86	0.70	0.88	2.39	1.85	0.77	1.02
Degenerative (SR)		1.83	1.34	0.70	0.82	1.68	1.17	0.69	0.79	1.64	1.13	0.66	0.75	1.62	1.29	0.69	0.87
Fusion	L5S1	1.55	0.81	0.56	0.61	1.47	0.83	0.58	0.65	1.41	0.82	0.57	0.72	1.35	0.99	0.61	0.78
	L4L5	1.91	1.55	0.69	0.89	1.93	1.56	0.67	0.88	1.86	1.51	0.64	0.84	1.81	1.46	0.67	0.90
	L4S1	1.81	1.52	1.37	1.38	1.75	1.52	1.43	1.50	1.90	1.61	1.48	1.61	2.24	1.86	1.77	1.88
	L3L5	0.95	0.79	0.81	0.82	0.92	0.77	0.79	0.81	0.91	0.77	0.78	0.79	0.88	0.75	0.74	0.89
HDS	L4S1	1.31	1.14	0.89	1.00	1.16	1.01	0.81	0.88	1.17	1.04	0.86	0.96	1.11	1.03	0.82	0.95
LADR	L5S1	2.04	0.90	0.67	0.74	1.94	0.87	0.68	0.74	1.74	0.82	0.65	0.73	1.67	0.89	0.70	0.85

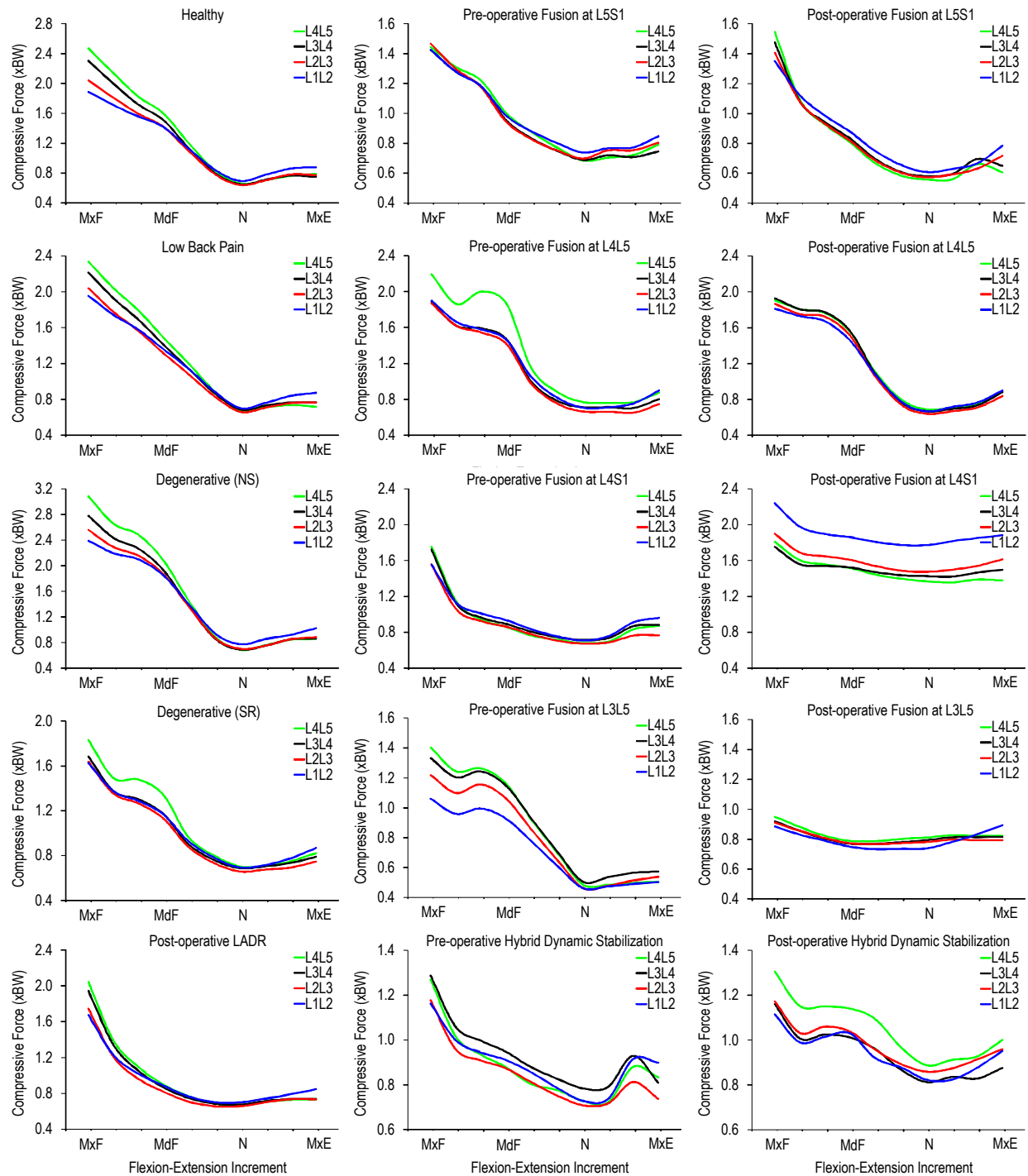


Figure 6.5 Average compressive force profiles normalized with respect to body weight during FE for both native and surgically implanted lumbar spines with comparisons pre- and post-operatively.

indicate muscle force patterns change following rigid fixation. Thus, for patients having instrumented fusion at L5S1, an average maximum compressive force of 1.55 x BW was predicted at L4L5 level. And although this was less than the average maximum compressive forces observed in the native lumbar spine, it represented a 7.6% increase over pre-operative evaluations in the same subjects at the same level. Further investigation of patients having fusion at either L4L5, L4 through S1, or L3 through L5 levels revealed average maximum compressive forces of 1.93 x BW, 2.24 x BW, and 0.95 x BW, respectively. Specifically, when the lumbar spine was fused at L4L5, average maximum compressive forces were found to be the greatest at the first adjacent L3L4 level, which represented a 2.1% increase over pre-operative forces derived at the same level. In a similar fashion, when fusion was performed at L4 through S1, the largest average maximum compressive force was at L1L2, which was also adjacent to fusion, but more superior than when L4L5 fusion. At this most superior lumbar level and at the more inferior adjacent L2L3 and L3L4 levels, compressive force magnitudes were calculated to be higher than those derived for pre-operative evaluations. These translated into a 1.7% increase of the average maximum compressive force at L3L4, a 21.8% increase at L2L3, and a 44.5% increase at L1L2.

Contrary to the findings described for the other fusion types, vertebral lumbar fusion at L3 through L5 resulted in the calculation of much lower average maximum compressive forces. In fact, at the first and second superior adjacent L2L3 and L1L2 levels, maximum compressive forces decreased, on average, 25.4% and 17.0%, respectively, compared to pre-operative magnitudes. However, these same patients also experienced a 57% loss in global ROM following multi-level fusion, which was not recovered post-operatively at the adjacent levels. Therefore,

this significant loss of motion was thought to be the main contributor for the prediction of these lower compressive force magnitudes.

Finally, relative to the groups having various degrees of fixation in the lumbar region, the HDS group with rigid fixation at L5S1 and a semi-rigid construct at L4L5, was predicted to experience an average maximum compressive force of $1.31 \times \text{BW}$ at the dynamically stabilized L4L5 level. This represented only a 3.2% increase over pre-operative magnitudes at the same level and resulted in slightly decreased average maximum compressive forces at more superior adjacent levels, compared to pre-operative magnitudes.

The remaining patients evaluated in this research study had previously been implanted with a LADR at L5S1 for approximately 10 years. In this patient group, an average maximum compressive force of $2.04 \times \text{BW}$ was predicted at L4L5 level. In addition, and contrary to patients with rigid fusion, compressive forces progressively decreased moving superiorly up the lumbar vertebral levels, a pattern which was found to be consistent in subjects having a native lumbar spine.

Interestingly, additional analysis of the average compressive forces during FE of the lumbar spine revealed substantially higher magnitudes at the upright, standing position in patients implanted with instrumentation at multiple lumbar levels. These patients, which included L4S1 fusion, L3L5 fusion and HDS groups, were found to average $1.05 \times \text{BW}$ at the neutral position. In comparison, average compressive force magnitudes in patients having either a native or surgically implanted lumbar spine at a single-level were calculated to experience $0.66 \times \text{BW}$ at the upright, neutral position. This difference was attributed to the constraining effects associated with fixation of multiple levels, which was thought to have influenced muscle firing patterns and

prompted the use of alternative muscle groups to actively stabilize the trunk around the neutral position during this activity.

In general during the FE maneuver, determination of *in vivo* compressive forces were found to be relatively sensitive to the kinematic inputs, especially those rotational magnitudes occurring in the FE motion plane. Patients achieving larger segmental ROMs tended to exhibit higher compressive force magnitudes at the associated level. This was observed in healthy, LBP, and non-surgical degenerative subjects. As motion at vertebral levels decreased, the predicted compressive force magnitudes also tended to be lower, which was evident in many of the fused and HDS spines. In addition, patients having a native lumbar spine, regardless of symptoms or pathologies, were found to have the largest compressive force magnitude at the most inferior L4L5 level with decreasing compressive forces moving from L5 to L1. However, in patients having instrumented fixation at one or more levels, the largest average maximum force magnitudes were calculated at levels adjacent to fusion and exhibited inconsistent loading patterns moving superiorly away from L5 level.

The AP forces occurring along the 1-direction were also evaluated and found to be smaller in magnitude compared to the compressive forces. In general, AP forces acted posteriorly at maximum flexion but decreased in magnitude, while still acting posteriorly, as the patient moved through neutral and progressed into extension (Figure 6.6). The largest average AP forces were most often experienced at L4L5 level. Hence, in the native spine at L4L5, patients classified as healthy, LBP, degenerative without the need for surgery, and degenerative requiring surgery, achieved force magnitudes ranging between -0.58 to $-0.26 \times \text{BW}$, -0.63 to $-0.33 \times \text{BW}$, -0.76 to $-0.27 \times \text{BW}$, and -0.42 to $-0.26 \times \text{BW}$, respectively. Likewise, in patients

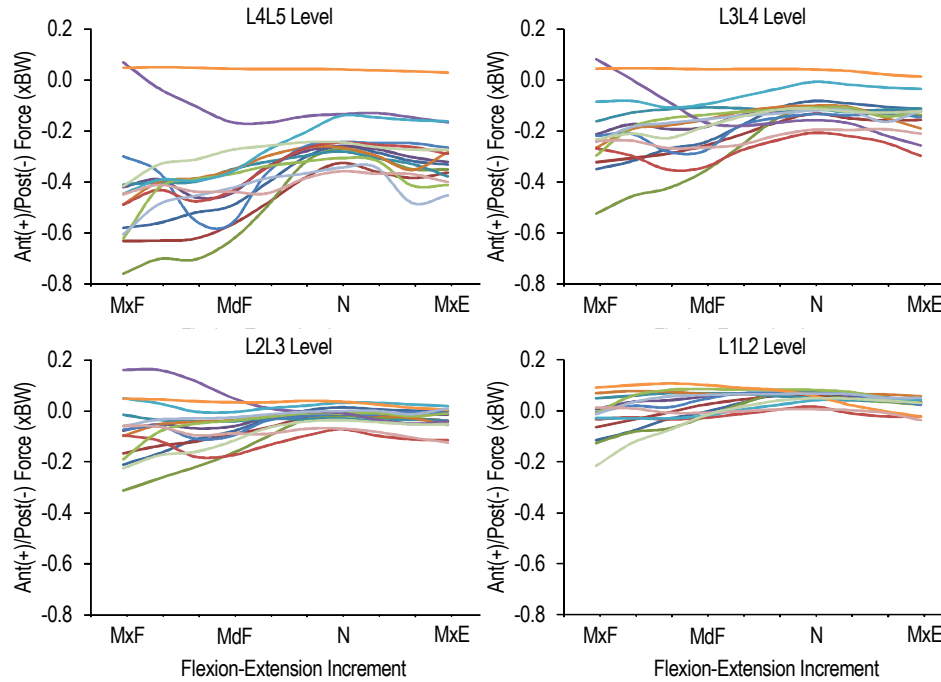


Figure 6.6 Average AP forces at each intervertebral level for all native and surgically implanted lumbar spine conditions while performing FE.

having fusion at either L5S1 or L4L5 levels, average AP forces ranged between -0.49 to -0.26 x BW and -0.49 to -0.24 x BW, respectively. However, when the lumbar spine was fused at L4 through S1 or L3 through L5, maximum AP forces were found at the L1L2 level and ranged between 0.23 to 0.47 x BW and from -0.02 to 0.09 x BW, respectively. Under these lumbar spine conditions, the AP force was also found to be inverted relative to the other spine groups, meaning that in the L4S1 and L3L5 fusion groups, the AP force was anteriorly directed at maximum flexion and became more posteriorly directed while moving through neutral and into extension.

The smallest of the forces in all the lumbar spine groups was found along the transverse plane in the lateral LR direction. These lateral forces were substantially smaller in terms of magnitude, compared to both the compressive and AP forces, thereby providing minimal

contribution to the overall resultant joint force experienced at vertebral levels in the lumbar spine. Both the derived force patterns and magnitudes across each of the lumbar spine conditions and at all lumbar levels were relatively consistent, ranging between -0.14 to $0.08 \times BW$, as such, no significant trends were observed (Figure 6.7).

The theoretical muscle forces predicted by the mathematical model followed somewhat similar profiles as predicted for the compressive contact forces, typically resulting in the peak force occurring at maximum flexion and declining to reach a minimum near the upright neutral, standing position (Figure 6.8). As subjects continued into extension, total muscle forces increased slightly with respect to the neutral position. Normalization of the muscle forces revealed the most dominant muscle throughout the FE activity was generally the MUL muscle for nearly all subjects. However, fusion of the lumbar spine between L4 and S1 resulted in the prediction of the largest force magnitudes in the IO muscles. These muscles remained active throughout the entire FE activity, dominating all other predicted muscle forces. Likewise, fusion at L3 through L5 also prompted the prediction of larger peak forces in the oblique muscles but, this time, in the EO muscles. The MUL generated the largest force between maximum flexion and mid-flexion, but the remainder of the motion was dominated by the EO. In general, patients having a native, non-implanted condition of the lumbar spine, inclusive of the healthy, LBP, and non-surgical degenerative spines were predicted to experience smoother force profiles in the muscles, whereas those patients requiring surgery tended to experience fluctuation in the predicted muscle forces which contributed to the motions, both pre- and post-operatively.

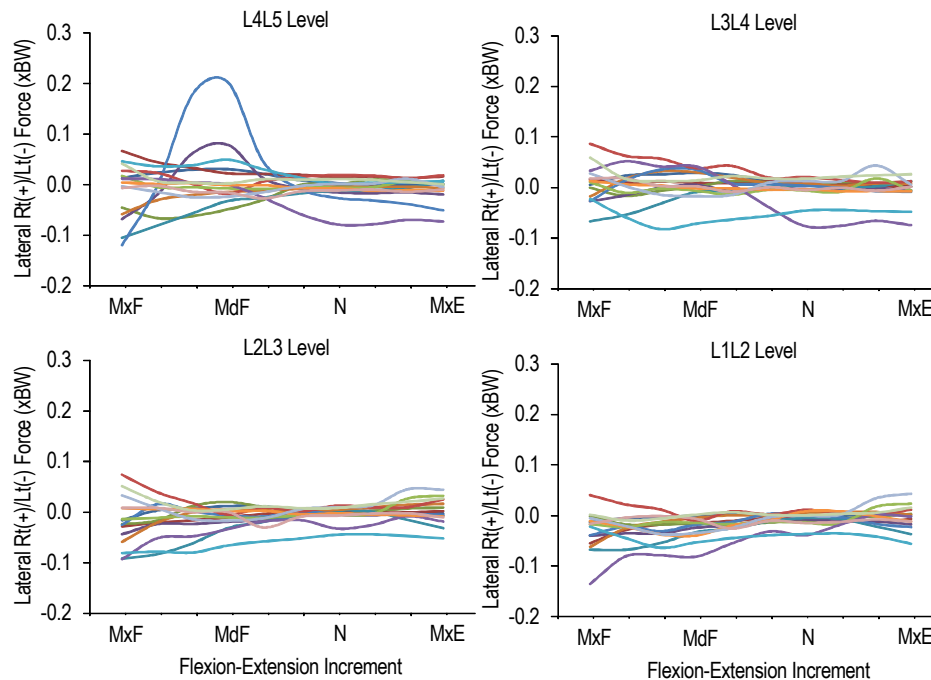


Figure 6.7 Average LR forces at each intervertebral level for all native and surgically implanted lumbar spine conditions while performing FE.

6.2.2 Lateral Flexion Activity

During LF of the lumbar spine, patients were analyzed while moving between maximum left laterally flexed position and maximum right laterally flexed position. Throughout the motion, the highest compressive forces were calculated at maximum laterally flexed positions, while the minimum force occurred as patients approached and moved through the neutral, upright standing position. Table 6.8 lists these average force magnitudes during the LF activity for native and surgically implanted lumbar spine conditions.

For the native lumbar spine in non-symptomatic, healthy patients, the average maximum compressive force was calculated to be 1.87 x BW and occurred at L4L5 level. As you moved superiorly from L5 to L1, the average maximum compressive force at each level progressively decreased. In addition, the bilateral motion of the LF activity resulted in mainly symmetric

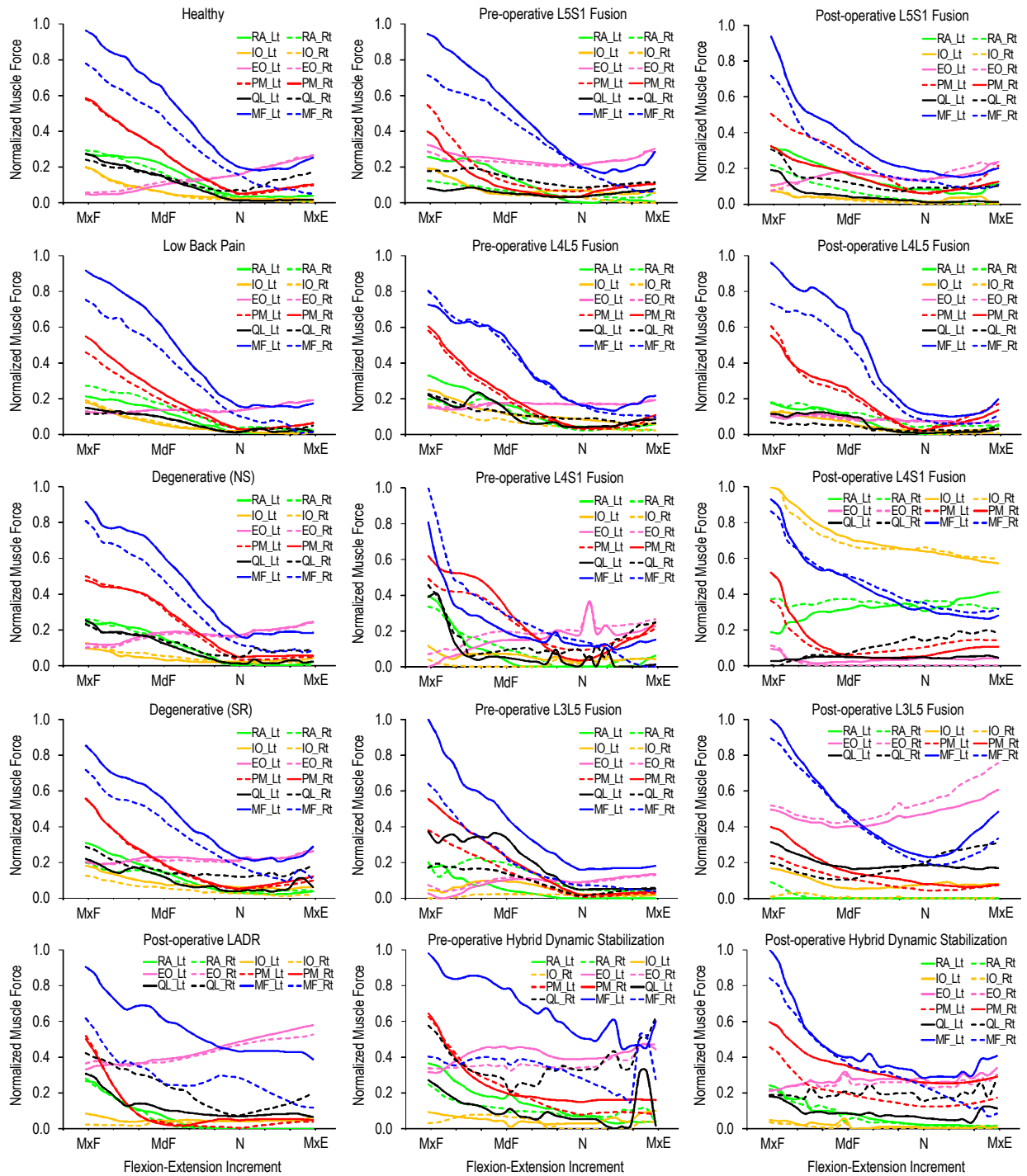


Figure 6.8 Average profiles for the theoretical muscle forces normalized with respect to muscle predicted to generate the largest force during FE for both native and surgically implanted lumbar spines with comparisons pre- and post-operatively.

Table 6.8 Average intersegmental compressive forces relative to body weight during LF activity for all lumbar spine conditions at each increment captured during the motion.

Lumbar Spine Condition	L4L5			L3L4			L2L3			L1L2			
	MxLt	N	MxRt	MxLt	N	MxRt	MxLt	N	MxRt	MxLt	N	MxRt	
Healthy	1.87	0.70	1.87	1.75	0.69	1.72	1.63	0.67	1.63	1.64	0.72	1.58	
LBP	1.54	0.74	1.74	1.48	0.70	1.64	1.43	0.67	1.53	1.52	0.74	1.52	
Degenerative (NS)	1.45	0.67	1.74	1.39	0.67	1.63	1.40	0.65	1.67	1.42	0.69	1.63	
Degenerative (SR)	1.28	0.76	1.40	1.21	0.71	1.27	1.18	0.69	1.22	1.17	0.71	1.23	
Fusion	L5S1	0.97	0.59	0.83	0.94	0.56	0.83	1.06	0.54	0.84	1.03	0.56	0.88
	L4L5	1.23	0.71	1.14	1.27	0.69	1.08	1.28	0.67	1.12	1.24	0.68	1.18
	L4S1	0.89	0.59	0.98	0.92	0.56	1.02	1.07	0.54	1.07	1.10	0.59	1.11
	L3L5	0.86	0.66	0.86	0.85	0.63	0.83	0.90	0.63	0.99	0.91	0.64	0.97
HDS	L4S1	1.40	0.79	1.10	1.57	0.80	1.08	1.53	0.72	1.11	1.34	0.71	0.97
LADR	L5S1	1.40	0.68	1.32	1.33	0.65	1.29	1.16	0.61	1.26	1.16	0.65	1.24

loading profiles with variations of the average maximum compressive force magnitudes between the left and right sides averaging less than 3.2% at all levels (Figure 6.9). However, in the native spine with the onset of LBP and/or degenerative pathologies classified as both non-surgical and surgical, average maximum compressive loads began to decrease slightly and became more asymmetrical between the left and right sides compared to healthy spines. While the average maximum compressive force in these groups was found to occur at L4L5, which was the same as in the healthy spine group, maximum compressive force magnitudes decreased to 1.74 x BW in the LBP group, 1.74 x BW in the degenerative group not requiring surgery, and 1.40 x BW in the group consisting of degenerative spines requiring surgery. Additionally, these average maximum compressive force magnitudes were not equal bilaterally and instead varied, on average, as much as 13.0% from the left and right side in the LBP group, 19.9% in the non-surgical degenerative group, and up to 9.4% in the degenerative group requiring surgery.

The compressive forces derived for the native lumbar spine conditions during LF were largely dependent upon the rotational magnitudes in the LF motion plane. As a result, the lower average compressive force magnitudes calculated in the degenerative group requiring surgery corresponded with the significantly smaller rotational magnitudes previously documented. Similarly, instances of pain and/or instability related to degenerative pathologies impacted the amount of left and right LF in the aforementioned native lumbar spine conditions and contributed to the non-congruent bilateral compressive joint forces in the symptomatic and pathological spines.

In patients undergoing surgery and having instrumented rigid or semi-rigid constructs implanted in the lumbar spine, previously documented cases of asymmetry were apparent along

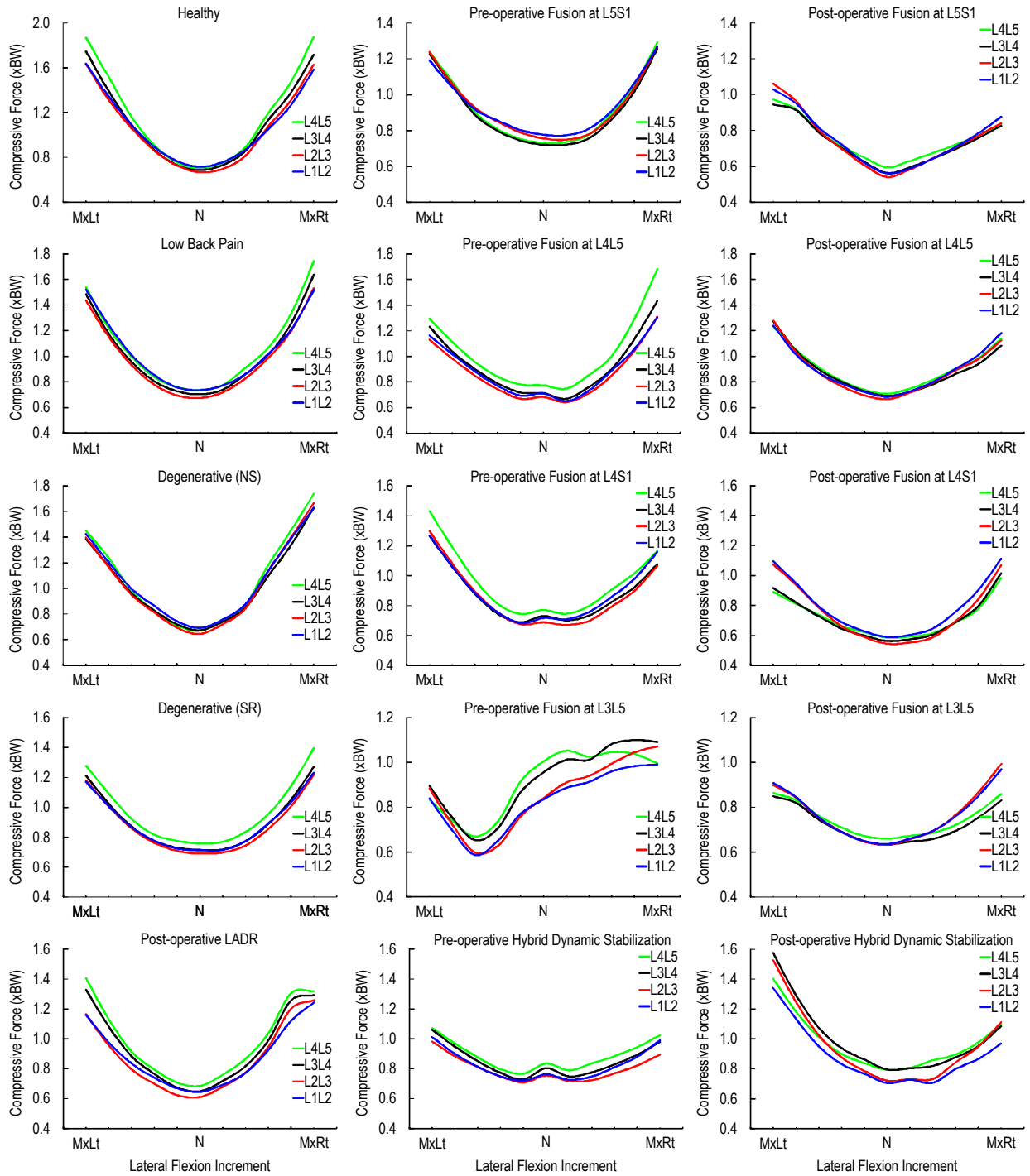


Figure 6.9 Average compressive force profiles normalized with respect to body weight during LF for both native and surgically implanted lumbar spines with comparisons pre- and post-operatively.

with instances of the largest average maximal compressive force occurring at more superior versus lower subadjacent lumbar levels. As an example, when the spine was fused at L5S1, L4L5, or L3 through L5 the largest average maximum compressive force occurred at L2L3 with magnitudes of 1.06 x BW, 1.28 x BW, and 0.99 x BW, respectively. Similarly, with fusion at L4 through S1, the highest average maximum compressive force was at the more superior adjacent L1L2 level having a magnitude of 1.11 x BW. Although, these magnitudes were smaller compared to pre-operative conditions and versus those calculated in the healthy lumbar spine, irregularities in the loading of the vertebral segments developed as a result of fusion. The decrease in the observed average compressive forces post-operatively in all fusion groups was generally predicted to correspond with the smaller segmental ROMs previously reported. However, L5S1 fusion patients experienced considerable increases in post-operative ROMs at the segmental levels, which was contrary to lower compressive forces predicted post-operatively. This finding was rather peculiar, as previous occurrences of increased ROM were accompanied with the calculation of larger compressive force magnitudes. However, despite this anomaly, further analysis of patients having HDS exhibited greater average maximum compressive forces which paralleled the increased segmental ROMs observed post-operatively. In addition, the greatest average compressive force of 1.57 x BW occurred at the adjacent L3L4 level, thereby continuing the trend where instrumented rigid and semi-rigid fixation resulted in the largest compressive force being found at levels other than the most inferior L4L5 level.

Conversely, in patients implanted with LADR, forces were observed to be more symmetrical from left to right compared to the fused and dynamically stabilized spines. In the LADR patient group, the variation of the average maximum compressive forces between the left and right sides

was less than 8.0% at all levels, on average. In addition, the highest average maximal compressive force magnitude occurred at L4L5 and decreased moving superiorly from L5 to L1, which was similar to the trend observed in patients having a native lumbar spine.

Subsequent analyses of the average AP forces during LF of the spine were found to be smaller in magnitude compared to compressive forces. In general, near neutral position, forces in the AP direction were quite small and mostly oriented in the posterior direction. LF of the lumbar spine to either the left or right side prompted an increase in the posterior force magnitudes. Generally, the largest average AP forces were experienced at the L4L5 level, except in patients where the lumbar spine was fused at L4 through S1 or had undergone HDS. The magnitudes of posteriorly directed forces were greatest in healthy patients at L4L5, whereas average maximum forces in the anterior direction were observed at L1L2, post-operatively, in patients having fusion of L4 through S1. However, despite these small differences, overall force patterns and magnitudes were determined to be relatively similar across various spine conditions and were not found to influence any significant changes in the calculated AP forces (Figure 6.10).

Relatively speaking, the forces derived along the transverse plane and acting in the lateral LR direction at each intervertebral level were quite trivial compared to the forces acting in the other directions. In all patients and across the various lumbar spine conditions analyzed, consistent lateral force patterns were observed during LF (Figure 6.11). In general, when the lumbar spine was flexed to one side, lateral forces at the inferior lumbar levels were directed to the same side, while at the more superior levels the forces were generally opposite to the

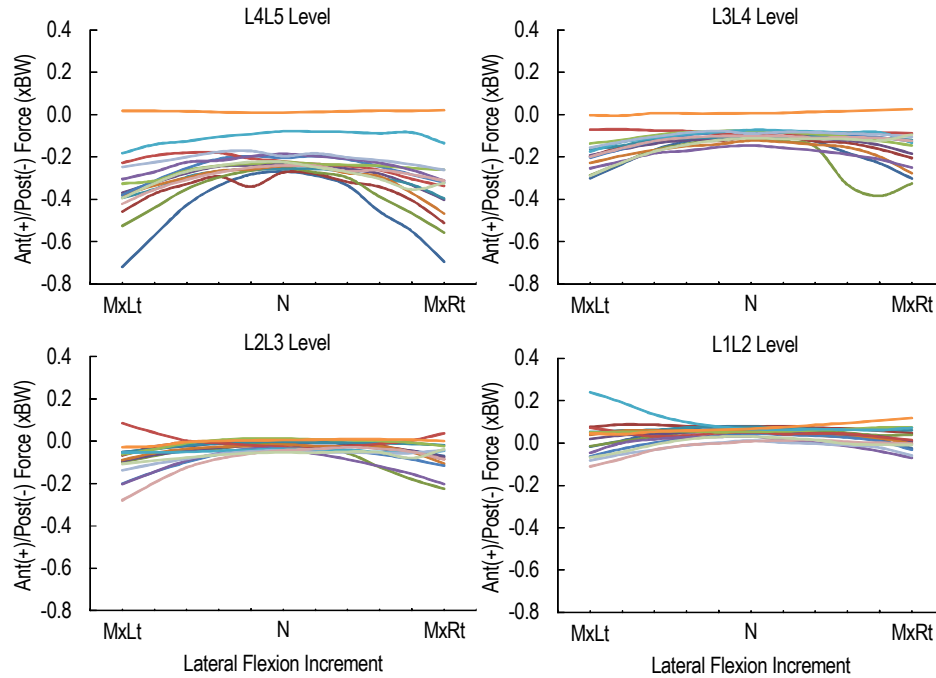


Figure 6.10 Average AP forces at each intervertebral level for all native and surgically implanted lumbar spine conditions while performing LF.

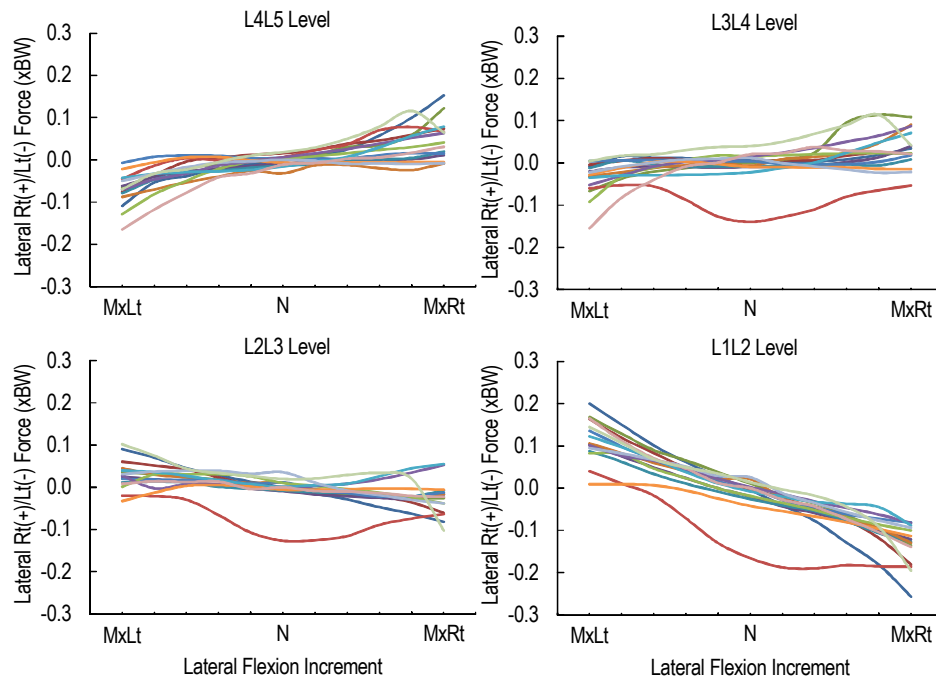


Figure 6.11 Average lateral right and left forces at each intervertebral level for all native and surgically implanted lumbar spine conditions while performing LF.

direction of LF. In addition, lateral forces calculated in the lumbar spine were generally greatest at the L1L2 levels in all lumbar spine conditions and ranged between -0.26 to $0.20 \times BW$.

Again, the muscle forces predicted by the mathematical model exhibited similar profiles as those predicted for the compressive contact forces, with the peak forces occurring at the maximum left and right laterally flexed position and decreasing near the upright, neutral position (Figure 6.12). The MUL and EO muscles typically generated the largest forces, while contributions from the PM and QL muscles were typically less but exhibited some fluctuation, depending upon the patient's lumbar spine condition. In addition, the model generally predicted smaller forces in the RA and IO muscles. However, higher muscle forces were predicted for the IO muscles in pre-operative L3L5 fusion patients during LF to the right side. Less symmetric muscle force profiles for pre- and post-operative conditions of the lumbar spine were also predicted.

6.2.3 Axial Rotation Activity

During AR of the lumbar spine, analyses were conducted while patients performed rotation of the trunk within the transverse plane between the maximum left and maximum right axially rotated positions. Similar to the generalized trends observed during LF, the largest compressive forces were predicted at the maximum axially rotated positions, while the minimum force occurred as patients moved through the upright neutral position. Table 6.9 lists the average compressive force magnitudes during the AR activity for native and surgically implanted lumbar spine conditions.

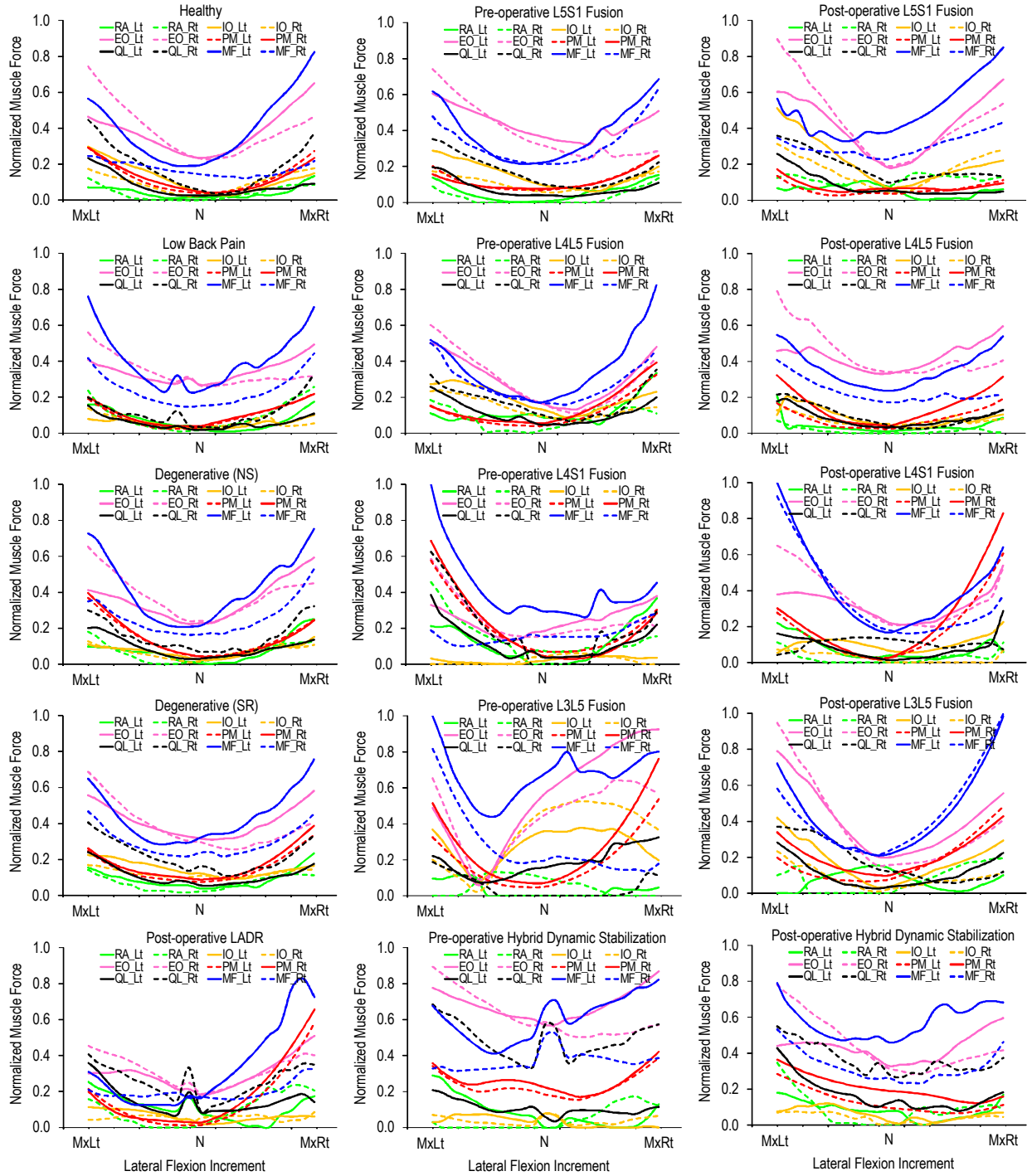


Figure 6.12 Average profiles for the theoretical muscle forces normalized with respect to the muscle predicted to generate the largest force during AR for both native and surgically implanted lumbar spines with comparisons pre- and post-operatively.

Table 6.9 Average intersegmental compressive forces relative to body weight during AR activity for all lumbar spine conditions at each increment captured during the motion.

Lumbar Spine Condition		L4L5			L3L4			L2L3			L1L2		
		MxLt	N	MxRt	MxLt	N	MxRt	MxLt	N	MxRt	MxLt	N	MxRt
Healthy		1.16	0.76	1.07	1.18	0.76	1.11	1.11	0.74	1.09	1.13	0.80	1.12
Low Back Pain		1.34	0.70	1.32	1.27	0.70	1.30	1.26	0.68	1.28	1.29	0.73	1.31
Degenerative (NS)		1.51	0.70	1.70	1.47	0.70	1.61	1.45	0.69	1.55	1.52	0.73	1.54
Degenerative (SR)		1.30	0.76	1.26	1.21	0.72	1.16	1.18	0.70	1.14	1.16	0.73	1.14
Fusion	L5S1	1.24	0.58	1.09	1.19	0.58	1.03	1.21	0.55	1.05	1.15	0.59	1.05
	L4L5	0.94	0.71	0.86	0.92	0.69	0.88	0.90	0.66	0.94	0.92	0.68	0.88
	L4S1	1.33	0.60	0.87	1.26	0.59	0.81	1.35	0.57	0.90	1.35	0.68	0.93
	L3L5	0.81	0.71	0.85	0.78	0.69	0.83	0.78	0.68	0.80	0.70	0.64	0.75
HDS	L4S1	0.86	0.85	1.08	0.82	0.71	1.02	0.77	0.68	0.89	0.72	0.66	0.87
LADR	L5S1	1.21	0.70	1.29	1.12	0.64	1.14	1.03	0.63	1.06	1.08	0.66	1.06

However, despite the generalized trends previously discussed, more in-depth analyses did reveal some variation in compressive force magnitudes and patterns among the different lumbar spine conditions and also between pre- and post-operative evaluations (Figure 6.13).

One important point relative to the compressive forces derived during AR, was the increased sensitivity of the 3D mathematical model to not only in-plane segmental ROM, but also the coupled FE and LF rotations. This was in contrast to the behavior of the model during both FE and LF activities, where in-plane segmental ROMs tended to primarily influence the model calculations. In part, this newfound sensitivity was attributed to the ligaments included in the model due to the directional orientation of the bundles, which seemed to be better suited to engage during FE and LF motion. AR motion, on the other hand, was limited more so by the zygapophyseal joints and to some extent by the muscles. As a result, ligament and muscle contributions toward the compressive force calculations were likely more variable during AR. In turn, the relationships between the observed kinematics and the predicted forces were difficult to discern.

Despite these added complexities, some observations were made among the various spine conditions. For the native lumbar spine, healthy patients normally exhibited maximum compressive forces at the L4L5 level. However during AR, L3L4 experienced the greatest compressive forces having an average magnitude of $1.18 \times \text{BW}$. However, since the compressive forces were very similar across all lumbar levels this finding was rather insignificant. However, as the native lumbar spine became more symptomatic, the maximum compressive forces increased to $1.34 \times \text{BW}$ in the LBP group, $1.70 \times \text{BW}$ in the non-surgical degenerative group, and $1.30 \times \text{BW}$ in the degenerative group requiring surgery. Though these increased compressive

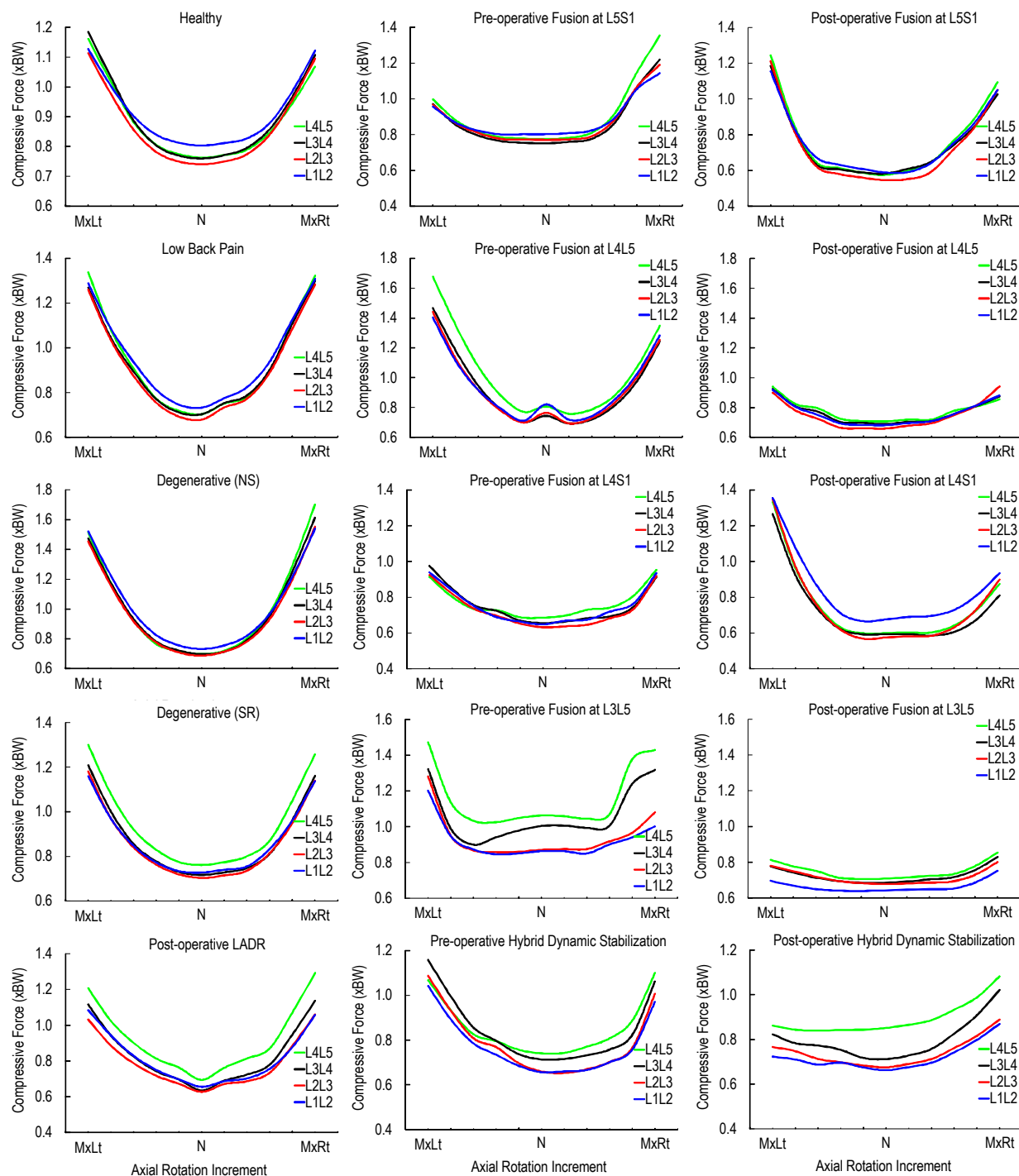


Figure 6.13 Average compressive force profiles normalized with respect to body weight during AR for both native and surgically implanted lumbar spines with comparisons pre- and post-operatively.

force magnitudes were not significantly different from the healthy lumbar spines, the larger contribution of coupled rotations toward the AR ROM in the symptomatic and pathologic spines may have contributed to the higher magnitudes. Furthermore, analysis of the bilateral motion during AR revealed mainly symmetric loading profiles for all conditions of the native lumbar spine with variations between the left and right side averaging less than 4.2% across all levels.

Post-operative analysis in patients undergoing either stand-alone fusion or HDS of the pathological segments revealed variable results. On average, patients fused at L5S1 or L4 through S1, experienced maximum compressive forces of 1.24 x BW and 1.35 x BW, respectively, which were comparable to those calculated in healthy subjects. However, post-operative maximum compressive force magnitudes at the same levels increased 9.0%, on average, when fusion occurred at L5S1 and 46.7% when patients were fused at L4 through S1. In contrast, patients having instrumented fusion at L4L5 or L3 through L5, had considerably smaller maximum compressive force magnitudes at all levels compared to healthy subjects. In fact, at the first and second superior adjacent levels, compressive forces decreased an average of 56.4% with L4L5 fusion and 60.0% with L3L5 fusion. It is unclear the cause for this significant decrease in the calculated compressive force; however, it is worth noting that both L4L5 and L3L5 fusion groups experienced decreased amounts of AR ROM with larger coupled motions following surgery. Similarly, in patients having HDS, average maximum compressive forces decreased post-operatively and in comparison with healthy patients, exhibited smaller magnitudes. Furthermore, several types of fusion groups were found to experience more symmetric loading profiles post-operatively. Contrary to this finding was with rigid fusion or

HDS of L4 through S1 levels, in which case, average maximum compressive force magnitudes between the left and right side varied by an average of 36.7% across all levels.

Finally, in LADR patients, the maximum compressive force magnitude occurred at L4L5 level with a magnitude of 1.29 x BW. Although, this compressive force was slightly increased compared to healthy subjects, its magnitude was similar to that experienced by the native spine group with LBP. As in the LBP group, increased amounts of coupled motions relative to AR ROM were experienced at some intervertebral segments in LADR patients and likely attributed to the increased compressive force magnitudes. In addition, the maximum compressive forces experienced on the left and right sides were mostly symmetrical, with a variability of less than 7.0%.

Analysis of the forces in the AP direction during AR revealed similar patterns as those observed during the LF activity. At the upright or neutral position, average AP forces were less than those generally experienced at maximum rotation to the left and right sides. In general, the calculated forces increased posteriorly with greater AR rotation of the spine, with the highest of these forces generally found to occur at L4L5 (Figure 6.14). For the native lumbar spine in healthy, LBP, and non-surgical degenerative subjects, the maximum average AP force at L4L5 was -0.46 x BW, -0.48 x BW, and -0.59 x BW, respectively. In patients having severe degeneration which would require surgery to stabilize the dysfunctional segment, the average maximum force was -0.40 x BW. Post-operatively, those patients having fusion at L5S1 experienced a maximum AP force of -0.47 x BW, while others fused at L4L5, L4 through S1, and L3 through L5 achieved a maximum force of -0.27 x BW, -0.15 x BW, and 0.13 x BW, respectively. Contrary to the other groups, the greatest force in the L3 through L5 fused spines

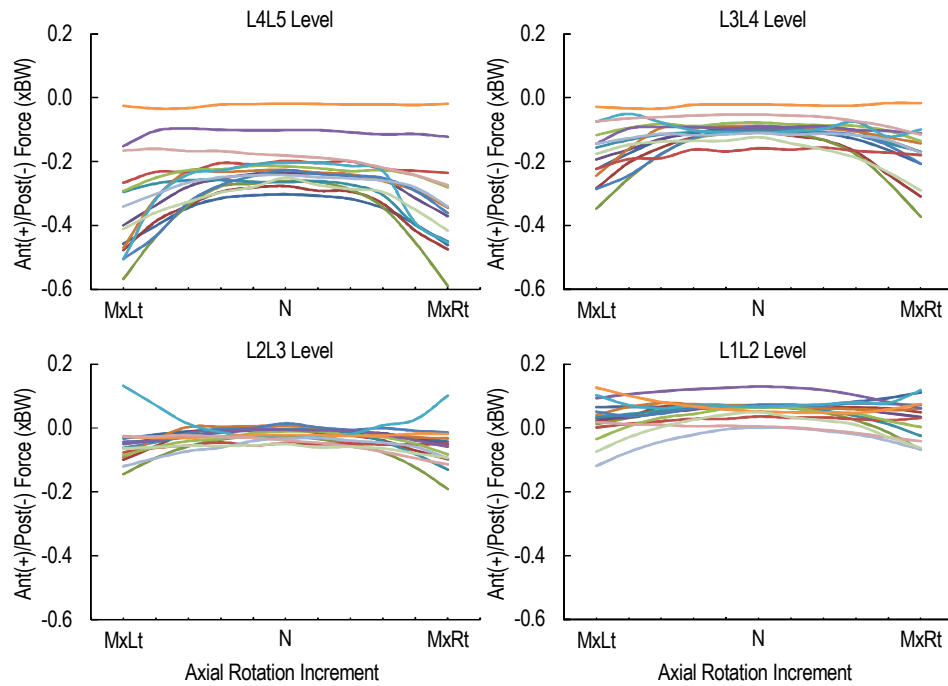


Figure 6.14 Average AP forces at each intervertebral level for all native and surgically implanted lumbar spine conditions while performing AR.

occurred at L1L2. Patients having HDS or LADR, experienced a maximum AP force at L4L5 of $-0.27 \times \text{BW}$ and $-0.42 \times \text{BW}$, respectively.

Forces in the transverse direction were again found to be very small relative to the other forces. In addition, the patterns and magnitudes observed in patients across all lumbar spine conditions were consistent at all lumbar levels (Figure 6.15). The overall range for the LR forces in all groups was between -0.19 to $0.06 \times \text{BW}$ and no significant trends were observed.

The contribution of the muscles during axial rotation continued to mimic the force profiles predicted for the compressive contact forces, with the peak forces typically occurring at the maximum left and right laterally flexed position and decreasing near the upright, neutral position (Figure 6.16). Again, the MUL and EO muscles tended to generate the peak forces

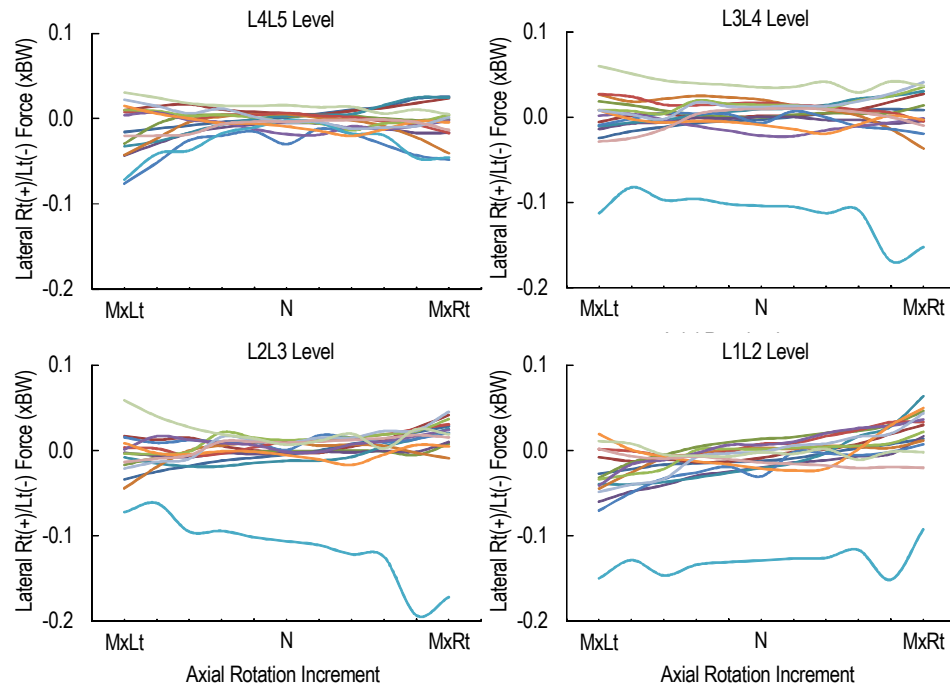


Figure 6.15 Average lateral LR forces at each intervertebral level for all native and surgically implanted lumbar spine conditions while performing AR.

required to axially rotate the spine, especially in the healthy, LBP, non-surgical degenerative, and degenerative subjects requiring surgery. However, for many of the pre-operative and post-operative conditions in the lumbar spine, AR maneuvers elicited the use of other muscles, with continued production of force in the MUL and EO muscles, but also involved increased force production in the PM muscle. In addition, the native lumbar spine conditions were predicted to have smoother muscle profiles. However, pre- and post-operative fusion and HDS, as well as post-operative LADR conditions were found to produce muscle force profiles that were rather sporadic throughout the AR activity.

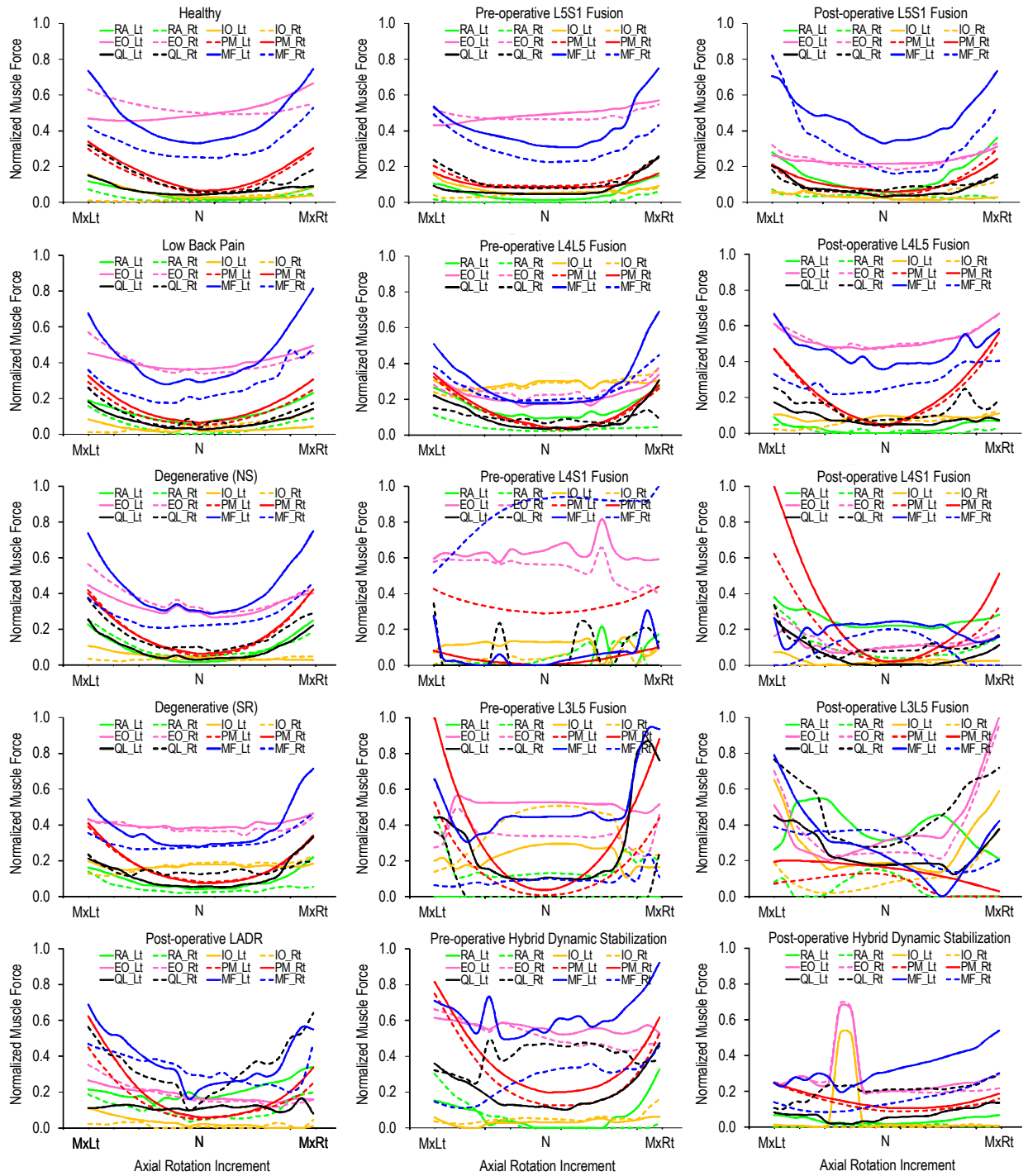


Figure 6.16 Average profiles for the theoretical muscle forces normalized with respect to the muscle predicted to generate the largest force during AR for both native and surgically implanted lumbar spines with comparisons pre- and post-operatively.

6.3 Validation of the Mathematical Model

6.3.1 Telemetry vs Theoretically Derived Forces

Comparison of the forces measured directly using telemetry [83] with forces predicted from the mathematical model and averaged among the various lumbar conditions revealed considerable variation (Figure 6.17). During flexion, the theoretically derived mean compressive force profiles with respect to the force calculated at the upright, neutral position revealed average errors ranging from 4.8% in the degenerative group requiring surgery up to 30.1% in patients having fusion at L3L5. The maximum error within these groups was 9.4% and 48.6%, respectively.

Since averaging can sometimes skew results, further analysis was conducted in the healthy and LBP groups on a patient-to-patient basis. Cases were found where the mathematical model performed very well relative to the measured telemetry data (Figure 6.18). The forces predicted for sample patients H4, H5, and LBP6 had an average error of 3.6%, 7.9%, and 5.8%, respectively, while the an average maximum error was less than 13.1%.

In vivo force data was also collected using telemetry while a patient performed LF to the right side. Again, when comparing the average predicted force profiles according to lumbar spine condition, the average calculated error increased and ranged from 4.2% up to 25.2%, with maximum errors between 12% and 47.9% (Figure 6.19). However, predicted force profiles in sample patients H8, H10, and LBP5 were predicted with an average error of 6.5%, 6.6%, and 10.4%, respectively (Figure 6.20). The maximum error for force prediction in these patients averaged 15.9%.

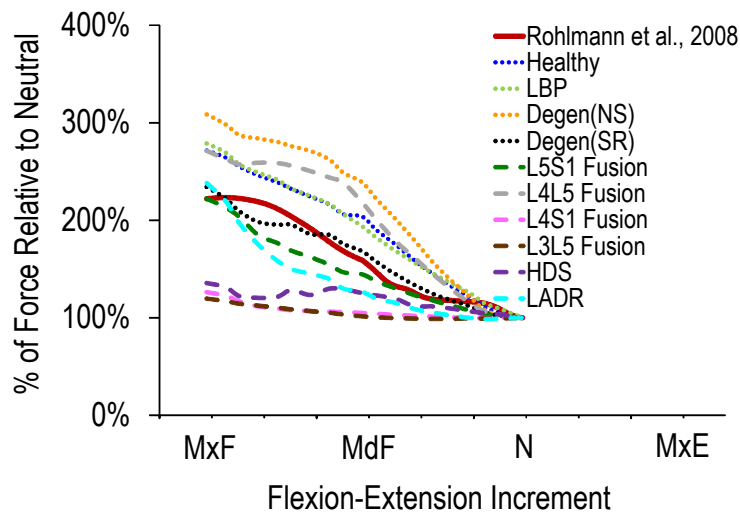


Figure 6.17 Comparison of the theoretically derived forces, averaged across various lumbar spine conditions at L1L2, with force data directly measured using a telemeterized vertebral body replacement between T12 and L2 while moving between maximum flexion and upright, neutral position.

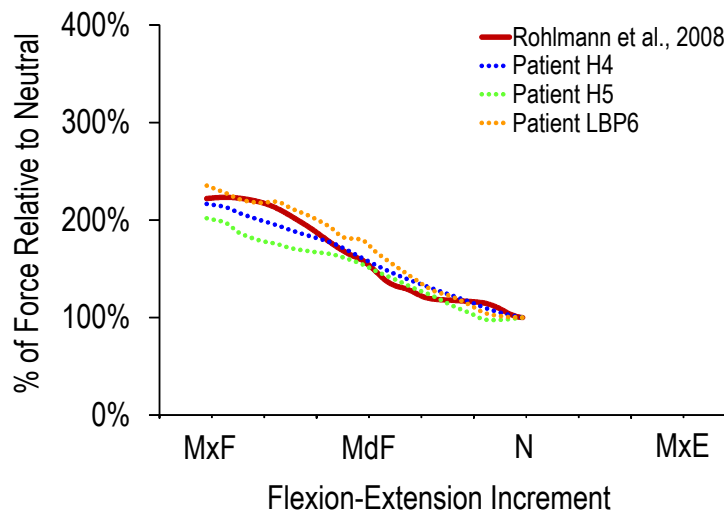


Figure 6.18 Comparison of the theoretically derived forces for three sample patients at L1L2 with force data directly measured using a telemeterized vertebral body replacement between T12 and L2 while moving between maximum flexion and upright, neutral position.

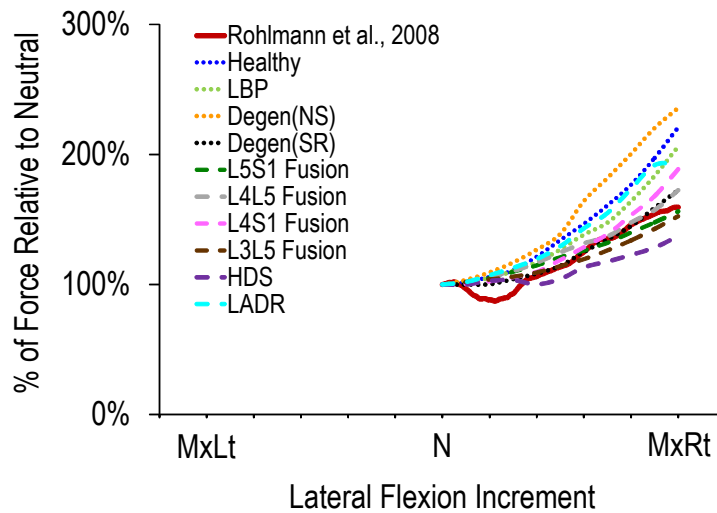


Figure 6.19 Comparison of the theoretically derived forces, averaged across various lumbar spine conditions at L1/L2, with force data directly measured using a telemeterized vertebral body replacement between T12 and L2 while performing LF to the right side.

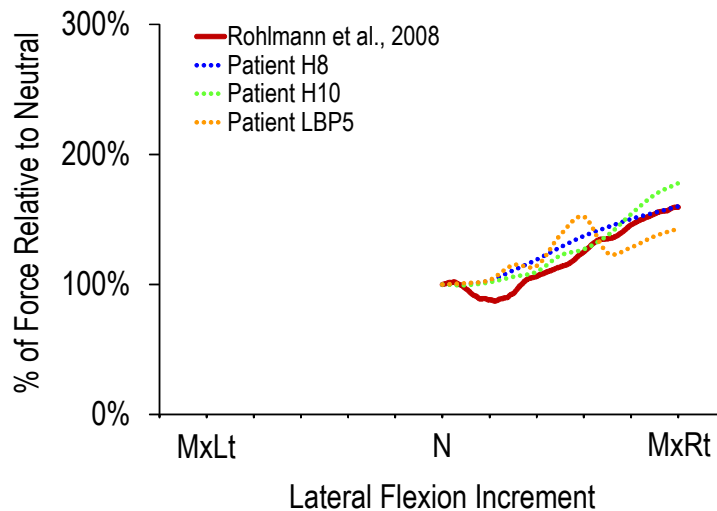


Figure 6.20 Comparison of theoretically derived forces for three sample patients at L1/L2 with force data measured using a telemeterized vertebral body replacement between T12 and L2 while performing LF to the right-side.

6.3.2 Intervertebral Disc Pressure vs Theoretically Derived Forces

In vivo disc pressures at the L4L5 level were previously reported in a single healthy subject performing FE, LF, and AR [112]. Following the conversion of the measured pressures to equivalent force values, comparative analysis were conducted at the L4L5 level on the forces derived using the mathematical model. As evident with the telemetry data, considerable variability between the predicted and measured forces was observed when comparing force profiles averaged across varying lumbar spine conditions (Figures 16.21 – 16.23). During FE, the average error for all spine groups ranged between 8.1% and 50.2%. Modeling of the forces during LF and AR activities were slightly improved; however, the average error between the averaged theoretical forces and those measured *in vivo* ranged from 3.0% to 30.0% and 3.6% to 23.4%, respectively. The maximum error of the predicted forces during FE was 103.9%, while LF and AR resulted in as much as 66.3% and 81.6% deviation from the *in vivo* data measured using pressure sensors, respectively.

Though the average force profiles for many of the spine groups differed from those collected *in vivo* using the pressure sensor, the model did predict some individual patient force profiles which corresponded well with the reported measurements at L4L5. During FE, sample patients H4, H6, and H10 had their L4L5 forces predicted with an average error of 6.9%, 8.2%, and 5.9%, respectively (Figure 16.24). For LF activity, the mathematical model was able to predict forces for sample patients H7, H8, and LBP5 with relatively small average errors less than 9.6% with maximum errors not exceeding 18.2% (Figure 16.25). In Figure 16.26, a similar scenario was observed, demonstrating the even with axial rotation, which normally exhibits smaller ROM

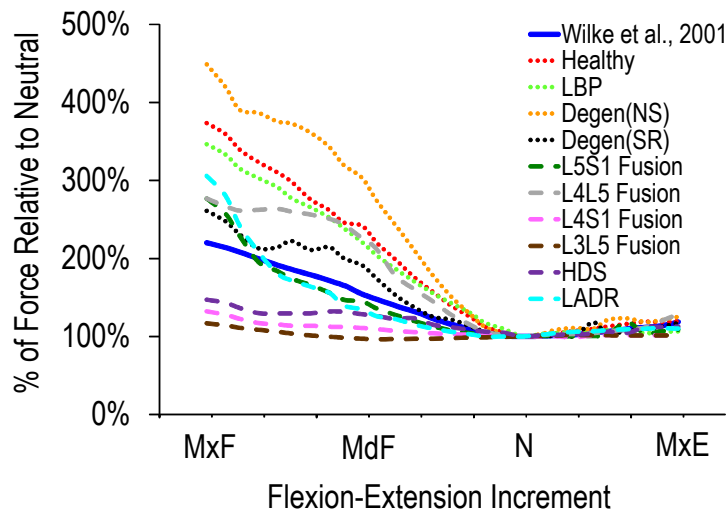


Figure 6.21 Comparison of theoretically derived forces averaged across various lumbar spine conditions at L4L5 with data reported in the literature, measuring *in vivo* loads using pressure sensors placed in the L4L5 intervertebral disc while performing FE.

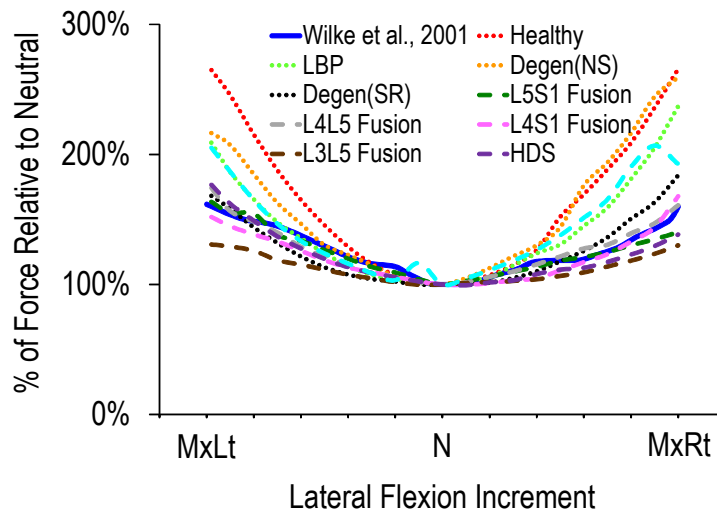


Figure 6.22 Comparison of theoretically derived forces averaged across various lumbar spine conditions at L4L5 with data reported in the literature, measuring *in vivo* loads using pressure sensors placed in the L4L5 intervertebral disc while performing left-to right LF.

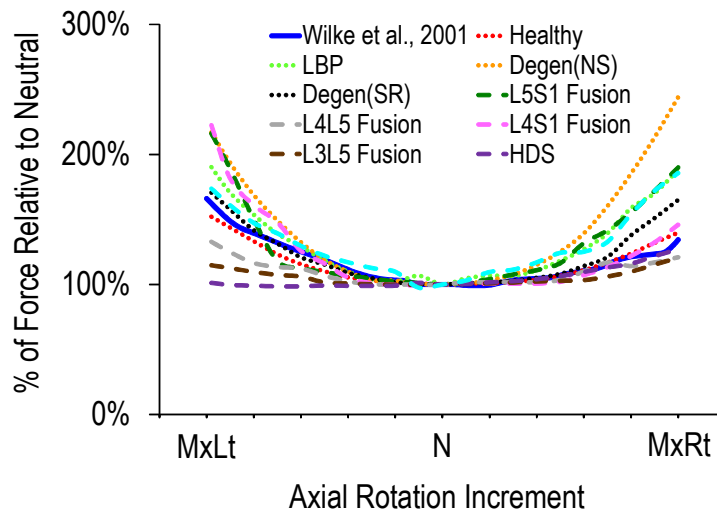


Figure 6.23 Comparison of theoretically derived forces averaged across various lumbar spine condition at L4L5 with data reported in the literature, measuring *in vivo* loads using pressure sensors placed in the L4L5 intervertebral disc while performing left-to right AR.

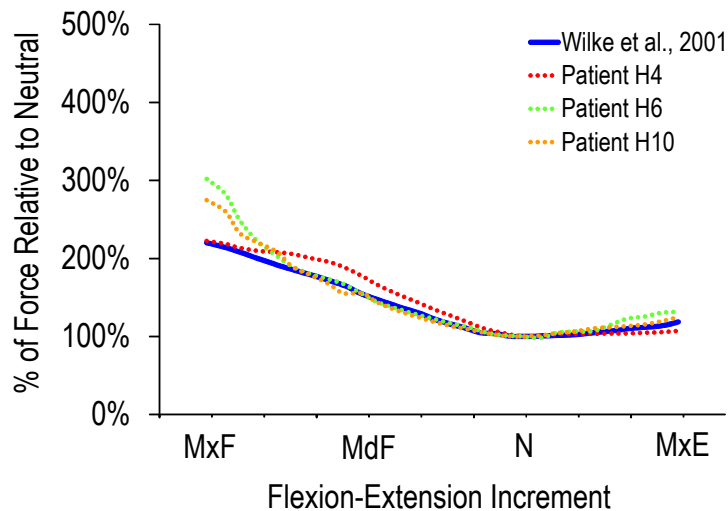


Figure 6.24 Comparison of theoretically derived forces for three sample patients at L4L5 with data reported in the literature, measuring *in vivo* loads using pressure sensors placed in the L4L5 intervertebral disc while performing FE.

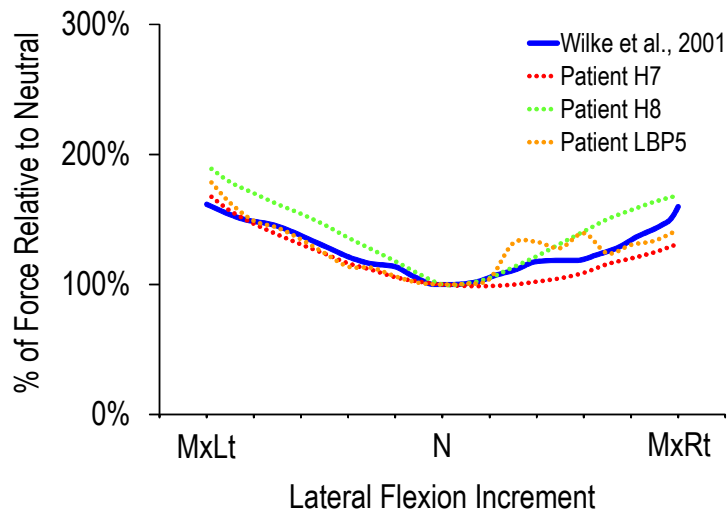


Figure 6.25 Comparison of theoretically derived forces for three sample patients at L4L5 with data reported in the literature measuring *in vivo* loads using pressure sensors placed in the L4L5 intervertebral disc while performing left-to-right LF.

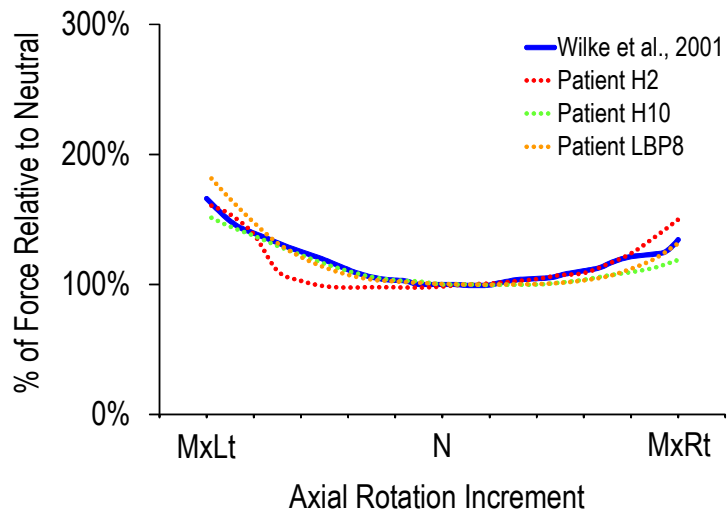


Figure 6.26 Comparison of theoretically derived force data for three sample patients at L4L5 with data reported in the literature, measuring *in vivo* loads using pressure sensors placed in the L4L5 intervertebral disc while performing left-to-right AR.

the model was able to perform well and predict forces with minimal error. Relative to the reported *in vivo* data measured using pressure sensors, AR of the spine resulted in the mathematical model achieving an average and maximum error of 6.3% and 17.1%, respectively, for sample patient H2. Likewise, the average errors in the theoretically derived forces for sample patients H10 and LBP8 were 4.7% and 3.8%, respectively, with maximum errors less than 11.6% for H10, and 9.3% for LBP8.

Chapter 7

Discussion

In the human body, a number of joints exist that allow for movement while also providing mechanical support. However, with advancing age and traumatic injury, problems can develop that impact the functionality of the joint and result in pain. Therefore, it is important for the development of tools which enhance understanding of the joint mechanics while also aiding in the diagnosis, prevention, and treatment strategies for various joint pathologies. In the past, dynamic fluoroscopy coupled with mathematical modeling techniques have shown to be successful methodologies for investigating both the kinematics and kinetics of specific joints. In fact, a considerable amount of research has been conducted by colleagues within our own laboratory to evaluate the knee [95], hip [32] and cervical spine [52].

This dissertation extended upon the methodologies used previously for other joints and focused on the evaluation of the *in vivo* mechanics in the lumbar spine. As a result, the kinematic characteristics of the healthy, symptomatic, pathological and pre- and post-operative lumbar spines were analyzed. Furthermore, the development of a computationally efficient, multi-body, 3D mathematical model was derived, using the *in vivo* kinematics as input data to drive the model. These theoretically derived loading characteristics may possibly serve as a tool to help progress the understanding and knowledge base for the mechanical characteristics of the many native and surgically implanted conditions in the lumbar spine.

7.1 Kinematics Analysis

Although numerous *in vivo* and *in vitro* studies have been conducted to describe both the clinical and biomechanical characteristics for the native lumbar spine in healthy, LBP, and non-surgical degenerative subjects, few studies have analyzed a large cohort of patients representing all these groups as well as other clinically defined conditions within a single study. In addition, patients stratified as having severe degeneration and instability at one or more levels and requiring surgery to stabilize dysfunctional lumbar segments were evaluated pre- and post-operatively. These evaluations were performed on patients have both a stand-alone fusion and in those having HDS. Patients were also assessed who had previously undergone LADR. In total, 44 subjects, across ten different lumbar spine conditions were evaluated for their *in vivo* kinematics.

The kinematic results investigated global ROM, intersegmental ROM, as well as coupled motions for the prescribed activities. Traditional kinematics analyses derive the maximum absolute rotational magnitude between the two end ROM during the prescribed activities. However, novel techniques were also implemented which isolated the rotational paths of the vertebrae at each FSU in the lumbar spine. Analyses of the global ROM across all lumbar spine groups found that patients having a native lumbar spine tended to experience greater ROM compared to patient groups having either a rigid and/or semi-rigid instrumented fixation. This was also observed in patients having motion preserving type implants. During FE, native lumbar spines averaged more than 40° of global FE motion between L1 and L5, while patients having surgically altered spines averaged considerably smaller ROM. Although, these differences were mainly statistically insignificant as a result of the smaller sample sizes, a dichotomy was

apparent when comparing native lumbar spines with those that had been surgically altered. With both LF and AR, the measured amount of global ROM between groups was not significantly different and no discernible trends seemed to exist. However, these findings were not completely unexpected as others have also reported on overall ROMs along the primary activity path and have suggested that rotational magnitudes are non-differentiable characteristics for identifying pathologies across various conditions of the spine [55, 66, 107]. In addition considerable amounts of variability in ROM have been observed and correlated with differences in age and gender [12].

However, assessment of the coupled motions in the spine groups defined in the current study revealed general monotonic increases in the out-of-plane motion as patients progressed into more symptomatic and pathologically advanced conditions of the low back. Even with the inherent increase in the amount of coupled motion with LF and AR, differences among the various lumbar spine conditions were observed. It is believed that this may serve as an indicator for certain patient pathologies where out-of-plane maneuvers are used to compensate for inefficiencies when performing activities which normally require dominant rotations within a single motion plane. This phenomenon was also observed by Johnson *et al.* [39], which used a portion of the kinematics derived in this dissertation to define coefficients relating the combined out-of-plane motion with the total in-plane motion. A classification scheme was then implemented to successfully differentiate among healthy, symptomatic and degenerative conditions.

Lund *et al.* [56] also evaluated the 3D motions of the lumbar spine in chronic LBP patients using percutaneous transpedicular screws to track vertebral motions during FE, bilateral AR, and

bilateral LF. He too suggested that coupled motion may be an indicator for different spinal pathologies. Other reports observing similar motion patterns have linked coupled motion at a functional lumbar segment with instability, and the increased risk for developing pathogenic disc degeneration [25]. Although, the exact mechanisms involved are not clear, it is hypothesized that prolonged exposure of the vertebral joint to excessive and aberrant motion patterns can slowly degrade the intervertebral disc, specifically the nuclear matrix. Over time, changes in this nuclear area can minimize its ability to retain fluids, thereby decreasing the relative disc height. As a result, ligaments, which are normally taut and work to constrain excessive amounts of motion, can become lax, possibly leading to what is commonly referred to as joint instability and contribute to the observed increase in coupled motion.

The motion characteristics of the lumbar spine may be influenced by a number of factors, including but not limited to muscle strains, which could possibly impact muscle activation patterns or other sources of localized pain that can be perturbed with increasing amounts of motion. Mechanical instability of the vertebral joint, in theory, could possibly be both a cause and an effect of these associated pathologies relating to the experience of pain. However, while the current study was not focused on specifically measuring instability in the spine, which has often been linked to a defined neutral zone, it is worth further investigation to determine if the increased coupled rotational motions observed in patients having LBP, degenerative conditions (both non-surgical and surgical), and surgically implanted devices experience clinically defined spinal instabilities.

White et al. [109] previously conducted an *in vitro* study investigating kinematics of the spine and proposed that the presence of motion characteristics which deviated from those

observed in healthy subjects were likely the result of instability. Furthermore, published literature has also reported on the possible link of segmental instability with increasing disc degeneration [24, 25]. These reports all maintain the current kinematic findings in this dissertation and suggest that increased amounts of out-of-plane motion may be critical in further understanding the complex etiologies for pain and related symptoms in the lower back region.

An effective treatment aimed at addressing the abnormal motions and perceived instabilities at dysfunctional levels has been the use of instrumentation to fuse parts of the spine. However, this often results in loss of motion and may have detrimental effects on adjacent segments. Findings in the current study revealed that for patients undergoing rigid fusion, regardless of level, always experienced a rotational magnitude and percentage loss, both globally and within at least one of the vertebral levels while performing the prescribed activities and compared to pre-operative evaluations. This occurrence has also been documented in numerous other studies in patients not only having fusion [28, 96], but also in subjects having dynamic stabilization [68, 69, 75]. In the current study, patients having a dynamically stabilized level at L4L5 were also implanted with a rigid fusion at L5S1. Theoretically, the HDS design was for providing a mechanical advantage at the adjacent level so as to limit stress above or below rigid fusion, thereby decreasing the incidence of adjacent segment level disease. In the current study, motion at the superior adjacent level in HDS patients was maintained post-operatively with minimal amounts of motion during all three activities; however, this finding may be limited due to the evaluation of only two patients. On the contrary, a study conducted by Mageswaran *et al.* [59] using cadaver lumbar spines having hybrid dynamic stabilization and reported that the dynamically stabilized levels behaved more like fusion, and likely would not have provided a

successful transition zone between the fused level and the more superior levels untouched by surgery.

7.2 Kinetics Analysis

To the author's knowledge, no study has been conducted quantifying the *in vivo* contact forces at multiple lumbar vertebral levels and compared them among healthy, symptomatic, pathological and various pre- and post-operative conditions in the lumbar spine. However, as the prevalence of LBP and its association with possible degenerative pathologies continues to impact large percentages of the population, studies which evaluate the etiology of LBP and its correlation with biomechanical effects are needed. Gaining an understanding for the interactive joint forces that the spinal structures are subjected to on a daily basis, in terms of the magnitude and direction of the forces, is critical in determining the distribution of stress and its effect on the intervertebral discs and the facet joints. In addition, the use of rigid implants, which are commonly utilized to address instability at dysfunctional segments in the lumbar spine, may be contributing to accelerated failure in adjacent segments and determination of the loading scenarios at these levels may be beneficial [25]. Therefore, this research set forth to develop a computationally efficient, multi-body, 3D mathematical model for the predicting the *in vivo* biomechanics inherent in the lumbar spine.

The vertebral joint contact forces were evaluated across a variety of conditions in the lumbar spine while patients performed FE, LF, and AR. On average, during FE, the degenerative subjects without the need for surgery exhibited the highest force magnitudes, followed by healthy, LBP, LADR, degenerative with required surgery, and then the fusion and HDS.

Interestingly, the order of maximum force magnitudes experienced by each patient group was contrary to our initial hypothesis, which supported the idea that patients having a loss of motion at a segment, as is the case with fusion and HDS, should experience significantly greater loads at the adjacent levels with possible effects further up the lumbar spine, compared to healthy patients. However, in the current study, rotational changes between pre- and post-operative conditions at levels adjacent to fusion were generally not sufficiently increased to magnitudes larger than those experienced in subjects having an intact lumbar spine. As a result, the kinematics input into the model were still representative of relatively smaller magnitudes of rotation, especially in-plane rotation, which the model seemed to be extremely sensitive to, thereby resulting in the prediction of decreased force magnitudes in surgically implanted subjects.

The sensitivity of the mathematical model to the kinematics, which served as one of the primary inputs, should have enabled for a direct correspondence of the derived motions with the theoretical contact forces predicted in each patient group. However, this relationship was not necessarily evident using the kinematics data as it was presented earlier in this dissertation. It was later discovered that describing the kinematics using rotational and translational magnitudes for each group offered negligible statistically significant evidence allowing for any type of differentiation among the various clinical conditions of the spine. Therefore, alternative methodologies were explored to determine if the kinematics data could, indeed, be arranged in such a way to extract more relevant information that might correlate with the predicted forces .

Results of this analysis have previously been described by Johnson *et al.* [39], which used a portion the rotational kinematics derived in this dissertation for the development of motion

coefficients aimed at differentiating among patients having clinically identifiable pathologies. The motion coefficients calculated for each prescribed activity represented the ratios between the amount of coupled out-of-plane and in-plane rotations. Analysis of the kinematics for the native lumbar spine groups demonstrated a monotonic increase moving from healthy to LBP to non-surgical degenerative to degenerative requiring surgery.

In general, it was assumed that the patient group having the smallest motion coefficient ratio for a prescribed activity would have the greatest force magnitudes predicted by the mathematical model. This generalization was based on the theory that patient groups having the lowest calculated motion coefficient ratio would also have sufficiently larger in-plane motions capable of disguising any reasonable amounts of coupled out-of-plane motions. Since the model seemed to be rather sensitive to the overall in-plane rotational magnitudes, then higher forces would be predicted. Therefore, using the coefficient ratios to predict how the model may perform, suggested that the healthy patient group should exhibit the highest forces, followed by LBP, non-surgical degenerative, and degenerative requiring surgery groups. However, actual results predicted by the computational model show the highest peak forces were experienced in the non-surgical degenerative group, followed by healthy, LBP, and the degenerative group requiring surgery. This discrepancy was likely due to the model's pronounced sensitivity to the larger in-plane motions, which were greatest in the non-surgical degenerative patients and decreased following the same trend as the predicted compressive contact forces. The motion coefficients on the other hand, were sensitive not only to in-plane motions but also the coupled out-of-plane motions. In addition, the non-surgical degenerative pathologies may have experienced some mild degree of instability in the spine linked with the greater amounts of coupled out-of-plane, as well

as in-plane motion. This instability could possibly be the result of small amounts of ligament laxity, which must be compensated for by the muscles and resulting in the prediction of higher loads.

On the contrary, during LF, the mathematical model's prediction of forces were highest in the healthy group and decreased following exactly the coefficients monotonic increase from healthy to degenerative requiring surgery patient groups. However, the prediction of forces in the native spine groups during axial rotation, were not found to exhibit any type of direct correspondence with the motion coefficients derived by Johnson *et al.* (Johnson, 2012). This was likely due the smaller in-plane motions measured relative to the out-of-plane rotations during the axial rotation activity. As a result, the mean coefficient ratios were calculated to be significantly greater in all spine groups and although still increasing monotonically, the difference between each group were smaller compared to the coefficients derived for FE and AR activities.

Other factors possibly influencing the model's predicted force magnitudes during AR deals with the muscles anatomical locations. It is well known that the features of the lumbar vertebrae are not conducive to large amounts of axial rotation, which is why coupled motions are more prominent during this activity. In addition, the muscles which insert in the various locations on the vertebrae are not ideally positioned to provide the most efficient lever arm needed to rotate the vertebra relative to one another. As a result, various muscle firing scenarios may be used to generate the appropriate torques in the defined patient groups, depending on how much a patient is flexed, extended, or laterally flexed during the maneuver. These varying muscle force profiles may lead to the prediction of loading patterns that are less correlated with motion and more of a function of the anatomic variables and geometries selected for use in the model.

Prediction of the kinetics in the lower back is not trivial, as the complex motions and structures can influence a number of conditions that go into the calculation of the vertebral joint forces. As previously discussed, soft tissue structures such as ligaments and muscles can substantially influence the kinetic outputs. These tissue structures were added to the patient-specific model not only to serve as anatomically correct constraints for stabilizing the vertebrae and disc structure making up the spinal unit, but also to provide active structures which generate torques driving and control motion at the intervertebral joint. As a result of these added parameters, the input of larger segmental motions can prompt larger soft tissue forces and ultimately, larger contact force magnitudes. As an example, in patients having fusion, the predicted forces in the IO and EO muscles tended to increase post-operatively. Consequently, these abdominal muscles have also been correlated with increased intra-abdominal pressures (IAP) [17] and although, the possible biomechanical role of the IAP has been debated, some have hypothesized that the IAP is a mechanism for creating an extensor moment which can result in decreased lumbar compressive forces [59]. This may be a contributing factor that led to decreased intervertebral contact forces in fused patients, and is evidence of how the soft tissues can contribute to the predicted contact forces.

In addition, derivation of the muscle force patterns often supported the observed speed and smoothness at which a patient performed a maneuver. In many of the patients having one of the native lumbar spine conditions, the activity was performed at increased rates of speed and to greater ROMs, with smoother force profiles. These increased velocities could have generated larger accelerations and possibly have led to the prediction of higher forces. On the other hand, patients having severe lumbar complications with instrumentation implanted in the spine

typically had greater difficulty performing the prescribed activities. This may have been the result of improper firing of their muscles, thereby producing slower motion cycles with smaller ROMs and possibly influencing the prediction for decreased force magnitudes.

In general, the determination of *in vivo* lumbar vertebral loads has been a challenging endeavor for the spine field, and assessing the accuracy and reliability of the results remains experimental due to the complexities of the spine. Limitations in new investigational technologies, as well as inherent risks which may be associated with assessing *in vivo* measurements directly have hampered recent progress aimed at measuring loading conditions in the spine. However, some advancements have been designed which allow for the measurement of *in vivo* loading conditions in the lumbar region. These telemetric type implants were first introduced using internal spinal fixation devices capable of collecting both forces and moments [82]. However, these devices were placed posteriorly along the spine, thus limiting the measurement of forces only for posterior elements of the vertebra. As a result, subsequent studies by the same group, led to the development of a new implantable telemetric device which replaced the anterior vertebral body between at levels between T12 and L2 or L2 and L4 [83, 84, 86, 87] and provided a way to measure the *in vivo* forces acting on the anterior side of the spine. However, implantation of the VBR implant also required posterior fixation rods to stabilize the spine. Unfortunately, these posterior rods were not equipped with telemetry and strain gauges to measure the posterior loads as well. However, in spite of these deficiencies, these instrumented devices have provided a baseline for *in vivo* loading conditions present at the intervertebral joint and have been invaluable tools for describing what force profiles in the spine should “look like” as well as an evaluation of the magnitudes.

In order to strengthen and validate the methodologies used by the computational model developed over the course of this research, generalized comparisons of the *in vivo* forces collected from a patient implanted with VBR and having performed similar activities were used to help validate the results predicted in the present study. In lieu of a direct comparison, maximum peak forces as well as loading profiles could be used to assess the model's effectiveness in predicting contact forces during the activities.

Patients implanted with VBR were evaluated at one month and six months post-operatively while performing a number of activities, which included flexion, LF and AR [83]. The resultant loads in the spine at the level of T12 through L2 spine were reported as a percentage of the force measured while the patient was in the upright, standing or neutral position. During the flexion maneuver, these forces ranged between 224% and 241%, with peak forces produced while the patient was in forward flexion at around 35°. During LF and AR, peak values were found to range from 127% to 145% and 103% to 104%, respectively. Conversion of the maximum predicted forces at L1L2 in the healthy group from the current study to percentage of standing resulted in a value of 286% for FE, 227% for LF, and 141% for AR.

The differences between the *in vivo* data measured in Rohlmann's study compared to the forces predicted in the current study may appear rather large, especially with the predicted forces during LF and AR. However, it is important to note that this validation was not a direct comparison of the data using the same patient, thus considerable variation is likely to exist. In addition, Rohlmann's study described the telemetry results from a VBR placed between T12 and L2. However, T12 through L2 level was not specifically modeled during this research. Hence, the forces predicted by the computational model at L1L2 were used for comparative purposes

instead. As a result of this change, we would expect that force magnitudes at L1L2 level to be higher than those measured by the telemetric implant between T12 and L2 due to increased body weight borne by the more inferior level. Additionally, this comparison used the average maximum healthy force magnitude at L1L2 for each activity, which generally included force magnitudes derived in patients that achieved far greater ranges-of-motion than the patient described in Rohlmann's study. Lastly, the computational model described here has been designed to output the total force in each of the principle directions acting at a specified vertebral level. However, data measured from the VBR does not represent the total load carried in the spine at the T12 through L1 level. Instead, the load is shared not only by the VBR, but also by the posterior fixation rods, the remaining parts of the native vertebral structure and the bone graft. Despite the many experimental limitations, Rohlmann *et al.* [83] provided data which was helpful in validating the pattern of the force for each of the activities, as well as, the relative magnitudes, which have been predicted in other non-specific spine models to have a rather considerable range.

Aside from instrumented telemetric VBR, only one other known method is available for direct measurement of loading conditions in the lower back region. This involves the use of pressure sensors implanted between the vertebral joint space as way to measure intradiscal pressures [63, 91, 112]. Ideally, this technique would allow for assessment of *in vivo* pressures and stresses within the disc. However, given the approximate area of the intervertebral disc through the use of MRI, force magnitudes acting on the intervertebral disc can be extrapolated from the measured pressure data. As a result, *in vivo* data collected using these pressure measurements were used as a second type of validation.

The research conducted by Wilke et al. [112] was selected for comparative purposes and reported results on a single healthy patient implanted with a pressure-sensing probe at L4L5. Data was generated pertaining to intervertebral disc pressures while performing a wide array of dynamic activities and mimicked the FE, LF, and AR maneuvers performed by patients in the current study. During FE, they reported peak disc pressures at L4L5 equal to 1.08 MPa during flexion at an angle of 36°, 0.6 MPa during extension at an angle of 19°, and 0.43-0.50 MPa while standing in the upright, neutral position. Similarly, during LF and AR, peak forces at the maximal left and right lateral positions were 0.59 MPa while during AR the measured disc pressures were 0.7 MPa to the left and 0.6 MPa to the right. Conversion of the pressure data to forces using the reported patient's disc area of 18 cm² and body mass of 70 kg, revealed peak forces during FE to be around 2.83 x BW in flexion, 1.57 x BW during extension, and 1.2 x BW at neutral. During LF, the maximum force to the left and right sides was 1.55 x BW, while peak forces during AR were calculated to be 1.83 x BW to the left and 1.57 x BW to the right. Comparatively, the average maximum forces calculated at L4L5 by the mathematical model in the healthy spine group during FE were 2.47 x BW, 0.79 x BW, and 0.66 x BW, respectively. During LF, healthy subjects were predicted to experience a force 1.87 x BW on the left and right side, while during AR the average peak force was 1.16 x BW to the left and 1.07 x BW to right.

While the force derived at maximum flexion was relatively similar to the average force predicted by the mathematical model for healthy patients at maximum flexion, there was considerable variability between the predicted and measured forces at the upright, neutral position and at full extension. These differences are likely the result of the experimental setup in the study conducted by Wilke *et al.* [112], which measured pressure profiles only in the disc.

Whereas the forces computed by the mathematical model are representative of the overall force at the vertebral level.

During flexion, this difference between the model and the measured data is smaller, as a large percentage of the total load carried in the spine typically passes through the anterior portion of the vertebra. However, at neutral and maximum extension, the posterior elements of the vertebrae likely are responsible for bearing more substantial forces. The results from the mathematical model account for the load distribution changes during the motion, while the pressure sensors only measure the effects happening at the intervertebral disc. The same also holds true during lateral bending and axial rotation; however, the motions become increasing complex, thereby requiring increasing loads to be carried by both the anterior vertebral body and the posterior zygapophyseal joint. However, despite these differences in magnitude, the force profiles predicted by the computational model at L4L5 were almost identical for all three activities reported on by Wilke *et al.* [112].

The telemetric vertebral implant and the intervertebral disc pressure sensors are currently the only methodologies offered for experimentally *in vivo* loading conditions in the lumbar spine. However, with instrumented VBR, the invasiveness of the procedure limits its use as a tool for direct measurement in the spine. Additionally, only surgically altered spine conditions can be assessed. With the use of pressure sensors, these too are invasive and only allow for temporary monitoring. Implantation of the sensor may also cause pain and result in increased muscle contraction or conversely, if area is anesthetized, pain may be absent, but the firing patterns in the muscles may be affected and could change the way the disc is “normally” loaded. Pressure sensors are also reliant on fluid to transmit pressure evenly. This limits its use in patients having

other defined pathologies due to the loss of hydration in the nucleus, thereby possibly altering the hydrostatic characteristics and artificially lowering intradiscal pressure readings [5, 100].

Since limitations are associated with telemetry and the use of pressure sensors, mathematical modeling has shown to be an alternative methodology for determining *in vivo* joint forces. Komistek et al. [42, 43] pioneered computational modeling techniques for the calculation of *in vivo* joint forces in the knee and hip, and did so with reliable accuracy. These same methodologies previously utilized have now been extended to the spine. However, many of the mathematical models for the spine have been developed based on generic musculoskeletal models and utilize optimization techniques to solve for joint and soft tissue forces [22,80, 100]. While other models have also been conducted which attempt to incorporate muscle co-contraction and activation patterns using EMG [27]. Hybrid type models also exist that combine both optimization and EMG methodologies [15, 16, 30]. However, none of these techniques have described a truly patient-specific model which utilizes unique kinematics and ground reaction forces for predicting loads in the spine.

In the current work, a non-invasive tool was developed to enable the determination of *in vivo* vertebral joint forces. In addition, the methodologies and results described here have established a basis for calculating relevant forces that correspond with force magnitudes and patterns collected using telemetry and pressure sensors. However, unlike telemetry, mathematical modeling of the lumbar spine can be applied to both native spine conditions as well as implanted intervertebral joints. In addition, mathematical models are capable of deriving the total load at a given spine level, whereas telemetry and pressure sensors are deficient in this regard. As a whole, the current research enables for a better understanding of the intervertebral joint forces

throughout the entire lumbar spine and helps in determining what parameters impact loading conditions. These methods provide more efficient ways for evaluating the lumbar spine and may contribute not only to future development of spinal prostheses designed to correct the dysfunctional segment, but also help explore more conservative therapies designed to prevent progressive and debilitating pathologies in the lower spine.

Chapter 8

Limitations and Future Work

In total, 44 subjects were stratified into six defined categories representing various conditions of the lumbar spine. However, because of the wide range of distinct clinical pathologies and treatment options which can be performed in multiple combinations at the different lumbar levels, enrollment of patients into categories which precisely represented the condition of the lumbar region was difficult. Initially, our goal was to enroll 10 patients into each lumbar classification group. However, over the course of this research study, patient enrollment in some of the groups proved to be challenging. As a result, some groups only included one or two patients and did not allow for statistical analyses, which are important for building strong evidence to support any findings. In addition, the enrollment parameters for each classification group should be well defined prevent ambiguities and create a much stronger data pool. To rectify these problems, a plan needs to be developed which details specific patient inclusion criteria for each of the enrollment groups. Specifically, more controlled requirements for age, clinical assessment scores, and pathologies at specified levels, as well as surgical intervention types should be well documented to enhance the outcomes for the study. Once these parameters are set, a stringent selection process should commence that seeks to increase the number of patients enrolled in each lumbar classification group. Implementation of these will hopefully

strengthen the data collected over the course of the study and allow for more definitive conclusions to be made.

Throughout this current work and many studies preceding it, fluoroscopy served as a valuable tool for evaluating any number of joints under in vivo, weight-bearing conditions. However, the complexity of the vertebral bone geometries coupled with greater tissue mass that x-ray must pass through to visualize the lower spine hinders the use of single-plane fluoroscopy. Coupled with the use of fluoroscopy is an important technique which requires precise registration of 3D bone models to 2D fluoroscopy images. Present methods are user-intensive and require ample amounts of time. Therefore, more advanced techniques such as the use of bi-planar fluoroscopy should be explored to determine if more characteristic features of the vertebra are visible and can aid the 3D-to-2D registration process. Further enhancements would be to update the registration algorithms that allow for more rapid registration without as much user intervention. This would also enable for more images to be captured from the dynamic motion video and possibly improve the resulting kinematics used as input for the developed mathematical model.

Additional improvements that is likely to enhance the understanding of the lumbar spine involves the analyses of the levels where the lumbar vertebrae interface with other areas of the spinal column. The current work evaluated only the portion of the lumbar spine between L5 and L1 vertebrae. However, inclusion of additional levels in the spine such as L5S1 and L1T12 may be beneficial for further development of the mathematical model and enhance the overall understanding of the how loads are transferred through the spinal column. Initially, this current study sought to analyze these spinal segments along with those between L5 and L1, but it was

soon discovered that our capabilities were limited by the size of the image intensifier and the field of view of the fluoroscopy C-Arm. In the future, as new technologies emerge, it may become possible to capture additional segments so as to include the entire low back architecture. This would enable for additional kinematic parameters to be derived and entered into the model, thereby possibly improving the prediction of the in vivo forces.

While the motions analyzed using fluoroscopy are important for deriving the kinematics at various levels of the vertebral column, effective methods that allow for better association and representation of the collected data at the joint level are essential. One suggested technique to aid in this process would be to capture the gross motions of the trunk during the prescribed activities. Since the kinematic patterns can vary considerably from patient to patient, collection of gross motion would allow for more effective normalization of the data for comparative purposes. Furthermore, the ranges-of-motion would be relatively simple to collect using a goniometer specifically designed to measure low back rotation. More advanced techniques may also be utilized such as the inertial measurement units attached to the back, which allow for tracking the position of the lower spine throughout an activity.

Many of the previously discussed limitations and future work have focused on enhancing practices for the collection and processing of data. Ultimately, these improvements impact the quality of data being input into the mathematical model. The current has shown to provide reliable methodologies for predicting joint reaction forces at each intervertebral level for any motion parameter defined by the user. However, the current model is the first step in advancing the understanding of the in vivo forces in the lumbar spine. Future enhancements for more closely approximating physiological conditions would be to change the way ligaments are

defined in the model. Currently, ligament tissues act as linear springs, using stiffness values, approximate cross-sectional areas, and initial slack lengths collected from the literature and input into the model. However, it is widely known that ligaments within the body exist as tough, fibrous collagen tissues that can best be modeled as viscoelastic materials. Under most normal conditions, ligaments function in the linear portion of the curve. However, instances may occur when the ligament is stretched beyond the linear zone, thereby generating greater forces. Conditions could also exist when the ligament is stretched beyond its elastic length and over time develops laxity. Implementing these simple changes may improve the model's accuracy and provide better explanations for the derived force patterns.

Additional improvements for modeling the lumbar region would be for the further development of understanding how the segments are loaded. This information would provide more relevant information for researchers developing finite element models of the spine and also enable for better correlation of clinical findings with forces at a particular location of a vertebral level. To implement this methodology, the interactive contact force which is currently defined at a single point on the body, could be decomposed to represent loading patterns at the intervertebral disc and on the articulating facet surfaces. However, using traditional Newtonian and Kane methods, likely will not enable for the large number of unknowns to be solved. Possible solutions would be to redefine the model using a number of assumptions and/or simplifications which allow for the derivation of equations that accurately represent the loading distributions on the vertebrae. These equations could then be equated using the variables solved for in the inverse model. Another possible solution may be to further implement the use of the pseudo-inverse methodology, which is currently utilized in the present model.

Finally, the methodologies for the development of the current lumbar mathematical model has yielded predicted lumbar forces which concur with existing literature reporting on the use of telemetry and pressure sensors to measure loads in the spine. However, it is important to have direct validation of the model and its predicted outputs. The best method currently available for verifying the calculated vertebral forces is through the use telemetrized implants. This type of analysis would allow for direct comparison of the calculated forces with magnitudes measured by the implant under in vivo conditions and provide important information for future iterations.

Bibliography

- [1] Abbott JH, Fritz JM, McCane B, *et al.* (2006). Lumbar segmental mobility disorders: comparison of two methods of defining abnormal displacement kinematics in a cohort of patients with non-specific mechanical low back pain. *BMC Musculoskelet Disord*, 7(45), doi:10.1186/1471-2474-7-45.
- [2] Adams, MA. (2004). Biomechanis of back pain. *Acupunct Med*, 22(4), 178-188.
- [3] Akamaru T, Kawahara N, Yoon T, *et al.* (2003). Adjacent Segment Motion After a Stimulated Lumbar Fusion in Different Sagittal Alignments. *Spine*, 28(14), 1560-1566.
- [4] Anderson PA, Rouleau JP. (2004). Intervertebral disc arthroplasty. *Spine*, 29(23), 2779-2786.
- [5] Antoniou J, Steffen T, Nelson F, *et al.* (1996). The human lumbar intervertebral disc: evidence for changes in the biosynthesis and denaturation of the extracellular matrix with growth, maturation, ageing, and degeneration. *J Clin Invest*, 98, 996-1003.
- [6] Auerbach JD, Wills BPD, McIntosh TC, *et al.* (2007). Evaluation of Spinal Kinematics Following Lumbar Total Disc Replacement and Circumferential Fusion Using In Vivo Fluoroscopy. *Spine*, 32(5), 527-536.
- [7] Axelsson P, Karlsson BS. (2005). Standardized Provocation of Lumbar Spine Mobility: Three Methods Compared by Radiostereometric Analysis. *Spine*, 30(7), 792-797.
- [8] Bakker EWP, Verhagen AP, van Trijffel E, *et al.* (2009). Spinal mechanical load as a risk factor for low back pain: a systematic review of prospective cohort studies. *Spine*, 34, E281-293.
- [9] Belkoff SM. (2007). *Biomechanics of the Spine*. Springer Berlin Heidelberg
- [10] Bogduk, N. (2005). *Clinical Anatomy of the Lumbar Spine and Sacrum* (4 ed.). Elsevier.
- [11] Burton AK, Battie MC, Gibbons L, *et al.* (1996). Lumbar disc degeneration and sagittal flexibility. *J Spinal Disord*, 9, 418-424.
- [12] Burton AK, Tillotson KM, Troup JDG (1989). Variation in lumbar sagittal mobility with low back troubles. *Spine*, 14, 584-590.
- [13] Busscher I, van Dieen JH, Kingma I, *et al.* (2009). Biomechanical Characteristics of Different Regions of the Human Spine. *Spine*, 34(26), 2858-2864.
- [14] Chen S, Zhong Z, Chen C, *et al.* (2009). Biomechanical comparison between lumbar disc arthroplasty and fusion. *Med Eng Phys*, 31, 244-253.

- [15] Cholewicki J, McGill SM, Norman RW. (1995). Comparison of Muscle Forces And Joint Load From An Optimiation and EMG Assisted Lumbar Spine Model: Towards Development Of A Hybrid Approach. *J Biomech*, 28(3), 321-331.
- [16] Cholewicki J, McGill SM. (1996). Mechanical stability of the in vivo lumbar spine: implications for injury and chronic low back pain. *Clin Biomech*, 11(1), 1-15.
- [17] Cresswell AG, Grundstrom H, Thorstensson A. (1992). Observations on intra-abdominal pressure and patterns of abdominal intra-muscular activity in man. *Acta Physiol Scand*, 144(4), 409-418.
- [18] Cunningham BW, Gordon JD, Dmitriev AE, *et al.* (2003). Biomechanical evaluation of total disc replacement arthroplasty: An in vitro human cadaveric model. *Spine*, 28, S110-S117.
- [19] Cunningham BW, Kotani Y, McNulty PS, *et al.* (1997). The Effect of Spinal Destabilization and Instrumentation on Lumbar Intradiscal Pressure: An In Vitro Biomechanical Analysis. *Spine*, 22(22), 2655-2663.
- [20] Dennis DA, Komistek RD, Hoff WA, *et al.* (1996). In vivo knee kinematics derived using an inverse perspective technique. *Clin Orthop Rel Rsh*, 331, 107-117.
- [21] Deyo RA, Weinstein JN. (2001). Low Back Pain. *New England J Med*, 344, 363-370.
- [22] De Zee M, Hansen L, Wong C, *et al.* (2007). A generic detailed rigid-body lumbar spine model. *J Biomech*, 40, 1219-1227.
- [23] Dooris AP, Goel VK, Grosland NM, *et al.* (2005). Load-sharing between anterior and posterior elements in a lumbar motion segment implanted with an artificial disc. *Spine*, 30(24), 2755-2764.
- [24] Dvorak J, Panjabi MM, Novotny JE, *et al.* (1991). Clinical validation of functional flexion-extension roentgenograms of the lumbar spine. *Spine*, 16, 943-950.
- [25] Dvorak J, Panjabi MM, Chang DG. *et al.* (1991). Functional radiographic diagnosis of the lumbar spine: Flexion-extension and lateral bending. *Spine*, 16, 562-571.
- [26] Edmondston SJ, Song S, Bricknell RV, *et al.* (2000). MRI evaluation of lumbar spine flexion and extension in asymptomatic individuals. *Manual Ther*, 5(3), 158-164.
- [27] El-Rich M, Shirazi-Adl A, Arjmand N. (2004). Muscle activity, internal loads, and stability of the human spine in standing postures: combined model and in vivo studies. *Spine*, 29(23), 2633-2642.

- [28] Esses S, Doherty BJ, Crawford MJ, *et al.* (1996). Kinematic Evaluation of Lumbar Fusion Techniques. *Spine*, 21(6), 676-684.
- [29] Fay L, Wu J, Tsai T, *et al.* (2012). Dynamic stabilization for degenerative spondylolisthesis: Evaluation of radiographic and clinical outcomes. *Clin Neurol Neurosurg*, <http://dx.doi.org/10.1016/j.clineuro.2012.05.036>.
- [30] Gagnon D, Lariviere C, Loisel P. (2001). Comparative ability of EMG, optimization, and hybrid modelling approaches to predict trunk muscle forces and lumbar spine loading during dynamic sagittal plane lifting. *Clin Biomech*, 16, 359-372.
- [31] Gertzbein SD, Seligman J, Holtby R, *et al.* (1985). Centrode patterns and segmental instability in degenerative disc disease. *Spine*, 10, 257-261.
- [32] Glaser, D. (2008). Mathematical Modeling, Vibration and Acoustic Emission Technique to Correlate In Vivo Kinematics, Kinetics and Sound in Total Hip Arthroplasty with Different Bearing Surfaces. (Unpublished doctoral dissertation). University of Tennessee, Knoxville, Tennessee.
- [33] Gomez, TT. (1994). Symmetry of lumbar rotation and lateral flexion range of motion and isometric strength in subjects with and without low back pain. *J Orthop Sports Phys Ther*, 19, 42-48.
- [34] Hall H, McIntosh G, Wilson L, *et al.* (1998). The spontaneous onset of back pain. *Clin J Pain*, 14, 129-133.
- [35] Hansen L, De Zee M, Rasmussen J, *et al.* (2006). Anatomy and Biomechanics of the Back Muscles in the Lumbar Spine with Reference to Biomechanical Modeling. *Spine*, 31(17), 1888-1899.
- [36] Harrop JS, Youssef JA, Maltenfort M, *et al.* (2008). Lumbar adjacent segment degeneration and disease after arthrodesis and total disc arthroplasty. *Spine*, 33(25), 1701-1707.
- [37] Hirsch C, Waugh T (1968). The Introduction of Force Measurements Guiding Instrumental Correction of Scoliosis. *Acta Orthop Scand*, 39, 136-144.
- [38] Inman V, Ralston H, De CM, *et al.* (1952). Relation of human electromyogram to muscular tension. *Electroencephal Clin Neurophysiol*, 4, 187-194.
- [39] Johnson MJ, Mahfouz M, Battaglia NV, *et al.* (2012). Clinical and statistical correlation of various lumbar pathological conditions. *J Biomech*, 46, 683-688.

- [40] Kane TR, Levinson DA. (1996). *Dynamics Online: Theory and Implementation with Autolev*. Sunnyvale, CA: Online Dynamics, Inc.
- [41] Knudson, D. (2003). *Fundamentals of Biomechanics*. New York, NY: Kluwer Academic/Plenum Publishers.
- [42] Komistek RD, Kane TR, Mahfouz M, *et al.* (2005). Knee mechanics: a review of past and present techniques to determine in vivo loads. *J Biomech*, 38, 215-228.
- [43] Komistek RD, Stiehl JB, Dennis DA, *et al.* (1998). Mathematical model of the lower extremity joint reaction forces using Kane's method of dynamics. *J Biomech*, 31, 185-189.
- [44] Kong WZ, Goel VK, Gilbertson LG, *et al.* (1996). Effects of muscle dysfunction on lumbar spine mechanics. A finite element study based on a two motion segments model. *Spine*, 21(19), 2197-2206.
- [45] Kozanke M, Wang S, Passias PG, *et al.* (2009). Range of Motion and Orientation of the Lumbar Facet Joints In Vivo. *Spine*, 34(19), E689-E696.
- [46] Kulig K, Powers CM, Landel RF, *et al.* (2007). Segmental lumbar mobility in individuals with low back pain: in vivo assessment during manual and self-imposed motion using dynamic MRI. *BMC Musculoskel Disord*, 8(8), doi:10.1186/1471-2474-8-8.
- [47] Lee BW, Lee J, Lee S, *et al.* (2011). Kinematic Analysis of the Lumbar Spine by Digital Videofluoroscopy in 18 Asymptomatic Subjects and 9 Patients With Herniated Nucleus Pulposus. *J Manip Physiol Ther*, 34(4), 221-230.
- [48] Lee, CK. (1988). Accelerated degeneration of the segment adjacent to a lumbar fusion. *Spine*, 13, 375-377.
- [49] Lee RYW, Laprade J, Fung EHK. (2003). A real-time gyroscopic system for three-dimensional measurement of lumbar spine motion. *Med Eng Phys*, 25, 817-824.
- [50] Li G, Wang S, Passias P, *et al.* (2009). Segmental in vivo vertebral motion during functional human lumbar spine activities. *Eur Spine J*, 18, 1013-1021.
- [51] Lim TH, Eck JC, An HS, *et al.* (1996). Biomechanics of transfixation in pedicle screw instrumentation. *Spine*, 21(19), 2224-2229.

- [52] Liu F. (2007). Theoretical Modeling and Experimental Validation of In Vivo Mechanics for Subjects Having Variable Cervical Spine Conditions (Unpublished doctoral dissertation). University of Tennessee, Knoxville, Tennessee.
- [53] Liu, F, Cheng J, Komistek RD, *et al.* (2007). In Vivo Evaluation of Dynamic Characteristics of the Normal, Fused, and Disc Replacement Cervical Spines. *Spine*, 32, 2578-2584.
- [54] Lorenz M, Patwardhan A, Vanderby R. (1983). Load Bearing Characteristics of Lumbar Facets in Normal and Surgically Altered Spinal Segments. *Spine*, 8(2), 122-130.
- [55] Lowery WD, Horn TJ, Boden SD, *et al.* (1992). Impairment evaluation based on spinal range of motion in normal subjects. *J Spinal Disord*, 5, 398-402.
- [56] Lund T, Nydegger T, Schlenzka D, *et al.* (2002). Three-Dimensional Motion Patterns During Active Bending in Patients with Chronic Low Back Pain. *Spine*, 27(17), 1865-1874.
- [57] Mahfouz MR, Hoff WA, Komistek RD, *et al.* (2003). A robust method for registration of three-dimensional knee implant models to two-dimensional fluoroscopy images. *IEEE: Trans Med Imaging*, 22, 1561-1574.
- [58] Mannion A, Troke M. (1999). A comparison of two motion analysis devices used in the measurement of lumbar spinal mobility. *Clin Biomech*, 14, 612-619.
- [59] Mageswaran P, Techy F, Colbrunn RW, *et al.* (2012). Hybrid dynamic stabilization: A biomechanical assessment of adjacent and suprajacent levels of the lumbar spine. *J Neurosurg Spine*, 17, 232-242.
- [60] Morris JM, Lucas DB, Bresler B. (1961). The role of the trunk in the stability of the spine. *J Bone Joint Surg*, 43, 327.
- [61] Nabhani F, Wake M. (2002). Computer modelling and stress analysis of the lumbar spine. *J Mater Process Technol*, 127(1), 40-47.
- [62] Nachemson A, Morris JM. (1964). In Vivo Measurement of Intradiscal Pressure. *JBJS*, 45(5), 1077-1092.
- [63] Nachemson A. (1965). The Effect of Forward Leaning on Lumbar Intradiscal Pressure. *Acta Orthop Scandinav*, 35, 314-328.
- [64] Nachemson A. (1976). The Lumbar Spine An Orthopaedic Challenge. *Spine*, 1(1), 59-71.

- [65] Natarajan RN, Andersson GBJ, Patwardhan AG, *et al.* (2002). Effect of annular incision type on the change in the biomechanical properties in a herniated lumbar intervertebral disc. *J Biomech Eng*, 124(2), 229-236.
- [66] Nattrass CL, Nitschke JE, Disler PB, *et al.* (1999). Lumbar spine range of motion as a measure of physical and functional impairment: An investigation of validity. *Clin Rehab*, 13, 211-218.
- [67] Nelson J, O'Neil C, Richardson CJ. (December 2011). *Treatment of Low Back Pain Exploring the Costs*. Retrieved from Healthy & Wellness: <http://www.resultsphysiotherapy.com/treatment-of-low-back-pain>
- [68] Niosi CA, Zhu QA, Wilson DC, *et al.* (2006). Biomechanical characterization of the three-dimensional kinematic behavior of the Dynesys dynamic stabilization system: an in vitro study. *Eur Spine J*, 15, 913-922.
- [69] Ohta H, Matsumoto Y, Morishita Y, *et al.* (2011). Surgical results of dynamic nonfusion stabilization with the Segmental Spinal Correction System for degenerative lumbar spinal diseases with instability: Minimum 2-year follow-up. *SAS J*, 5, 69-74.
- [70] Okawa A, Shinomiya K, Komori H, *et al.* (1998). Dynamic motion study of the whole lumbar spine by vidofluoroscopy. *Spine*, 23, 1743-1749.
- [71] Ordway NR, Fayyazi AH, Abjornson C, *et al.* (2008). Twelve-Month Follow-up of Lumbar Spine Range of Motion Following Intervertebral Disc Replacement Using Radiostereometric Analysis. *SAS J*, 2, 9-15.
- [72] Panjabi, MM. (2003). Clinical spinal instability and low back pain. *J Electromyogr Kinesiol*, 13, 371-379.
- [73] Panjabi MM, Krag MH, Chung TQ (1984). Effects of disc injury on mechanical behavior of the lumbar spine. *Spine*, 9, 707-713.
- [74] Panjabi MM, Oxland TR, Lin RM, *et al.* (1994). Thoracolumbar burst fracture: A biomechanical investigation of its multidirectional flexibility. *Spine*, 19, 578-585.
- [75] Park S, Fayyazi AH, Yonemura KS, *et al.* (2012). An in vivo kinematic comparison of dynamic lumbar stabilization to lumbar disectomy and posterior lumbar fusion using radiostereometric analysis. *International Society Adv Spine Surg*, doi:10.1016/j.ijsp.2012.02.003.

- [76] Park S, Ordway NR, Fayyazi AH, *et al.* (2009). Comparison of Cobb Technique, Quantative Motion Analysis, and Radiostereometric Analysis in Measurement of Segmental Range of Motions After Lumbar Total Disc Arthroplasty. *J Spinal Disord Tech*, 22, 602-609.
- [77] Pearcy MJ, Tibrewal SB. (1984). Axial rotation and lateral bending in the normal lumbar spine measured by three-dimensional radiography. *Spine*, 9(6), 582-587.
- [78] Pearsall DJ, Reid JG, Livingston LA. (1996). Segmental Inertial Parameters of the Human Trunk as Determined from Computed Tomography. *Ann Biomed Eng*, 24, 198-210.
- [79] Pintar FA, Yoganandan N, Myers T, *et al.* (1992). Biomechanical Properties of Human Lumbar Spine Ligaments. *J Biomech*, 25(11), 1351-1356.
- [80] Rasmussen J, Damsgaard M, Voigt M. (2001). Muscle recruitment by the min/max criterion - a comparative numerical study. *J Biomech*, 34, 409-415.
- [81] Roffey DM, Wai EK, Bishop P, *et al.* (2010). Causal assessment of awkward occupational postures and low back pain: results of a systematic review. *Spine J*, 10, 89-99.
- [82] Rohlmann A, Graichen F, Weber U, *et al.* (2000). Monitoring In Vivo Implant Loads With a Telemeterized Internal Spinal Fixation Device. *Spine*, 25(23), 2981-2986.
- [83] Rohlmann A, Graichen F, Kayser R, *et al.* (2008). Loads on a Telemeterized Vertebral Body Replacement Measured in Two Patients. *Spine*, 33(11), 1170-1179.
- [84] Rohlmann A, Peterson R, Schwachmeyer V, *et al.* (2012). Spinal loads during position changes. *Clin Biomech*, doi:10.1016/j.clinbiomech.2012.04.006.
- [85] Rohlmann A, Zander T, Bergmann G. (2006). Spinal loads after osteoporotic vertebral fractures treated by vertebroplasty or kyphoplasty. *Eur Spine J*, 15(8), 1255-1264.
- [86] Rohlmann A, Zander T, Graichen F, *et al.* (2011). Measured loads on a vertebral body replacement during sitting. *Spine J*, 11, 870-875.
- [87] Rohlmann G, Graichen F, Bender A, *et al.* (2008). Loads on a telemeterized vertebral body replacement measured in three patients with the first postoperative month. *Clin Biomech*, 23, 147-158.
- [88] Rozumalski A, Schwartz MH, Wervej R, *et al.* (2008). The in vivo three-dimensional motion of the human lumbar spine during gait. *Gait Posture*, 28, 378-384.

- [89] Rubin, DI. (2007). Epidemiology and Risk Factors for Spine Pain. *Neurol Clin*, 25, 353-371.
- [90] Sairyo K, Goel VK, Masuda A, *et al.* (2005). Biomechanical rationale of endoscopic decompression for lumbar spondylolysis as an effective minimally invasive procedure - A study based on the finite element analysis. *Minim Invasive Neurosurg*, 48(2), 119-122.
- [91] Sato K, Kikuchi S, Yonezawa T. (1999). In Vivo Intradiscal Pressure Measurements in Healthy Individuals and in Patients With Ongoing Back Problems. *Spine*, 24(23), 2468-2474.
- [92] Schache AG, Blanch P, Rath D, *et al.* (2002). Three-dimensional angular kinematics of the lumbar spine and pelvis during running. *Hum Mov Sci*, 21, 273-293.
- [93] Schoenfeld, AJ. (2011). Adjacent segment degeneration after lumbar spinal fusion: risk factors and implications for clinical practice. *Spine J*, 11, 21-23.
- [94] Sears WR, Sergides IG, Kazemi N, *et al.* (2011). Incidence and prevalence of surgery at segments adjacent to a previous posterior lumbar arthrodesis. *Spine J*, 11, 11-20.
- [95] Sharma A. (2008). Development of a Computational Model to Predict the In Vivo Contact Mechanics of Modern Total Knee Arthroplasty. (Unpublished doctoral dissertation). University of Tennessee, Knoxville, Tennessee
- [96] Sim HB, Murovic JA, Cho BY, *et al.* (2010). Biomechanical comparison of single-level posterior versus transforaminal lumbar interbody fusions with bilateral pedicle screw fixation: segmental stability and the effects on adjacent motion segments. *J Neurosurg Spine*, 12, 700-708.
- [97] Slosar PJ, Reynolds JB, Schofferman JS, *et al.* (2000). Patient Satisfaction After Circumferential Lumbar Fusion. *Spine*, 25(6), 722-726.
- [98] Soni A. (July 2010). *Back Problems: Use and Expenditures for the U.S. Adult Population, 2007. Statistical Brief #289*. Retrieved from Agency for Healthcare Research and Quality: http://www.meps.ahrq.gov/mepsweb/data_files/publications/st289/stat289.pdf
- [99] Steffen T, Rubin RK, Baramki HG, *et al.* (1997). A New Technique for Measuring Lumbar Segmental Motion In Vivo: Method, Accuracy, and Preliminary Results. *Spine*, 22(2), 156-166.

- [100] Stokes IA, Gardner-Morse M. (1994). Lumbar Spine Maximum Efforts And Muscle Recruitment Patterns Predicted By A Model With Multijoint Muscles and Joints With Stiffness. *J Biomech*, 28(2), 173-186.
- [101] Stokes IAF, Iatridis JC. (2004). Mechanical Conditions That Accelerate Intervertebral Disc Degeneration: Overload Versus Immobilization. *Spine*, 29(23), 2724-2732.
- [102] Sullivan MS, Dickinson CE, Troup JDG. (1994). The influence of age and gender on lumbar spine sagittal plane range of motion. *Spine*, 19, 682-686.
- [103] Thompson RE, Pearcy MJ, Downing KJ, *et al.* (2000). Disc lesions and the mechanics of the intervertebral joint complex. *Spine*, 25, 3026-3035.
- [104] Turner JA, Ersek M, Herron L, *et al.* (1992). Patient Outcomes After Lumbar Spinal Fusions. *JAMA*, 268(7), 907-911.
- [105] Untch C, Liu D, Hart R. (2004). Segmental Motion Adjacent to an Instrumented Lumbar Fusion. *Spine*, 29(21), 2376-2381.
- [106] Van Herp G, Rowe P, Salter P, *et al.* (2000). Three-dimensional lumbar spinal kinematics: a study of range of movement in 100 healthy subjects aged 20 to 60+ years. *Rheumatology*, 39, 1337-1340.
- [107] Waddell G, Somervill D, Henderson I, *et al.* (1992). Objective clinical evaluation of physical impairment in chronic low back pain. *Spine*, 17, 617-628.
- [108] Waugh TR. (1966). Intravital Measurements During Instrumental Correction of Idiopathic Scoliosis. *Acta Orthop Scand*, 93.
- [109] White AA, Panjabi MM. (1990). *Clinical Biomechics of the Spine* (2nd ed.). Lippincott Williams & Wilkins.
- [110] Whittle MW, Levine D. (1997). Measurement of lumbar lordosis as a component of clinical gait analysis. *Gait Posture*, 5, 101-107.
- [111] Wigfield C, Gill S, Nelson R, *et al.* (2002). Influence of an artificial cervical joint compared with fusion on adjacent-level motion in the treatment of degenerative cervical disc disease. *J Neurosurg Spine*, 96, 17-21.
- [112] Wilke H, Neff P, Hinz B, *et al.* (2001). Intradiscal pressure together with anthropometric data - a data set for the validation of models. *Clin Biomech*, 16(Supplement No. 1), S111-S126.

- [113] Yamaguchi GT, Moran D, Si J. (1995). A computationally efficient method for solving the redundant problem in biomechanics. *J Biomech*, 28(8), 999-1005.
- [114] Yamaguchi, G. (2005). *Dynamic modeling of musculoskeletal motion: a vectorized approach for biomechanical analysis in three dimensions*. Springer Verlag.
- [115] Yamamoto I, Panjabi MM, Crisco T, *et al.* (1989). Three-Dimensional Movements of the Whole Lumbar Spine and Lumbosacral Joint. *Spine*, 14(11), 1256-1260.
- [116] Yoganandan N, Kumaresan S, Pintar FA. (2001). Biomechanics of the cervical spine Part 2. Cervical spine soft tissue responses and biomechanical modeling. *Clin Biomech*, 16(1), 1-27.
- [117] Youdas JW, Hollman JH, Krause DA. (2006). The effects of gender, age, and body mass index on standing lumbar curvature in persons without current low back pain. *Physiother Theory Pract*, 22(5), 229-237.
- [118] Zander T, Rohlmann A, Burra NK, *et al.* (2006). Effect of a posterior dynamic implant adjacent to a rigid spinal fixator. *Clin Biomech*, 21(8), 767-774.
- [119] Zander T, Rohlmann A, Bergmann G. (2009). Influence of different artificial disc kinematics on spine biomechanics. *Clin Biomech*, 24(2), 135-142.
- [120] Zander T, Rohlmann A, Calisse J, *et al.* (2001). Estimation of muscle forces in the lumbar spine during upper-body inclination. *Clin Biomech*, 16(Supplement No. 1), S73-S80.

Appendix

Detailed Analysis of Patients' Results

A.1 Patient 1H

Age: 30 years

Gender: Male

Height: 1.78 m

Mass: 70 kg

Condition: Healthy

A.1.1 Flexion-Extension Activity

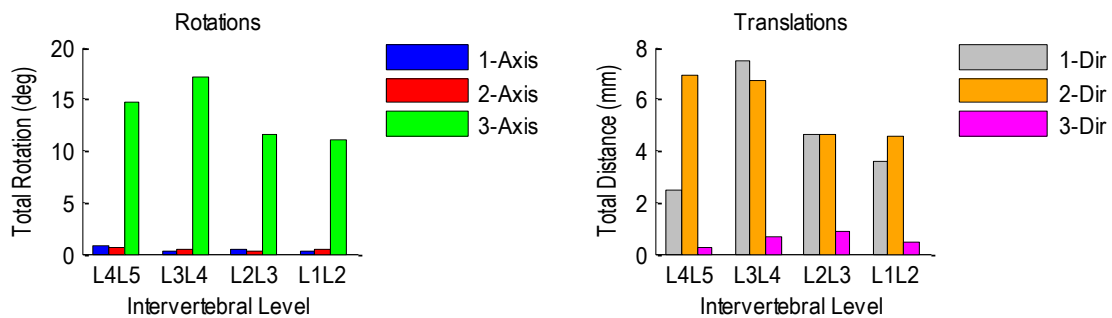


Figure A.1 Patient 1H relative rotations (left) and translations (right) at each vertebral level during flexion-extension.

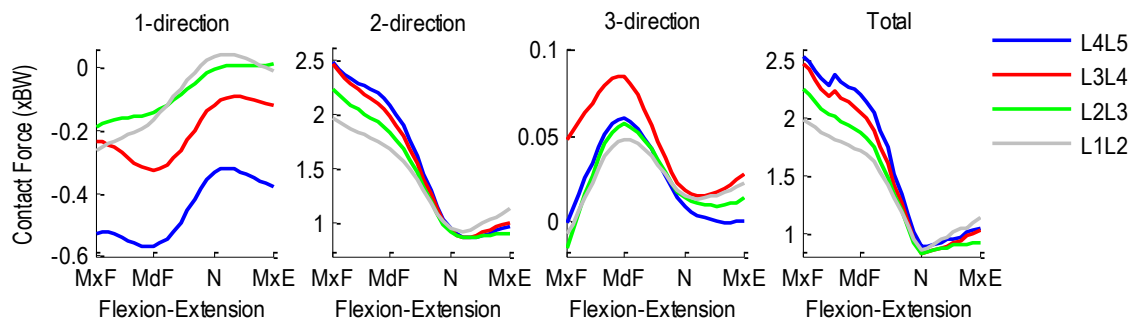


Figure A.2 Patient 1H intervertebral contact forces normalized with respect to body weight during flexion-extension. 1-dir=Ant(+)/Post(-), 2-dir=Sup(+)/Inf(-), 3-dir=Rt(+)/Lt(-).

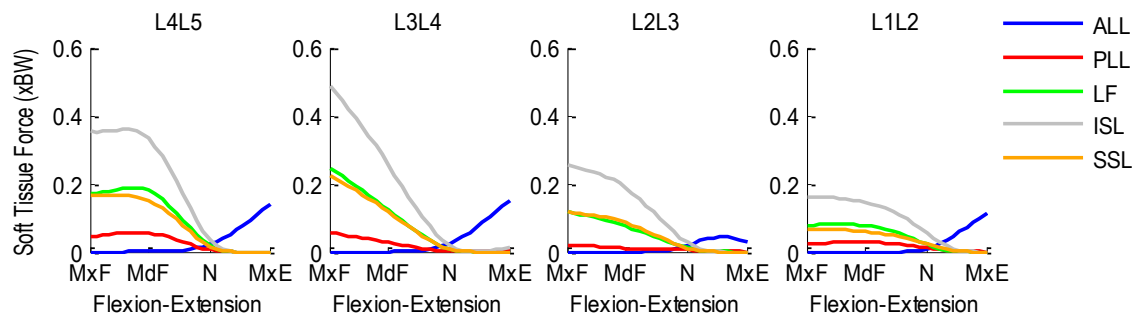


Figure A.3 Patient 1H segmental ligament forces normalized with respect to body weight during flexion-extension.

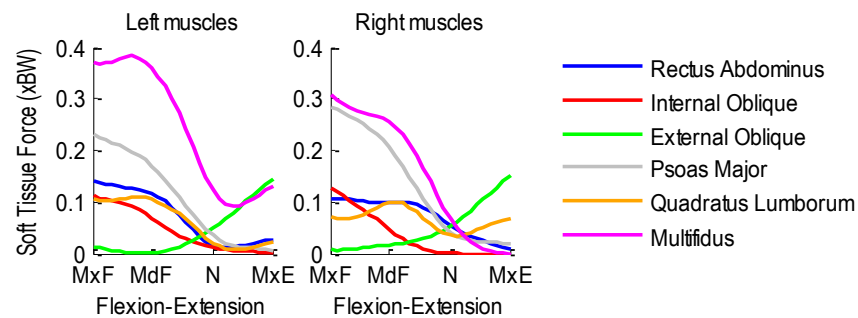


Figure A.4 Patient 1H bilateral muscle forces normalized with respect to body weight during flexion-extension.

A.1.2 Lateral Flexion Activity

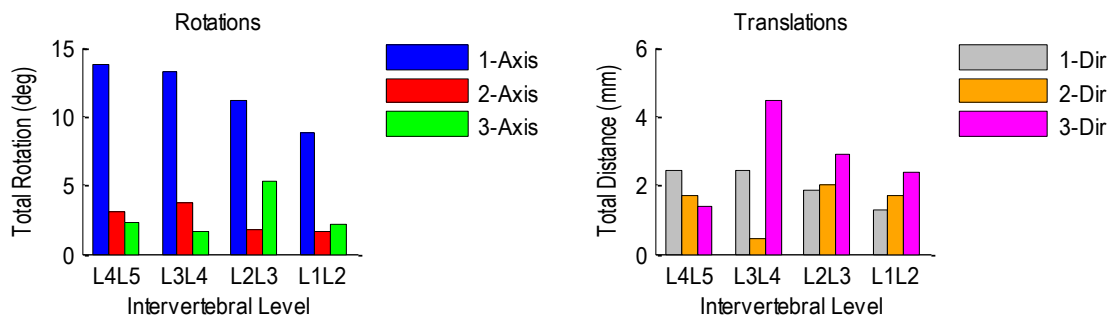


Figure A.5 Patient 1H relative rotations (left) and translations (right) at each vertebral level during lateral flexion.

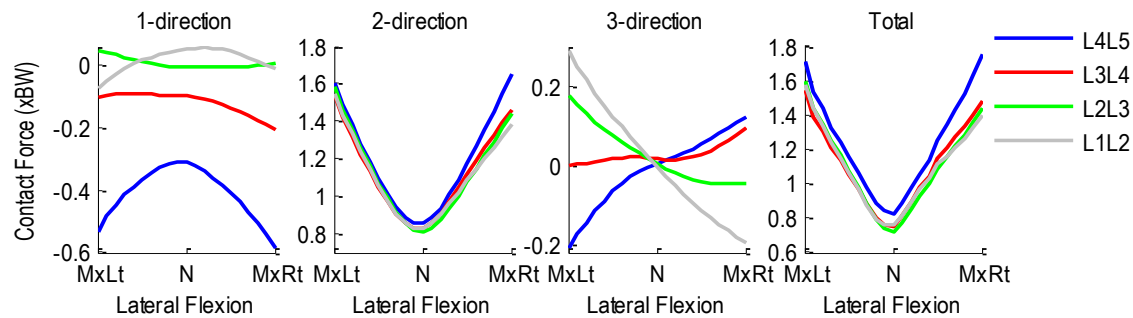


Figure A.6 Patient 1H intervertebral contact forces normalized with respect to body weight during right-to-left lateral flexion. 1-dir=Ant(+)/Post(-), 2-dir=Sup(+)/Inf(-), 3-dir=Rt(+)/Lt(-).

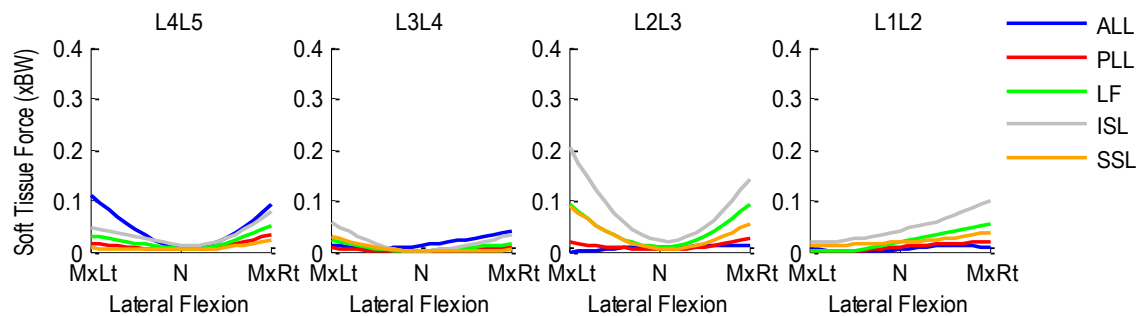


Figure A.7 Patient 1H segmental ligament forces normalized with respect to body weight during left-to-right lateral flexion.

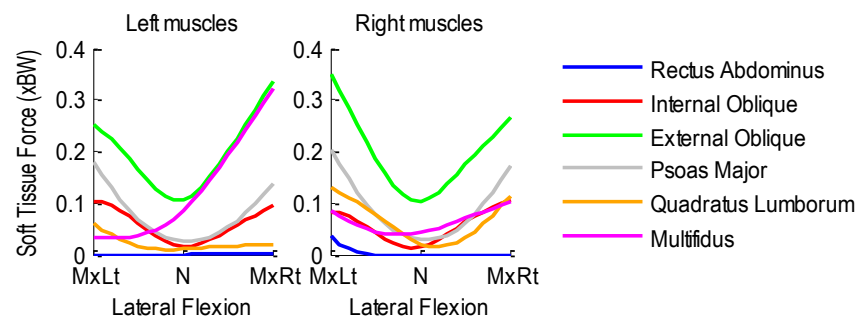


Figure A.8 Patient 1H bilateral muscle forces normalized with respect to body weight during left-to-right lateral flexion.

A.1.3 Axial Rotation Activity

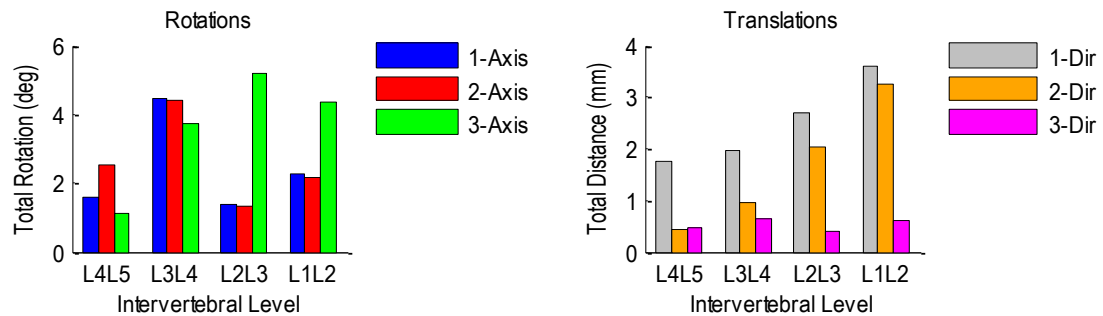


Figure A.9 Patient 1H relative rotations (left) and translations (right) at each vertebral level during axial rotation.

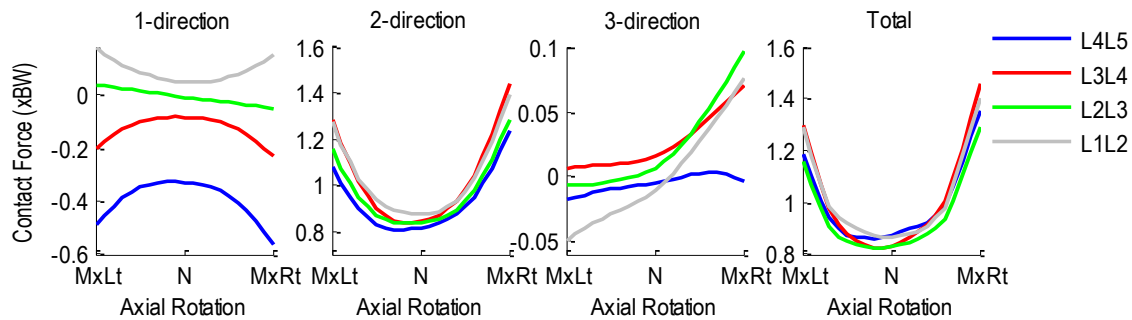


Figure A.10 Patient 1H intervertebral contact forces normalized with respect to body weight during left-to-right axial rotation. 1-dir=Ant(+)/Post(-), 2-dir=Sup(+)/Inf(-), 3-dir=Rt(+)/Lt(-).

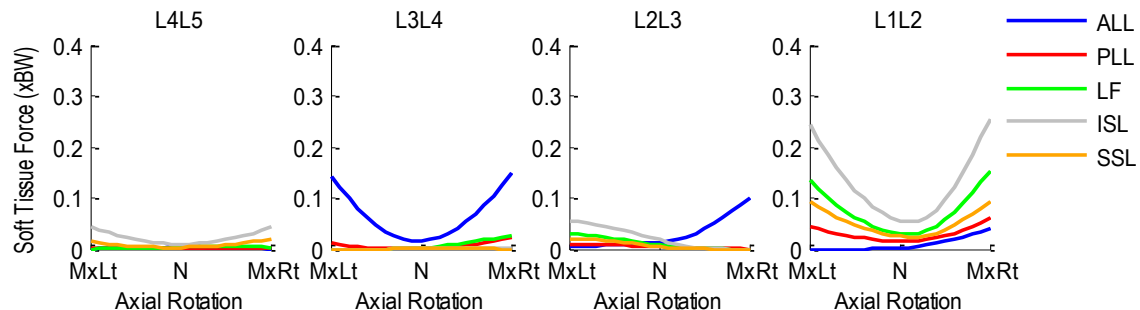


Figure A.11 Patient 1H segmental ligament forces normalized with respect to body weight during left-to-right axial rotation.

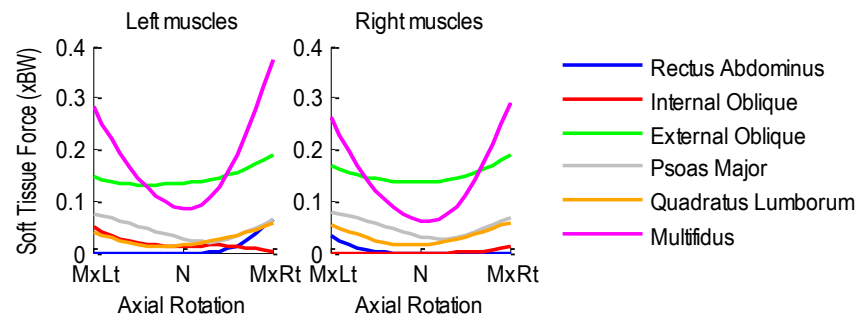


Figure A.12 Patient 1H bilateral muscle forces normalized to body weight during left-to-right axial rotation.

A.2 Patient 2H

Age: 37 years

Gender: Female

Height: 1.70 m

Mass: 73 kg

Condition: Healthy

A.2.1 Flexion-Extension Activity

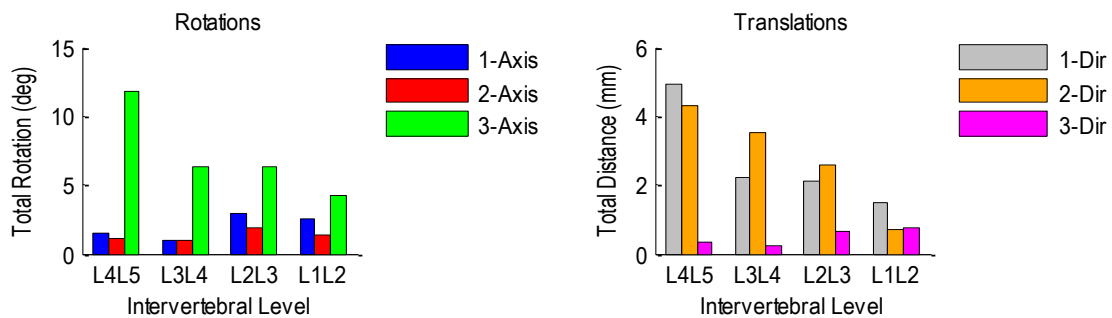


Figure A.13 Patient 2H relative rotations (left) and translations (right) at each vertebral level during flexion-extension.

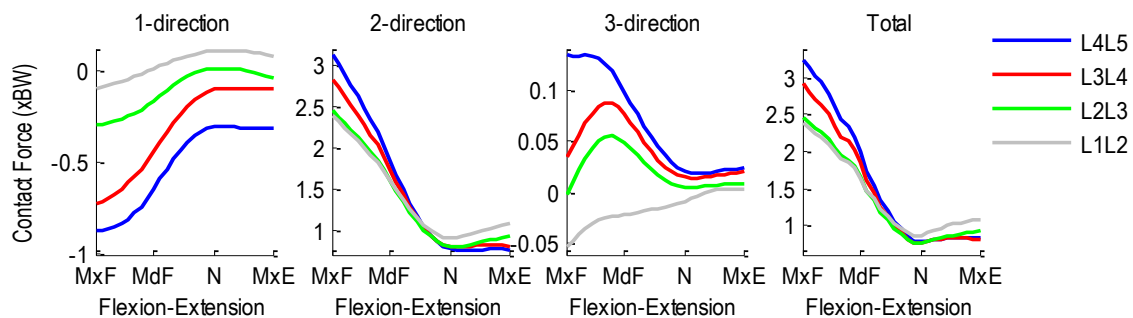


Figure A.14 Patient 2H intervertebral contact forces normalized with respect to body weight during flexion-extension. 1-dir=Ant(+)/Post(-), 2-dir=Sup(+)/Inf(-), 3-dir=Rt(+)/Lt(-).

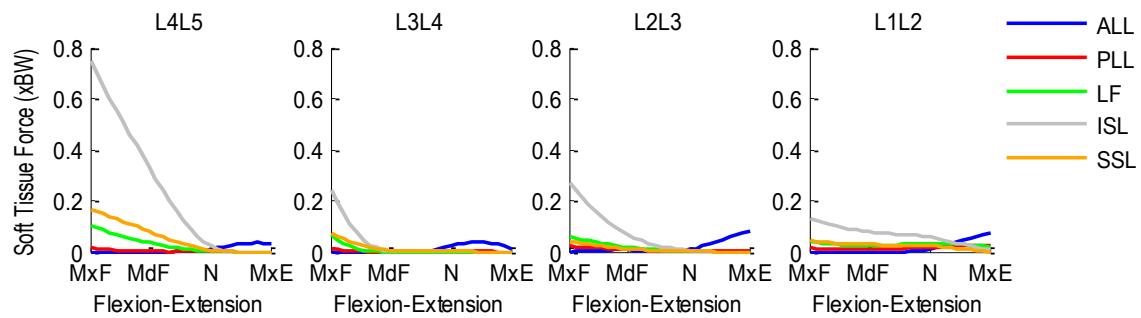


Figure A.15 Patient 2H segmental ligament forces normalized with respect to body weight during flexion-extension.

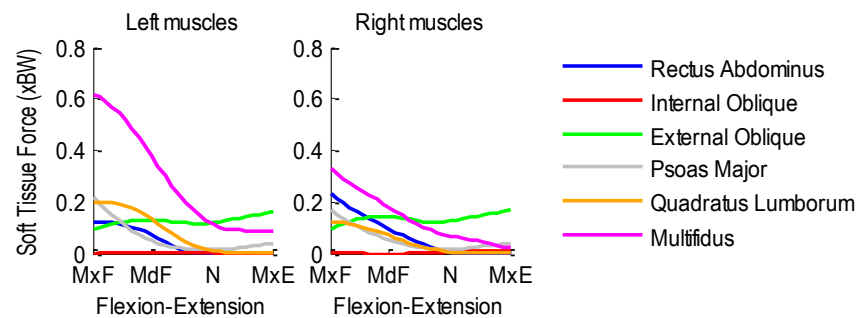


Figure A.16 Patient 2H bilateral muscle forces normalized with respect to body weight during flexion-extension.

A.2.2 Lateral Flexion Activity

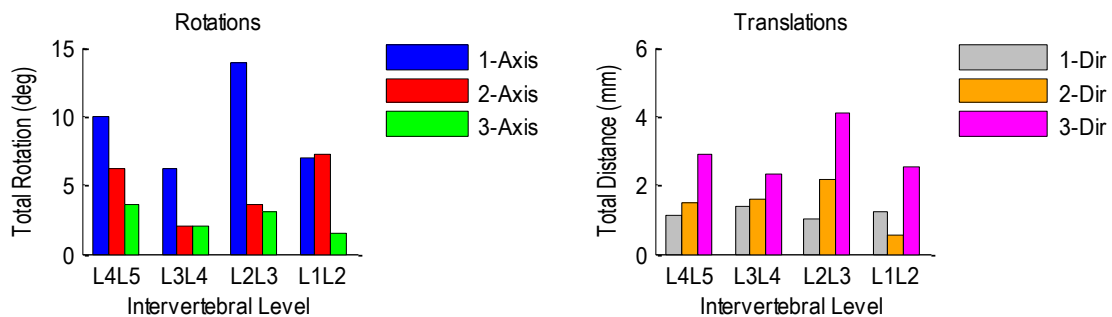


Figure A.17 Patient 2H relative rotations (left) and translations (right) at each vertebral level during left-to-right lateral flexion.

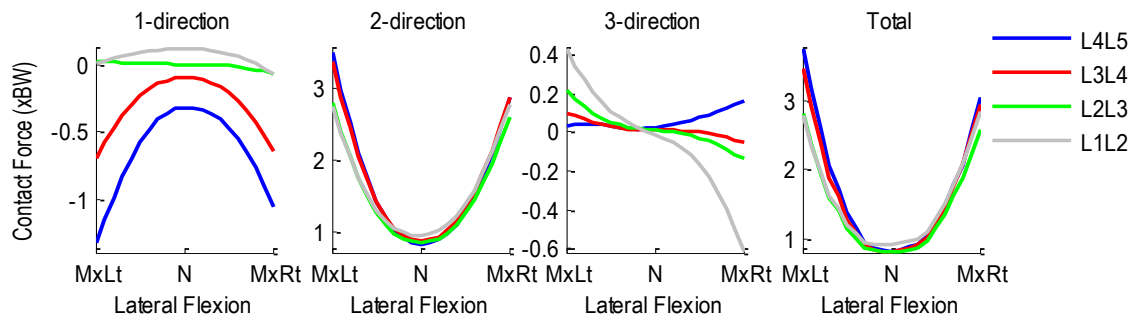


Figure A.18 Patient 2H intervertebral contact forces normalized with respect to body weight during right-to-left lateral flexion. 1-dir=Ant(+)/Post(-), 2-dir=Sup(+)/Inf(-), 3-dir=Rt(+)/Lt(-).

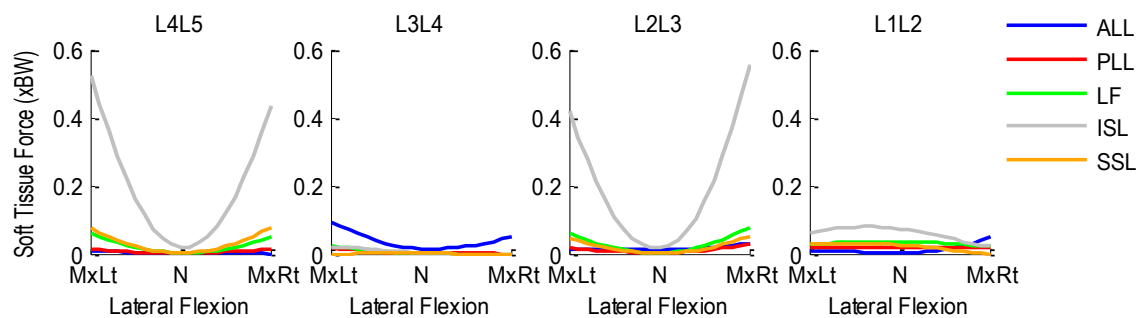


Figure A.19 Patient 2H segmental ligament forces normalized with respect to body weight during left-to-right lateral flexion.

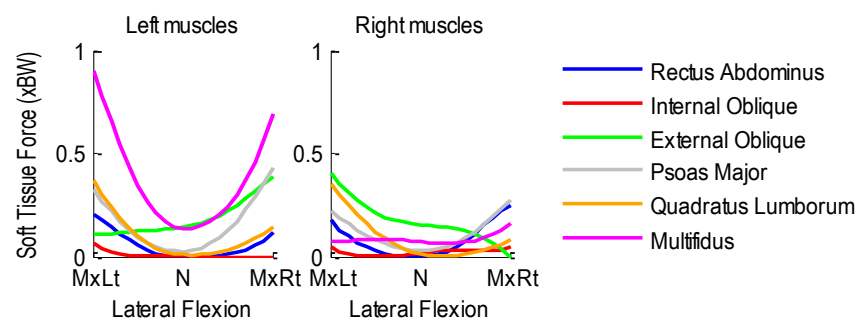


Figure A.20 Patient 2H bilateral muscle forces normalized with respect to body weight during left-to-right lateral flexion.

A.2.3 Axial Rotation Activity

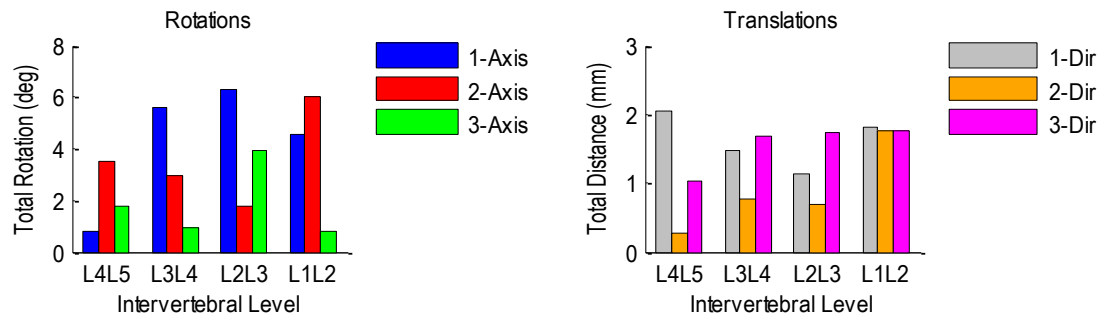


Figure A.21 Patient 2H relative rotations (left) and translations (right) at each vertebral level during left-to-right axial rotation.

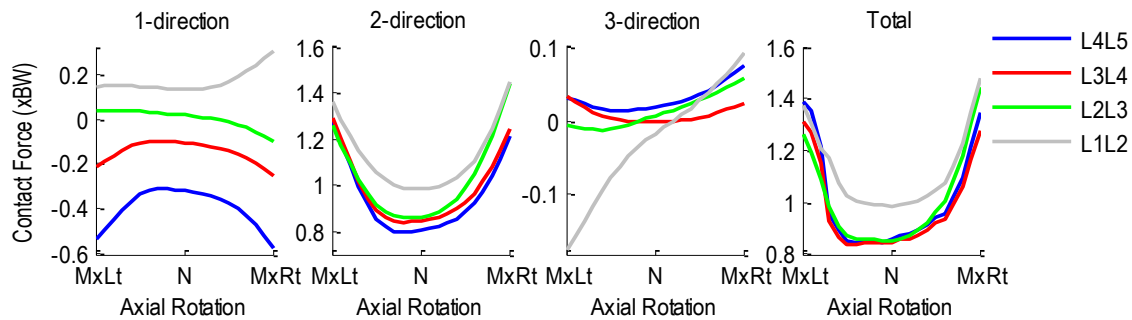


Figure A.22 Patient 2H intervertebral contact forces normalized with respect to body weight during left-to-right axial rotation. 1-dir=Ant(+)/Post(-), 2-dir=Sup(+)/Inf(-), 3-dir=Rt(+)/Lt(-).

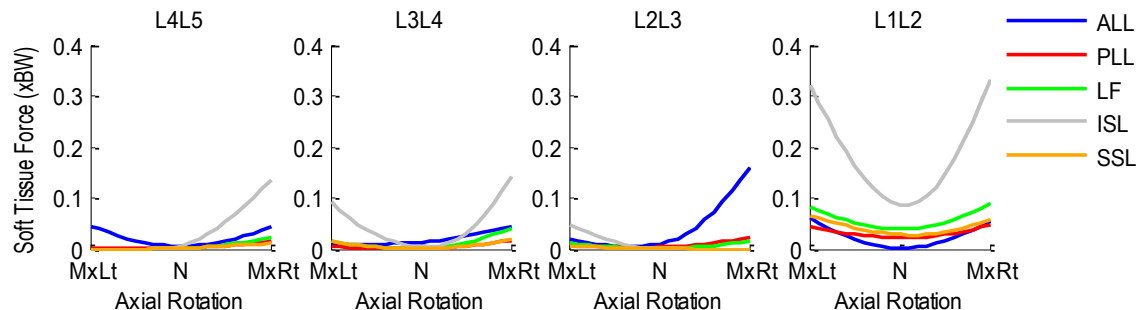


Figure A.23 Patient 2H segmental ligament forces normalized with respect to body weight during left-to-right axial rotation.

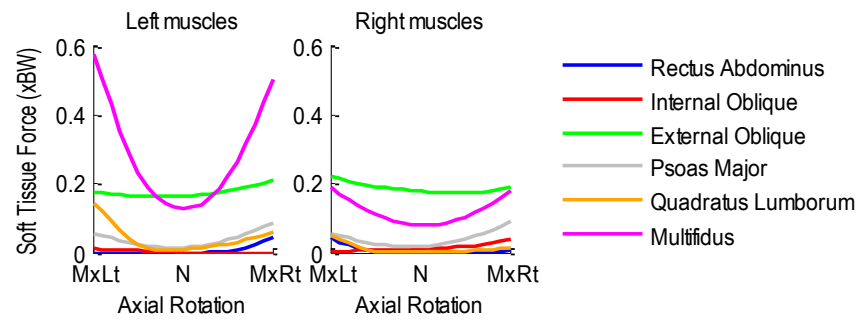


Figure A.24 Patient 2H bilateral muscle forces normalized to body weight during left-to-right axial rotation.

A.3 Patient 3H

Age: 30 years

Gender: Male

Height: 1.78 m

Mass: 84 kg

Condition: Healthy

A.3.1 Flexion-Extension Activity

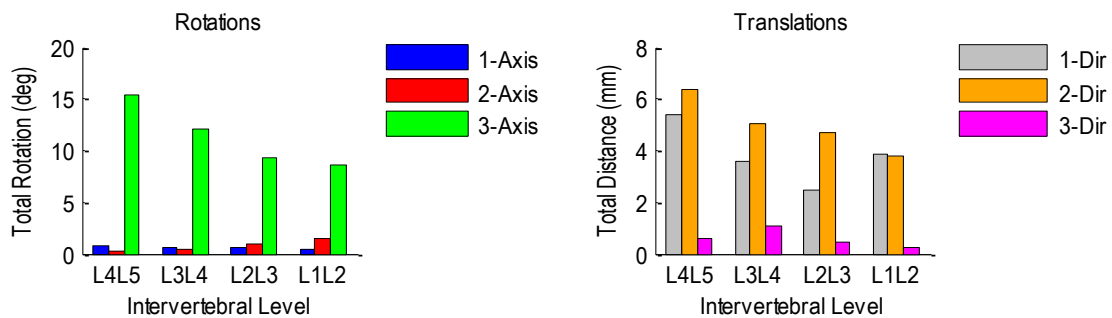


Figure A.25 Patient 3H relative rotations (left) and translations (right) at each vertebral level during flexion-extension.

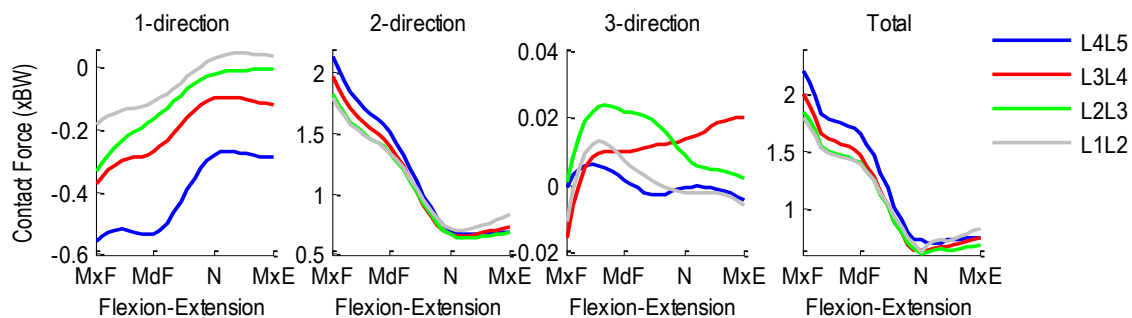


Figure A.26 Patient 3H intervertebral contact forces normalized with respect to body weight during flexion-extension. 1-dir=Ant(+)/Post(-), 2-dir=Sup(+)/Inf(-), 3-dir=Rt(+)/Lt(-).

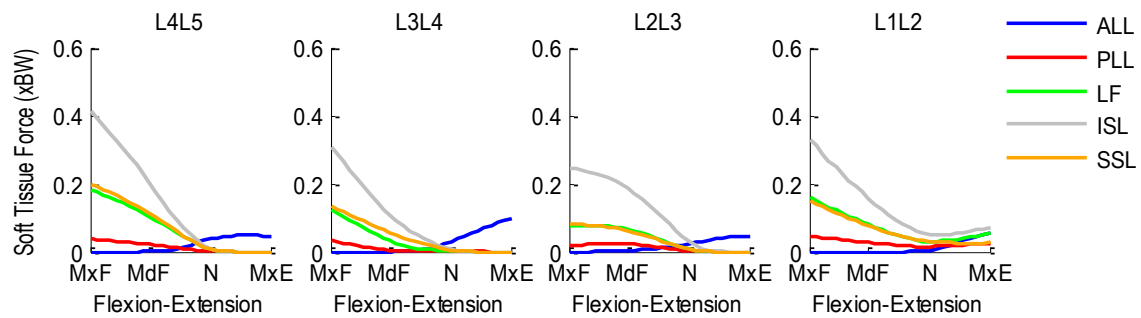


Figure A.27 Patient 3H segmental ligament forces normalized with respect to body weight during flexion-extension.

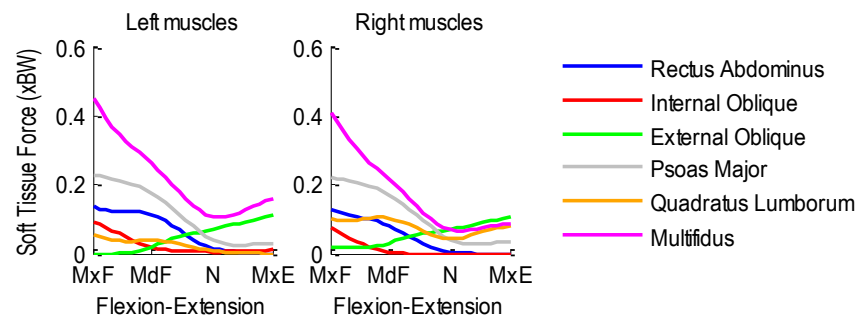


Figure A.28 Patient 3H bilateral muscle forces normalized with respect to body weight during flexion-extension.

A.3.2 Lateral Flexion Activity

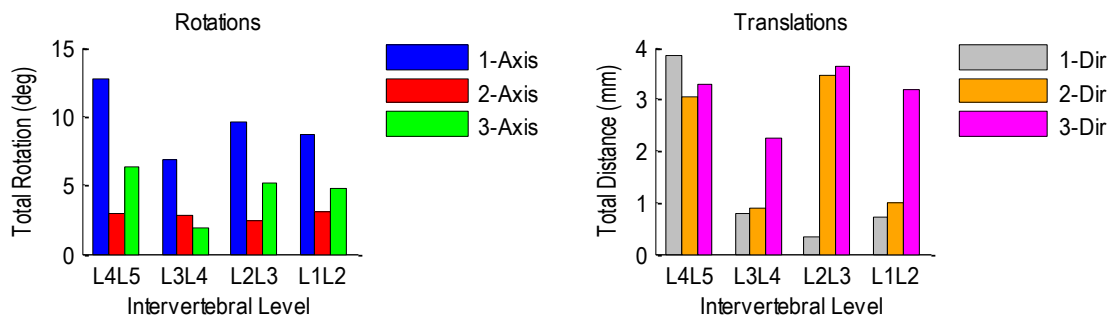


Figure A.29 Patient 3H relative rotations (left) and translations (right) at each vertebral level during left-to-right lateral flexion.

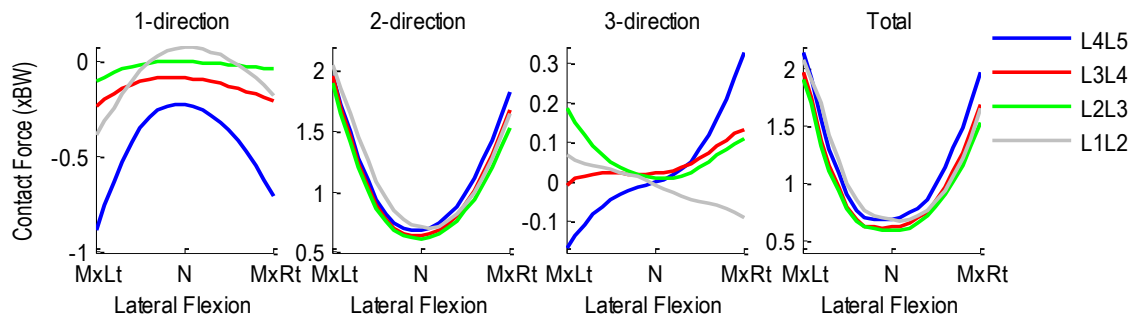


Figure A.30 Patient 3H intervertebral contact forces normalized with respect to body weight during right-to-left lateral flexion. 1-dir=Ant(+)/Post(-), 2-dir=Sup(+)/Inf(-), 3-dir=Rt(+)/Lt(-).

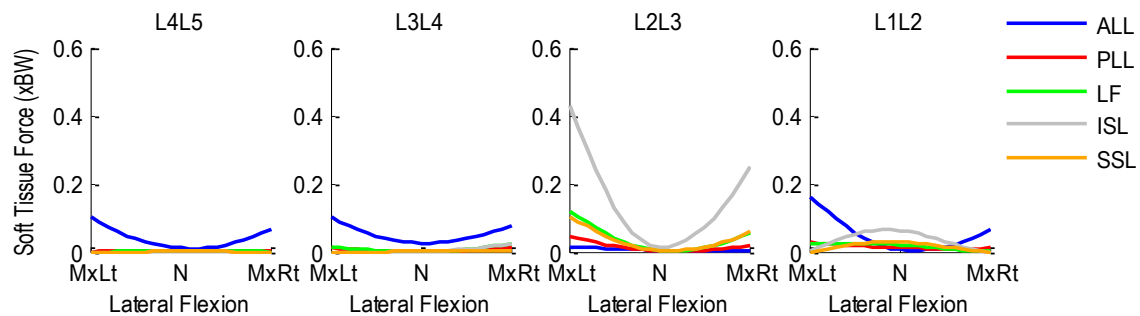


Figure A.31 Patient 3H segmental ligament forces normalized with respect to body weight during left-to-right lateral flexion.

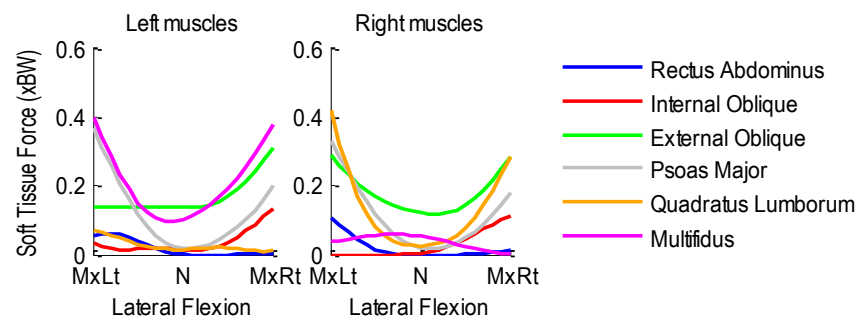


Figure A.32 Patient 3H bilateral muscle forces normalized with respect to body weight during left-to-right lateral flexion.

A.3.3 Axial Rotation Activity

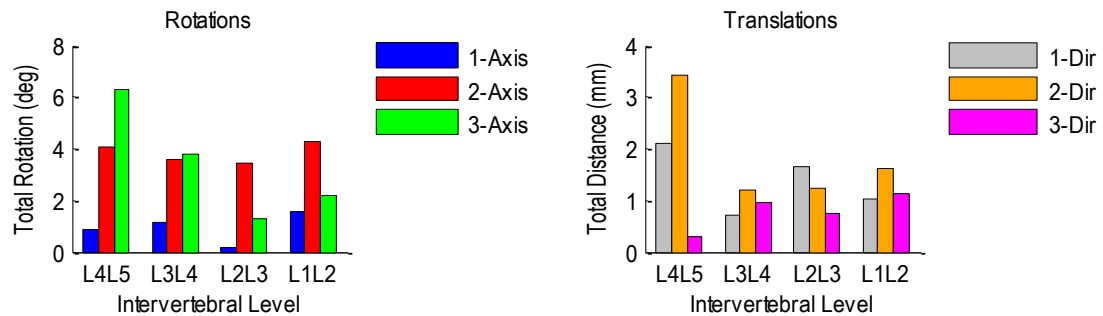


Figure A.33 Patient 3H relative rotations (left) and translations (right) at each vertebral level during left-to-right axial rotation.

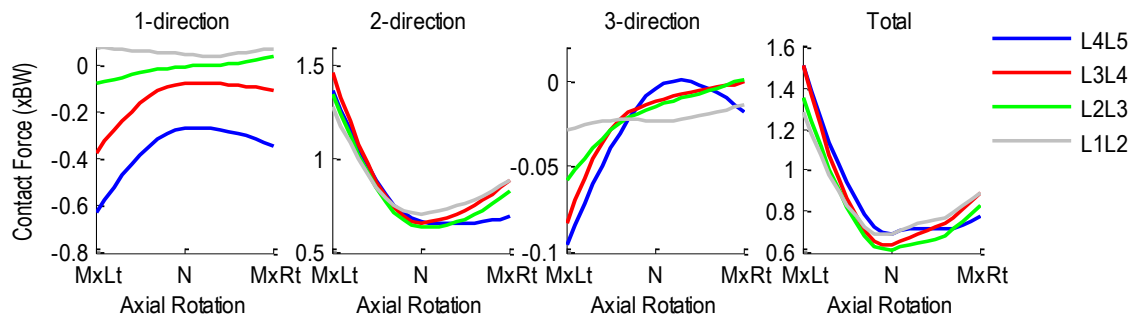


Figure A.34 Patient 3H intervertebral contact forces normalized with respect to body weight during left-to-right axial rotation. 1-dir=Ant(+)/Post(-), 2-dir=Sup(+)/Inf(-), 3-dir=Rt(+)/Lt(-).

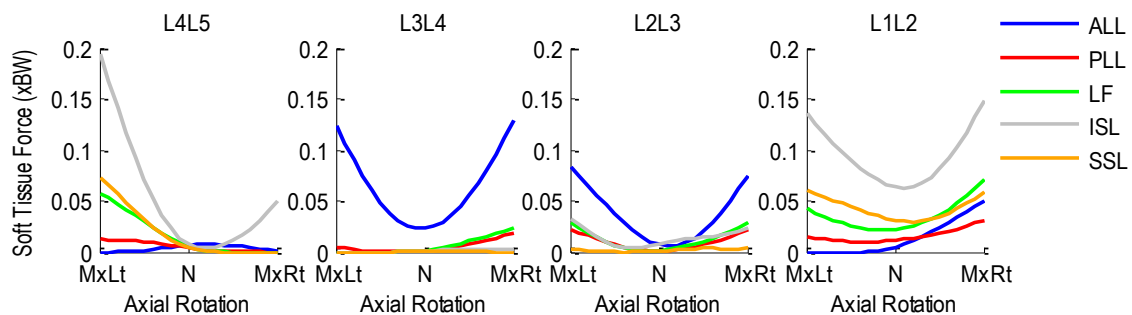


Figure A.35 Patient 3H segmental ligament forces normalized with respect to body weight during left-to-right axial rotation.

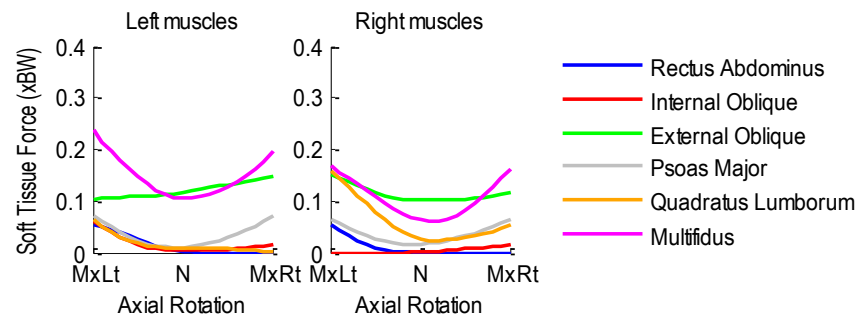


Figure A.36 Patient 3H bilateral muscle forces normalized to body weight during left-to-right axial rotation.

A.4 Patient 4H

Age: 50 years

Gender: Female

Height: 1.70 m

Mass: 84 kg

Condition: Healthy

A.4.1 Flexion-Extension Activity

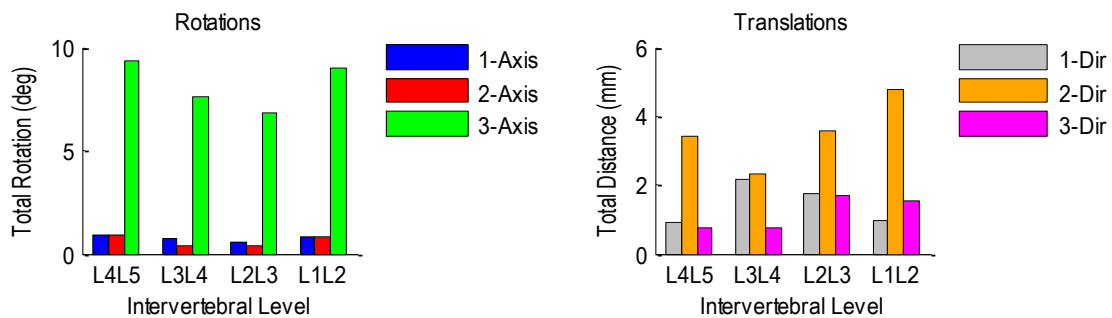


Figure A.37 Patient 4H relative rotations (left) and translations (right) at each vertebral level during flexion-extension.

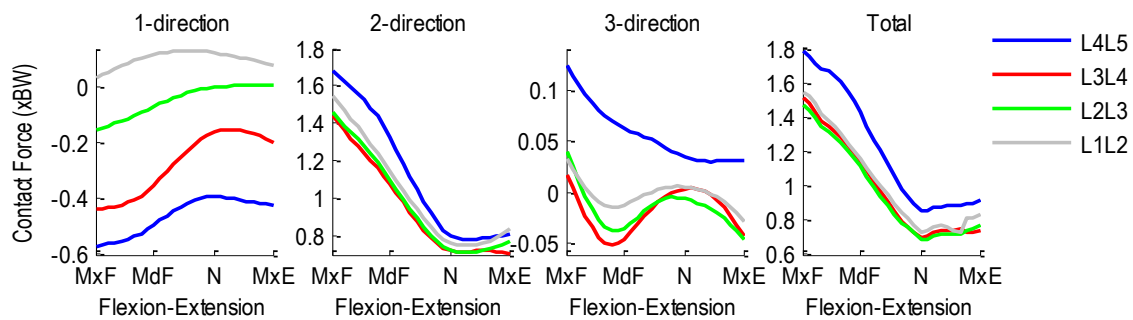


Figure A.38 Patient 4H intervertebral contact forces normalized with respect to body weight during flexion-extension. 1-dir=Ant(+)/Post(-), 2-dir=Sup(+)/Inf(-), 3-dir=Rt(+)/Lt(-).

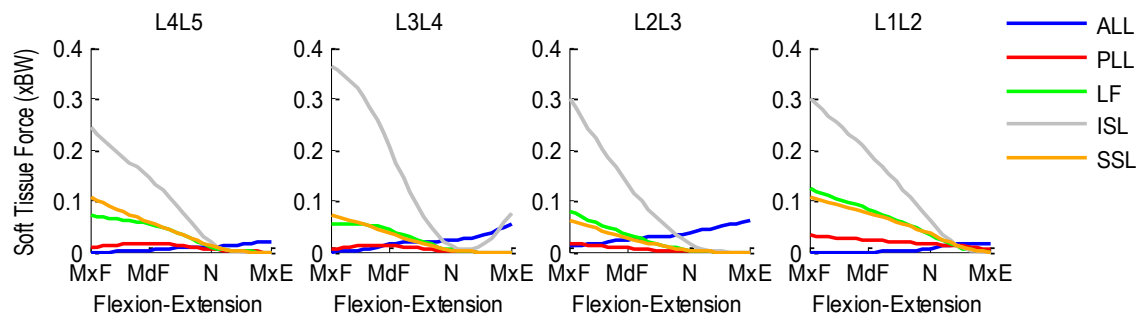


Figure A.39 Patient 4H segmental ligament forces normalized with respect to body weight during flexion-extension.

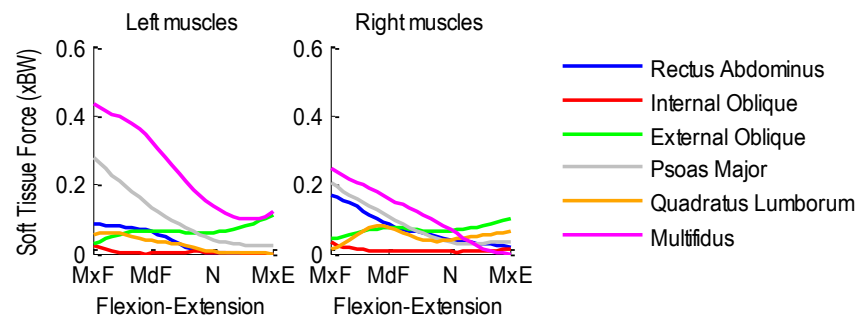


Figure A.40 Patient 1H bilateral muscle forces normalized with respect to body weight during flexion-extension.

A.4.2 Lateral Flexion Activity

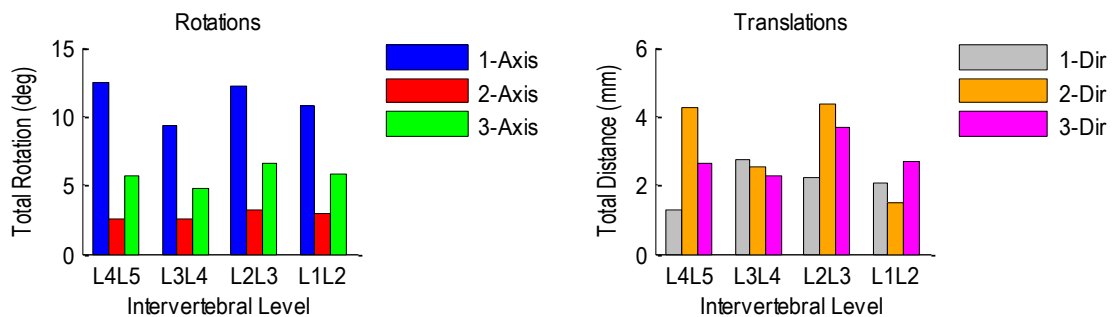


Figure A.41 Patient 4H relative rotations (left) and translations (right) at each vertebral level during left-to-right lateral flexion.

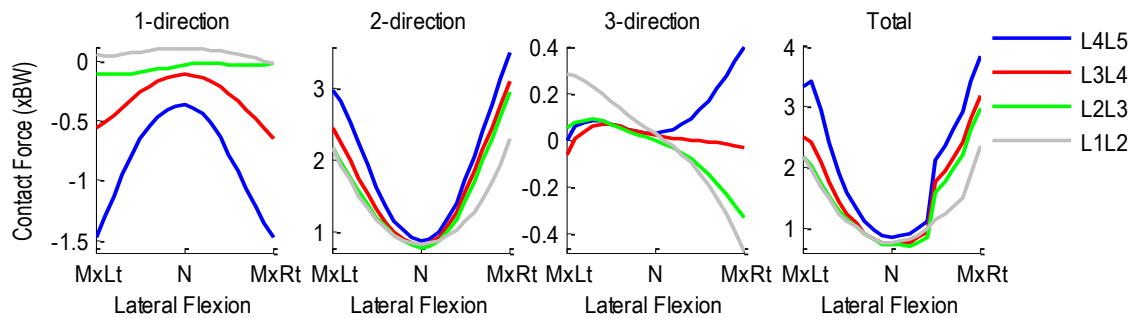


Figure A.42 Patient 4H intervertebral contact forces normalized with respect to body weight during right-to-left lateral flexion. 1-dir=Ant(+)/Post(-), 2-dir=Sup(+)/Inf(-), 3-dir=Rt(+)/Lt(-).

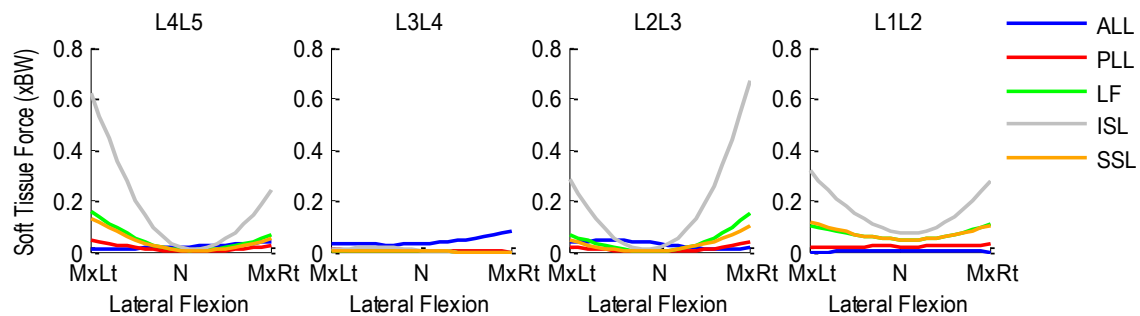


Figure A.43 Patient 4H segmental ligament forces normalized with respect to body weight during left-to-right lateral flexion.

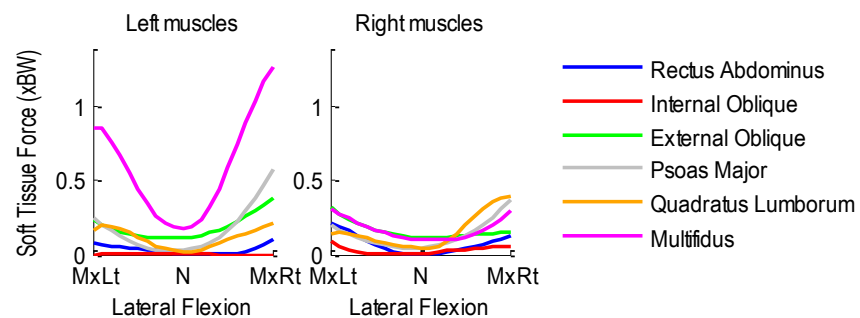


Figure A.44 Patient 4H bilateral muscle forces normalized with respect to body weight during left-to-right lateral flexion.

A.4.3 Axial Rotation Activity

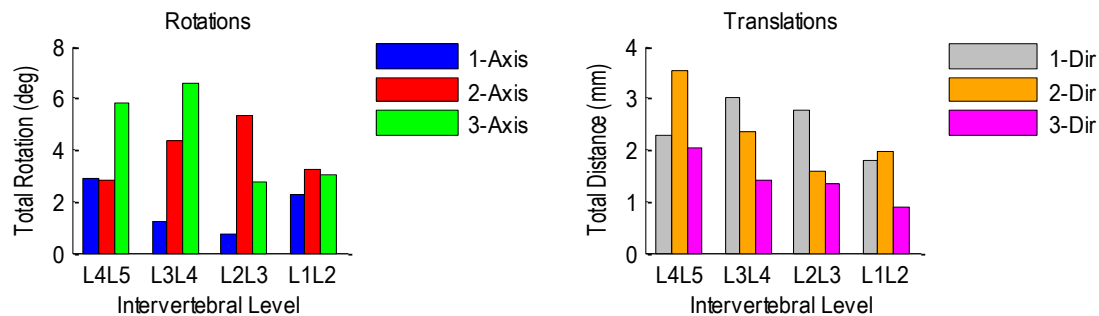


Figure A.45 Patient 4H relative rotations (left) and translations (right) at each vertebral level during left-to-right axial rotation.

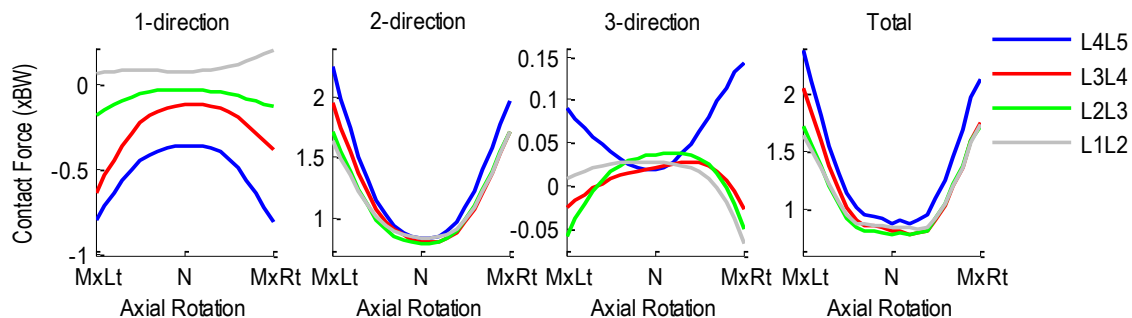


Figure A.46 Patient 4H intervertebral contact forces normalized with respect to body weight during left-to-right axial rotation. 1-dir=Ant(+)/Post(-), 2-dir=Sup(+)/Inf(-), 3-dir=Rt(+)/Lt(-).

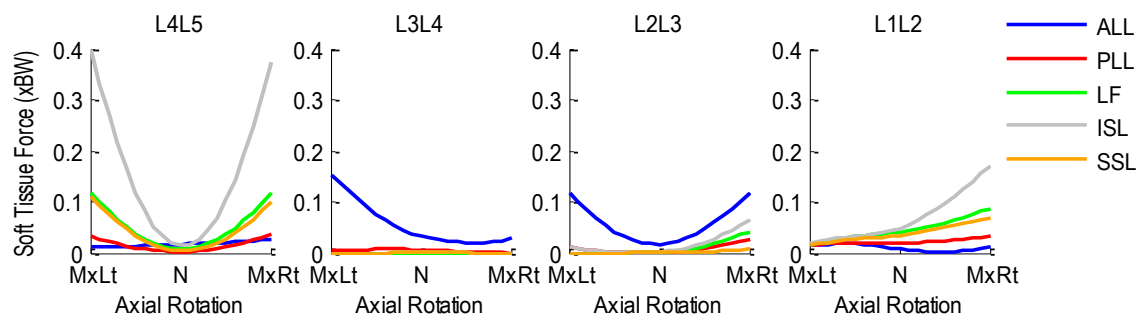


Figure A.47 Patient 4H bilateral muscle forces normalized to body weight during left-to-right axial rotation.

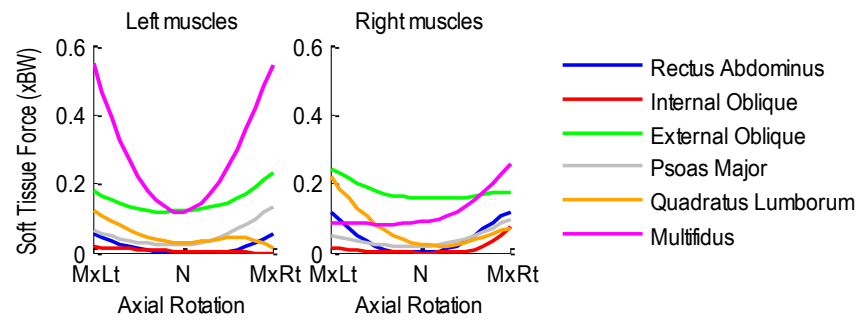


Figure A.48 Patient 4H bi-lateral muscle forces normalized to patient's body weight (BW) during left-to-right axial rotation.

A.5 Patient 5H

Age: 50 years

Gender: Male

Height: 1.91 m

Mass: 113 kg

Condition: Healthy

A.5.1 Flexion-Extension Activity

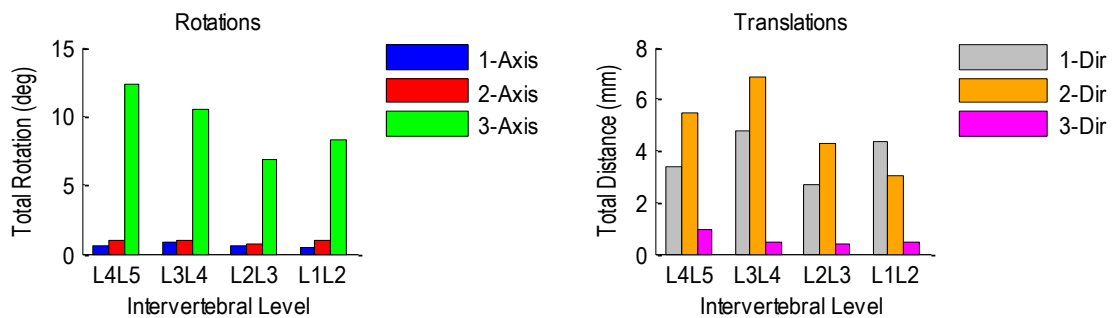


Figure A.49 Patient 5H relative rotations (left) and translations (right) at each vertebral level during flexion-extension.

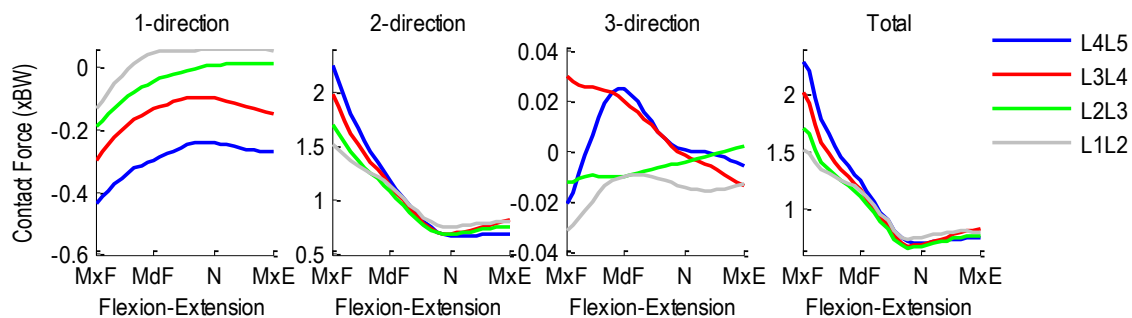


Figure A.50 Patient 5H intervertebral contact forces normalized with respect to body weight during flexion-extension. 1-dir=Ant(+)/Post(-), 2-dir=Sup(+)/Inf(-), 3-dir=Rt(+)/Lt(-).

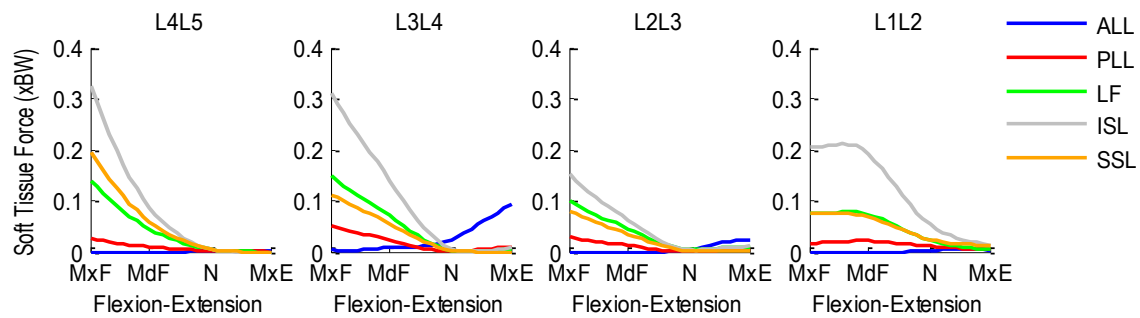


Figure A.51 Patient 5H segmental ligament forces normalized with respect to body weight during flexion-extension.

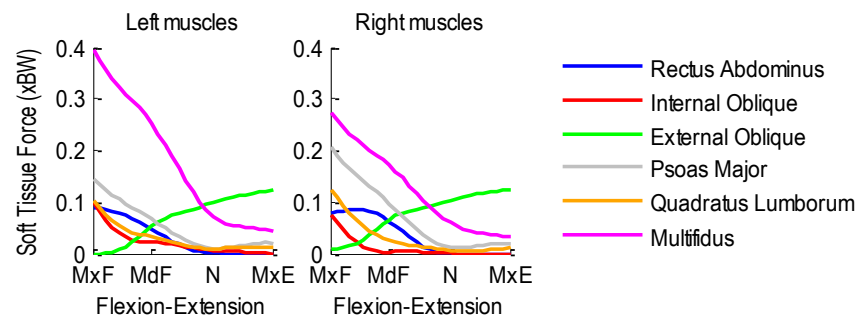


Figure A.52 Patient 5H bilateral muscle forces normalized with respect to body weight during flexion-extension.

A.5.2 Lateral Flexion Activity

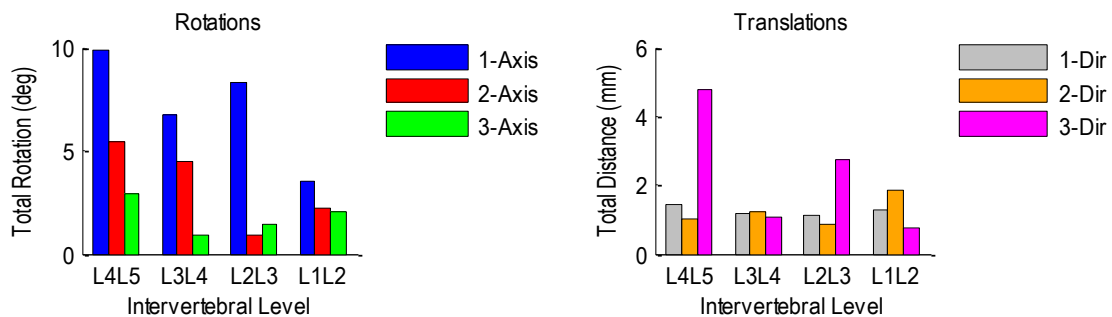


Figure A.53 Patient 5H relative rotations (left) and translations (right) at each vertebral level during left-to-right lateral flexion.

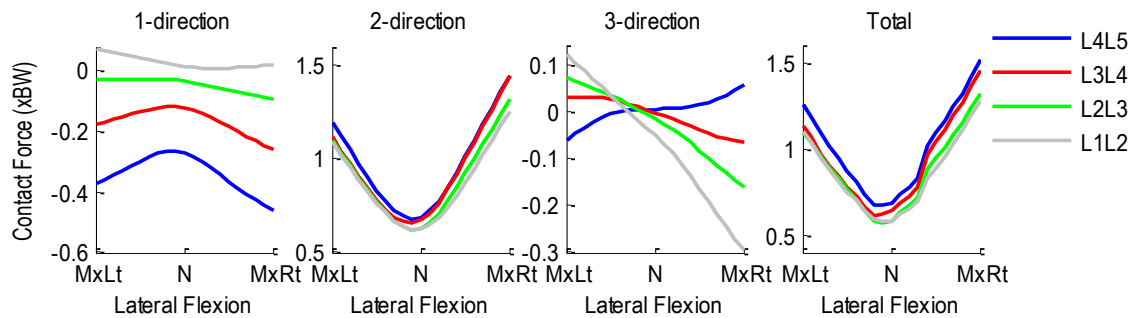


Figure A.54 Patient 5H intervertebral contact forces normalized with respect to body weight during right-to-left lateral flexion. 1-dir=Ant(+)/Post(-), 2-dir=Sup(+)/Inf(-), 3-dir=Rt(+)/Lt(-).

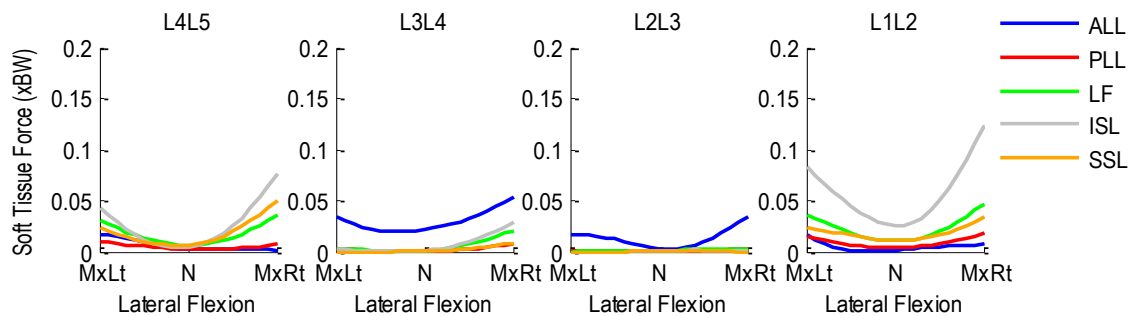


Figure A.55 Patient 2H segmental ligament forces normalized with respect to body weight during left-to-right lateral flexion.

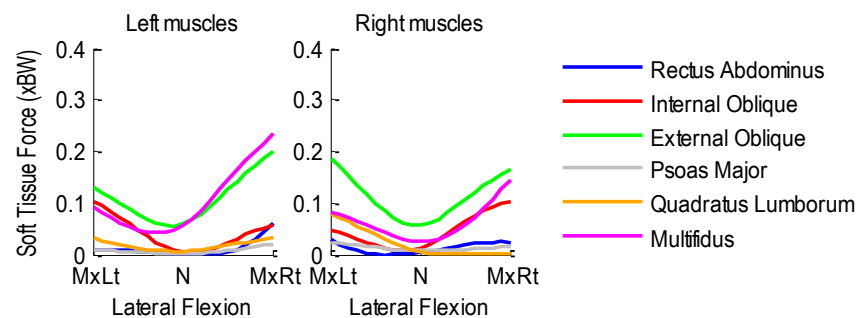


Figure A.56 Patient 5H bilateral muscle forces normalized with respect to body weight during left-to-right lateral flexion.

A.5.3 Axial Rotation Activity

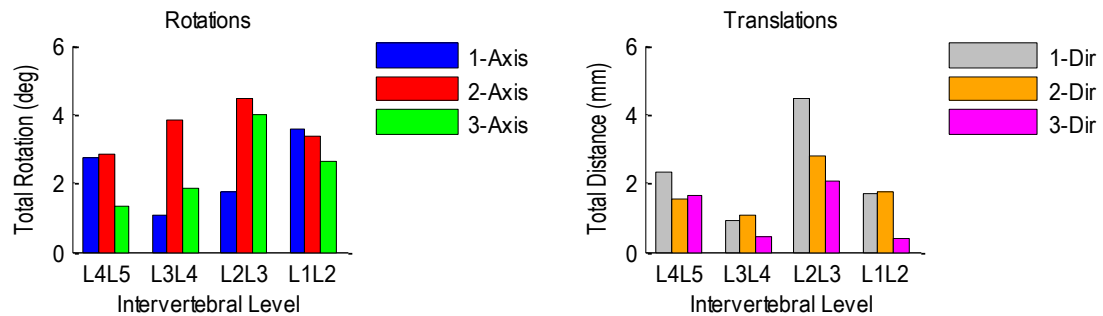


Figure A.57 Patient 5H relative rotations (left) and translations (right) at each vertebral level during left-to-right axial rotation.

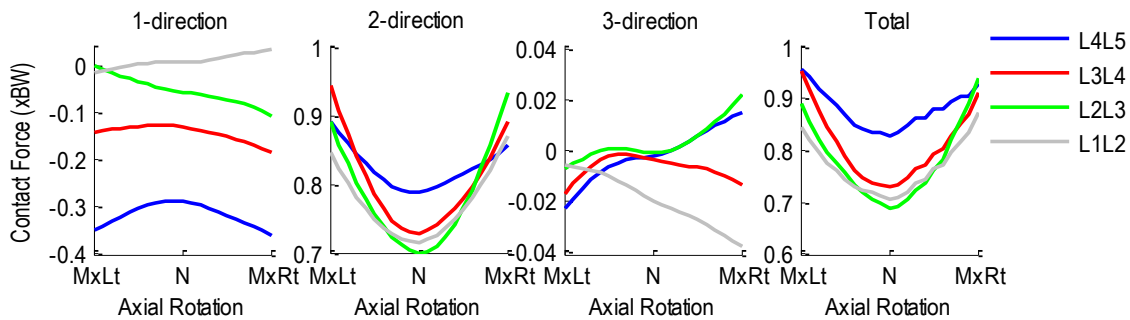


Figure A.58 Patient 5H intervertebral contact forces normalized with respect to body weight during left-to-right axial rotation. 1-dir=Ant(+)/Post(-), 2-dir=Sup(+)/Inf(-), 3-dir=Rt(+)/Lt(-).

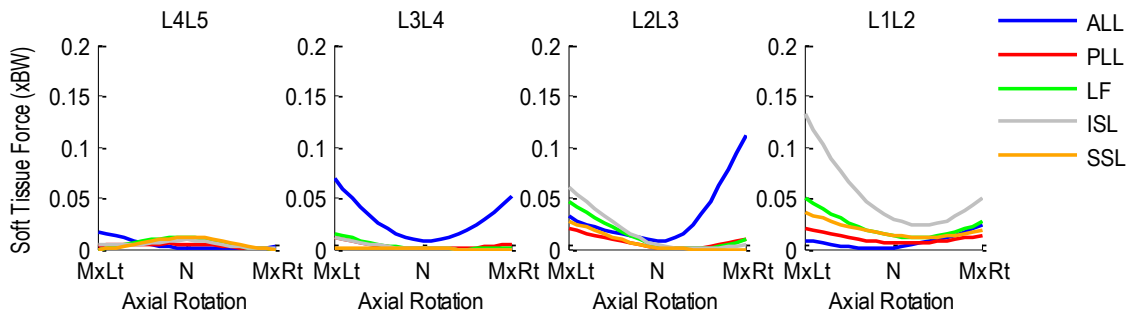


Figure A.59 Patient 5H segmental ligament forces normalized with respect to body weight during left-to-right axial rotation.

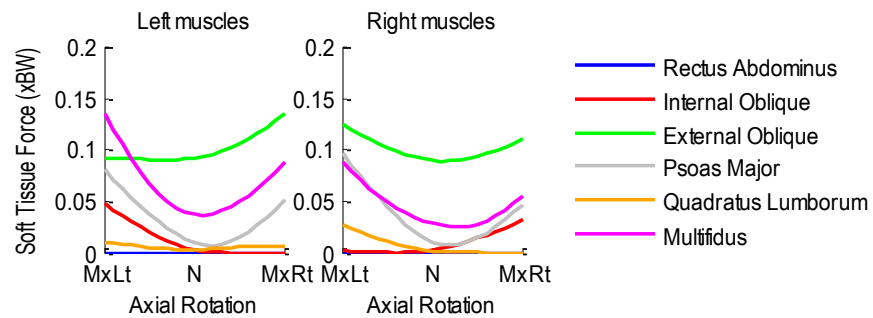


Figure A.60 Patient 5H bilateral muscle forces normalized to body weight during left-to-right axial rotation.

A.6 Patient 6H

Age: 46 years

Gender: Male

Height: 1.85 m

Mass: 108 kg

Condition: Healthy

A.6.1 Flexion-Extension Activity

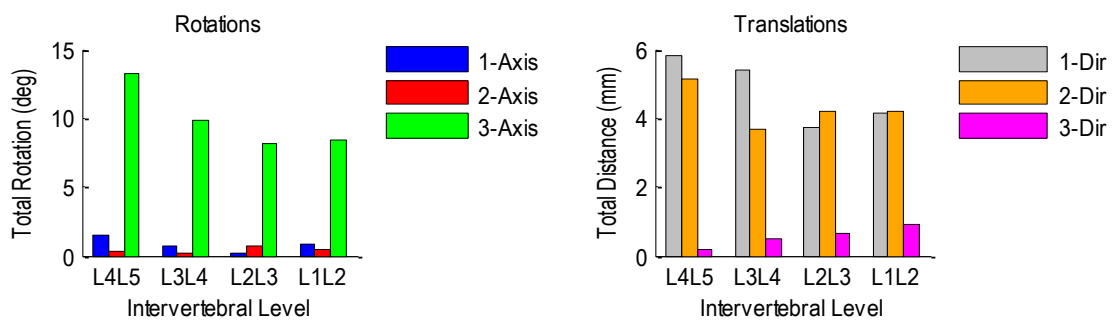


Figure A.61 Patient 6H relative rotations (left) and translations (right) at each vertebral level during flexion-extension.

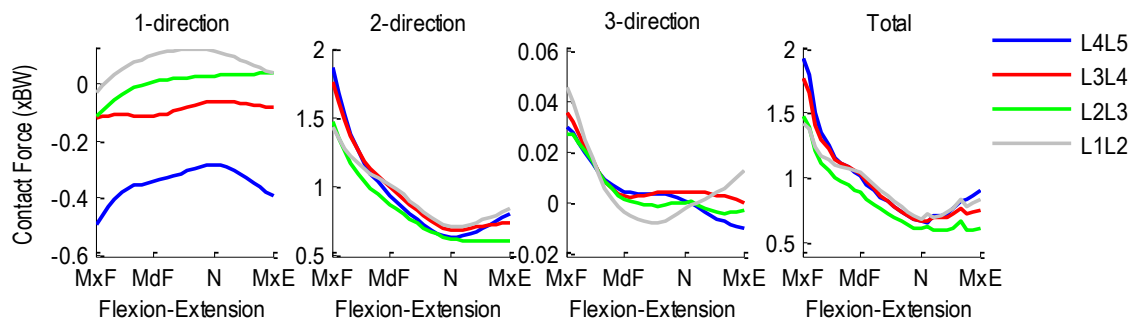


Figure A.62 Patient 6H intervertebral contact forces normalized with respect to body weight during flexion-extension. 1-dir=Ant(+)/Post(-), 2-dir=Sup(+)/Inf(-), 3-dir=Rt(+)/Lt(-).

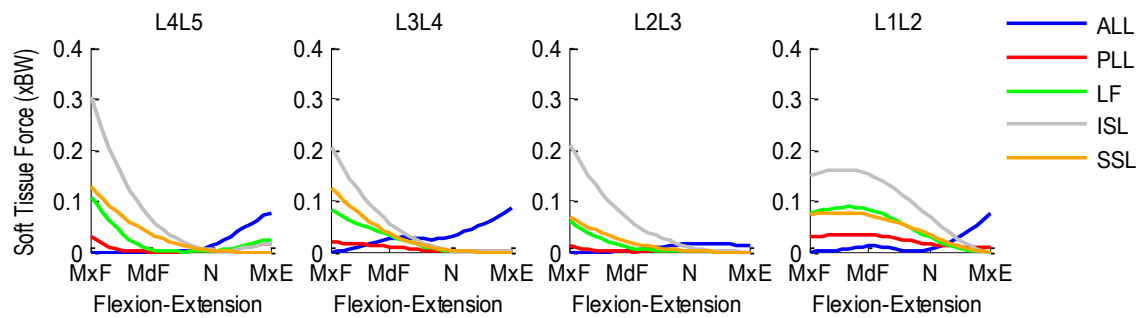


Figure A.63 Patient 6H segmental ligament forces normalized with respect to body weight during flexion-extension.

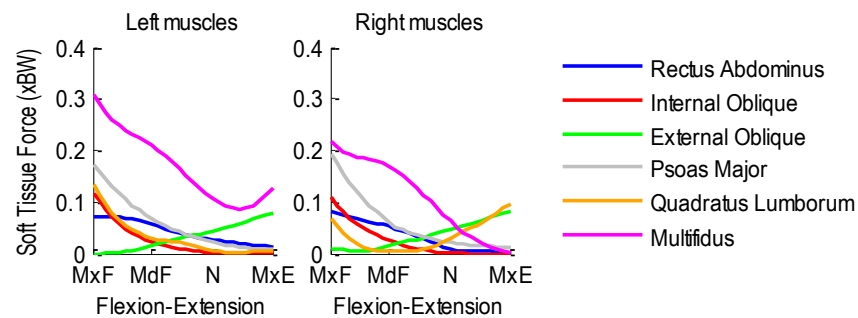


Figure A.64 Patient 6H bilateral muscle forces normalized with respect to body weight during flexion-extension.

A.6.2 Lateral Flexion Activity

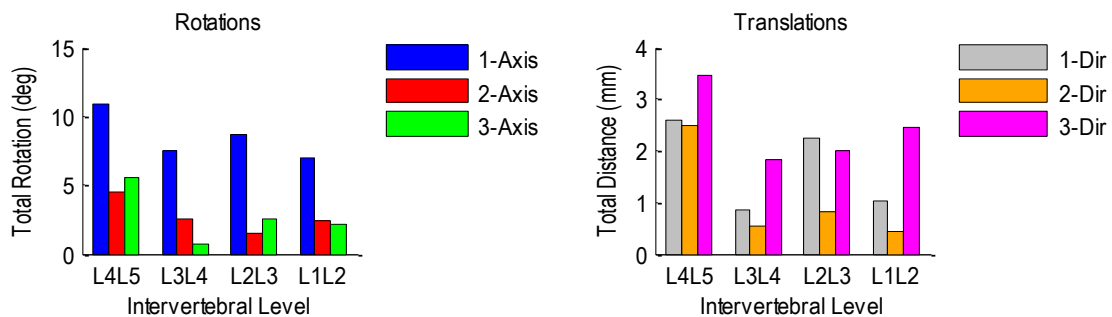


Figure A.65 Patient 6H relative rotations (left) and translations (right) at each vertebral level during left-to-right lateral flexion.

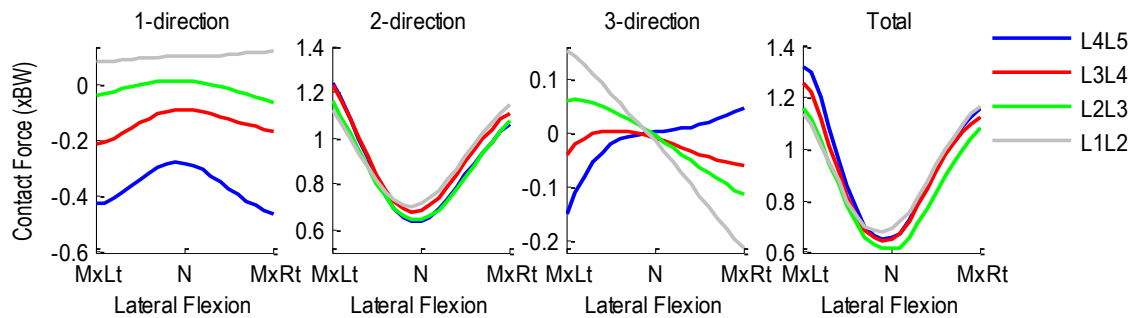


Figure A.66 Patient 6H intervertebral contact forces normalized with respect to body weight during right-to-left lateral flexion. 1-dir=Ant(+)/Post(-), 2-dir=Sup(+)/Inf(-), 3-dir=Rt(+)/Lt(-).

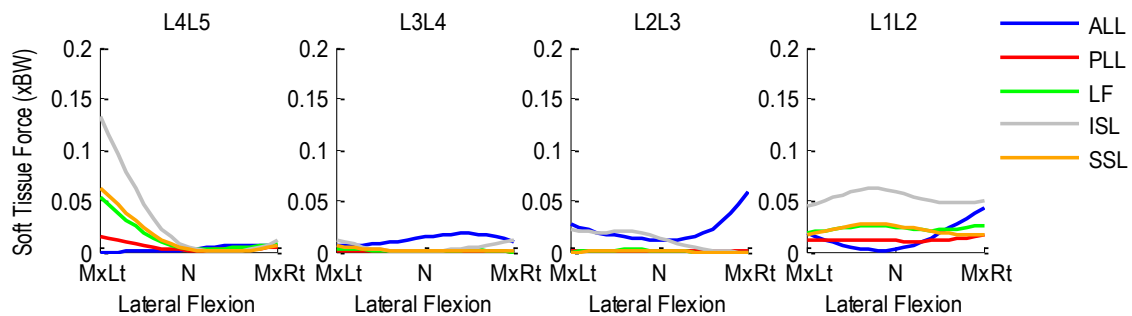


Figure A.67 Patient 6H segmental ligament forces normalized with respect to body weight during left-to-right lateral flexion.

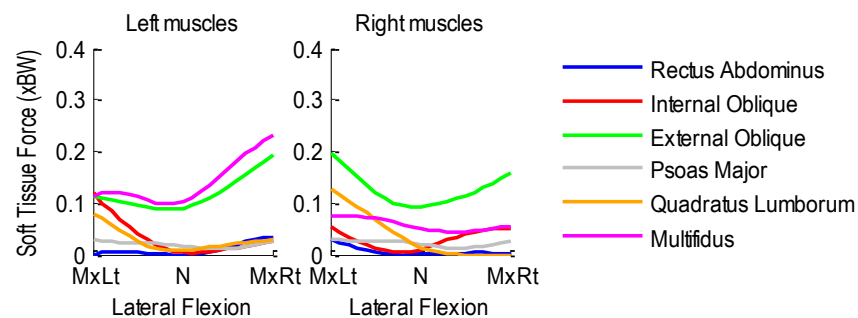


Figure A.68 Patient 6H bilateral muscle forces normalized with respect to body weight during left-to-right lateral flexion.

A.6.3 Axial Rotation Activity

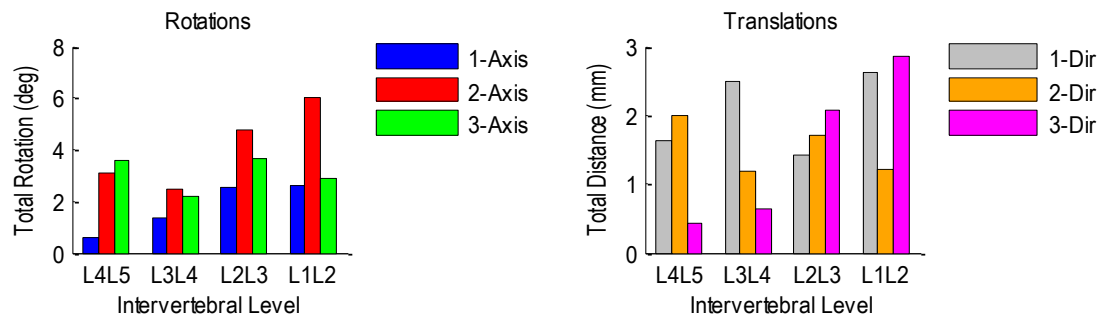


Figure A.69 Patient 6H relative rotations (left) and translations (right) at each vertebral level during left-to-right axial rotation.

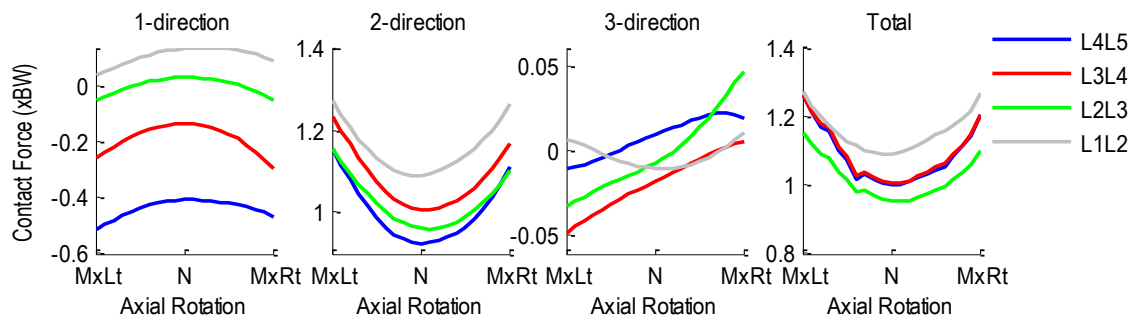


Figure A.70 Patient 6H intervertebral contact forces normalized with respect to body weight during left-to-right axial rotation. 1-dir=Ant(+)/Post(-), 2-dir=Sup(+)/Inf(-), 3-dir=Rt(+)/Lt(-).

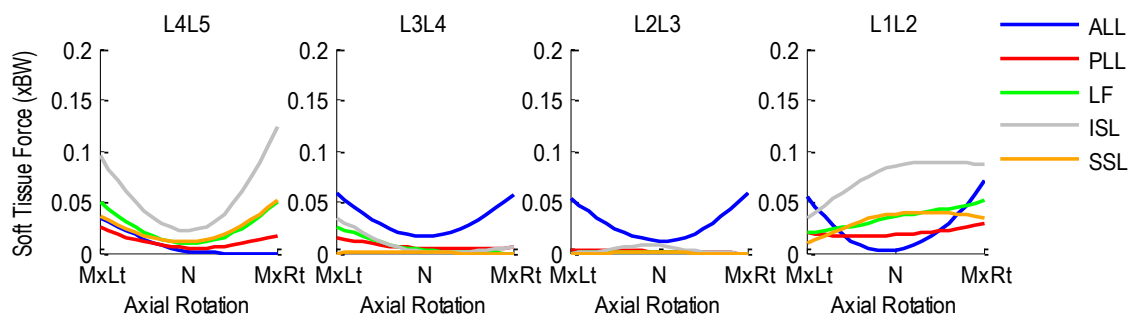


Figure A.71 Patient 6H segmental ligament forces normalized with respect to body weight during left-to-right axial rotation.

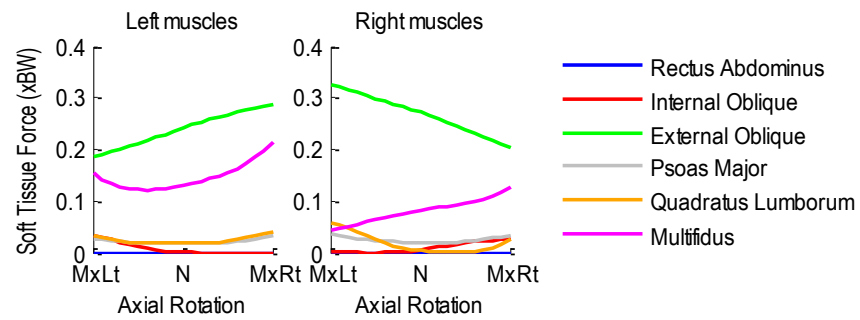


Figure A.72 Patient 6H bilateral muscle forces normalized to body weight during left-to-right axial rotation.

A.7 Patient 7H

Age: 65 years

Gender: Female

Height: 1.63 m

Mass: 77 kg

Condition: Healthy

A.7.1 Flexion-Extension Activity

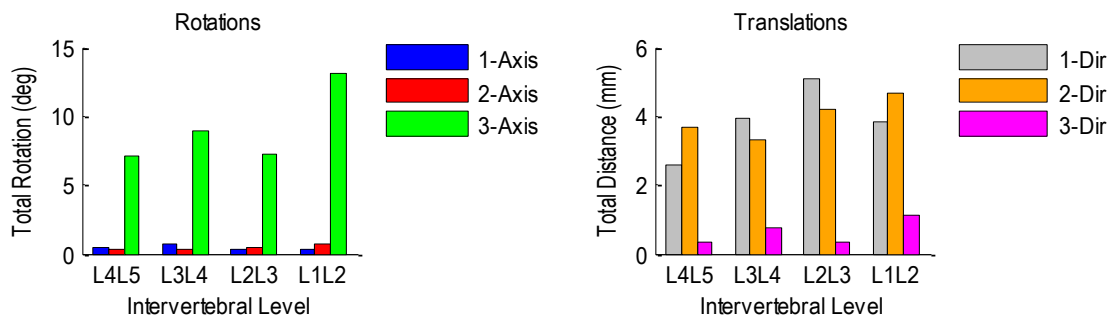


Figure A.73 Patient 7H relative rotations (left) and translations (right) at each vertebral level during flexion-extension.

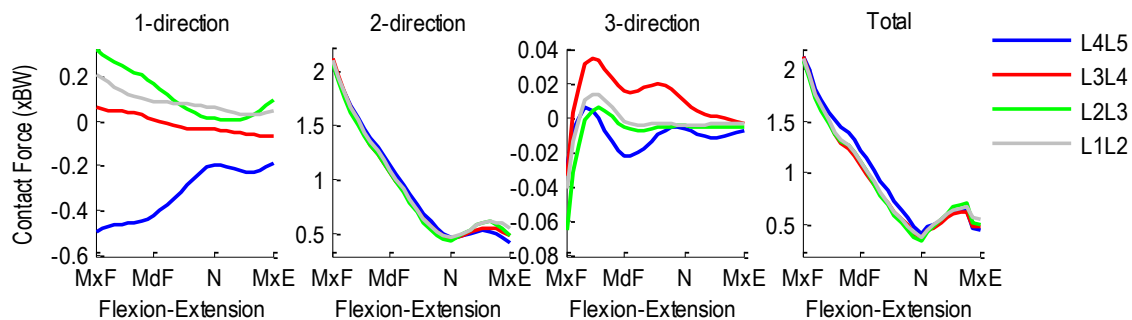


Figure A.74 Patient 7H intervertebral contact forces normalized with respect to body weight during flexion-extension. 1-dir=Ant(+)/Post(-), 2-dir=Sup(+)/Inf(-), 3-dir=Rt(+)/Lt(-).

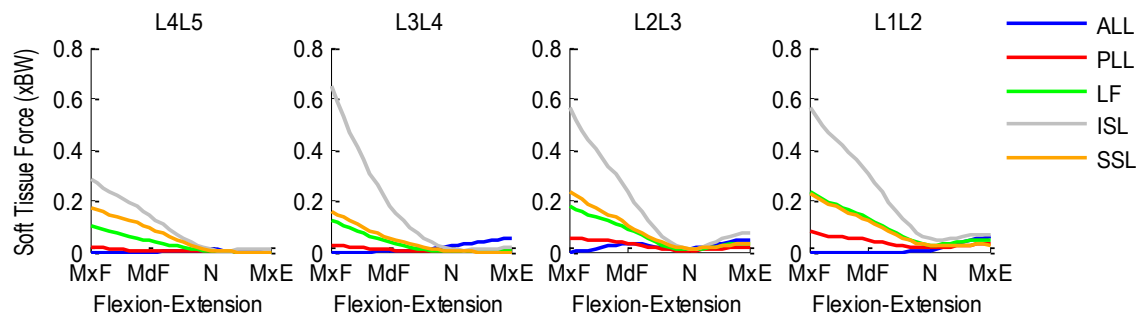


Figure A.75 Patient 7H segmental ligament forces normalized with respect to body weight during flexion-extension.

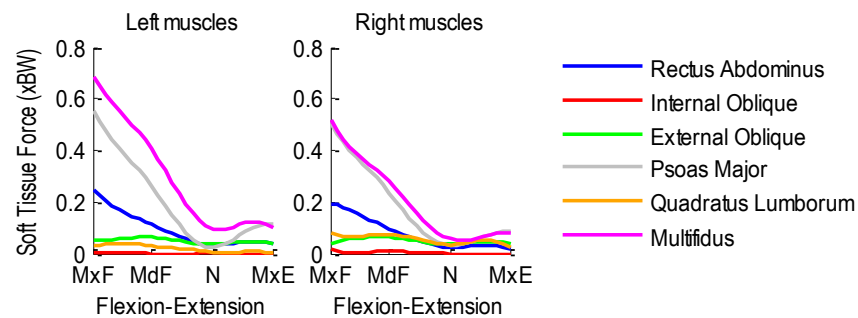


Figure A.76 Patient 7H bilateral muscle forces normalized with respect to body weight during flexion-extension.

A.7.2 Lateral Flexion Activity

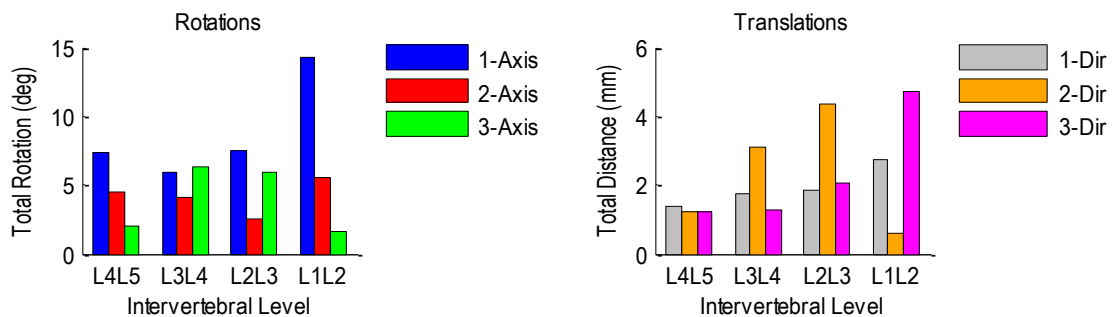


Figure A.77 Patient 7H relative rotations (left) and translations (right) at each vertebral level during left-to-right lateral flexion.

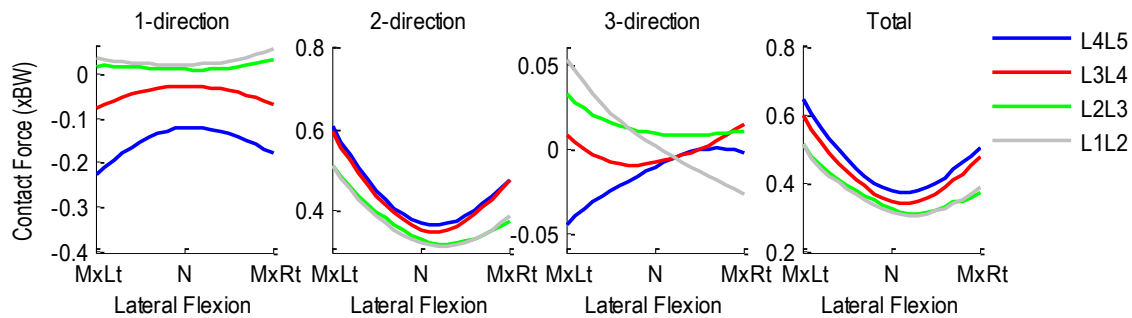


Figure A.78 Patient 7H intervertebral contact forces normalized with respect to body weight during right-to-left lateral flexion. 1-dir=Ant(+)/Post(-), 2-dir=Sup(+)/Inf(-), 3-dir=Rt(+)/Lt(-).

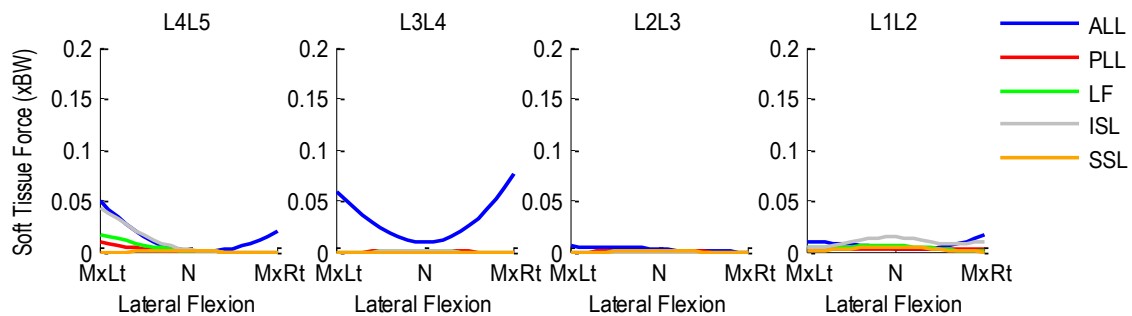


Figure A.79 Patient 7H segmental ligament forces normalized with respect to body weight during left-to-right lateral flexion.

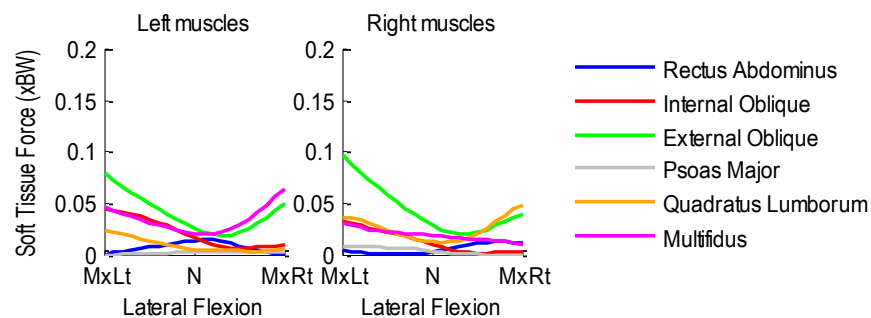


Figure A.80 Patient 7H bilateral muscle forces normalized with respect to body weight during left-to-right lateral flexion.

A.7.3 Axial Rotation Activity

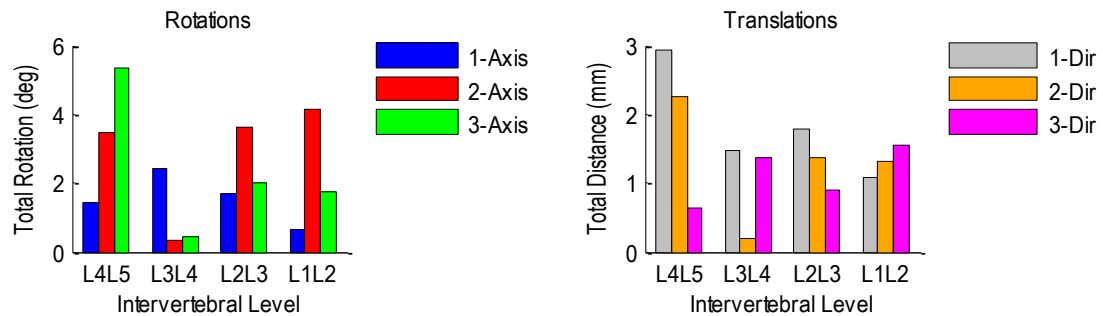


Figure A.81 Patient 7H relative rotations (left) and translations (right) at each vertebral level during left-to-right axial rotation.

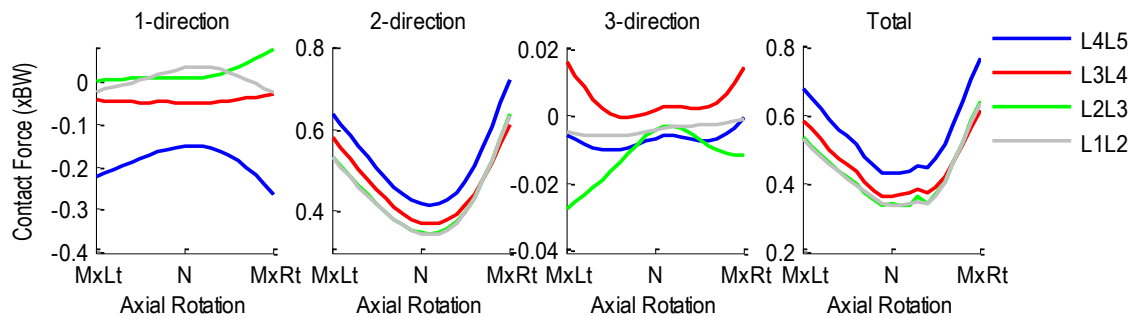


Figure A.82 Patient 7H intervertebral contact forces normalized with respect to body weight during left-to-right axial rotation. 1-dir=Ant(+)/Post(-), 2-dir=Sup(+)/Inf(-), 3-dir=Rt(+)/Lt(-).

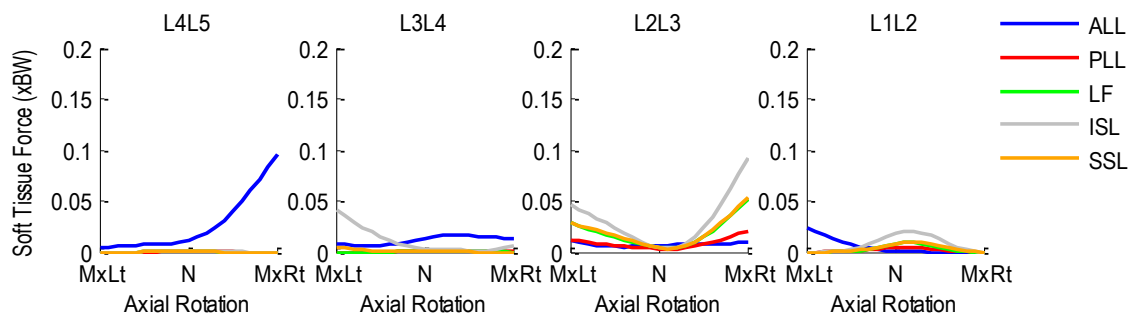


Figure A.83 Patient 7H segmental ligament forces normalized with respect to body weight during left-to-right axial rotation.

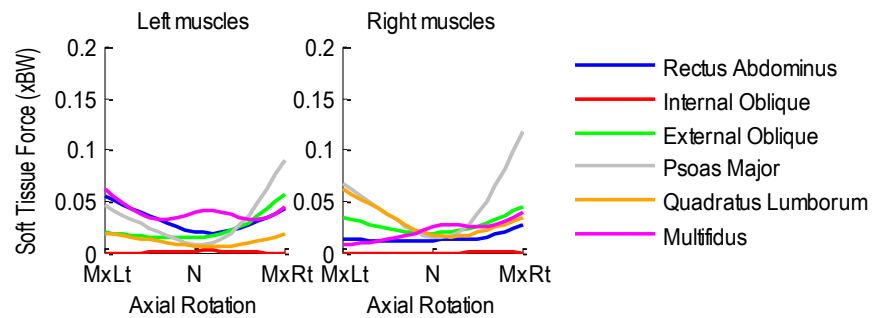


Figure A.84 Patient 7H bilateral muscle forces normalized to body weight during left-to-right axial rotation.

A.8 Patient 8H

Age: 32 years

Gender: Male

Height: 1.85 m

Mass: 88 kg

Condition: Healthy

A.8.1 Flexion-Extension Activity

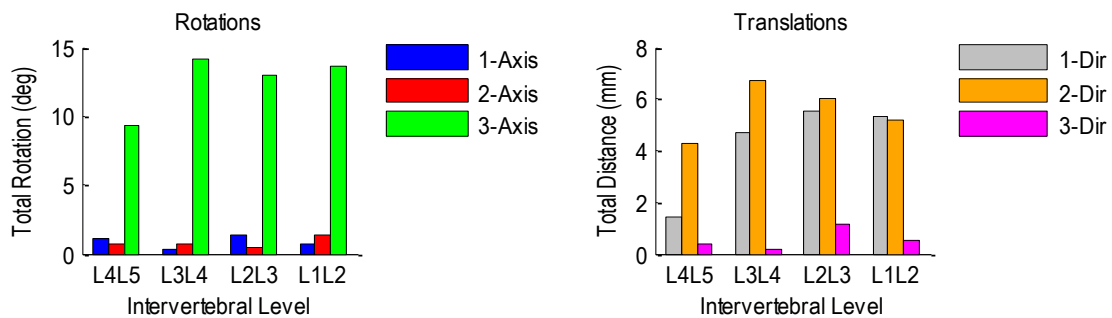


Figure A.85 Patient 8H relative rotations (left) and translations (right) at each vertebral level during flexion-extension.

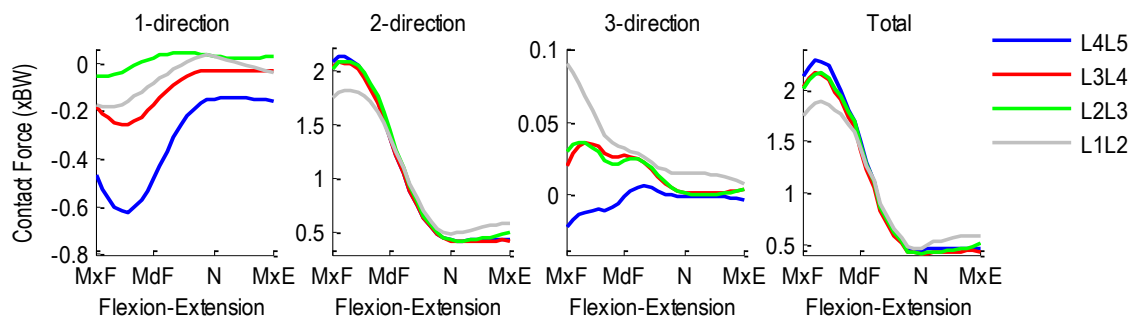


Figure A.86 Patient 8H intervertebral contact forces normalized with respect to body weight during flexion-extension. 1-dir=Ant(+)/Post(-), 2-dir=Sup(+)/Inf(-), 3-dir=Rt(+)/Lt(-).

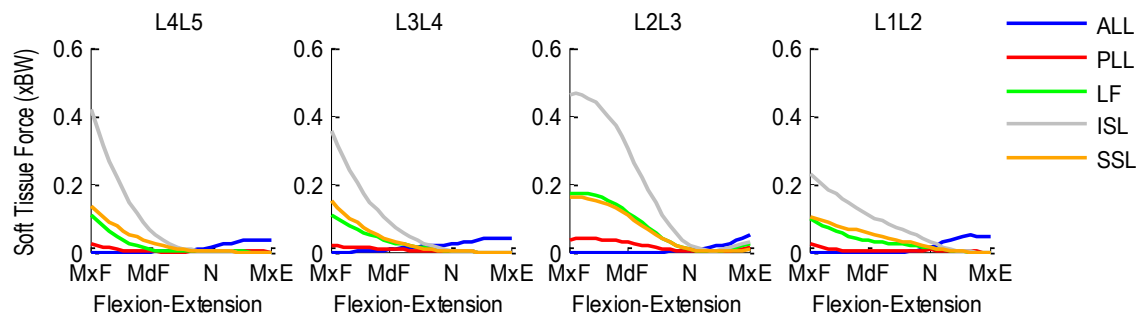


Figure A.87 Patient 8H segmental ligament forces normalized with respect to body weight during flexion-extension.

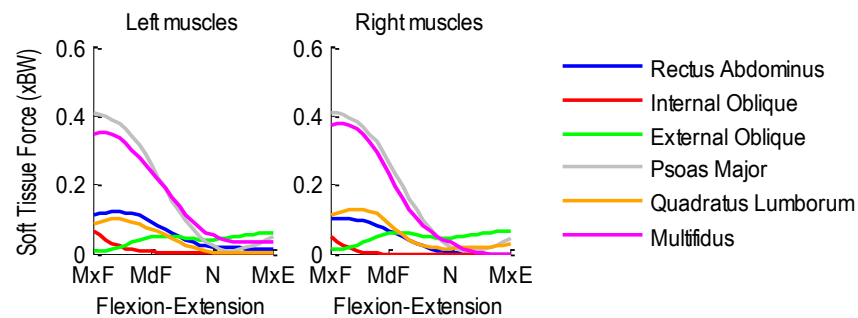


Figure A.88 Patient 8H bilateral muscle forces normalized with respect to body weight during flexion-extension.

A.8.2 Lateral Flexion Activity

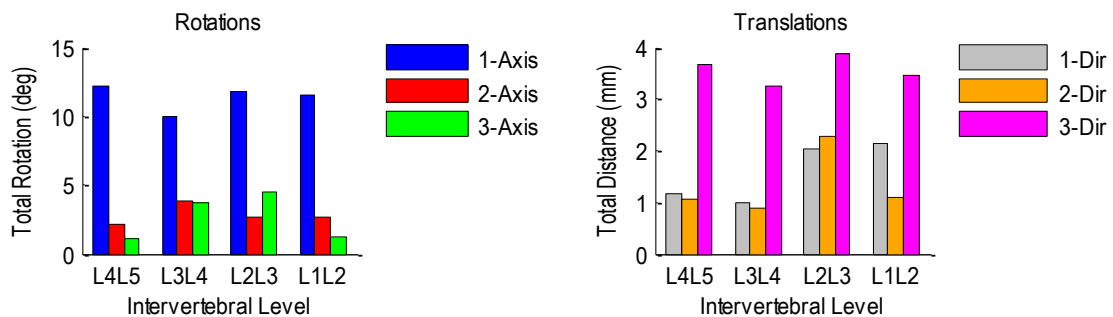


Figure A.89 Patient 8H relative rotations (left) and translations (right) at each vertebral level during left-to-right lateral flexion.

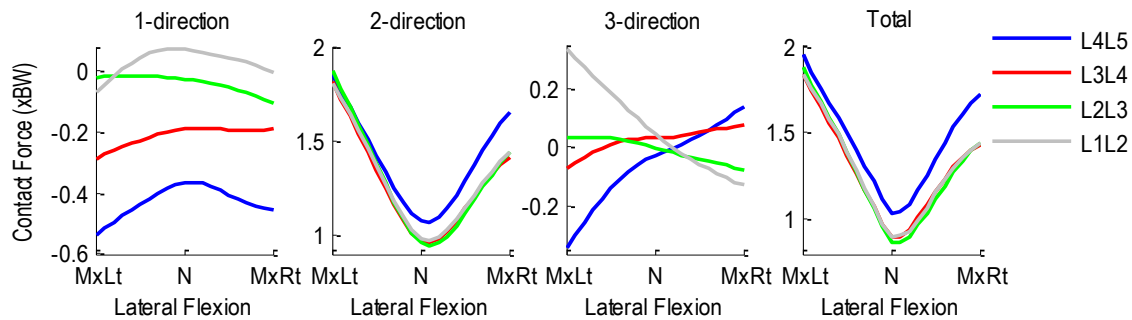


Figure A.90 Patient 8H intervertebral contact forces normalized with respect to body weight during right-to-left lateral flexion. 1-dir=Ant(+)/Post(-), 2-dir=Sup(+)/Inf(-), 3-dir=Rt(+)/Lt(-).

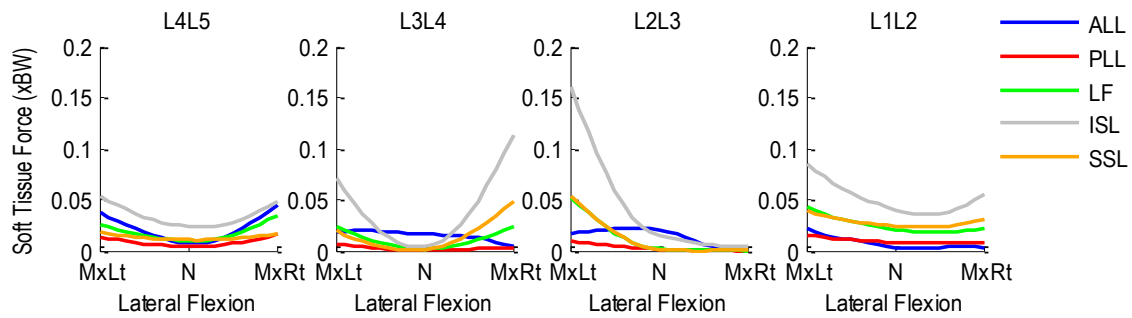


Figure A.91 Patient 8H segmental ligament forces normalized with respect to body weight during left-to-right lateral flexion.

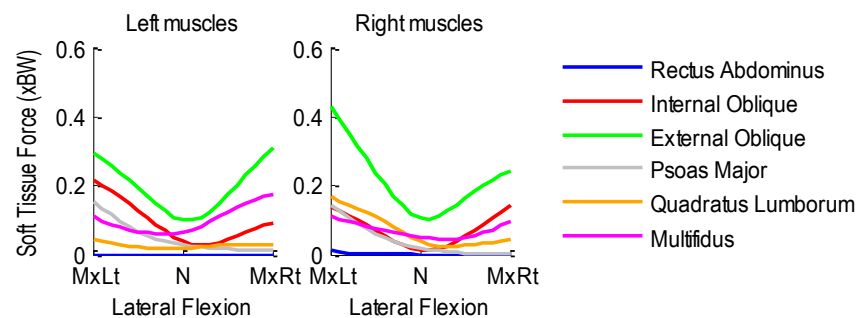


Figure A.92 Patient 8H bilateral muscle forces normalized with respect to body weight during left-to-right lateral flexion.

A.8.3 Axial Rotation Activity

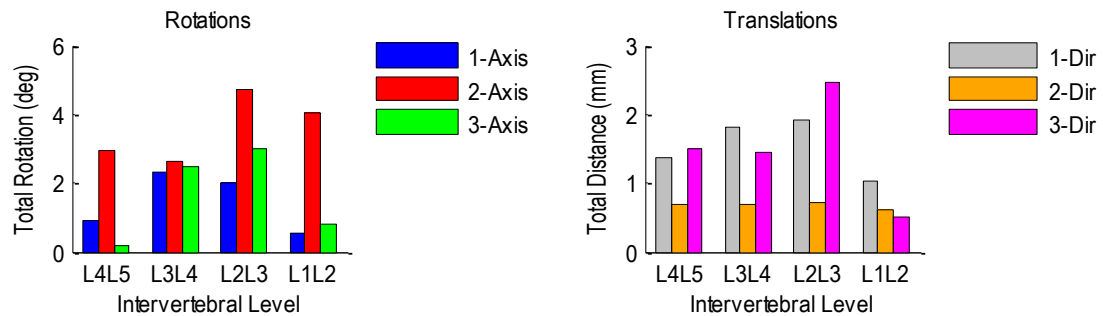


Figure A.93 Patient 8H relative rotations (left) and translations (right) at each vertebral level during left-to-right axial rotation.

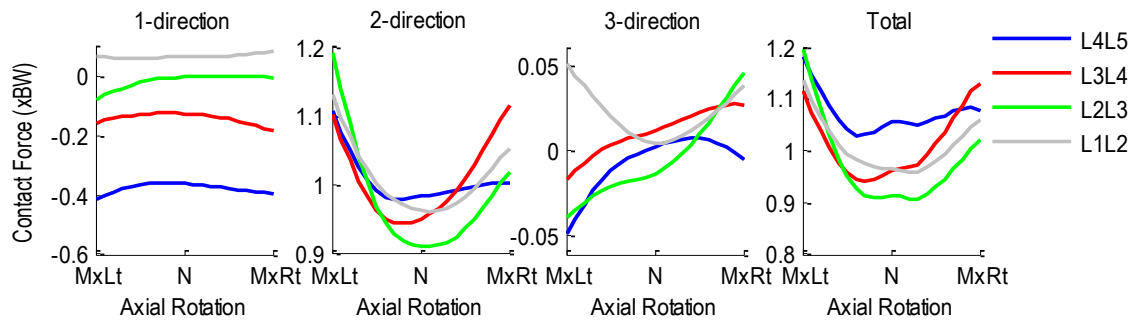


Figure A.94 Patient 8H intervertebral contact forces normalized with respect to body weight during left-to-right axial rotation. 1-dir=Ant(+)/Post(-), 2-dir=Sup(+)/Inf(-), 3-dir=Rt(+)/Lt(-).

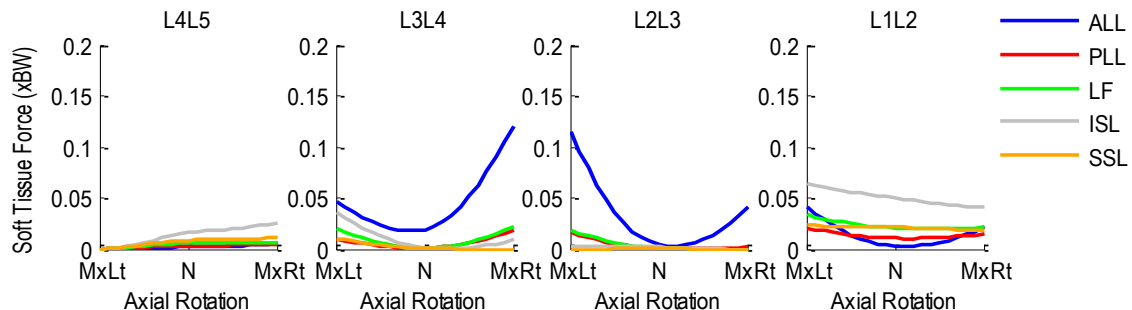


Figure A.95 Patient 8H segmental ligament forces normalized with respect to body weight during left-to-right axial rotation.

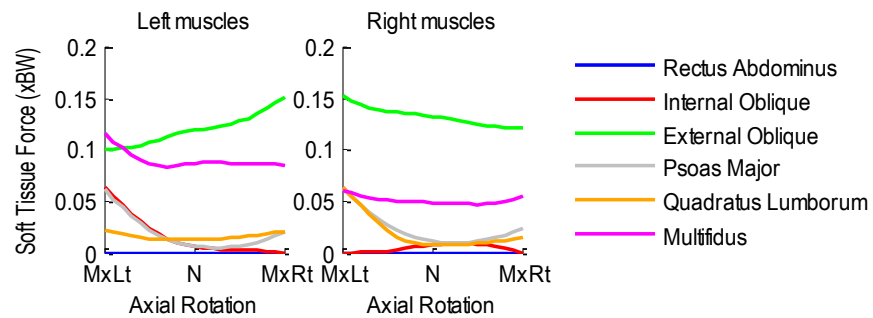


Figure A.96 Patient 8H bilateral muscle forces normalized to body weight during left-to-right axial rotation.

A.9 Patient 9H

Age: 23 years

Gender: Female

Height: 1.70 m

Mass: 57 kg

Condition: Healthy

A.9.1 Flexion-Extension Activity

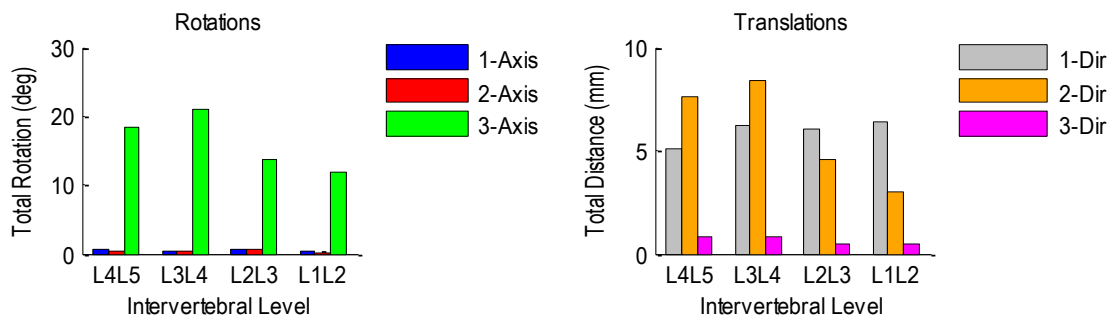


Figure A.97 Patient 9H relative rotations (left) and translations (right) at each vertebral level during flexion-extension.

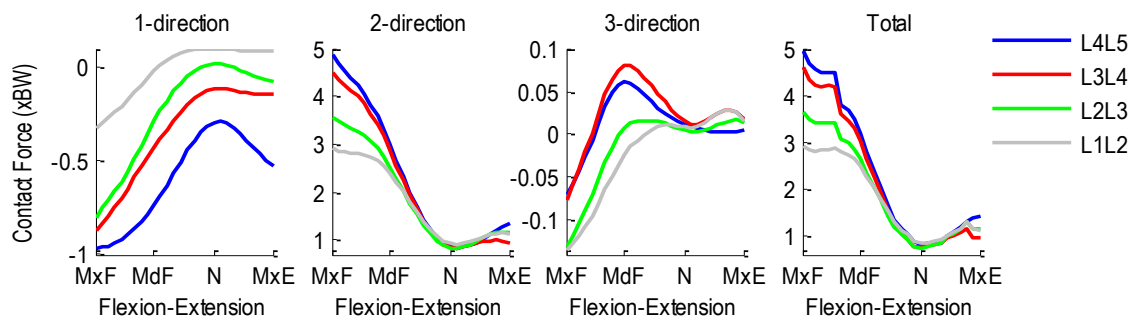


Figure A.98 Patient 9H intervertebral contact forces normalized with respect to body weight during flexion-extension. 1-dir=Ant(+)/Post(-), 2-dir=Sup(+)/Inf(-), 3-dir=Rt(+)/Lt(-).

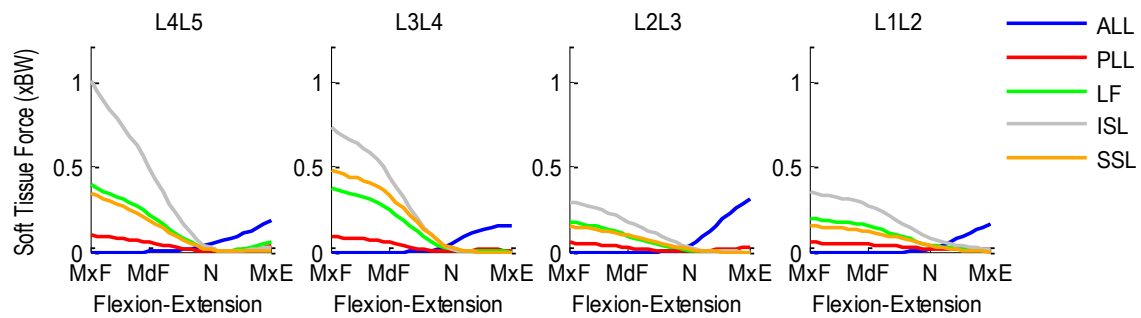


Figure A.99 Patient 9H segmental ligament forces normalized with respect to body weight during flexion-extension.

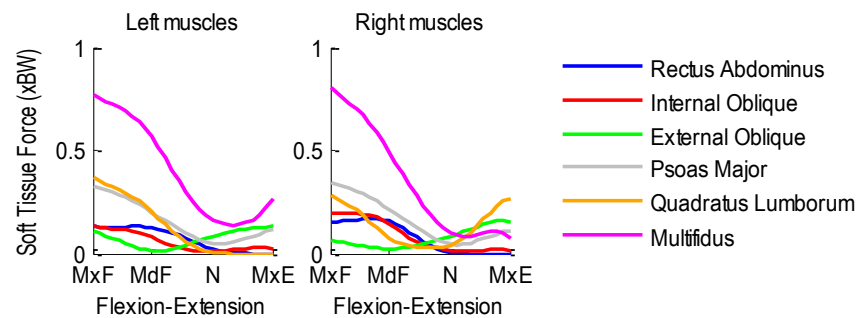


Figure A.100 Patient 9H bilateral muscle forces normalized with respect to body weight during flexion-extension.

A.9.2 Lateral Flexion Activity

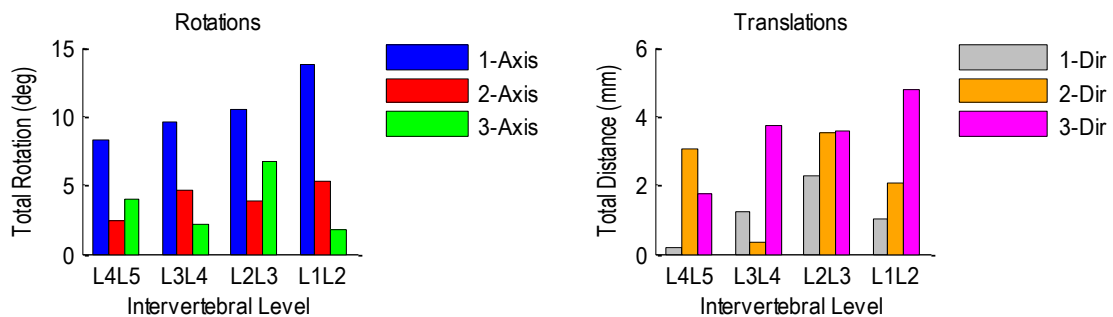


Figure A.101 Patient 9H relative rotations (left) and translations (right) at each vertebral level during left-to-right lateral flexion.

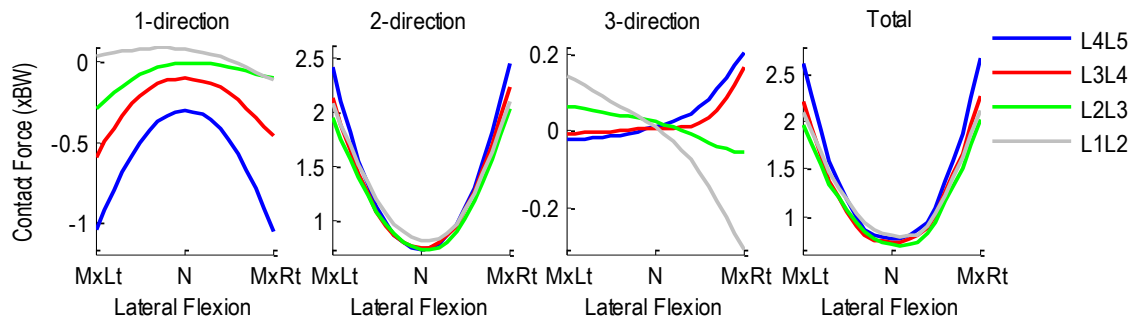


Figure A.102 Patient 9H intervertebral contact forces normalized with respect to body weight during right-to-left lateral flexion. 1-dir=Ant(+)/Post(-), 2-dir=Sup(+)/Inf(-), 3-dir=Rt(+)/Lt(-).

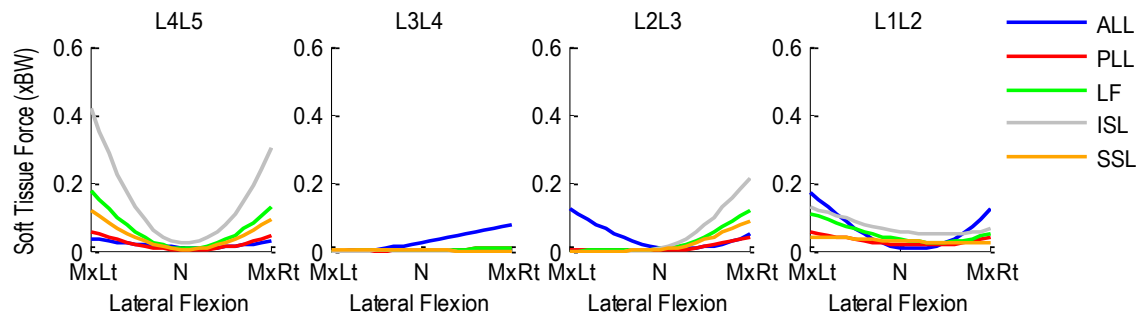


Figure A.103 Patient 9H segmental ligament forces normalized with respect to body weight during left-to-right lateral flexion.

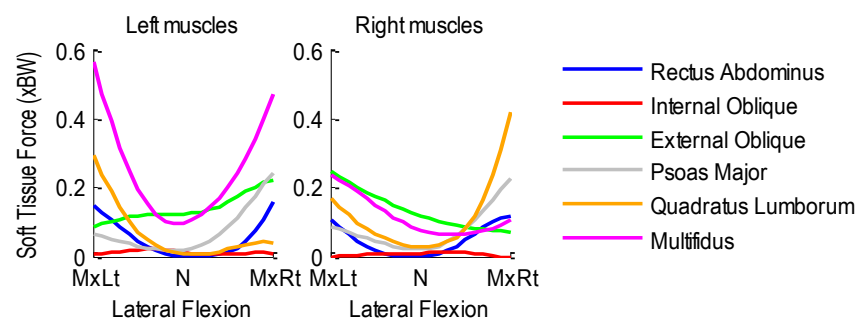


Figure A.104 Patient 9H bilateral muscle forces normalized with respect to body weight during left-to-right lateral flexion.

A.9.3 Axial Rotation Activity

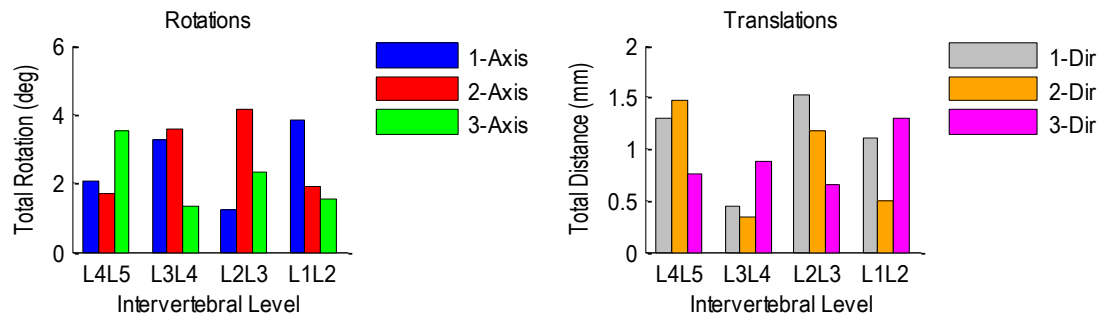


Figure A.105 Patient 9H relative rotations (left) and translations (right) at each vertebral level during left-to-right axial rotation.

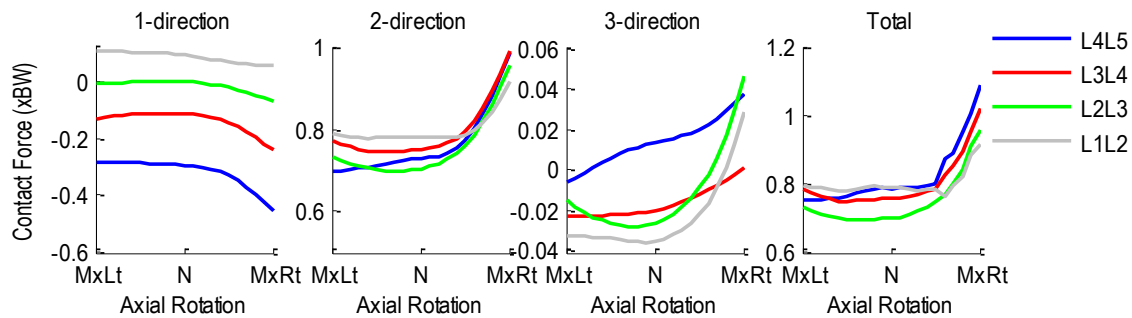


Figure A.106 Patient 9H intervertebral contact forces normalized with respect to body weight during left-to-right axial rotation. 1-dir=Ant(+)/Post(-), 2-dir=Sup(+)/Inf(-), 3-dir=Rt(+)/Lt(-).

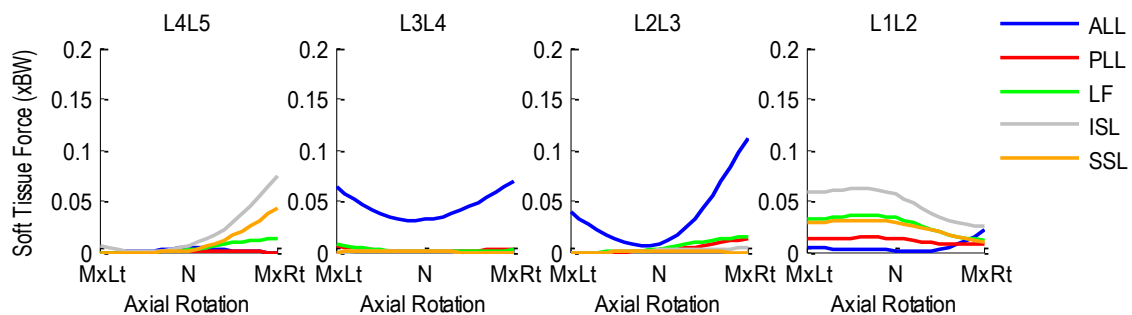


Figure A.107 Patient 9H segmental ligament forces normalized with respect to body weight during left-to-right axial rotation.

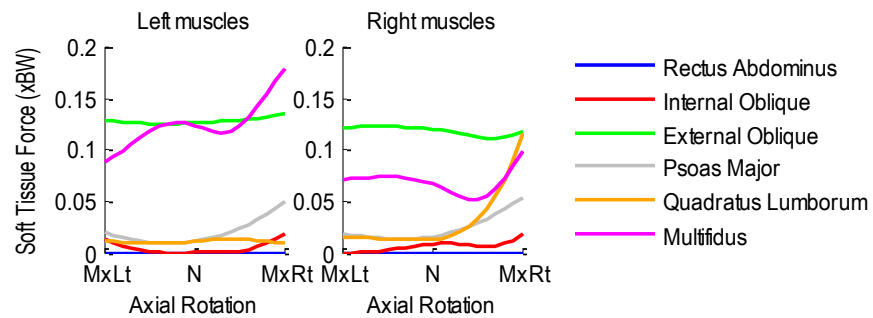


Figure A.108 Patient 9H bilateral muscle forces normalized to body weight during left-to-right axial rotation.

A.10 Patient 10H

Age: 28 years

Gender: Female

Height: 1.65 m

Mass: 82 kg

Condition: Healthy

A.10.1 Flexion-Extension Activity

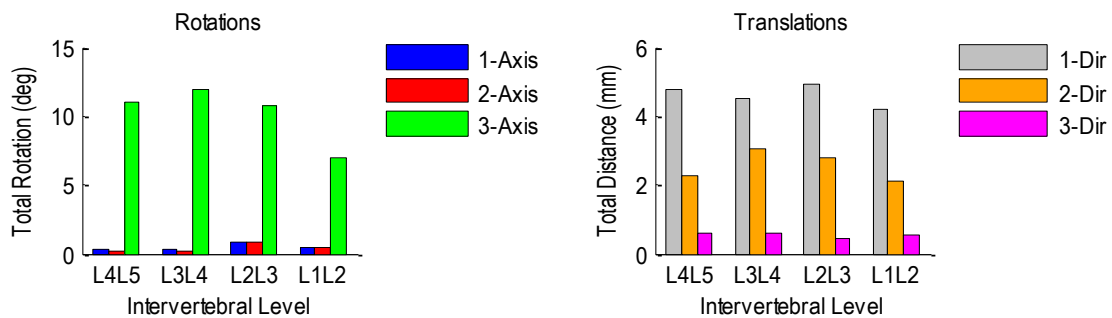


Figure A.109 Patient 10H relative rotations (left) and translations (right) at each vertebral level during flexion-extension.

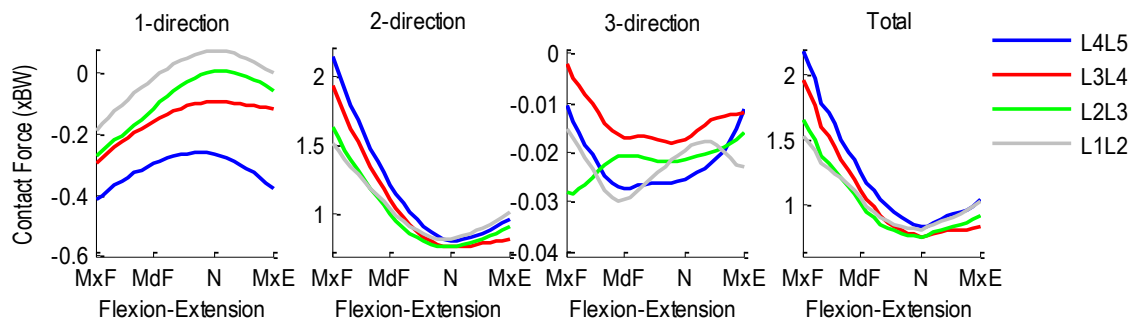


Figure A.110 Patient 10H intervertebral contact forces normalized with respect to body weight during flexion-extension. 1-dir=Ant(+)/Post(-), 2-dir=Sup(+)/Inf(-), 3-dir=Rt(+)/Lt(-).

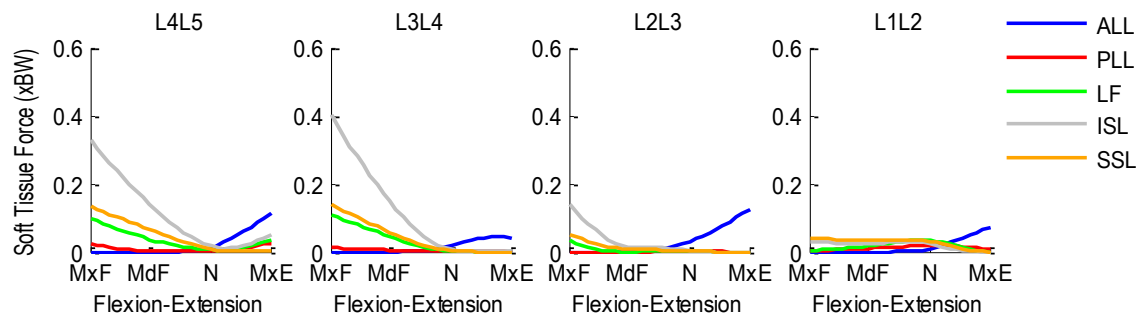


Figure A.111 Patient 10H segmental ligament forces normalized with respect to body weight during flexion-extension.

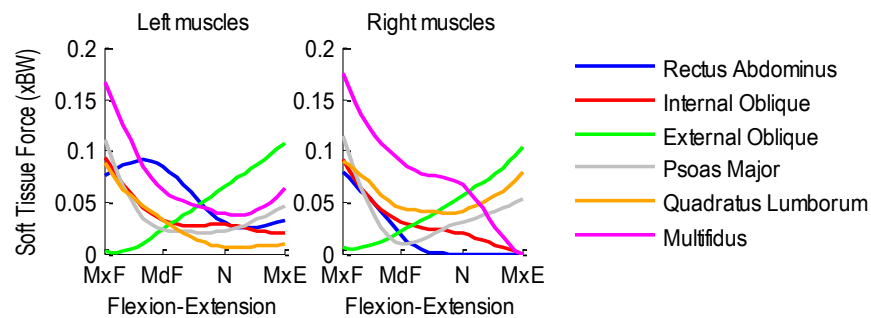


Figure A.112 Patient 10H bilateral muscle forces normalized with respect to body weight during flexion-extension.

A.10.2 Lateral Flexion Activity

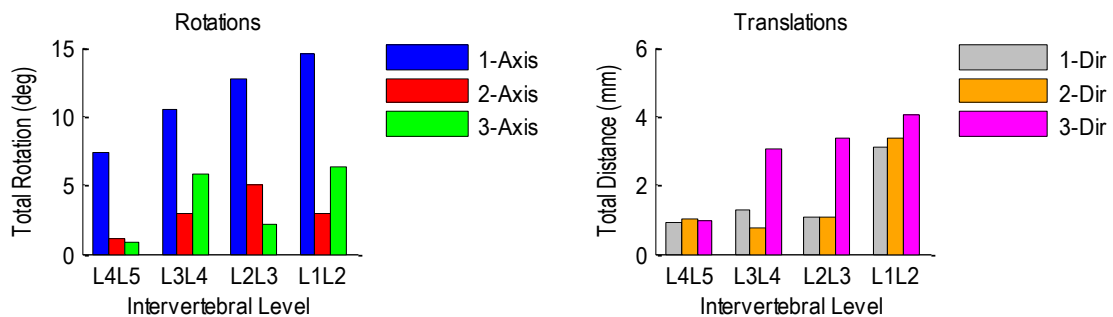


Figure A.113 Patient 10H relative rotations (left) and translations (right) at each vertebral level during left-to-right lateral flexion.

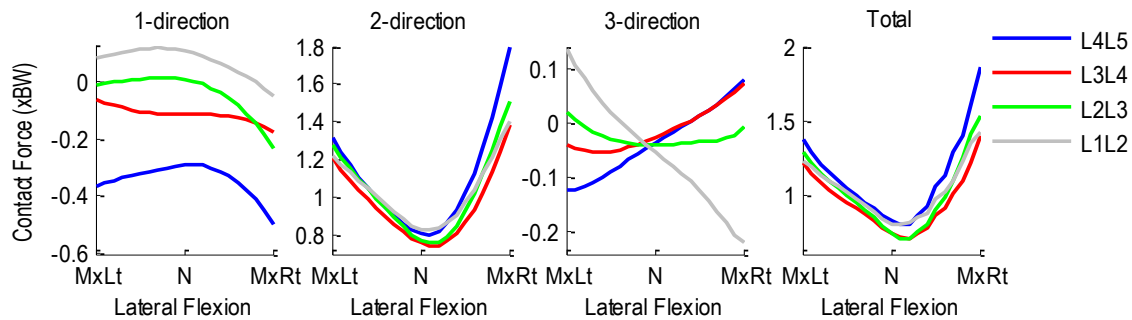


Figure A.114 Patient 10H intervertebral contact forces normalized with respect to body weight during left-to-right lateral flexion. 1-dir=Ant(+)/Post(-), 2-dir=Sup(+)/Inf(-), 3-dir=Rt(+)/Lt(-).

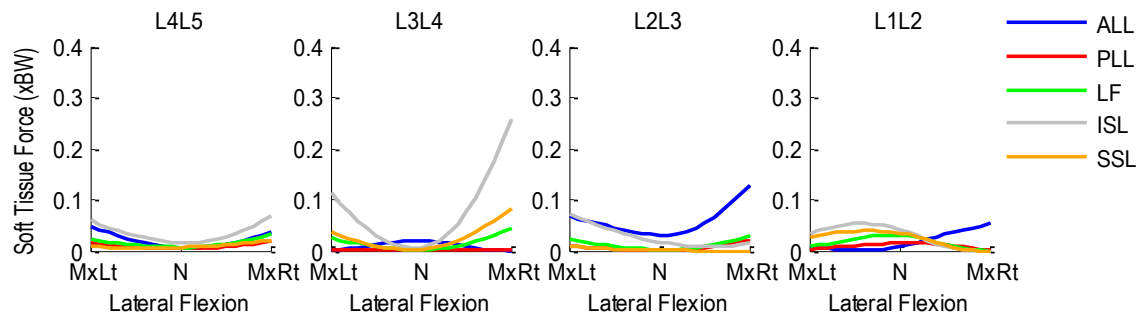


Figure A.115 Patient 10H segmental ligament forces normalized with respect to body weight during left-to-right lateral flexion.

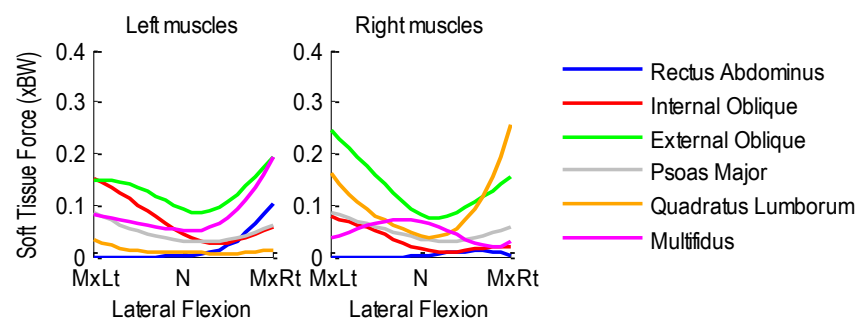


Figure A.116 Patient 10H bilateral muscle forces normalized with respect to body weight during left-to-right lateral flexion

A.10.3 Axial Rotation Activity

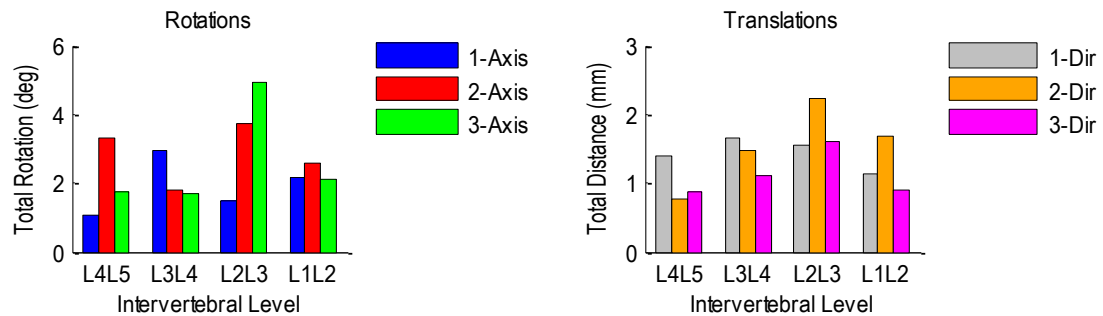


Figure A.117 Patient 10H relative rotations (left) and translations (right) at each vertebral level during left-to-right axial rotation.

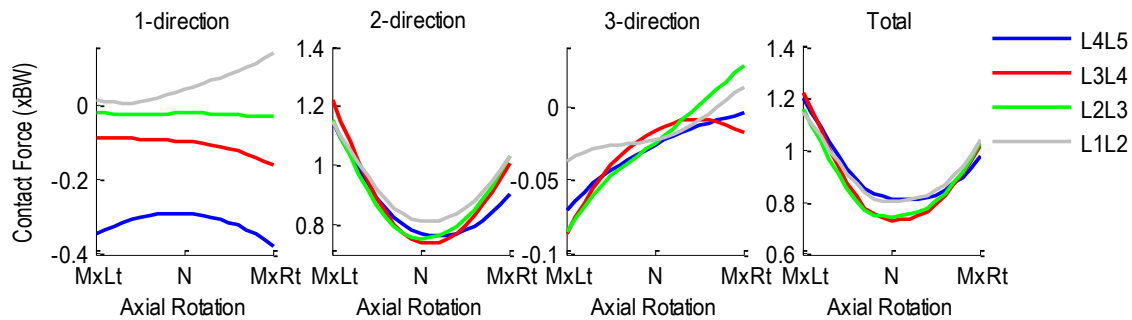


Figure A.118 Patient 1H intervertebral contact forces normalized with respect to body weight during left-to-right axial rotation. 1-dir=Ant(+)/Post(-), 2-dir=Sup(+)/Inf(-), 3-dir=Rt(+)/Lt(-).

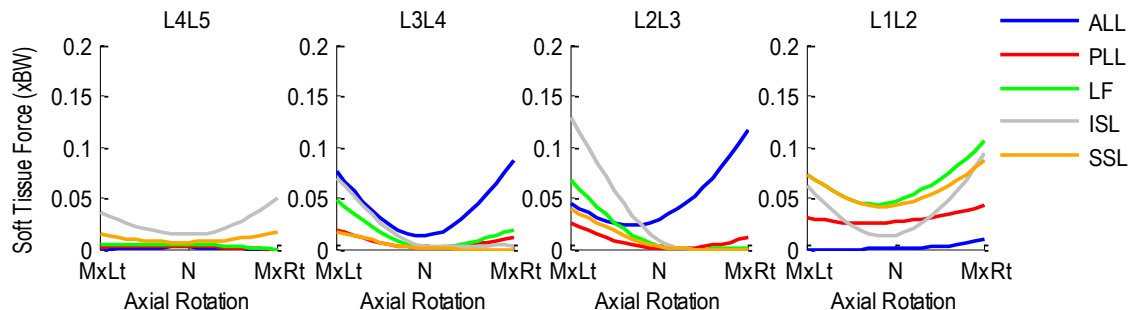


Figure A.119 Patient 10H segmental ligament forces normalized with respect to body weight during left-to-right axial rotation.

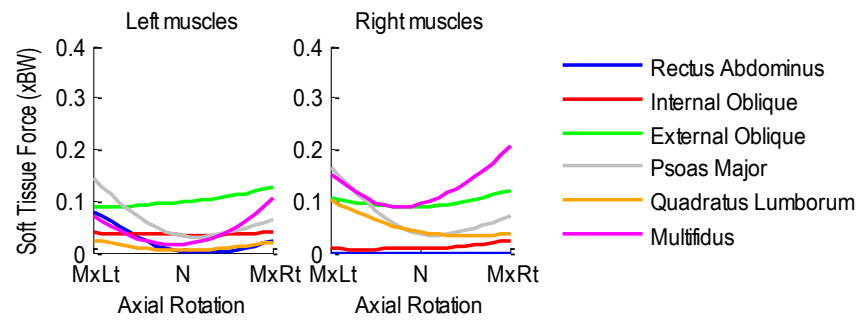


Figure A.120 Patient 10H bilateral muscle forces normalized to body weight during left-to-right axial rotation.

A.11 Patient 1LBP

Age: 44 years

Gender: Male

Height: 1.78 m

Mass: 89 kg

Condition: Low back pain

A.11.1 Flexion-Extension Activity

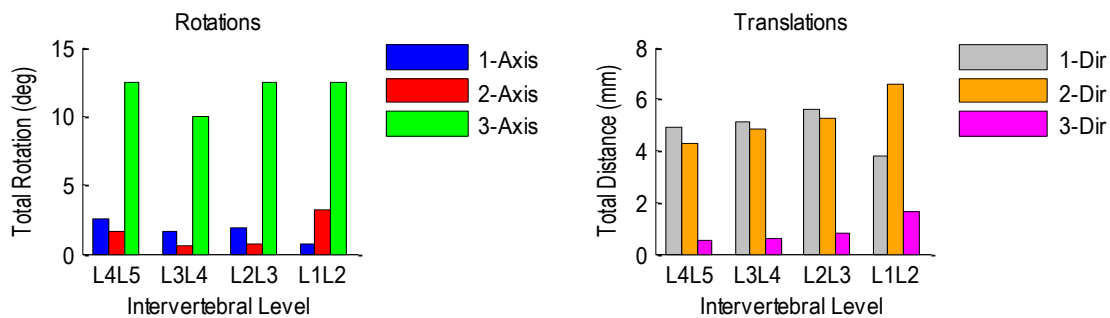


Figure A.121 Patient 1LBP relative rotations (left) and translations (right) at each vertebral level during flexion-extension.

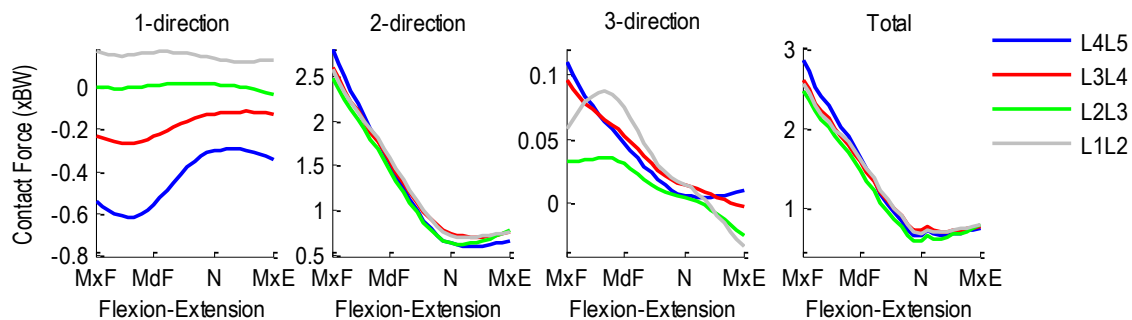


Figure A.122 Patient 1LBP intervertebral contact forces normalized with respect to body weight during flexion-extension. 1-dir=Ant(+)/Post(-), 2-dir=Sup(+)/Inf(-), 3-dir=Rt(+)/Lt(-).

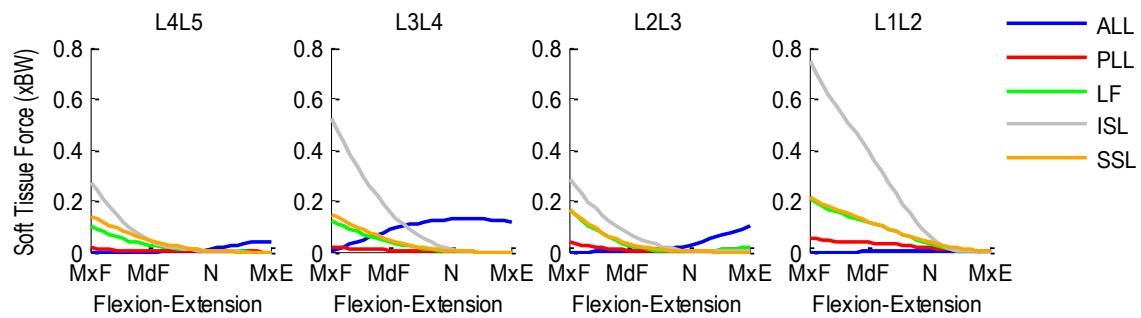


Figure A.123 Patient 1LBP segmental ligament forces normalized with respect to body weight during flexion-extension.

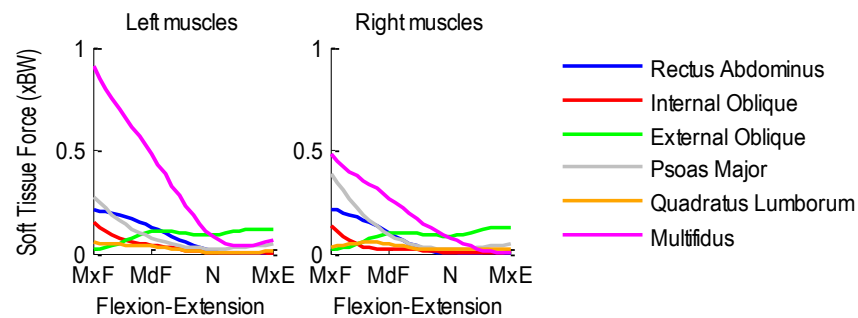


Figure A.124 Patient 1LBP bilateral muscle forces normalized with respect to body weight during flexion-extension.

A.11.2 Lateral Flexion Activity

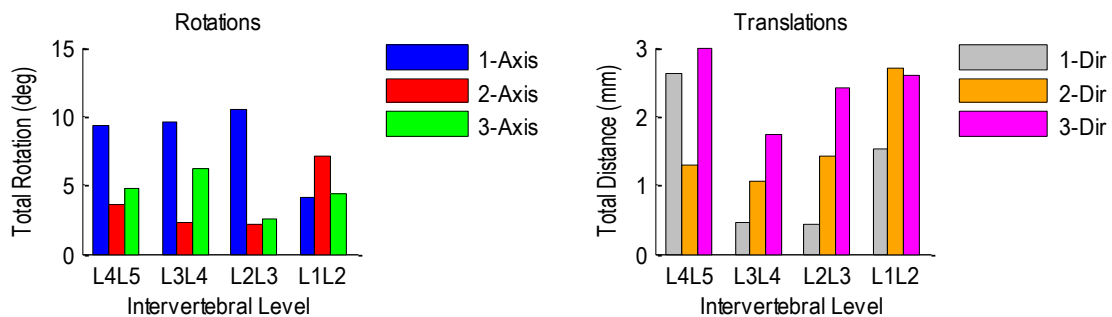


Figure A.125 Patient 1LBP relative rotations (left) and translations (right) at each vertebral level during left-to-right lateral flexion.

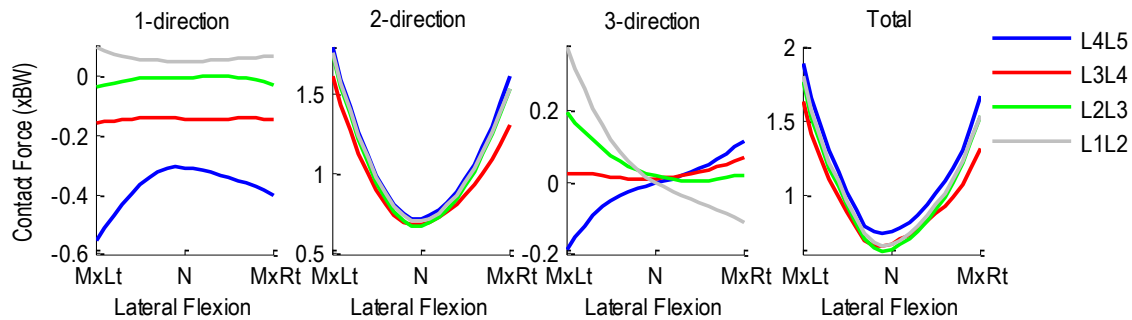


Figure A.126 Patient 1LBP intervertebral contact forces normalized with respect to body weight during left-to-right lateral flexion. 1-dir=Ant(+)/Post(-), 2-dir=Sup(+)/Inf(-), 3-dir=Rt(+)/Lt(-).

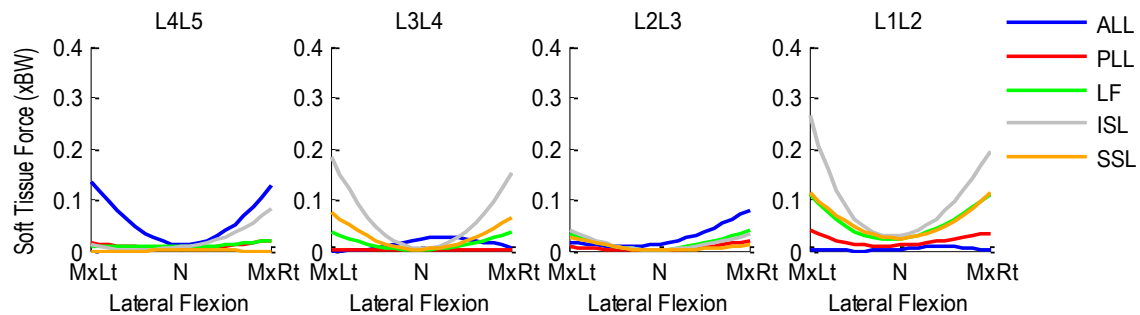


Figure A.127 Patient 1LBP segmental ligament forces normalized with respect to body weight during left-to-right lateral flexion.

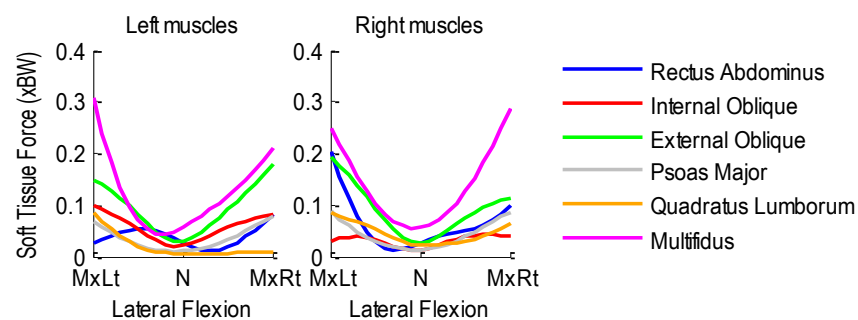


Figure A.128 Patient 1LBP bilateral muscle forces normalized to body weight during left-to-right lateral flexion.

A.11.3 Axial Rotation Activity

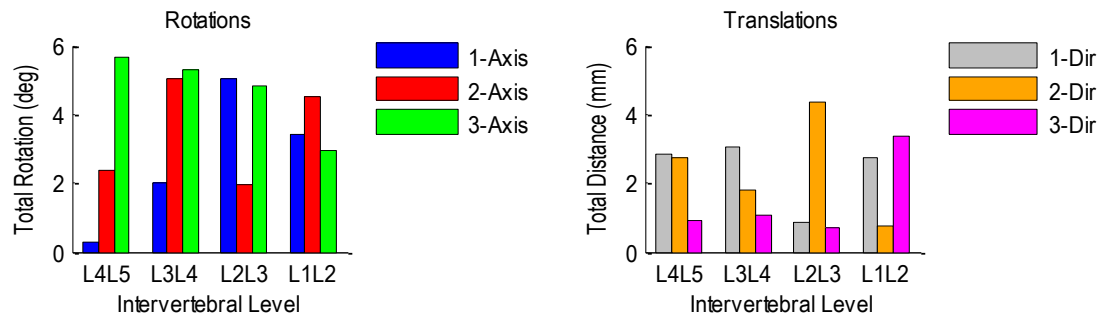


Figure A.129 Patient 1LBP relative rotations (left) and translations (right) at each vertebral level during left-to-right axial rotation.

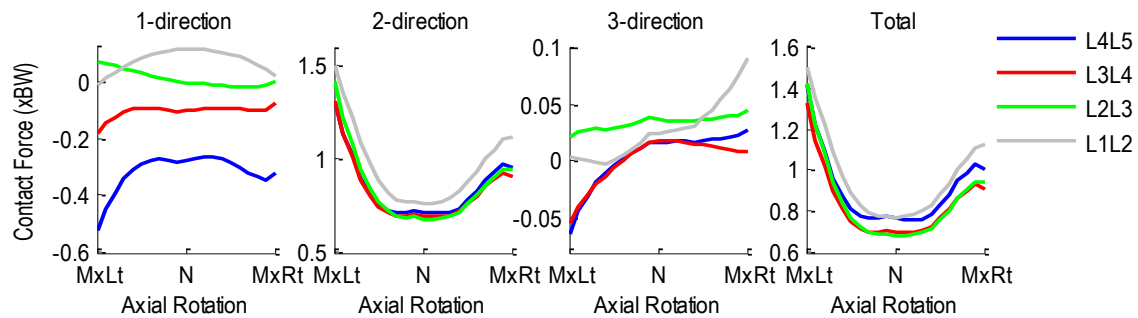


Figure A.130 Patient 1LBP intervertebral contact forces normalized with respect to body weight during left-to-right axial rotation. 1-dir=Ant(+)/Post(-), 2-dir=Sup(+)/Inf(-), 3-dir=Rt(+)/Lt(-).

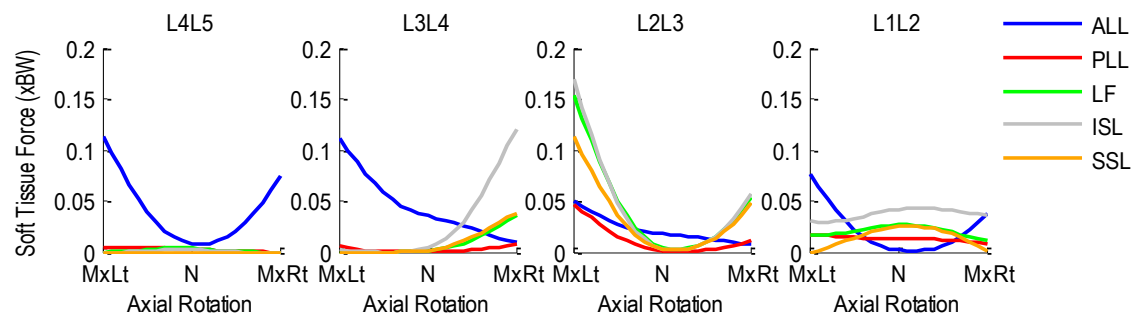


Figure A.131 Patient 1LBP segmental ligament forces normalized with respect to body weight during left-to-right axial rotation.

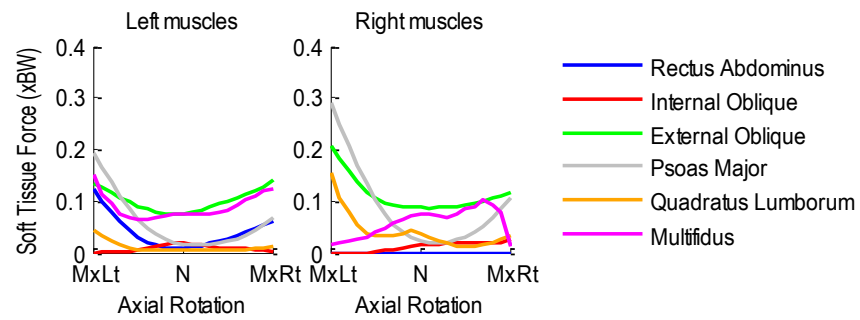


Figure A.132 Patient 1LBP bilateral muscle forces normalized with respect to body weight during left-to-right axial rotation.

A.12 Patient 2LBP

Age: 44 years

Gender: Male

Height: 1.85 m

Mass: 91 kg

Condition: Low back pain

A.12.1 Flexion-Extension Activity

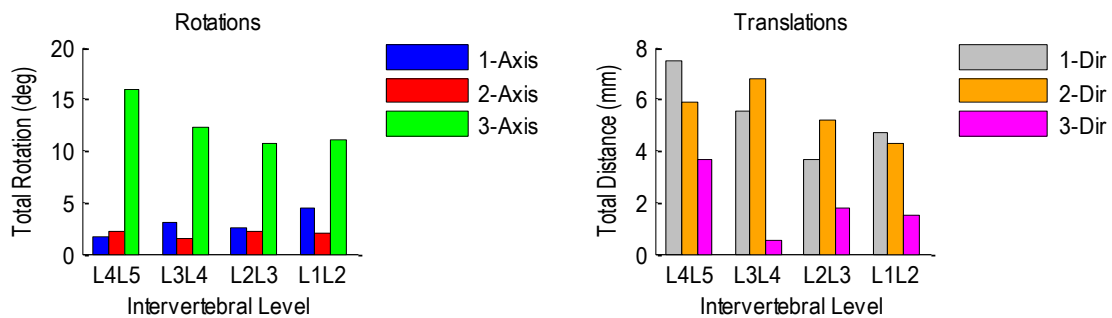


Figure A.133 Patient 2LBP relative rotations (left) and translations (right) at each vertebral level during flexion-extension.

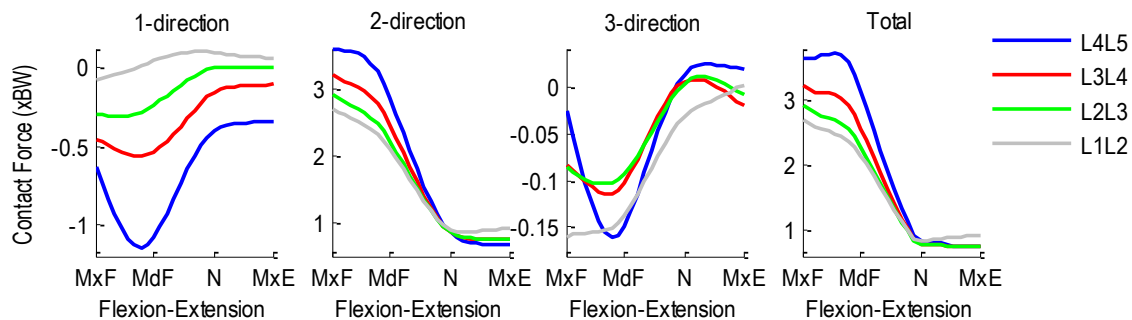


Figure A.134 Patient 2LBP intervertebral contact forces normalized with respect to body weight during flexion-extension. 1-dir=Ant(+)/Post(-), 2-dir=Sup(+)/Inf(-), 3-dir=Rt(+)/Lt(-).

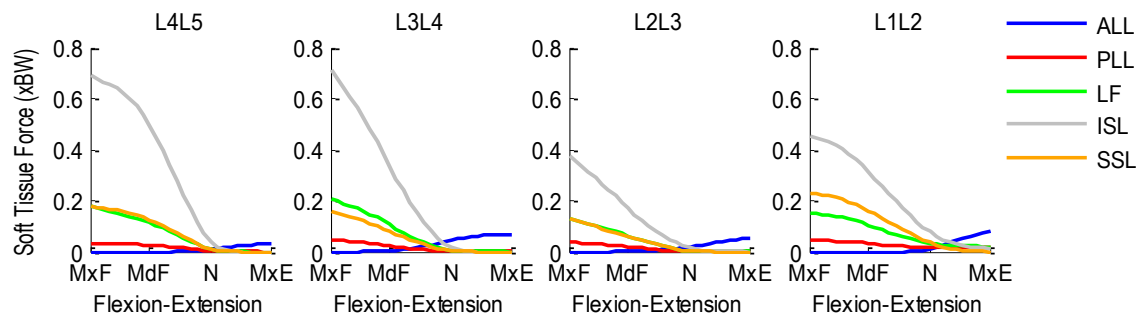


Figure A.135 Patient 2LBP segmental ligament forces normalized with respect to body weight during flexion-extension.

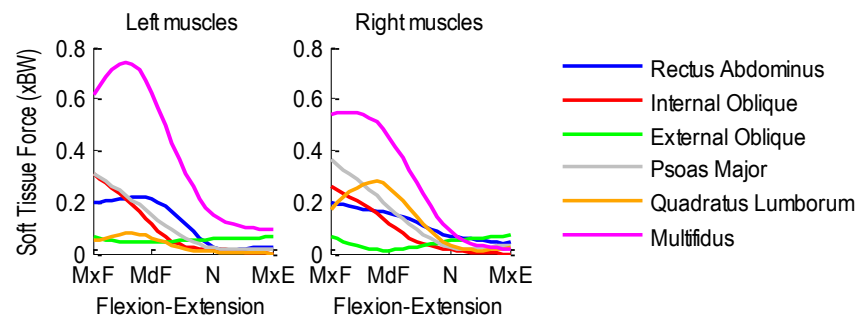


Figure A.136 Patient 2LBP bilateral muscle forces normalized with respect to body weight during flexion-extension.

A.12.2 Lateral Flexion Activity

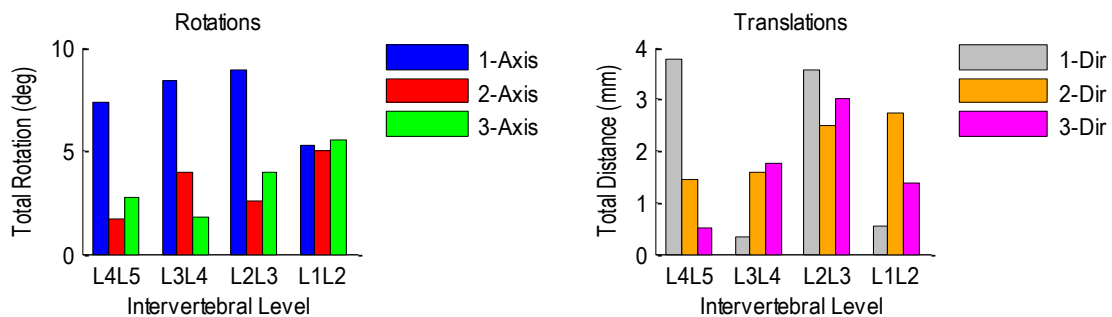


Figure A.137 Patient 2LBP relative rotations (left) and translations (right) at each vertebral level during left-to-right lateral flexion.

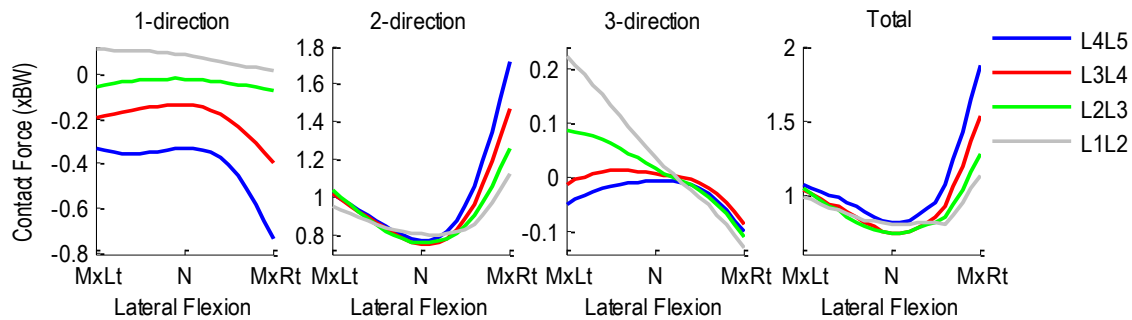


Figure A.138 Patient 2LBP intervertebral contact forces normalized with respect to body weight during left-to-right lateral flexion. 1-dir=Ant(+)/Post(-), 2-dir=Sup(+)/Inf(-), 3-dir=Rt(+)/Lt(-).

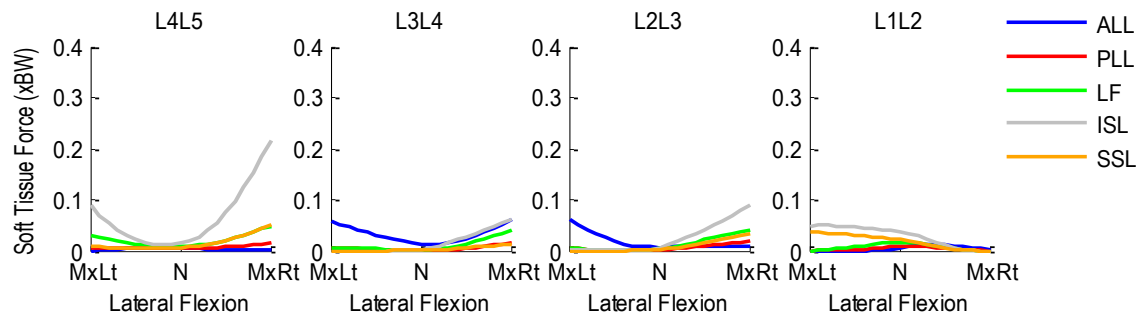


Figure A.139 Patient 2LBP segmental ligament forces normalized with respect to body weight during left-to-right lateral flexion.

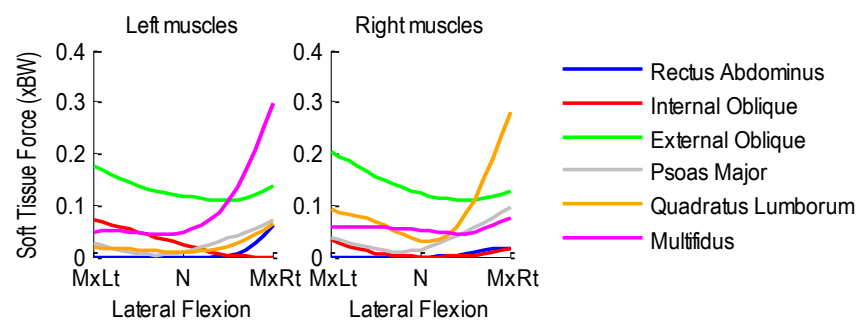


Figure A.140 Patient 2LBP bilateral muscle forces normalized to body weight during left-to-right lateral flexion.

A.12.3 Axial Rotation Activity

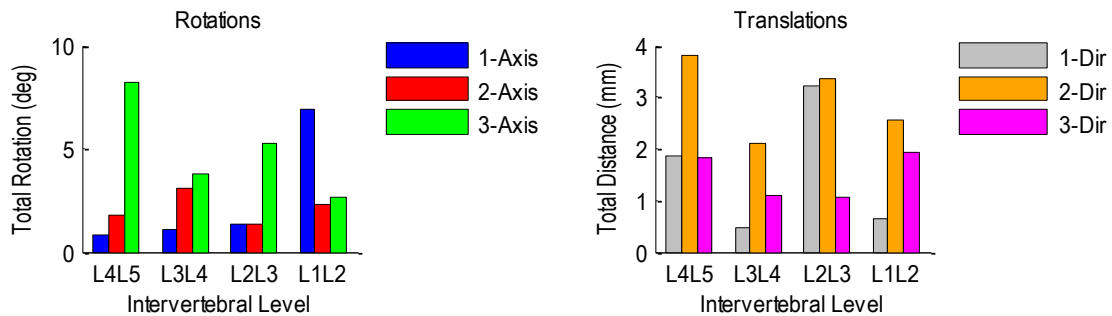


Figure A.141 Patient 2LBP relative rotations (left) and translations (right) at each vertebral level during left-to-right axial rotation.

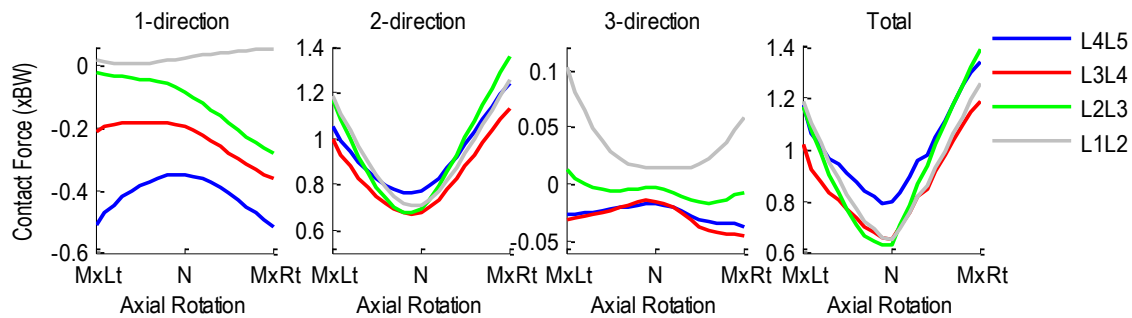


Figure A.142 Patient 2LBP intervertebral contact forces normalized with respect to body weight during left-to-right axial rotation. 1-dir=Ant(+)/Post(-), 2-dir=Sup(+)/Inf(-), 3-dir=Rt(+)/Lt(-).

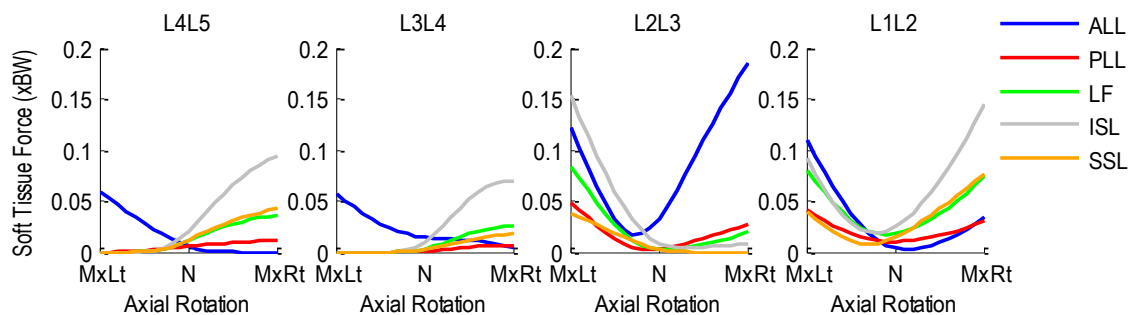


Figure A.143 Patient 2LBP segmental ligament forces normalized with respect to body weight during left-to-right axial rotation.

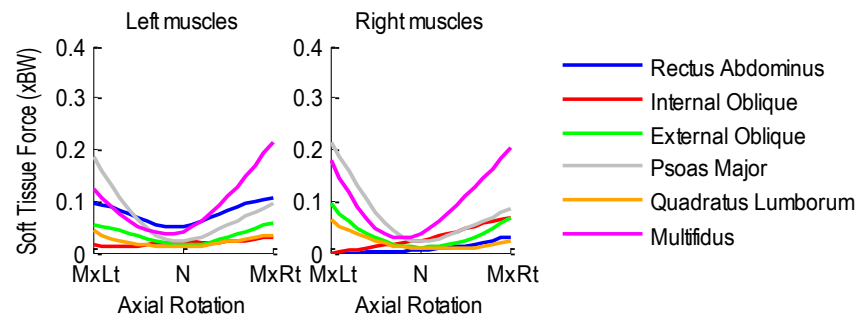


Figure A.144 Patient 2LBP bilateral muscle forces normalized with respect to body weight during left-to-right axial rotation.

A.13 Patient 3LBP

Age: 41 years

Gender: Male

Height: 1.75 m

Mass: 87 kg

Condition: Low back pain

A.13.1 Flexion-Extension Activity

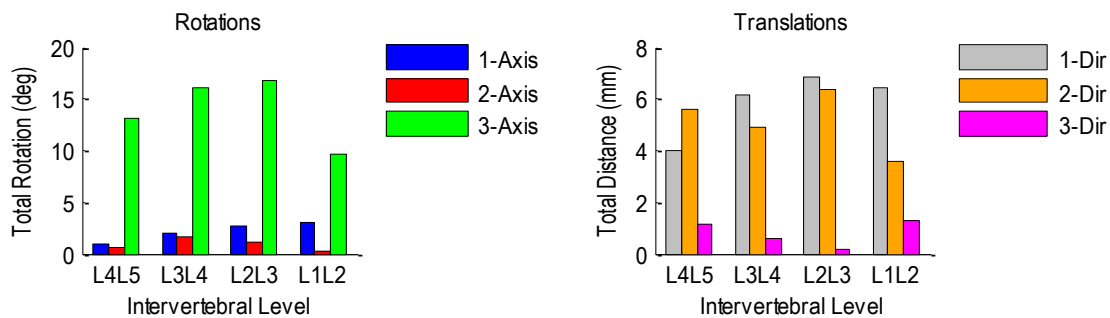


Figure A.145 Patient 3LBP relative rotations (left) and translations (right) at each vertebral level during flexion-extension.

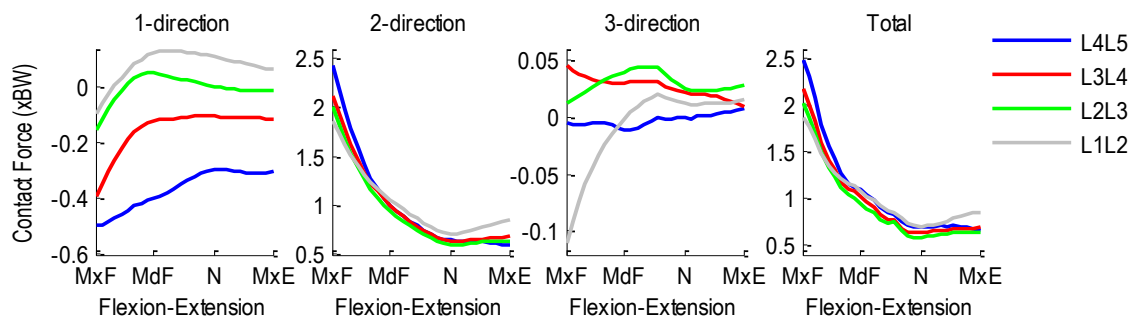


Figure A.146 Patient 3LBP intervertebral contact forces normalized with respect to body weight during flexion-extension. 1-dir=Ant(+)/Post(-), 2-dir=Sup(+)/Inf(-), 3-dir=Rt(+)/Lt(-).

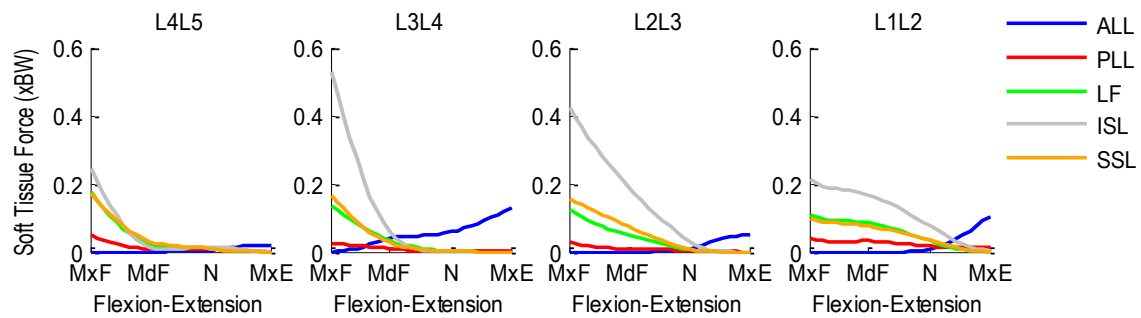


Figure A.147 Patient 3LBP segmental ligament forces normalized with respect to body weight during flexion-extension.

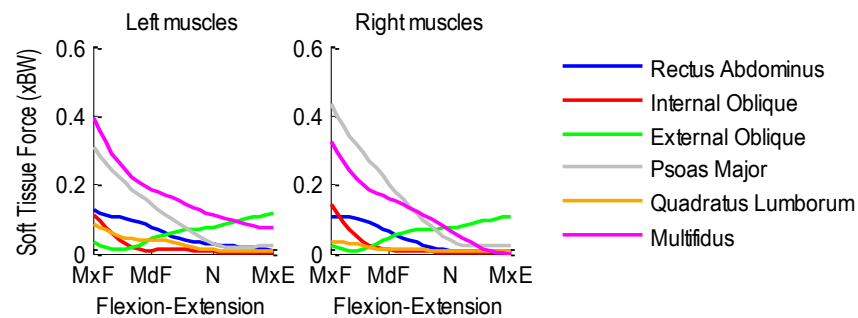


Figure A.148 Patient 3LBP bilateral muscle forces normalized with respect to body weight during flexion-extension.

A.13.2 Lateral Flexion Activity

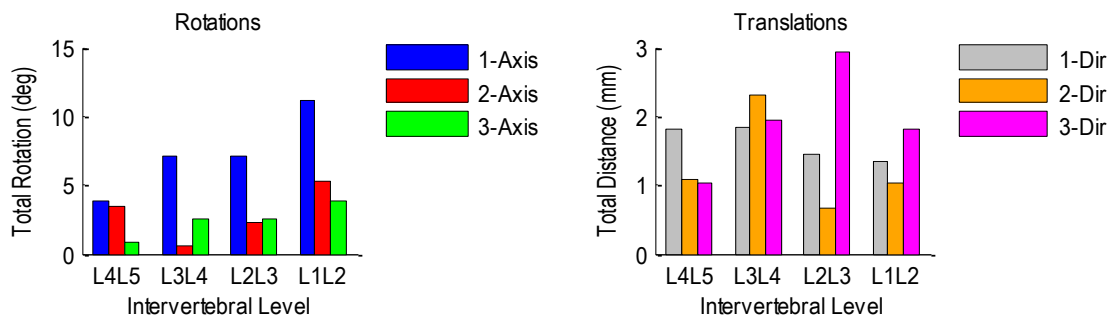


Figure A.149 Patient 3LBP relative rotations (left) and translations (right) at each vertebral level during left-to-right lateral flexion.

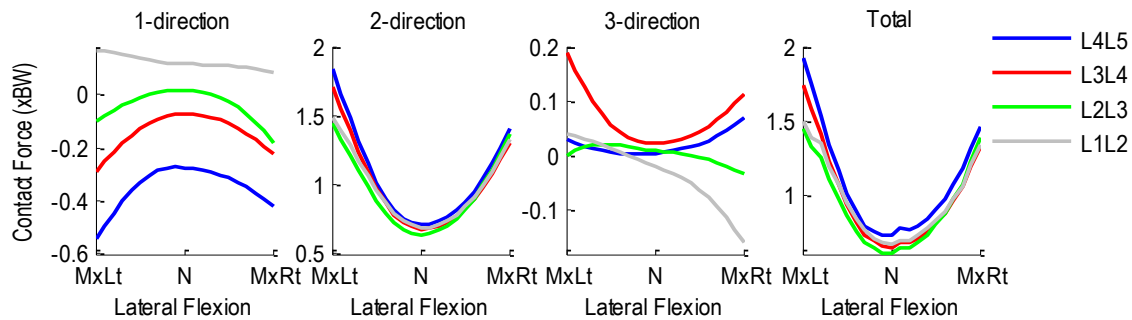


Figure A.150 Patient 3LBP intervertebral contact forces normalized with respect to body weight during left-to-right lateral flexion. 1-dir=Ant(+)/Post(-), 2-dir=Sup(+)/Inf(-), 3-dir=Rt(+)/Lt(-).

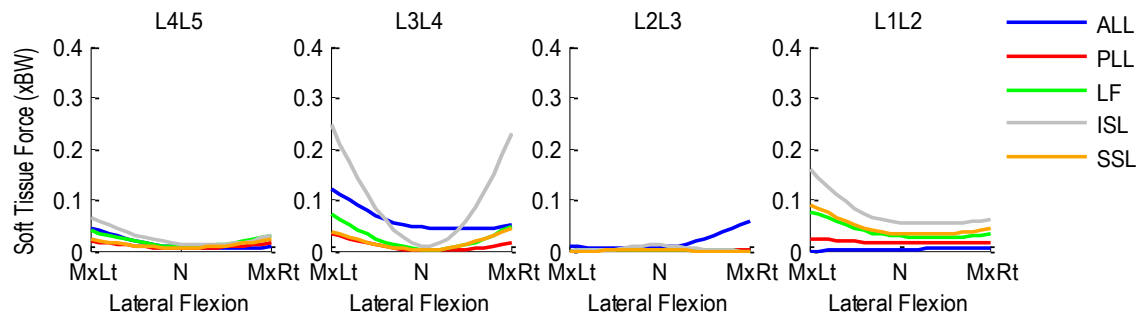


Figure A.151 Patient 3LBP segmental ligament forces normalized with respect to body weight during left-to-right lateral flexion.

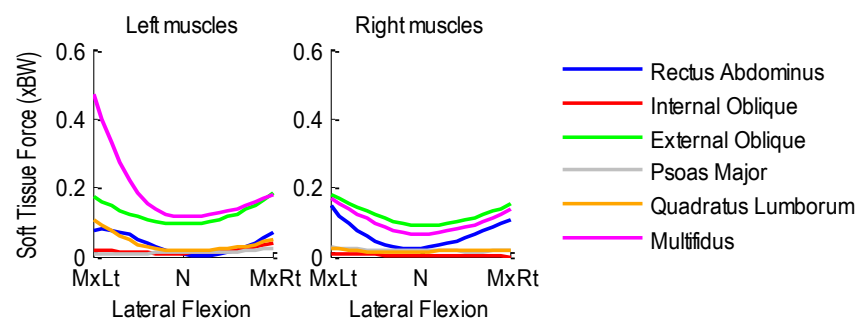


Figure A.152 Patient 3LBP bilateral muscle forces normalized to body weight during left-to-right lateral flexion.

A.13.3 Axial Rotation Activity

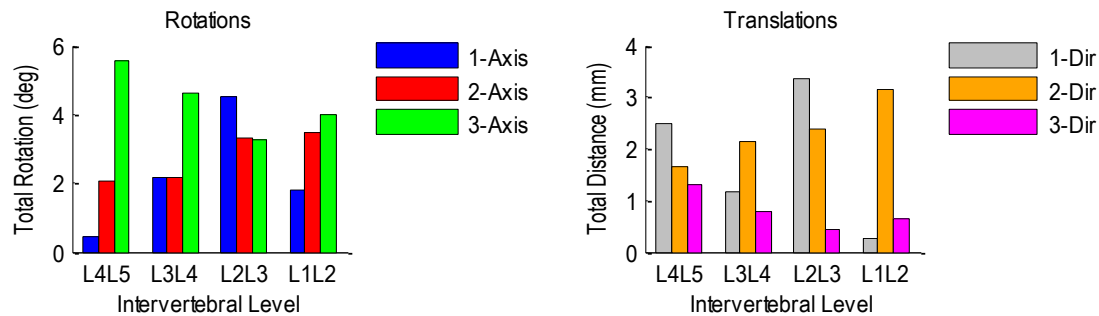


Figure A.153 Patient 3LBP relative rotations (left) and translations (right) at each vertebral level during left-to-right axial rotation.

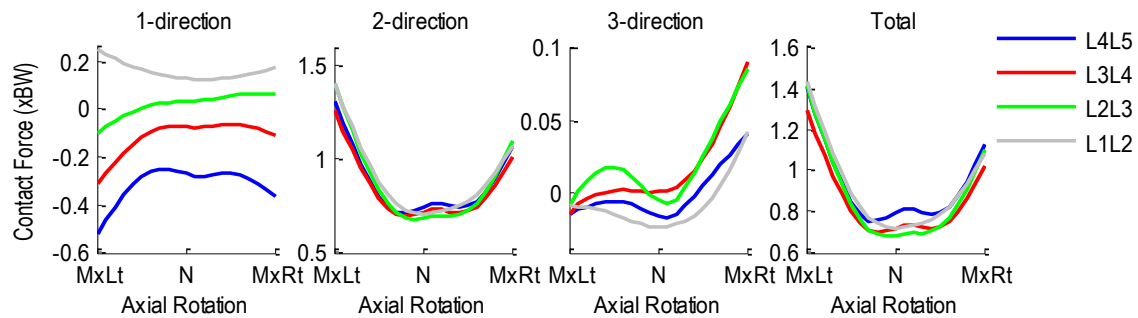


Figure A.154 Patient 3LBP intervertebral contact forces normalized with respect to body weight during left-to-right axial rotation. 1-dir=Ant(+)/Post(-), 2-dir=Sup(+)/Inf(-), 3-dir=Rt(+)/Lt(-).

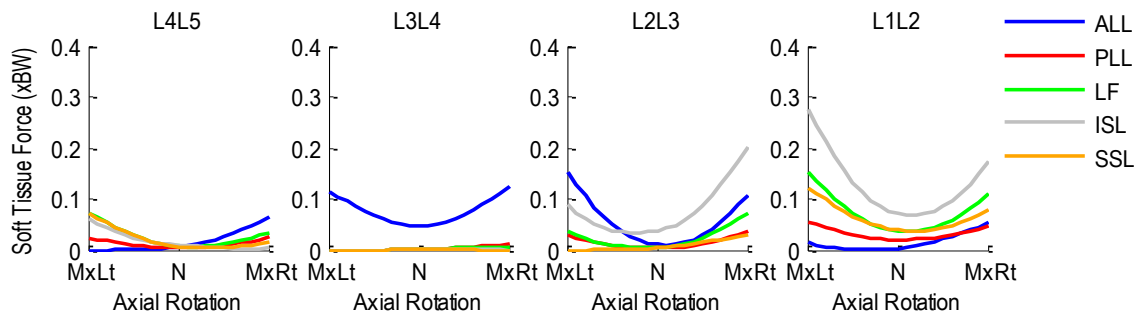


Figure A.155 Patient 3LBP segmental ligament forces normalized with respect to body weight during left-to-right axial rotation.

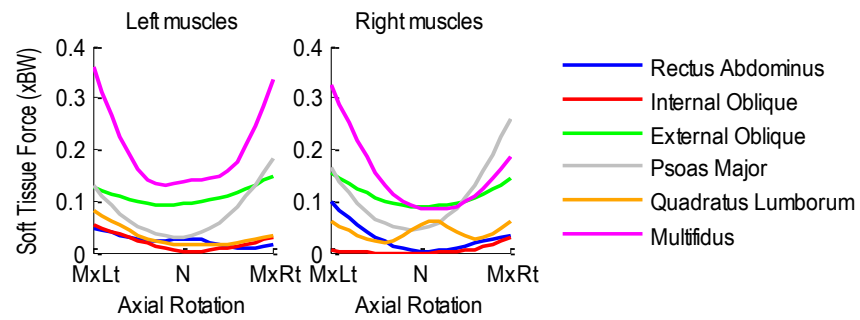


Figure A.156 Patient 3LBP bilateral muscle forces normalized with respect to body weight during left-to-right axial rotation.

A.14 Patient 4LBP

Age: 53 years

Gender: Female

Height: 1.60 m

Mass: 67 kg

Condition: Low back pain

A.14.1 Flexion-Extension Activity

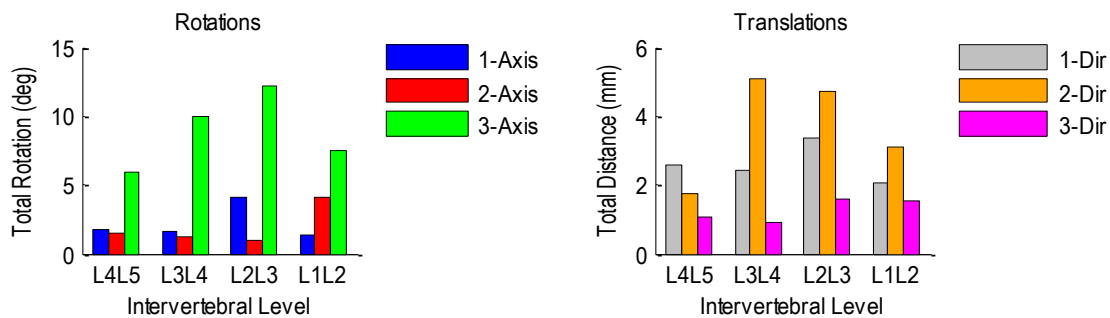


Figure A.157 Patient 4LBP relative rotations (left) and translations (right) at each vertebral level during flexion-extension.

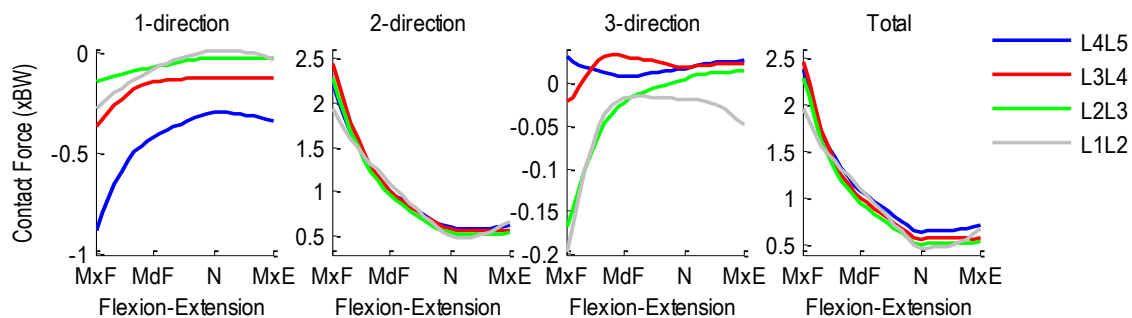


Figure A.158 Patient 4LBP intervertebral contact forces normalized with respect to body weight during flexion-extension. 1-dir=Ant(+)/Post(-), 2-dir=Sup(+)/Inf(-), 3-dir=Rt(+)/Lt(-).

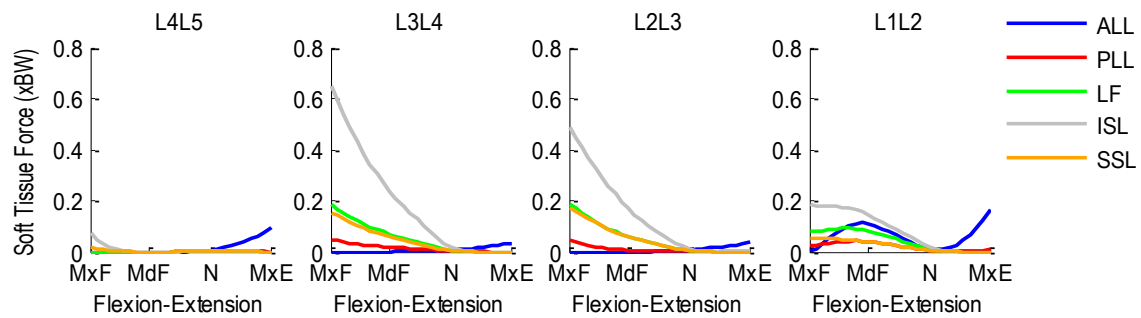


Figure A.159 Patient 4LBP segmental ligament forces normalized with respect to body weight during flexion-extension.

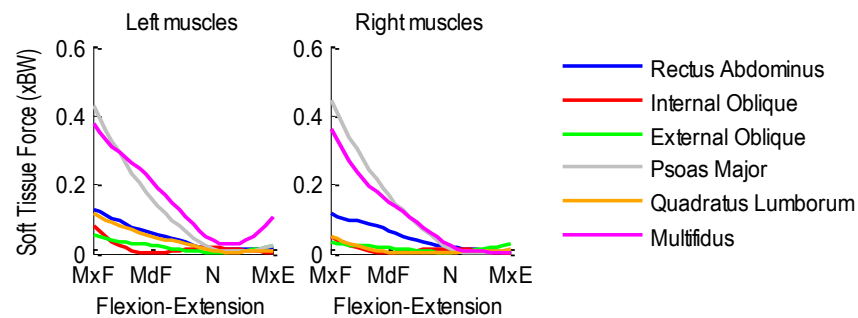


Figure A.160 Patient 4LBP bilateral muscle forces normalized with respect to body weight during flexion-extension.

A.14.2 Lateral Flexion Activity

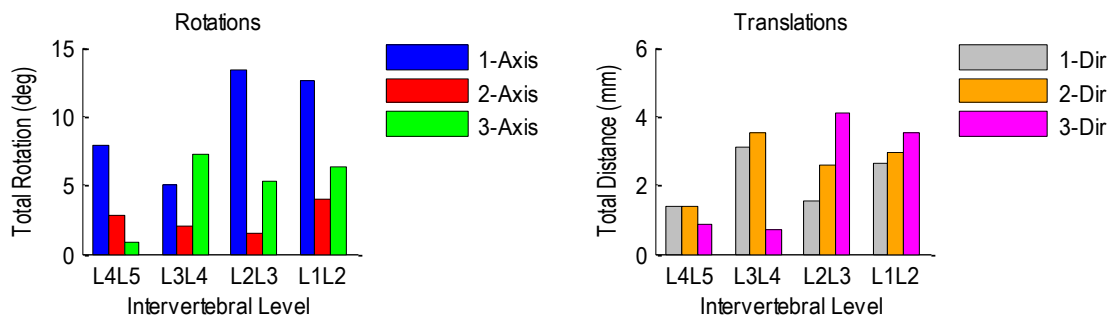


Figure A.161 Patient 4LBP relative rotations (left) and translations (right) at each vertebral level during left-to-right lateral flexion.

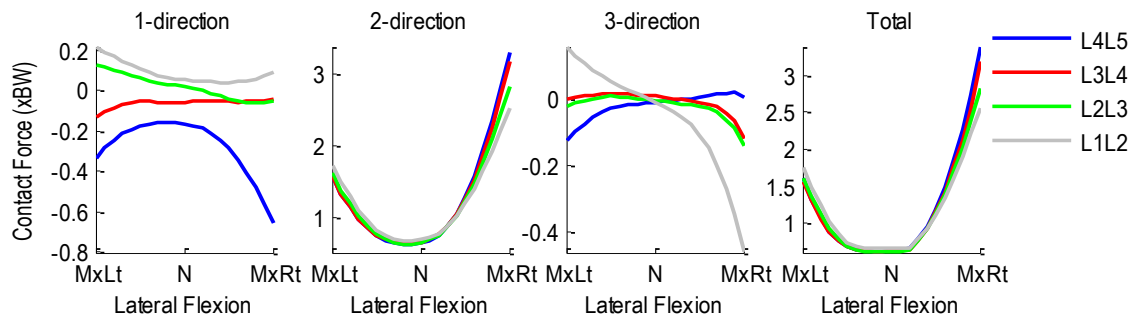


Figure A.162 Patient 4LBP intervertebral contact forces normalized with respect to body weight during left-to-right lateral flexion. 1-dir=Ant(+)/Post(-), 2-dir=Sup(+)/Inf(-), 3-dir=Rt(+)/Lt(-).

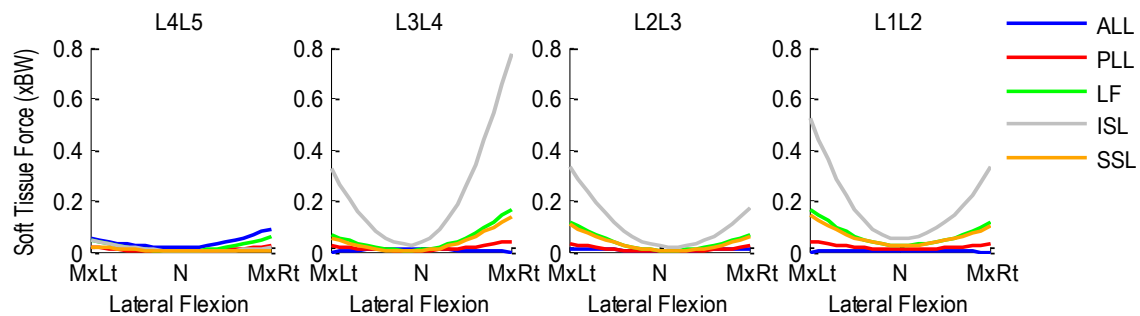


Figure A.163 Patient 4LBP segmental ligament forces normalized with respect to body weight during left-to-right lateral flexion.

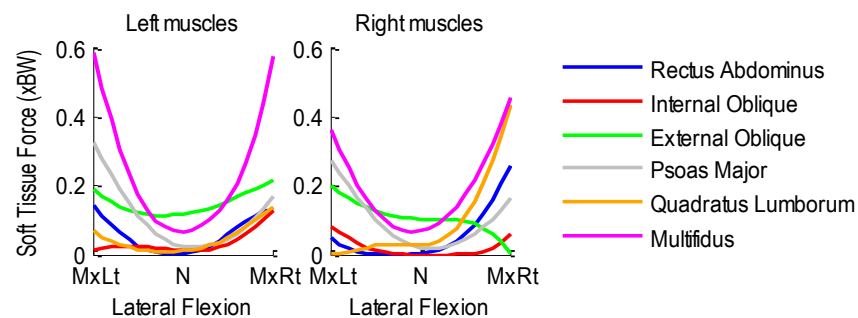


Figure A.164 Patient 4LBP bilateral muscle forces normalized to body weight during left-to-right lateral flexion.

A.14.3 Axial Rotation Activity

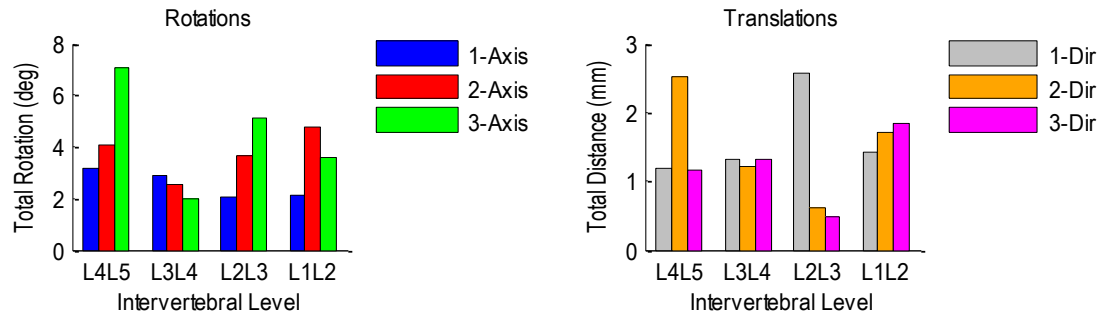


Figure A.165 Patient 4LBP relative rotations (left) and translations (right) at each vertebral level during left-to-right axial rotation.

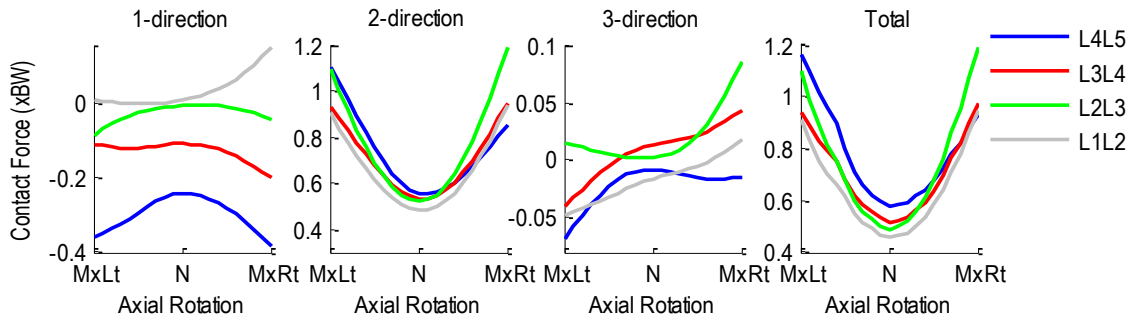


Figure A.166 Patient 4LBP intervertebral contact forces normalized with respect to body weight during left-to-right axial rotation. 1-dir=Ant(+)/Post(-), 2-dir=Sup(+)/Inf(-), 3-dir=Rt(+)/Lt(-).

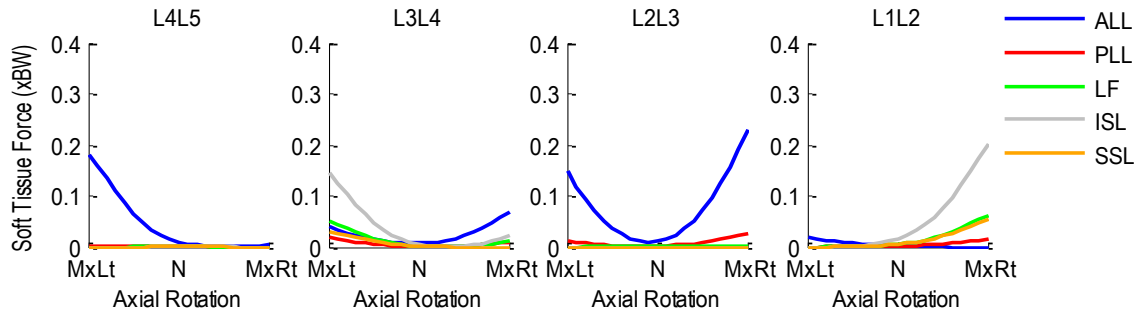


Figure A.167 Patient 4LBP segmental ligament forces normalized with respect to body weight during left-to-right axial rotation.

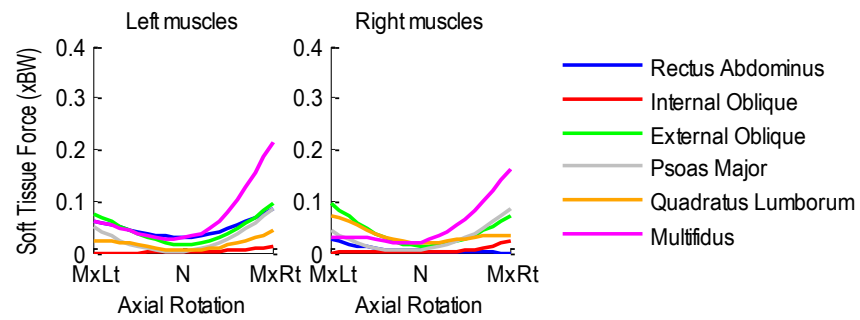


Figure A.168 Patient 4LBP bilateral muscle forces normalized with respect to body weight during left-to-right axial rotation.

A.15 Patient 5LBP

Age: 24 years

Gender: Male

Height: 1.78 m

Mass: 85 kg

Condition: Low back pain

A.15.1 Flexion-Extension Activity

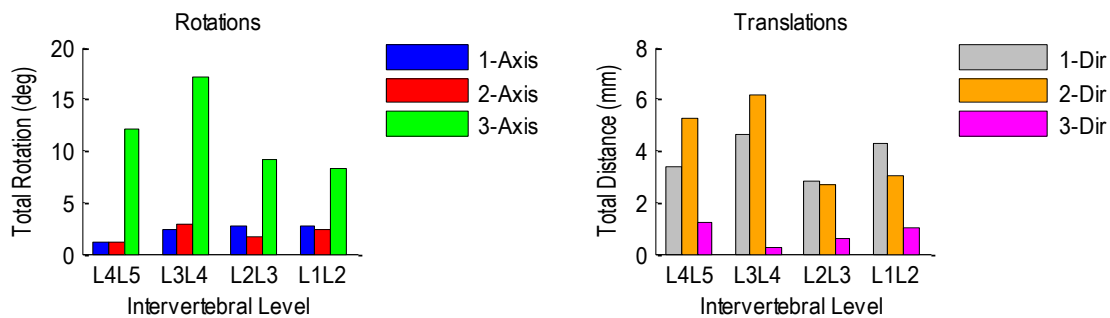


Figure A.169 Patient 5LBP relative rotations (left) and translations (right) at each vertebral level during flexion-extension.

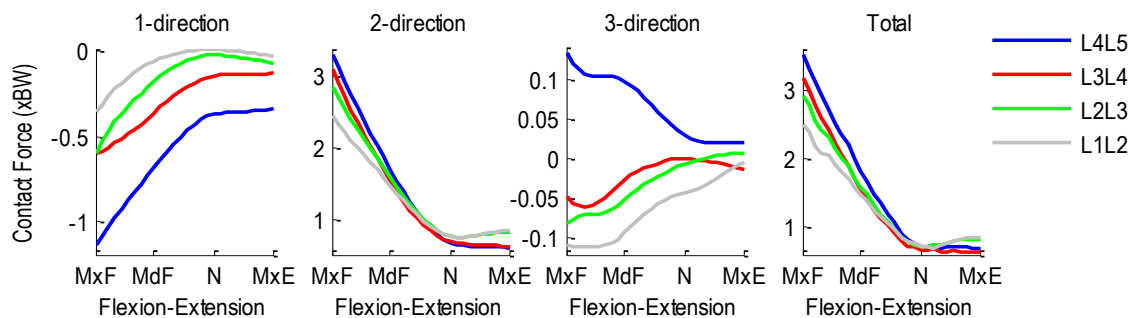


Figure A.170 Patient 5LBP intervertebral contact forces normalized with respect to body weight during flexion-extension. 1-dir=Ant(+)/Post(-), 2-dir=Sup(+)/Inf(-), 3-dir=Rt(+)/Lt(-).

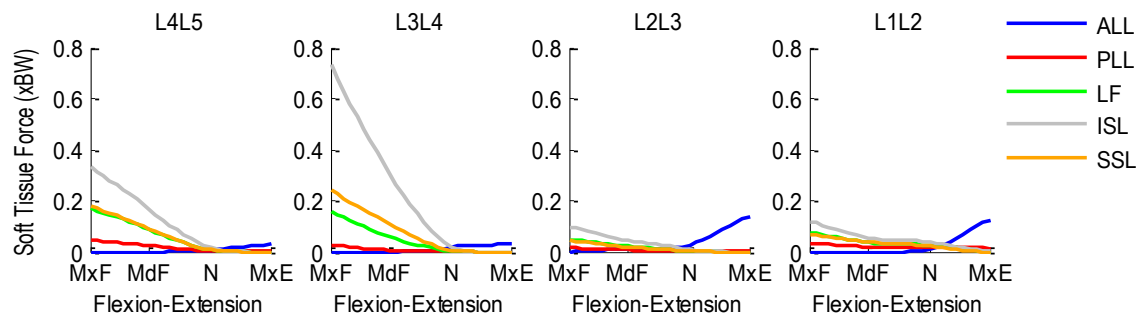


Figure A.171 Patient 5LBP segmental ligament forces normalized with respect to body weight during flexion-extension.

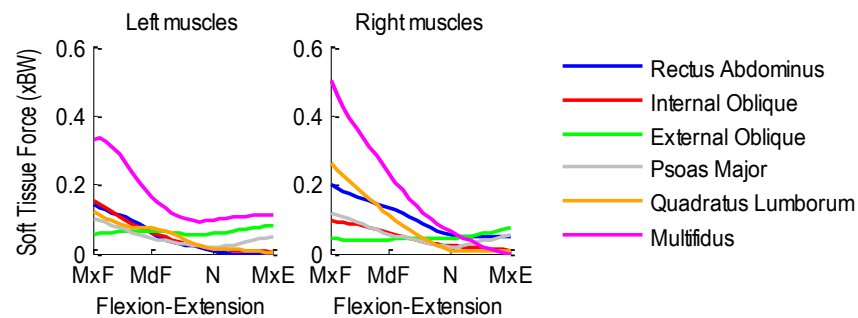


Figure A.172 Patient 5LBP bilateral muscle forces normalized with respect to body weight during flexion-extension.

A.15.2 Lateral Flexion Activity

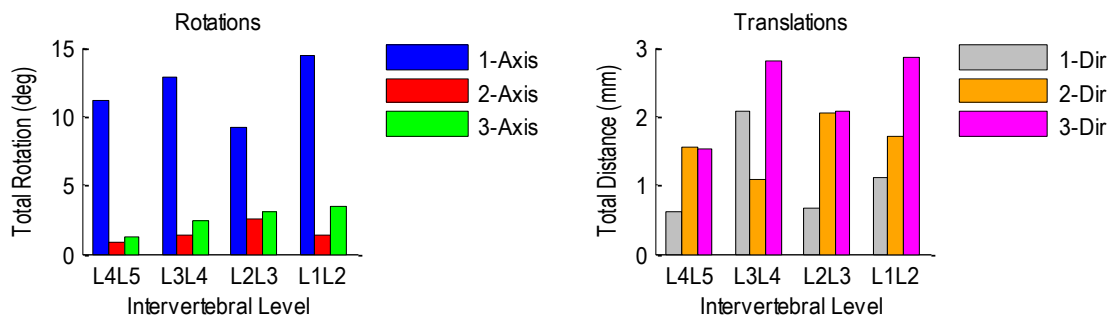


Figure A.173 Patient 5LBP relative rotations (left) and translations (right) at each vertebral level during left-to-right lateral flexion.

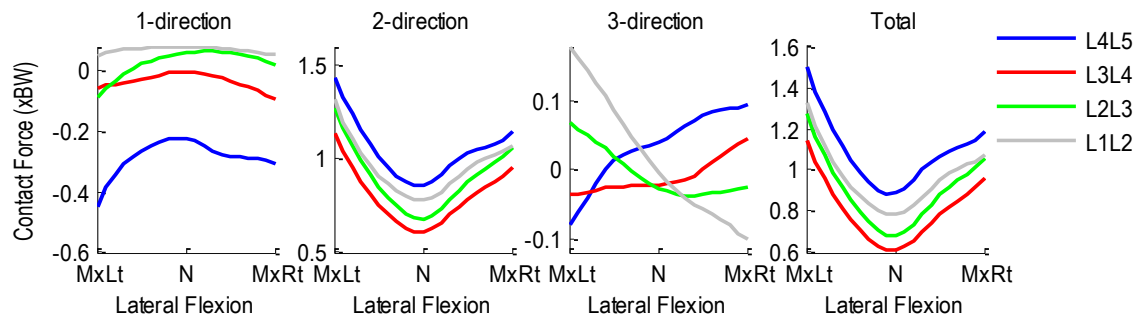


Figure A.174 Patient 5LBP intervertebral contact forces normalized with respect to body weight during left-to-right lateral flexion. 1-dir=Ant(+)/Post(-), 2-dir=Sup(+)/Inf(-), 3-dir=Rt(+)/Lt(-).

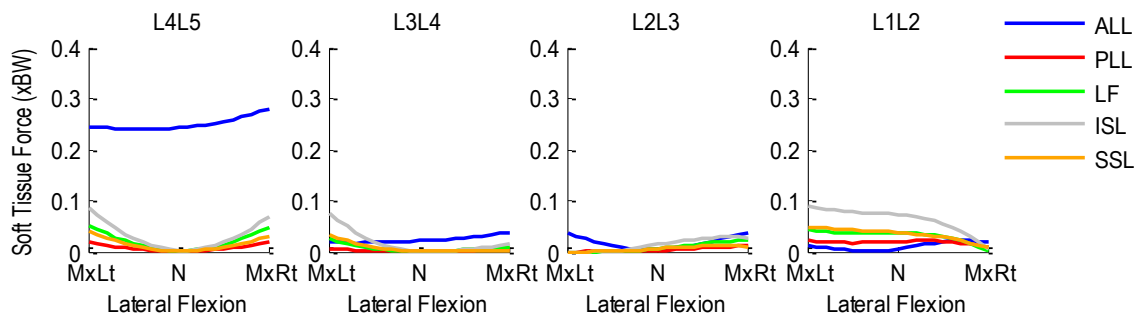


Figure A.175 Patient 5LBP segmental ligament forces normalized with respect to body weight during left-to-right lateral flexion.

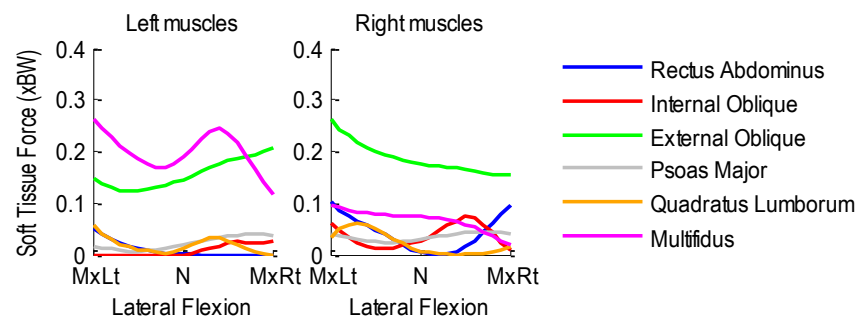


Figure A.176 Patient 5LBP bilateral muscle forces normalized to body weight during left-to-right lateral flexion.

A.15.3 Axial Rotation Activity

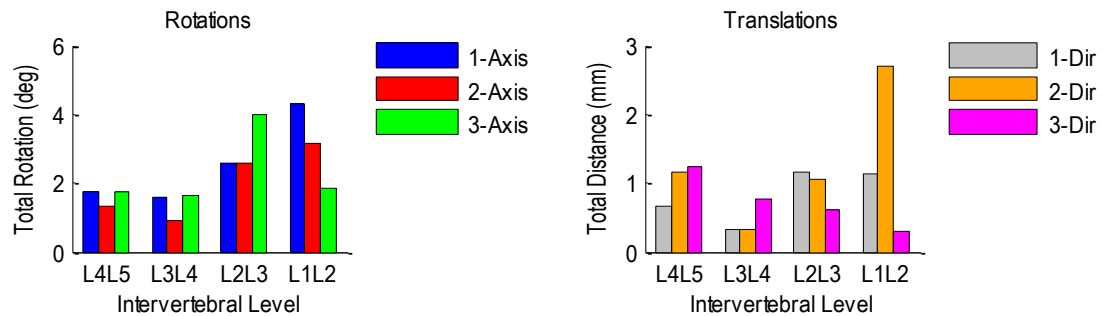


Figure A.177 Patient 5LBP relative rotations (left) and translations (right) at each vertebral level during left-to-right axial rotation.

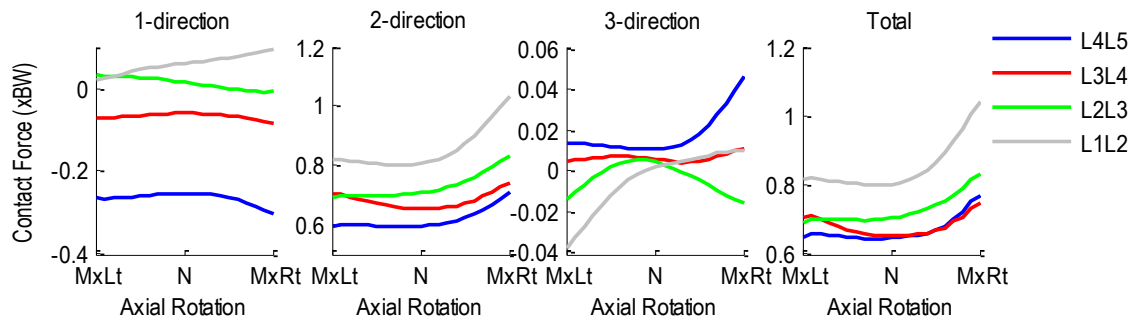


Figure A.178 Patient 5LBP intervertebral contact forces normalized with respect to body weight during left-to-right axial rotation. 1-dir=Ant(+)/Post(-), 2-dir=Sup(+)/Inf(-), 3-dir=Rt(+)/Lt(-).

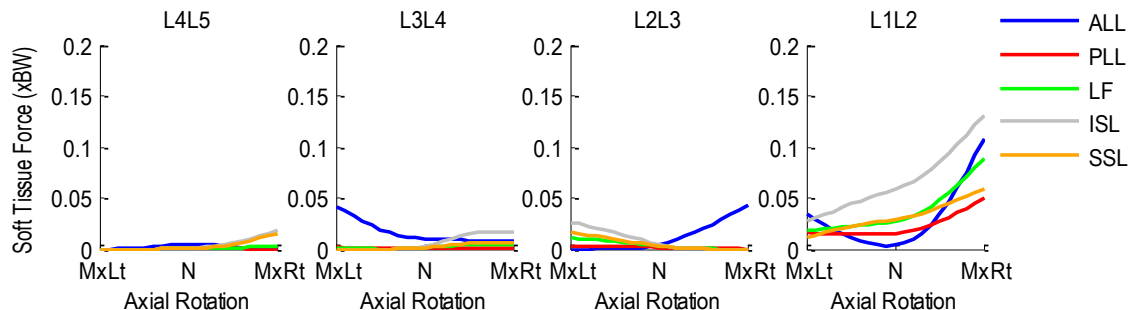


Figure A.179 Patient 5LBP segmental ligament forces normalized with respect to body weight during left-to-right axial rotation.

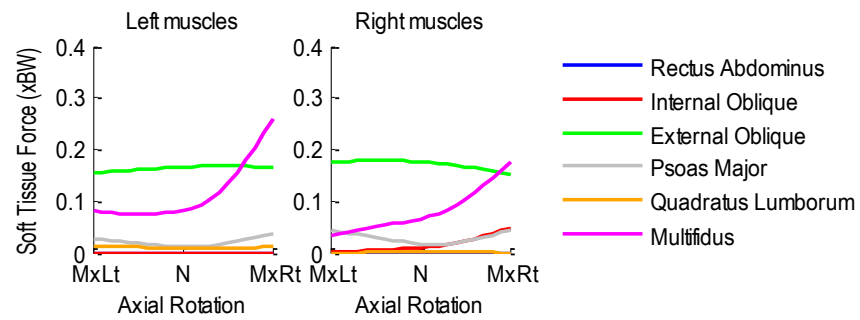


Figure A.180 Patient 5LBP bilateral muscle forces normalized with respect to body weight during left-to-right axial rotation.

A.16 Patient 6LBP

Age: 44 years

Gender: Male

Height: 1.73 m

Mass: 75 kg

Condition: Low back pain

A.16.1 Flexion-Extension Activity

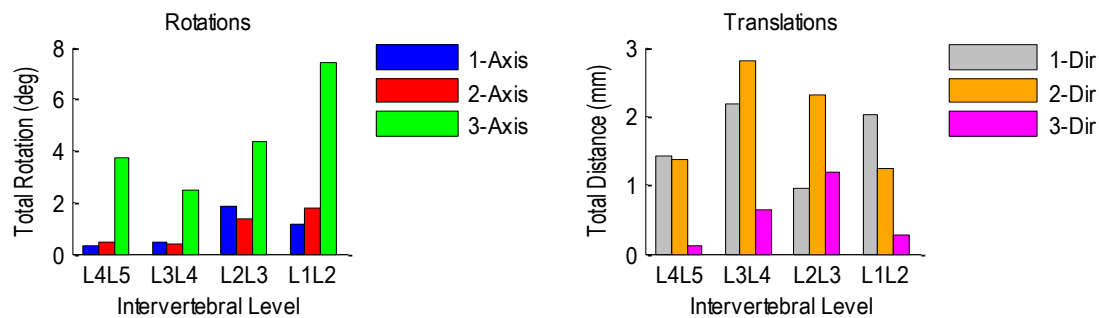


Figure A.181 Patient 6LBP relative rotations (left) and translations (right) at each vertebral level during flexion-extension.

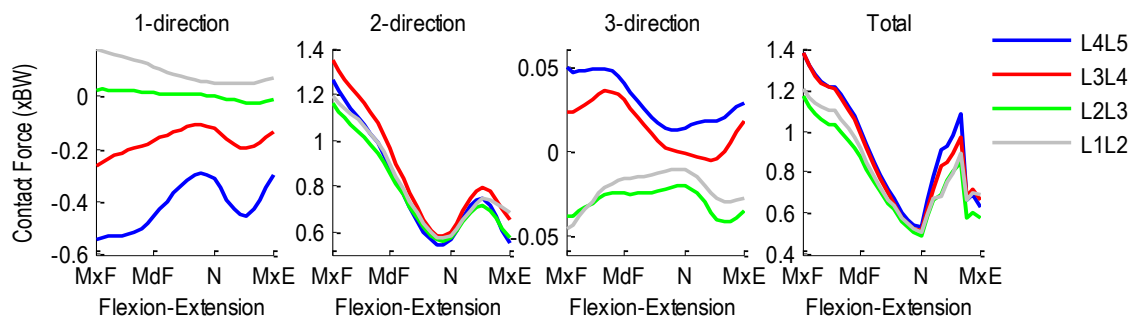


Figure A.182 Patient 6LBP intervertebral contact forces normalized with respect to body weight during flexion-extension. 1-dir=Ant(+)/Post(-), 2-dir=Sup(+)/Inf(-), 3-dir=Rt(+)/Lt(-).

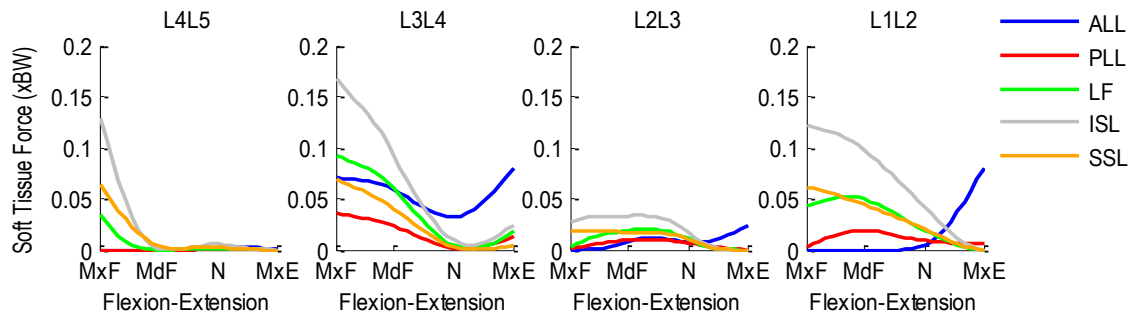


Figure A.183 Patient 6LBP segmental ligament forces normalized with respect to body weight during flexion-extension.

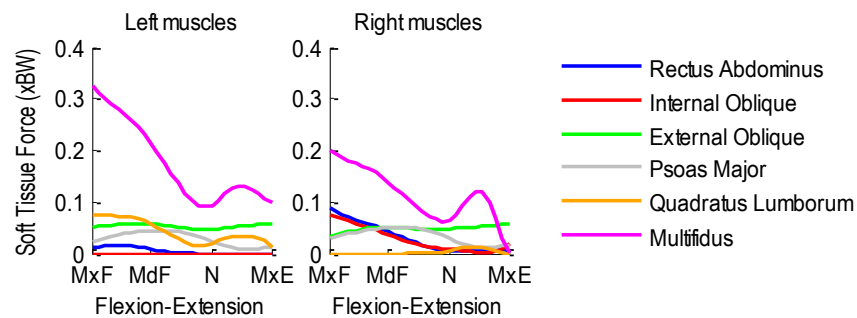


Figure A.184 Patient 6LBP bilateral muscle forces normalized with respect to body weight during flexion-extension.

A.16.2 Lateral Flexion Activity

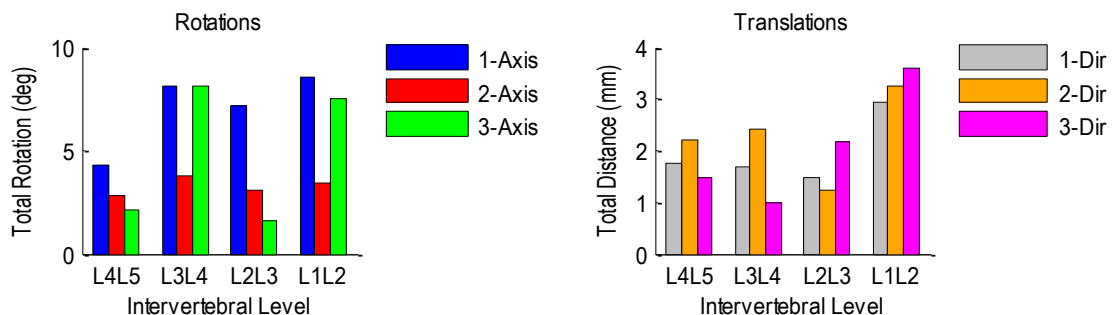


Figure A.185 Patient 6LBP relative rotations (left) and translations (right) at each vertebral level during left-to-right lateral flexion.

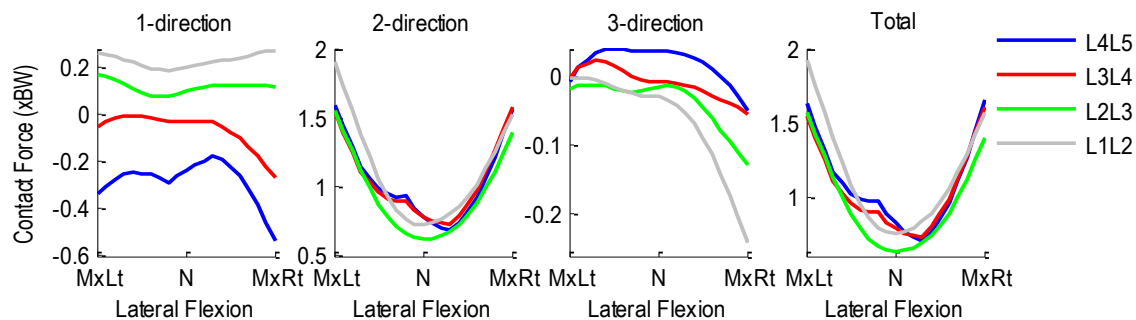


Figure A.186 Patient 6LBP intervertebral contact forces normalized with respect to body weight during left-to-right lateral flexion. 1-dir=Ant(+)/Post(-), 2-dir=Sup(+)/Inf(-), 3-dir=Rt(+)/Lt(-).

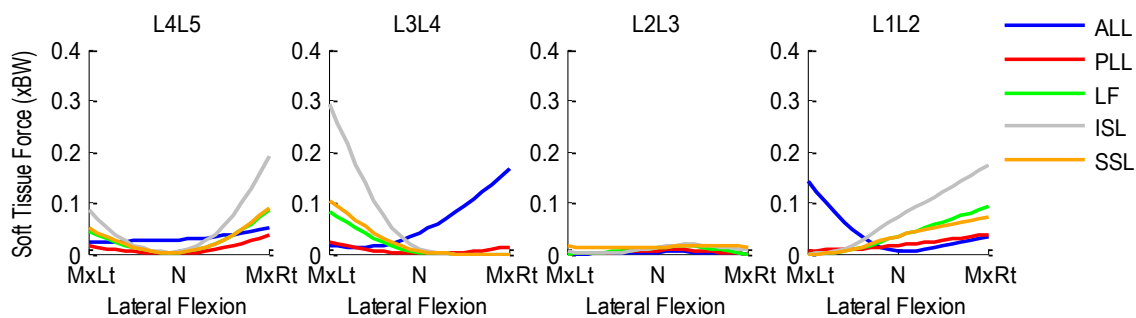


Figure A.187 Patient 6LBP segmental ligament forces normalized with respect to body weight during left-to-right lateral flexion.

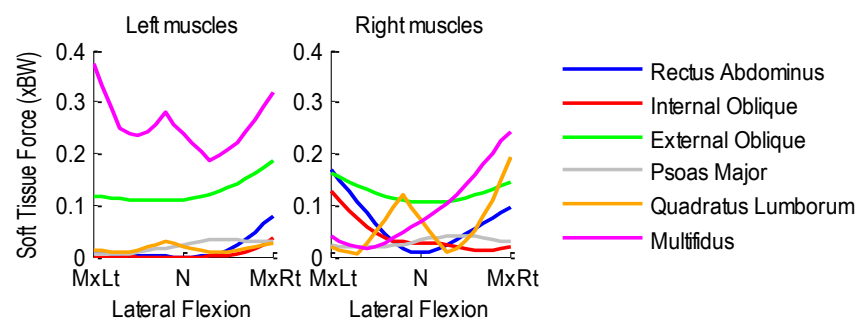


Figure A.188 Patient 6LBP bilateral muscle forces normalized to body weight during left-to-right lateral flexion.

A.16.3 Axial Rotation Activity

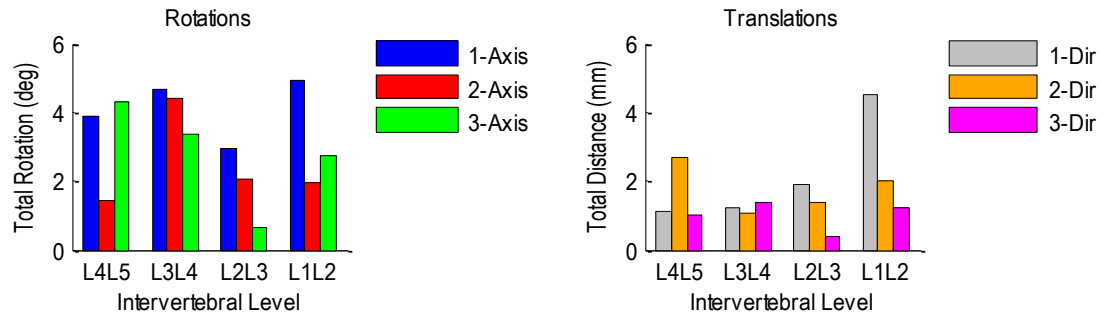


Figure A.189 Patient 6LBP relative rotations (left) and translations (right) at each vertebral level during left-to-right axial rotation.

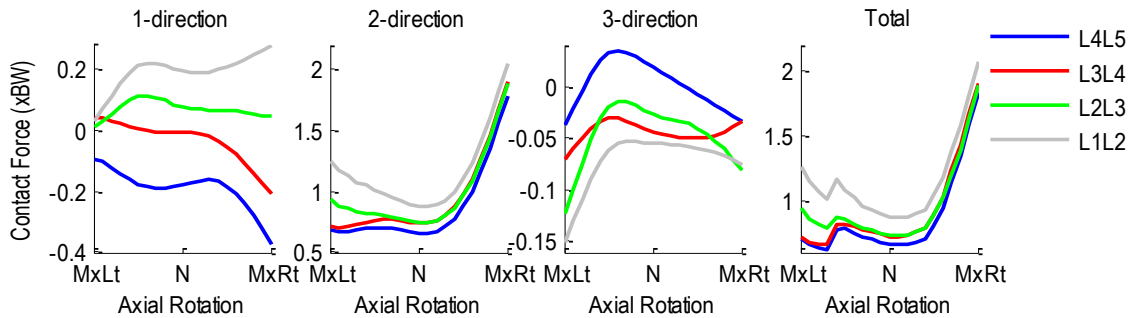


Figure A.190 Patient 6LBP intervertebral contact forces normalized with respect to body weight during left-to-right axial rotation. 1-dir=Ant(+)/Post(-), 2-dir=Sup(+)/Inf(-), 3-dir=Rt(+)/Lt(-).

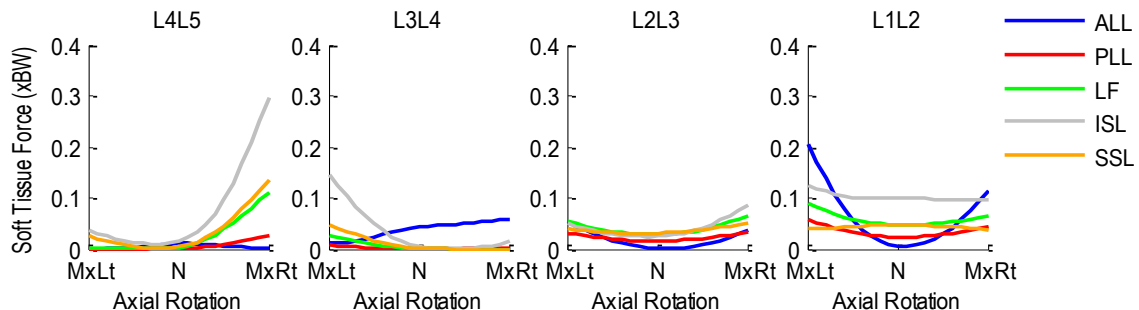


Figure A.191 Patient 6LBP segmental ligament forces normalized with respect to body weight during left-to-right axial rotation.

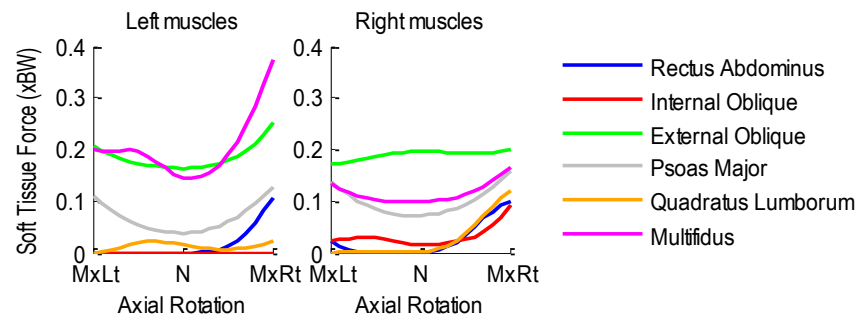


Figure A.192 Patient 6LBP bilateral muscle forces normalized with respect to body weight during left-to-right axial rotation.

A.17 Patient 7LBP

Age: 46 years

Gender: Female

Height: 1.60 m

Mass: 59 kg

Condition: Low back pain

A.17.1 Flexion-Extension Activity

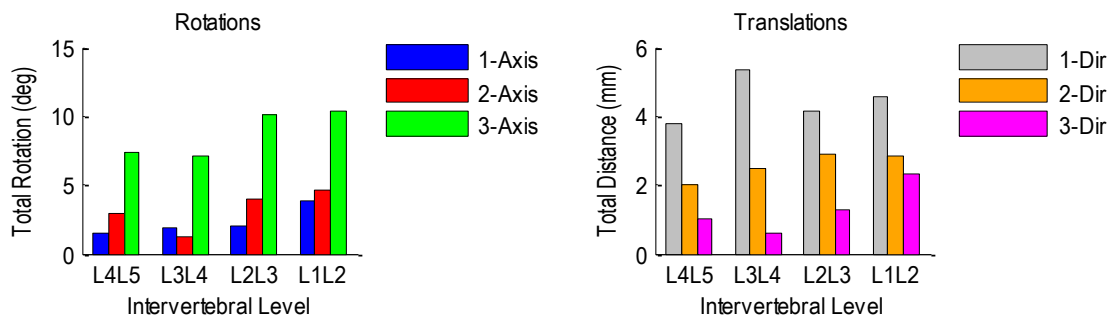


Figure A.193 Patient 7LBP relative rotations (left) and translations (right) at each vertebral level during flexion-extension.

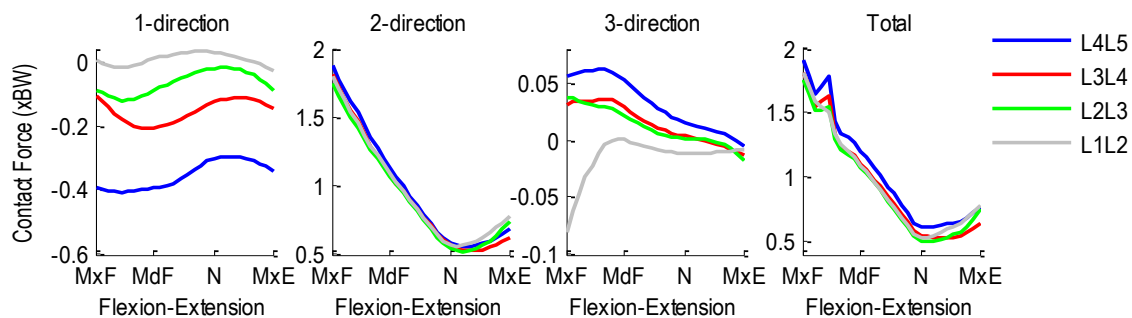


Figure A.194 Patient 7LBP intervertebral contact forces normalized with respect to body weight during flexion-extension. 1-dir=Ant(+)/Post(-), 2-dir=Sup(+)/Inf(-), 3-dir=Rt(+)/Lt(-).

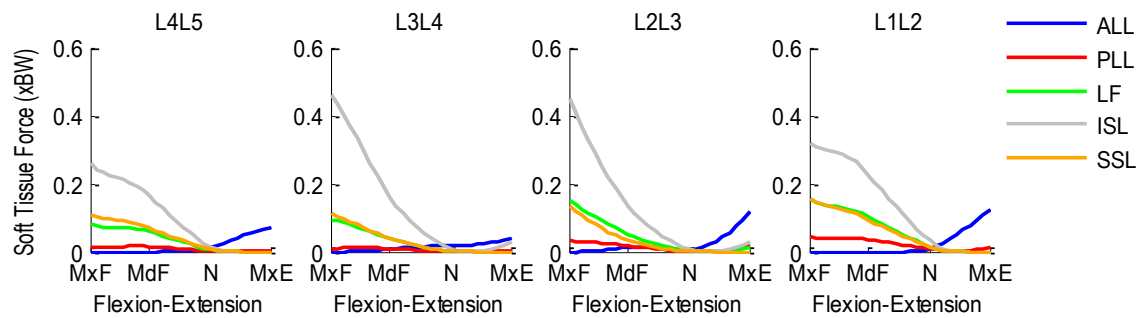


Figure A.195 Patient 7LBP segmental ligament forces normalized with respect to body weight during flexion-extension.

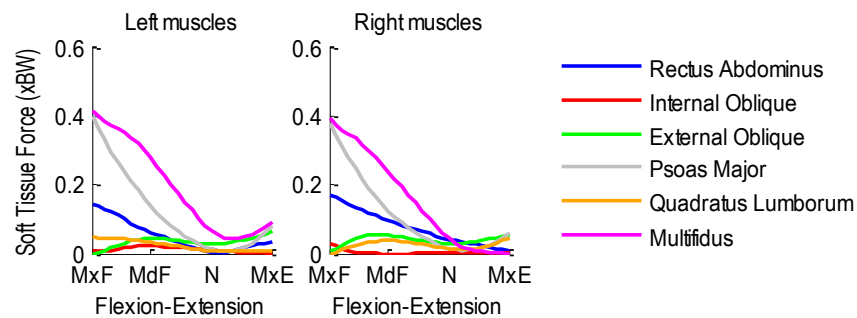


Figure A.196 Patient 7LBP bilateral muscle forces normalized with respect to body weight during flexion-extension.

A.17.2 Lateral Flexion Activity

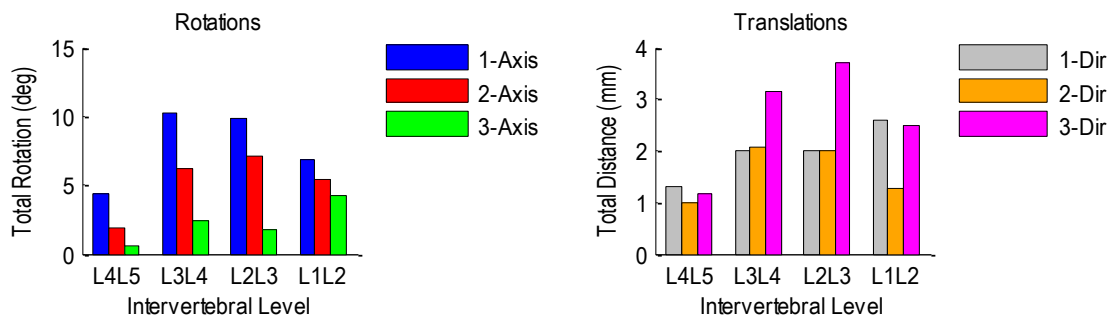


Figure A.197 Patient 7LBP relative rotations (left) and translations (right) at each vertebral level during left-to-right lateral flexion.

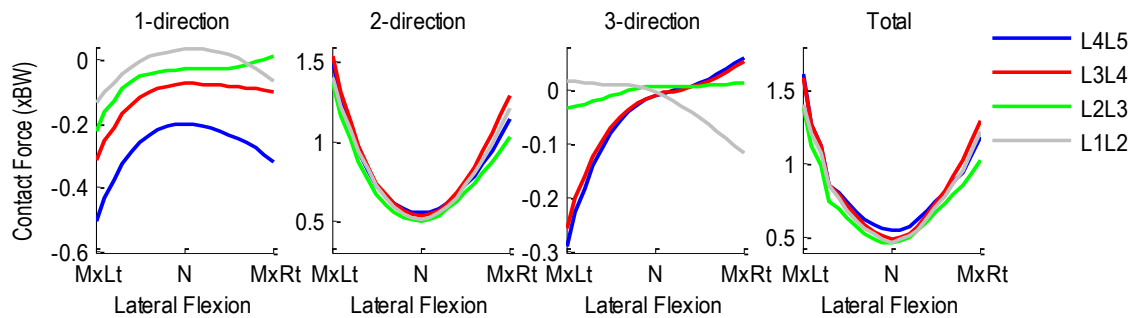


Figure A.198 Patient 7LBP intervertebral contact forces normalized with respect to body weight during left-to-right lateral flexion. 1-dir=Ant(+)/Post(-), 2-dir=Sup(+)/Inf(-), 3-dir=Rt(+)/Lt(-).

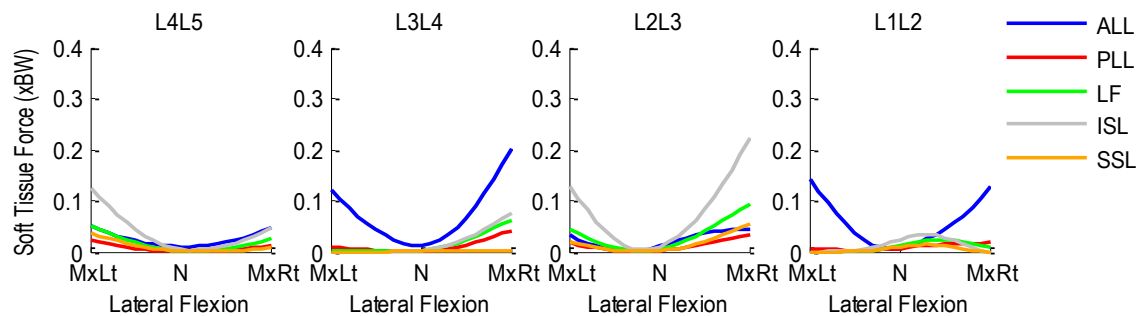


Figure A.199 Patient 7LBP segmental ligament forces normalized with respect to body weight during left-to-right lateral flexion.

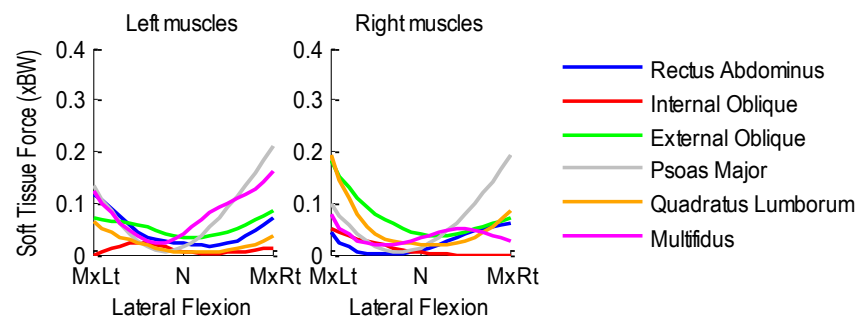


Figure A.200 Patient 7LBP bilateral muscle forces normalized to body weight during left-to-right lateral flexion.

A.17.3 Axial Rotation Activity

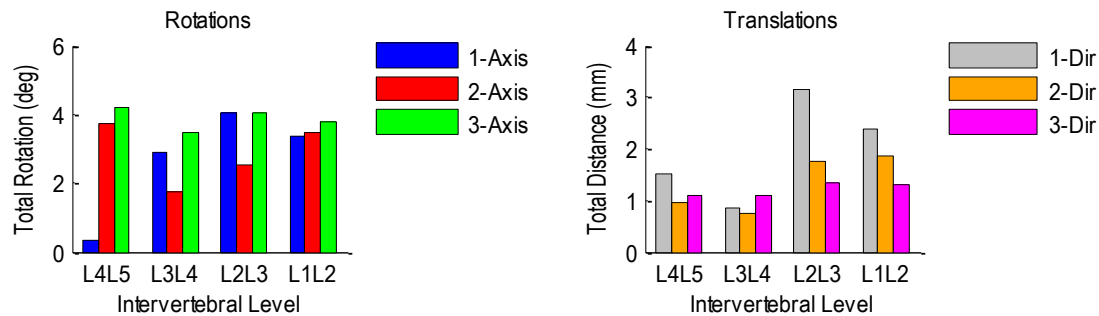


Figure A.201 Patient 7LBP relative rotations (left) and translations (right) at each vertebral level during left-to-right axial rotation.

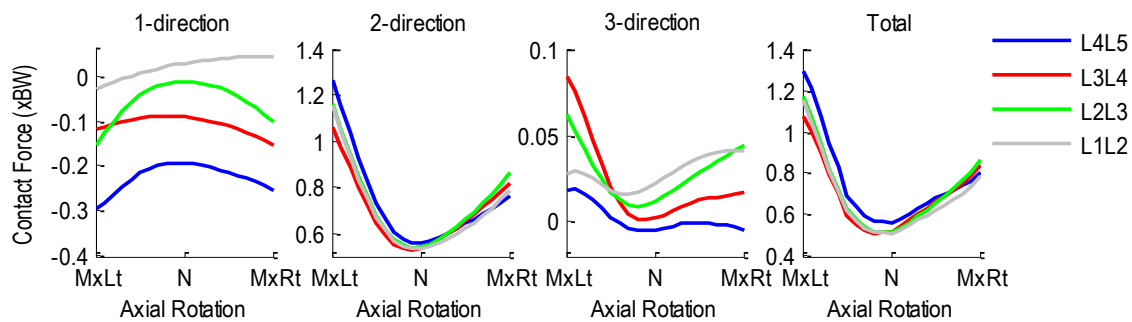


Figure A.202 Patient 7LBP intervertebral contact forces normalized with respect to body weight during left-to-right axial rotation. 1-dir=Ant(+)/Post(-), 2-dir=Sup(+)/Inf(-), 3-dir=Rt(+)/Lt(-).

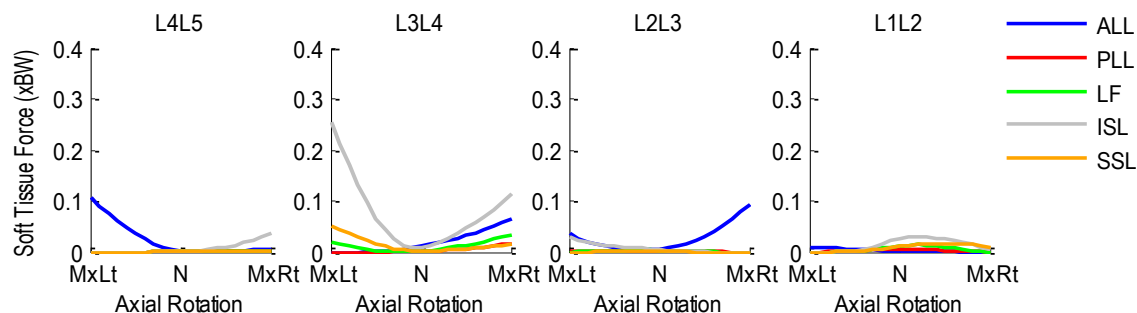


Figure A.203 Patient 7LBP segmental ligament forces normalized with respect to body weight during left-to-right axial rotation.

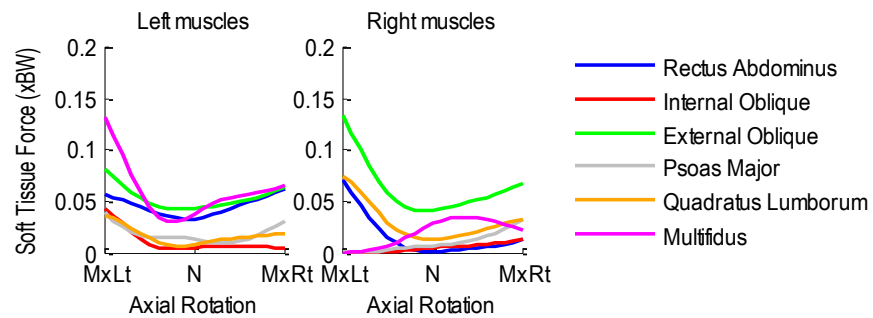


Figure A.204 Patient 7LBP bilateral muscle forces normalized with respect to body weight during left-to-right axial rotation.

A.18 Patient 8LBP

Age: 50 years

Gender: Female

Height: 1.68 m

Mass: 96 kg

Condition: Low back pain

A.18.1 Flexion-Extension Activity

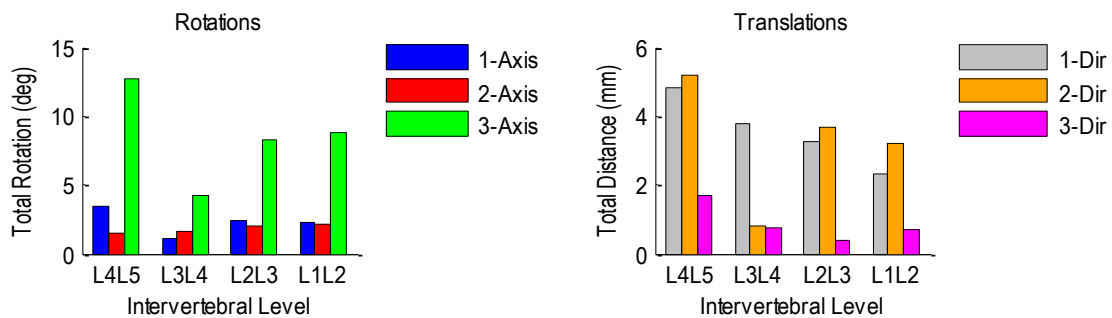


Figure A.205 Patient 8LBP relative rotations (left) and translations (right) at each vertebral level during flexion-extension.

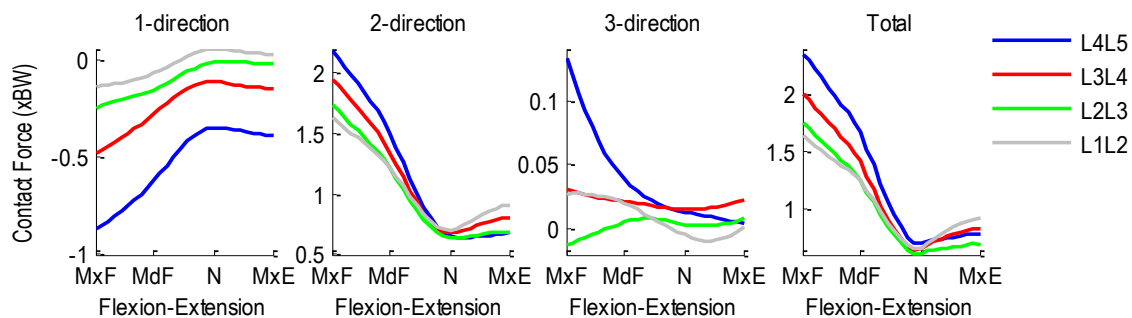


Figure A.206 Patient 8LBP intervertebral contact forces normalized with respect to body weight during flexion-extension. 1-dir=Ant(+)/Post(-), 2-dir=Sup(+)/Inf(-), 3-dir=Rt(+)/Lt(-).

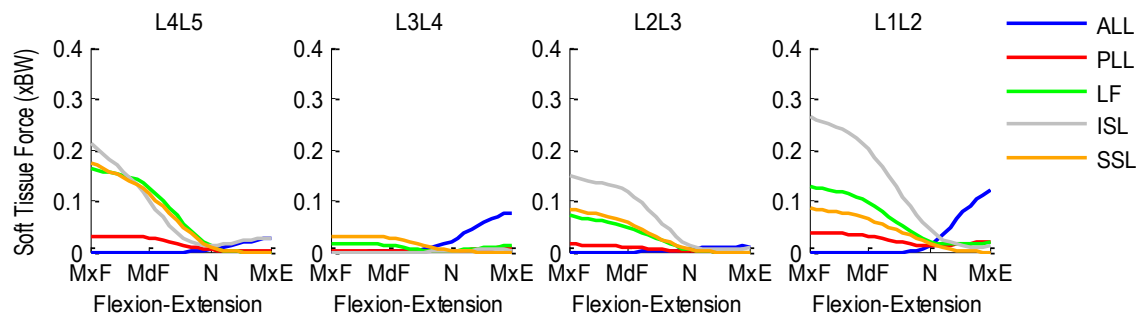


Figure A.207 Patient 8LBP segmental ligament forces normalized with respect to body weight during flexion-extension.

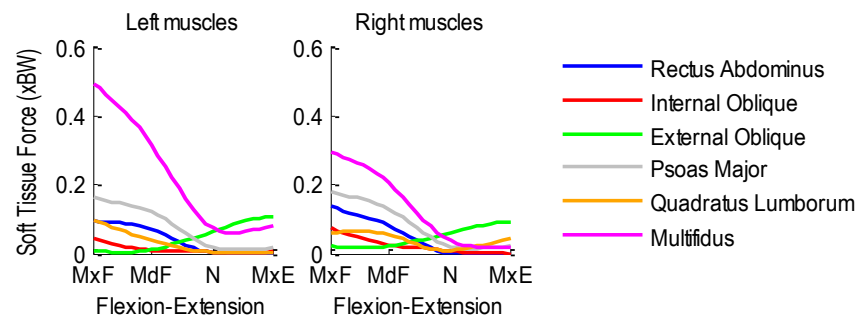


Figure A.208 Patient 8LBP bilateral muscle forces normalized with respect to body weight during flexion-extension.

A.18.2 Lateral Flexion Activity

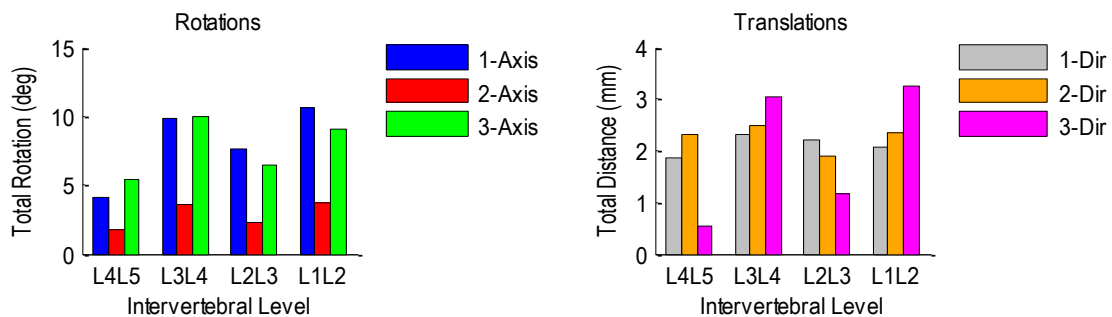


Figure A.209 Patient 8LBP relative rotations (left) and translations (right) at each vertebral level during left-to-right lateral flexion.

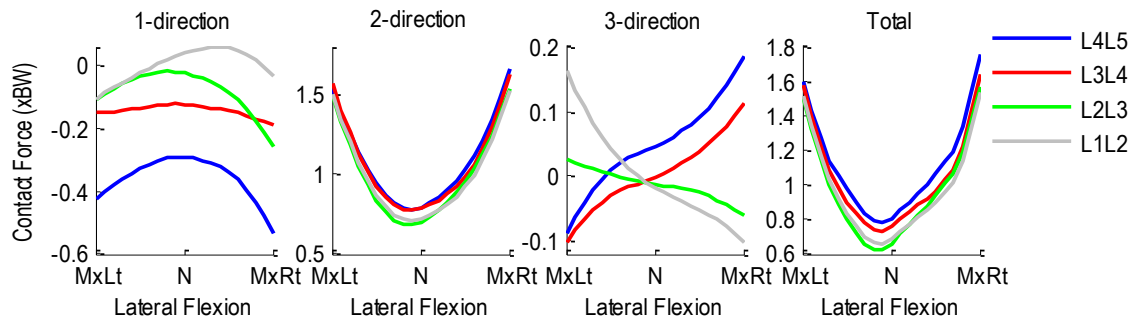


Figure A.210 Patient 8LBP intervertebral contact forces normalized with respect to body weight during left-to-right lateral flexion. 1-dir=Ant(+)/Post(-), 2-dir=Sup(+)/Inf(-), 3-dir=Rt(+)/Lt(-).

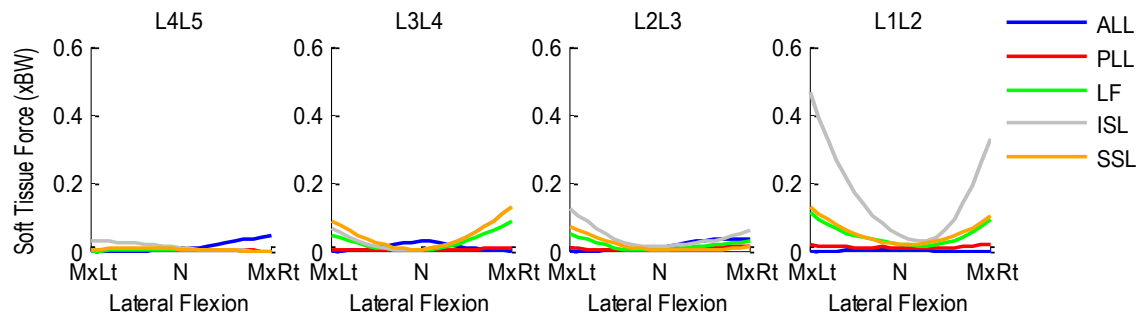


Figure A.211 Patient 8LBP segmental ligament forces normalized with respect to body weight during left-to-right lateral flexion.

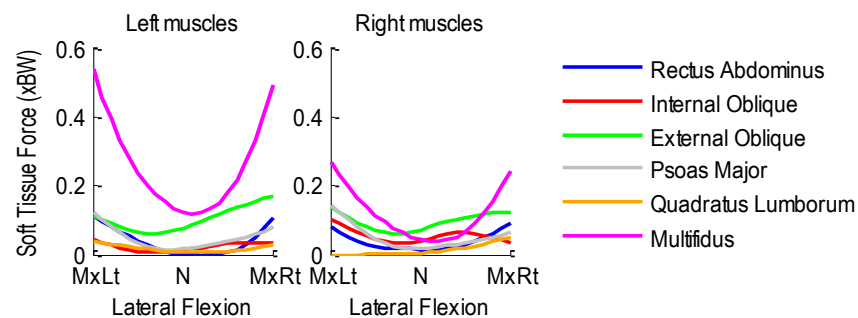


Figure A.212 Patient 8LBP bilateral muscle forces normalized to body weight during left-to-right lateral flexion.

A.18.3 Axial Rotation Activity

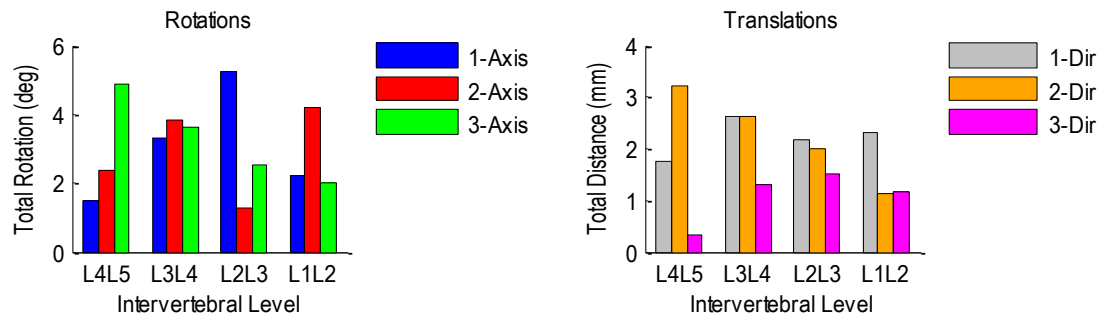


Figure A.213 Patient 8LBP relative rotations (left) and translations (right) at each vertebral level during left-to-right axial rotation.

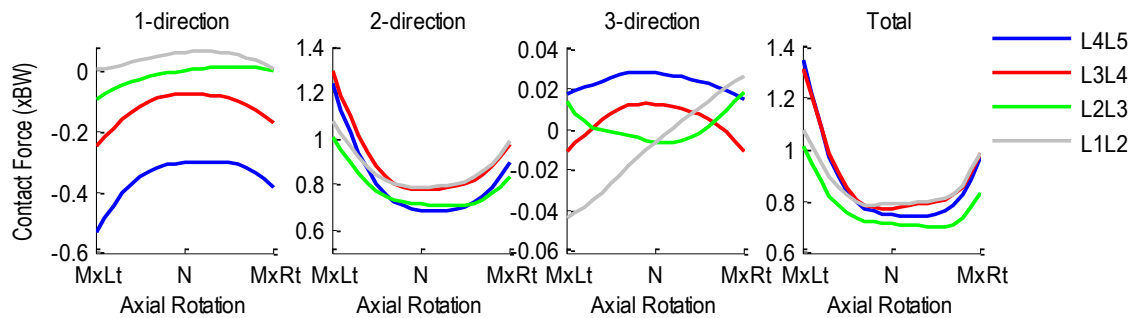


Figure A.214 Patient 8LBP intervertebral contact forces normalized with respect to body weight during left-to-right axial rotation. 1-dir=Ant(+)/Post(-), 2-dir=Sup(+)/Inf(-), 3-dir=Rt(+)/Lt(-).

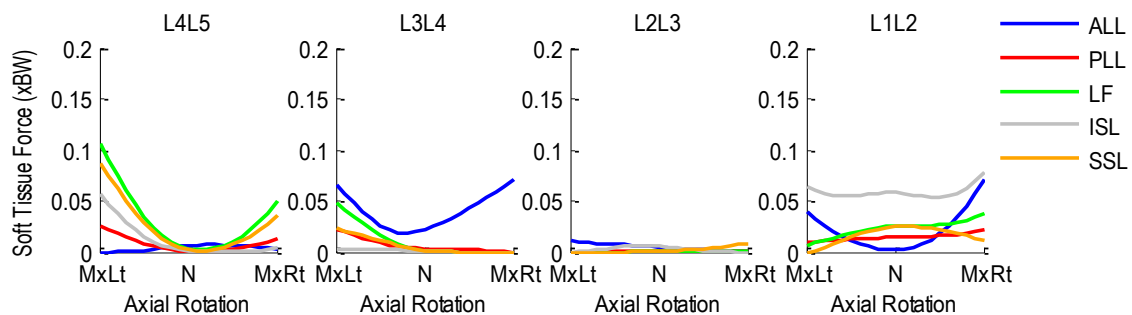


Figure A.215 Patient 8LBP segmental ligament forces normalized with respect to body weight during left-to-right axial rotation.

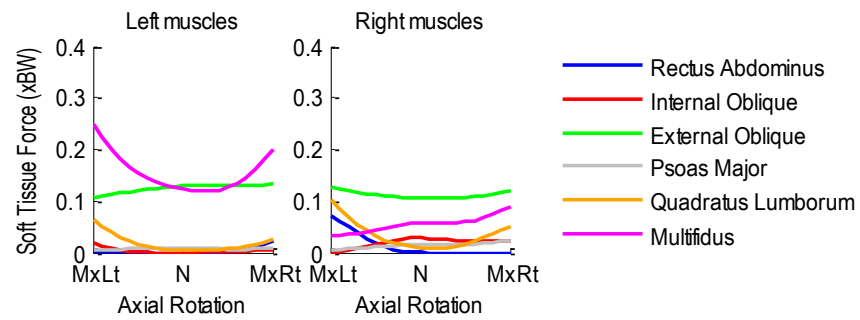


Figure A.216 Patient 8LBP bilateral muscle forces normalized with respect to body weight during left-to-right axial rotation.

A.19 Patient 9LBP

Age: 59 years

Gender: Female

Height: 1.70 m

Mass: 73 kg

Condition: Low back pain

A.19.1 Flexion-Extension Activity

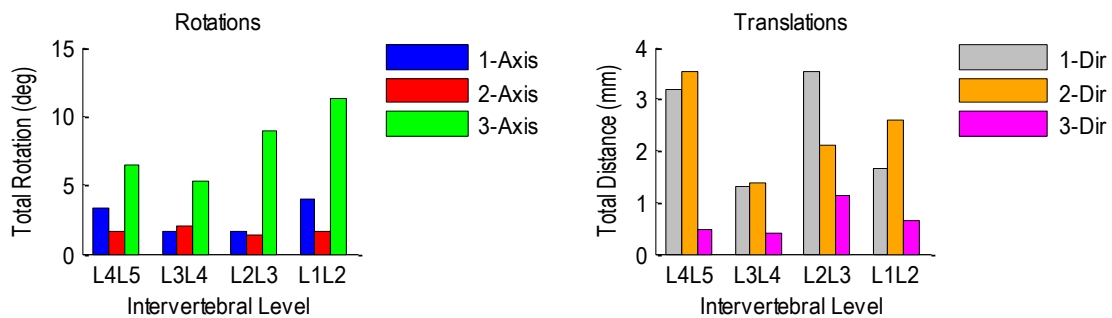


Figure A.217 Patient 9LBP relative rotations (left) and translations (right) at each vertebral level during flexion-extension.

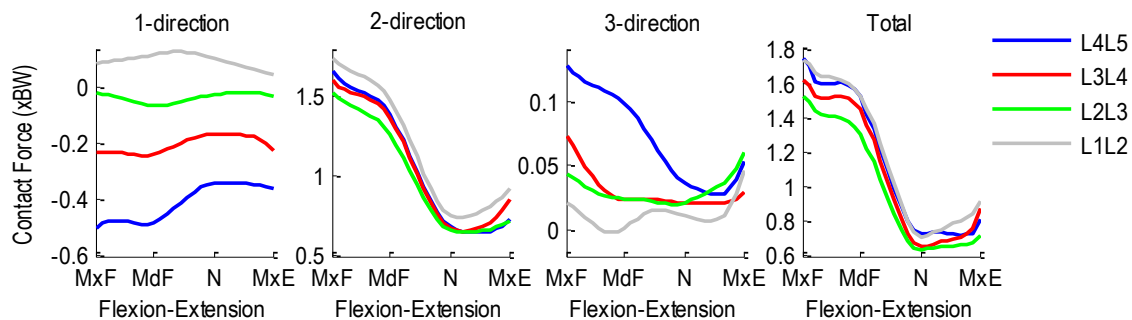


Figure A.218 Patient 9LBP intervertebral contact forces normalized with respect to body weight during flexion-extension. 1-dir=Ant(+)/Post(-), 2-dir=Sup(+)/Inf(-), 3-dir=Rt(+)/Lt(-).

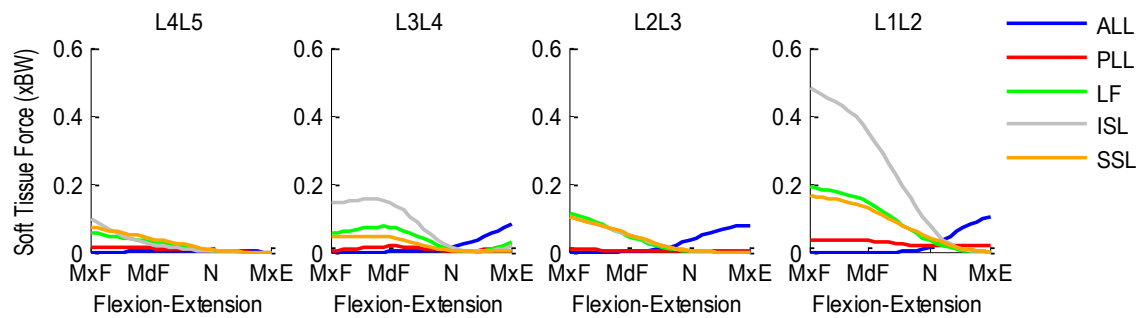


Figure A.219 Patient 9LBP segmental ligament forces normalized with respect to body weight during flexion-extension.

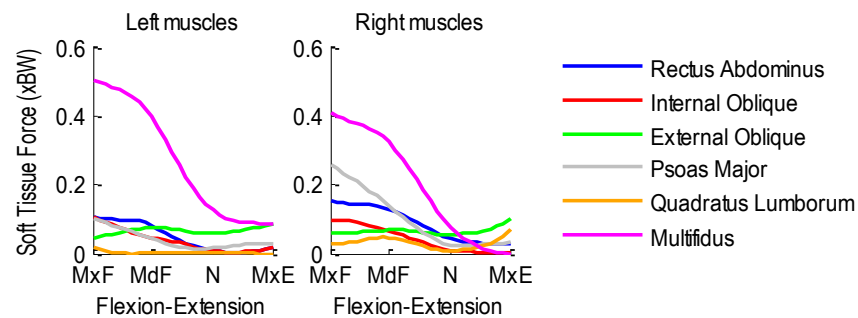


Figure A.220 Patient 9LBP bilateral muscle forces normalized with respect to body weight during flexion-extension.

A.19.2 Lateral Flexion Activity

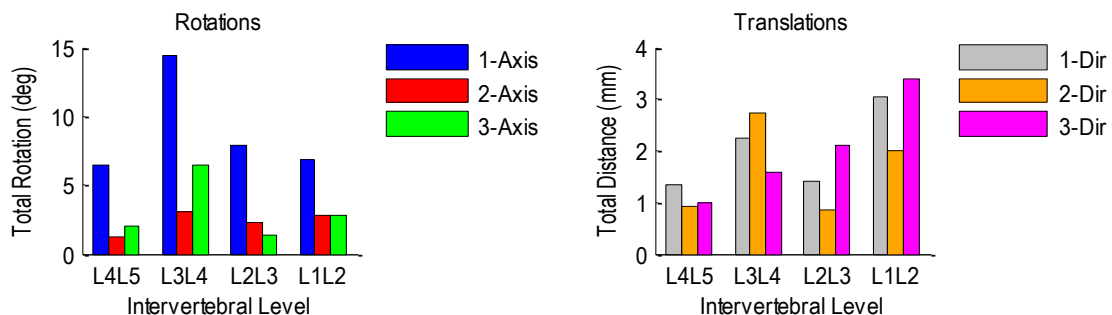


Figure A.221 Patient 9LBP relative rotations (left) and translations (right) at each vertebral level during left-to-right lateral flexion.

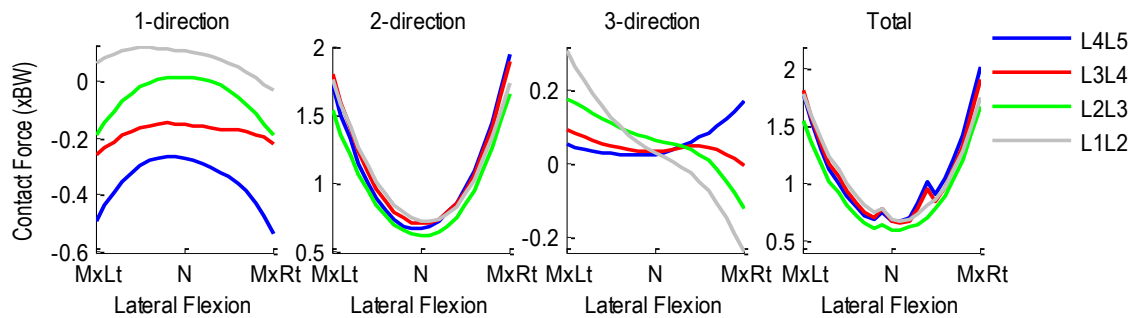


Figure A.222 Patient 9LBP intervertebral contact forces normalized with respect to body weight during left-to-right lateral flexion. 1-dir=Ant(+)/Post(-), 2-dir=Sup(+)/Inf(-), 3-dir=Rt(+)/Lt(-).

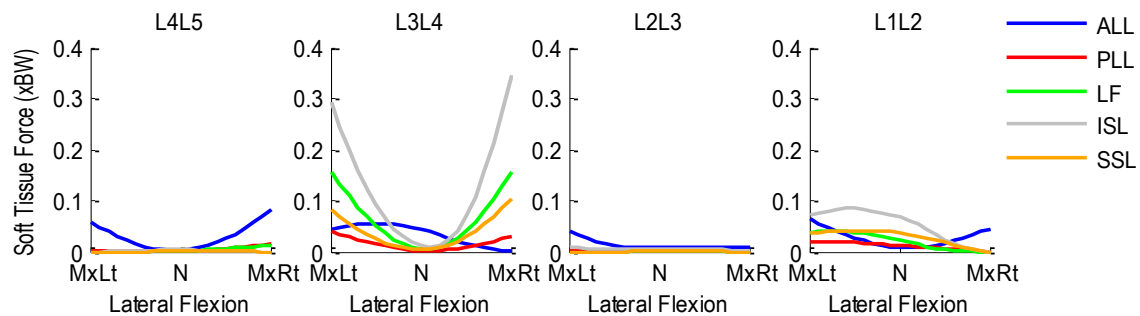


Figure A.223 Patient 9LBP segmental ligament forces normalized with respect to body weight during left-to-right lateral flexion.

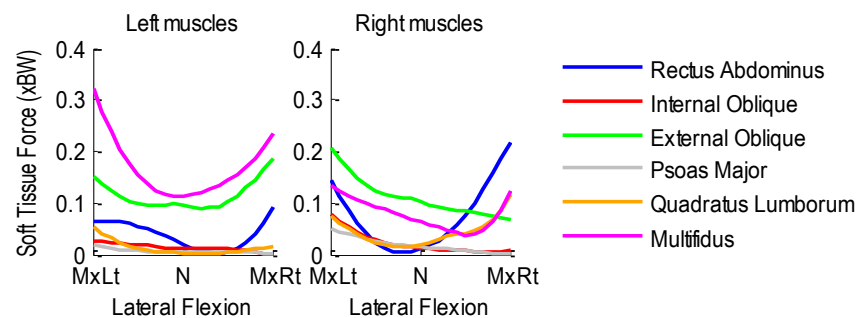


Figure A.224 Patient 9LBP bilateral muscle forces normalized to body weight during left-to-right lateral flexion.

A.19.3 Axial Rotation Activity

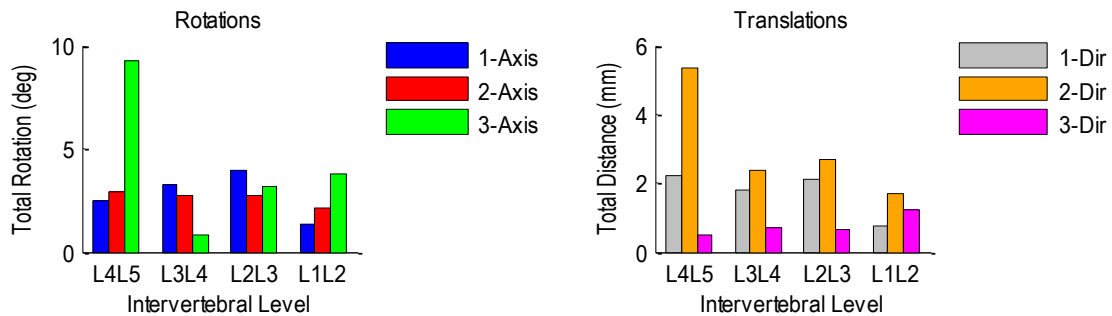


Figure A.225 Patient 9LBP relative rotations (left) and translations (right) at each vertebral level during left-to-right axial rotation.

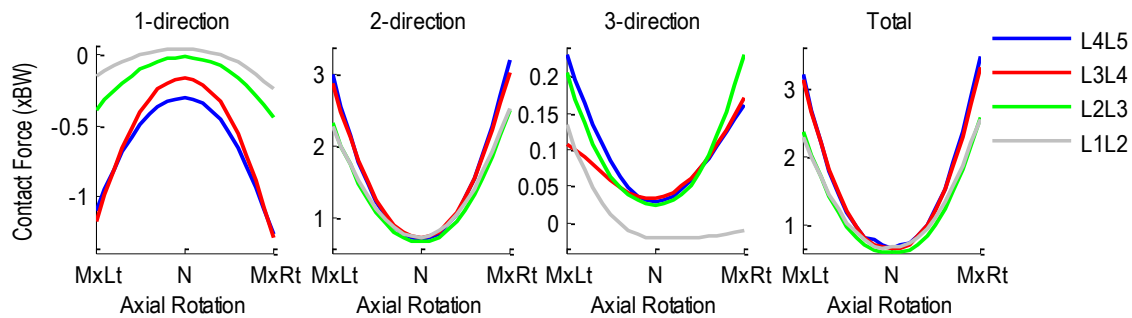


Figure A.226 Patient 9LBP intervertebral contact forces normalized with respect to body weight during left-to-right axial rotation. 1-dir=Ant(+)/Post(-), 2-dir=Sup(+)/Inf(-), 3-dir=Rt(+)/Lt(-).

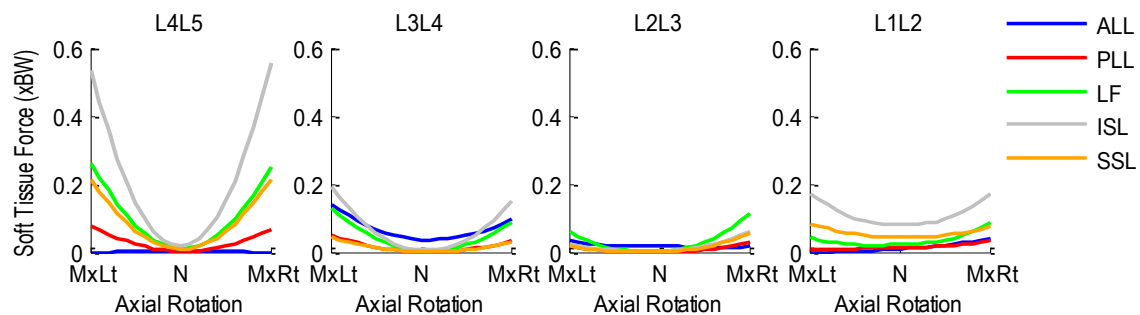


Figure A.227 Patient 9LBP segmental ligament forces normalized with respect to body weight during left-to-right axial rotation.

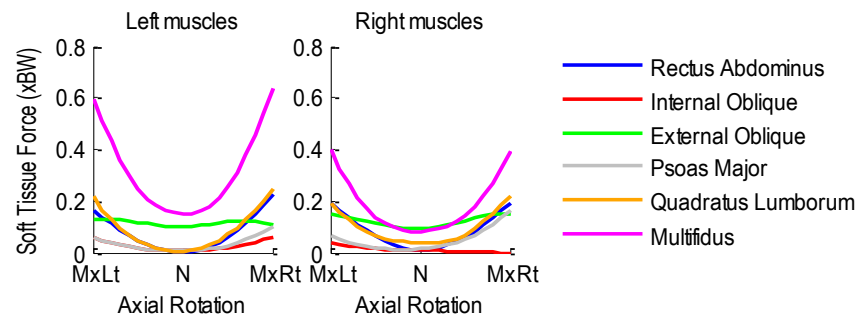


Figure A.228 Patient 9LBP bilateral muscle forces normalized with respect to body weight during left-to-right axial rotation.

A.20 Patient 10LBP

Age: 57 years

Gender: Female

Height: 1.67 m

Mass: 75 kg

Condition: Low back pain

A.20.1 Flexion-Extension Activity

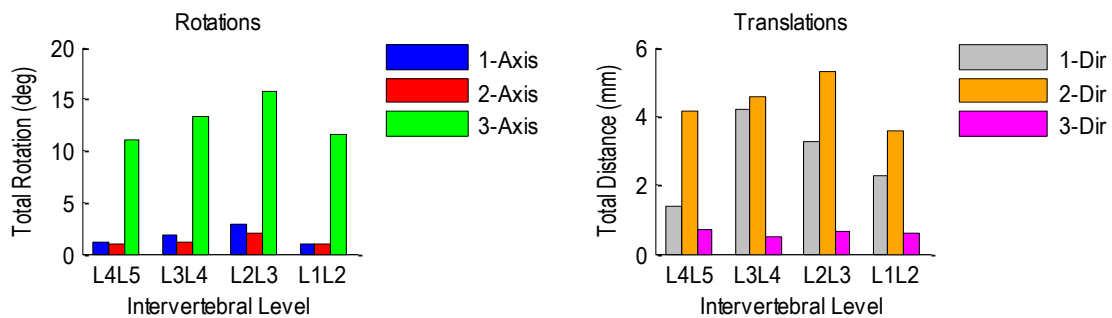


Figure A.229 Patient 10LBP relative rotations (left) and translations (right) at each vertebral level during flexion-extension.

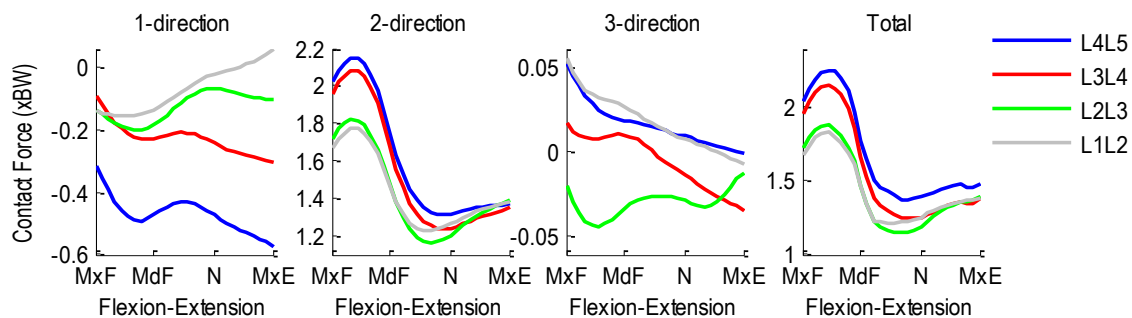


Figure A.230 Patient 10LBP intervertebral contact forces normalized with respect to body weight during flexion-extension. 1-dir=Ant(+)/Post(-), 2-dir=Sup(+)/Inf(-), 3-dir=Rt(+)/Lt(-).

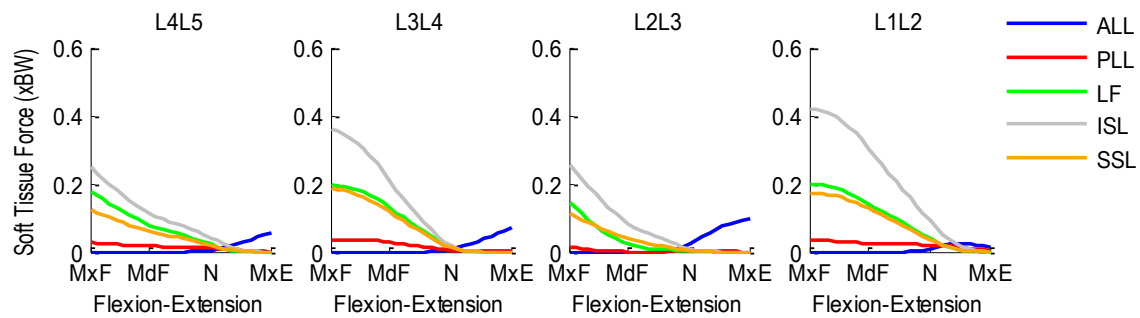


Figure A.231 Patient 10LBP segmental ligament forces normalized with respect to body weight during flexion-extension.

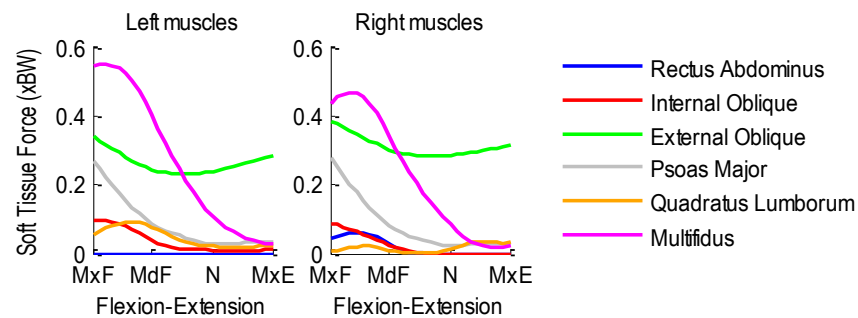


Figure A.232 Patient 10LBP bilateral muscle forces normalized with respect to body weight during flexion-extension.

A.20.2 Lateral Flexion Activity

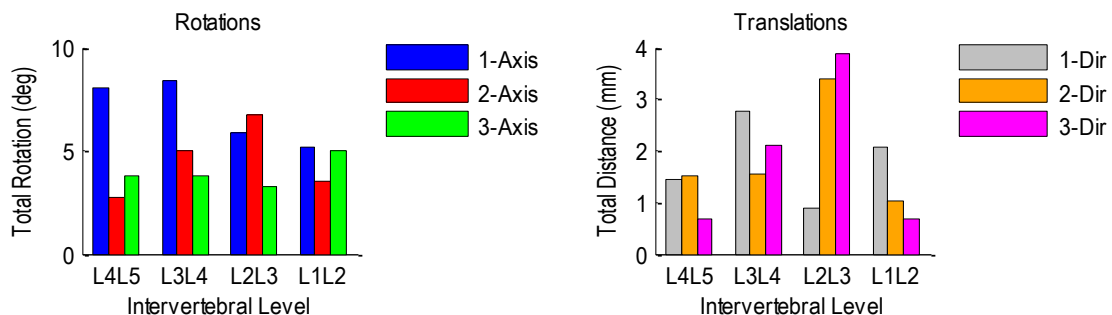


Figure A.233 Patient 10LBP relative rotations (left) and translations (right) at each vertebral level during left-to-right lateral flexion.

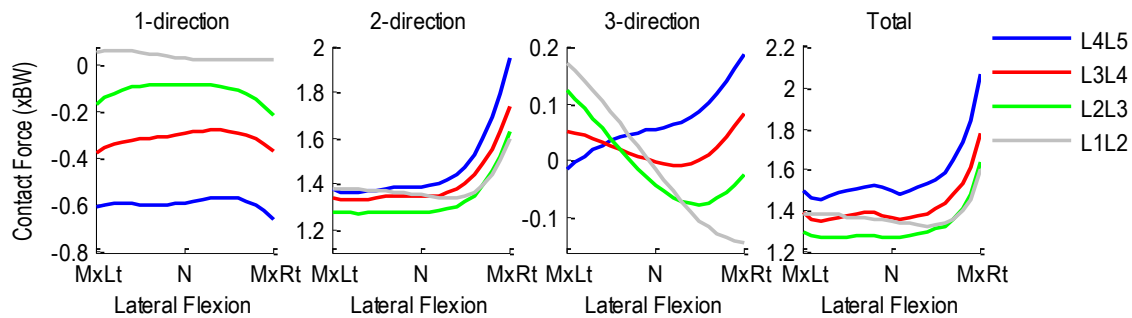


Figure A.234 Patient 10LBP intervertebral contact forces normalized with respect to body weight during left-to-right lateral flexion. 1-dir=Ant(+)/Post(-), 2-dir=Sup(+)/Inf(-), 3-dir=Rt(+)/Lt(-).

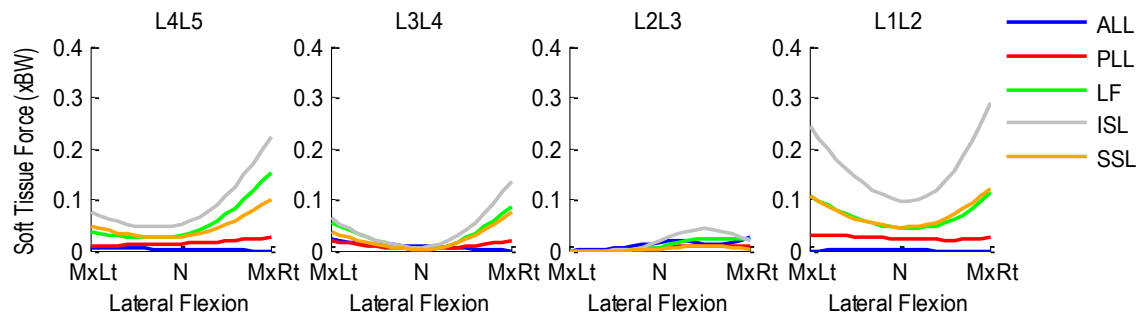


Figure A.235 Patient 10LBP segmental ligament forces normalized with respect to body weight during left-to-right lateral flexion.

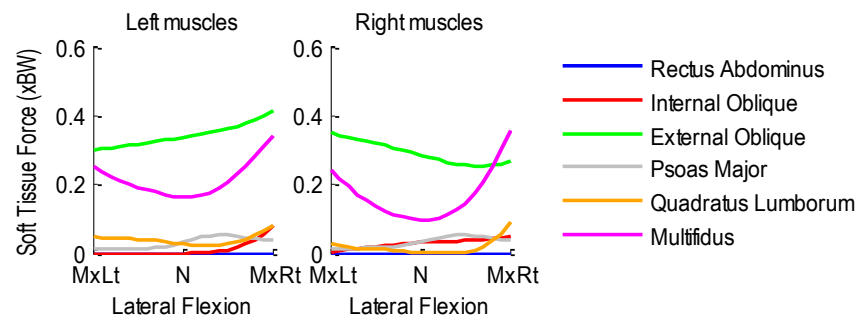


Figure A.236 Patient 10LBP bilateral muscle forces normalized to body weight during left-to-right lateral flexion.

A.20.3 Axial Rotation Activity

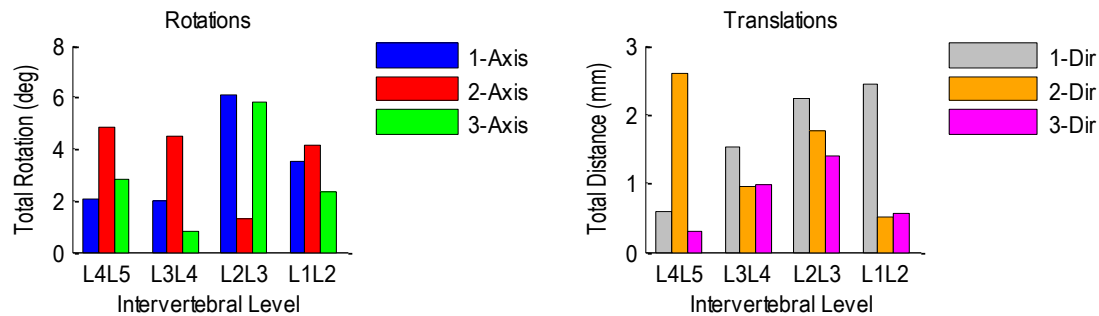


Figure A.237 Patient 10LBP relative rotations (left) and translations (right) at each vertebral level during left-to-right axial rotation.

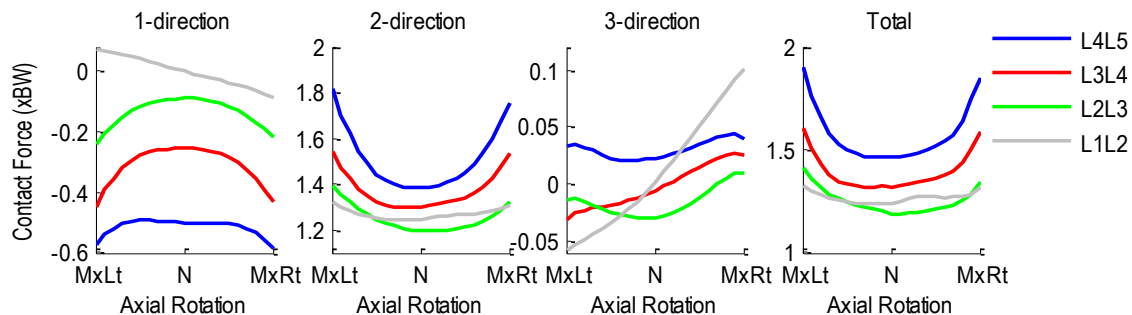


Figure A.238 Patient 10LBP intervertebral contact forces normalized with respect to body weight during left-to-right axial rotation. 1-dir=Ant(+)/Post(-), 2-dir=Sup(+)/Inf(-), 3-dir=Rt(+)/Lt(-).

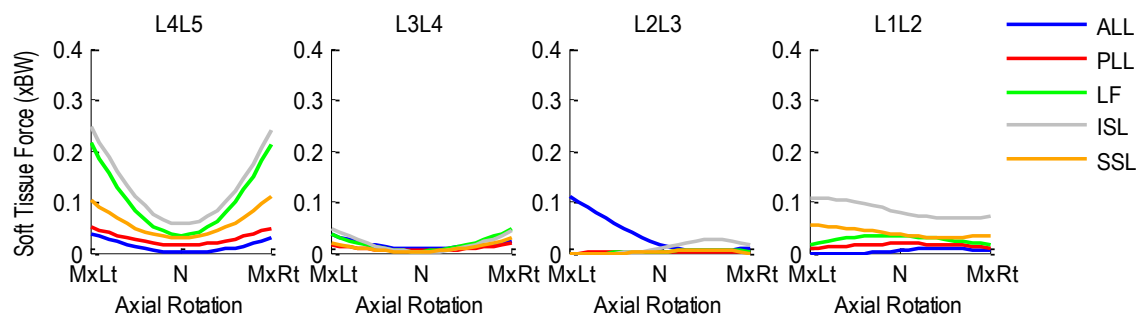


Figure A.239 Patient 10LBP segmental ligament forces normalized with respect to body weight during left-to-right axial rotation.

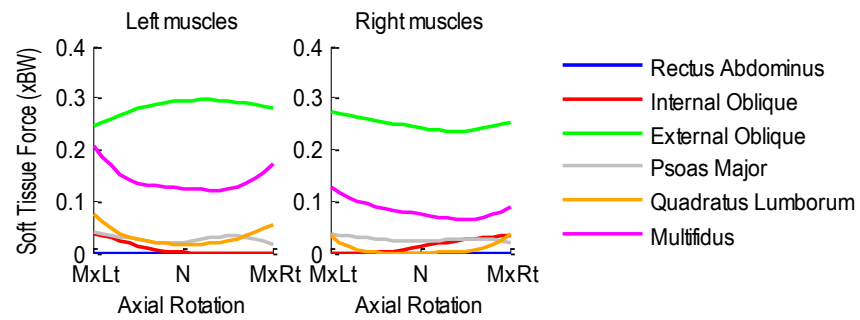


Figure A.240 Patient 10LBP bilateral muscle forces normalized with respect to body weight during left-to-right axial rotation.

A.21 Patient 1D

Age: 25 years

Gender: Male

Height: 1.80 m

Mass: 70 kg

Condition: Degenerative at L4L5

A.21.1 Flexion-Extension Activity

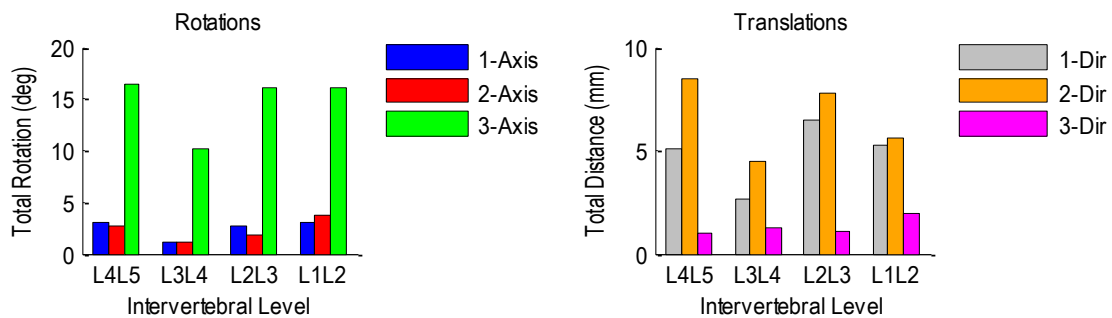


Figure A.241 Patient 1D relative rotations (left) and translations (right) at each vertebral level during flexion-extension.

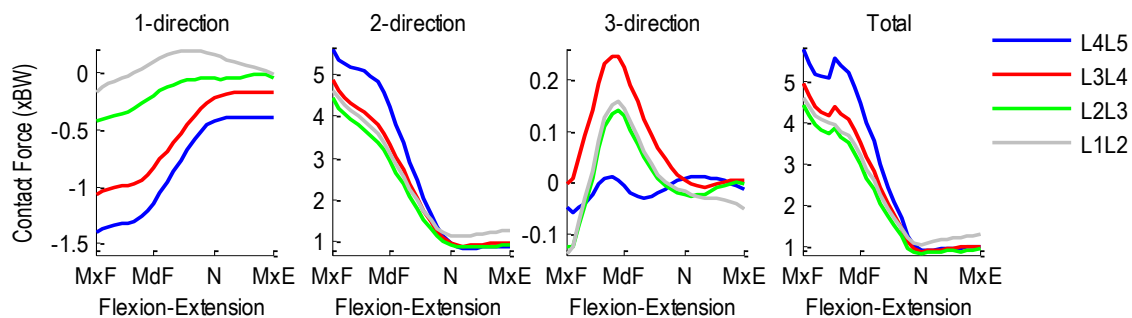


Figure A.242 Patient 1D intervertebral contact forces normalized with respect to body weight during flexion-extension. 1-dir=Ant(+)/Post(-), 2-dir=Sup(+)/Inf(-), 3-dir=Rt(+)/Lt(-).

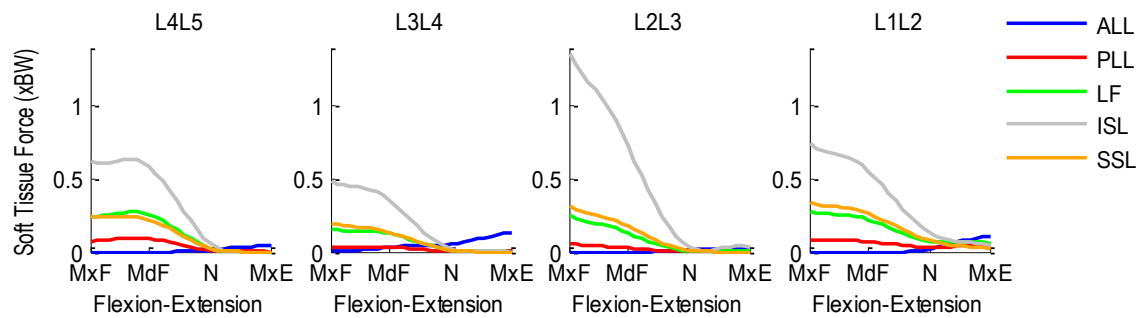


Figure A.243 Patient 1D segmental ligament forces normalized with respect to body weight during flexion-extension.

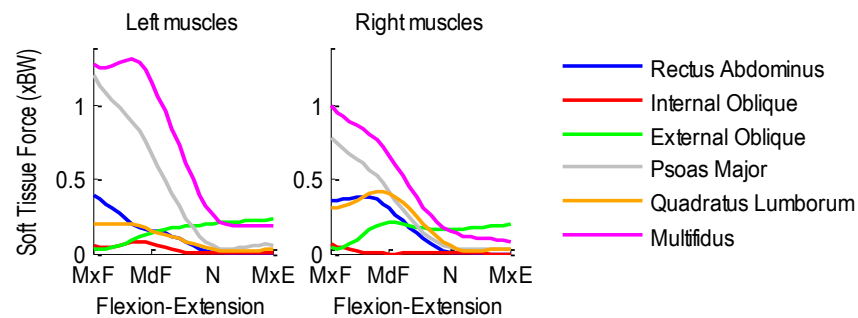


Figure A.244 Patient 1D bilateral muscle forces normalized with respect to body weight during flexion-extension.

A.21.2 Lateral Flexion Activity

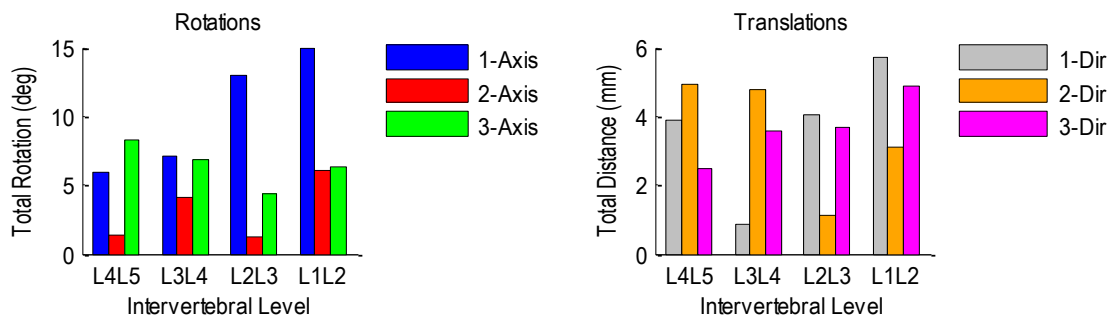


Figure A.245 Patient 1D relative rotations (left) and translations (right) at each vertebral level during left-to-right lateral flexion.

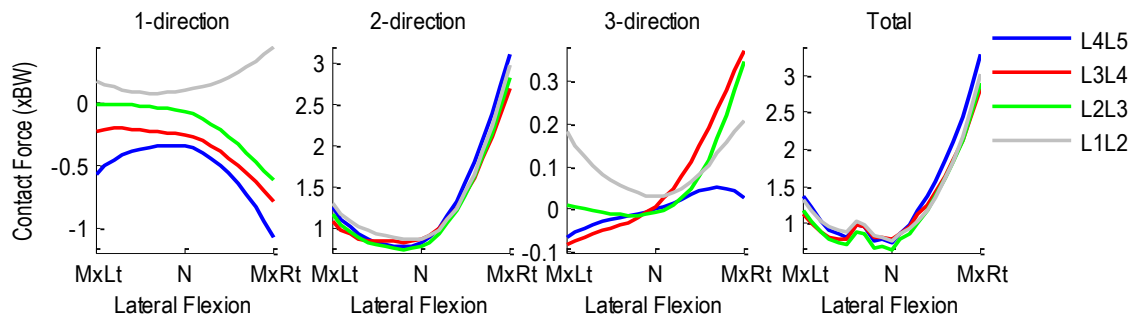


Figure A.246 Patient 1D intervertebral contact forces normalized with respect to body weight during left-to-right lateral flexion. 1-dir=Ant(+)/Post(-), 2-dir=Sup(+)/Inf(-), 3-dir=Rt(+)/Lt(-).

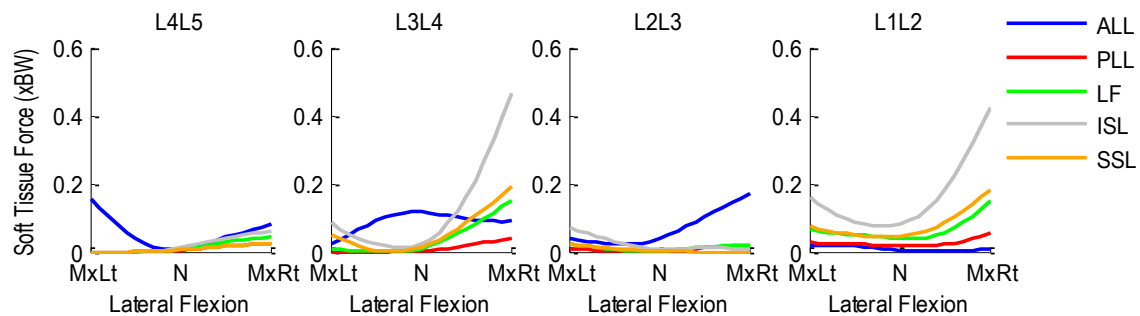


Figure A.247 Patient 1D segmental ligament forces normalized with respect to body weight during left-to-right lateral flexion.

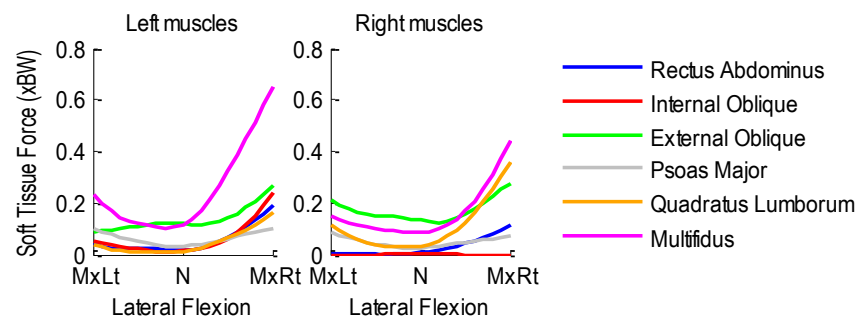


Figure A.248 Patient 1D bilateral muscle forces normalized with respect to body weight during left-to-right lateral flexion.

A.21.3 Axial Rotation Activity

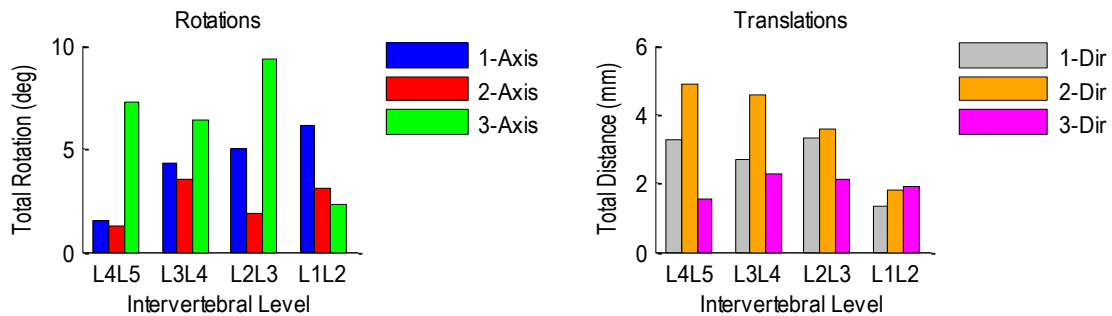


Figure A.249 Patient 1D relative rotations (left) and translations (right) at each vertebral level during left-to-right axial rotation.

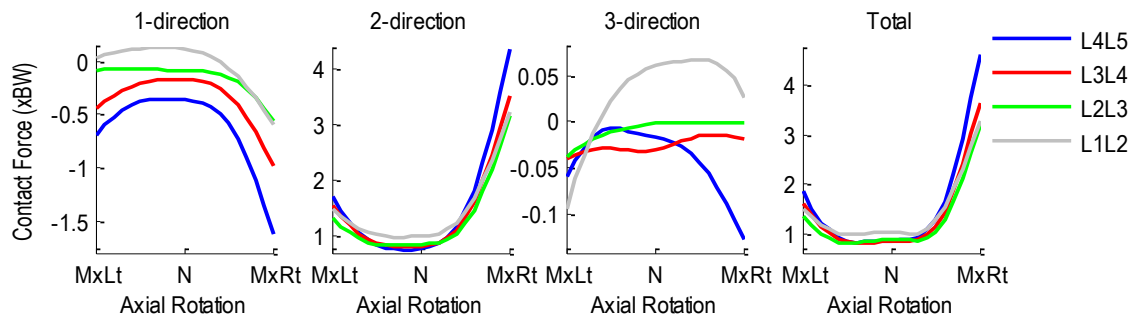


Figure A.250 Patient 1D intervertebral contact forces normalized with respect to body weight during left-to-right axial rotation. 1-dir=Ant(+)/Post(-), 2-dir=Sup(+)/Inf(-), 3-dir=Rt(+)/Lt(-).

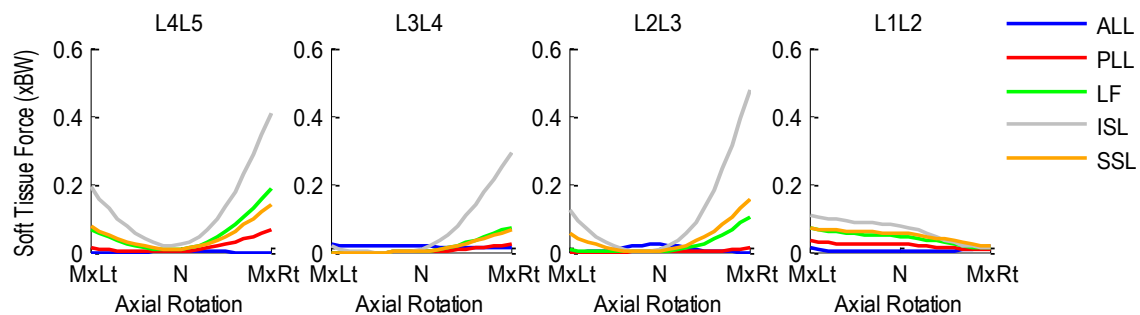


Figure A.251 Patient 1D segmental ligament forces normalized with respect to body weight during left-to-right axial rotation.

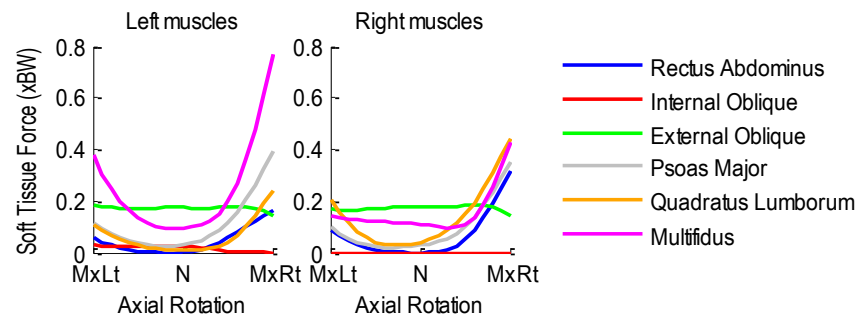


Figure A.252 Patient 1D bilateral muscle forces normalized with respect to body weight during left-to-right axial rotation.

A.22 Patient 2D

Age: 48 years

Gender: Female

Height: 1.70 m

Mass: 73 kg

Condition: Degenerative at L2L3

A.22.1 Flexion-Extension Activity

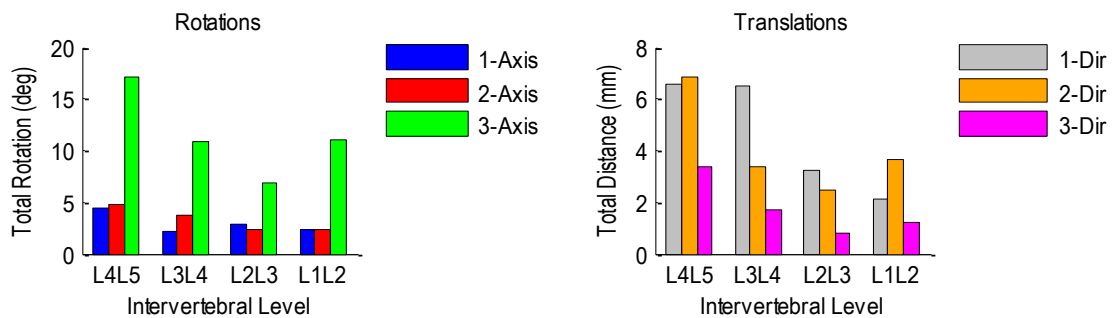


Figure A.253 Patient 2D relative rotations (left) and translations (right) at each vertebral level during flexion-extension.

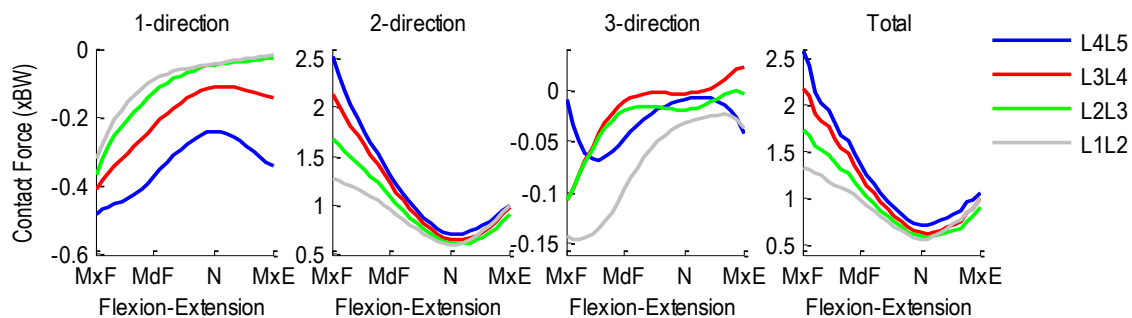


Figure A.254 Patient 2D intervertebral contact forces normalized with respect to body weight during flexion-extension. 1-dir=Ant(+)/Post(-), 2-dir=Sup(+)/Inf(-), 3-dir=Rt(+)/Lt(-).

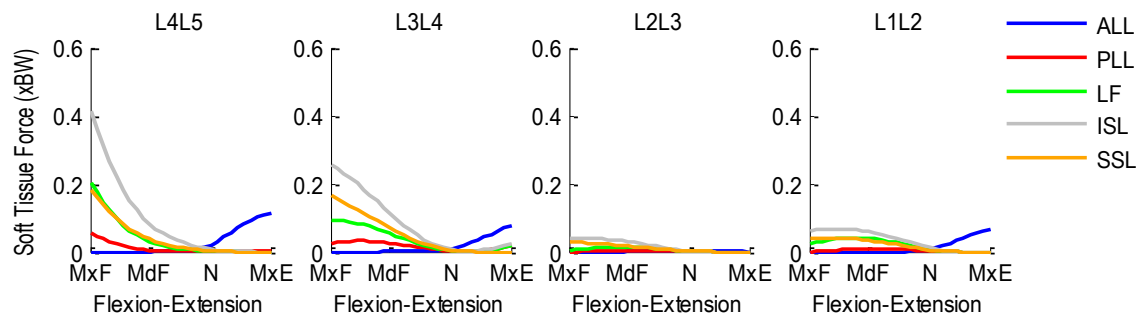


Figure A.255 Patient 2D segmental ligament forces normalized with respect to body weight during flexion-extension.

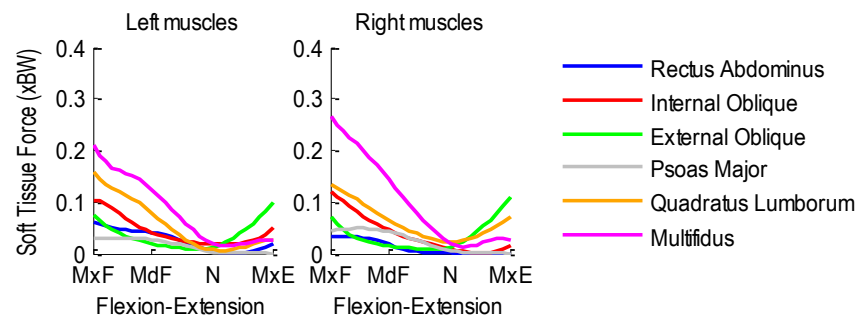


Figure A.256 Patient 2D bilateral muscle forces normalized with respect to body weight during flexion-extension.

A.22.2 Lateral Flexion Activity

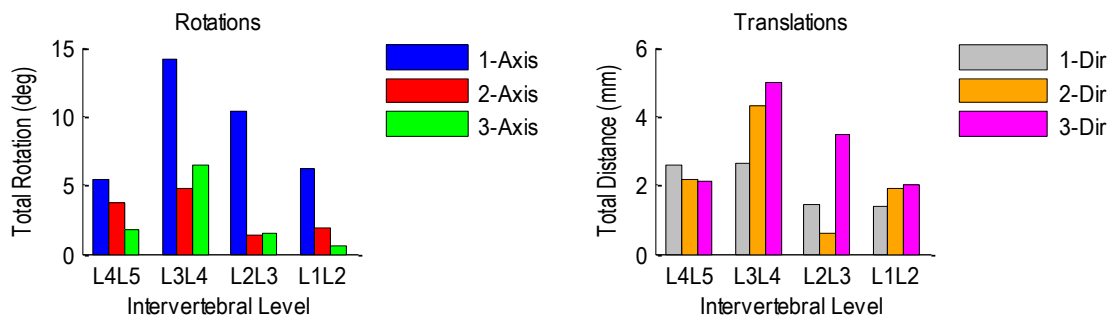


Figure A.257 Patient 2D relative rotations (left) and translations (right) at each vertebral level during left-to-right lateral flexion.

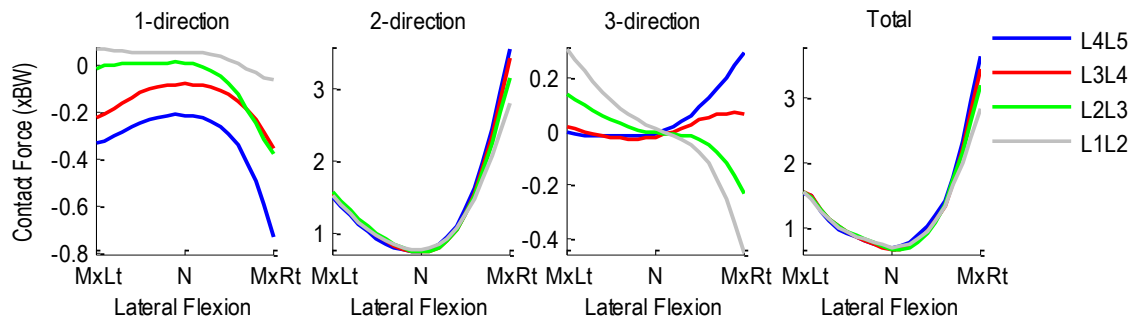


Figure A.258 Patient 2D intervertebral contact forces normalized with respect to body weight during left-to-right lateral flexion. 1-dir=Ant(+)/Post(-), 2-dir=Sup(+)/Inf(-), 3-dir=Rt(+)/Lt(-).

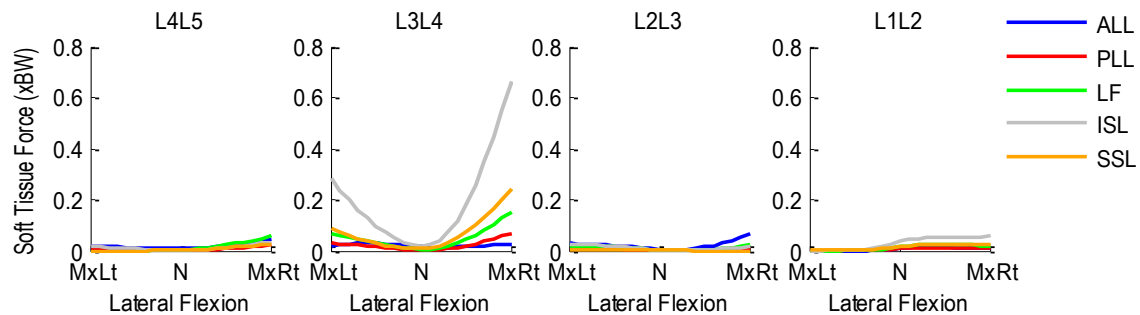


Figure A.259 Patient 2D segmental ligament forces normalized with respect to body weight during left-to-right lateral flexion.

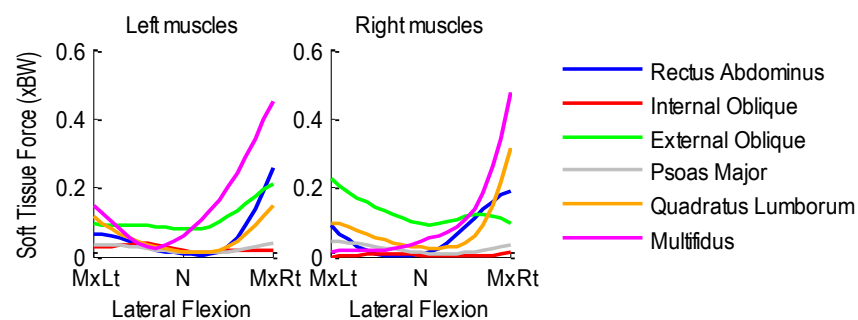


Figure A.260 Patient 2D bilateral muscle forces normalized with respect to body weight during left-to-right lateral flexion.

A.22.3 Axial Rotation Activity

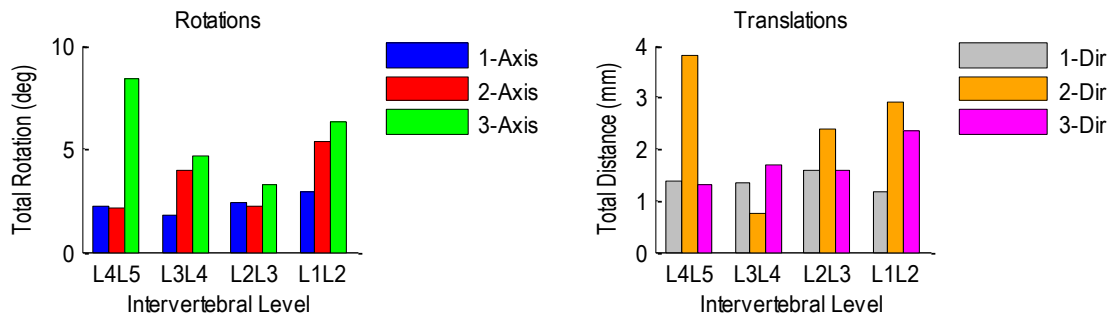


Figure A.261 Patient 2D relative rotations (left) and translations (right) at each vertebral level during left-to-right axial rotation.

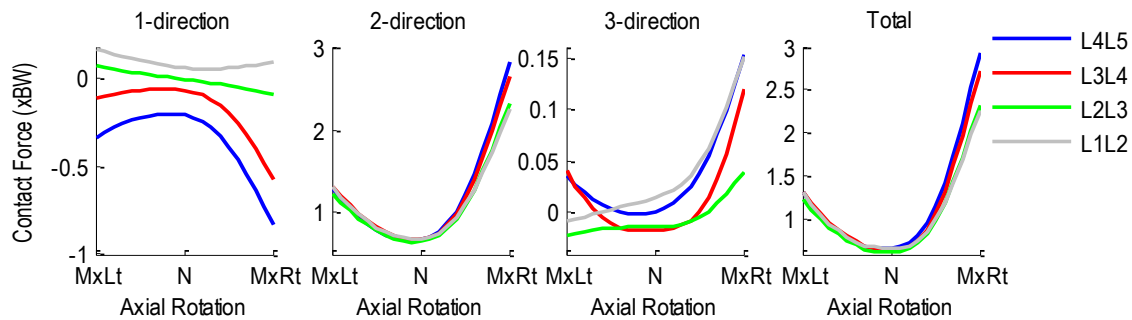


Figure A.262 Patient 2D intervertebral contact forces normalized with respect to body weight during left-to-right axial rotation. 1-dir=Ant(+)/Post(-), 2-dir=Sup(+)/Inf(-), 3-dir=Rt(+)/Lt(-).

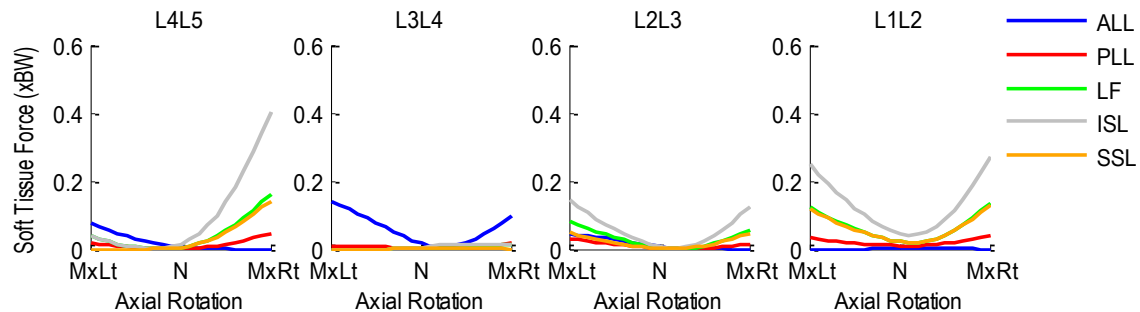


Figure A.263 Patient 2D segmental ligament forces normalized with respect to body weight during left-to-right axial rotation.

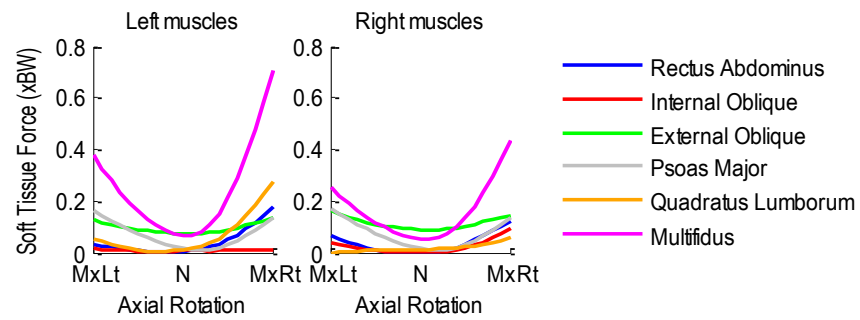


Figure A.264 Patient 2D bilateral muscle forces normalized with respect to body weight during left-to-right axial rotation.

A.23 Patient 3D

Age: 39 years

Gender: Male

Height: 1.83 m

Mass: 98 kg

Condition: Degenerative at L5S1

A.23.1 Flexion-Extension Activity

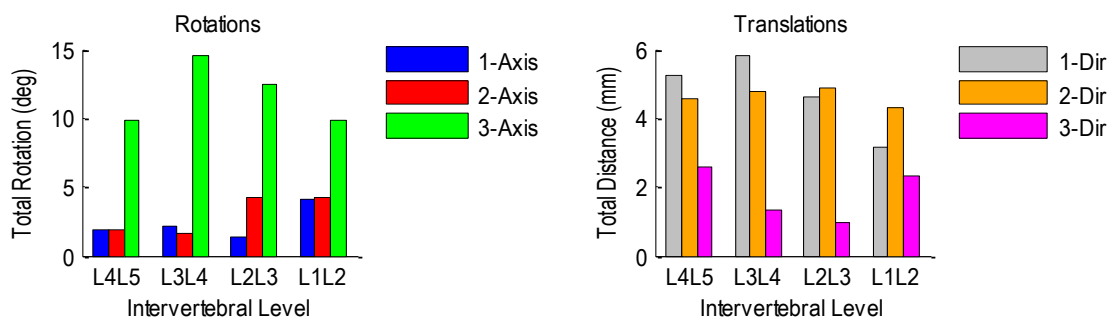


Figure A.265 Patient 3D relative rotations (left) and translations (right) at each vertebral level during flexion-extension.

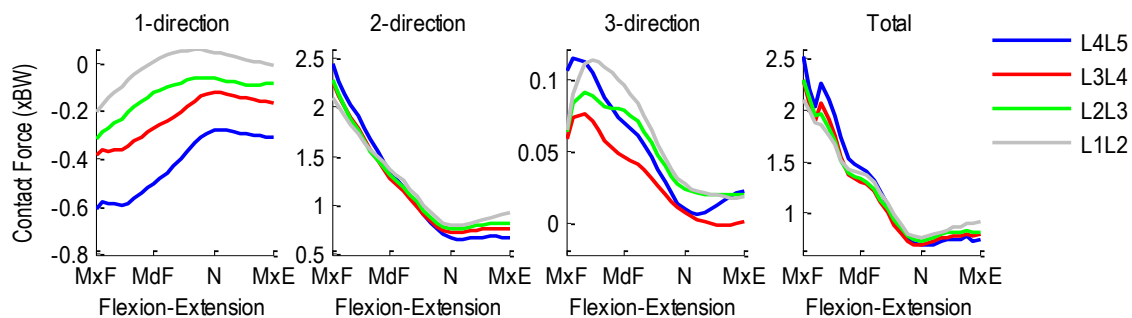


Figure A.266 Patient 3D intervertebral contact forces normalized with respect to body weight during flexion-extension. 1-dir=Ant(+)/Post(-), 2-dir=Sup(+)/Inf(-), 3-dir=Rt(+)/Lt(-).

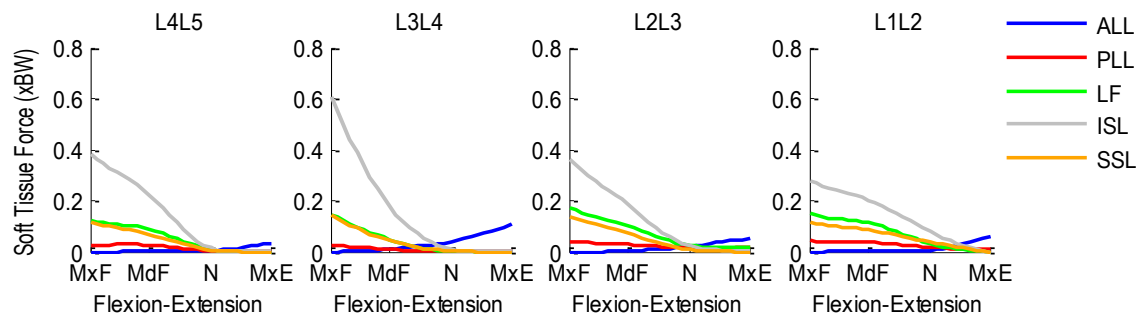


Figure A.267 Patient 3D segmental ligament forces normalized with respect to body weight during flexion-extension.

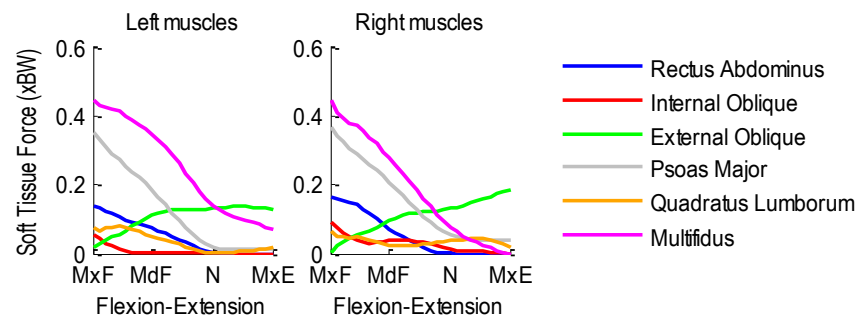


Figure A.268 Patient 3D bilateral muscle forces normalized with respect to body weight during flexion-extension.

A.23.2 Lateral Flexion Activity

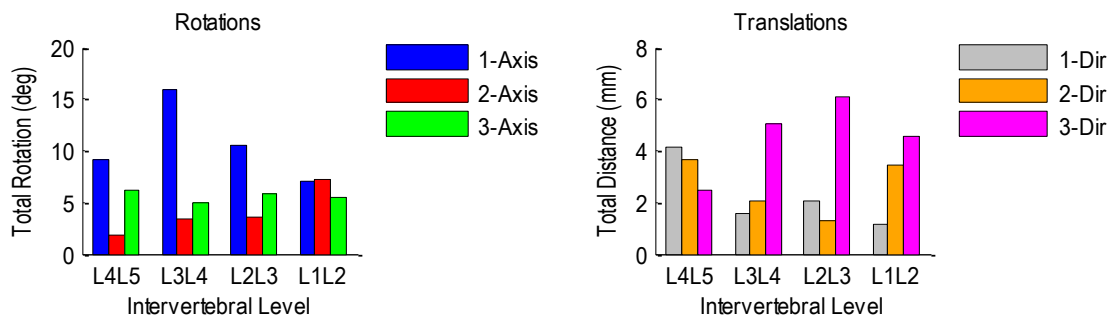


Figure A.269 Patient 3D relative rotations (left) and translations (right) at each vertebral level during left-to-right lateral flexion.

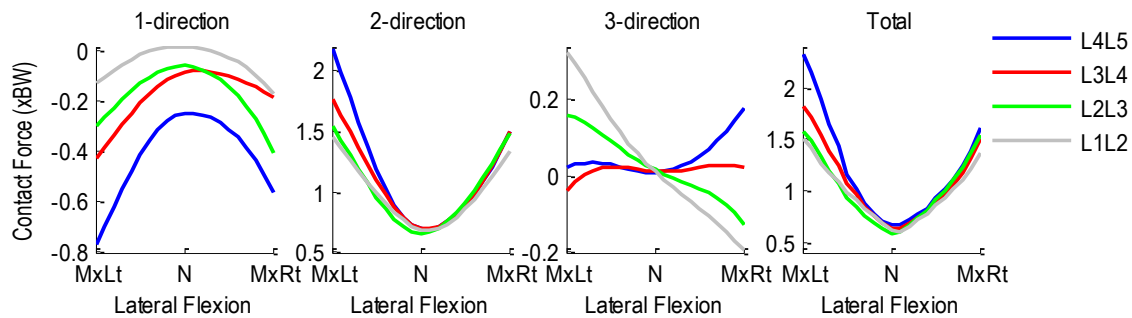


Figure A.270 Patient 3D intervertebral contact forces normalized with respect to body weight during left-to-right lateral flexion. 1-dir=Ant(+)/Post(-), 2-dir=Sup(+)/Inf(-), 3-dir=Rt(+)/Lt(-).

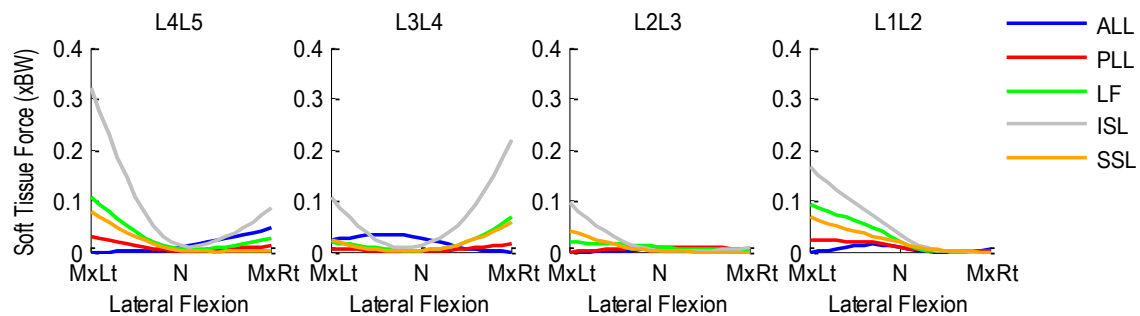


Figure A.271 Patient 3D segmental ligament forces normalized with respect to body weight during left-to-right lateral flexion.

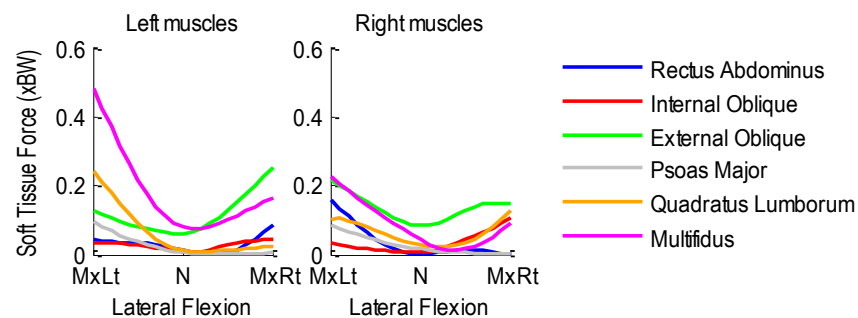


Figure A.272 Patient 3D bilateral muscle forces normalized with respect to body weight during left-to-right lateral flexion.

A.23.3 Axial Rotation Activity

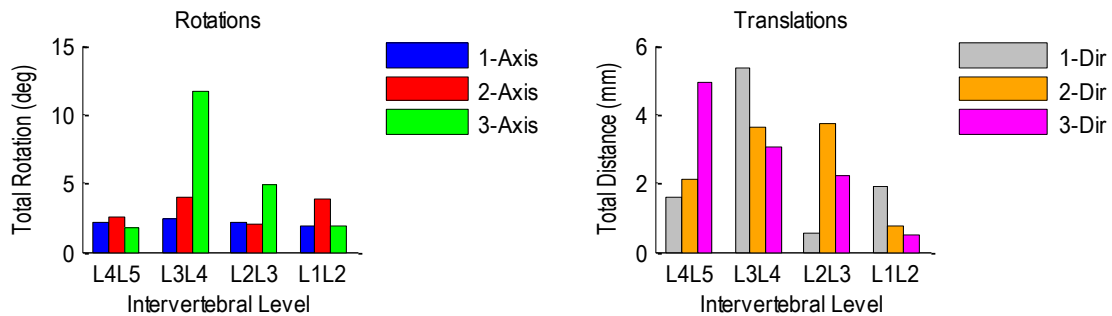


Figure A.273 Patient 3D relative rotations (left) and translations (right) at each vertebral level during left-to-right axial rotation.

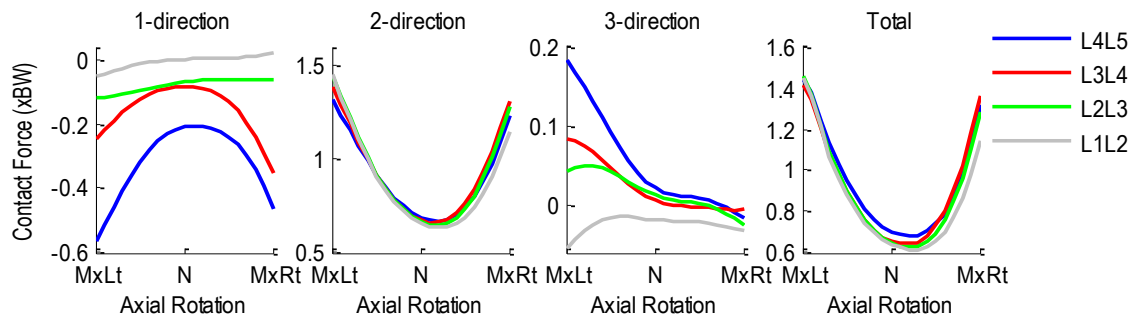


Figure A.274 Patient 3D intervertebral contact forces normalized with respect to body weight during left-to-right axial rotation. 1-dir=Ant(+)/Post(-), 2-dir=Sup(+)/Inf(-), 3-dir=Rt(+)/Lt(-).

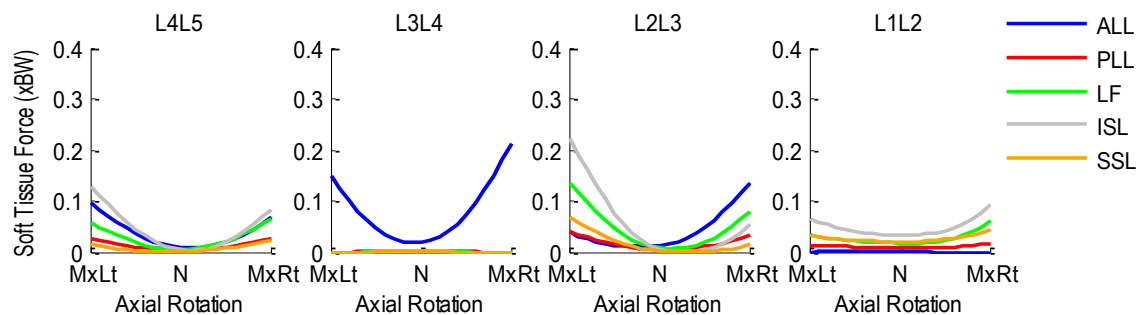


Figure A.275 Patient 3D segmental ligament forces normalized with respect to body weight during left-to-right axial rotation.

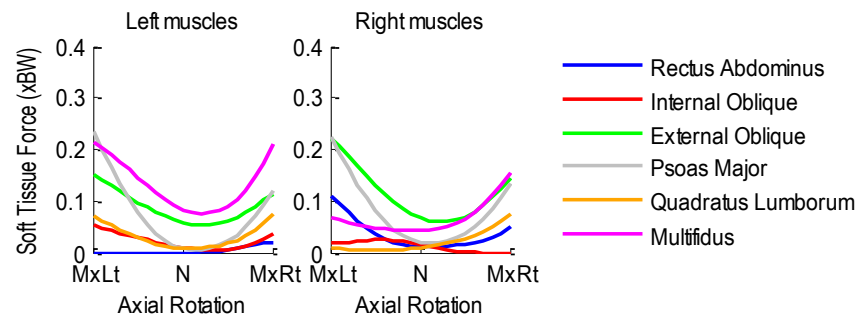


Figure A.276 Patient 3D bilateral muscle forces normalized with respect to body weight during left-to-right axial rotation.

A.24 Patient 4D

Age: 49 years

Gender: Male

Height: 1.88 m

Mass: 87 kg

Condition: Degenerative at L4L5 and L5S1

A.24.1 Flexion-Extension Activity

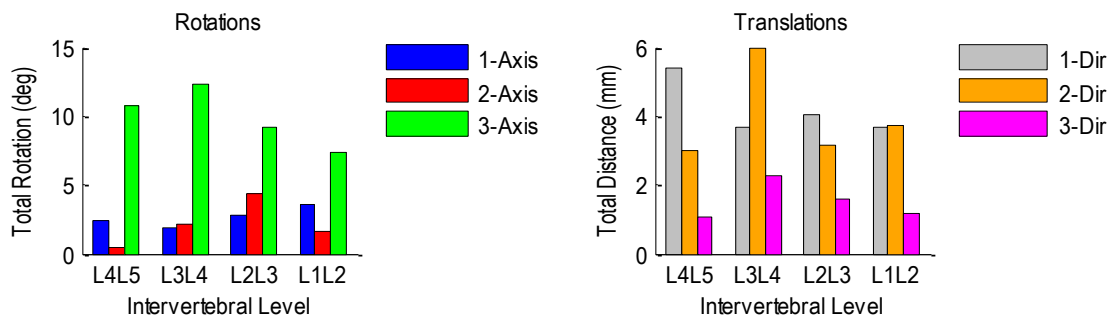


Figure A.277 Patient 4D relative rotations (left) and translations (right) at each vertebral level during flexion-extension.

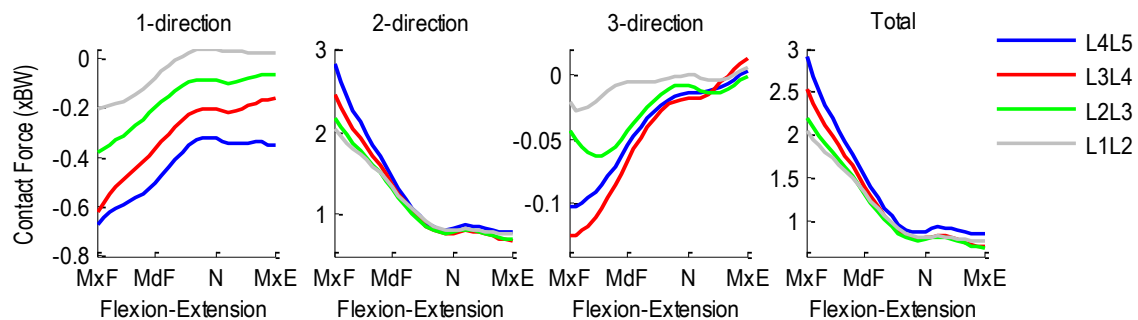


Figure A.278 Patient 4D intervertebral contact forces normalized with respect to body weight during flexion-extension. 1-dir=Ant(+)/Post(-), 2-dir=Sup(+)/Inf(-), 3-dir=Rt(+)/Lt(-).

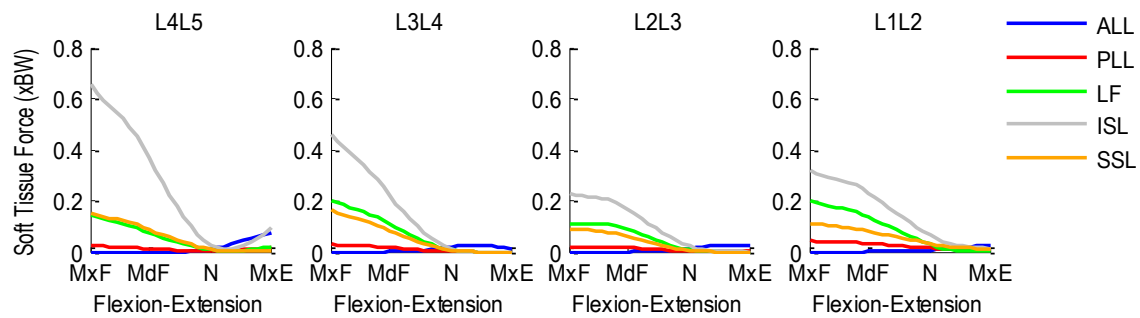


Figure A.279 Patient 4D segmental ligament forces normalized with respect to body weight during flexion-extension.

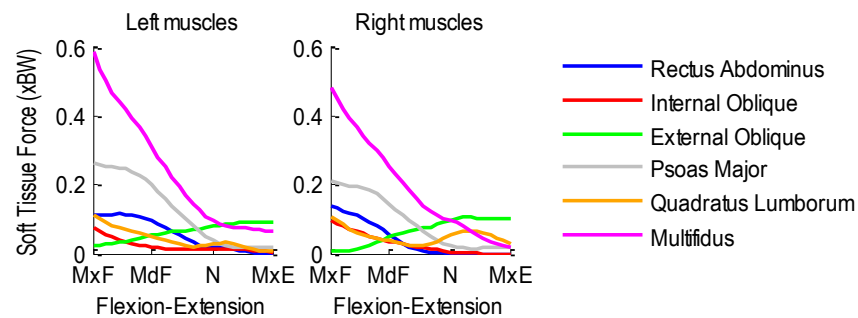


Figure A.280 Patient 4D bilateral muscle forces normalized with respect to body weight during flexion-extension.

A.24.2 Lateral Flexion Activity

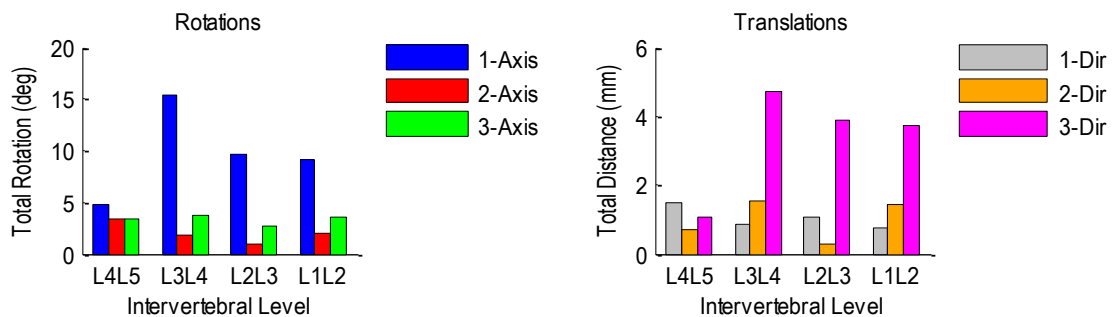


Figure A.281 Patient 4D relative rotations (left) and translations (right) at each vertebral level during left-to-right lateral flexion.

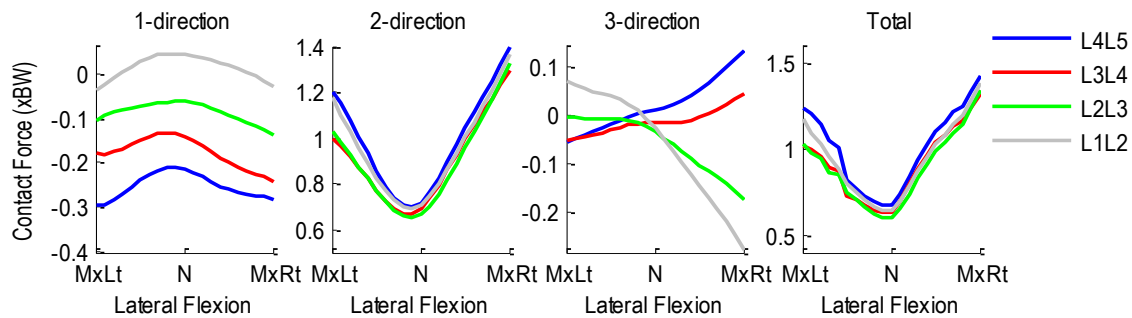


Figure A.282 Patient 4D intervertebral contact forces normalized with respect to body weight during left-to-right lateral flexion. 1-dir=Ant(+)/Post(-), 2-dir=Sup(+)/Inf(-), 3-dir=Rt(+)/Lt(-).

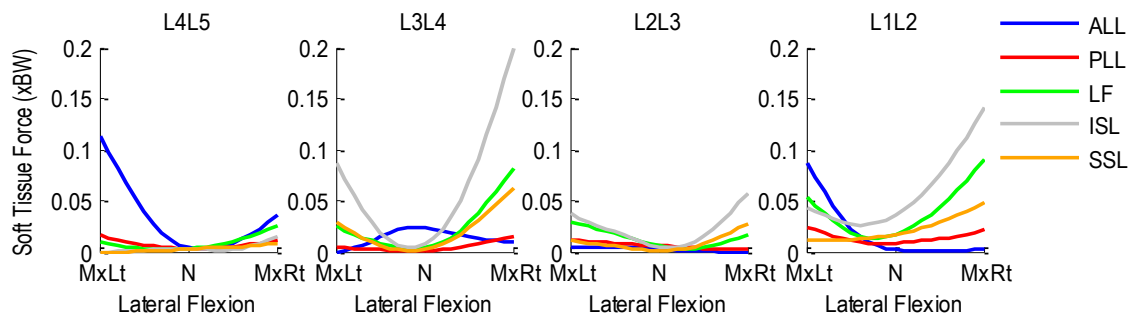


Figure A.283 Patient 4D segmental ligament forces normalized with respect to body weight during left-to-right lateral flexion.

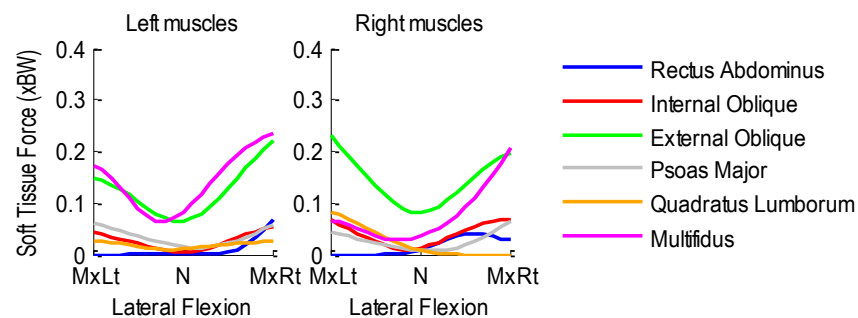


Figure A.284 Patient 4D bilateral muscle forces normalized with respect to body weight during left-to-right lateral flexion.

A.24.3 Axial Rotation Activity

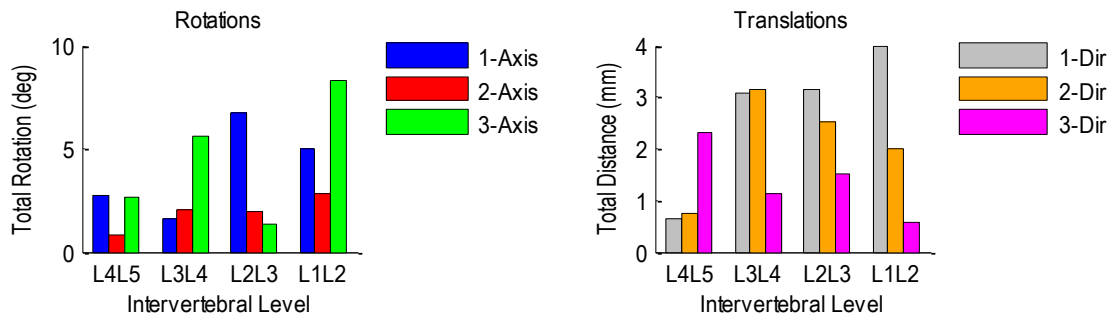


Figure A.285 Patient 4D relative rotations (left) and translations (right) at each vertebral level during left-to-right axial rotation.

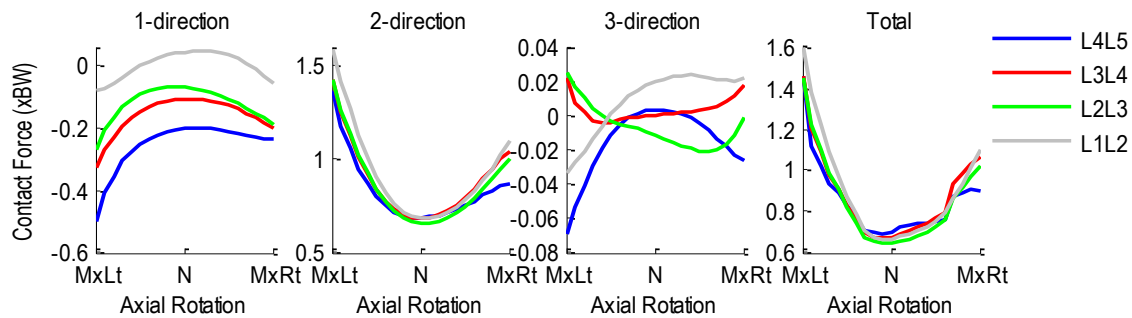


Figure A.286 Patient 4D intervertebral contact forces normalized with respect to body weight during left-to-right axial rotation. 1-dir=Ant(+)/Post(-), 2-dir=Sup(+)/Inf(-), 3-dir=Rt(+)/Lt(-).

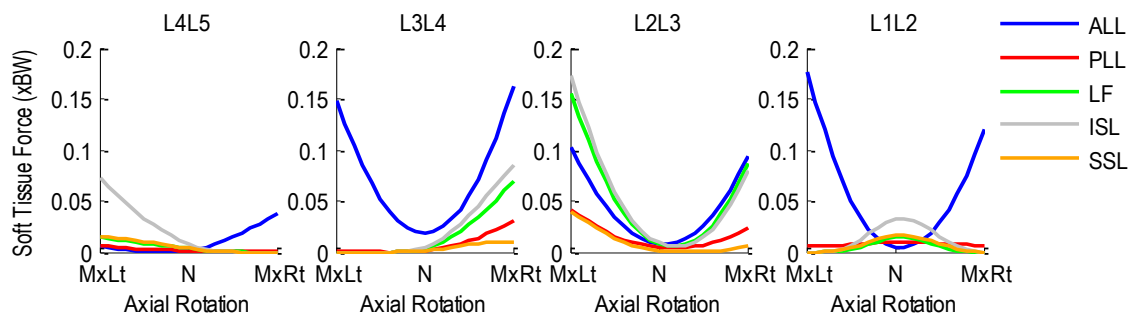


Figure A.287 Patient 4D segmental ligament forces normalized with respect to body weight during left-to-right axial rotation.

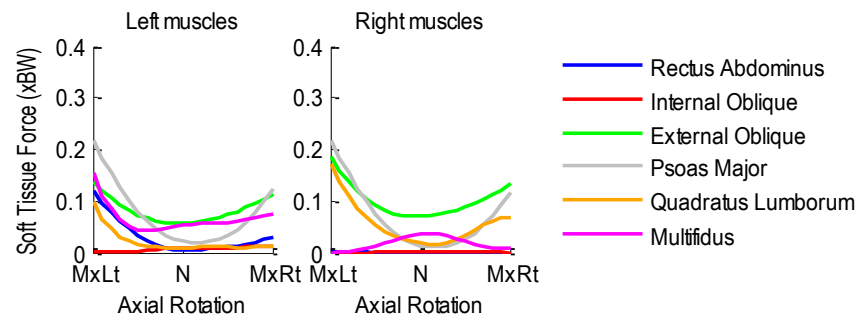


Figure A.288 Patient 4D bilateral muscle forces normalized with respect to body weight during left-to-right axial rotation.

A.25 Patient 5D

Age: 45 years

Gender: Male

Height: 1.78 m

Mass: 75 kg

Condition: Degenerative at L4L5

A.25.1 Flexion-Extension Activity

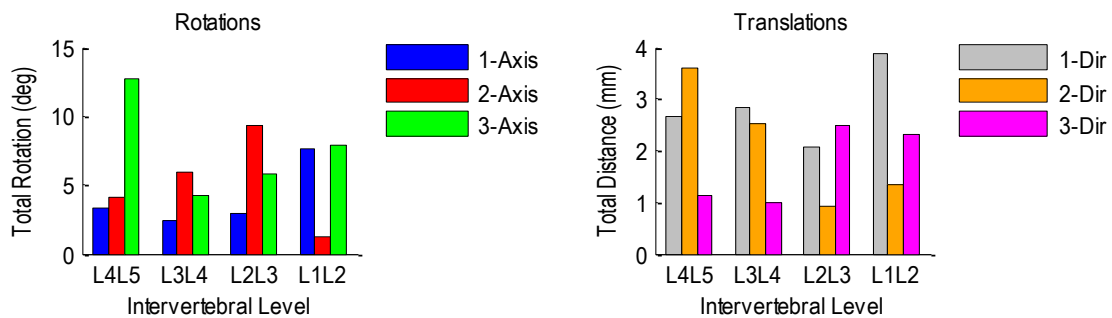


Figure A.289 Patient 5D relative rotations (left) and translations (right) at each vertebral level during flexion-extension.

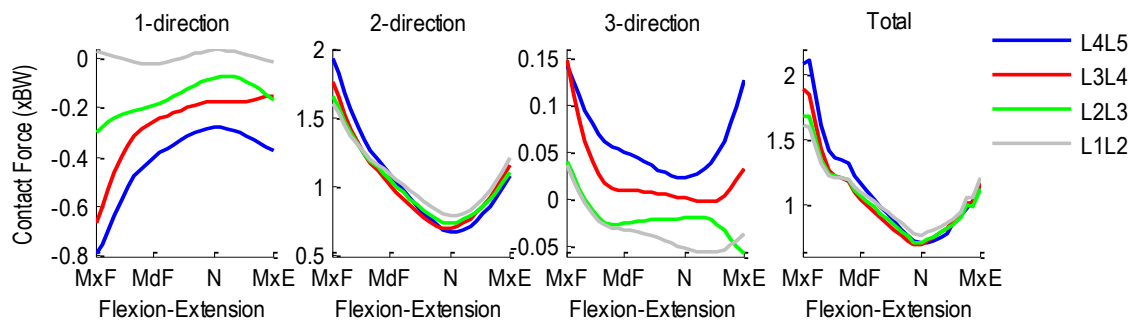


Figure A.290 Patient 5D intervertebral contact forces normalized with respect to body weight during flexion-extension. 1-dir=Ant(+)/Post(-), 2-dir=Sup(+)/Inf(-), 3-dir=Rt(+)/Lt(-).

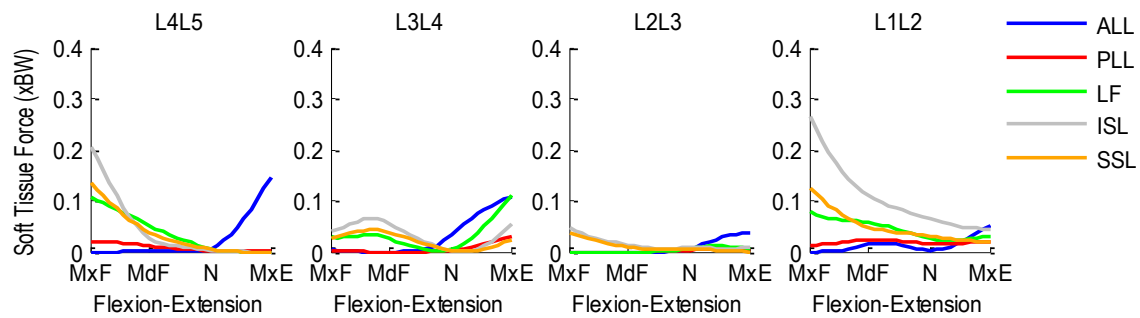


Figure A.291 Patient 5D segmental ligament forces normalized with respect to body weight during flexion-extension.

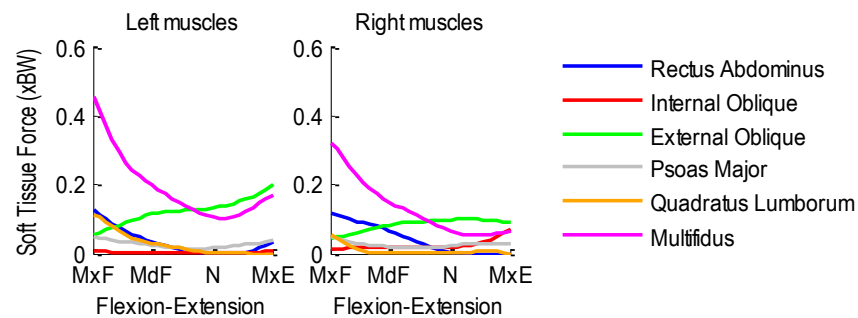


Figure A.292 Patient 5D bilateral muscle forces normalized with respect to body weight during flexion-extension.

A.25.2 Lateral Flexion Activity

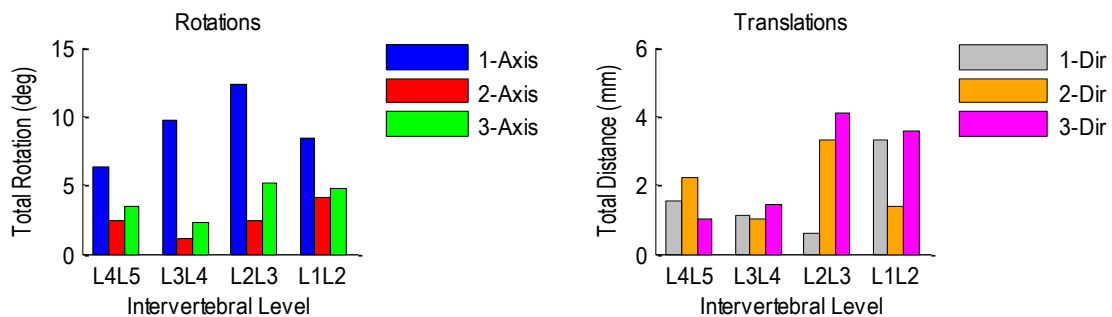


Figure A.293 Patient 5D relative rotations (left) and translations (right) at each vertebral level during left-to-right lateral flexion.

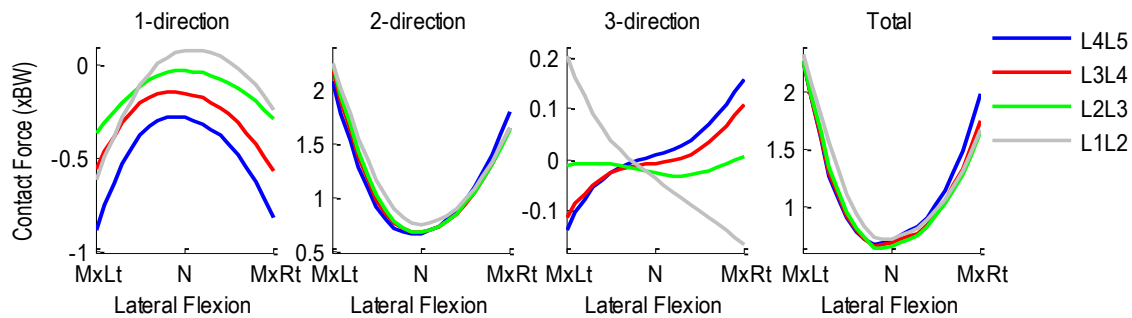


Figure A.294 Patient 5D intervertebral contact forces normalized with respect to body weight during left-to-right lateral flexion. 1-dir=Ant(+)/Post(-), 2-dir=Sup(+)/Inf(-), 3-dir=Rt(+)/Lt(-).

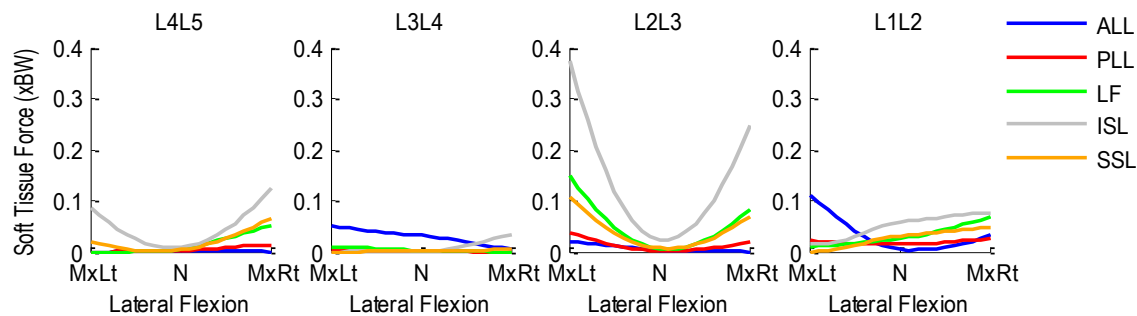


Figure A.295 Patient 5D segmental ligament forces normalized with respect to body weight during left-to-right lateral flexion.

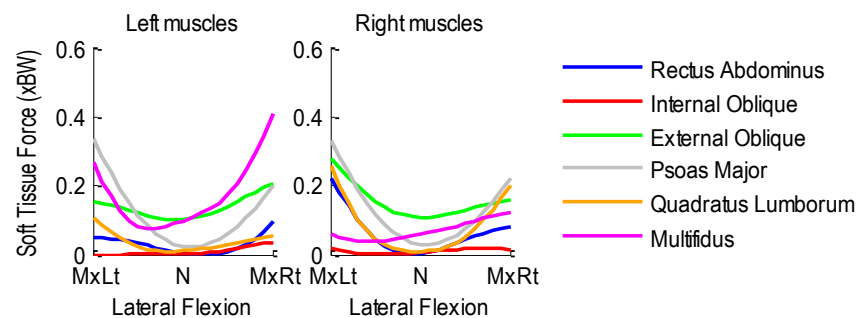


Figure A.296 Patient 5D bilateral muscle forces normalized with respect to body weight during left-to-right lateral flexion.

A.25.3 Axial Rotation Activity

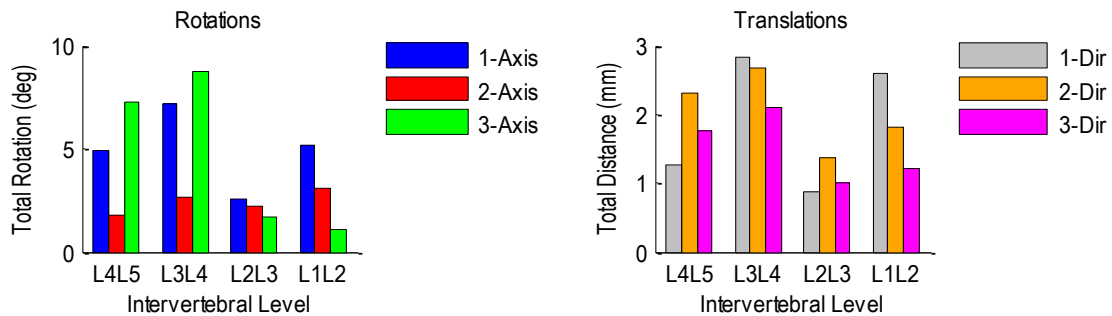


Figure A.297 Patient 5D relative rotations (left) and translations (right) at each vertebral level during left-to-right axial rotation.

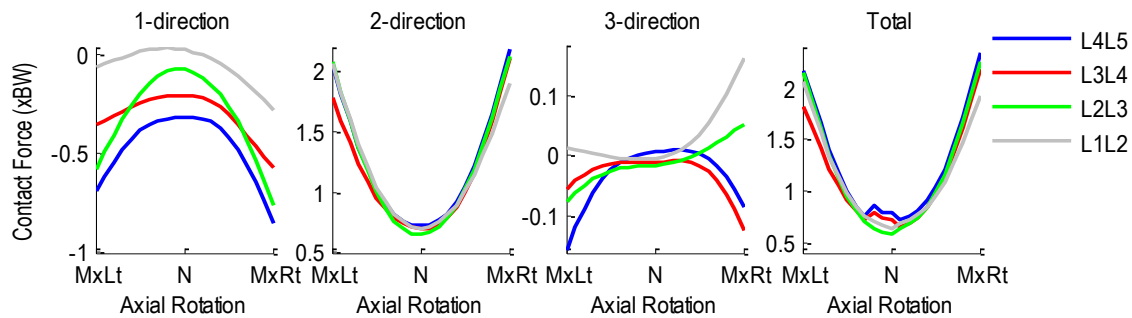


Figure A.298 Patient 5D intervertebral contact forces normalized with respect to body weight during left-to-right axial rotation. 1-dir=Ant(+)/Post(-), 2-dir=Sup(+)/Inf(-), 3-dir=Rt(+)/Lt(-).

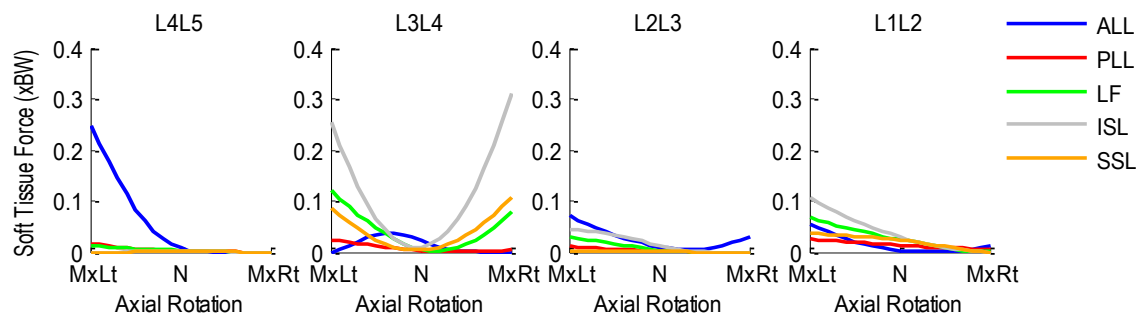


Figure A.299 Patient 5D segmental ligament forces normalized with respect to body weight during left-to-right axial rotation.

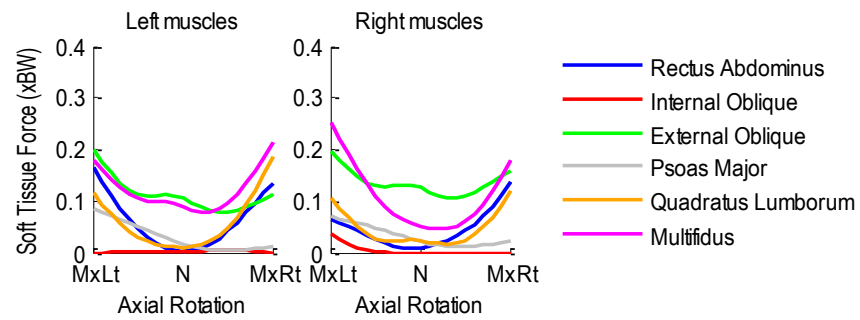


Figure A.300 Patient 5D bilateral muscle forces normalized with respect to body weight during left-to-right axial rotation.

A.26 Patient 6D

Age: 50 years

Gender: Female

Height: 1.60 m

Mass: 84 kg

Condition: Degenerative at L3L4 and L5S1

A.26.1 Flexion-Extension Activity

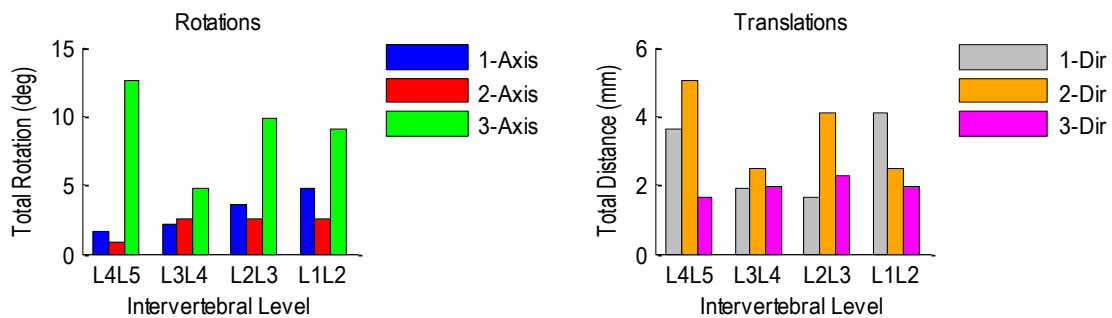


Figure A.301. Patient 6D relative rotations (left) and translations (right) at each vertebral level during flexion-extension.

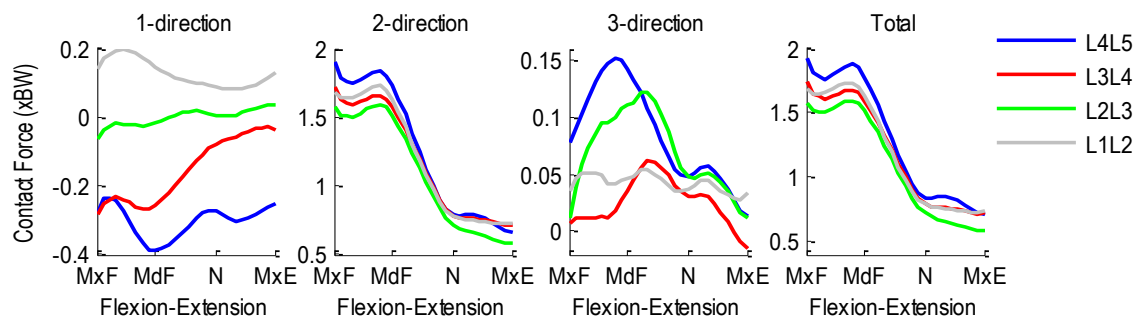


Figure A.302 Patient 6D intervertebral contact forces normalized with respect to body weight during flexion-extension. 1-dir=Ant(+)/Post(-), 2-dir=Sup(+)/Inf(-), 3-dir=Rt(+)/Lt(-).

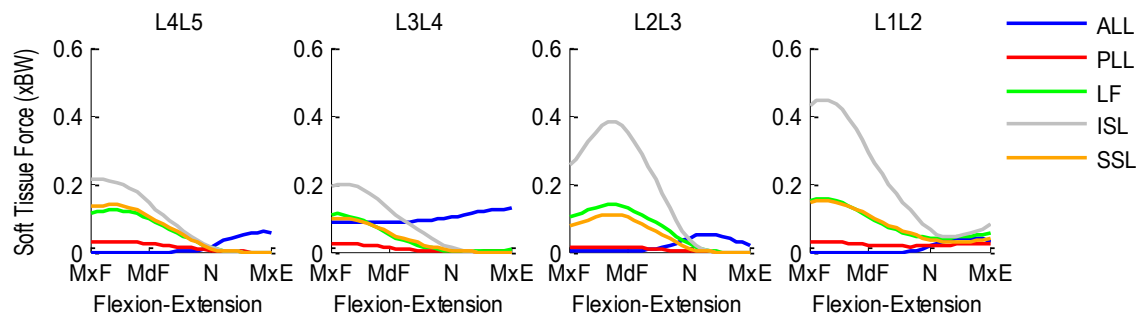


Figure A.303 Patient 6D segmental ligament forces normalized with respect to body weight during flexion-extension.

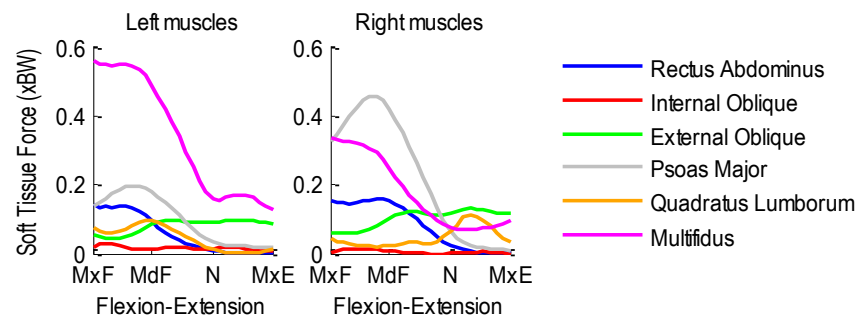


Figure A.304 Patient 6D bilateral muscle forces normalized with respect to body weight during flexion-extension.

A.26.2 Lateral Flexion Activity

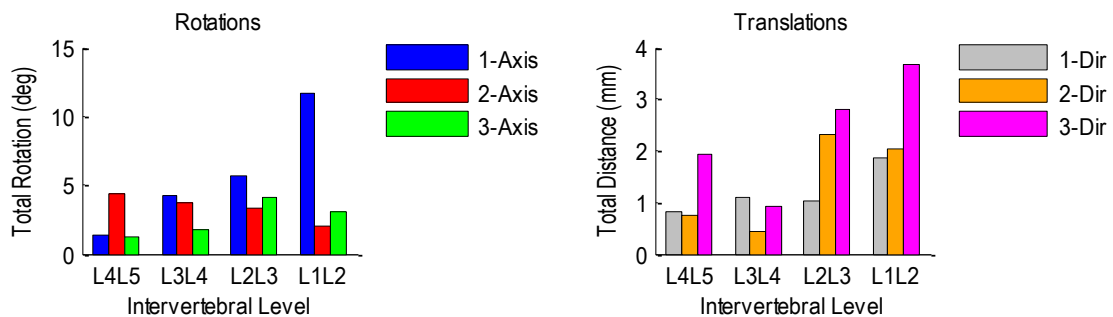


Figure A.305 Patient 6D relative rotations (left) and translations (right) at each vertebral level during left-to-right lateral flexion.

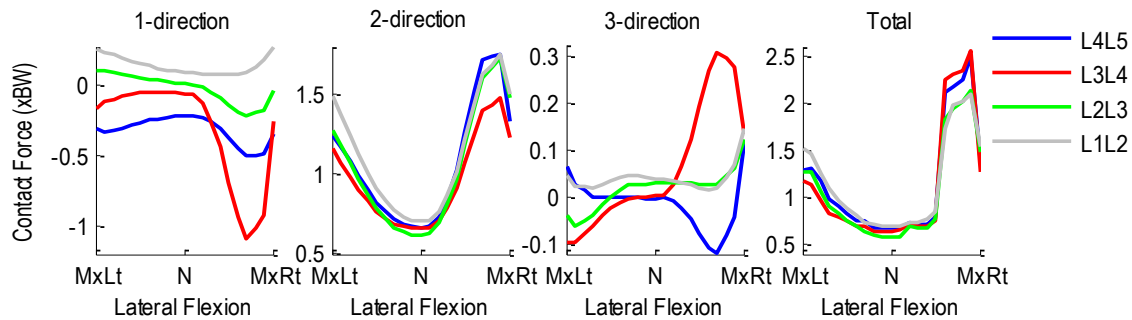


Figure A.306 Patient 6D intervertebral contact forces normalized with respect to body weight during left-to-right lateral flexion. 1-dir=Ant(+)/Post(-), 2-dir=Sup(+)/Inf(-), 3-dir=Rt(+)/Lt(-).

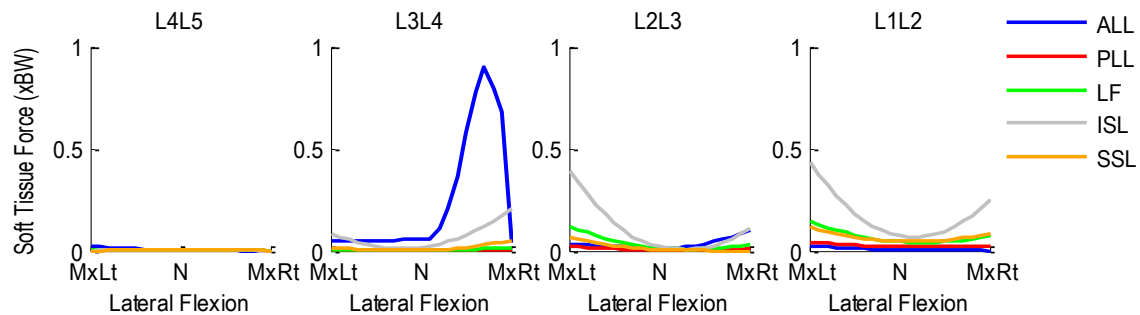


Figure A.307 Patient 6D segmental ligament forces normalized with respect to body weight during left-to-right lateral flexion.

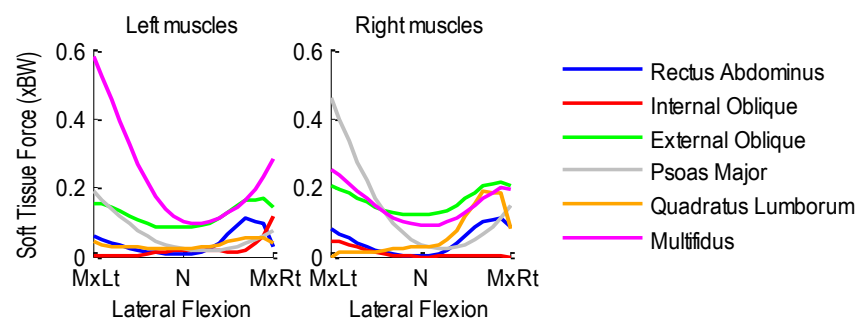


Figure A.308 Patient 6D bilateral muscle forces normalized with respect to body weight during left-to-right lateral flexion.

A.26.3 Axial Rotation Activity

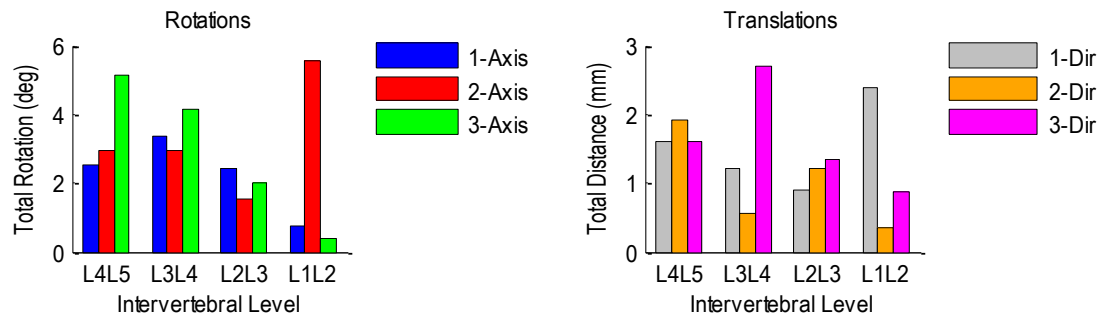


Figure A.309 Patient 6D relative rotations (left) and translations (right) at each vertebral level during left-to-right axial rotation.

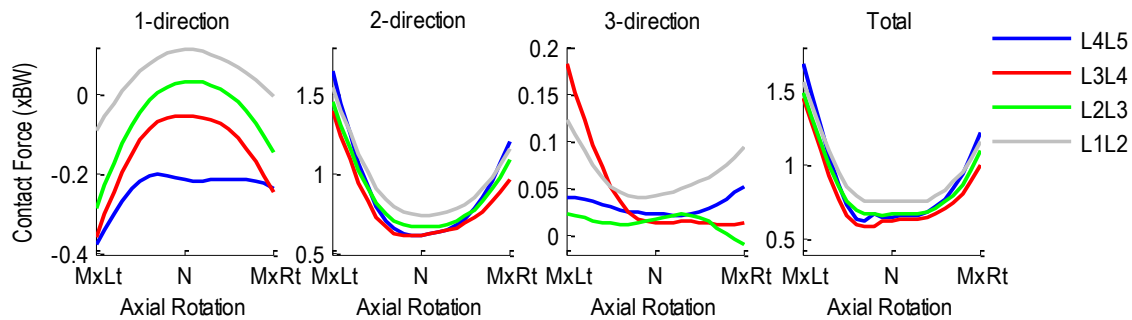


Figure A.310 Patient 6D intervertebral contact forces normalized with respect to body weight during left-to-right axial rotation. 1-dir=Ant(+)/Post(-), 2-dir=Sup(+)/Inf(-), 3-dir=Rt(+)/Lt(-).

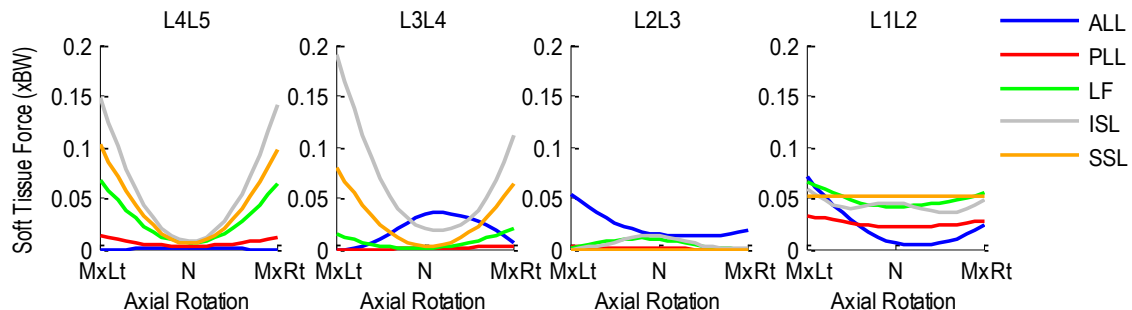


Figure A.311 Patient 6D segmental ligament forces normalized with respect to body weight during left-to-right axial rotation.

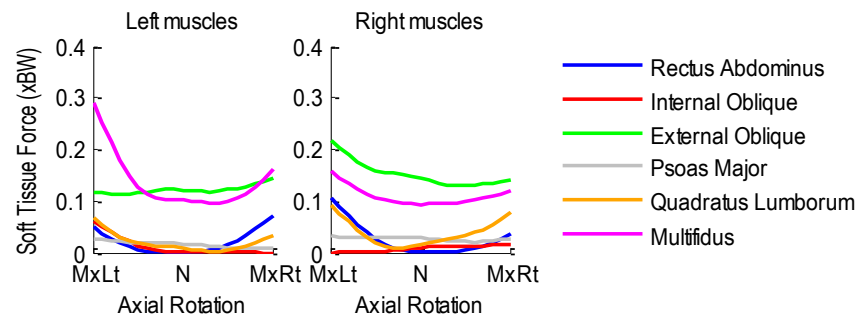


Figure A.312 Patient 6D bilateral muscle forces normalized with respect to body weight during left-to-right axial rotation.

A.27 Patient 7D

Age: 45 years

Gender: Female

Height: 1.68 m

Mass: 107 kg

Condition: Degenerative at L5S1

A.27.1 Flexion-Extension Activity

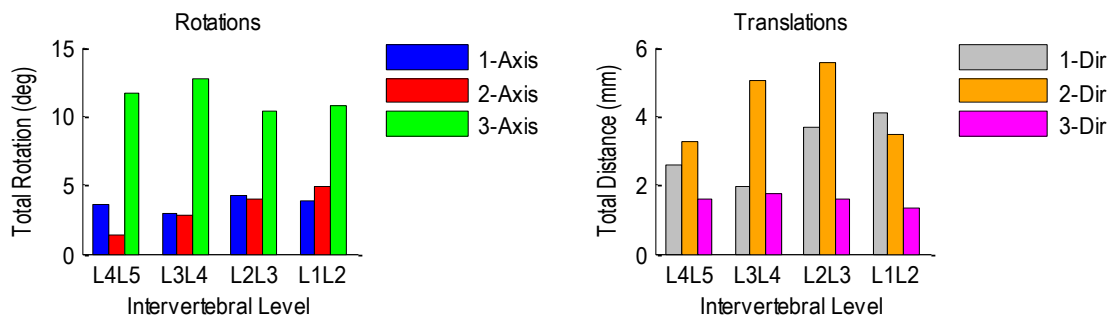


Figure A.313 Patient 7D relative rotations (left) and translations (right) at each vertebral level during flexion-extension.

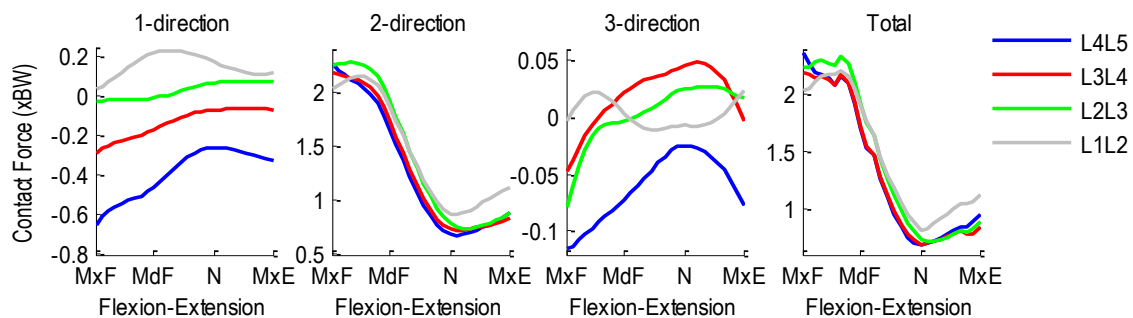


Figure A.314 Patient 7D intervertebral contact forces normalized with respect to body weight during flexion-extension. 1-dir=Ant(+)/Post(-), 2-dir=Sup(+)/Inf(-), 3-dir=Rt(+)/Lt(-).

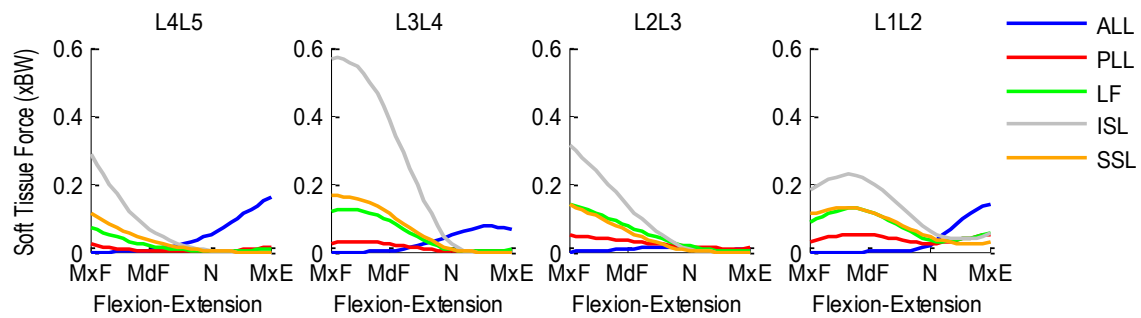


Figure A.315 Patient 7D segmental ligament forces normalized with respect to body weight during flexion-extension.

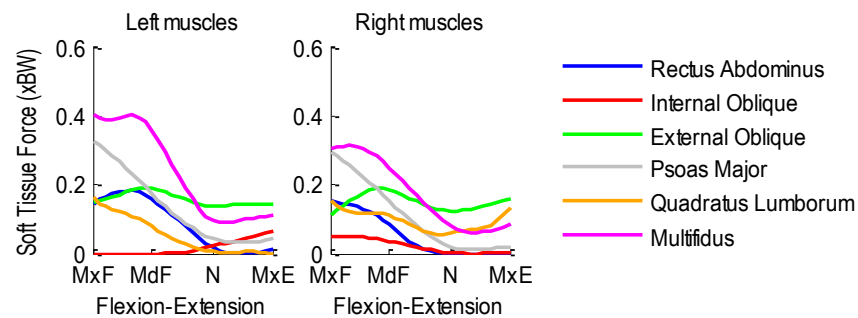


Figure A.316 Patient 7D bilateral muscle forces normalized with respect to body weight during flexion-extension.

A.27.2 Lateral Flexion Activity

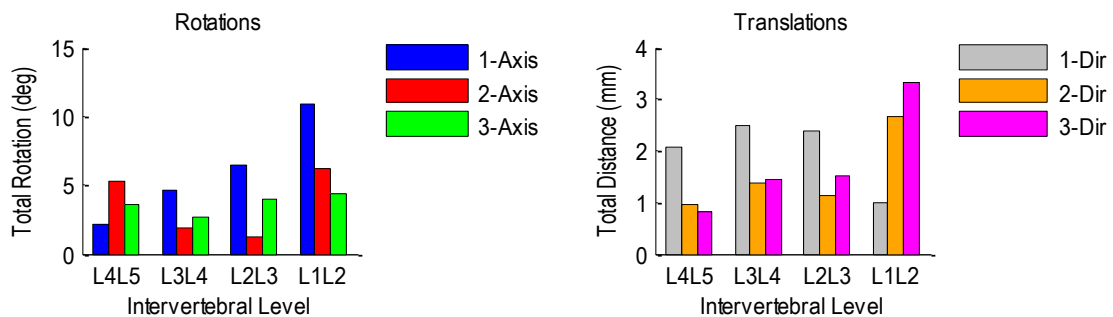


Figure A.317 Patient 7D relative rotations (left) and translations (right) at each vertebral level during left-to-right lateral flexion.

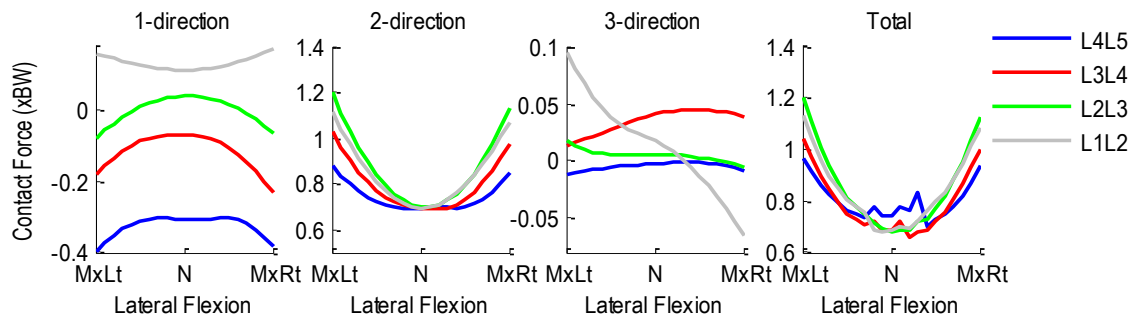


Figure A.318 Patient 7D intervertebral contact forces normalized with respect to body weight during left-to-right lateral flexion. 1-dir=Ant(+)/Post(-), 2-dir=Sup(+)/Inf(-), 3-dir=Rt(+)/Lt(-).

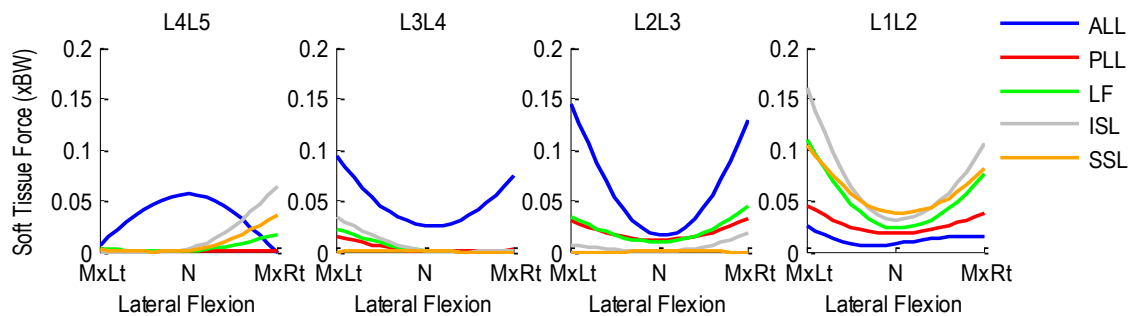


Figure A.319 Patient 7D segmental ligament forces normalized with respect to body weight during left-to-right lateral flexion.

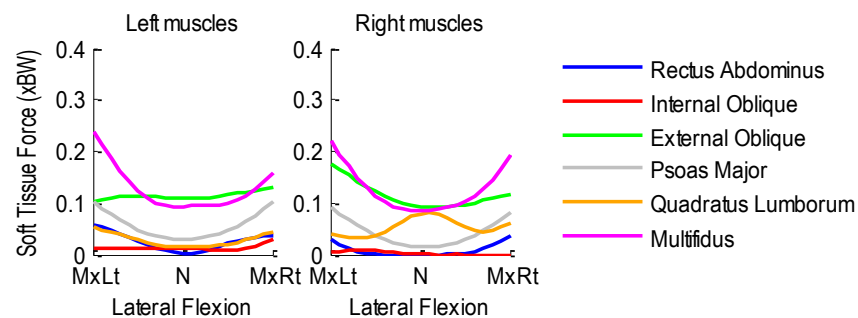


Figure A.320 Patient 7D bilateral muscle forces normalized with respect to body weight during left-to-right lateral flexion.

A.27.3 Axial Rotation Activity

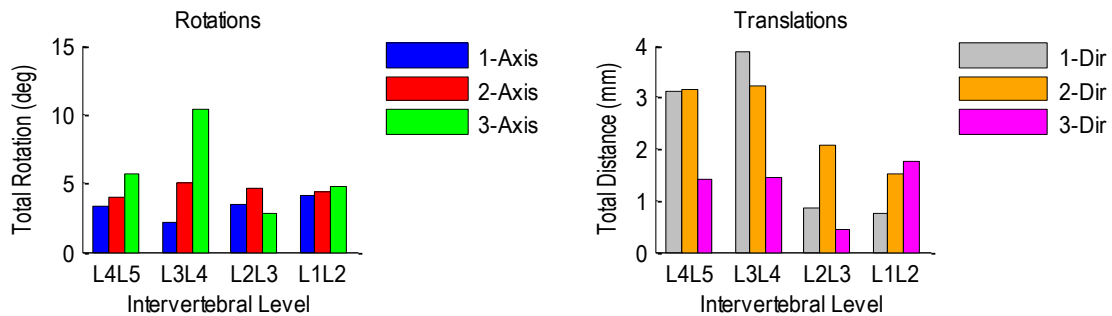


Figure A.321 Patient 7D relative rotations (left) and translations (right) at each vertebral level during left-to-right axial rotation.

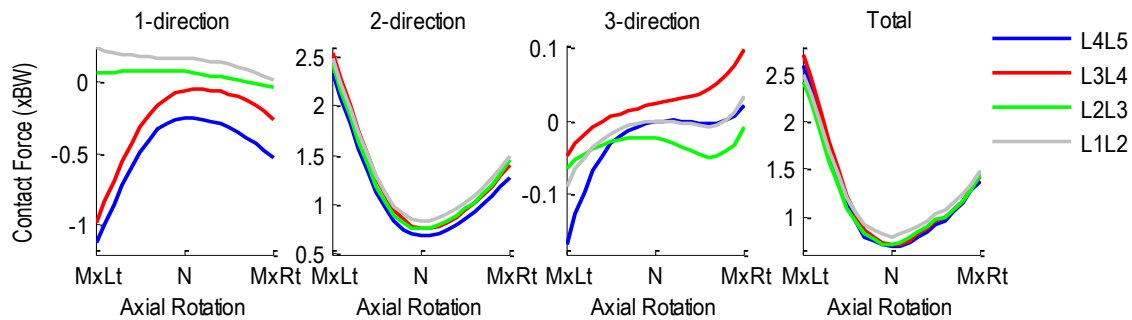


Figure A.322 Patient 7D intervertebral contact forces normalized with respect to body weight during left-to-right axial rotation. 1-dir=Ant(+)/Post(-), 2-dir=Sup(+)/Inf(-), 3-dir=Rt(+)/Lt(-).

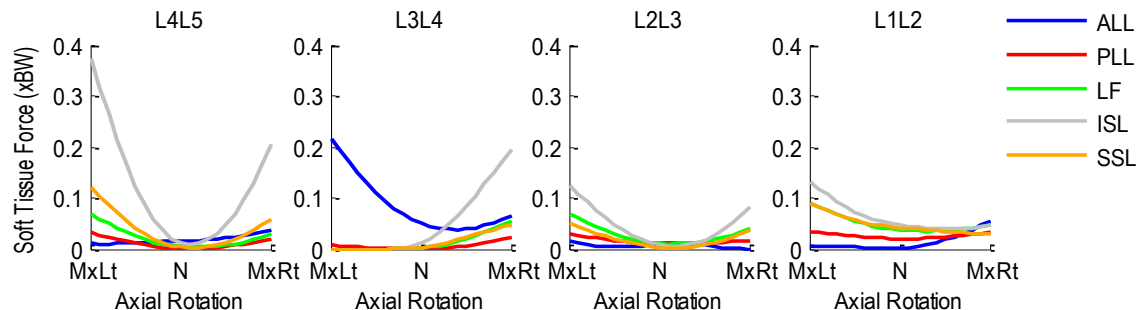


Figure A.323 Patient 7D segmental ligament forces normalized with respect to body weight during left-to-right axial rotation.

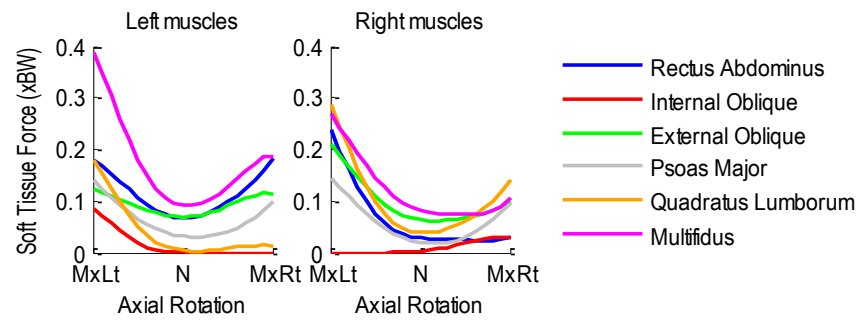


Figure A.324 Patient 7D bilateral muscle forces normalized with respect to body weight during left-to-right axial rotation.

A.28 Patient 8D

Age: 40 years

Gender: Female

Height: 1.73 m

Mass: 69 kg

Condition: Degenerative at L4L5

A.28.1 Flexion-Extension Activity

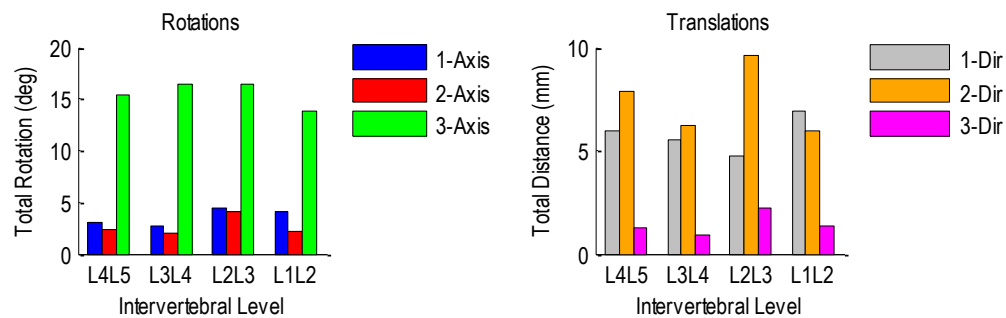


Figure A.325 Patient 8D relative rotations (left) and translations (right) at each vertebral level during flexion-extension.

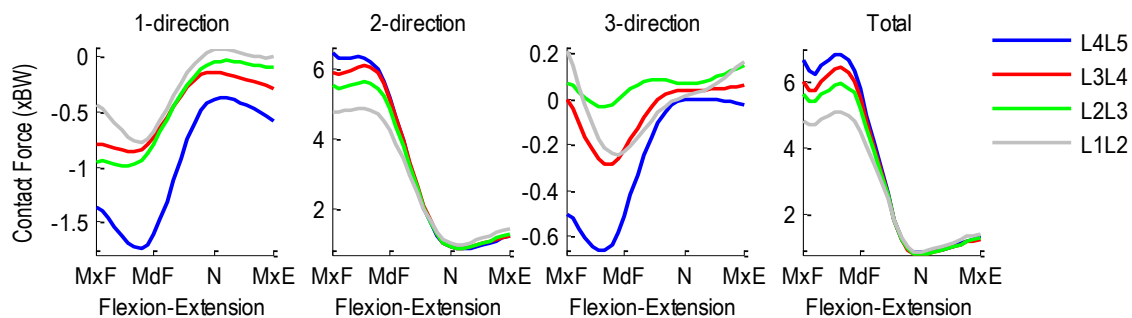


Figure A.326 Patient 8D intervertebral contact forces normalized with respect to body weight during flexion-extension. 1-dir=Ant(+)/Post(-), 2-dir=Sup(+)/Inf(-), 3-dir=Rt(+)/Lt(-).

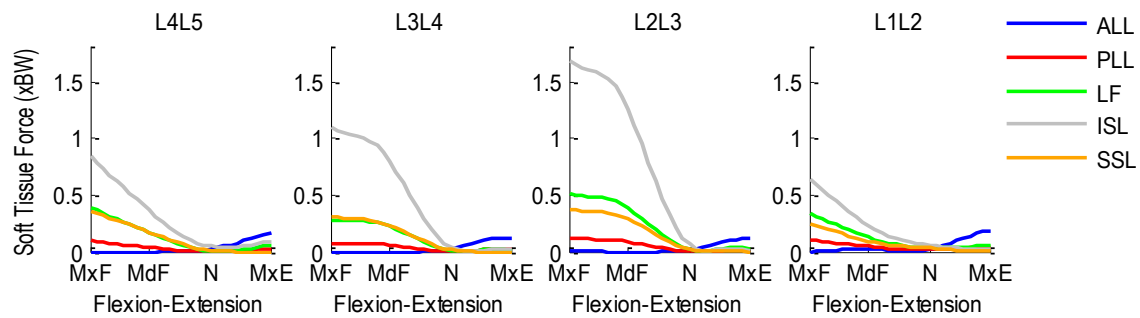


Figure A.327 Patient 8D segmental ligament forces normalized with respect to body weight during flexion-extension.

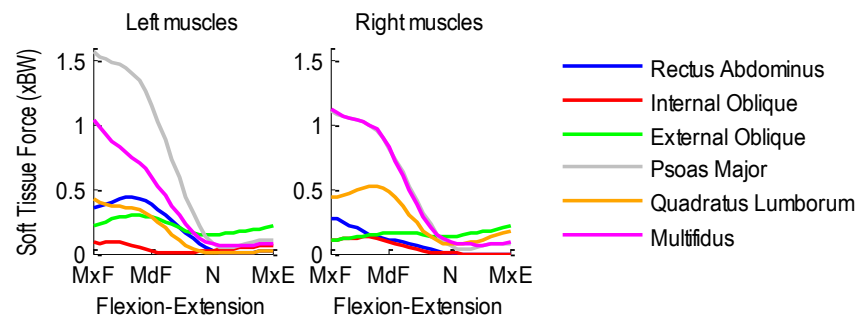


Figure A.328 Patient 8D bilateral muscle forces normalized with respect to body weight during flexion-extension.

A.28.2 Lateral Flexion Activity

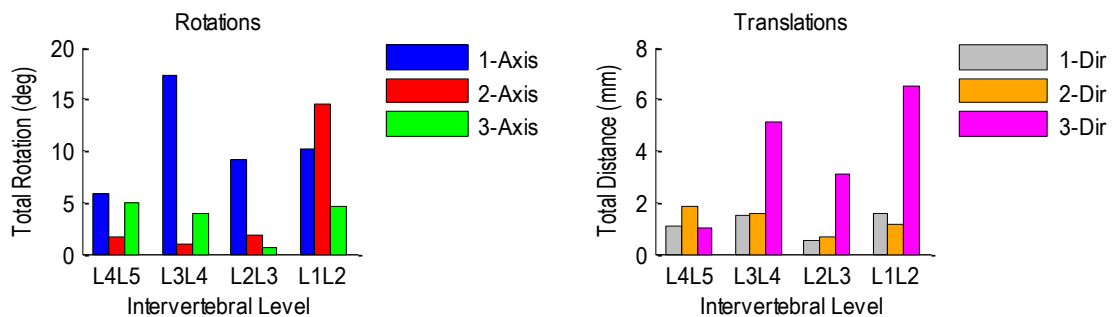


Figure A.329 Patient 8D relative rotations (left) and translations (right) at each vertebral level during left-to-right lateral flexion.

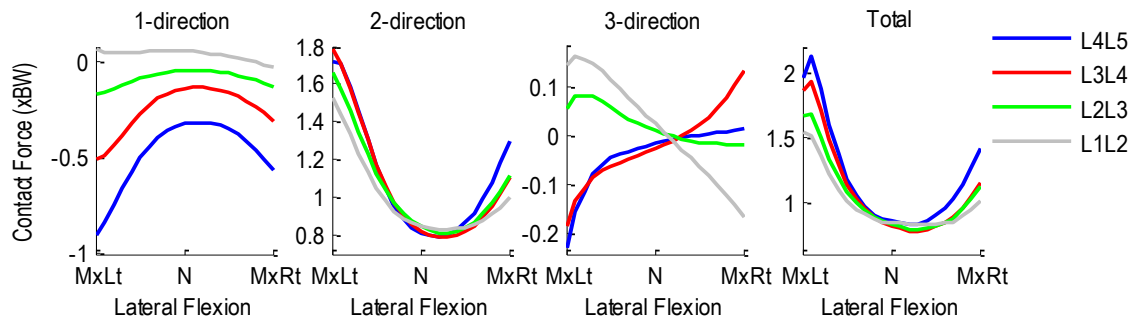


Figure A.330 Patient 8D intervertebral contact forces normalized with respect to body weight during left-to-right lateral flexion. 1-dir=Ant(+)/Post(-), 2-dir=Sup(+)/Inf(-), 3-dir=Rt(+)/Lt(-).

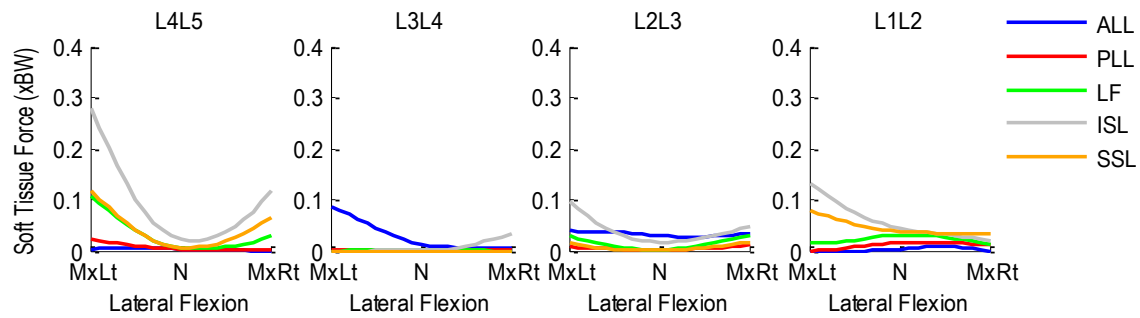


Figure A.331 Patient 8D segmental ligament forces normalized with respect to body weight during left-to-right lateral flexion.

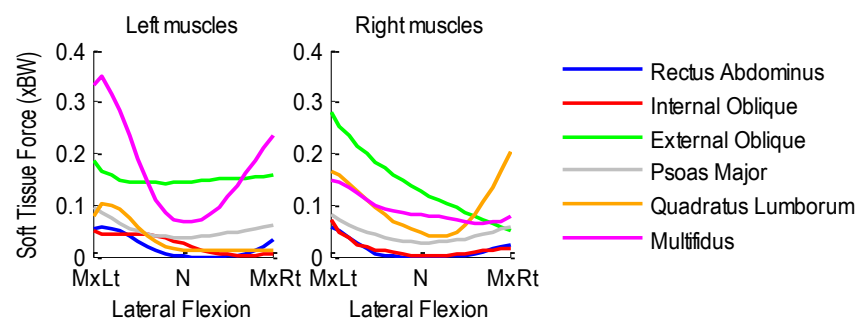


Figure A.332 Patient 8D bilateral muscle forces normalized with respect to body weight during left-to-right lateral flexion.

A.28.3 Axial Rotation Activity

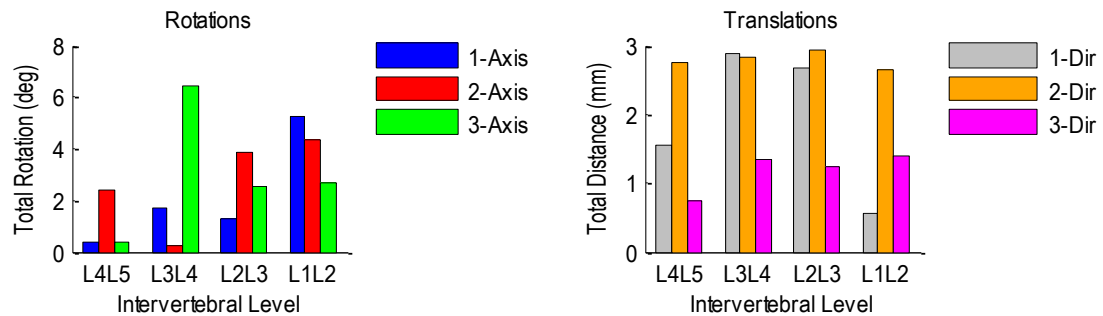


Figure A.333 Patient 8D relative rotations (left) and translations (right) at each vertebral level during left-to-right axial rotation.

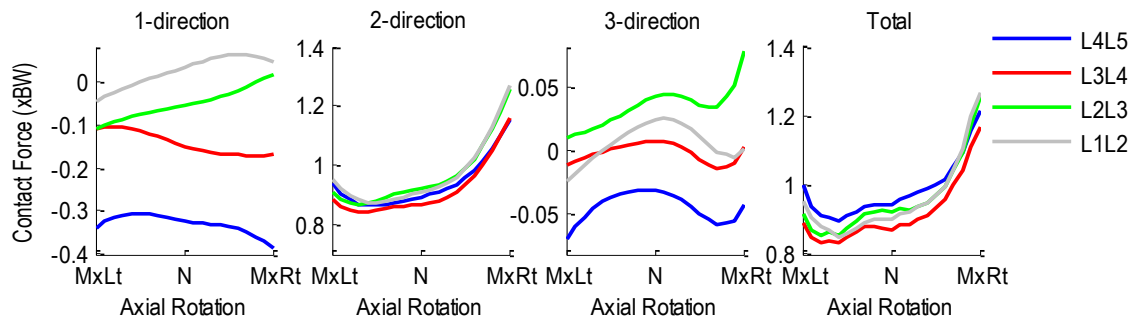


Figure A.334 Patient 8D intervertebral contact forces normalized with respect to body weight during left-to-right axial rotation. 1-dir=Ant(+)/Post(-), 2-dir=Sup(+)/Inf(-), 3-dir=Rt(+)/Lt(-).

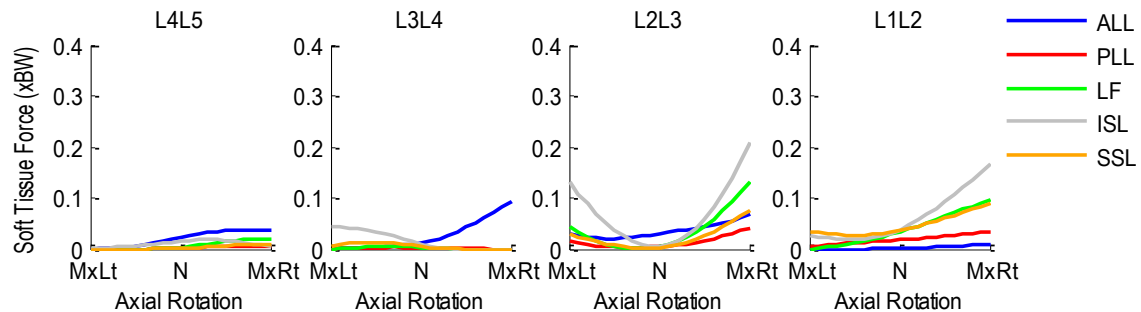


Figure A.335 Patient 8D segmental ligament forces normalized with respect to body weight during left-to-right axial rotation.

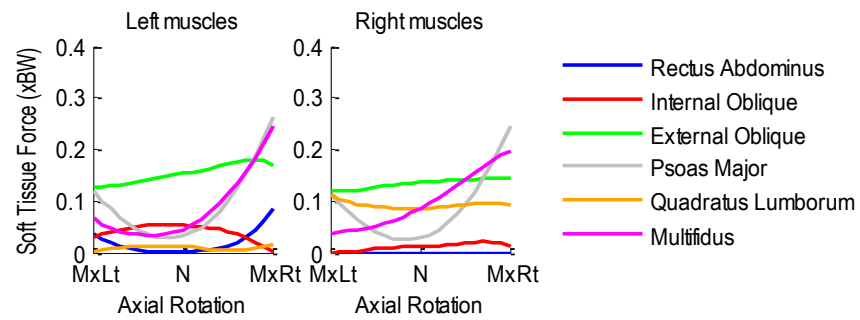


Figure A.336 Patient 8D bilateral muscle forces normalized with respect to body weight during left-to-right axial rotation.

A.29 Patient 9D

Age: 29 years

Gender: Male

Height: 1.78 m

Mass: 75 kg

Condition: Degenerative at L4L5 and L5S1

A.29.1 Flexion-Extension Activity

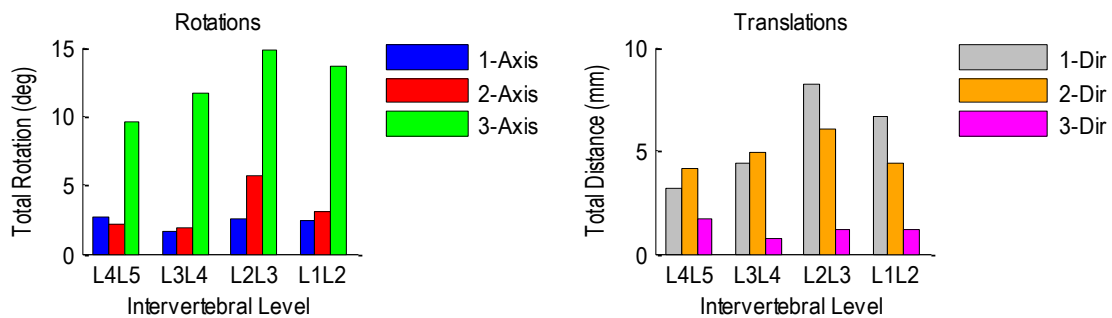


Figure A.337 Patient 9D relative rotations (left) and translations (right) at each vertebral level during flexion-extension.

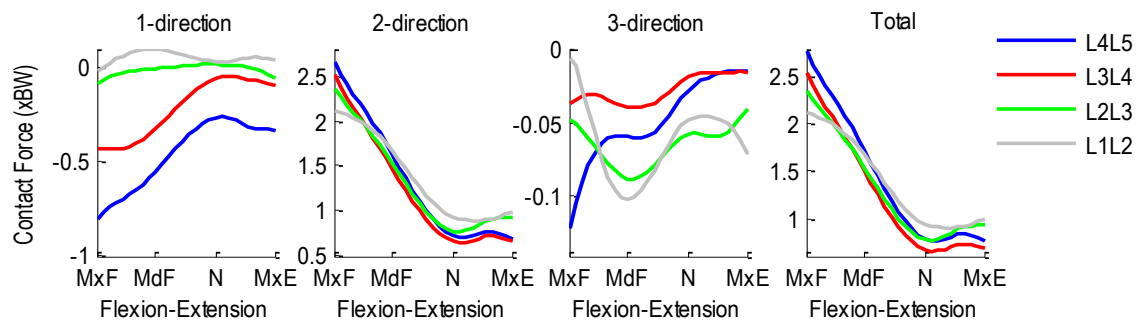


Figure A.338 Patient 9D intervertebral contact forces normalized with respect to body weight during flexion-extension. 1-dir=Ant(+)/Post(-), 2-dir=Sup(+)/Inf(-), 3-dir=Rt(+)/Lt(-).

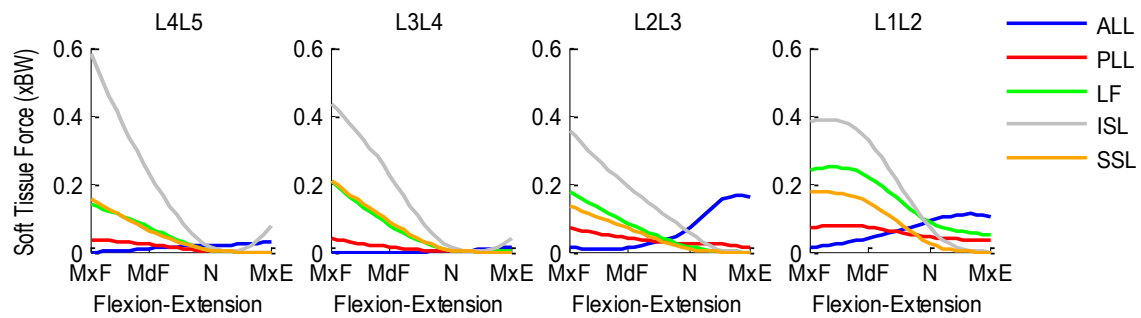


Figure A.339 Patient 9D segmental ligament forces normalized with respect to body weight during flexion-extension.

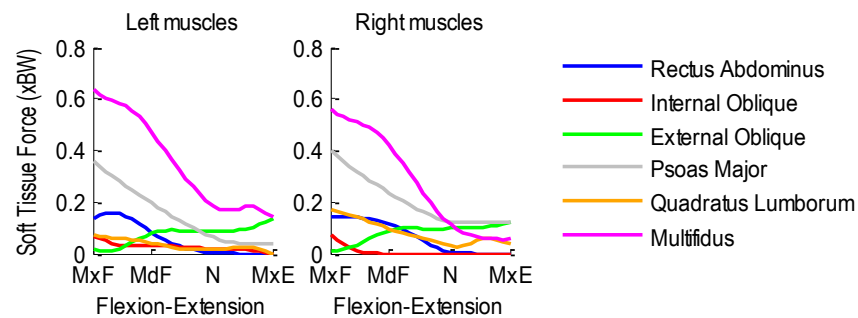


Figure A.340 Patient 9D bilateral muscle forces normalized with respect to body weight during flexion-extension.

A.29.2 Lateral Flexion Activity

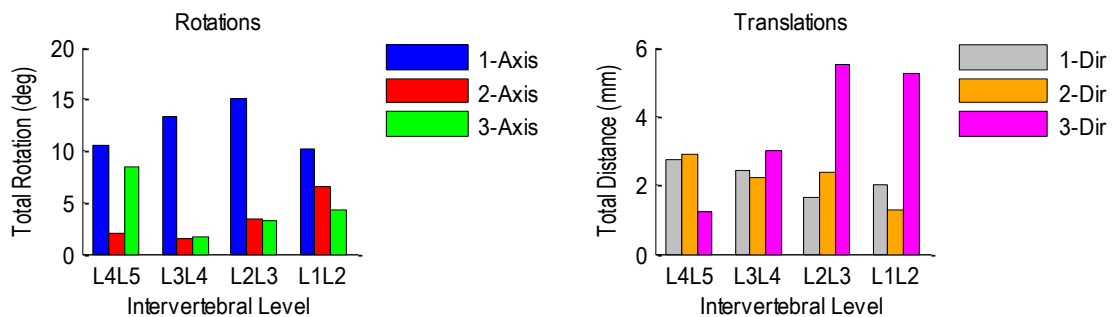


Figure A.341 Patient 9D relative rotations (left) and translations (right) at each vertebral level during left-to-right lateral flexion.

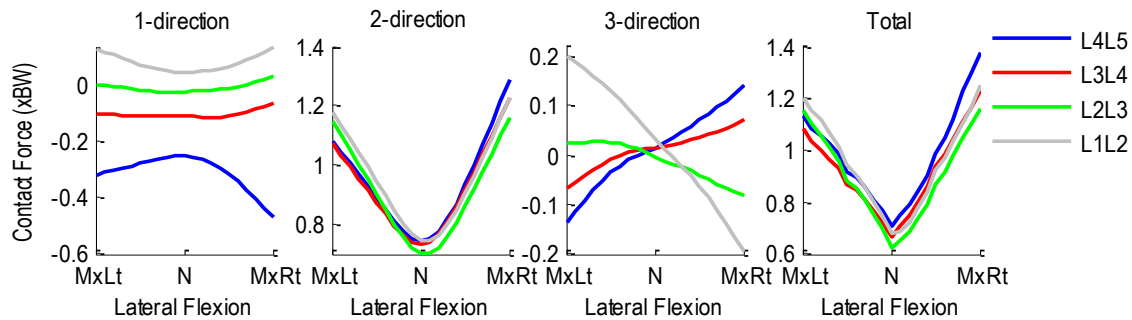


Figure A.342 Patient 9D intervertebral contact forces normalized with respect to body weight during left-to-right lateral flexion. 1-dir=Ant(+)/Post(-), 2-dir=Sup(+)/Inf(-), 3-dir=Rt(+)/Lt(-).

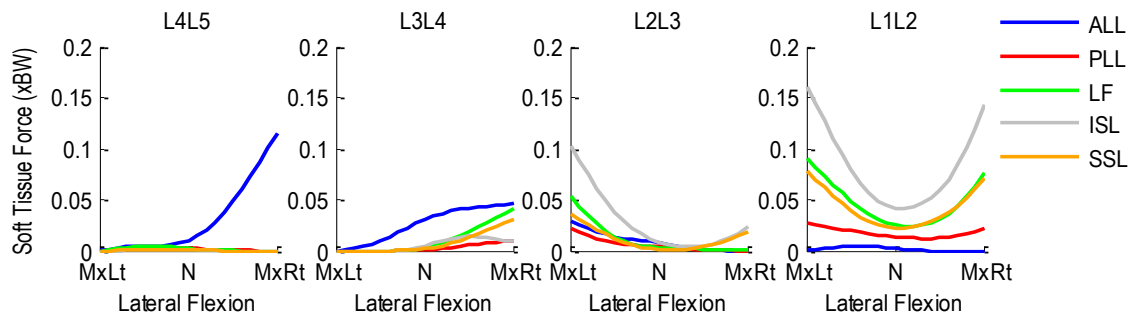


Figure A.343 Patient 9D segmental ligament forces normalized with respect to body weight during left-to-right lateral flexion.

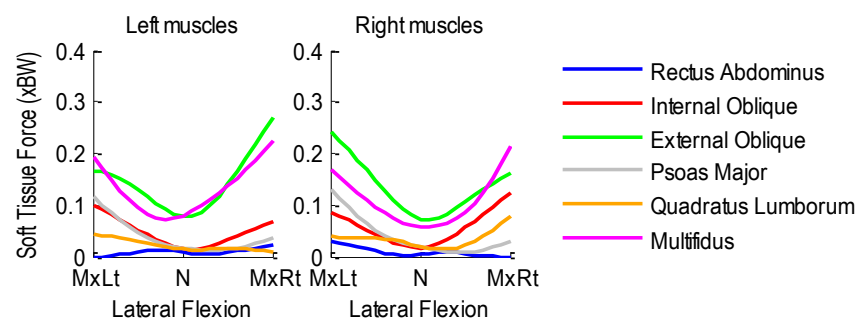


Figure A.344 Patient 9D bilateral muscle forces normalized with respect to body weight during left-to-right lateral flexion.

A.29.3 Axial Rotation Activity

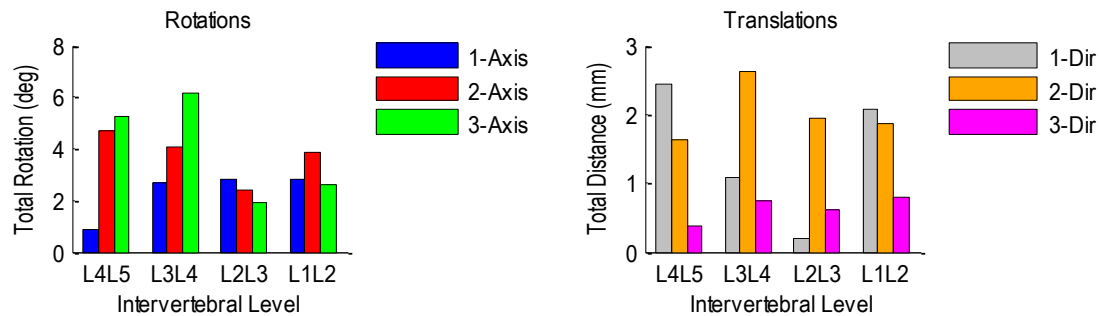


Figure A.345 Patient 9D relative rotations (left) and translations (right) at each vertebral level during left-to-right axial rotation.

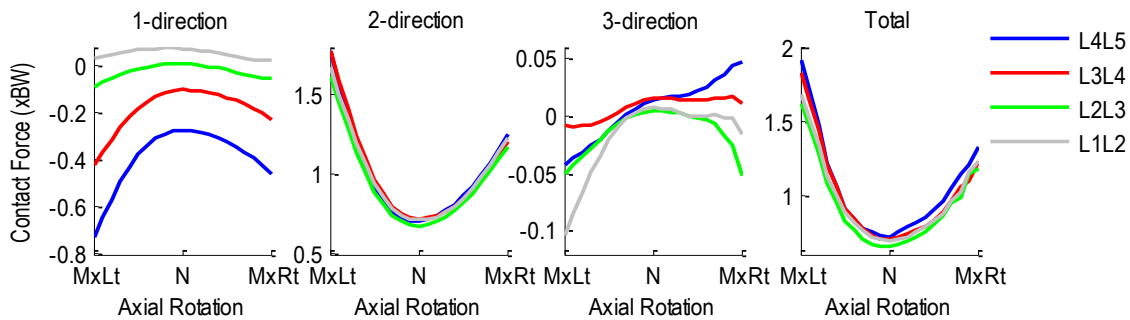


Figure A.346 Patient 9D intervertebral contact forces normalized with respect to body weight during left-to-right axial rotation. 1-dir=Ant(+)/Post(-), 2-dir=Sup(+)/Inf(-), 3-dir=Rt(+)/Lt(-).

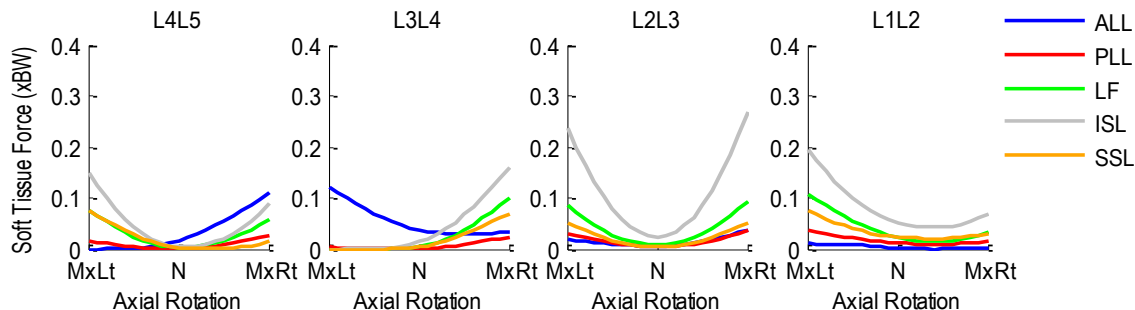


Figure A.347 Patient 9D segmental ligament forces normalized with respect to body weight during left-to-right axial rotation.

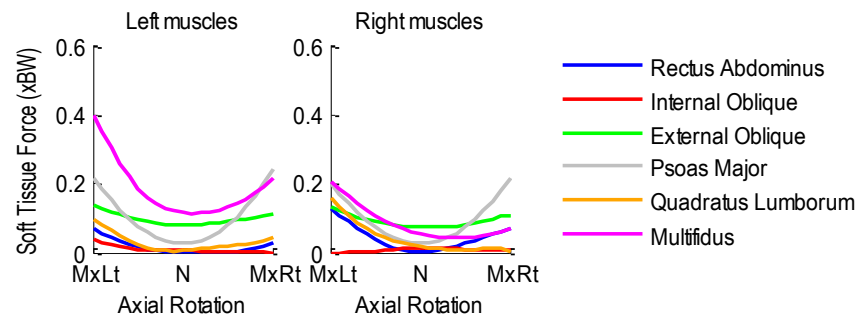


Figure A.348 Patient 9D bilateral muscle forces normalized with respect to body weight during left-to-right axial rotation.

A.30 Patient 10D

Age: 28 years

Gender: Male

Height: 1.85 m

Mass: 89 kg

Condition: Degenerative at L4L5 and L5S1

A.30.1 Flexion-Extension Activity

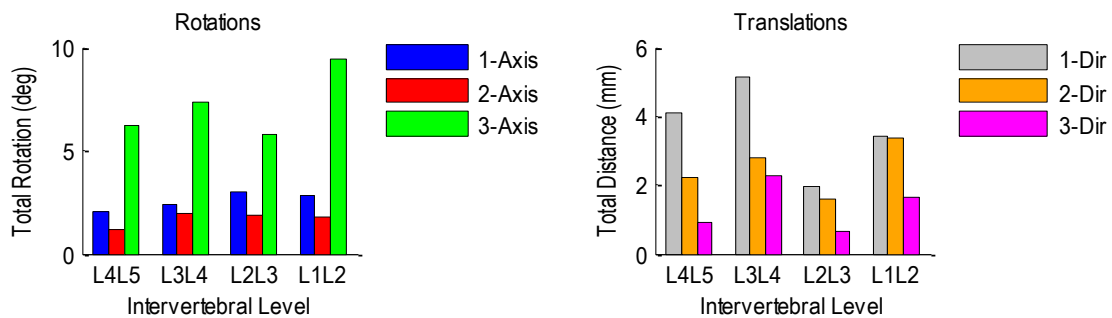


Figure A.349 Patient 10D relative rotations (left) and translations (right) at each vertebral level during flexion-extension.

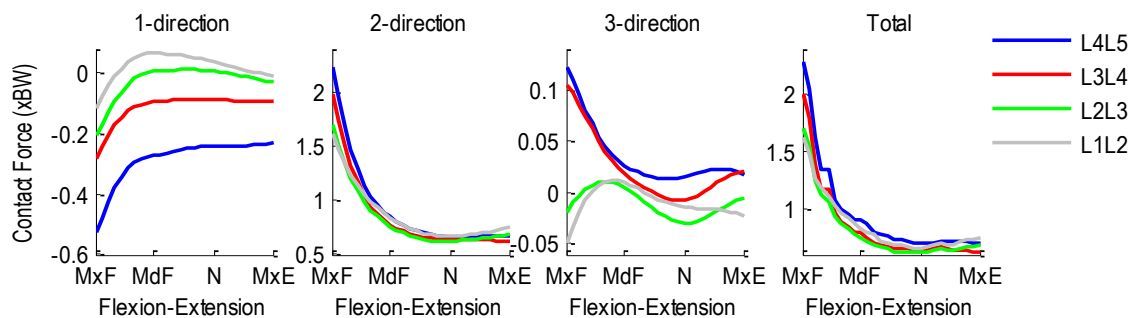


Figure A.350 Patient 10D intervertebral contact forces normalized with respect to body weight during flexion-extension. 1-dir=Ant(+)/Post(-), 2-dir=Sup(+)/Inf(-), 3-dir=Rt(+)/Lt(-).

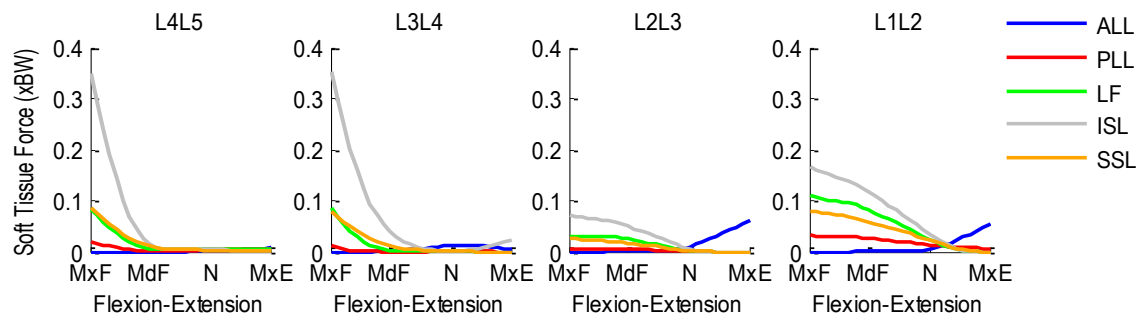


Figure A.351 Patient 10D segmental ligament forces normalized with respect to body weight during flexion-extension.

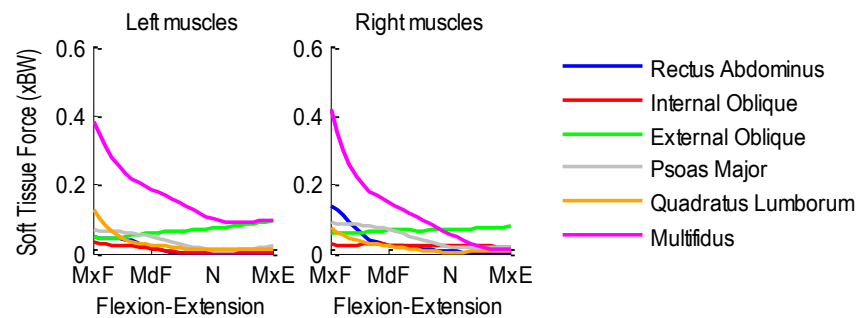


Figure A.352 Patient 10D bilateral muscle forces normalized with respect to body weight during flexion-extension.

A.30.2 Lateral Flexion Activity

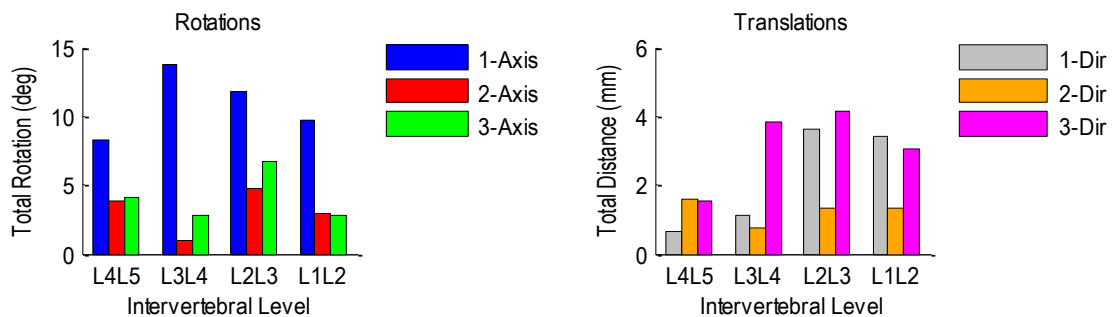


Figure A.353 Patient 10D relative rotations (left) and translations (right) at each vertebral level during left-to-right lateral flexion.

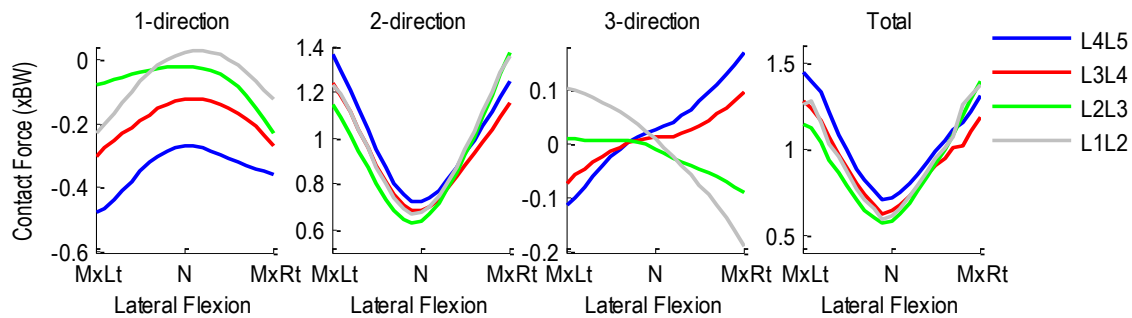


Figure A.354 Patient 10D intervertebral contact forces normalized with respect to body weight during left-to-right lateral flexion. 1-dir=Ant(+)/Post(-), 2-dir=Sup(+)/Inf(-), 3-dir=Rt(+)/Lt(-).

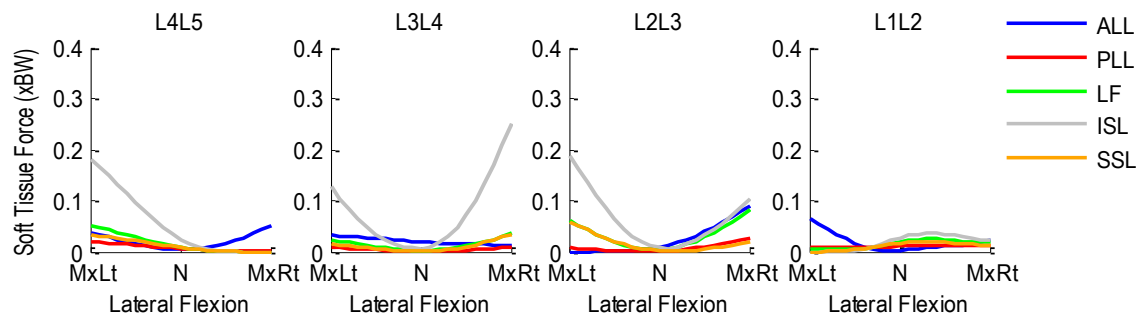


Figure A.355 Patient 10D segmental ligament forces normalized with respect to body weight during left-to-right lateral flexion.

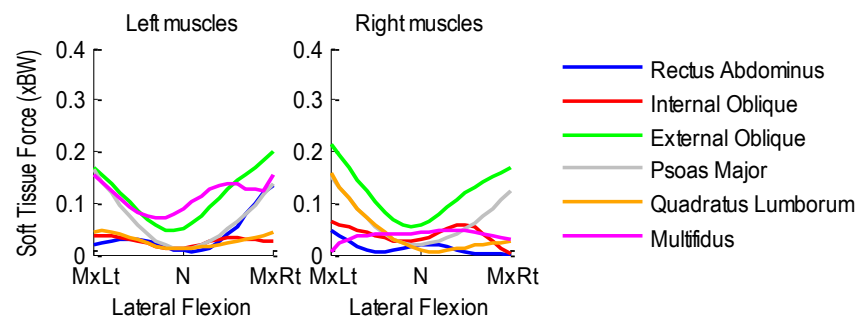


Figure A.356 Patient 10D bilateral muscle forces normalized with respect to body weight during left-to-right lateral flexion.

A.30.3 Axial Rotation Activity

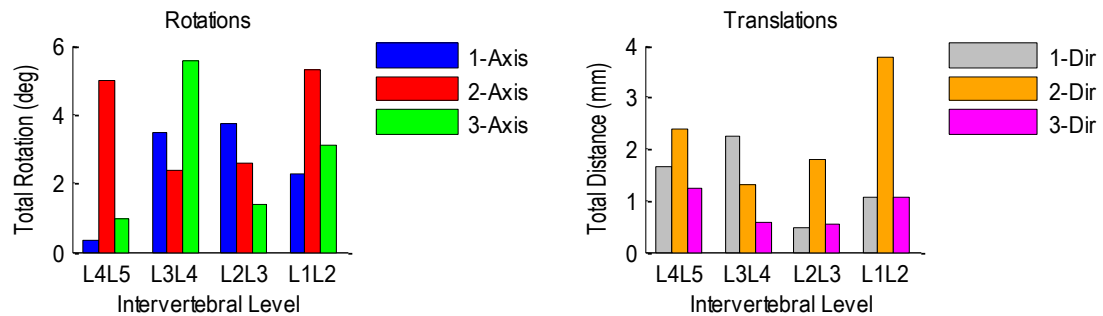


Figure A.357 Patient 10D relative rotations (left) and translations (right) at each vertebral level during left-to-right axial rotation.

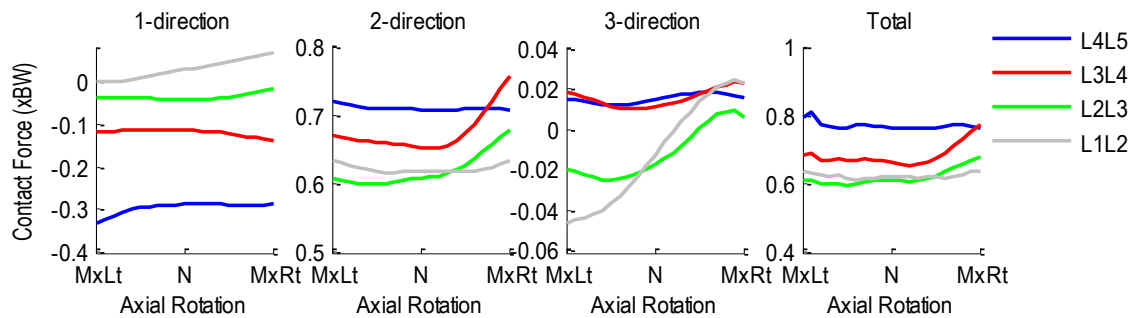


Figure A.358 Patient 10D intervertebral contact forces normalized with respect to body weight during left-to-right axial rotation. 1-dir=Ant(+)/Post(-), 2-dir=Sup(+)/Inf(-), 3-dir=Rt(+)/Lt(-).

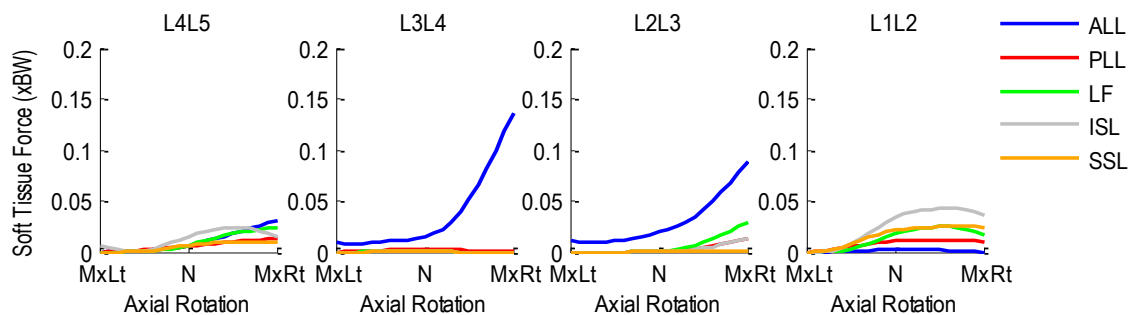


Figure A.359 Patient 10D segmental ligament forces normalized with respect to body weight during left-to-right axial rotation.

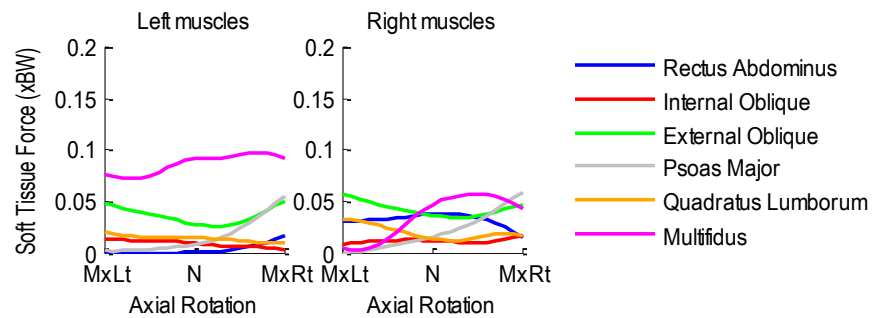


Figure A.360 Patient 10D bilateral muscle forces normalized with respect to body weight during left-to-right axial rotation.

A.31 Patient 1F

Age: 41 years

Gender: Male

Height: 1.78 m

Mass: 92 kg

Condition: Posterior lumbar interbody fusion at L4L5

A.31.1 Flexion-Extension Activity

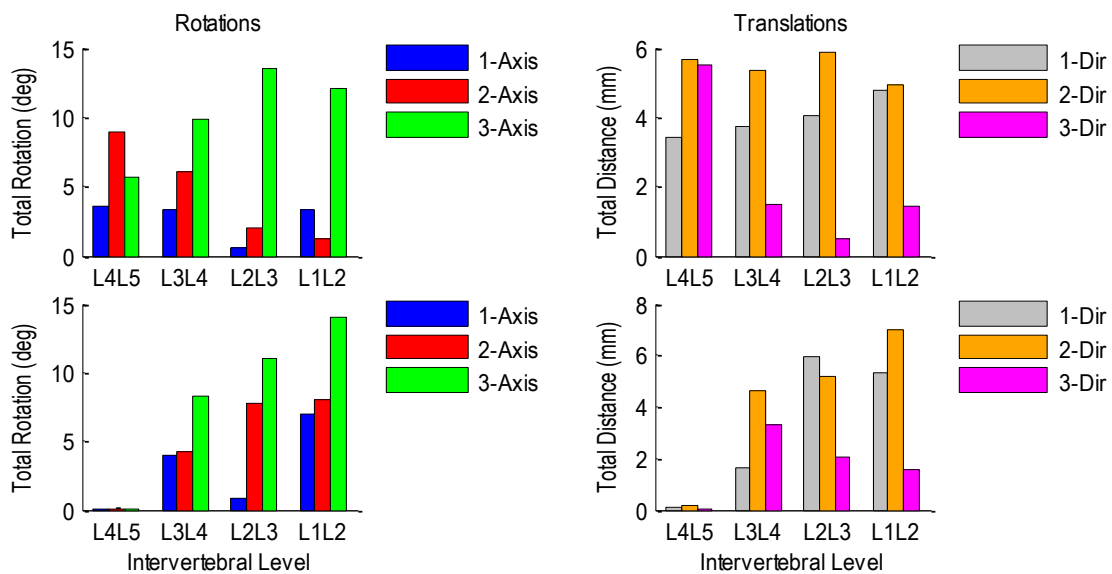


Figure A.361 Patient 1F pre-operative (top row) and post-operative (bottom row) relative rotations (left) and translations (right) at each vertebral level during flexion-extension.

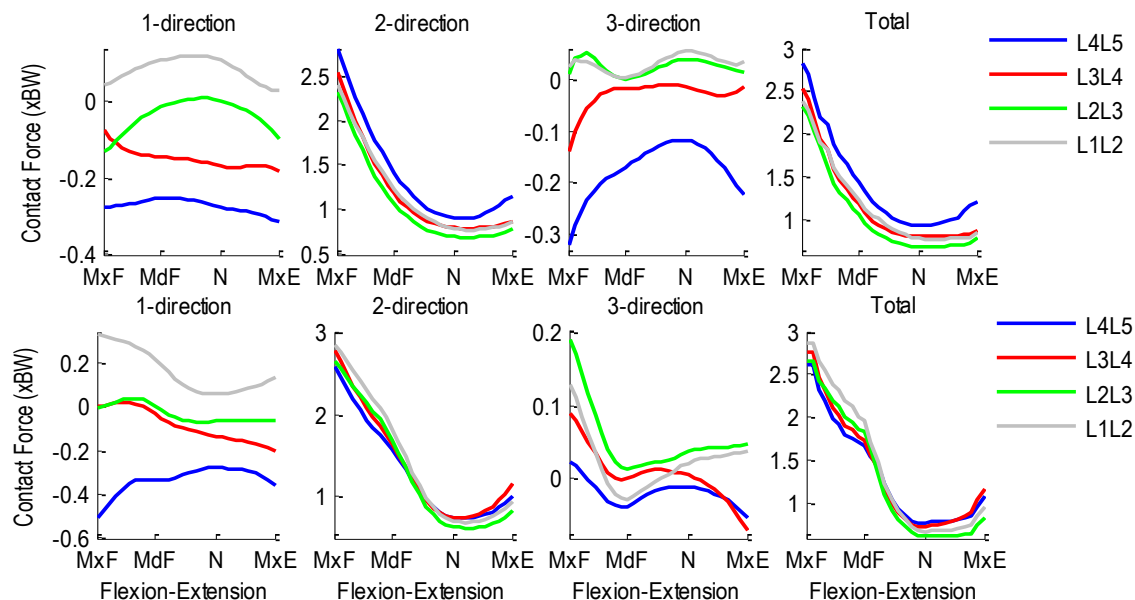


Figure A.362 Patient 1F pre- (top row) and post-operative (bottom row) intervertebral contact forces normalized with respect to body weight during flexion-extension. 1-dir=Ant(+)/Post (-), 2-dir=Sup(+)/Inf(-), 3-dir=Rt(+)/Lt(-).

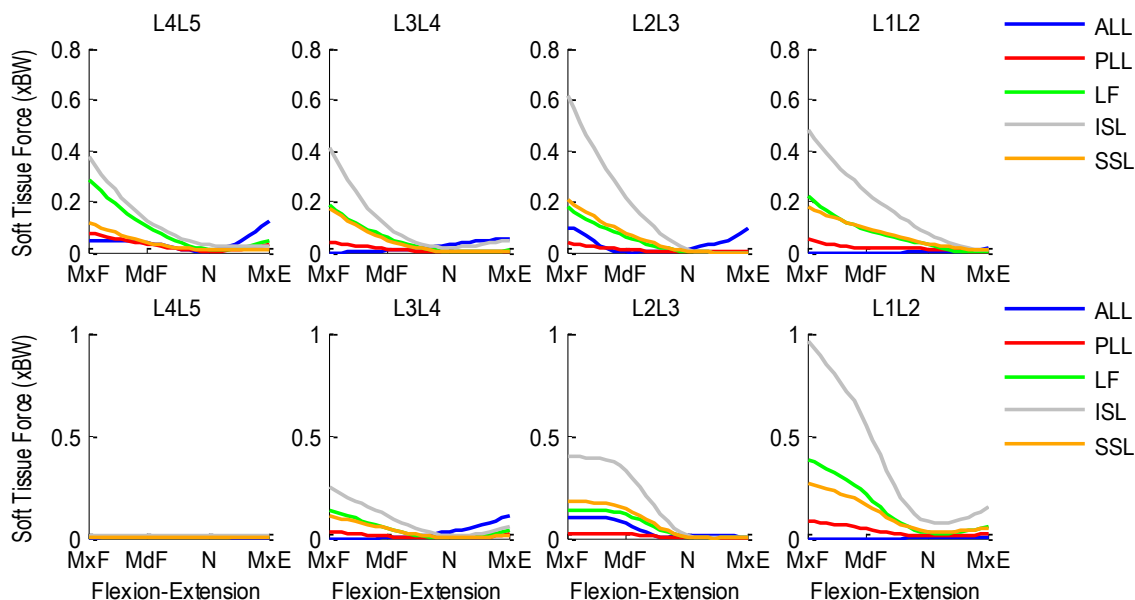


Figure A.363 Patient 1F pre- (top row) and post-operative (bottom row) segmental ligament forces normalized with respect to body weight during flexion-extension.

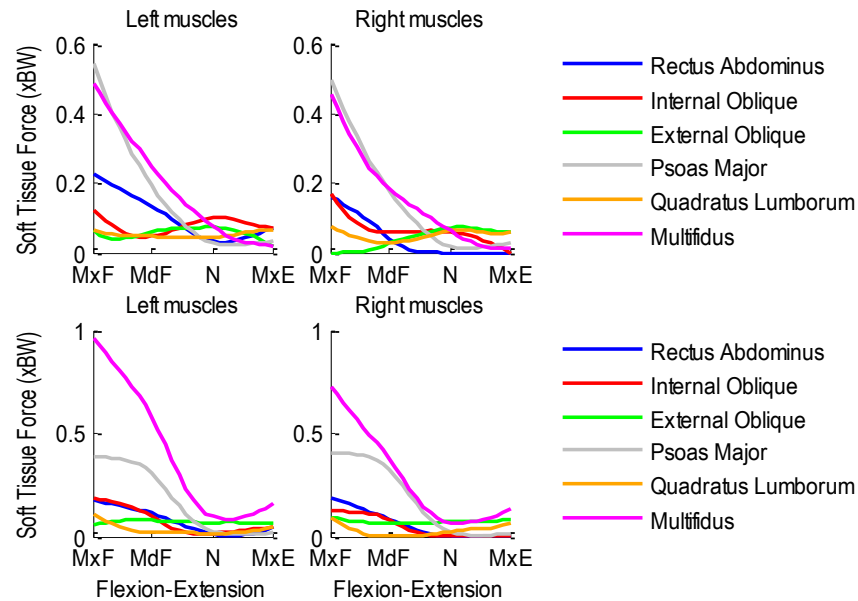


Figure A.364 Patient 1F pre- (top row) and post-operative (bottom row) bilateral muscle forces normalized with respect to body weight during flexion-extension.

A.31.2 Lateral Flexion Activity

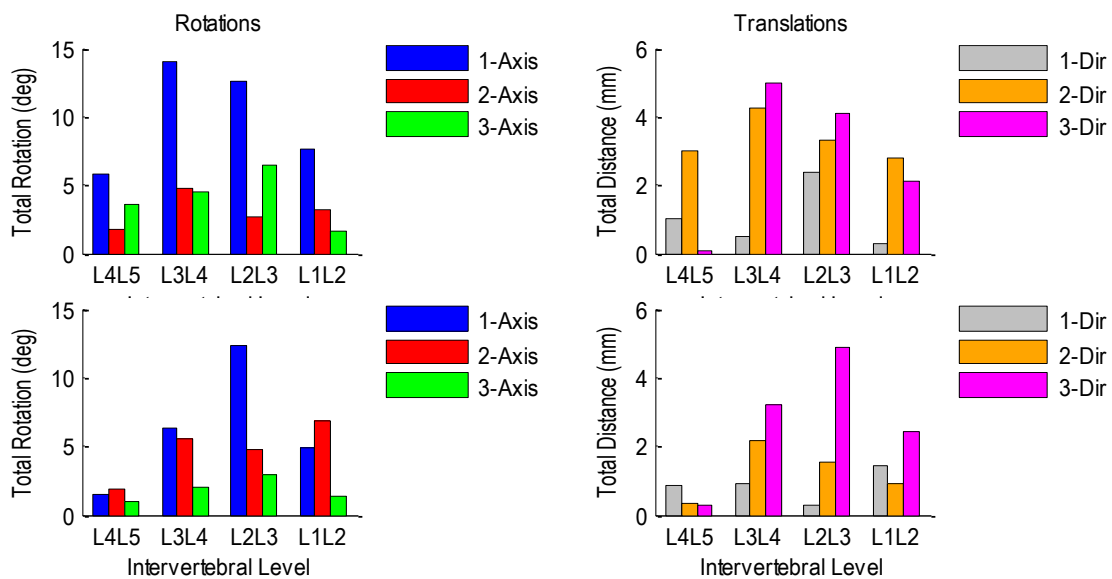


Figure A.365 Patient 1F pre-operative (top row) and post-operative (bottom row) relative rotations (left) and translations (right) at each vertebral level during left-to-right lateral flexion.

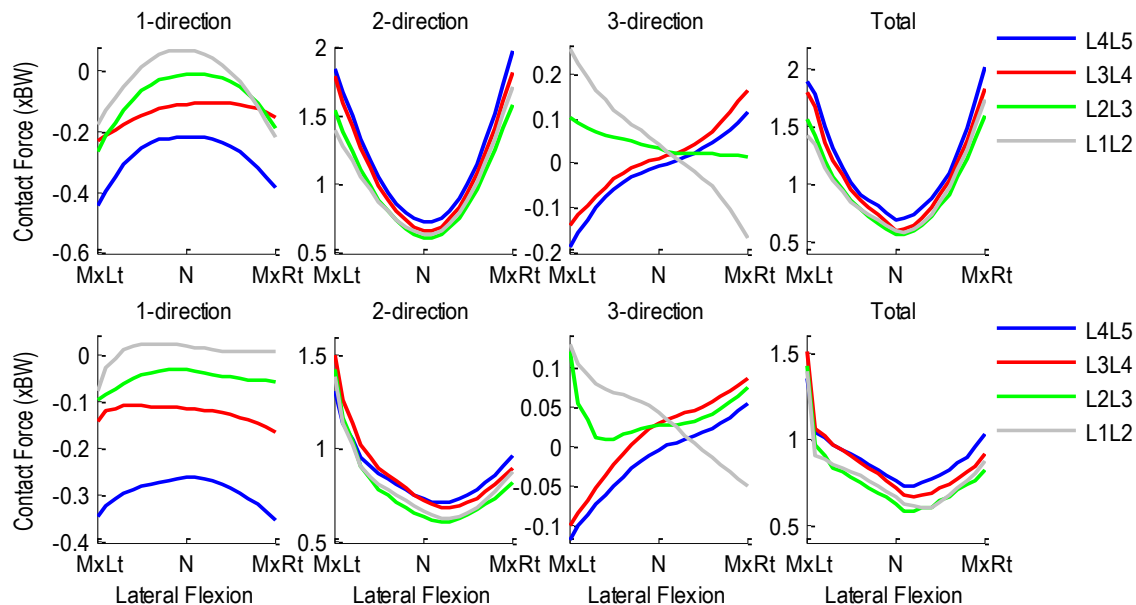


Figure A.366 Patient 1F pre- (top row) and post-operative (bottom row) intervertebral contact forces normalized with respect to body weight during right-to-left lateral flexion. 1-dir=Ant(+)/Post(-), 2-dir=Sup (+)/Inf(-), 3-dir=Rt(+)/Lt(-).

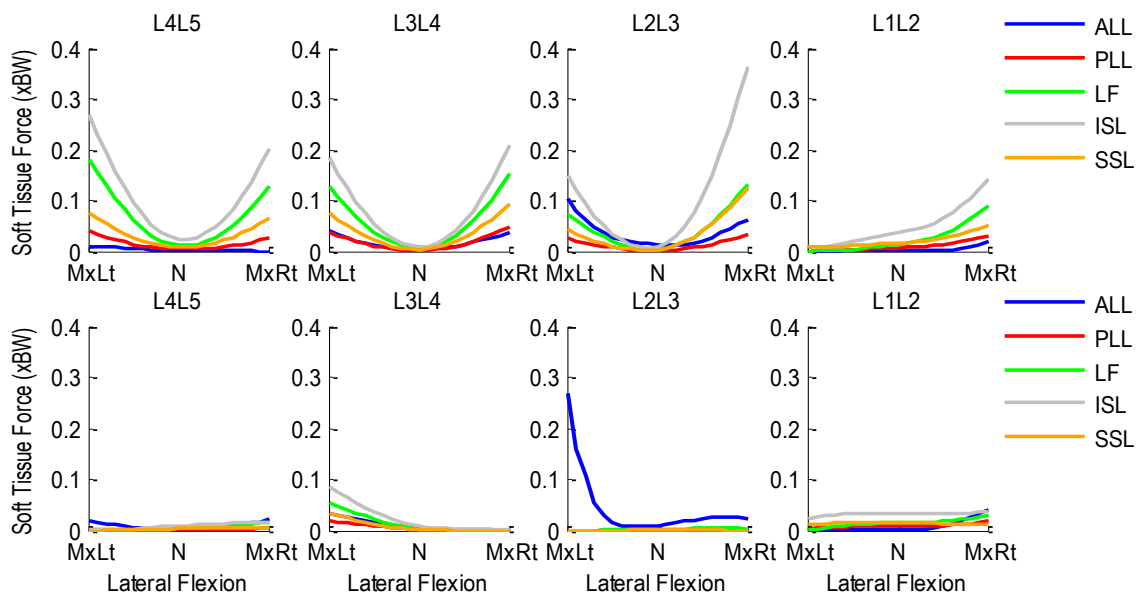


Figure A.367 Patient 1F pre- (top row) and post-operative (bottom row) segmental ligament forces normalized with respect to body weight during left-to-right lateral flexion.

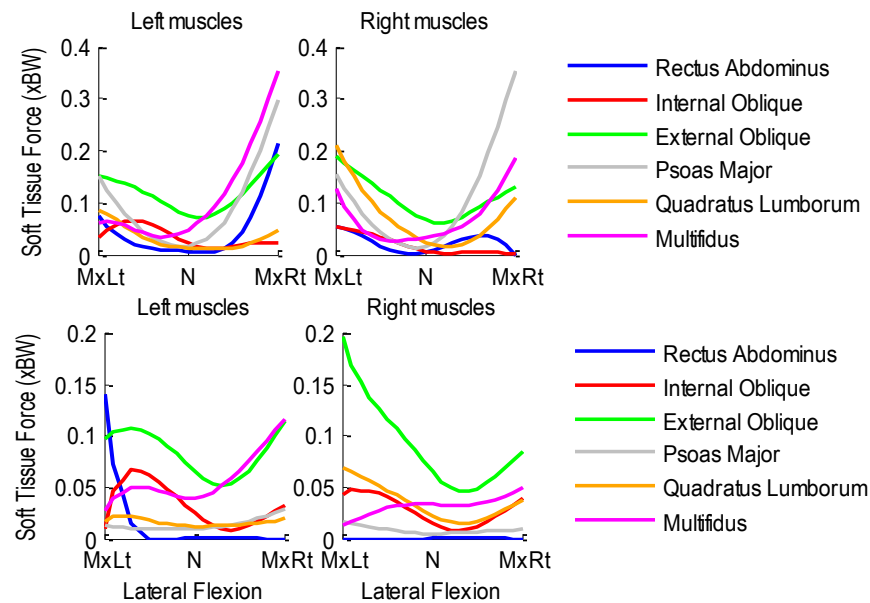


Figure A.368 Patient 1F pre- (top row) and post-operative (bottom row) bilateral muscle forces normalized with respect to body weight during left-to-right lateral flexion.

A.31.3 Axial Rotation Activity

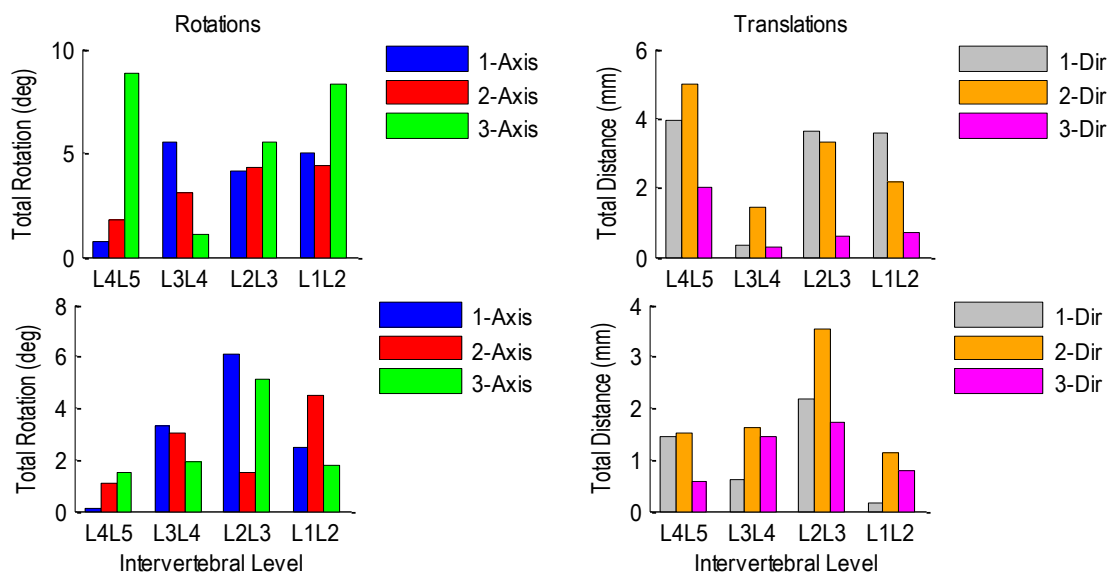


Figure A.369 Patient 1F pre-operative (top row) and post-operative (bottom row) relative rotations (left) and translations (right) at each vertebral level during left-to-right axial rotation.

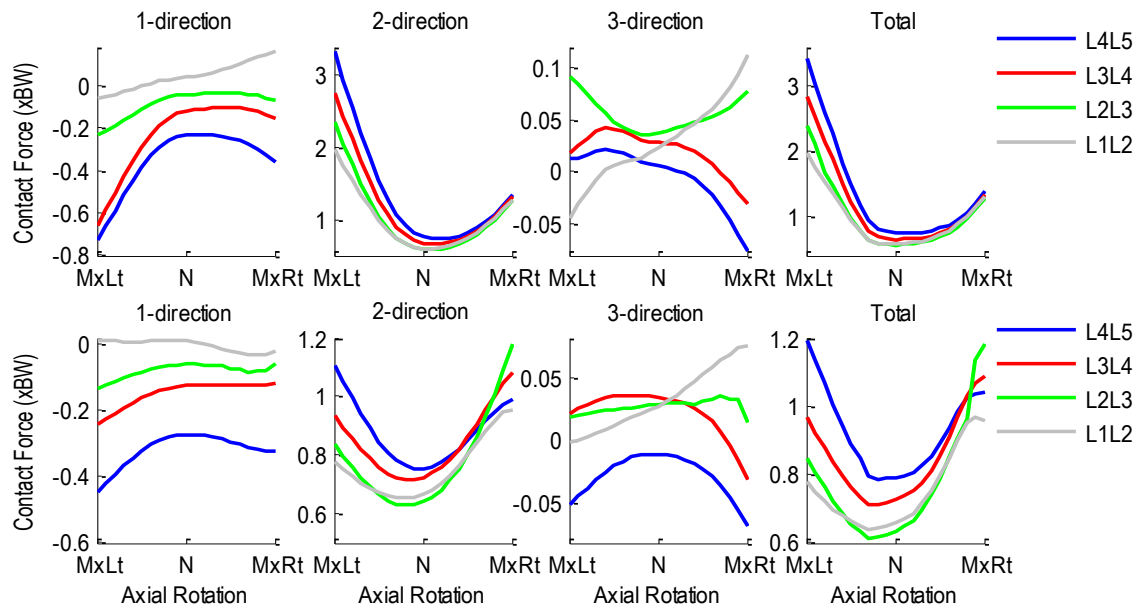


Figure A.370 Patient 1F pre- (top row) and post-operative (bottom row) normalized with respect to body weight during left-to-right axial rotation. 1-dir=Ant(+)/Post(-), 2-dir=Sup(+)/Inf(-), 3-dir=Rt(+)/Lt(-).

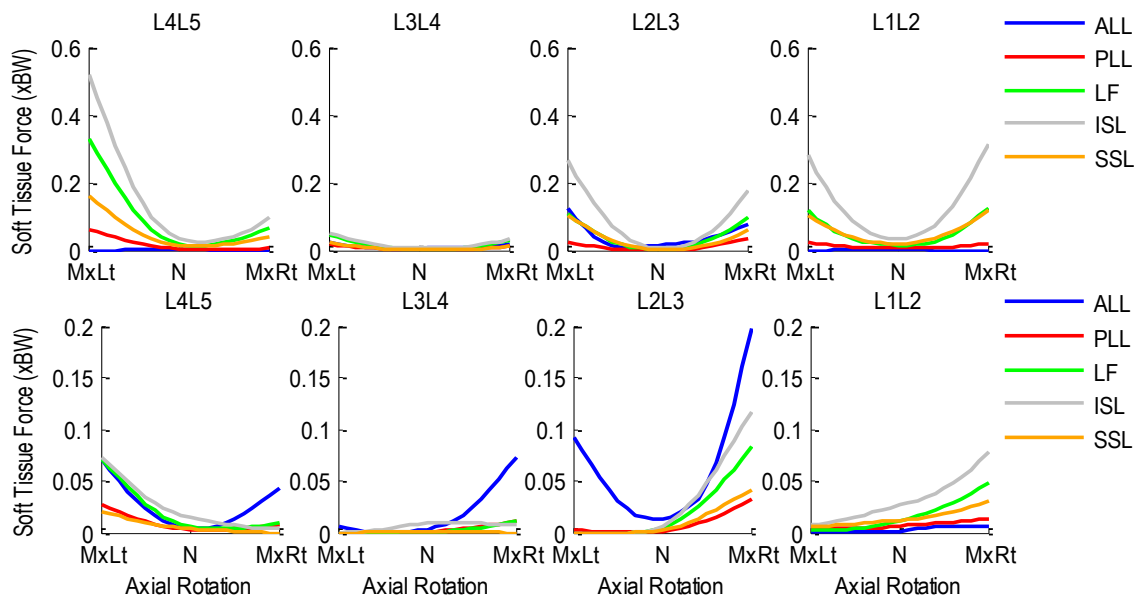


Figure A.371 Patient 1F pre- (top row) and post-operative (bottom row) segmental ligament forces normalized with respect to body weight during left-to-right axial rotation.

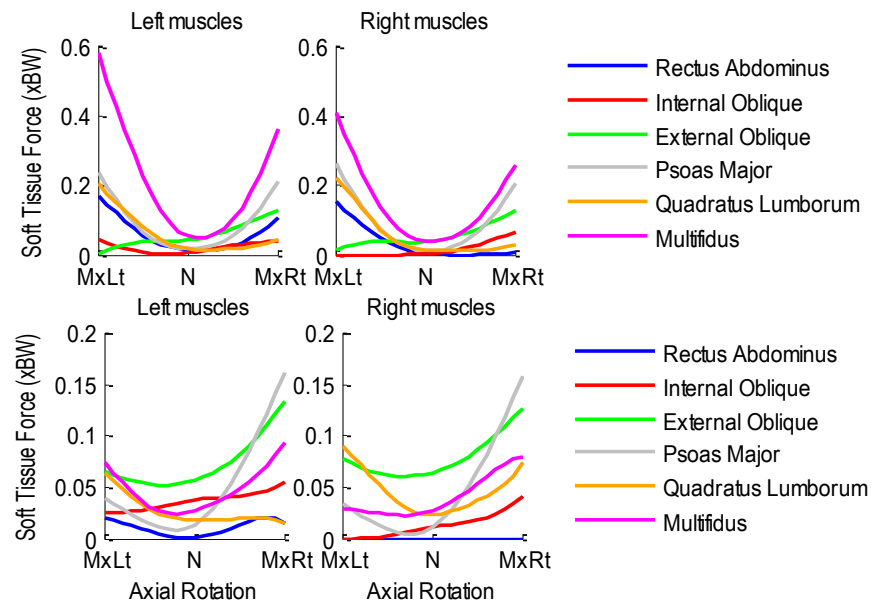


Figure A.372 Patient 1F pre- (top row) and post-operative (bottom row) bilateral muscle forces normalized with respect to body weight during left-to-right axial rotation.

A.32 Patient 2F

Age: 50 years

Gender: Male

Height: 1.75 m

Mass: 101 kg

Condition: Posterior lumbar interbody fusion at L5S1

A.32.1 Flexion-Extension Activity

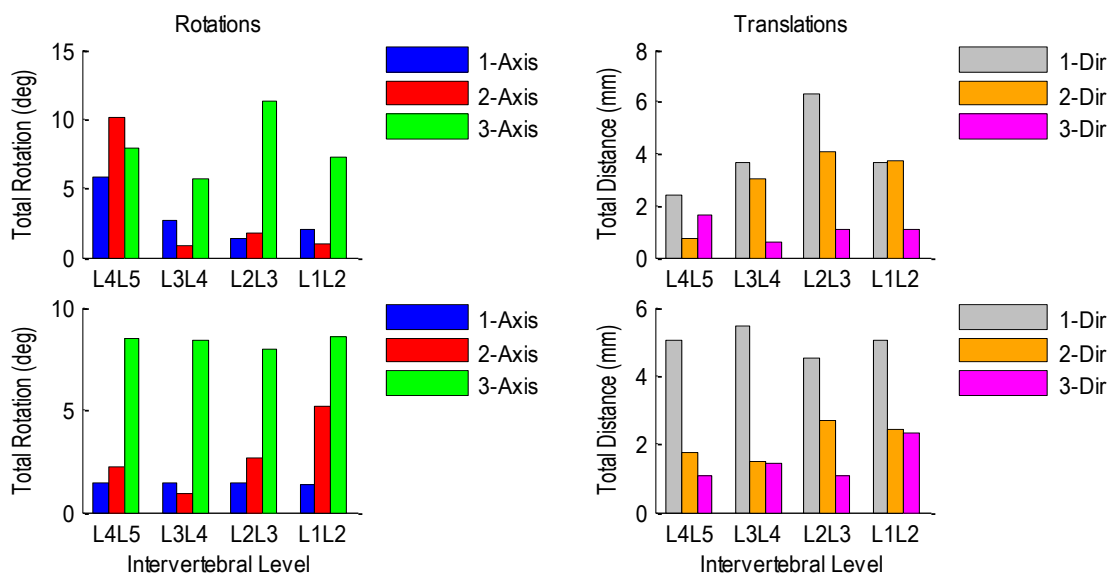


Figure A.373 Patient 2F pre-operative (top row) and post-operative (bottom row) relative rotations (left) and translations (right) at each vertebral level during flexion-extension.

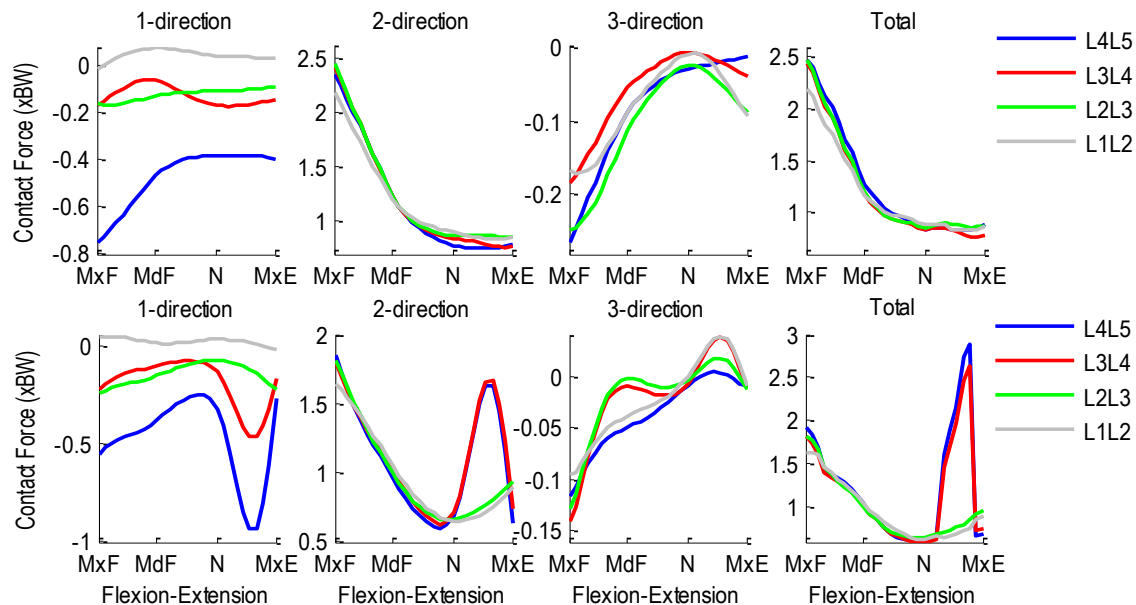


Figure A.374 Patient 2F pre- (top row) and post-operative (bottom row) segmental ligament forces normalized with respect to body weight during flexion-extension.

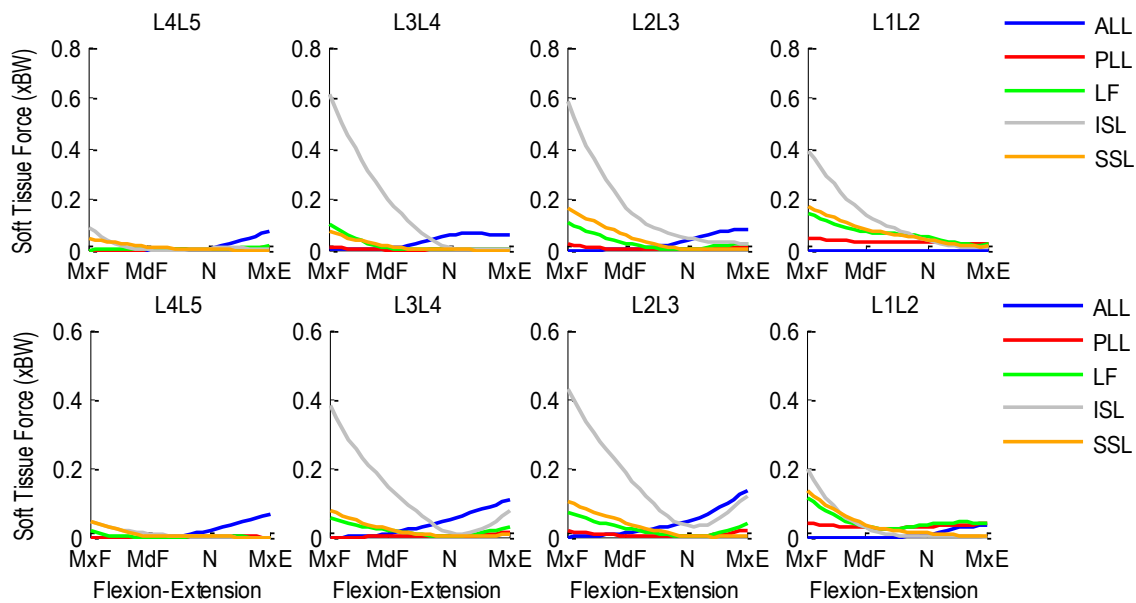


Figure A.375 Patient 2F pre- (top row) and post-operative (bottom row) segmental ligament forces normalized with respect to body weight during flexion-extension.

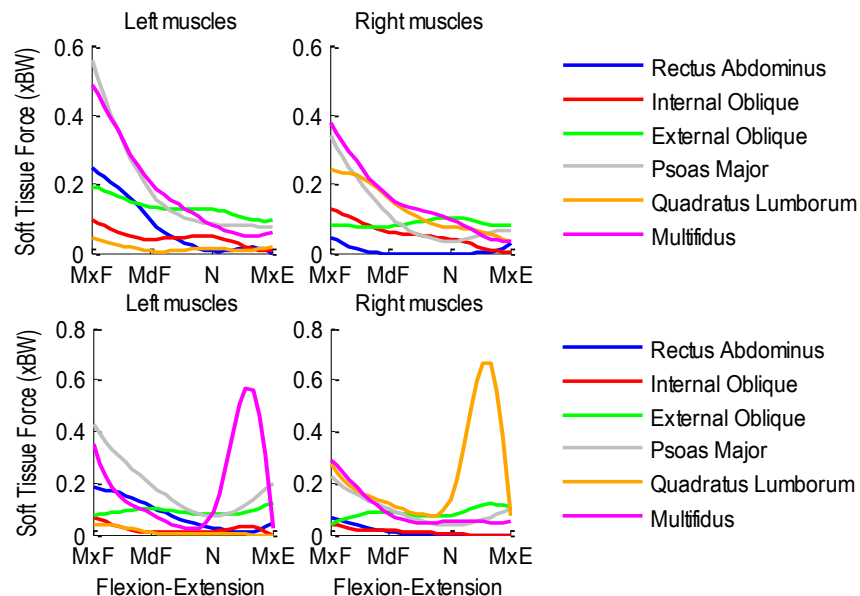


Figure A.376 Patient 2F pre- (top row) and post-operative (bottom row) bilateral muscle forces normalized with respect to body weight during flexion-extension.

A.32.2 Lateral Flexion Activity

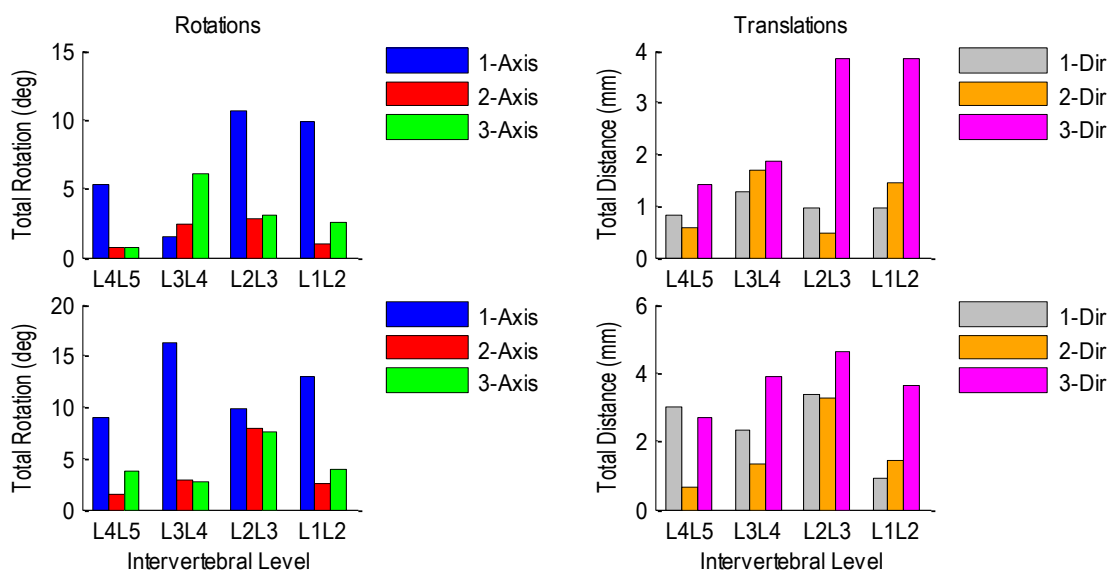


Figure A.377 Patient 2F pre-operative (top row) and post-operative (bottom row) relative rotations (left) and translations (right) at each vertebral level during left-to-right lateral flexion.

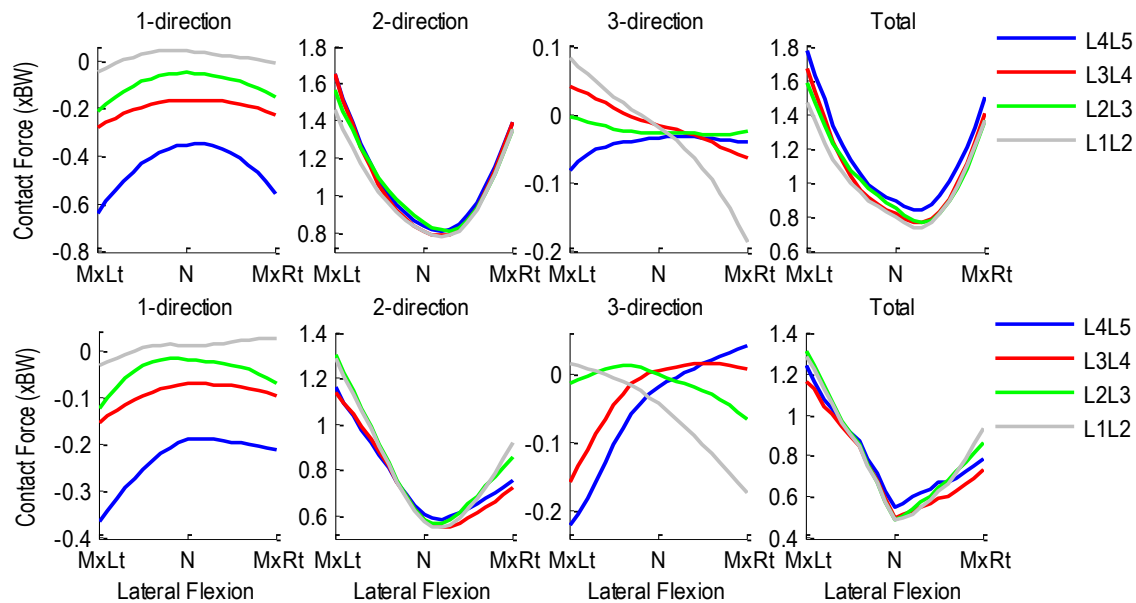


Figure A.378 Patient 2F pre- (top row) and post-operative (bottom row) intervertebral contact forces normalized with respect to body weight during right-to-left lateral flexion. 1-dir=Ant(+)/Post(-), 2-dir=Sup (+)/Inf(-), 3-dir=Rt(+)/Lt(-).

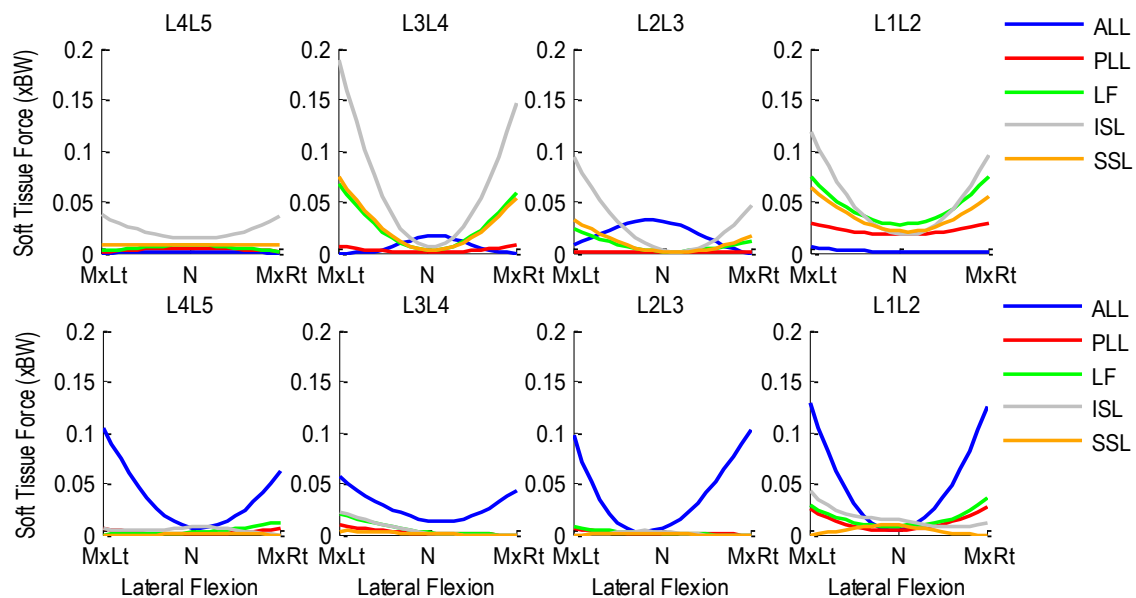


Figure A.379 Patient 2F pre- (top row) and post-operative (bottom row) segmental ligament forces normalized with respect to body weight during left-to-right lateral flexion.

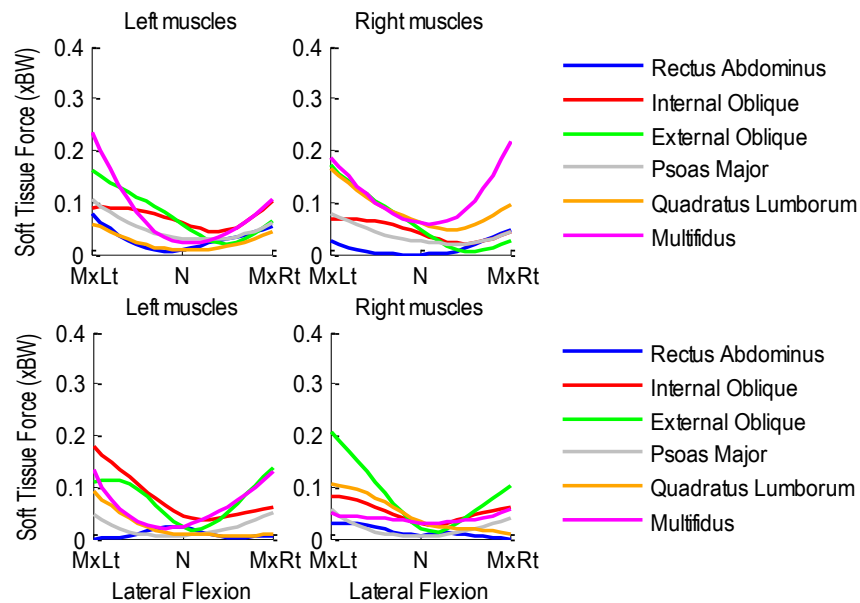


Figure A.380 Patient 2F pre- (top row) and post-operative (bottom row) bilateral muscle forces normalized with respect to body weight during left-to-right lateral flexion.

A.32.3 Axial Rotation Activity

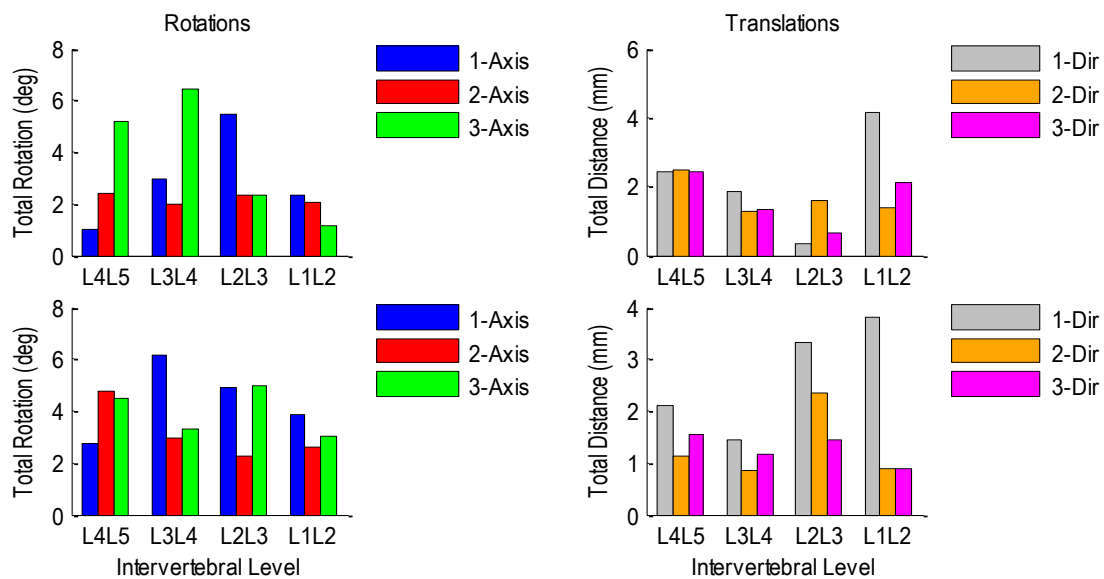


Figure A.381 Patient 2F pre-operative (top row) and post-operative (bottom row) relative rotations (left) and translations (right) at each vertebral level during left-to-right axial rotation.

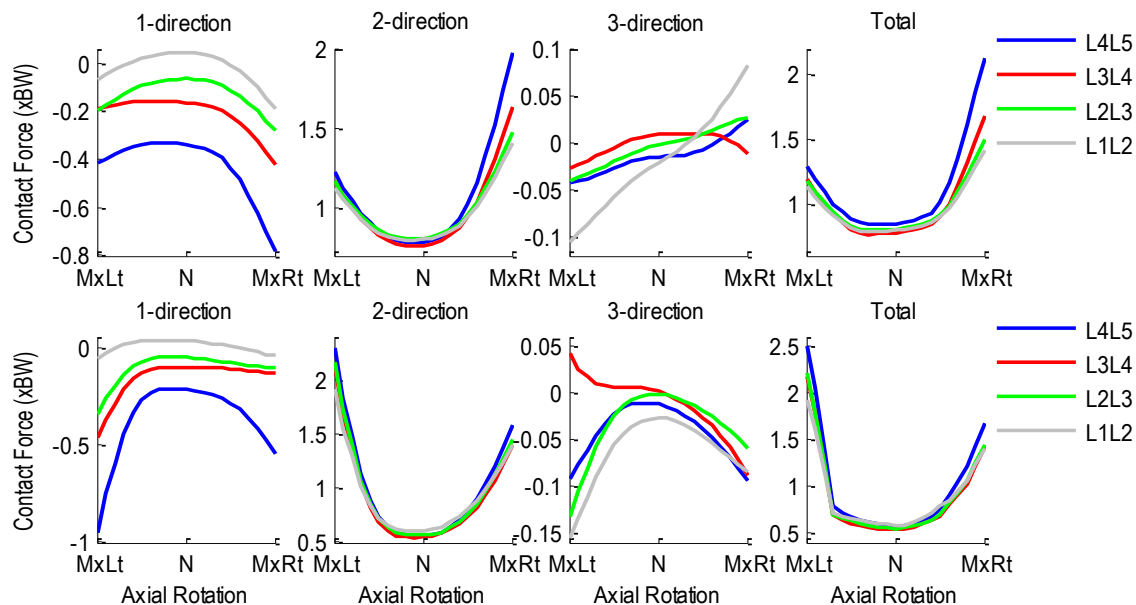


Figure A.382 Patient 2F pre- (top row) and post-operative (bottom row) intervertebral contact forces normalized with respect to body weight during left-to-right axial rotation. 1-dir=Ant(+)/Post(-), 2-dir=Sup(+)/Inf(-), 3-dir=Rt(+)/Lt(-).

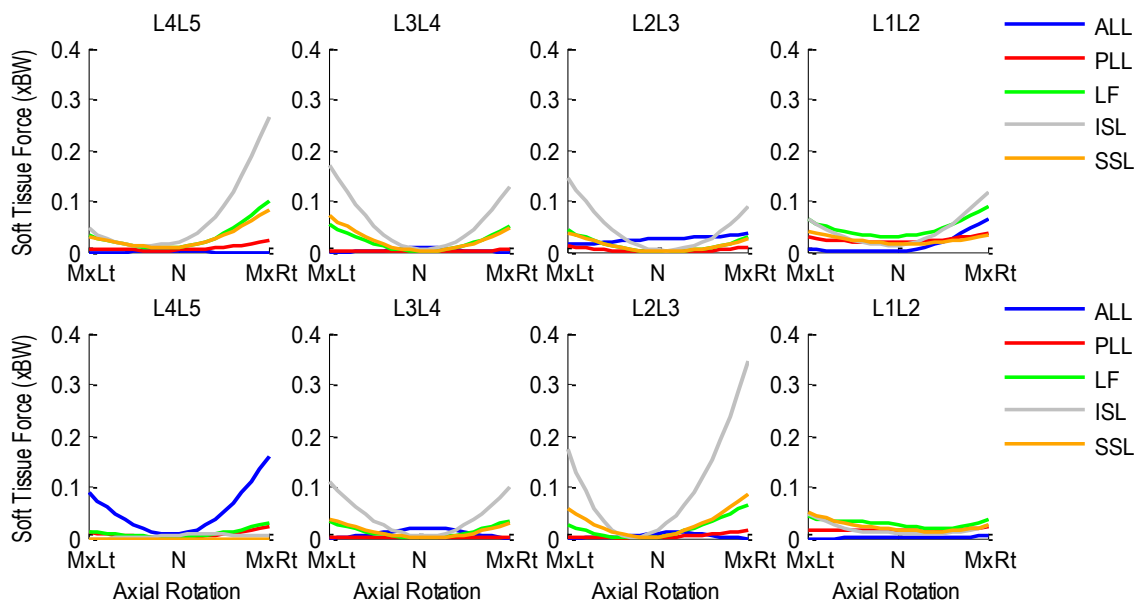


Figure A.383 Patient 2F pre- (top row) and post-operative (bottom row) segmental ligament forces normalized with respect to body weight during left-to-right axial rotation.

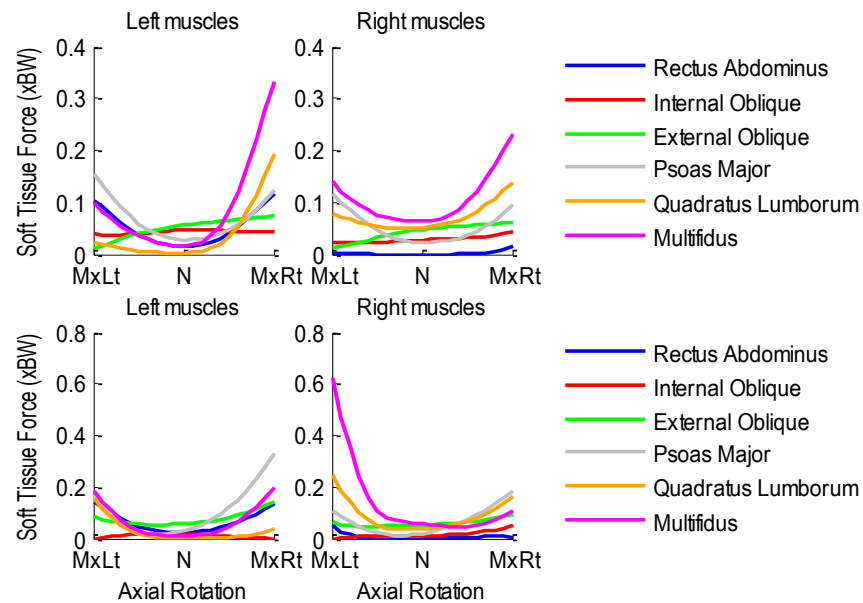


Figure A.384 Patient 2F pre- (top row) and post-operative (bottom row) bilateral muscle forces normalized with respect to body weight during left-to-right axial rotation.

A.33 Patient 3F

Age: 50 years

Gender: Female

Height: 1.60 m

Mass: 119 kg

Condition: Posterior lumbar interbody fusion at L5S1

A.33.1 Flexion-Extension Activity

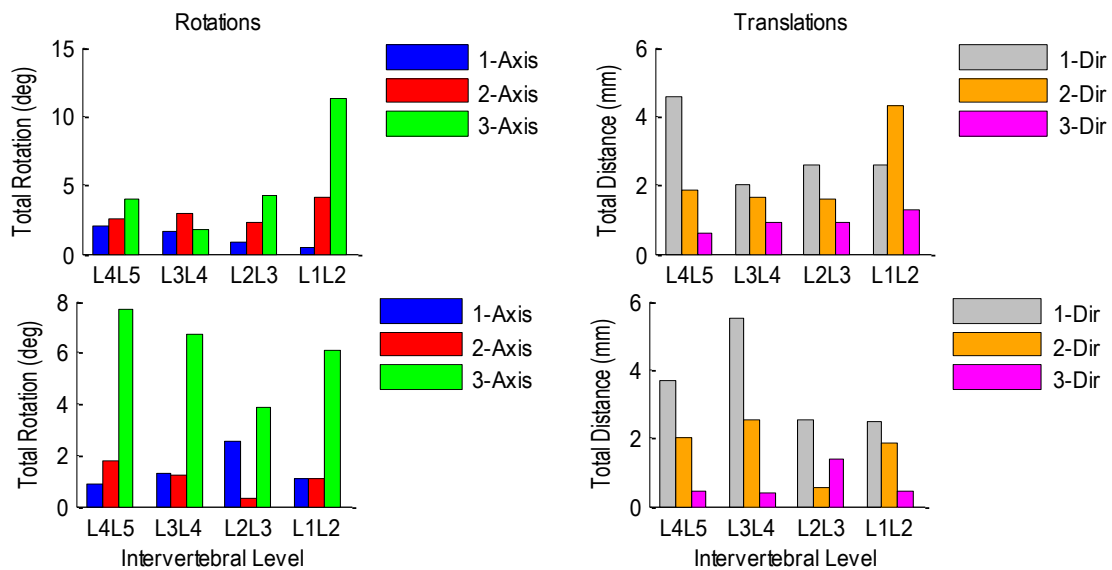


Figure A.385 Patient 3F pre-operative (top row) and post-operative (bottom row) relative rotations (left) and translations (right) at each vertebral level during flexion-extension.

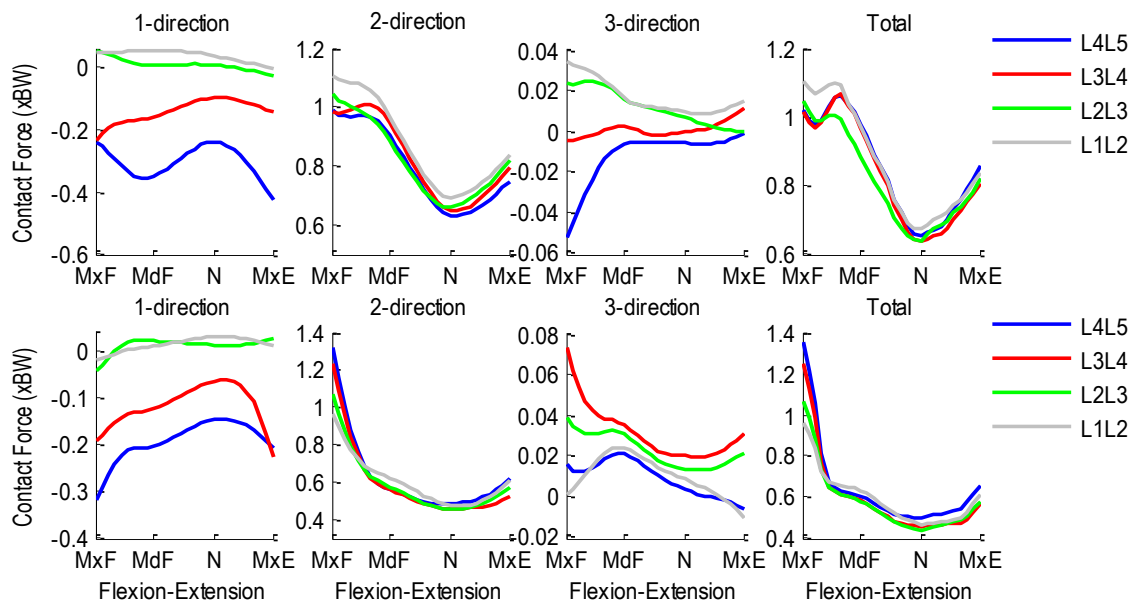


Figure A.386 Patient 3F pre- (top row) and post-operative (bottom row) segmental ligament forces normalized with respect to body weight during flexion-extension.

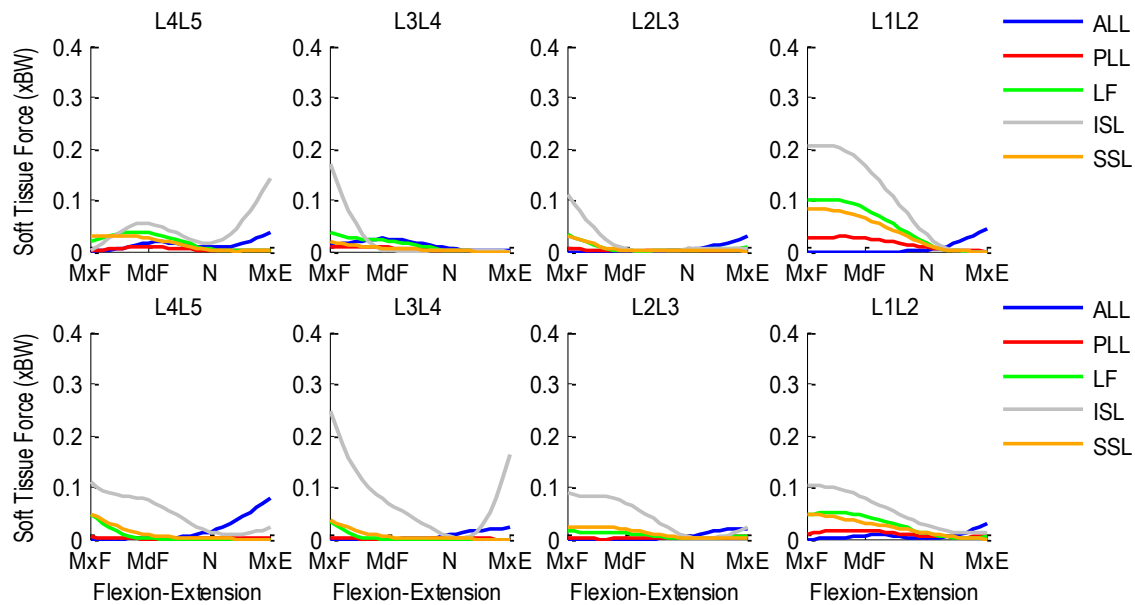


Figure A.387 Patient 3F pre- (top row) and post-operative (bottom row) segmental ligament forces normalized with respect to body weight during flexion-extension.

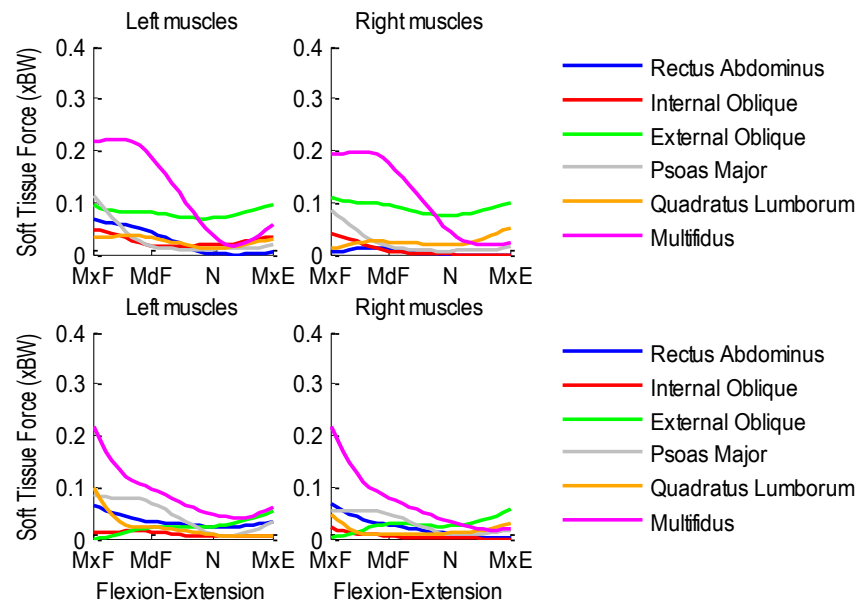


Figure A.388 Patient 3F pre- (top row) and post-operative (bottom row) bilateral muscle forces normalized with respect to body weight during flexion-extension.

A.33.2 Lateral Flexion Activity

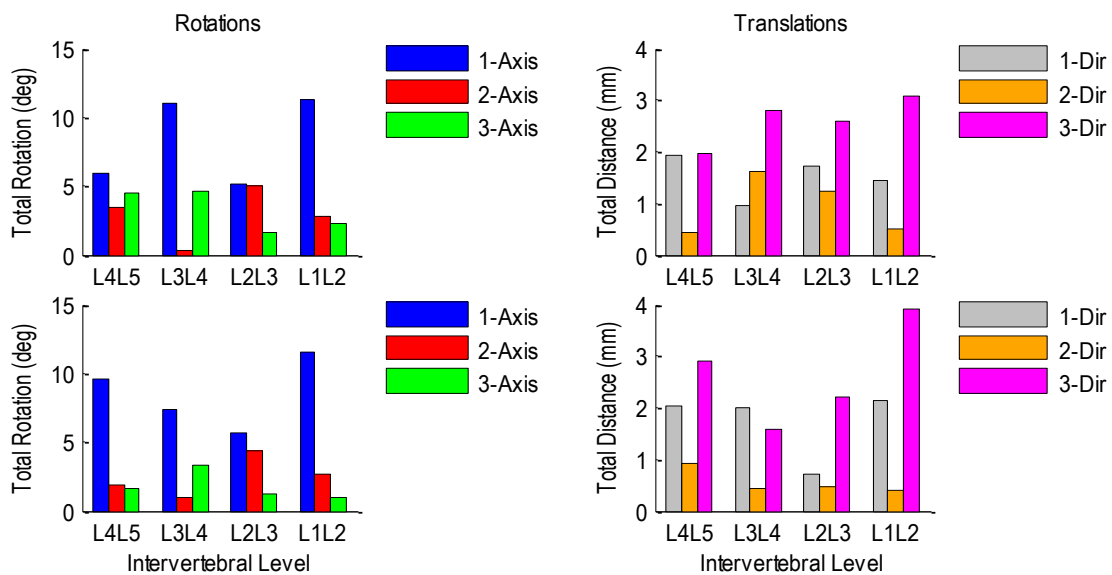


Figure A.389 Patient 3F pre-operative (top row) and post-operative (bottom row) relative rotations (left) and translations (right) at each vertebral level during left-to-right lateral flexion.

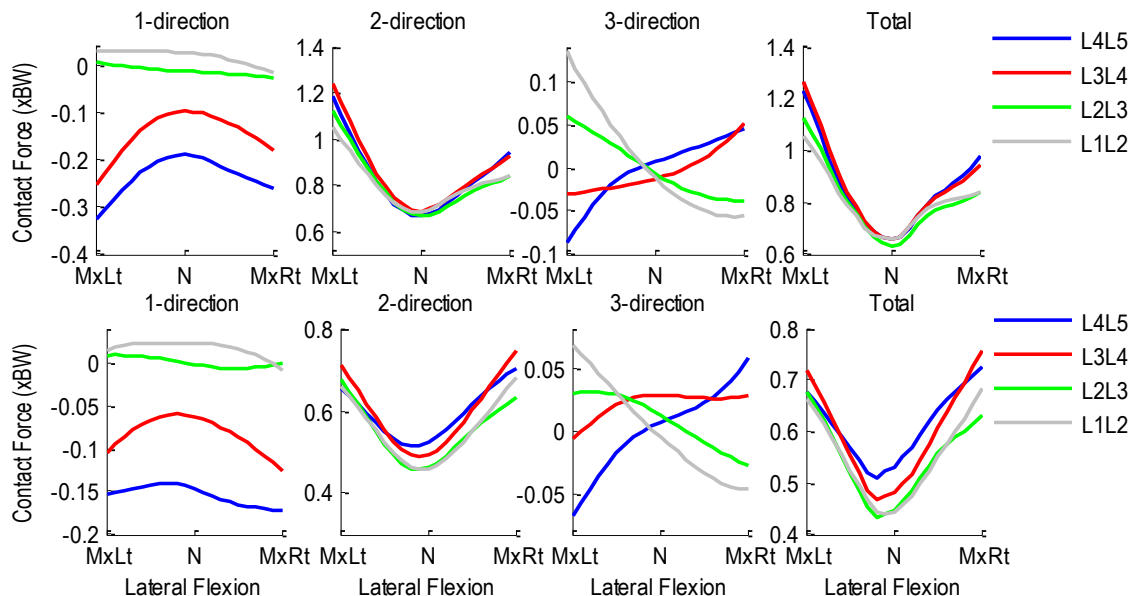


Figure A.390 Patient 3F pre- (top row) and post-operative (bottom row) intervertebral contact forces normalized with respect to body weight during right-to-left lateral flexion. 1-dir=Ant(+)/Post(-), 2-dir=Sup (+)/Inf(-), 3-dir=Rt(+)/Lt(-).

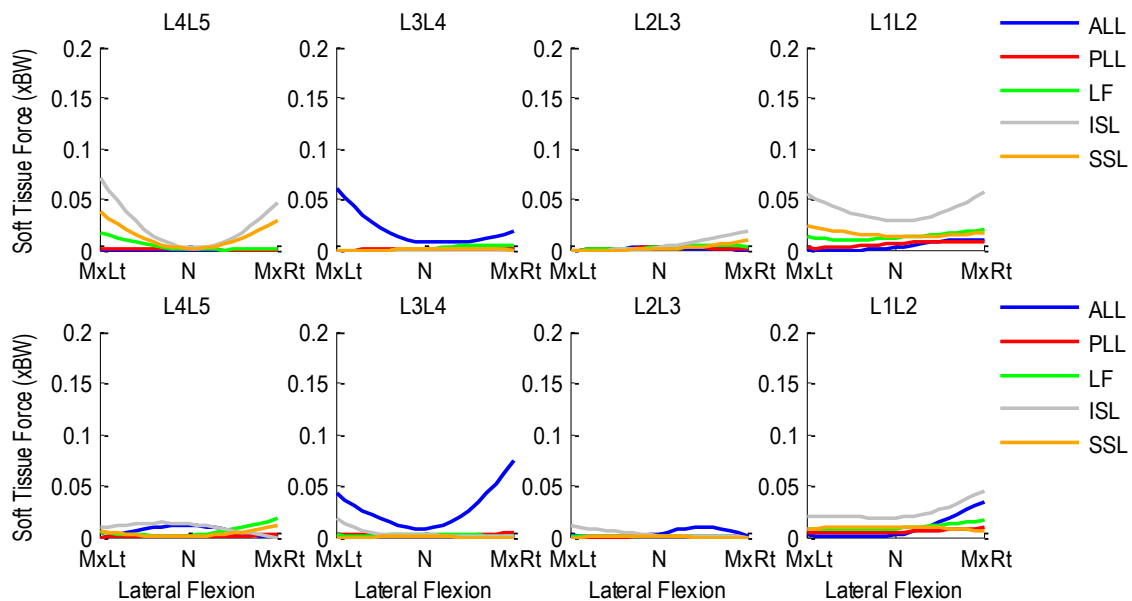


Figure A.391 Patient 3F pre- (top row) and post-operative (bottom row) segmental ligament forces normalized with respect to body weight during left-to-right lateral flexion.

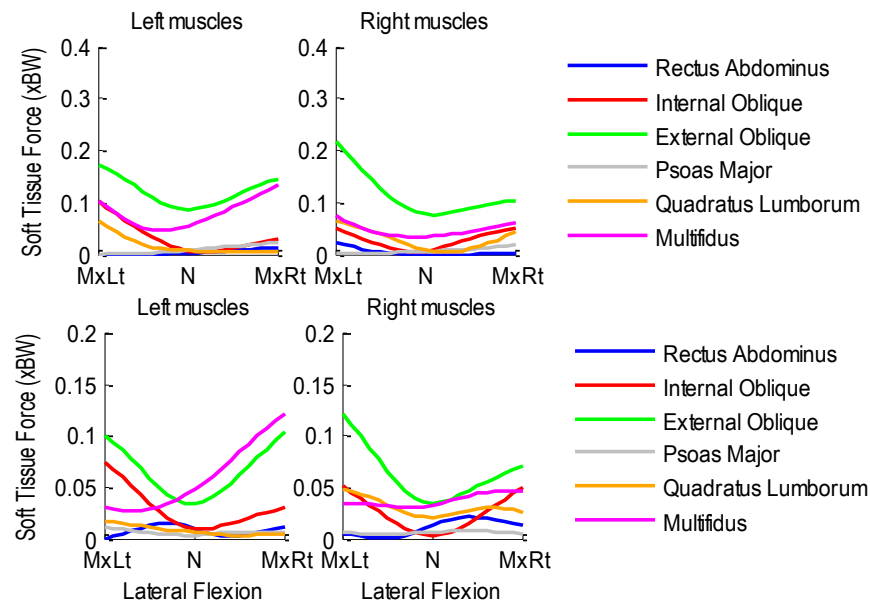


Figure A.392 Patient 3F pre- (top row) and post-operative (bottom row) bilateral muscle forces normalized with respect to body weight during left-to-right lateral flexion.

A.33.3 Axial Rotation Activity

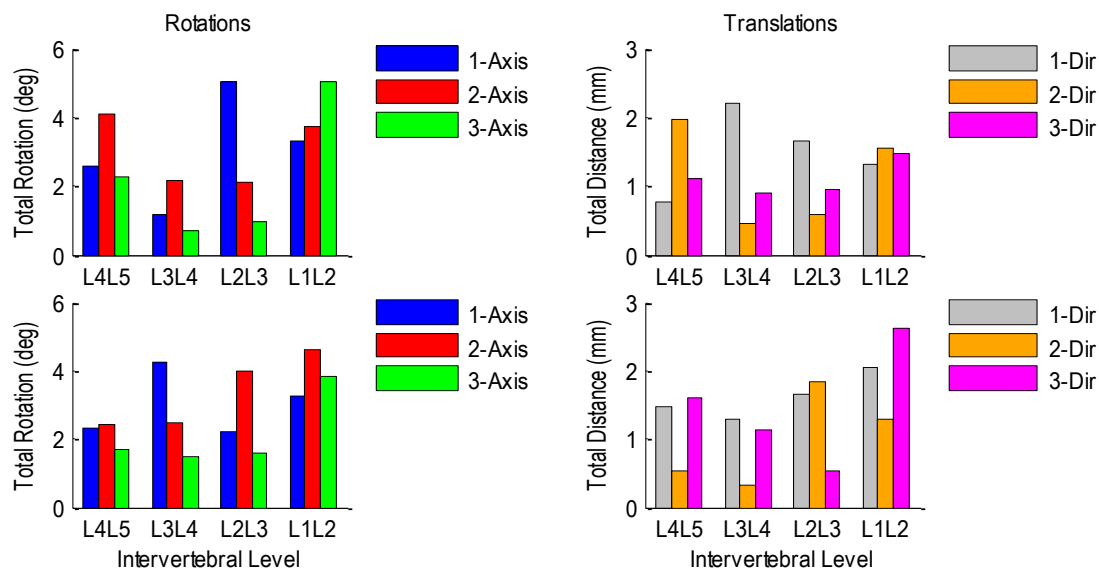


Figure A.393 Patient 3F pre-operative (top row) and post-operative (bottom row) relative rotations (left) and translations (right) at each vertebral level during left-to-right axial rotation.

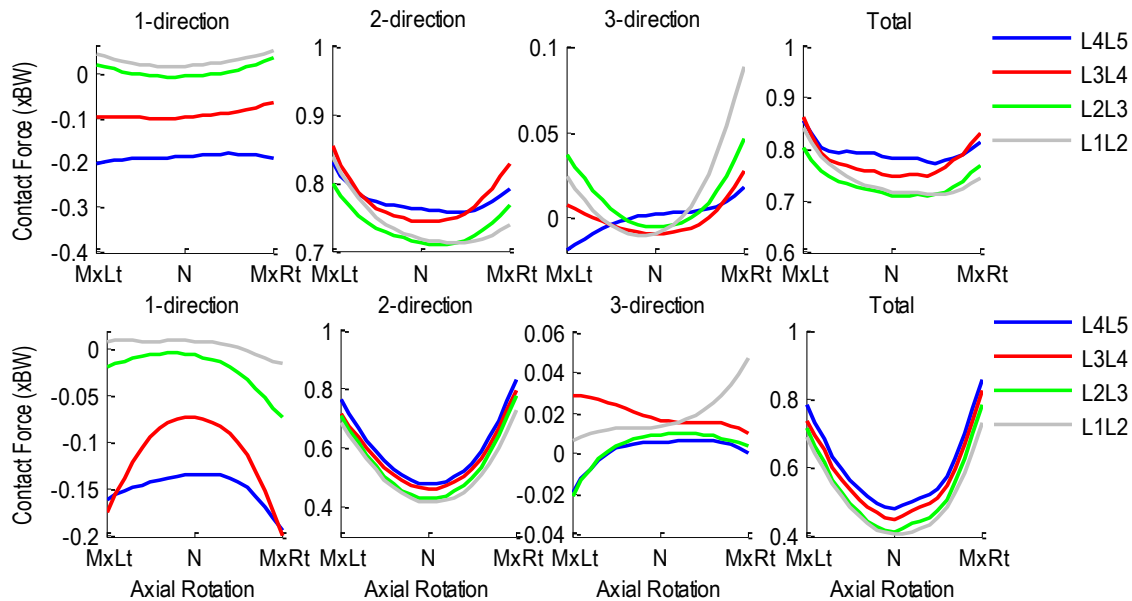


Figure A.394 Patient 3F pre- (top row) and post-operative (bottom row) intervertebral contact forces normalized with respect to body weight during left-to-right axial rotation. 1-dir=Ant(+)/Post(-), 2-dir=Sup(+)/Inf(-), 3-dir=Rt(+)/Lt(-).

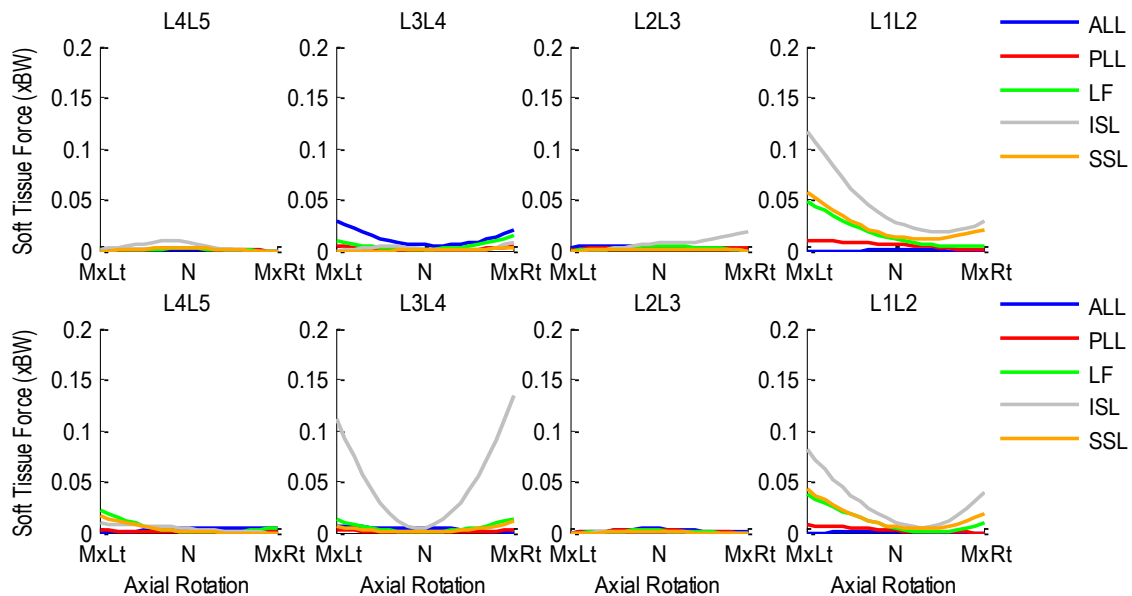


Figure A.395 Patient 3F pre- (top row) and post-operative (bottom row) segmental ligament forces normalized with respect to body weight during left-to-right axial rotation.

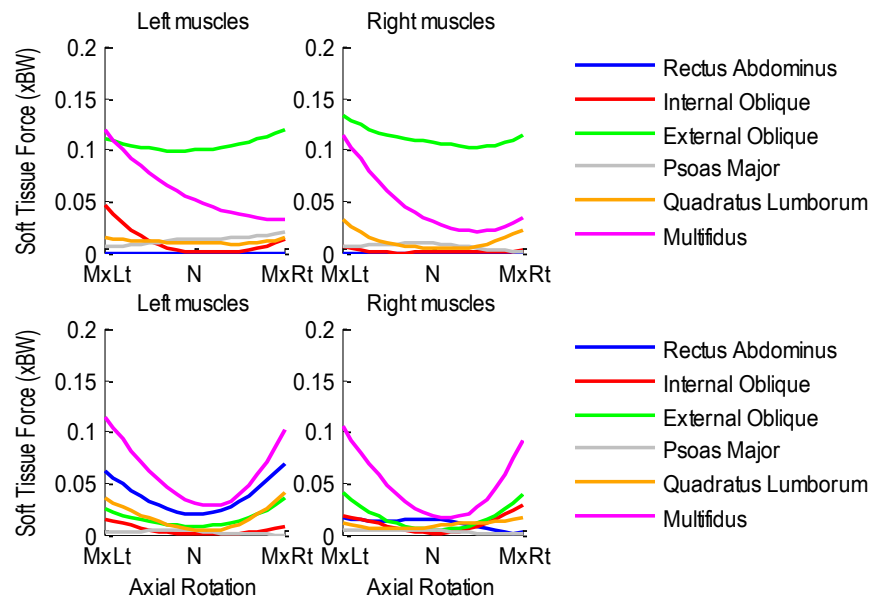


Figure A.396 Patient 3F pre- (top row) and post-operative (bottom row) bilateral muscle forces normalized with respect to body weight during left-to-right axial rotation.

A.34 Patient 4F

Age: 60 years

Gender: Female

Height: 1.45 m

Mass: 62 kg

Condition: Posterior lumbar interbody fusion at L4L5

A.34.1 Flexion-Extension Activity

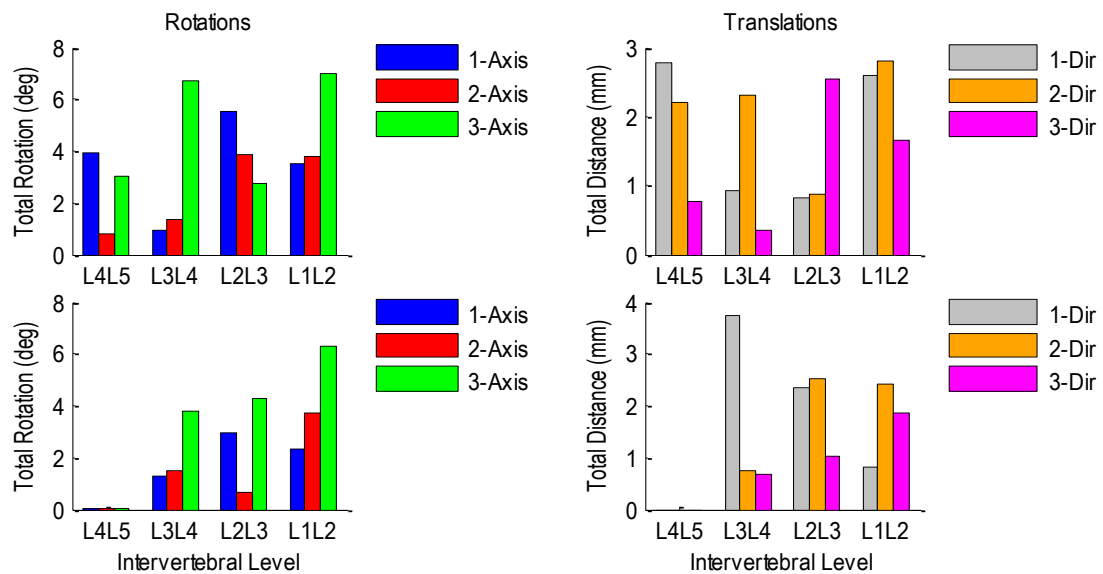


Figure A.397 Patient 4F pre-operative (top row) and post-operative (bottom row) relative rotations (left) and translations (right) at each vertebral level during flexion-extension.

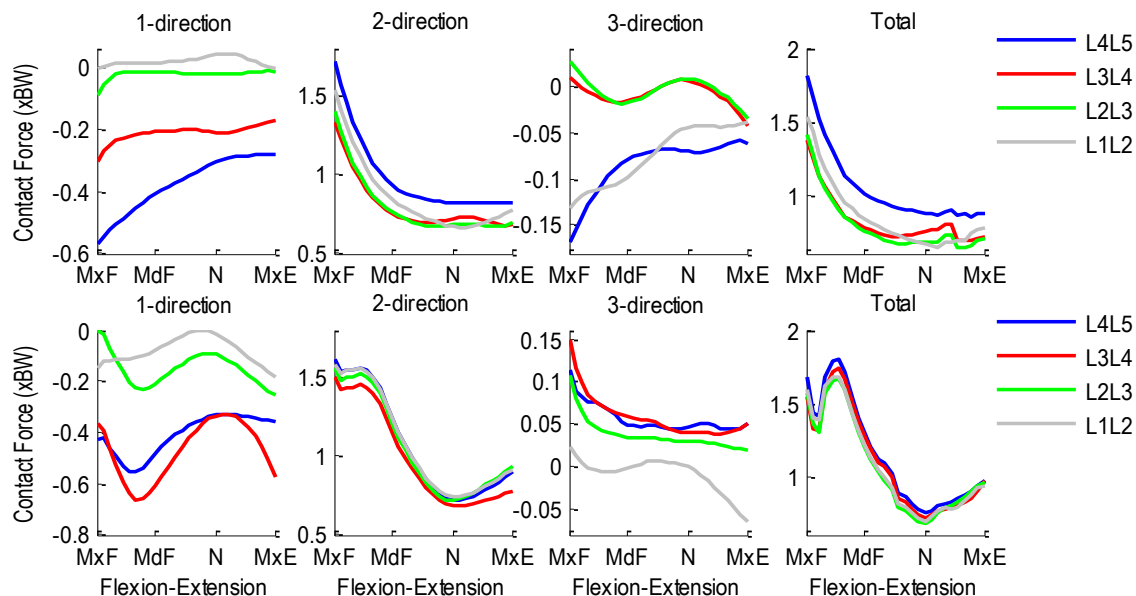


Figure A.398 Patient 4F pre- (top row) and post-operative (bottom row) segmental ligament forces normalized with respect to body weight during flexion-extension.

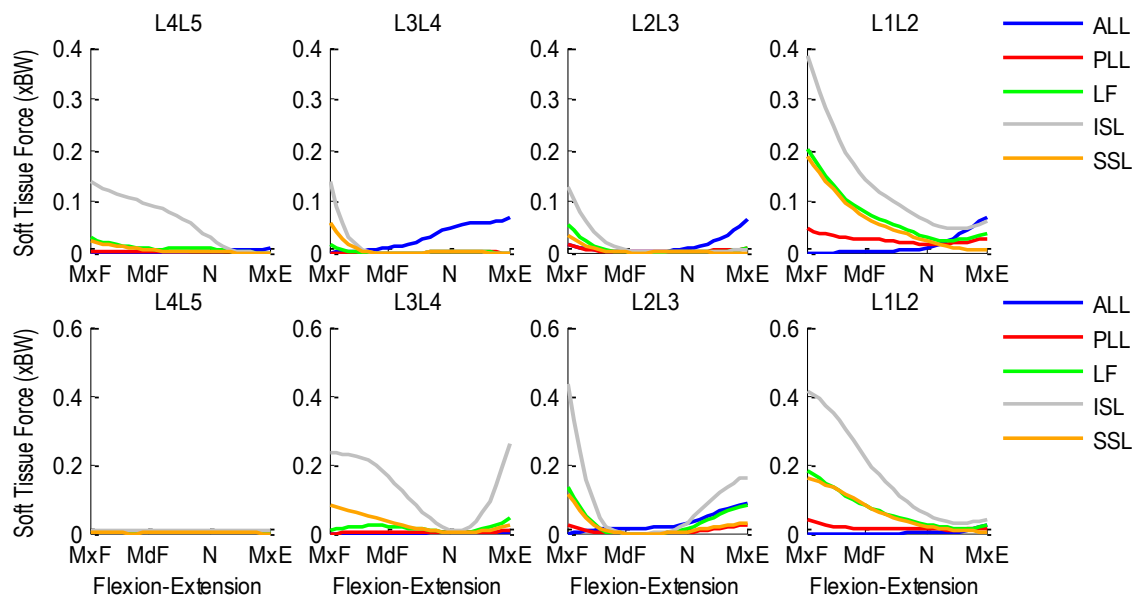


Figure A.399 Patient 4F pre- (top row) and post-operative (bottom row) segmental ligament forces normalized with respect to body weight during flexion-extension.

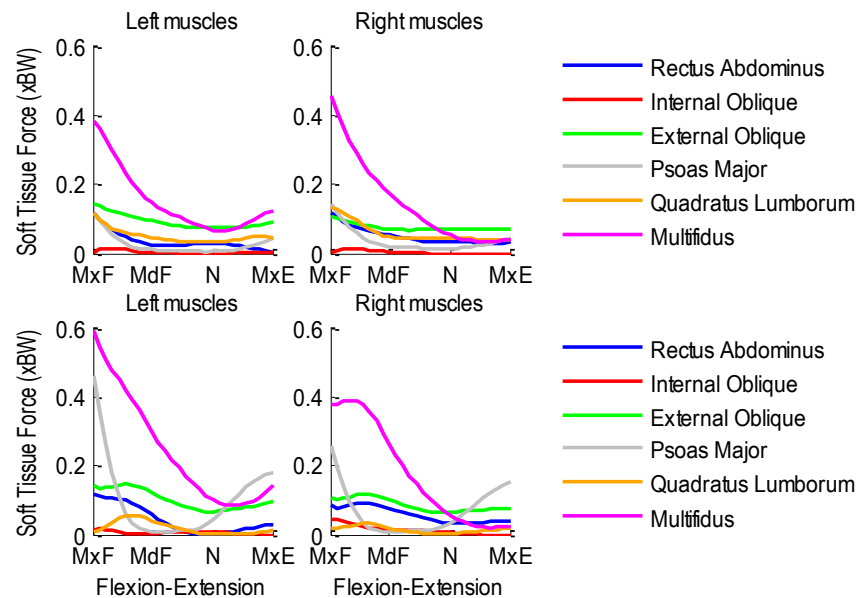


Figure A.400 Patient 4F pre- (top row) and post-operative (bottom row) bilateral muscle forces normalized with respect to body weight during flexion-extension.

A.34.2 Lateral Flexion Activity

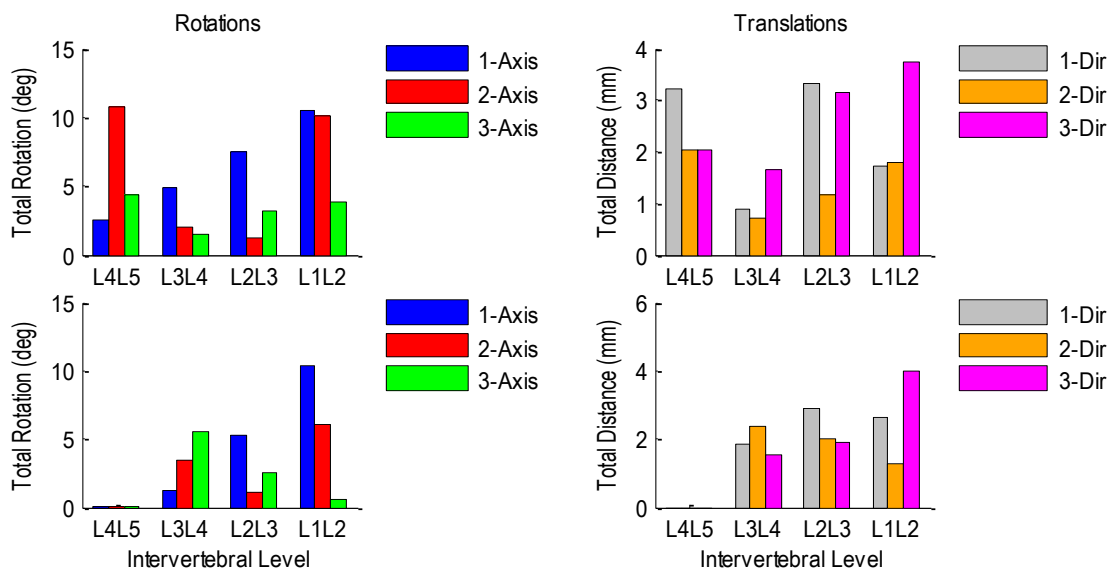


Figure A.401 Patient 4F pre-operative (top row) and post-operative (bottom row) relative rotations (left) and translations (right) at each vertebral level during left-to-right lateral flexion.

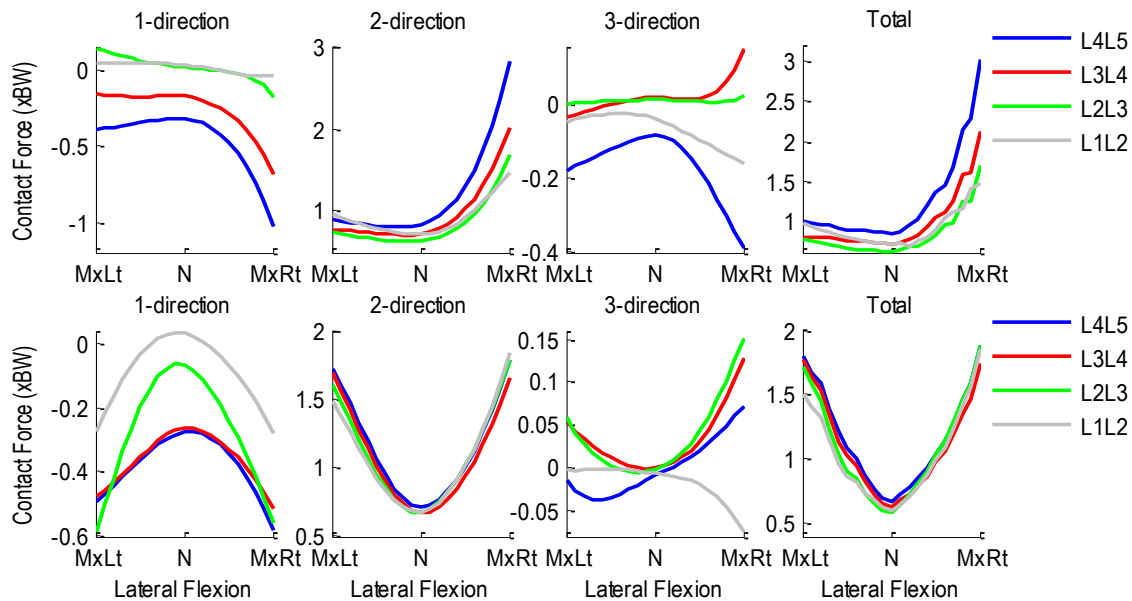


Figure A.402 Patient 4F pre- (top row) and post-operative (bottom row) intervertebral contact forces normalized with respect to body weight during right-to-left lateral flexion. 1-dir=Ant(+)/Post(-), 2-dir=Sup (+)/Inf(-), 3-dir=Rt(+)/Lt(-).

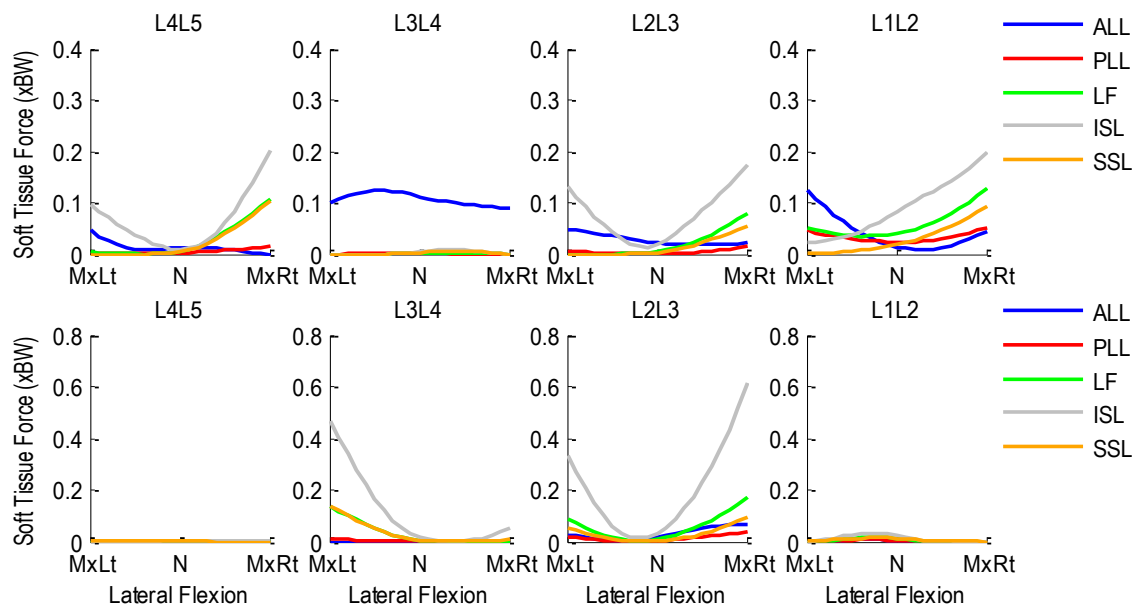


Figure A.403 Patient 4F pre- (top row) and post-operative (bottom row) segmental ligament forces normalized with respect to body weight during left-to-right lateral flexion.

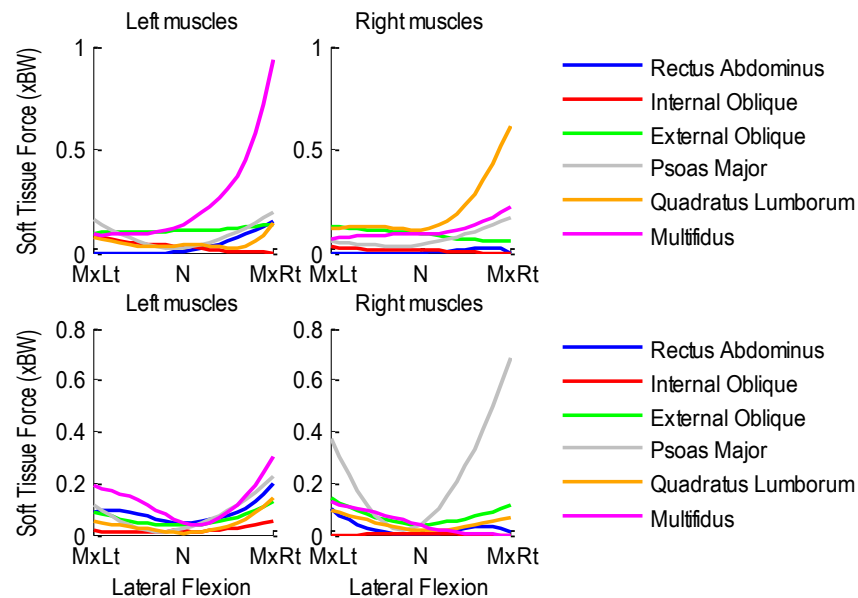


Figure A.404 Patient 4F pre- (top row) and post-operative (bottom row) bilateral muscle forces normalized with respect to body weight during left-to-right lateral flexion.

A.34.3 Axial Rotation Activity

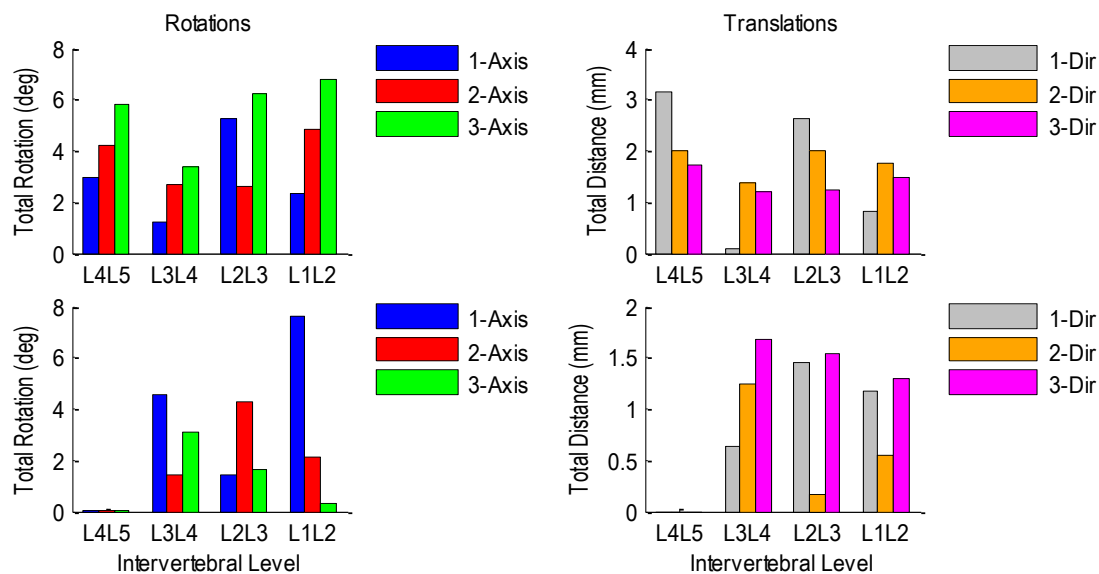


Figure A.405 Patient 4F pre-operative (top row) and post-operative (bottom row) relative rotations (left) and translations (right) at each vertebral level during left-to-right axial rotation.

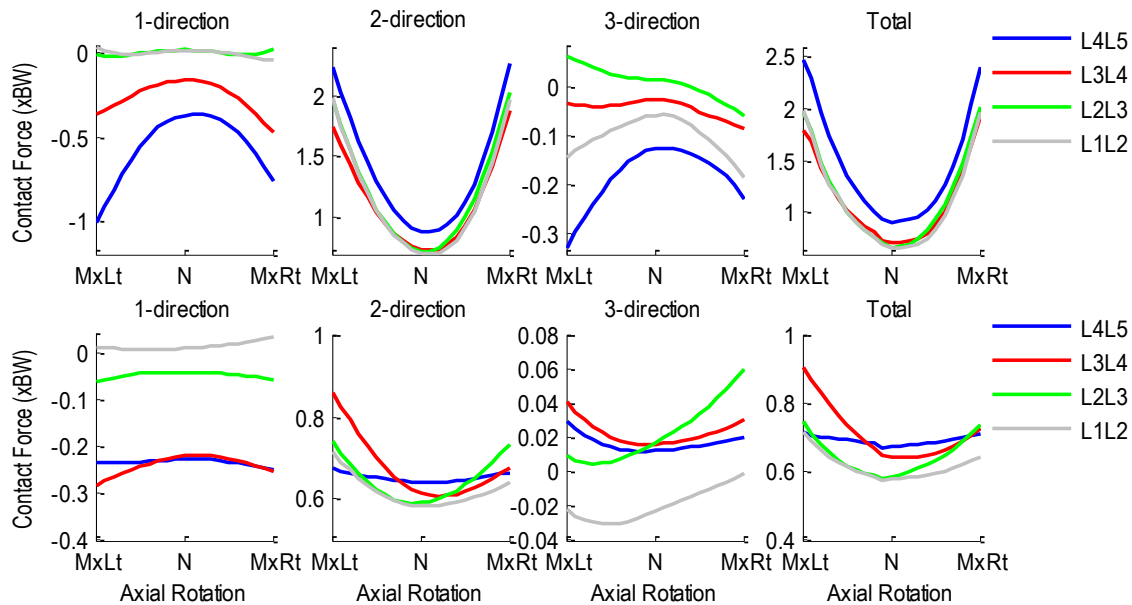


Figure A.406 Patient 4F pre- (top row) and post-operative (bottom row) intervertebral contact forces normalized with respect to body weight during left-to-right axial rotation. 1-dir=Ant(+)/Post(-), 2-dir=Sup(+)/Inf(-), 3-dir=Rt(+)/Lt(-).

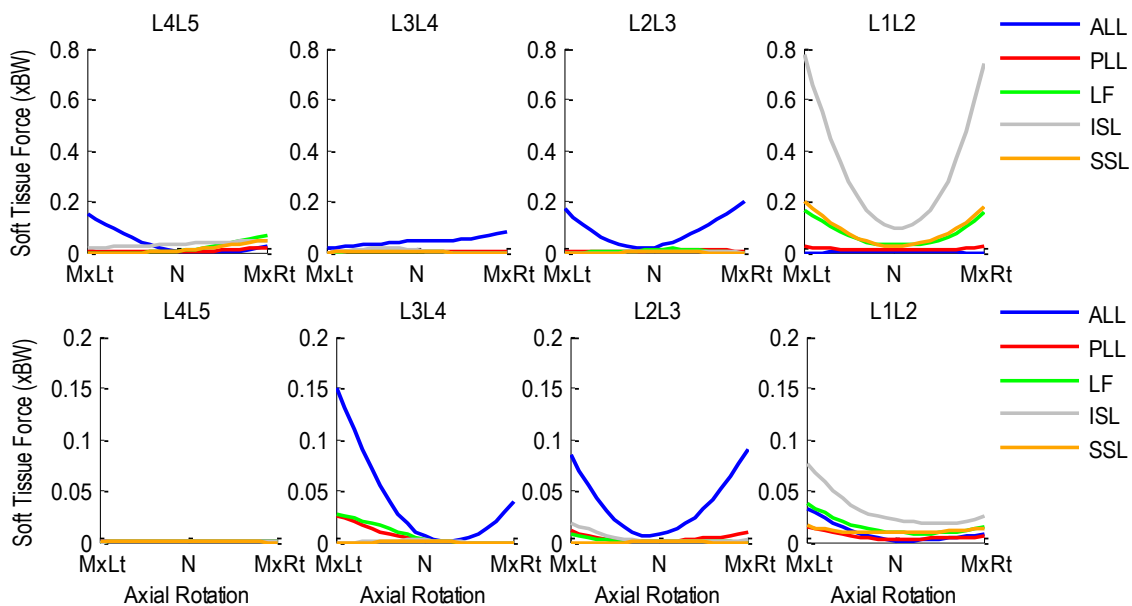


Figure A.407 Patient 4F pre- (top row) and post-operative (bottom row) segmental ligament forces normalized with respect to body weight during left-to-right axial rotation.

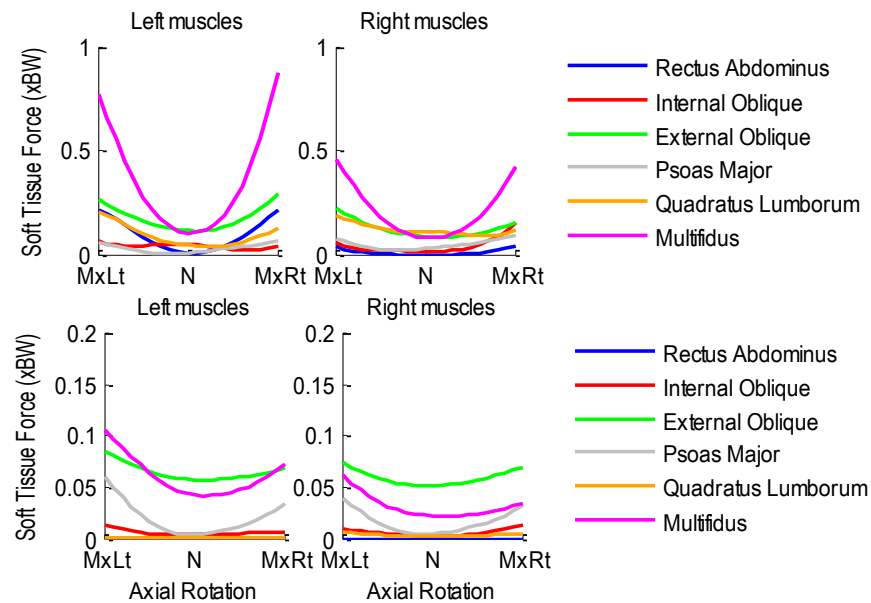


Figure A.408 Patient 4F pre- (top row) and post-operative (bottom row) bilateral muscle forces normalized with respect to body weight during left-to-right axial rotation.

A.35 Patient 5F

Age: 38 years

Gender: Female

Height: 1.70 m

Mass: 91 kg

Condition: Posterior lumbar interbody fusion at L4L5

A.35.1 Flexion-Extension Activity

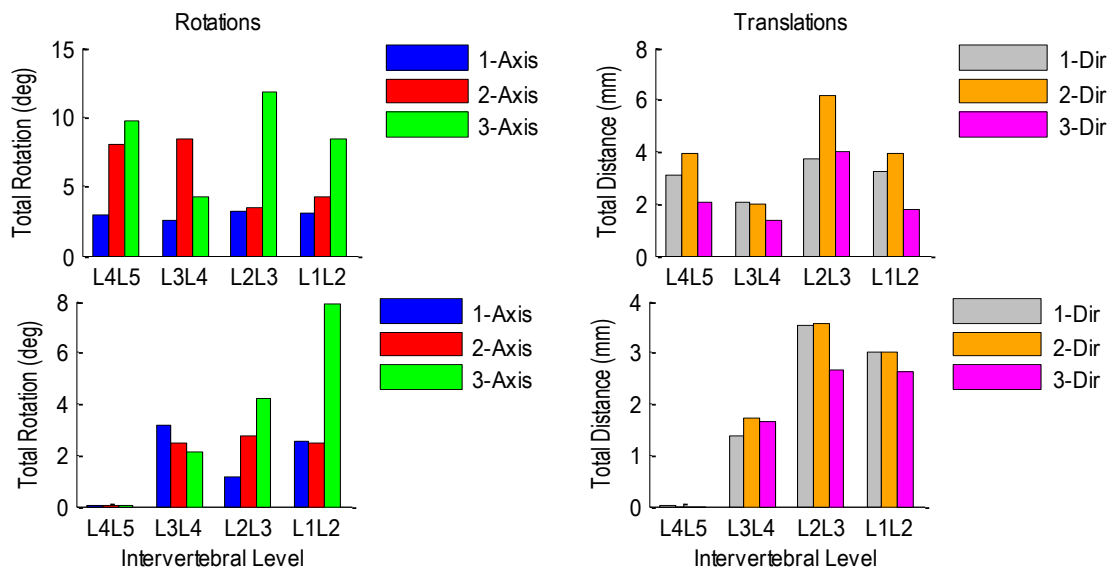


Figure A.409 Patient 5F pre-operative (top row) and post-operative (bottom row) relative rotations (left) and translations (right) at each vertebral level during flexion-extension.

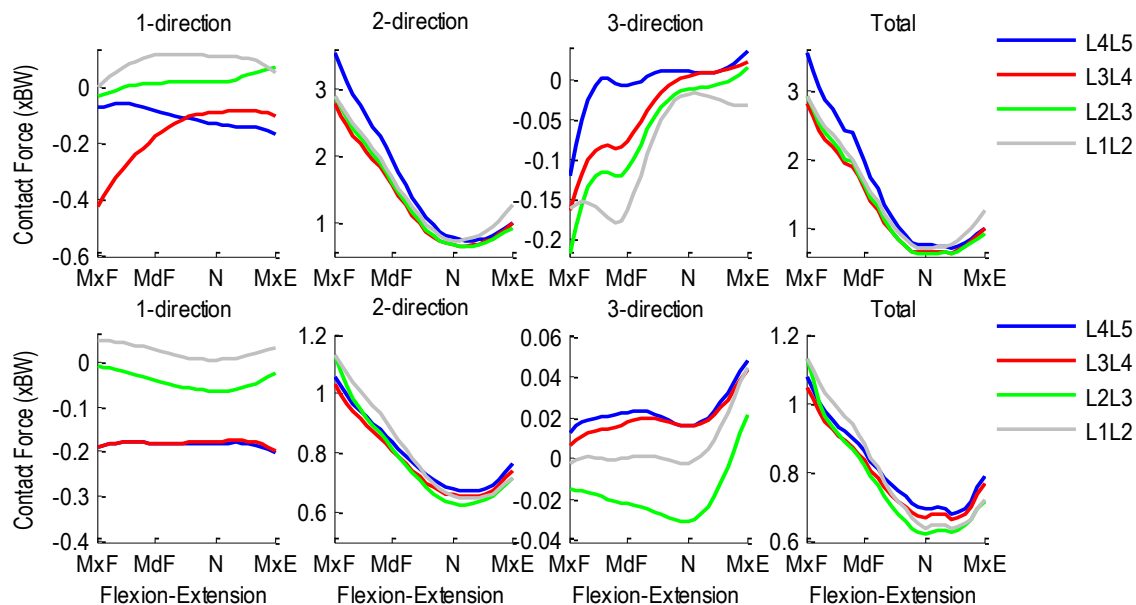


Figure A.410 Patient 5F pre- (top row) and post-operative (bottom row) segmental ligament forces normalized with respect to body weight during flexion-extension.

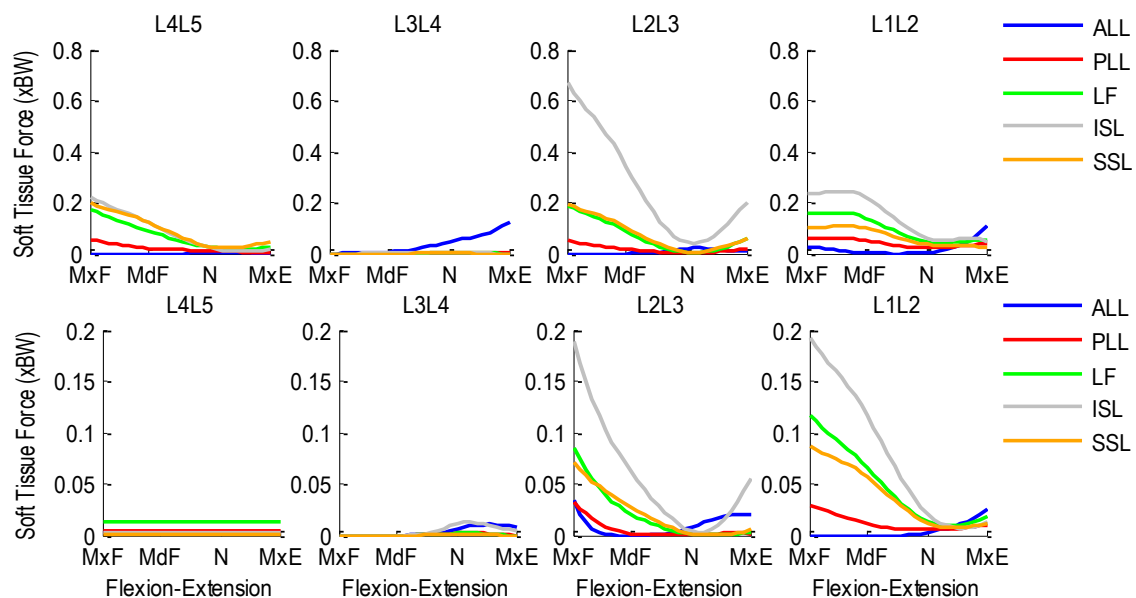


Figure A.411 Patient 5F pre- (top row) and post-operative (bottom row) segmental ligament forces normalized with respect to body weight during flexion-extension.

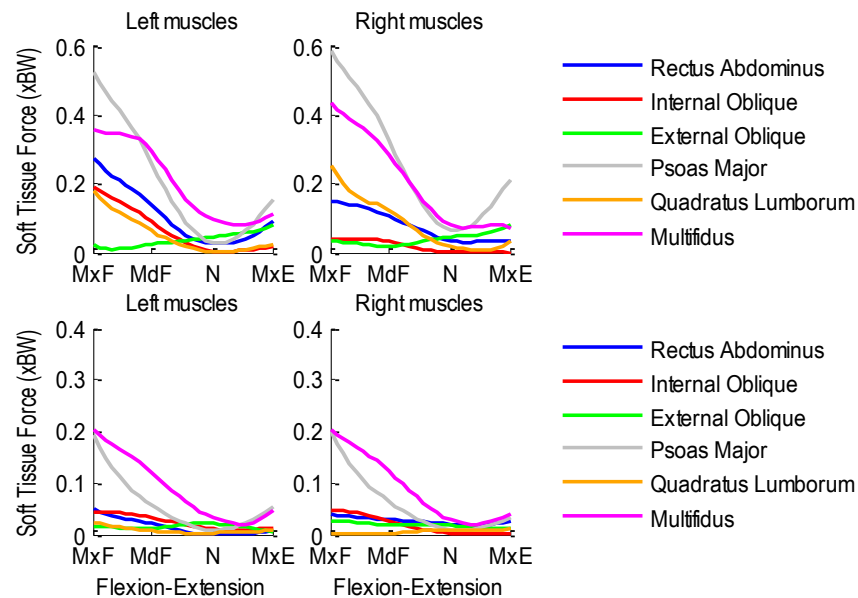


Figure A.412 Patient 5F pre- (top row) and post-operative (bottom row) bilateral muscle forces normalized with respect to body weight during flexion-extension.

A.35.2 Lateral Flexion Activity

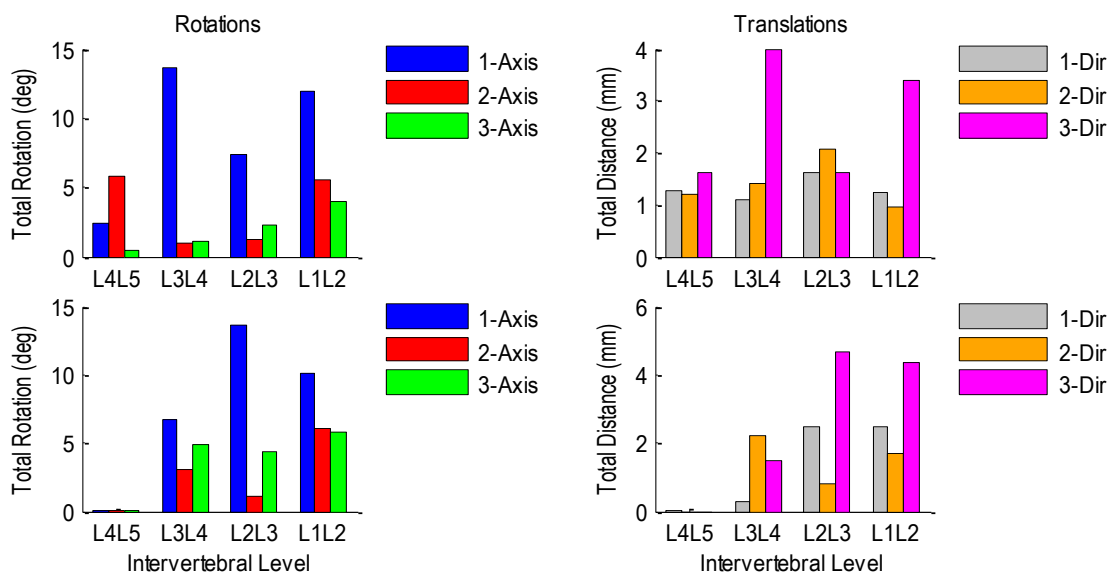


Figure A.413 Patient 5F pre-operative (top row) and post-operative (bottom row) relative rotations (left) and translations (right) at each vertebral level during left-to-right lateral flexion.

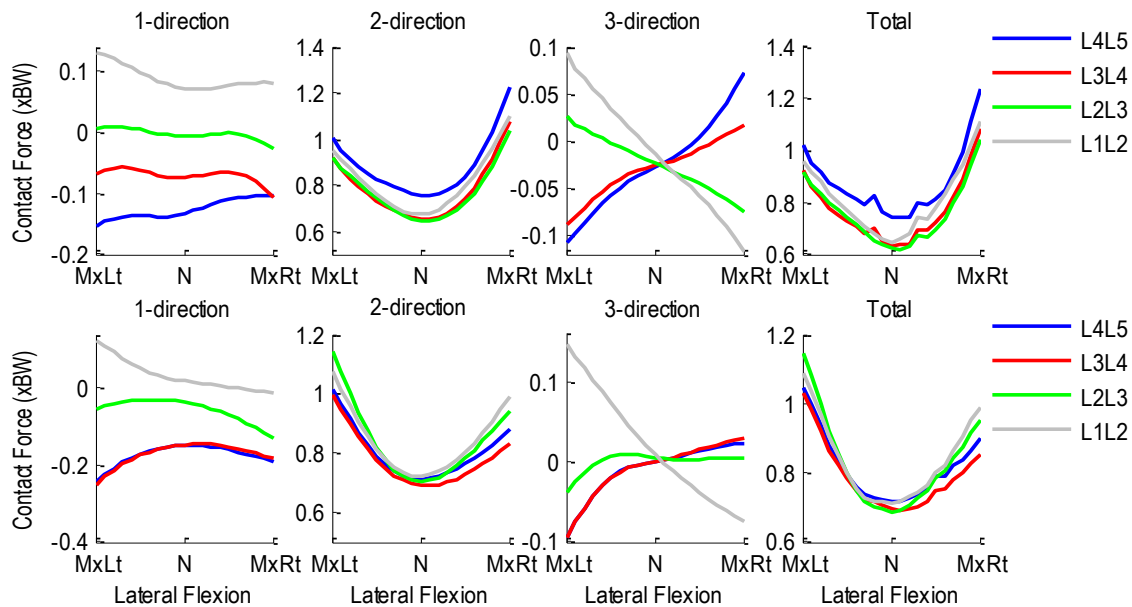


Figure A.414. Patient 5F pre- (top row) and post-operative (bottom row) intervertebral contact forces normalized with respect to body weight during right-to-left lateral flexion. 1-dir=Ant(+)/Post(-), 2-dir=Sup (+)/Inf(-), 3-dir=Rt(+)/Lt(-).

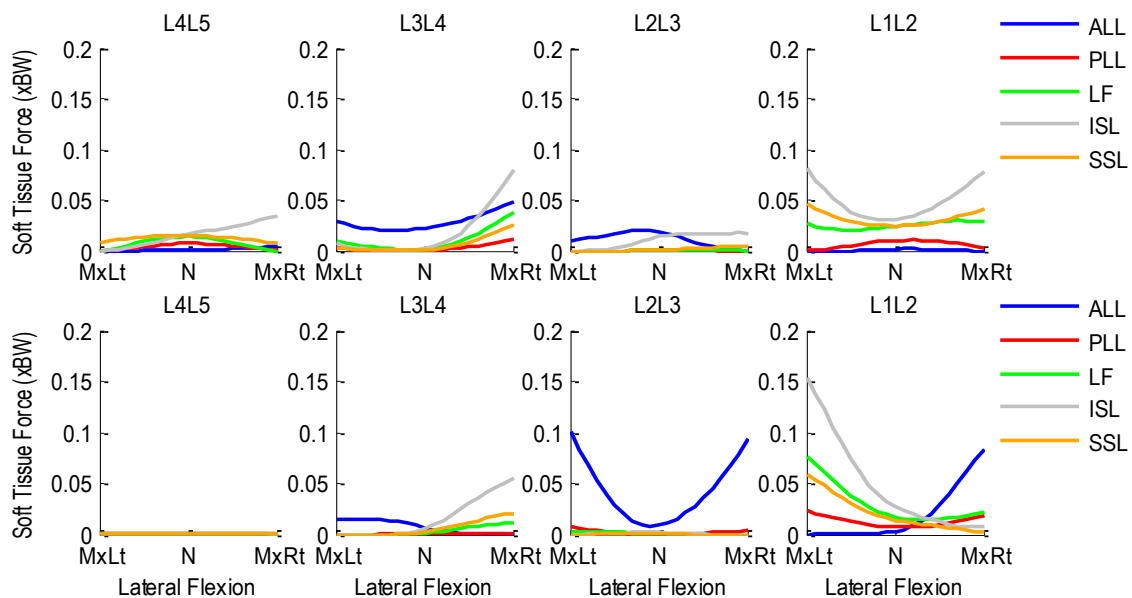


Figure A.415 Patient 5F pre- (top row) and post-operative (bottom row) segmental ligament forces normalized with respect to body weight during left-to-right lateral flexion.

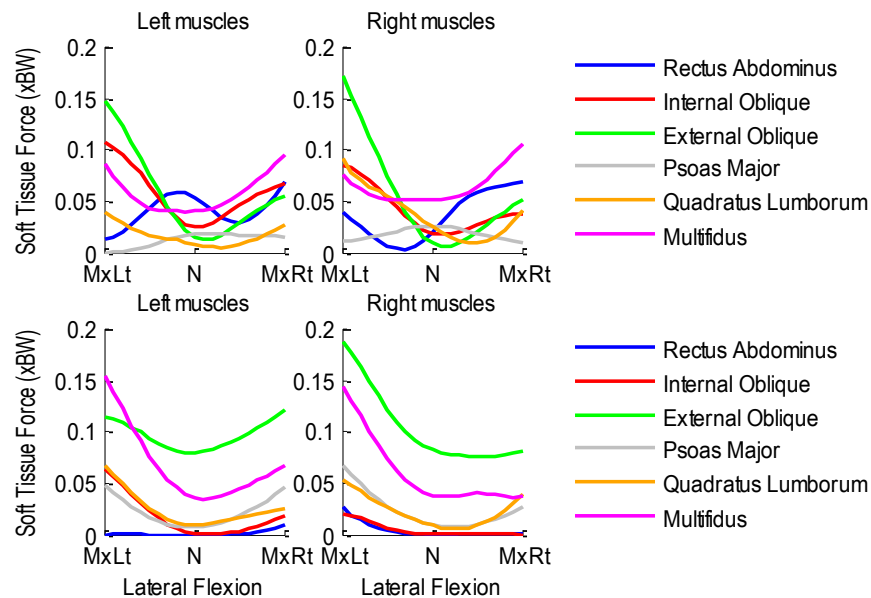


Figure A.416 Patient 5F pre- (top row) and post-operative (bottom row) bilateral muscle forces normalized with respect to body weight during left-to-right lateral flexion.

A.35.3 Axial Rotation Activity

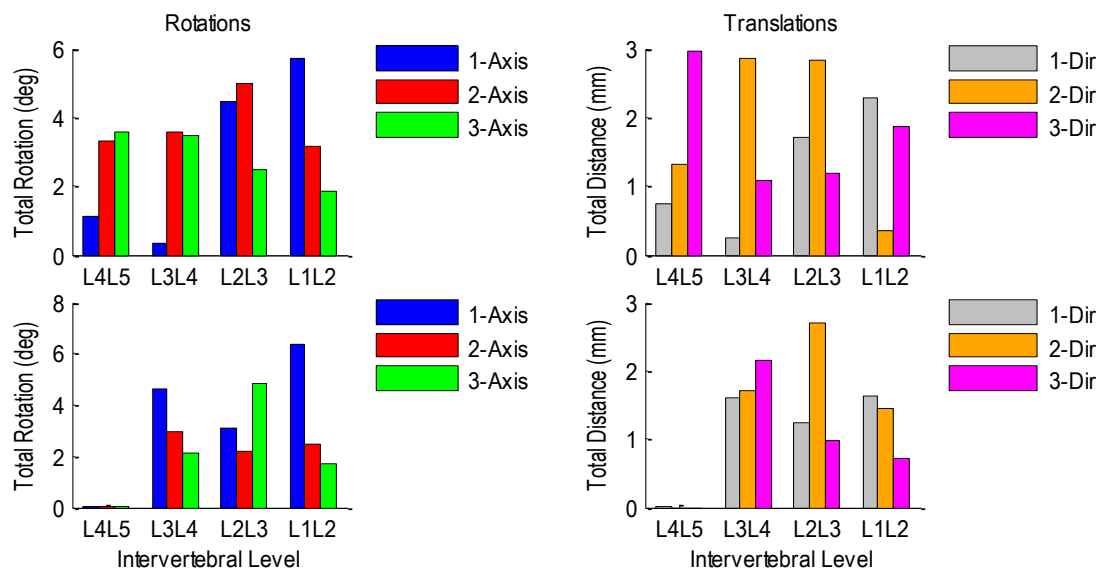


Figure A.417 Patient 5F pre-operative (top row) and post-operative (bottom row) relative rotations (left) and translations (right) at each vertebral level during left-to-right axial rotation.

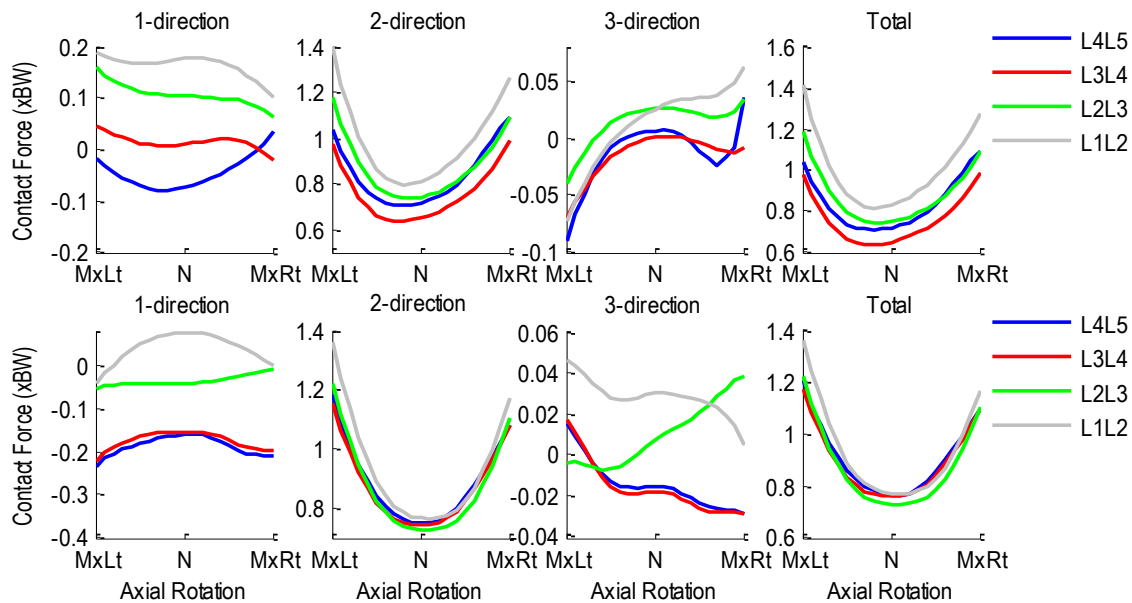


Figure A.418 Patient 5F pre- (top row) and post-operative (bottom row) intervertebral contact forces normalized with respect to body weight during left-to-right axial rotation. 1-dir=Ant(+)/Post(-), 2-dir=Sup(+)/Inf(-), 3-dir=Rt(+)/Lt(-).

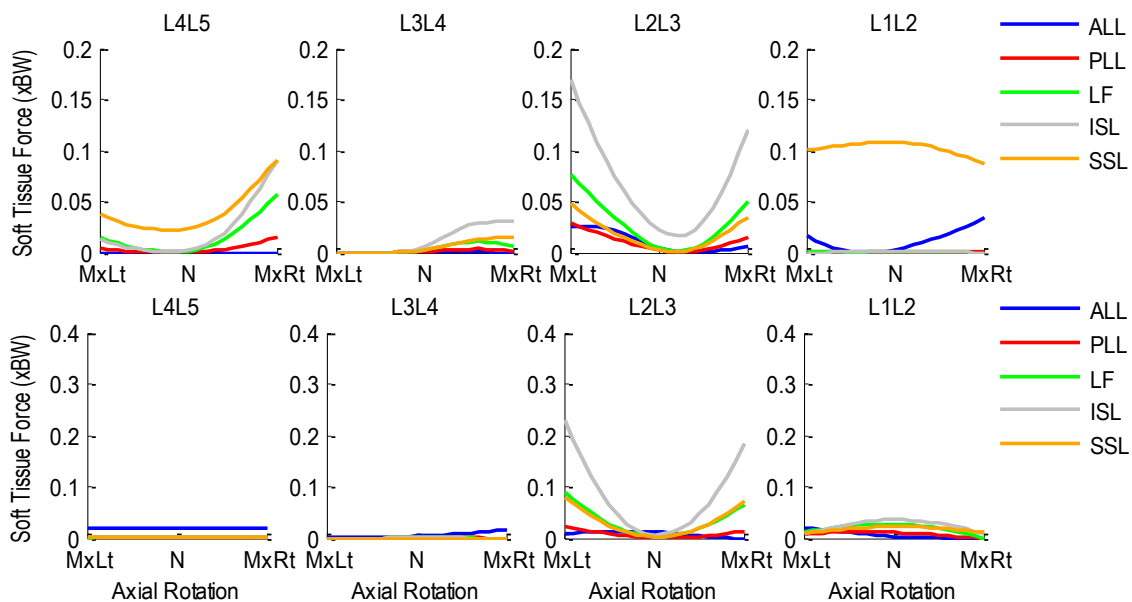


Figure A.419 Patient 5F pre- (top row) and post-operative (bottom row) segmental ligament forces normalized with respect to body weight during left-to-right axial rotation.

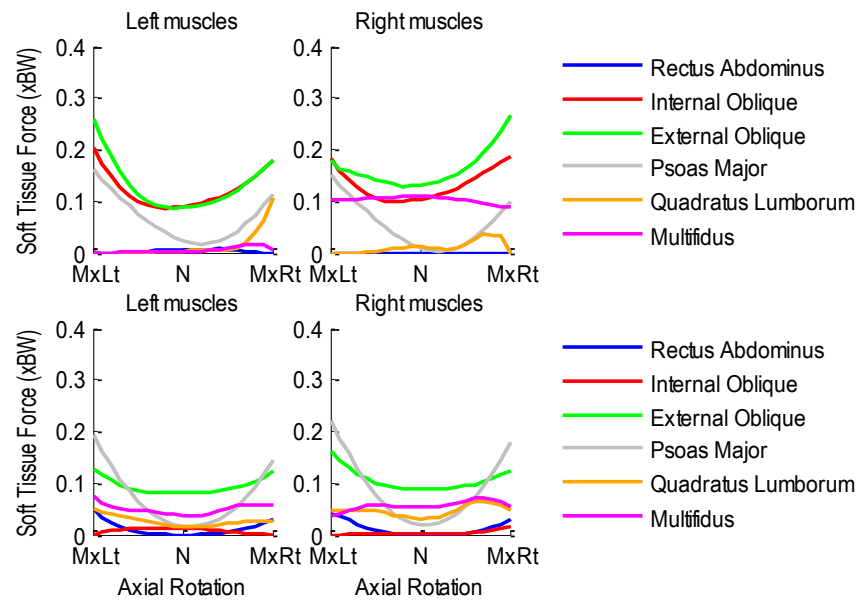


Figure A.420 Patient 5F pre- (top row) and post-operative (bottom row) bilateral muscle forces normalized with respect to body weight during left-to-right axial rotation.

A.36 Patient 6F

Age: 45 years

Gender: Male

Height: 1.83 m

Mass: 110 kg

Condition: Posterior lumbar interbody fusion at L5S1

A.36.1 Flexion-Extension Activity

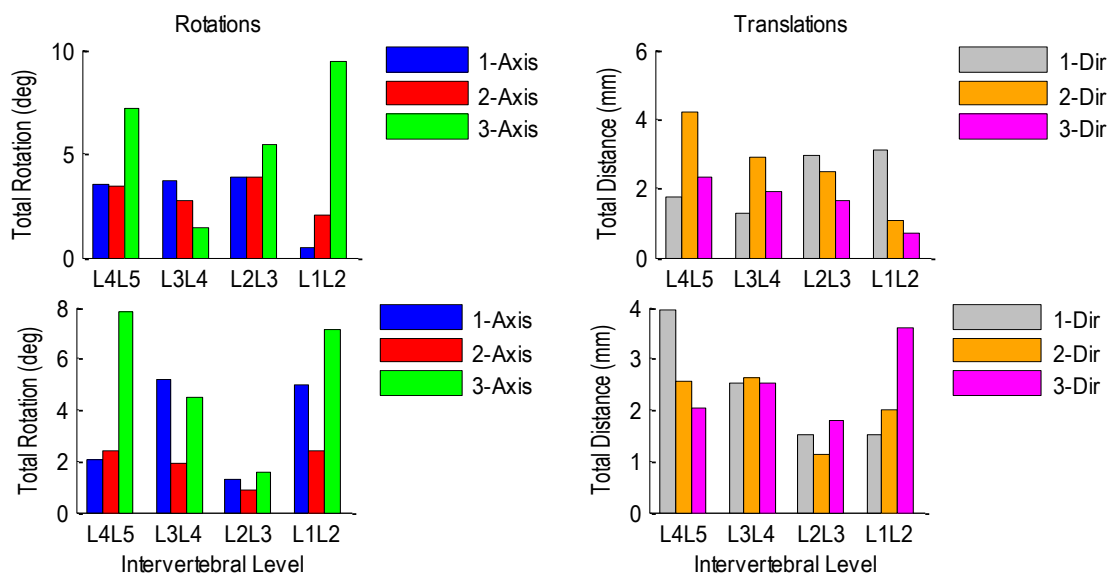


Figure A.421 Patient 6F pre-operative (top row) and post-operative (bottom row) relative rotations (left) and translations (right) at each vertebral level during flexion-extension.

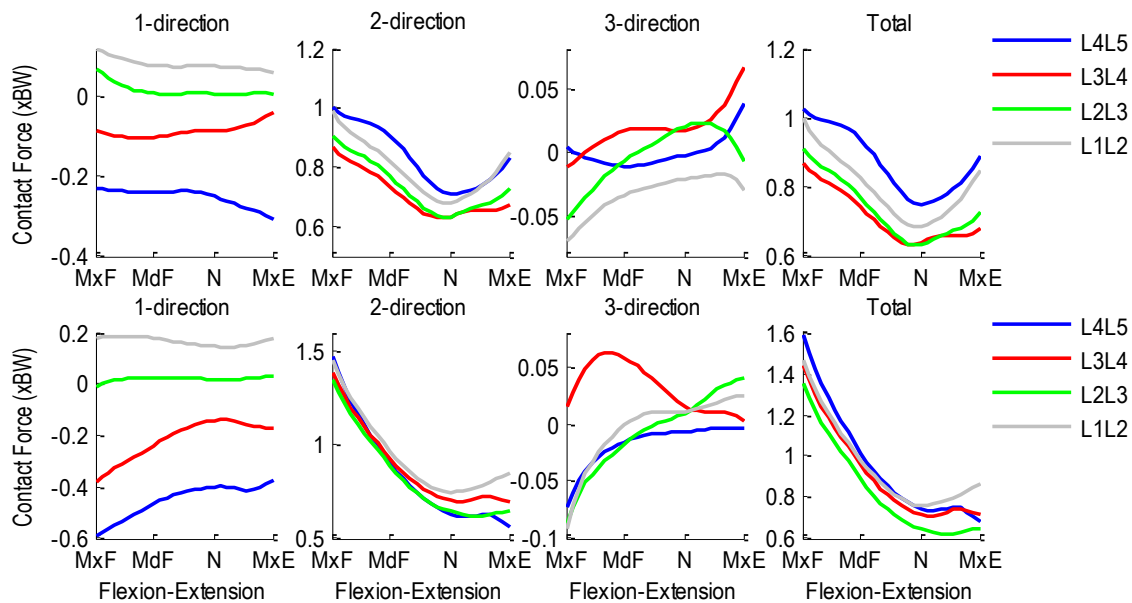


Figure A.422 Patient 6F pre- (top row) and post-operative (bottom row) segmental ligament forces normalized with respect to body weight during flexion-extension.

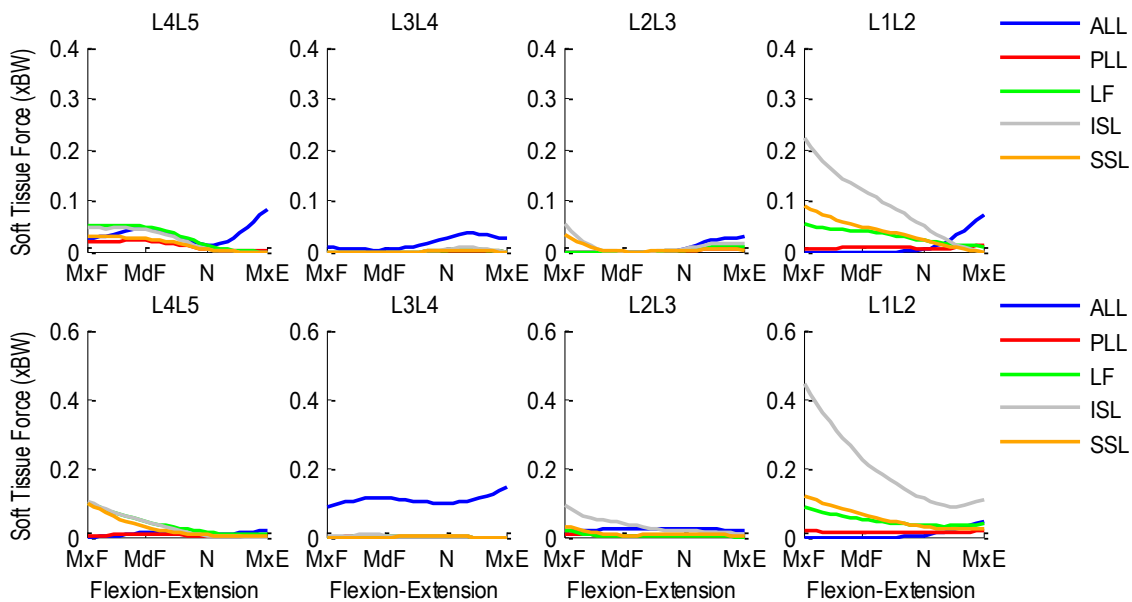


Figure A.423 Patient 6F pre- (top row) and post-operative (bottom row) segmental ligament forces normalized with respect to body weight during flexion-extension.

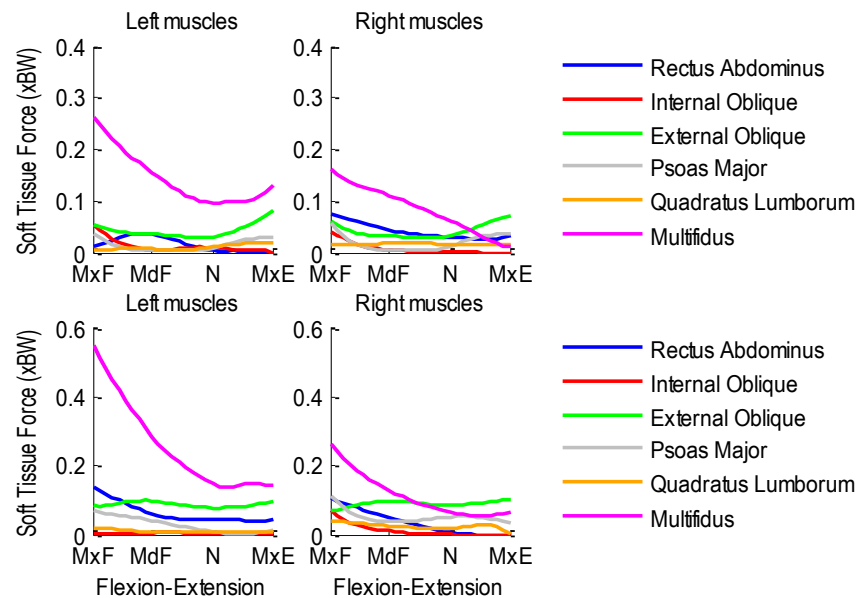


Figure A.424 Patient 6F pre- (top row) and post-operative (bottom row) bilateral muscle forces normalized with respect to body weight during flexion-extension.

A.36.2 Lateral Flexion Activity

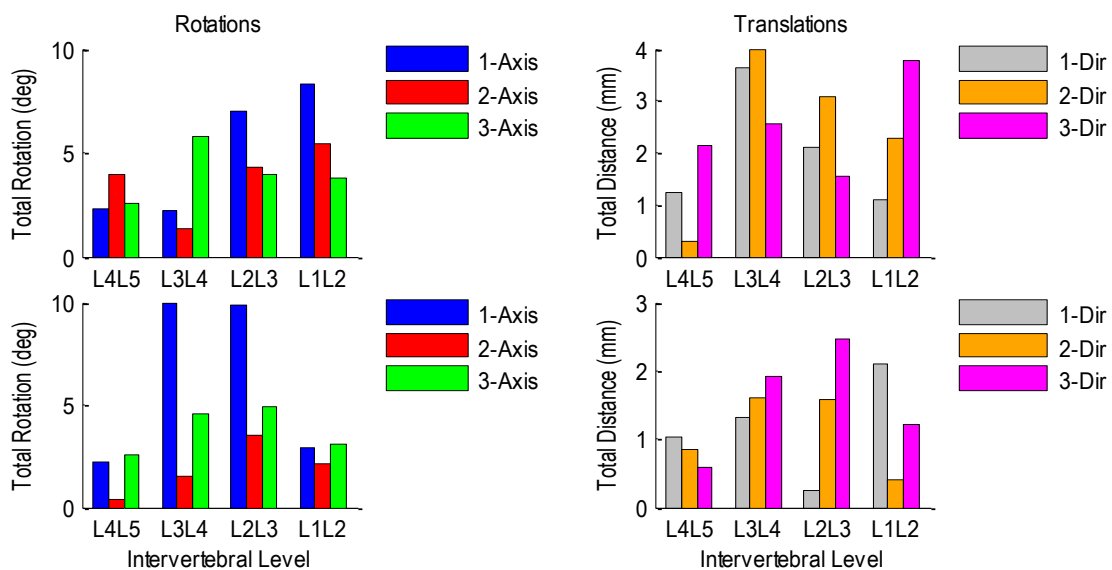


Figure A.425 Patient 6F pre-operative (top row) and post-operative (bottom row) relative rotations (left) and translations (right) at each vertebral level during left-to-right lateral flexion.

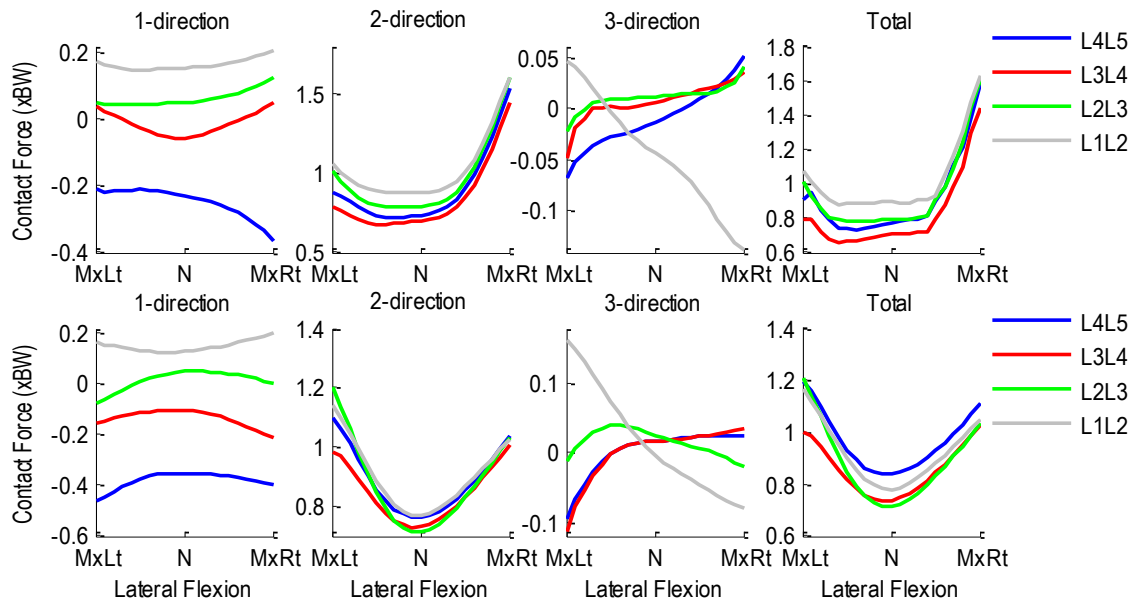


Figure A.426 Patient 6F pre- (top row) and post-operative (bottom row) intervertebral contact forces normalized with respect to body weight during right-to-left lateral flexion. 1-dir=Ant(+)/Post(-), 2-dir=Sup (+)/Inf(-), 3-dir=Rt(+)/Lt(-).

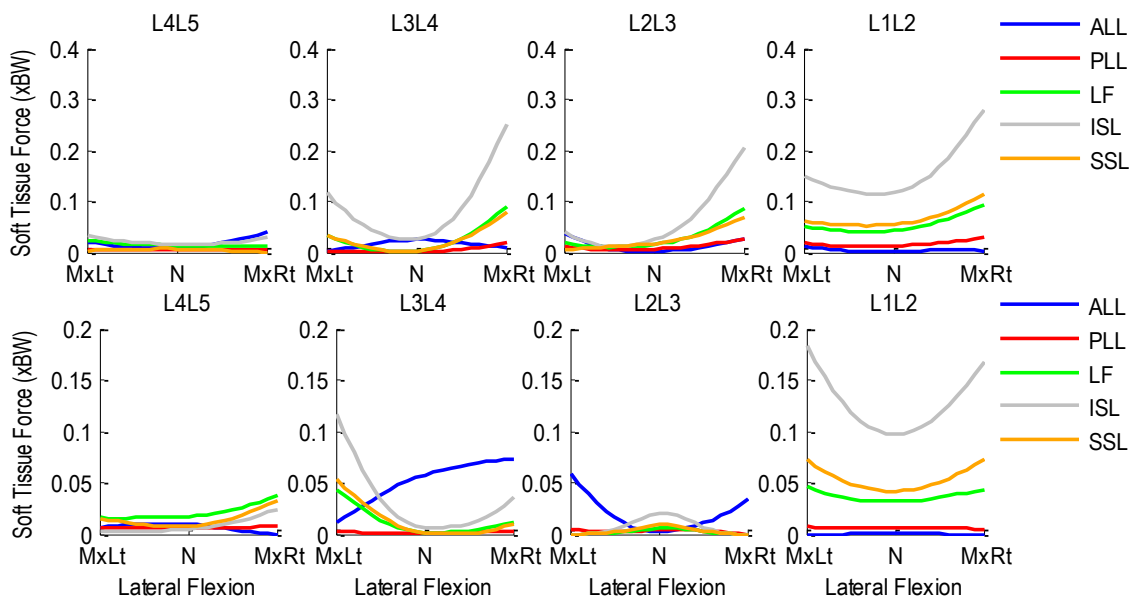


Figure A.427 Patient 6F pre- (top row) and post-operative (bottom row) segmental ligament forces normalized with respect to body weight during left-to-right lateral flexion.

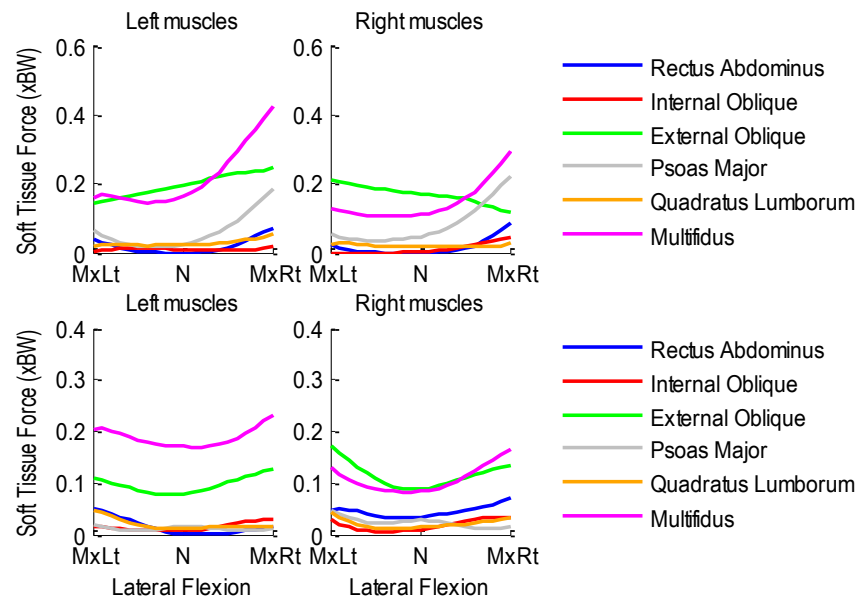


Figure A.428 Patient 6F pre- (top row) and post-operative (bottom row) bilateral muscle forces normalized with respect to body weight during left-to-right lateral flexion.

A.36.3 Axial Rotation Activity

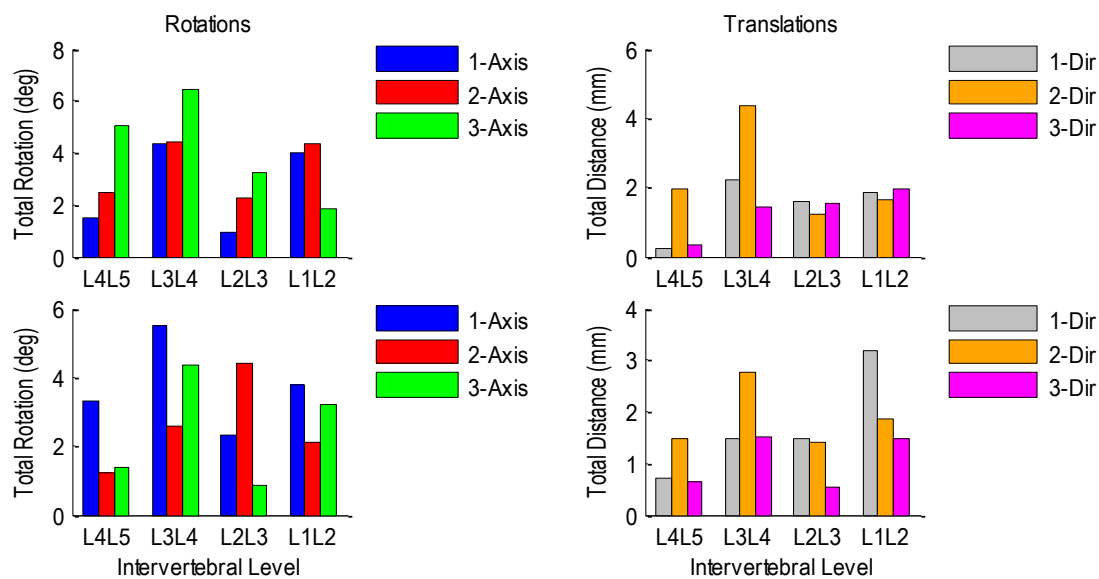


Figure A.429 Patient 6F pre-operative (top row) and post-operative (bottom row) relative rotations (left) and translations (right) at each vertebral level during left-to-right axial rotation.

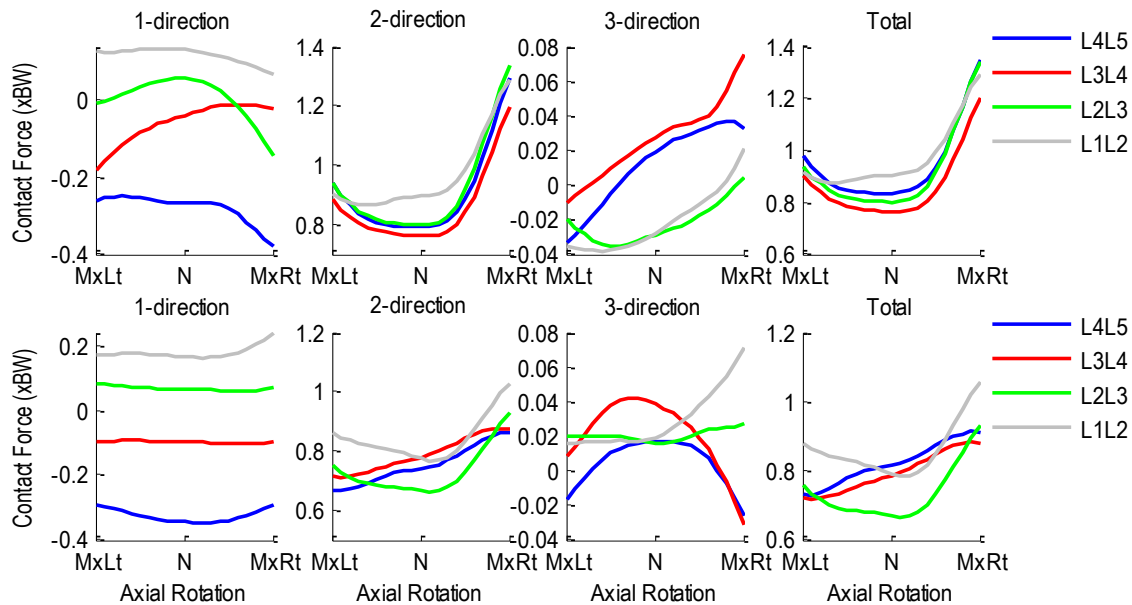


Figure A.430 Patient 6F pre- (top row) and post-operative (bottom row) intervertebral contact forces normalized with respect to body weight during left-to-right axial rotation. 1-dir=Ant(+)/Post(-), 2-dir=Sup(+)/Inf(-), 3-dir=Rt(+)/Lt(-).

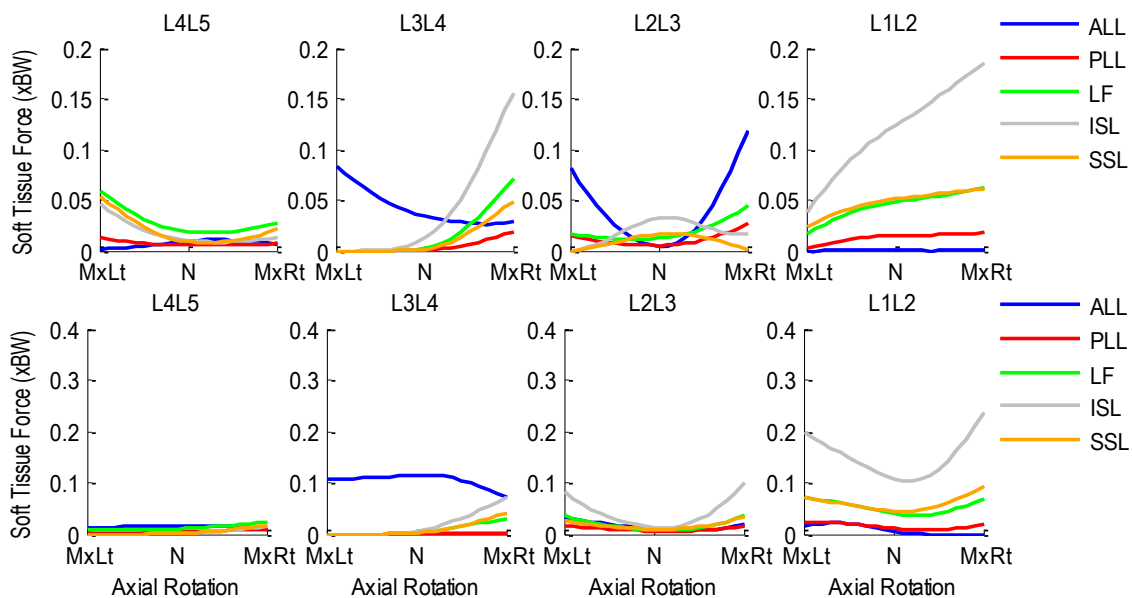


Figure A.431 Patient 6F pre- (top row) and post-operative (bottom row) segmental ligament forces normalized with respect to body weight during left-to-right axial rotation.

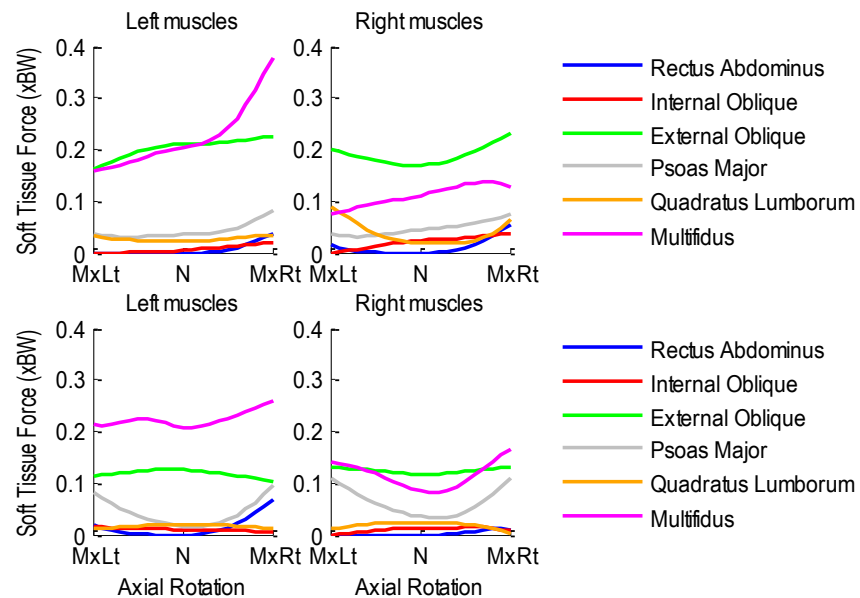


Figure A.432 Patient 6F pre- (top row) and post-operative (bottom row) bilateral muscle forces normalized with respect to body weight during left-to-right axial rotation.

A.37 Patient 7F

Age: 31 years

Gender: Female

Height: 1.70 m

Mass: 96 kg

Condition: Posterior lumbar interbody fusion at L4L5

A.37.1 Flexion-Extension Activity

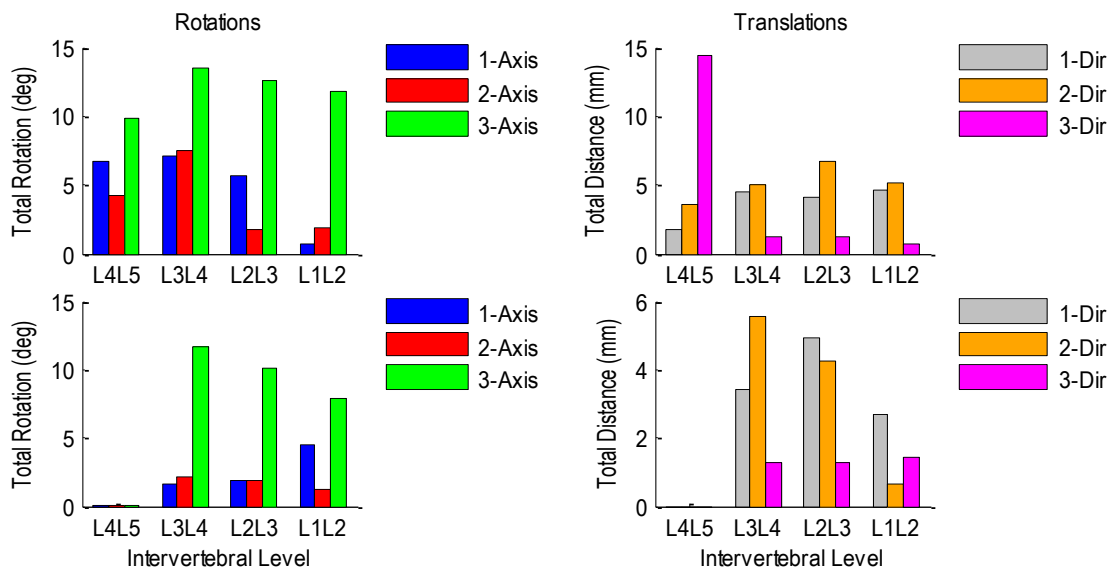


Figure A.433 Patient 7F pre-operative (top row) and post-operative (bottom row) relative rotations (left) and translations (right) at each vertebral level during flexion-extension.

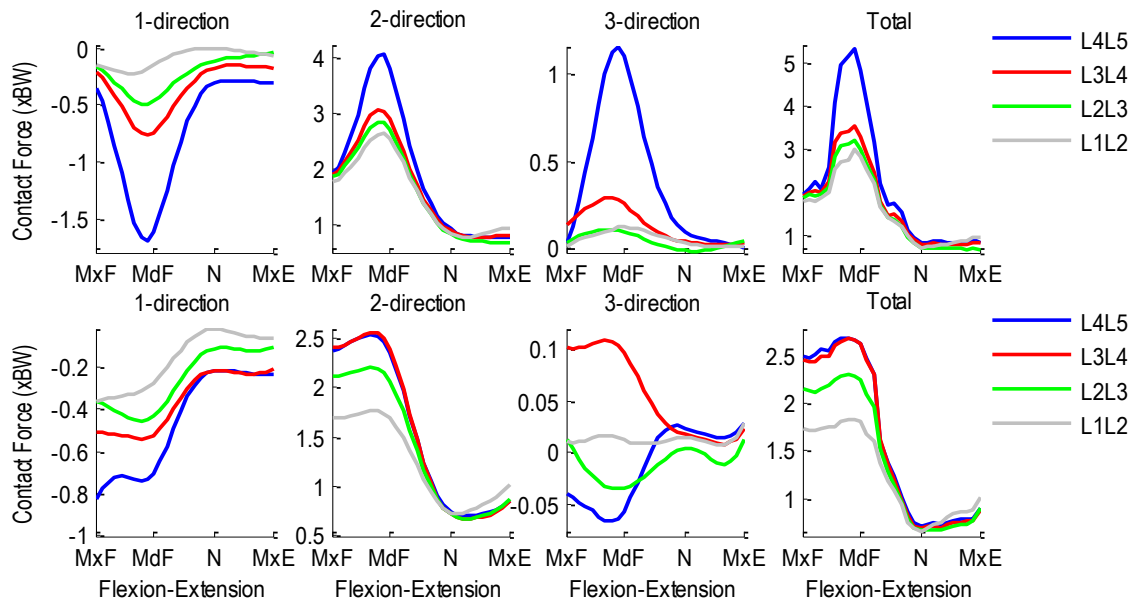


Figure A.434 Patient 7F pre- (top row) and post-operative (bottom row) segmental ligament forces normalized with respect to body weight during flexion-extension.

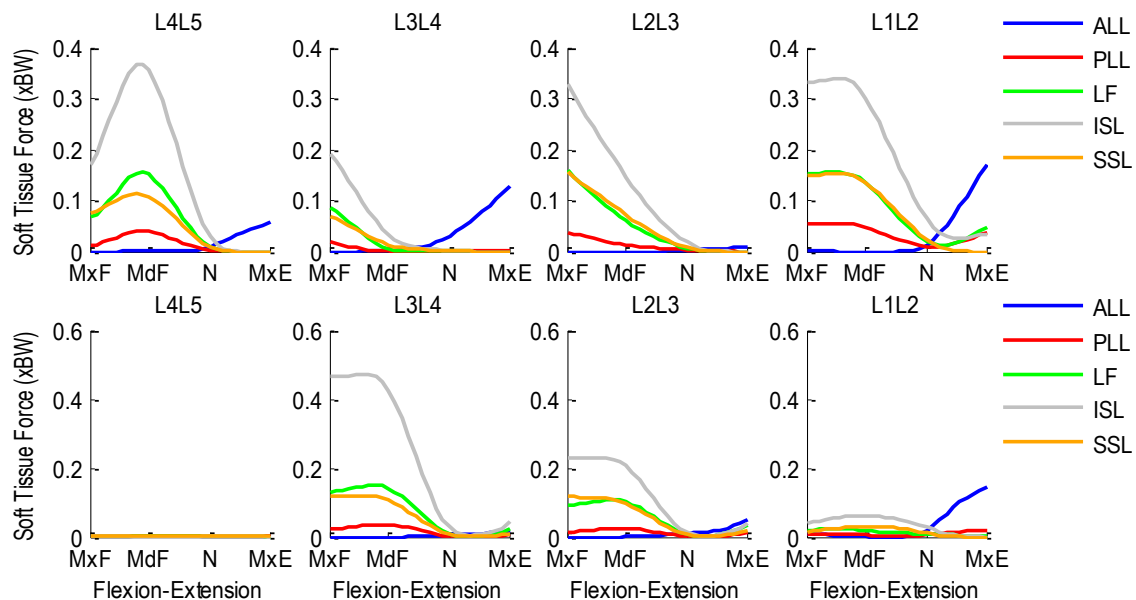


Figure A.435 Patient 7F pre- (top row) and post-operative (bottom row) segmental ligament forces normalized with respect to body weight during flexion-extension.

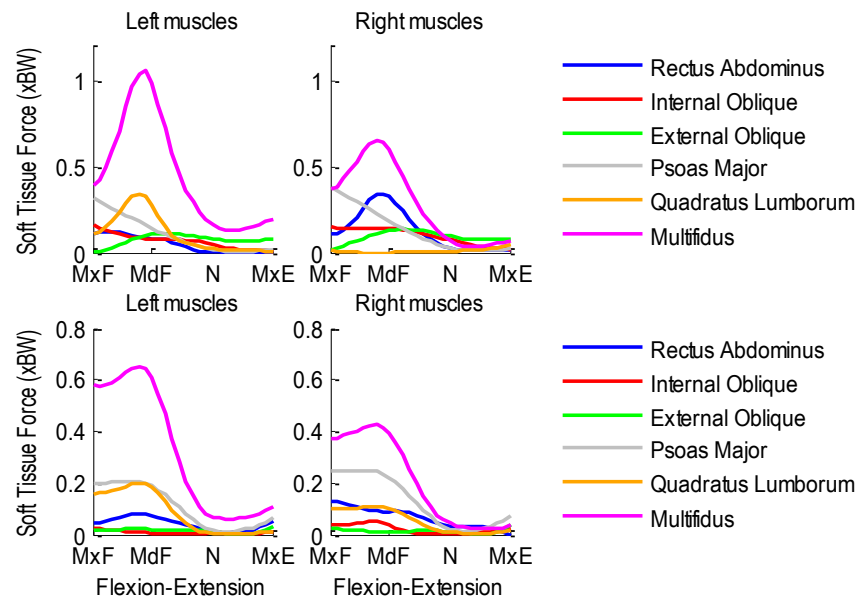


Figure A.436 Patient 7F pre- (top row) and post-operative (bottom row) bilateral muscle forces normalized with respect to body weight during flexion-extension.

A.37.2 Lateral Flexion Activity

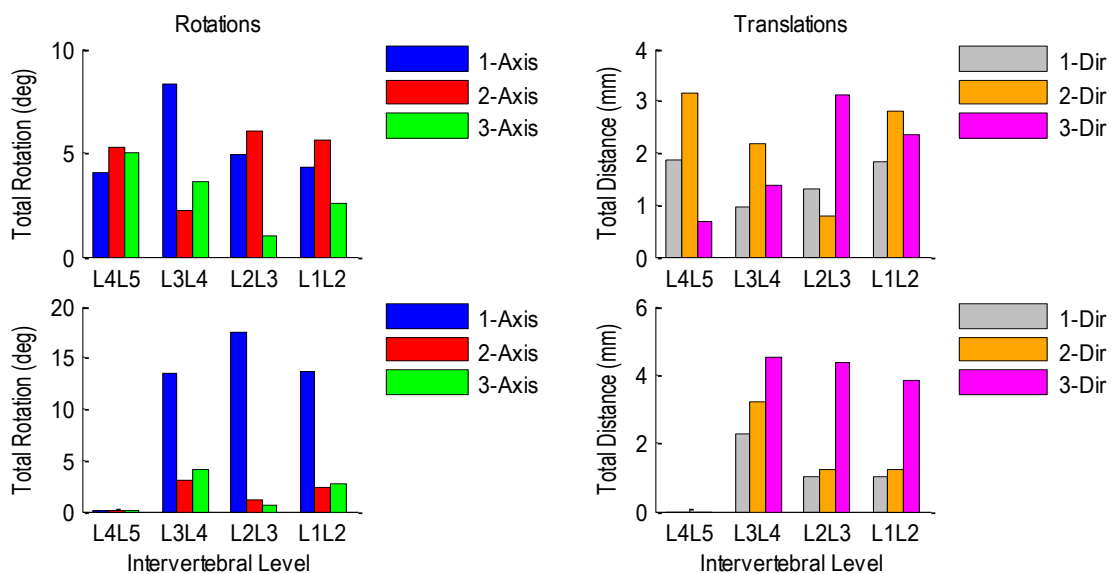


Figure A.437 Patient 7F pre-operative (top row) and post-operative (bottom row) relative rotations (left) and translations (right) at each vertebral level during left-to-right lateral flexion.

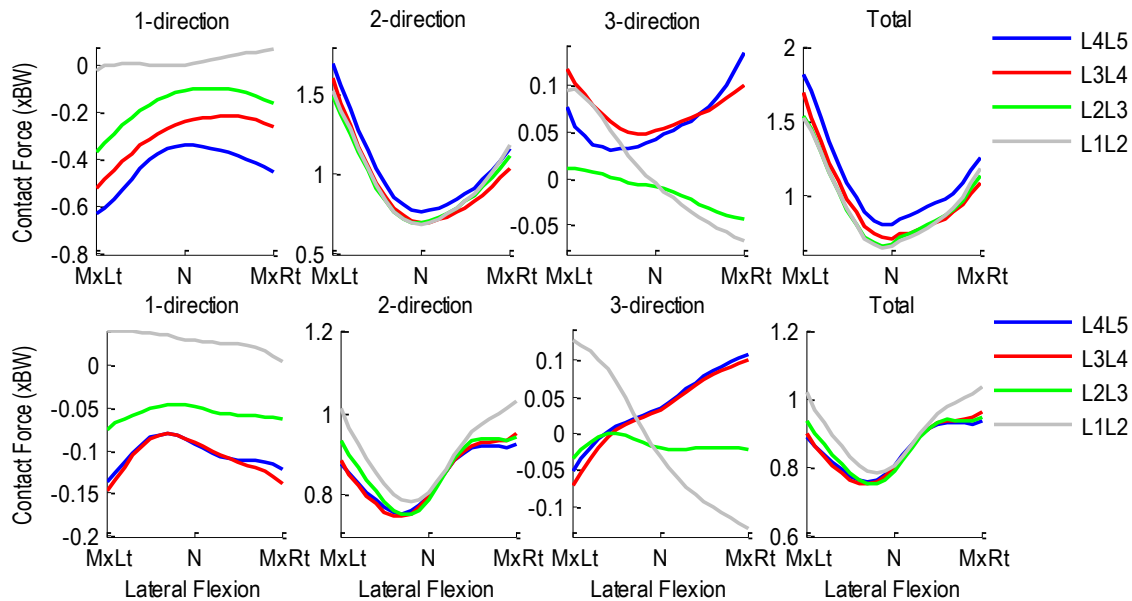


Figure A.438 Patient 7F pre- (top row) and post-operative (bottom row) intervertebral contact forces normalized with respect to body weight during right-to-left lateral flexion. 1-dir=Ant(+)/Post(-), 2-dir=Sup (+)/Inf(-), 3-dir=Rt(+)/Lt(-).

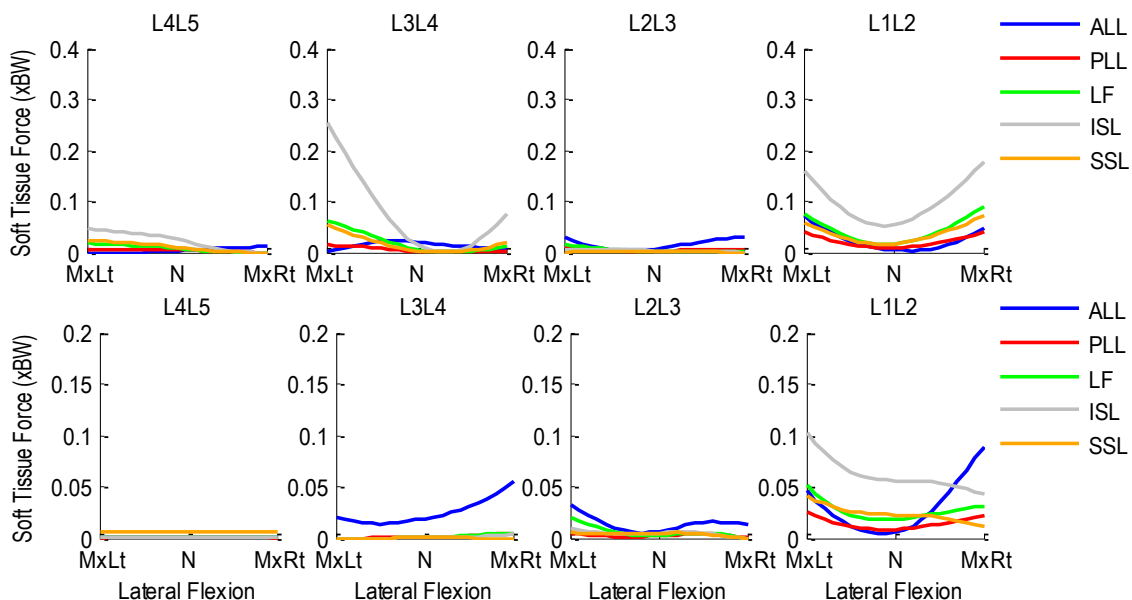


Figure A.439 Patient 7F pre- (top row) and post-operative (bottom row) segmental ligament forces normalized with respect to body weight during left-to-right lateral flexion.

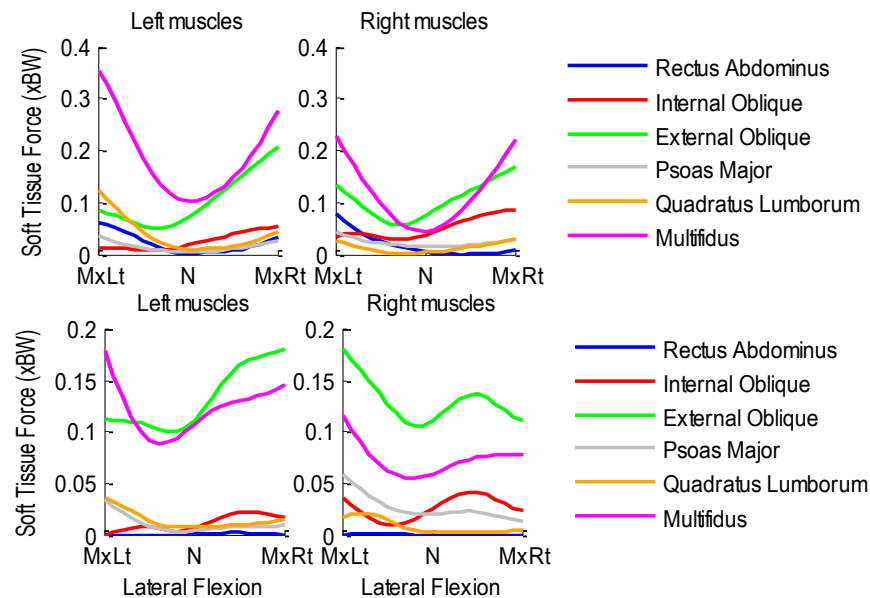


Figure A.440 Patient 7F pre- (top row) and post-operative (bottom row) bilateral muscle forces normalized with respect to body weight during left-to-right lateral flexion.

A.37.3 Axial Rotation Activity

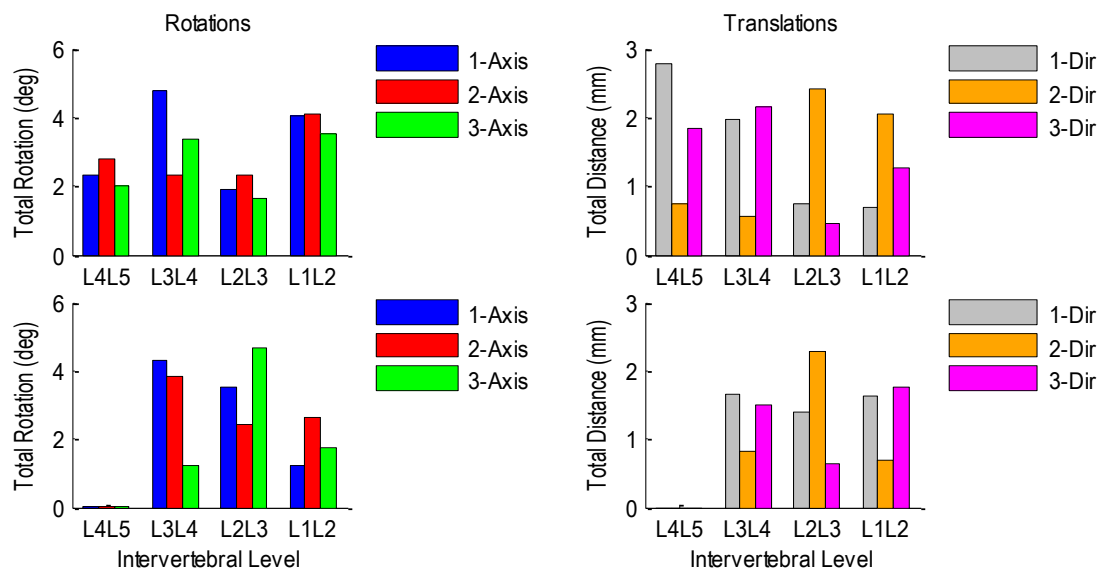


Figure A.441 Patient 7F pre-operative (top row) and post-operative (bottom row) relative rotations (left) and translations (right) at each vertebral level during left-to-right axial rotation.

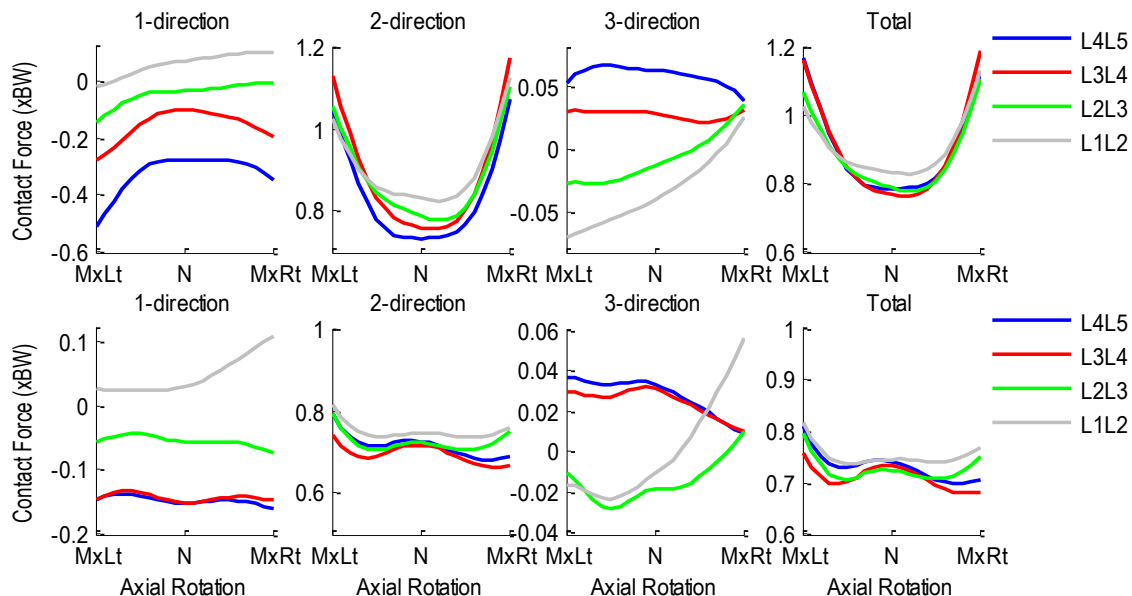


Figure A.442 Patient 7F pre- (top row) and post-operative (bottom row) intervertebral contact forces normalized with respect to body weight during left-to-right axial rotation. 1-dir=Ant(+)/Post(-), 2-dir=Sup(+)/Inf(-), 3-dir=Rt(+)/Lt(-).

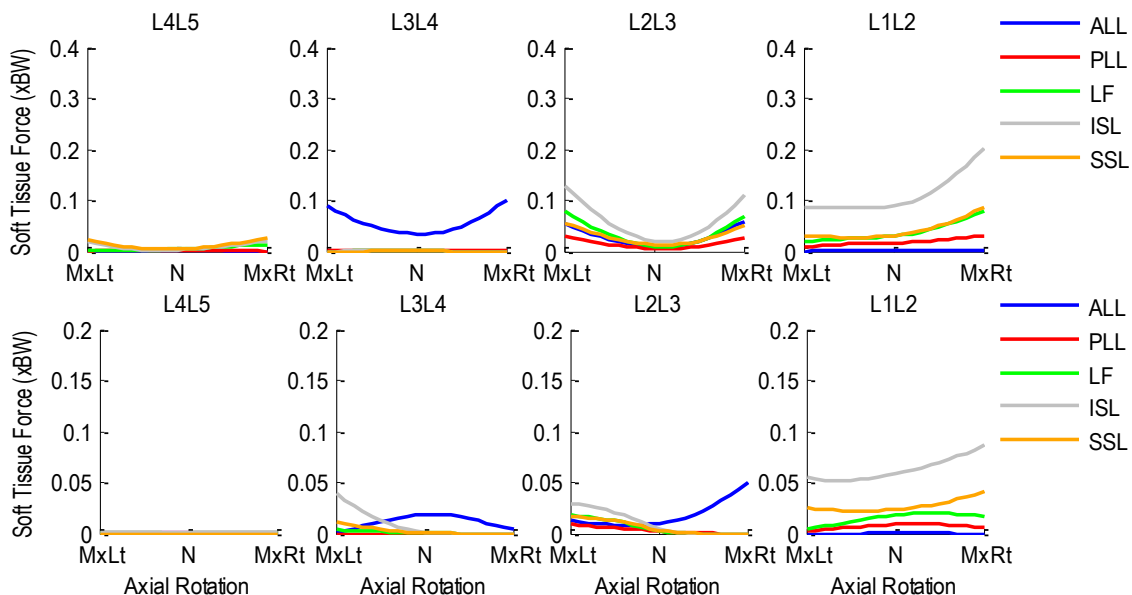


Figure A.443 Patient 7F pre- (top row) and post-operative (bottom row) segmental ligament forces normalized with respect to body weight during left-to-right axial rotation.

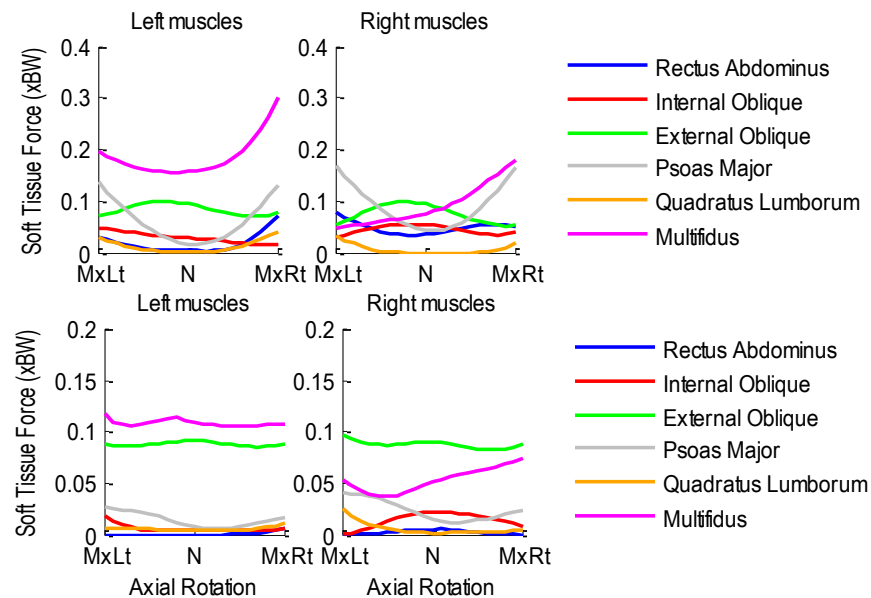


Figure A.444 Patient 7F pre- (top row) and post-operative (bottom row) bilateral muscle forces normalized with respect to body weight during left-to-right axial rotation.

A.38 Patient 8F

Age: 62 years

Gender: Male

Height: 1.85 m

Mass: 108 kg

Condition: Posterior lumbar interbody fusion at L3L4 and L4L5

A.38.1 Flexion-Extension Activity

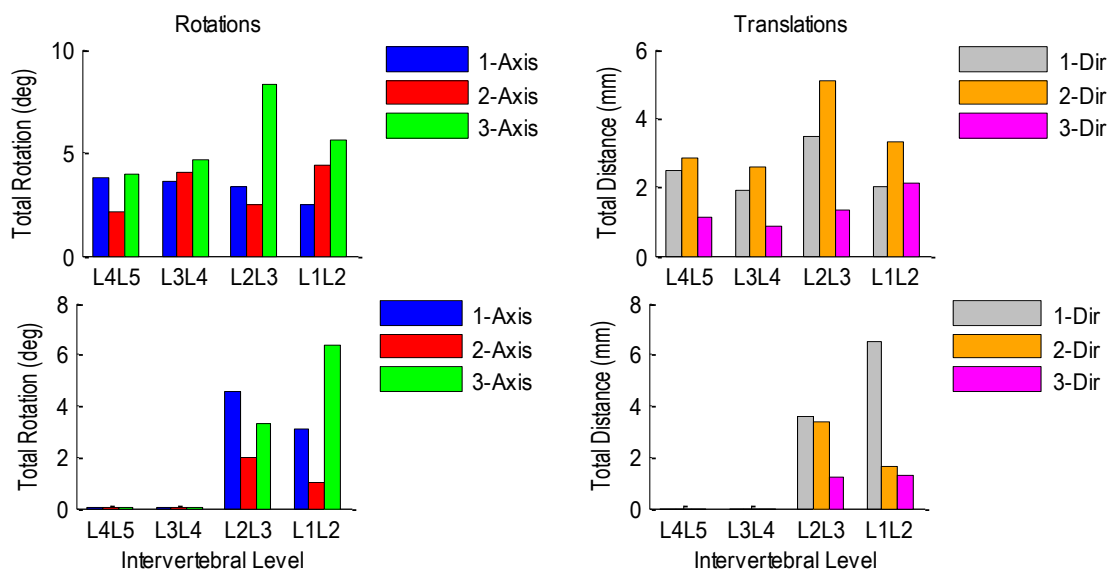


Figure A.445 Patient 8F pre-operative (top row) and post-operative (bottom row) relative rotations (left) and translations (right) at each vertebral level during flexion-extension.

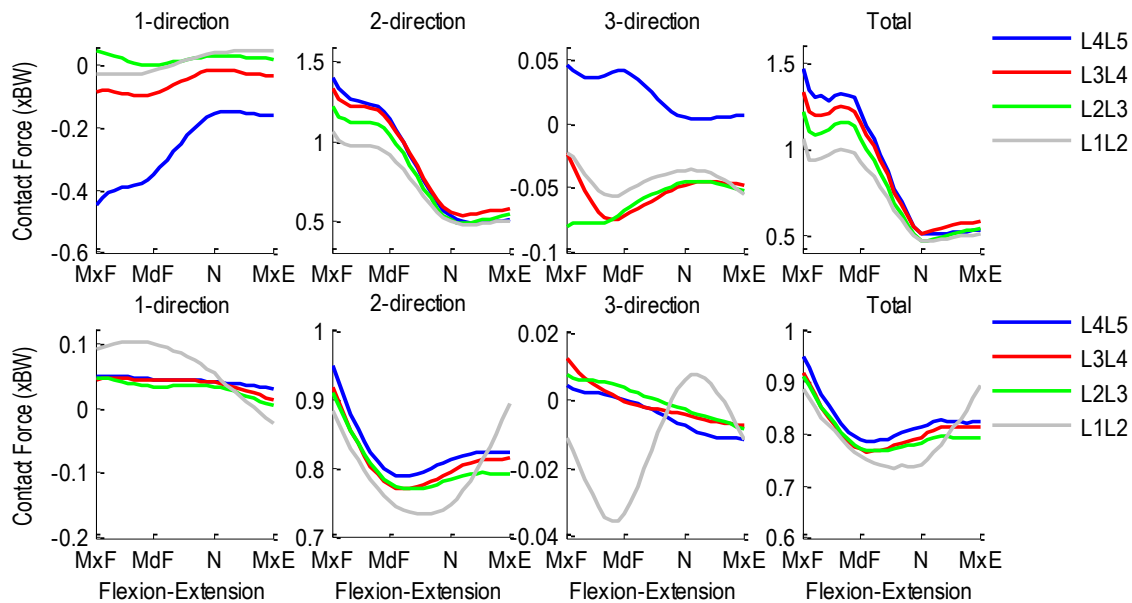


Figure A.446 Patient 8F pre- (top row) and post-operative (bottom row) segmental ligament forces normalized with respect to body weight during flexion-extension.

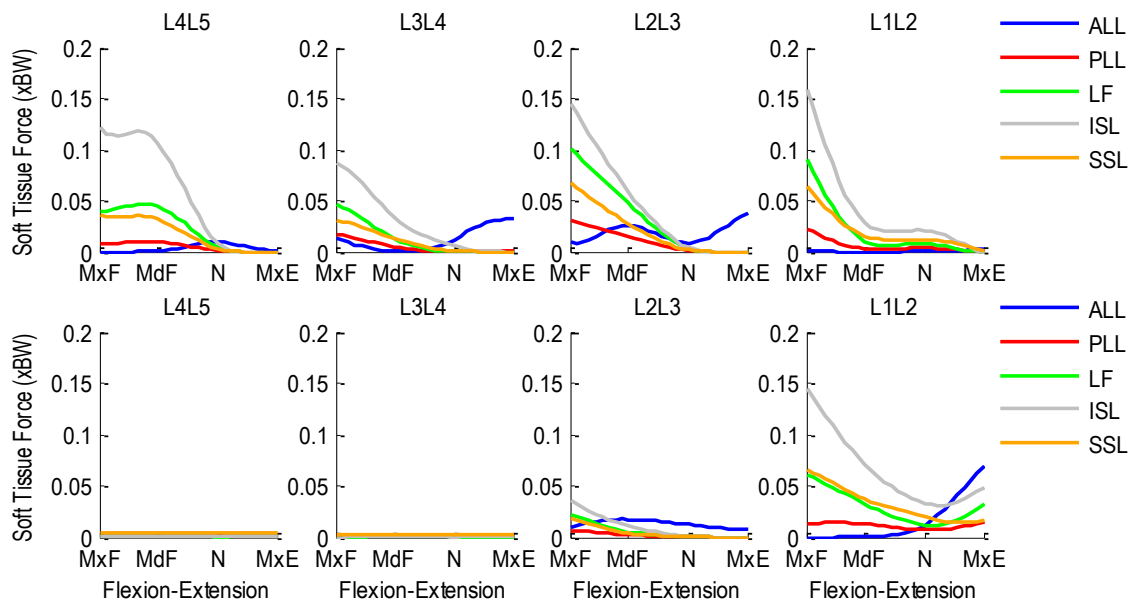


Figure A.447 Patient 8F pre- (top row) and post-operative (bottom row) segmental ligament forces normalized with respect to body weight during flexion-extension.

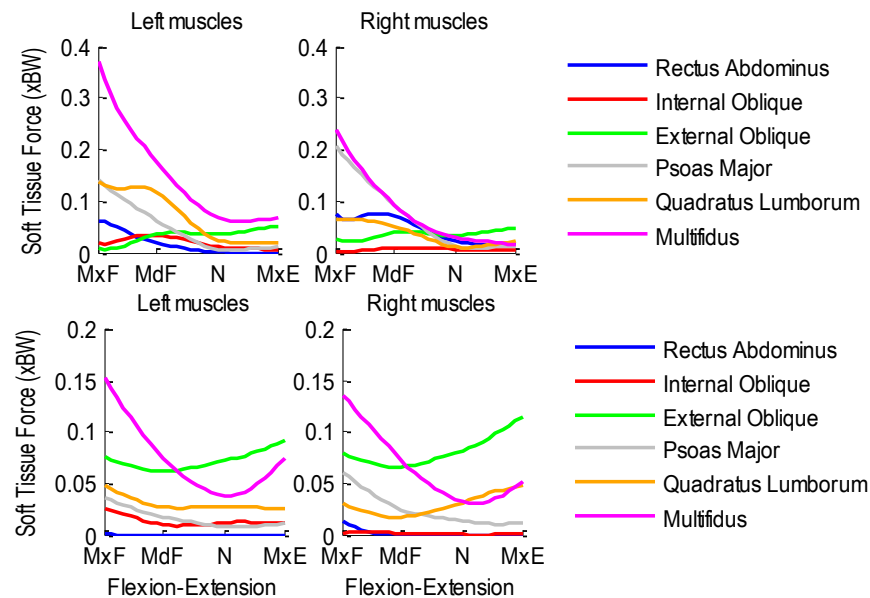


Figure A.448 Patient 8F pre- (top row) and post-operative (bottom row) bilateral muscle forces normalized with respect to body weight during flexion-extension.

A.38.2 Lateral Flexion Activity

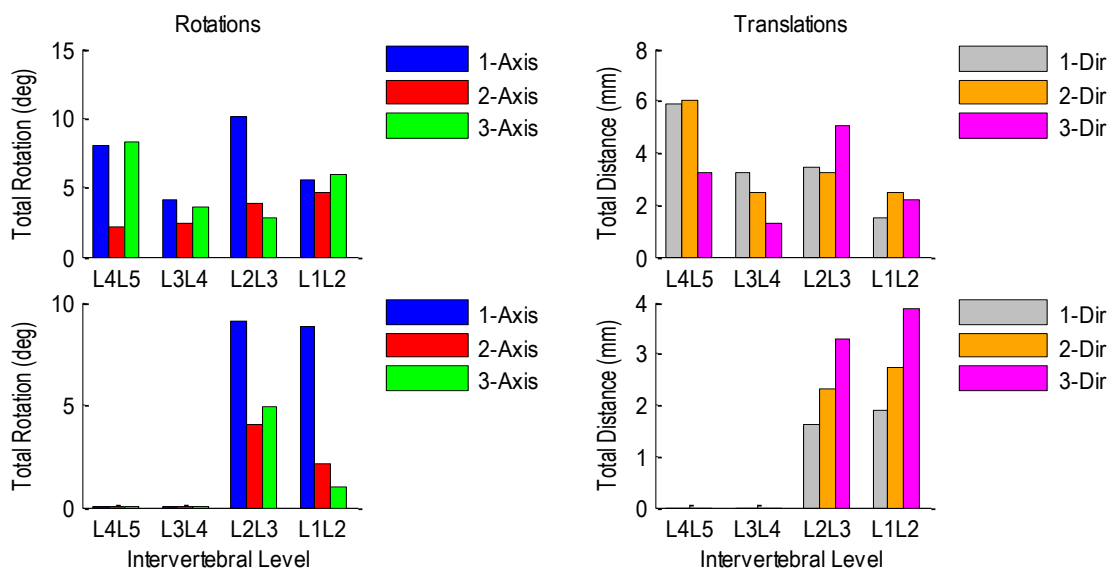


Figure A.449 Patient 8F pre-operative (top row) and post-operative (bottom row) relative rotations (left) and translations (right) at each vertebral level during left-to-right lateral flexion.

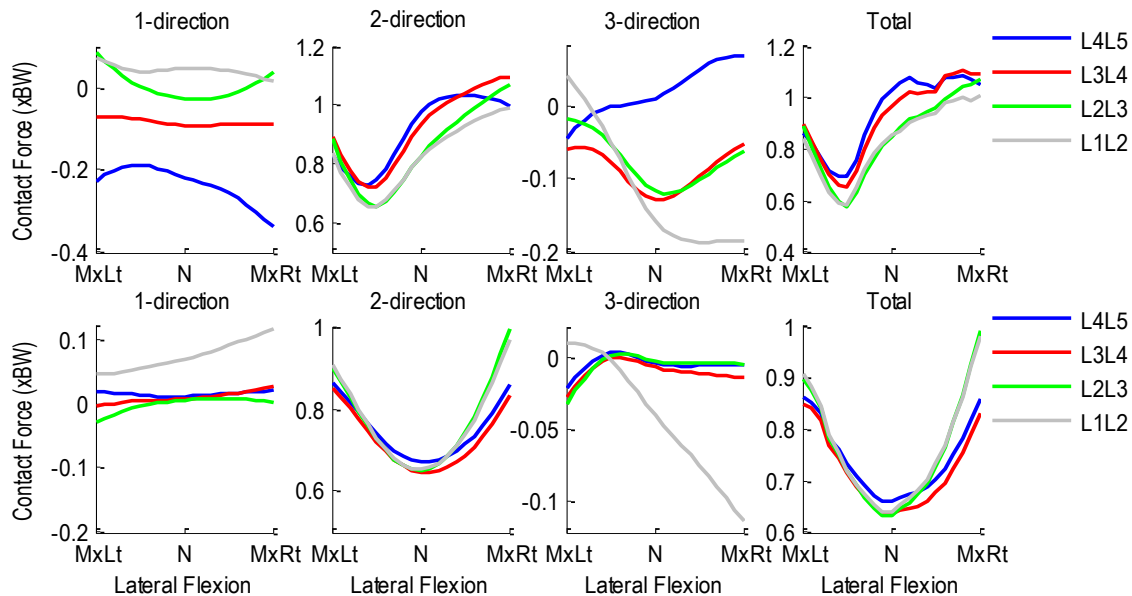


Figure A.450 Patient 8F pre- (top row) and post-operative (bottom row) intervertebral contact forces normalized with respect to body weight during right-to-left lateral flexion. 1-dir=Ant(+)/Post(-), 2-dir=Sup (+)/Inf(-), 3-dir=Rt(+)/Lt(-).

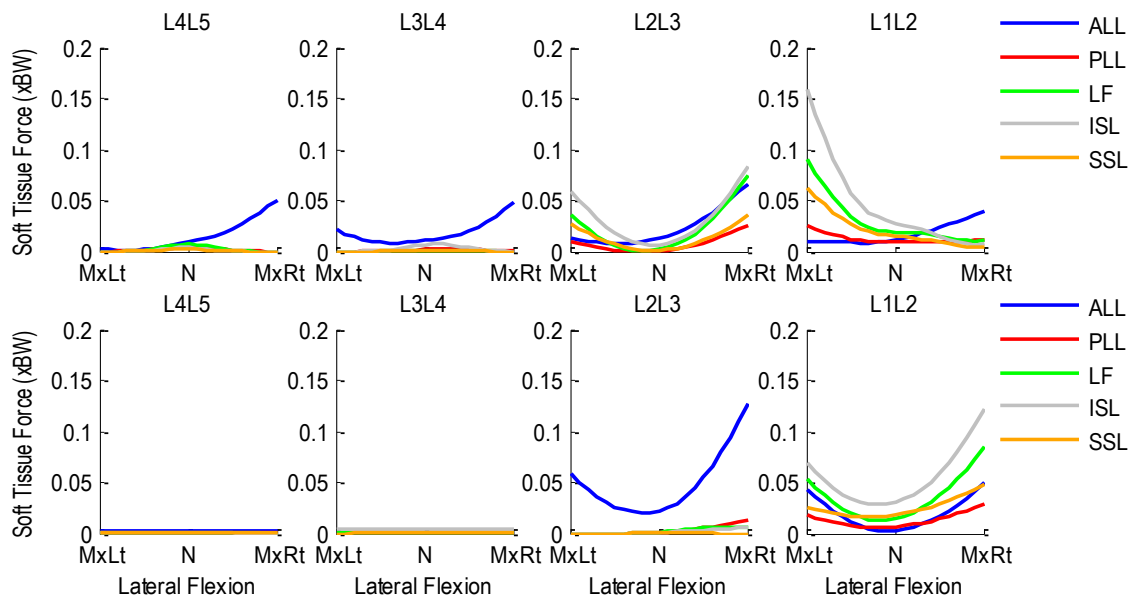


Figure A.451 Patient 8F pre- (top row) and post-operative (bottom row) segmental ligament forces normalized with respect to body weight during left-to-right lateral flexion.

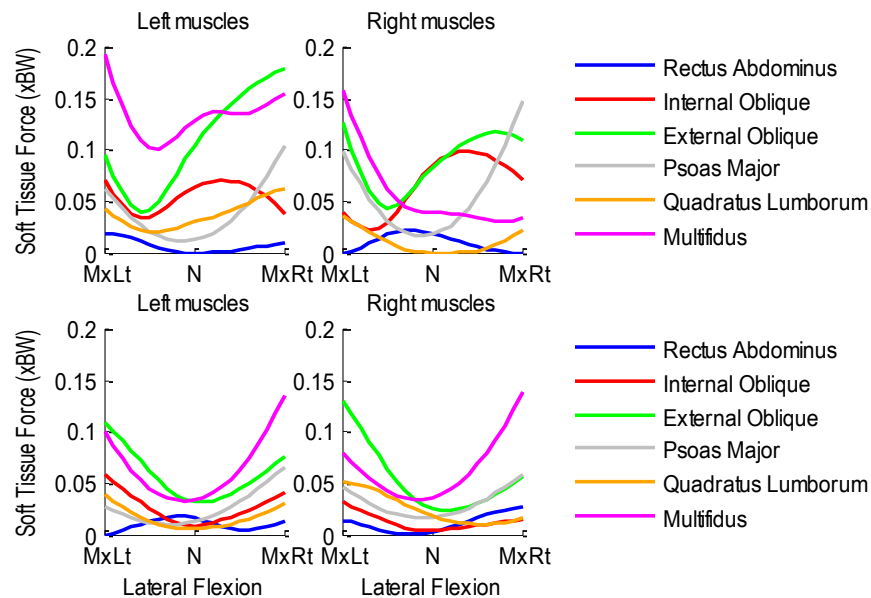


Figure A.452 Patient 8F pre- (top row) and post-operative (bottom row) bilateral muscle forces normalized with respect to body weight during left-to-right lateral flexion.

A.38.3 Axial Rotation Activity

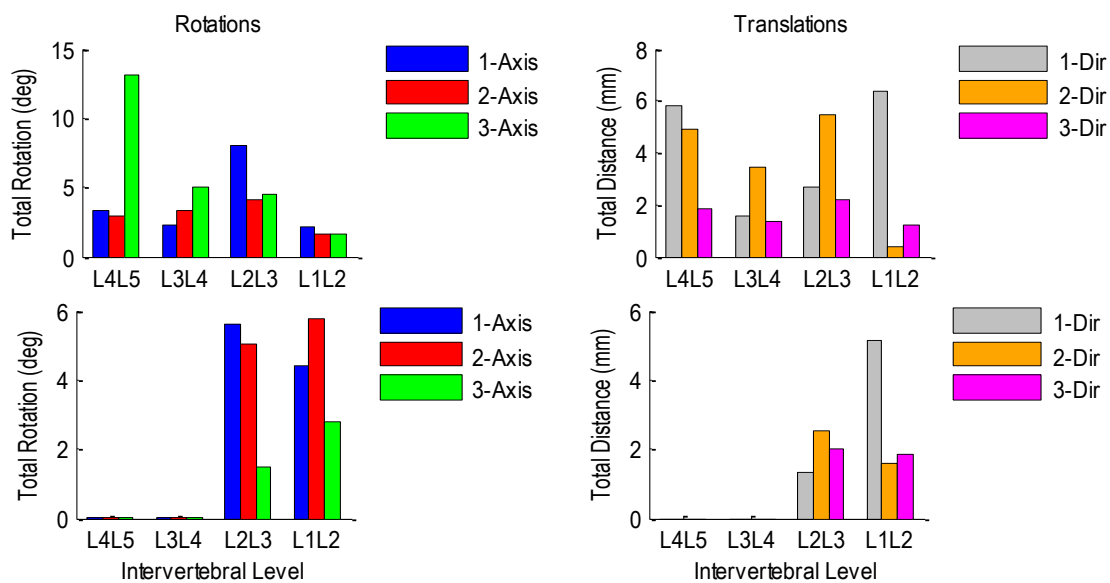


Figure A.453 Patient 8F pre-operative (top row) and post-operative (bottom row) relative rotations (left) and translations (right) at each vertebral level during left-to-right axial rotation.

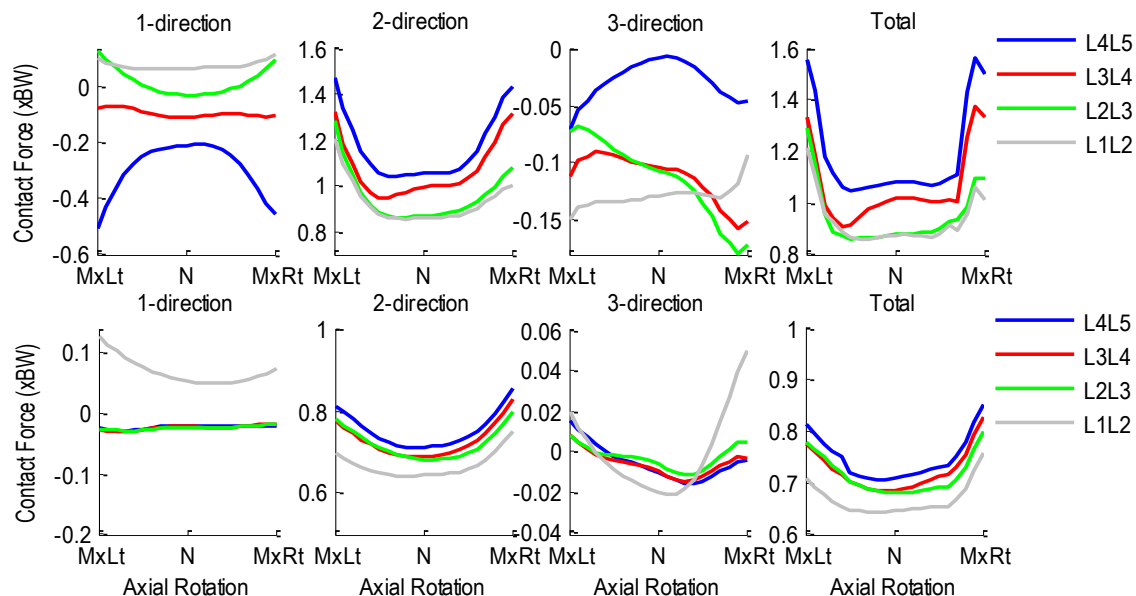


Figure A.454 Patient 8F pre- (top row) and post-operative (bottom row) intervertebral contact forces normalized with respect to body weight during left-to-right axial rotation. 1-dir=Ant(+)/Post(-), 2-dir=Sup(+)/Inf(-), 3-dir=Rt(+)/Lt(-).

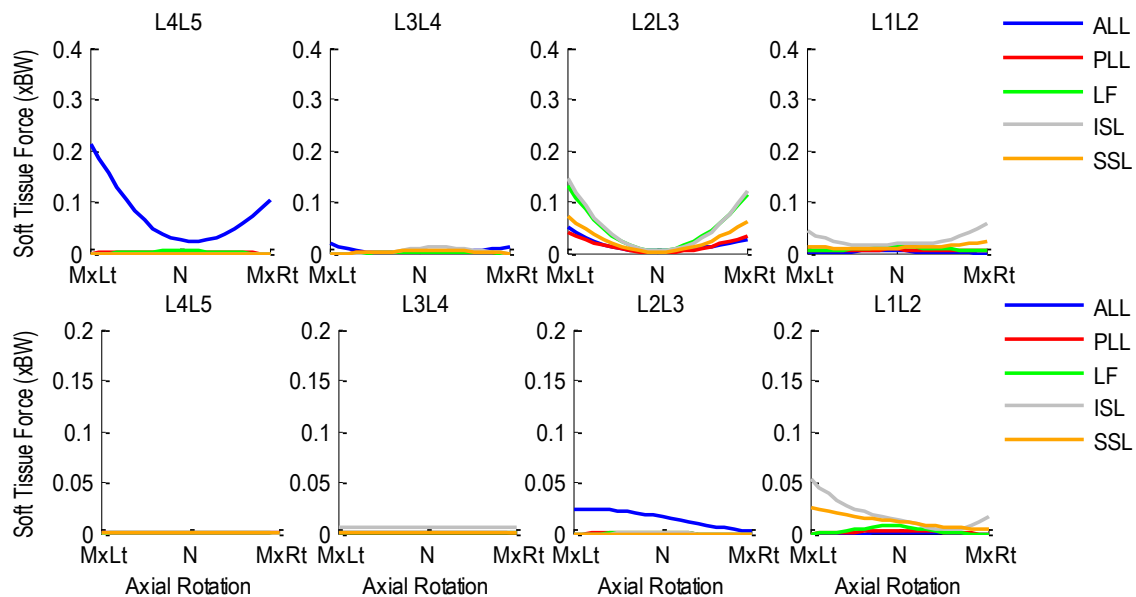


Figure A.455 Patient 8F pre- (top row) and post-operative (bottom row) segmental ligament forces normalized with respect to body weight during left-to-right axial rotation.

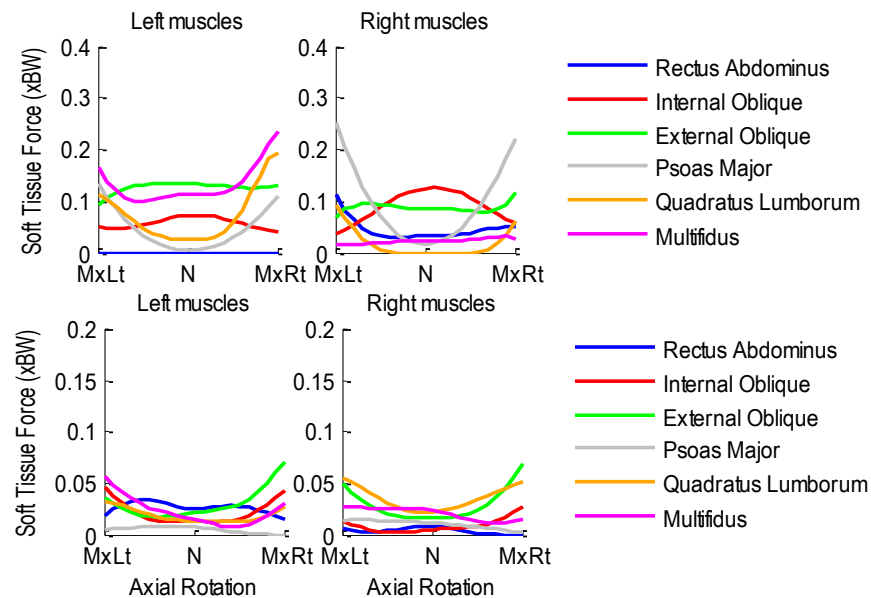


Figure A.456 Patient 8F pre- (top row) and post-operative (bottom row) bilateral muscle forces normalized with respect to body weight during left-to-right axial rotation.

A.39 Patient 9F

Age: 60 years

Gender: Male

Height: 1.78 m

Mass: 87 kg

Condition: Posterior lumbar interbody fusion at L4L5 and L5S1

A.39.1 Flexion-Extension Activity

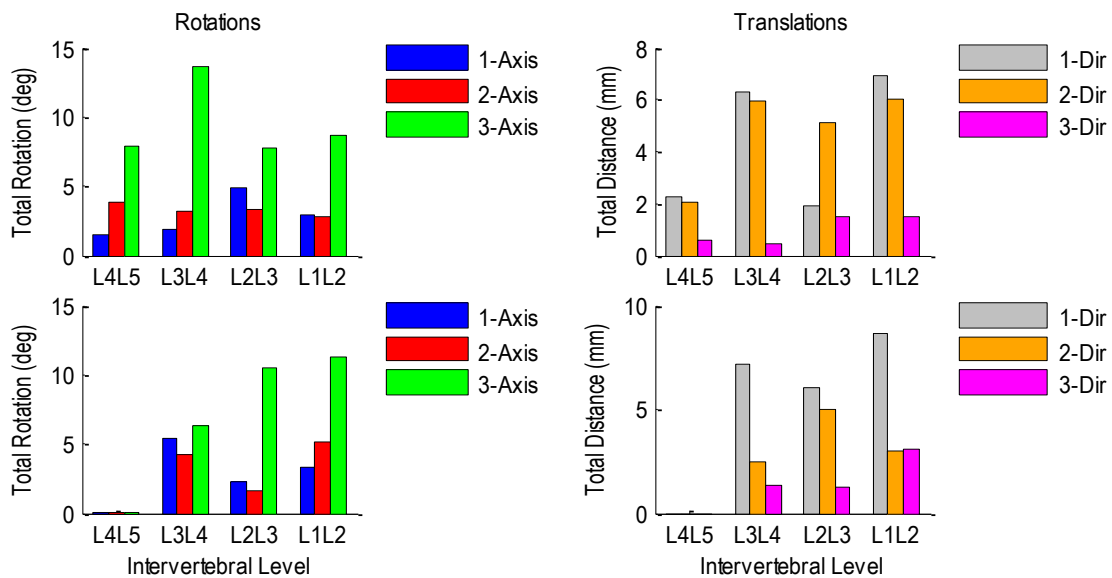


Figure A.457 Patient 9F pre-operative (top row) and post-operative (bottom row) relative rotations (left) and translations (right) at each vertebral level during flexion-extension.

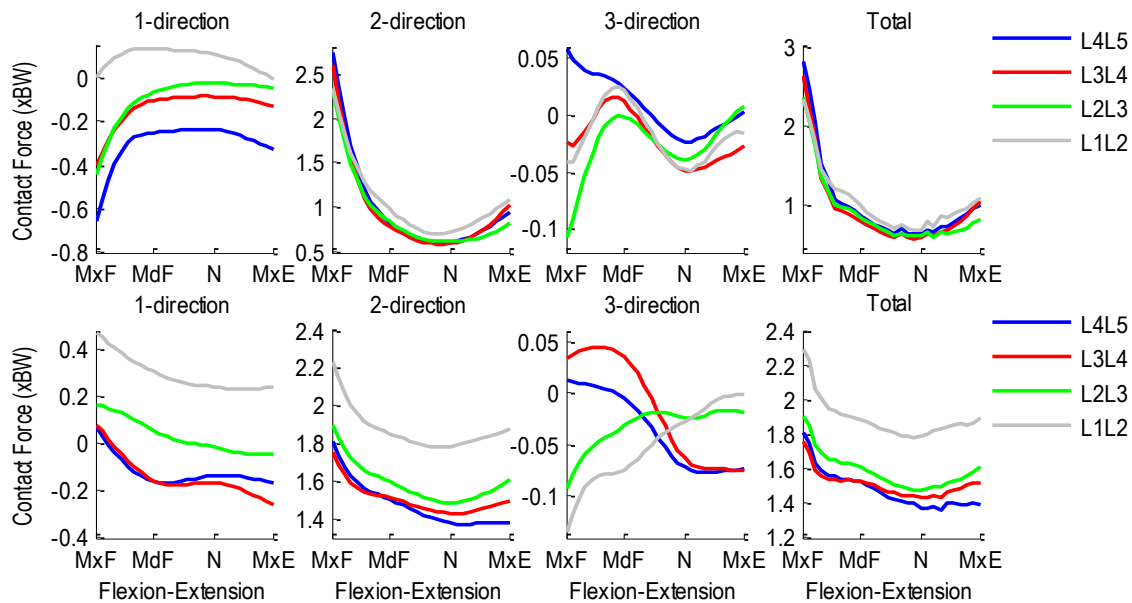


Figure A.458 Patient 9F pre- (top row) and post-operative (bottom row) segmental ligament forces normalized with respect to body weight during flexion-extension.

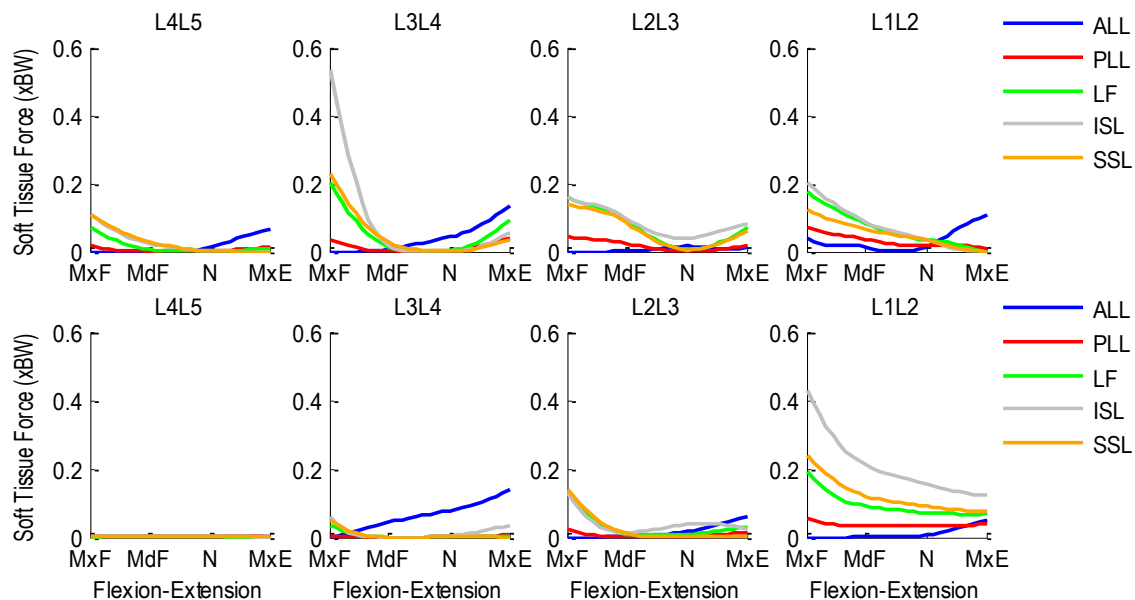


Figure A.459 Patient 9F pre- (top row) and post-operative (bottom row) segmental ligament forces normalized with respect to body weight during flexion-extension.

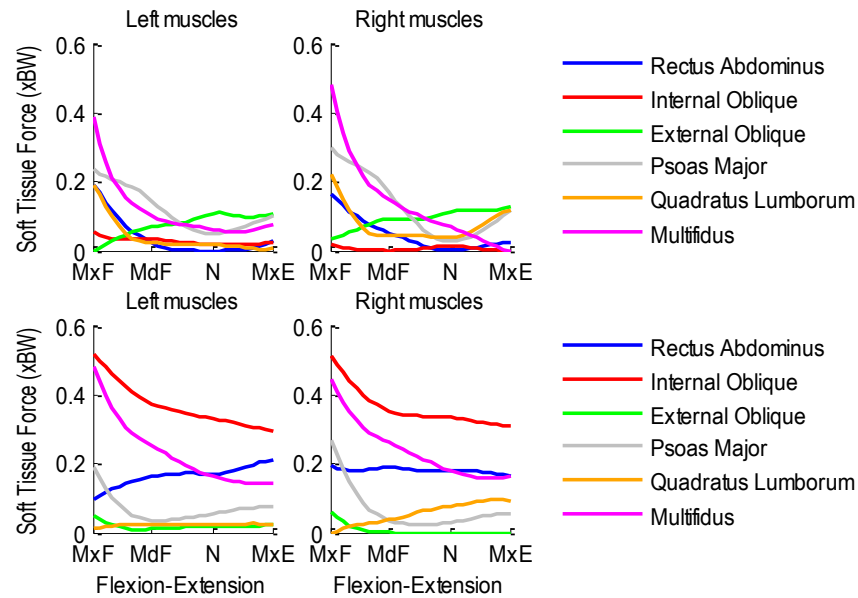


Figure A.460 Patient 9F pre- (top row) and post-operative (bottom row) bilateral muscle forces normalized with respect to body weight during flexion-extension.

A.39.2 Lateral Flexion Activity

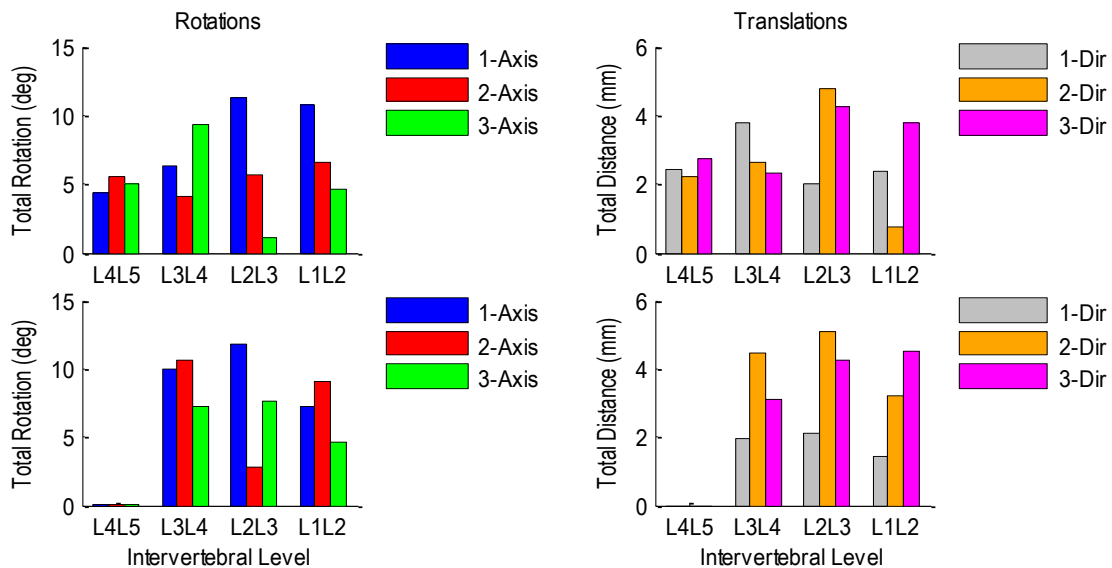


Figure A.461 Patient 9F pre-operative (top row) and post-operative (bottom row) relative rotations (left) and translations (right) at each vertebral level during left-to-right lateral flexion.

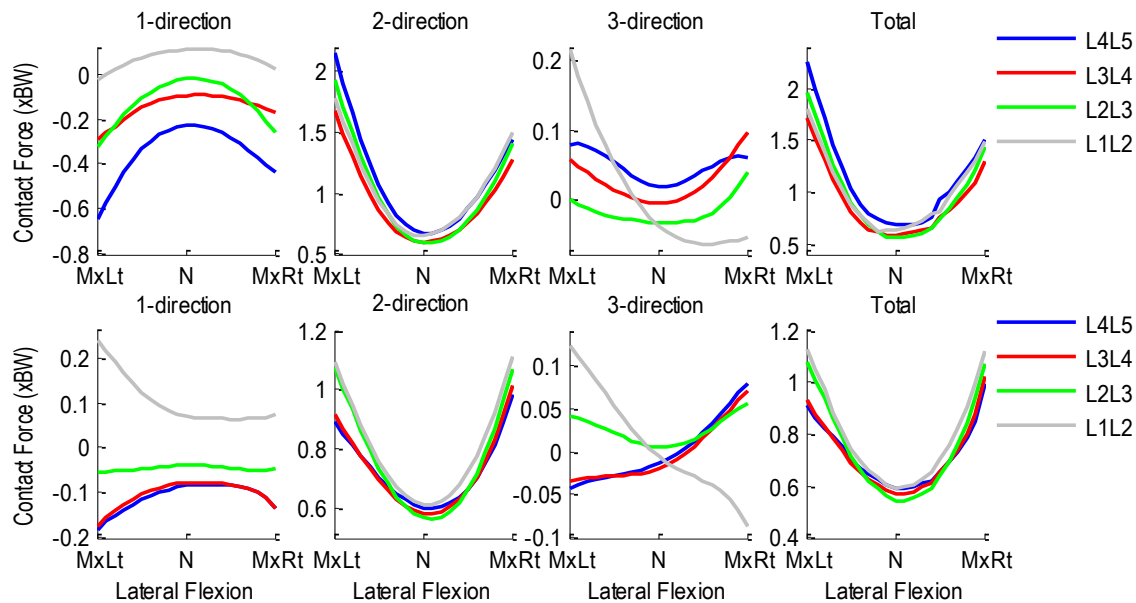


Figure A.462 Patient 9F pre- (top row) and post-operative (bottom row) intervertebral contact forces normalized with respect to body weight during right-to-left lateral flexion. 1-dir=Ant(+)/Post(-), 2-dir=Sup (+)/Inf(-), 3-dir=Rt(+)/Lt(-).

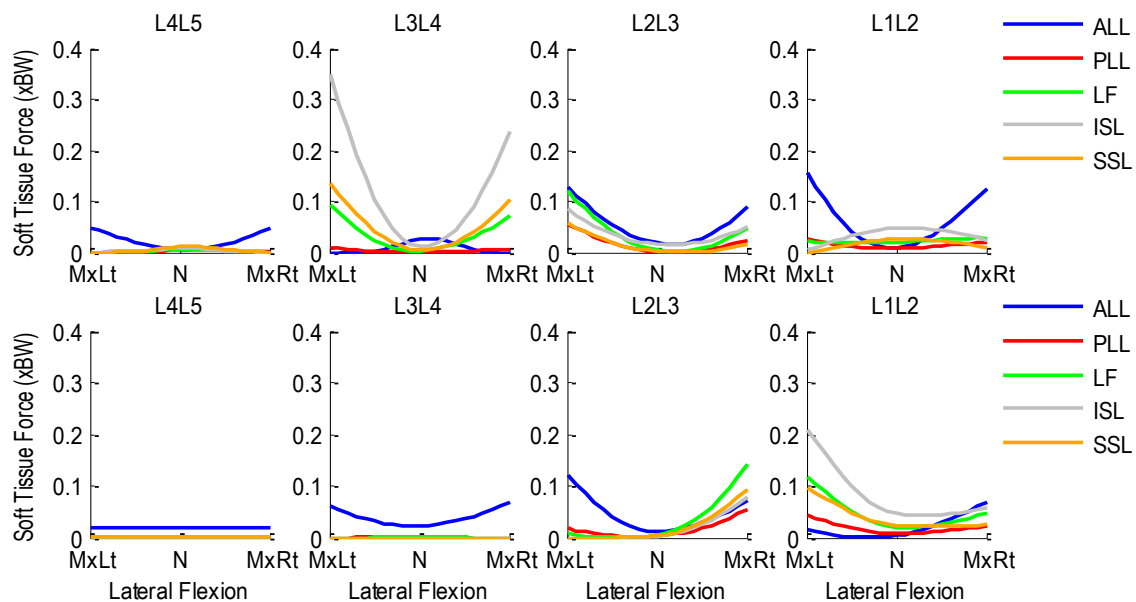


Figure A.463 Patient 9F pre- (top row) and post-operative (bottom row) segmental ligament forces normalized with respect to body weight during left-to-right lateral flexion.

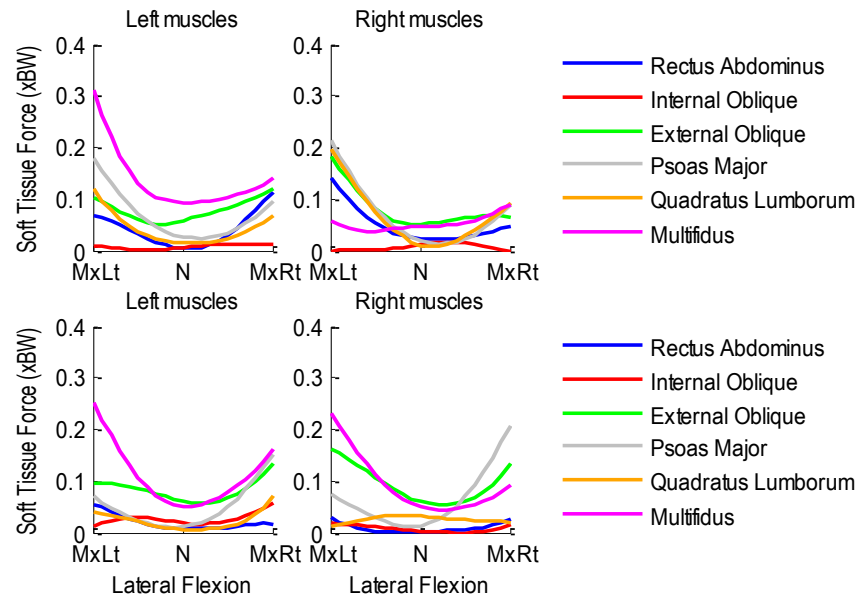


Figure A.464 Patient 9F pre- (top row) and post-operative (bottom row) bilateral muscle forces normalized with respect to body weight during left-to-right lateral flexion.

A.39.3 Axial Rotation Activity

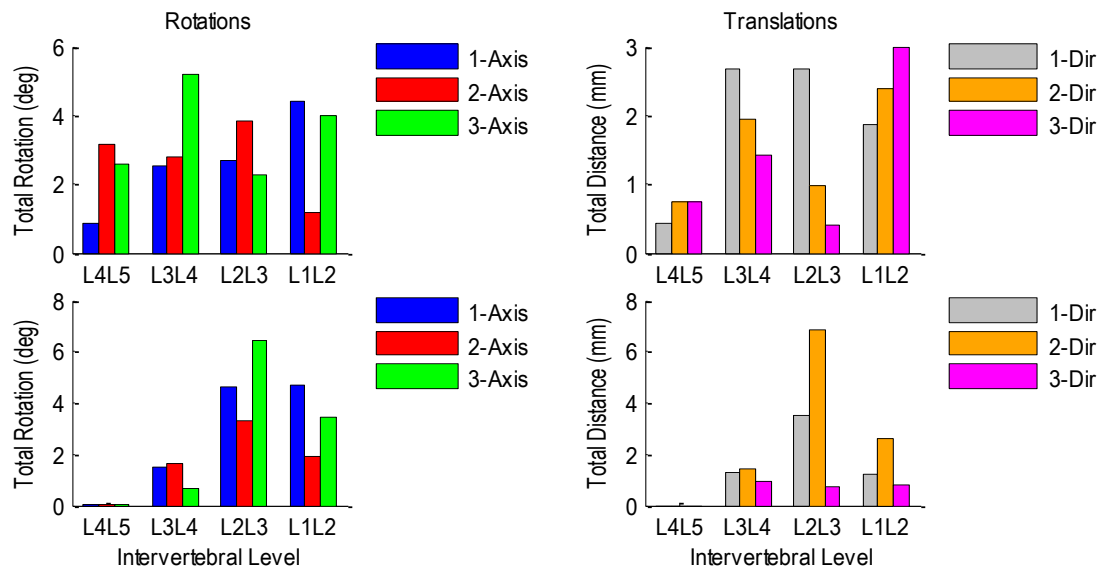


Figure A.465 Patient 9F pre-operative (top row) and post-operative (bottom row) relative rotations (left) and translations (right) at each vertebral level during left-to-right axial rotation.

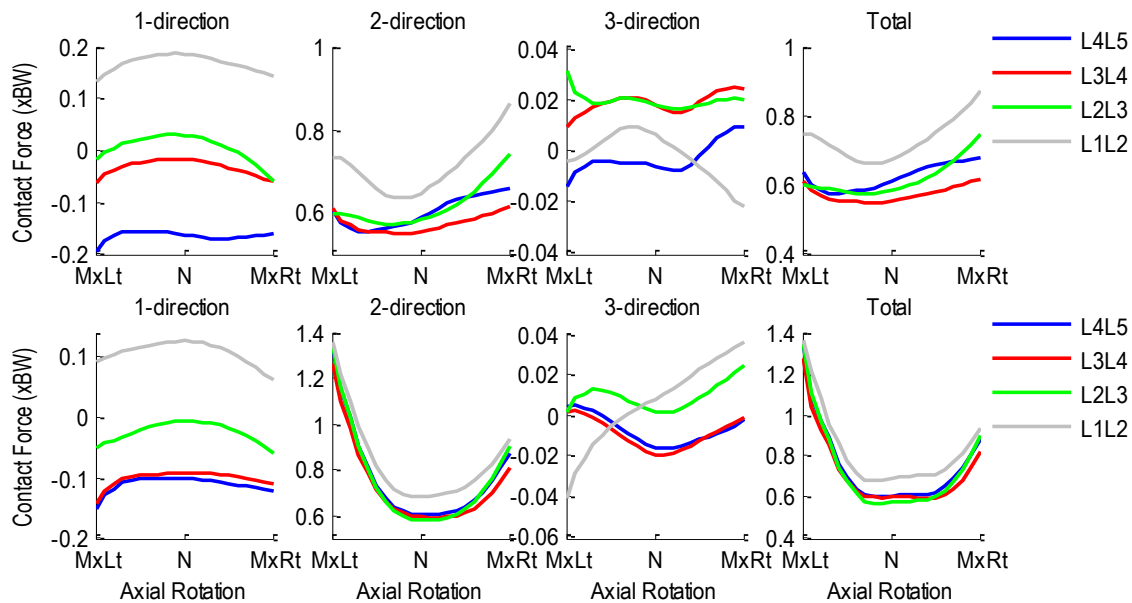


Figure A.466 Patient 9F pre- (top row) and post-operative (bottom row) intervertebral contact forces normalized with respect to body weight during left-to-right axial rotation. 1-dir=Ant(+)/Post(-), 2-dir=Sup(+)/Inf(-), 3-dir=Rt(+)/Lt(-).

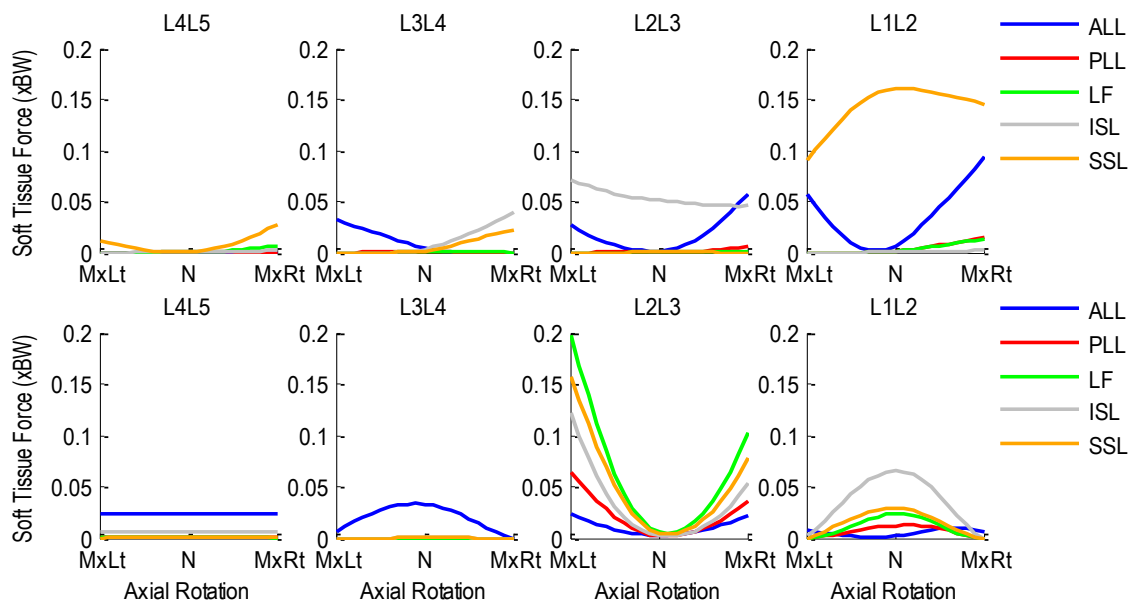


Figure A.467 Patient 9F pre- (top row) and post-operative (bottom row) segmental ligament forces normalized with respect to body weight during left-to-right axial rotation.

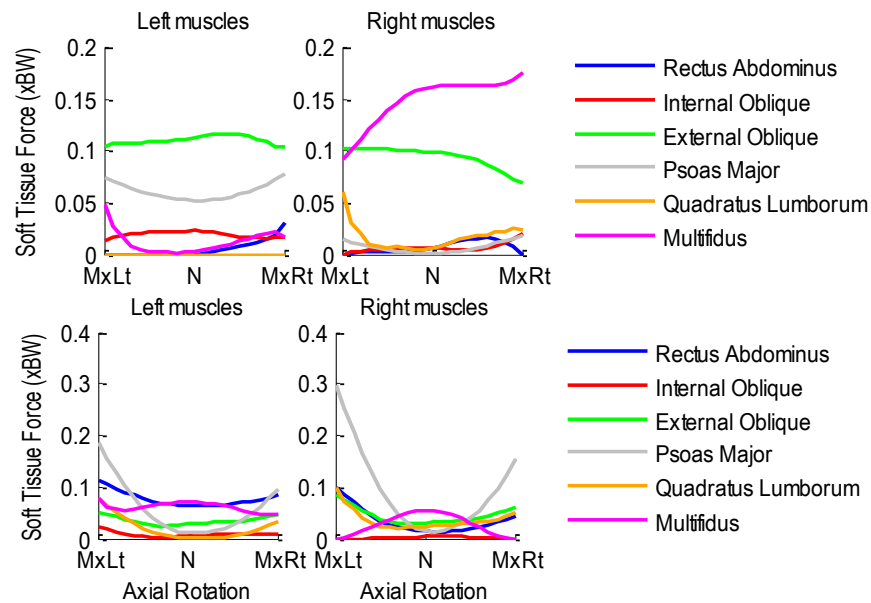


Figure A.468 Patient 9F pre- (top row) and post-operative (bottom row) bilateral muscle forces normalized with respect to body weight during left-to-right axial rotation.

A.40 Patient 10F

Age: 43 years

Gender: Male

Height: 1.88 m

Mass: 125 kg

Condition: Posterior lumbar interbody fusion at L5S1; Pt evaluated pre-operatively only

A.40.1 Flexion-Extension Activity

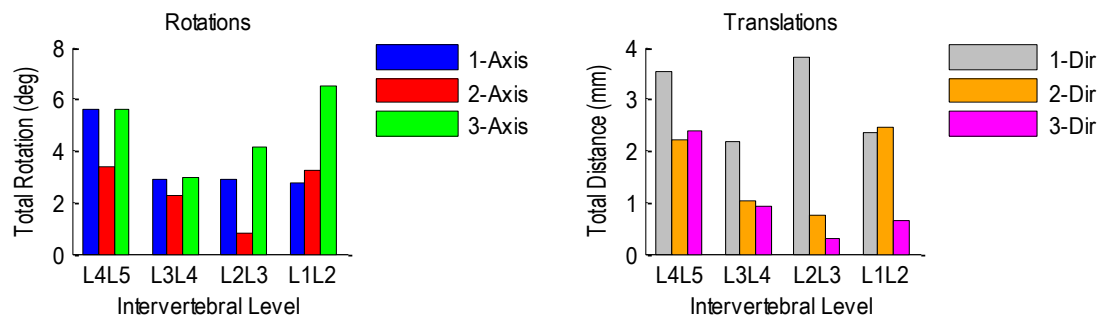


Figure A.469 Patient 10F pre-operative relative rotations (left) and translations (right) at each vertebral level during flexion-extension.

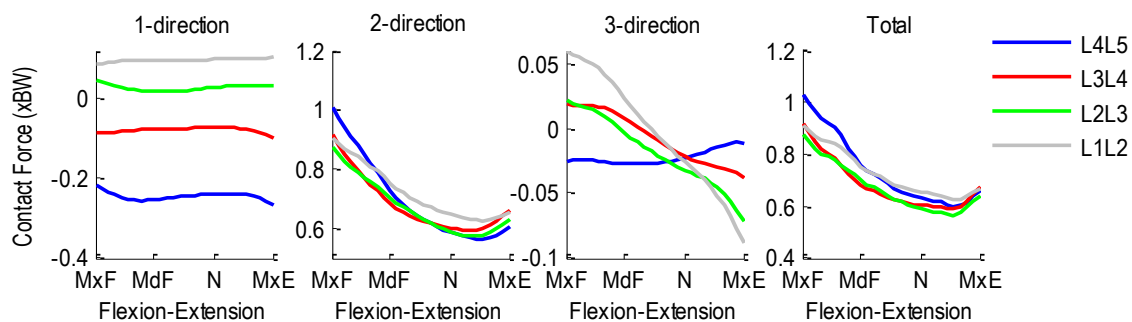


Figure A.470 Patient 10F pre-operative intervertebral contact forces normalized with respect to body weight during flexion-extension. 1-dir=Ant (+)/Post(-), 2-dir=Sup(+)/Inf(-), 3-dir=Rt (+)/Lt(-).

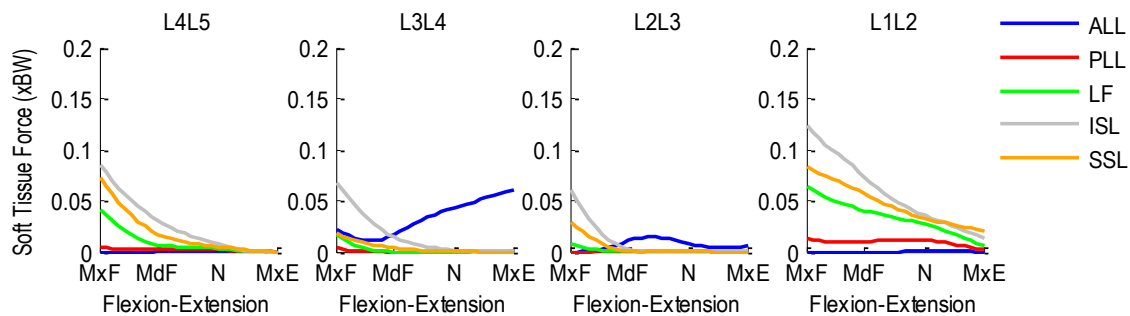


Figure A.471 Patient 10F pre-operative segmental ligament forces normalized with respect to body weight during flexion-extension

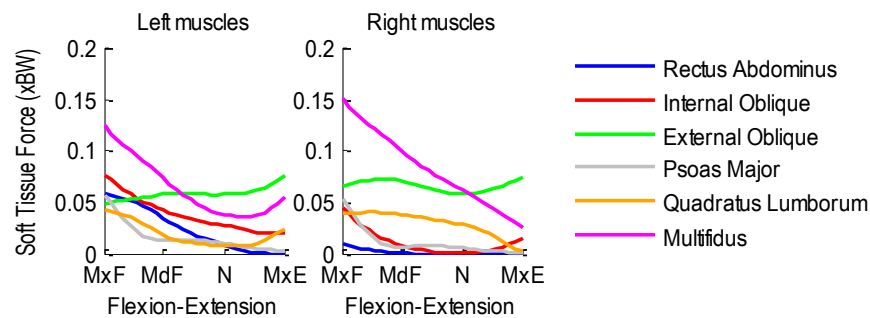


Figure A.472 Patient 10F pre-operative bilateral muscle forces normalized with respect to body weight during flexion-extension.

A.40.2 Lateral Flexion Activity

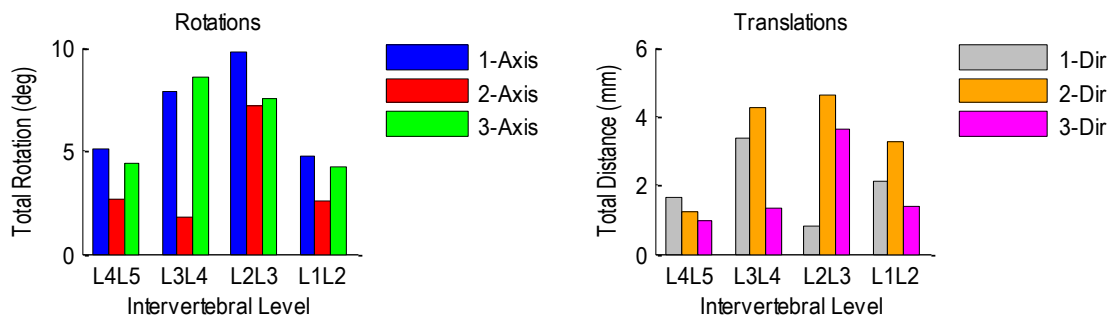


Figure A.473 Patient 10F pre-operative relative rotations (left) and translations (right) at each vertebral level during left-to-right lateral flexion.

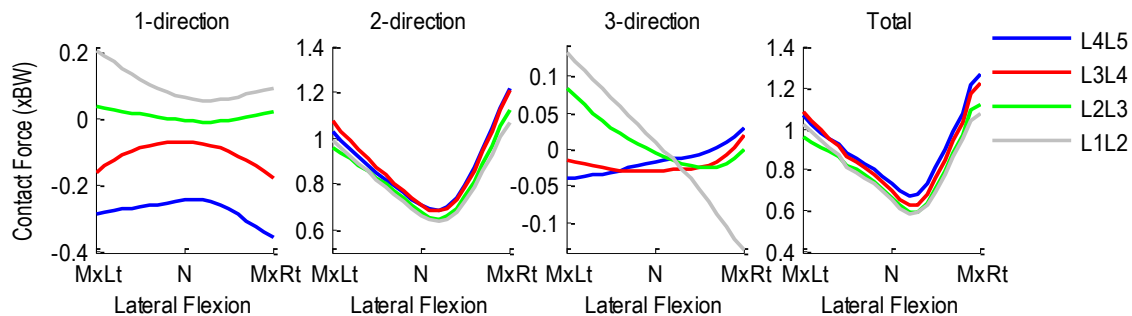


Figure A.474 Patient 10F pre-operative intervertebral contact forces normalized with respect to body weight during right-to-left lateral flexion. 1-dir= Ant (+)/Post (-), 2-dir=Sup (+)/Inf(-), 3-dir=Rt(+)/Lt(-).

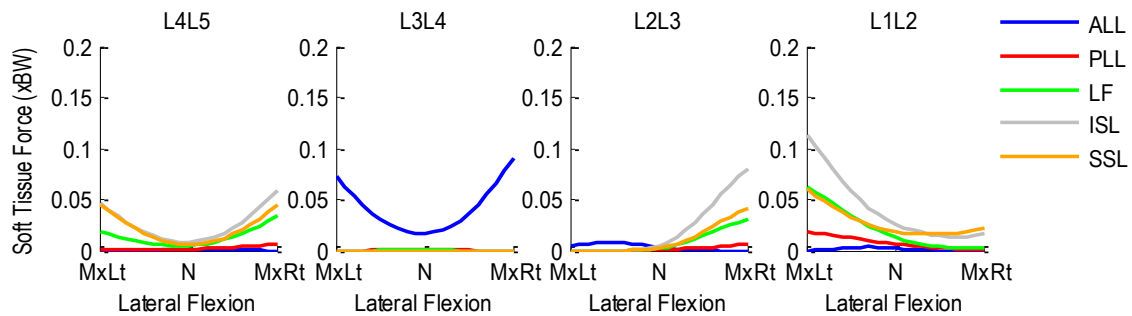


Figure A.475 Patient 10F pre-operative segmental ligament forces normalized with respect to body weight during left-to-right lateral flexion.

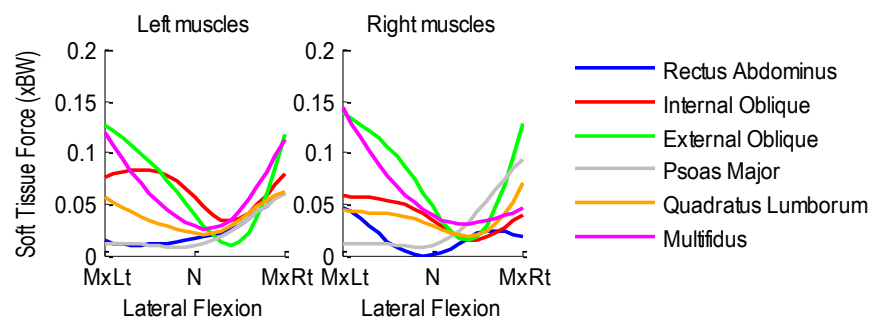


Figure A.476 Patient 10F pre-operative bilateral muscle forces normalized with respect to body weight during left-to-right lateral flexion.

A.40.3 Axial Rotation Activity

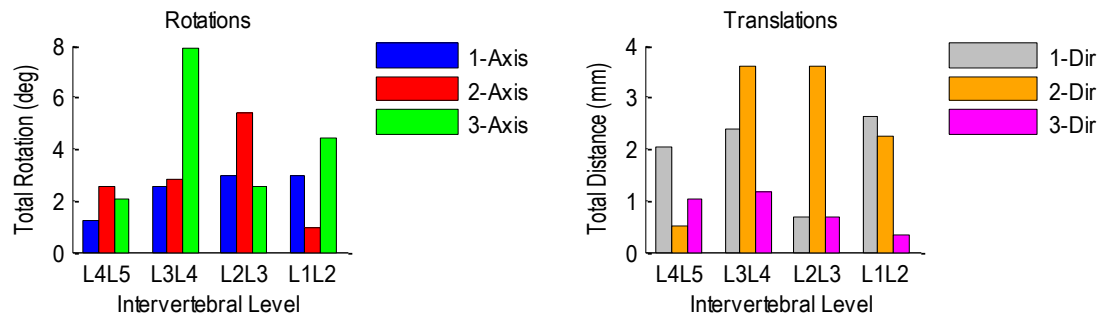


Figure A.477 Patient 10F pre-operative relative rotations (left) and translations (right) at each vertebral level during left-to-right axial rotation.

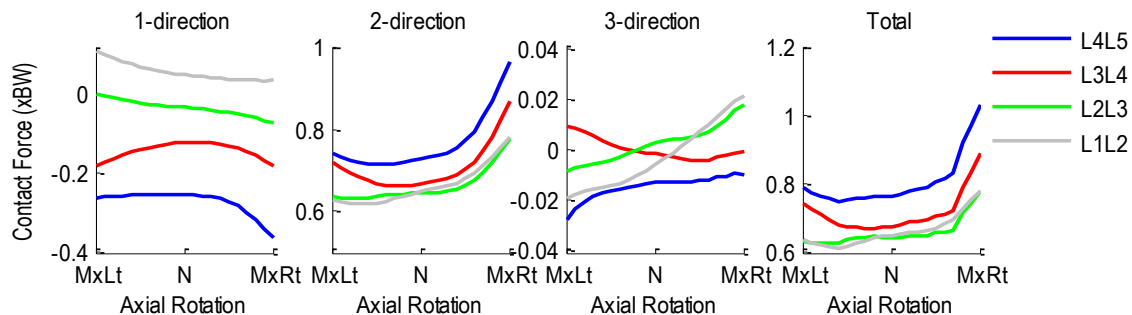


Figure A.478 Patient 10F pre-operative intervertebral contact forces normalized with respect to body weight (BW) during left-to-right axial rotation. 1-dir= Ant(+)/Post(-), 2-dir=Sup(+)/Inf(-), 3-dir=Rt(+)/Lt(-).

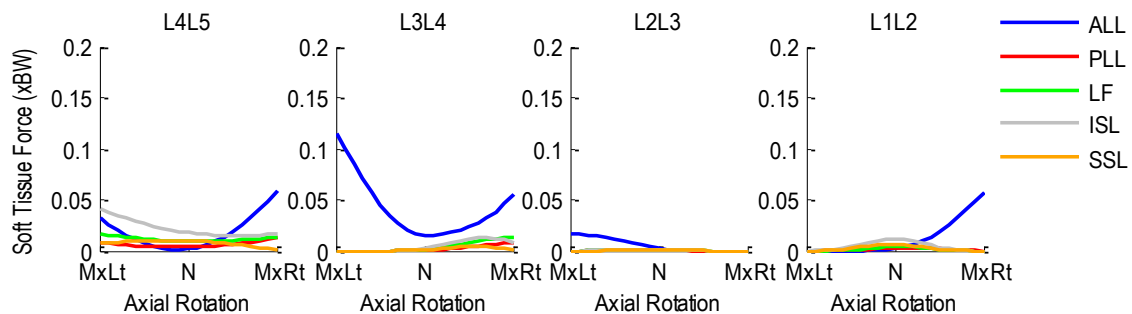


Figure A.479 Patient 10F pre-operative segmental ligament forces normalized with respect to body weight during left-to-right axial rotation.

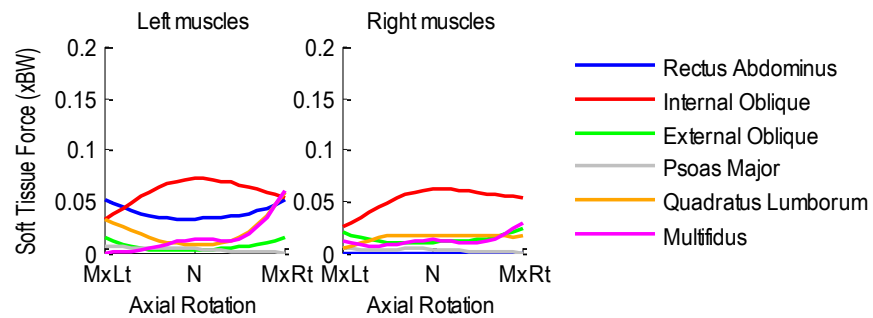


Figure A.480 Patient 10F pre-operative bilateral muscle forces normalized with respect to body weight during left-to-right axial rotation.

A.41 Patient 1HDS

Age: 41 years

Gender: Male

Height: 1.83 m

Mass: 97 kg

Condition: Posterior lumbar interbody fusion at L5S1 with dynamic stabilization at L4L5

A.41.1 Flexion-Extension Activity

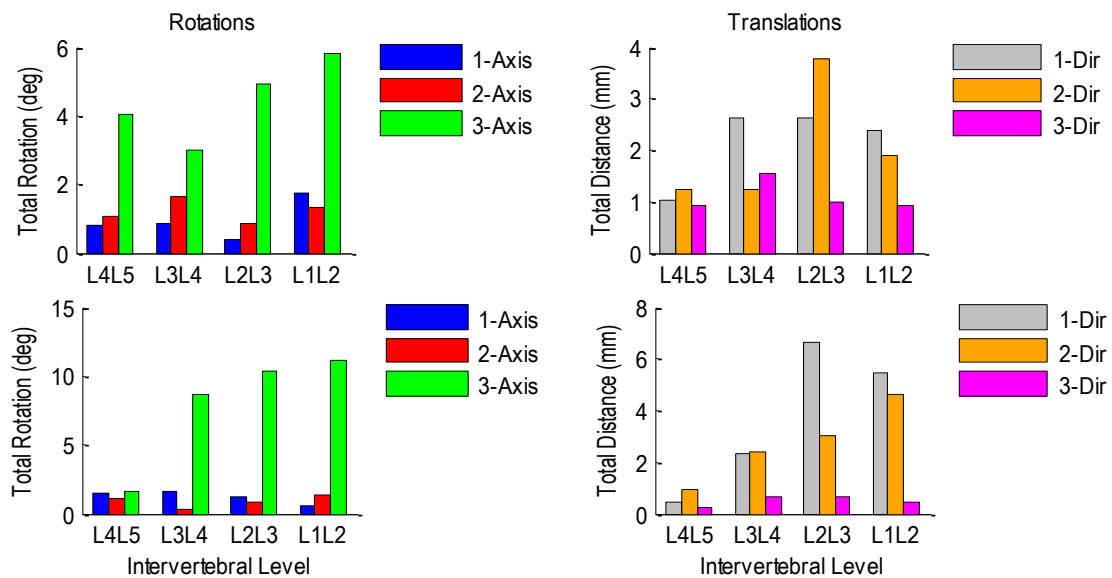


Figure A.481 Patient 1HDS pre-operative (top row) and post-operative (bottom row) relative rotations (left) and translations (right) at each vertebral level during flexion-extension.

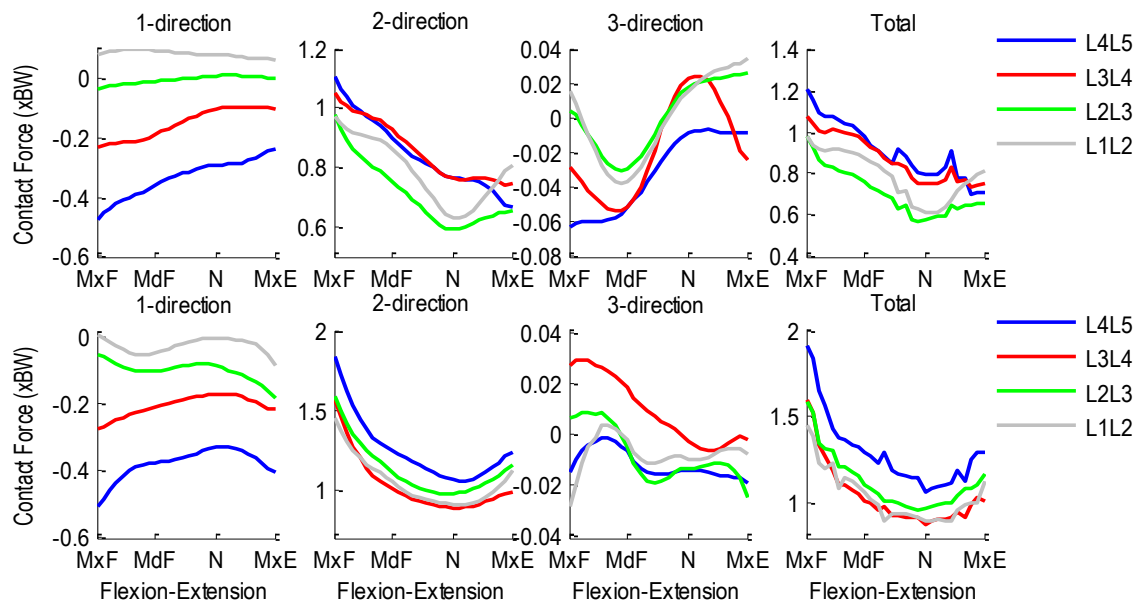


Figure A.482 Patient 1HDS pre- (top row) and post-operative (bottom row) intervertebral contact forces normalized with respect to body weight during flexion-extension. 1-dir=Ant (+)/Post(-), 2-dir=Sup(+)/Inf(-), 3-dir=Rt (+)/Lt(-).

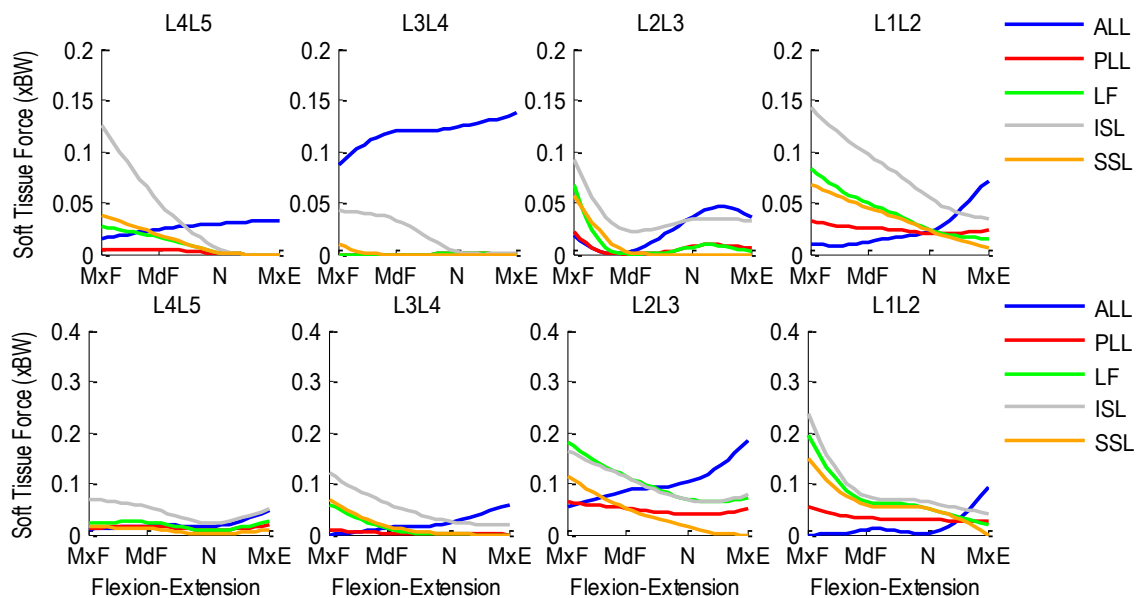


Figure A.483 Patient 1HDS pre- (top row) and post-operative (bottom row) segmental ligament forces normalized with respect to body weight during flexion-extension.

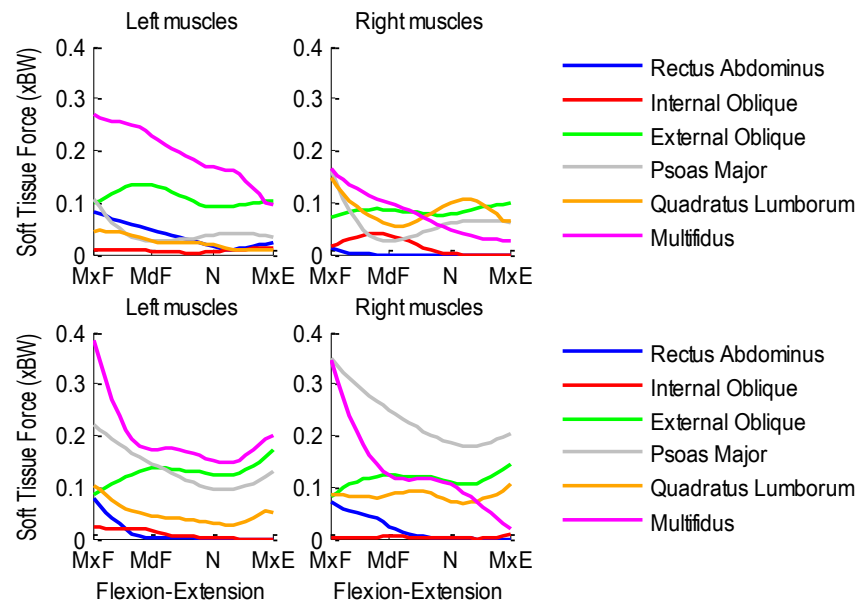


Figure A.484 Patient 1HDS pre- (top row) and post-operative (bottom row) bilateral muscle forces normalized with respect to body weight during flexion-extension.

A.41.2 Lateral Flexion Activity

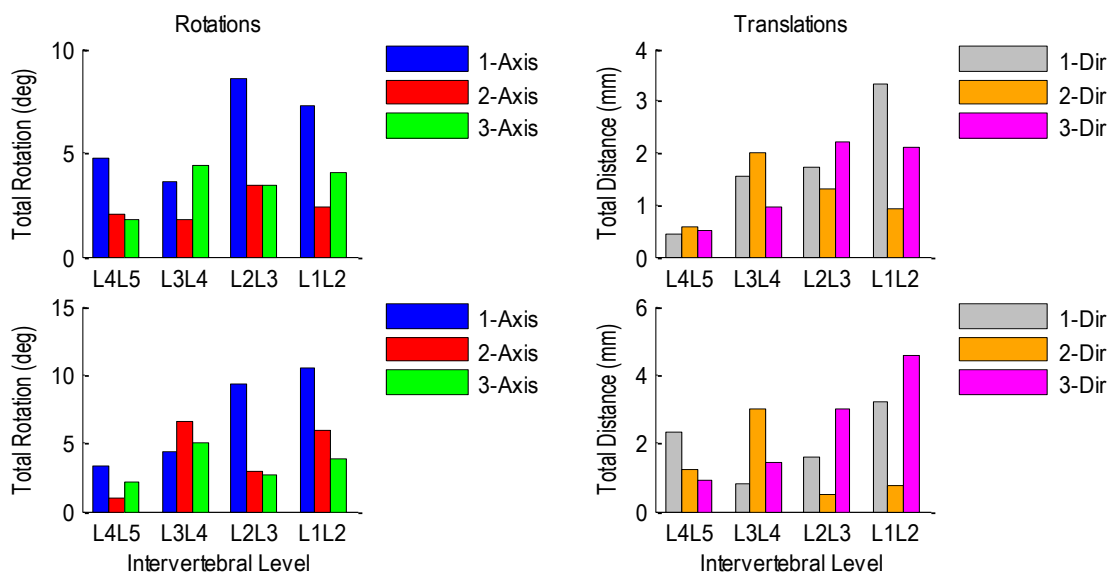


Figure A.485 Patient 1HDS pre-operative (top row) and post-operative (bottom row) relative rotations (left) and translations (right) at each vertebral level during left-to-right lateral flexion.

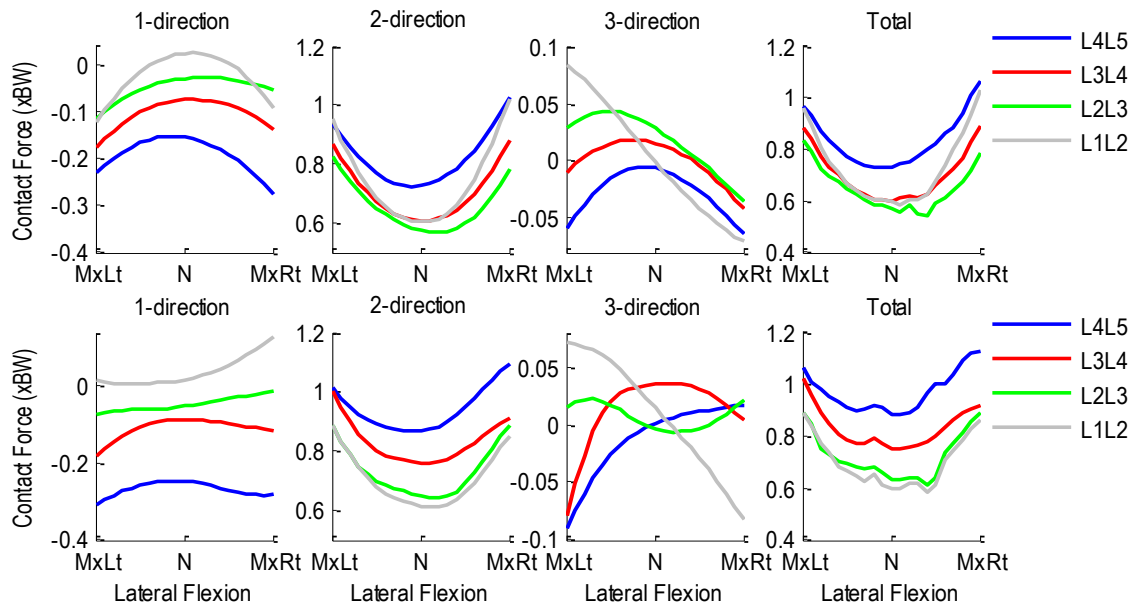


Figure A.486 Patient 1HDS pre- (top row) and post-operative (bottom row) intervertebral contact forces normalized with respect to body weight during right-to-left lateral flexion. 1-dir= Ant (+)/Post (-), 2-dir=Sup (+)/Inf(-),3-dir=Rt(+)/Lt(-).

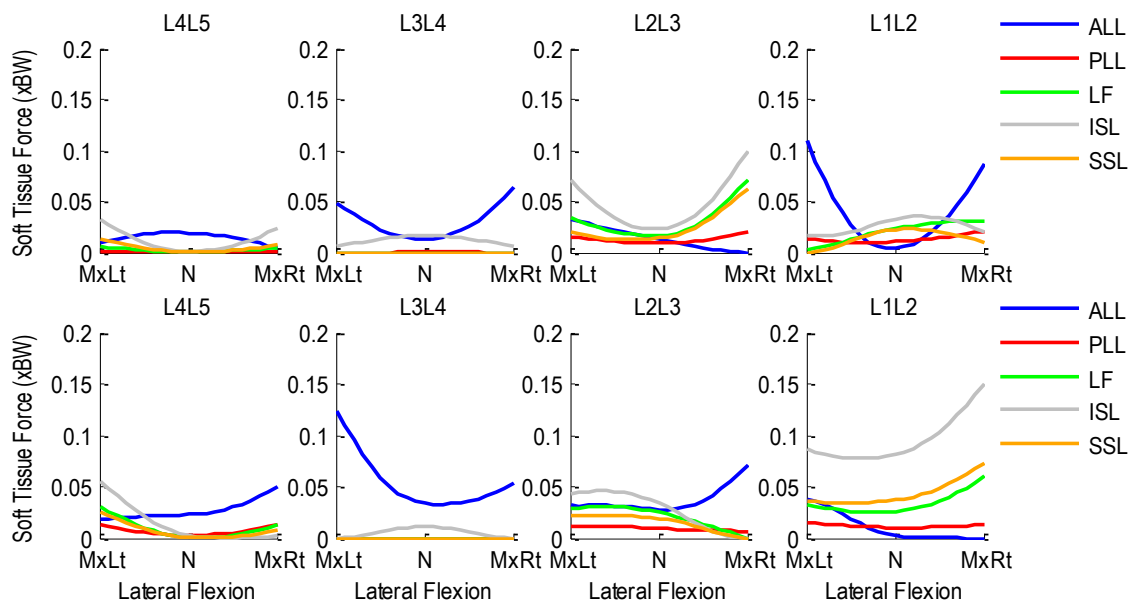


Figure A.487 Patient 1HDS pre- (top row) and post-operative (bottom row) segmental ligament forces normalized with respect to body weight during left-to-right lateral flexion.

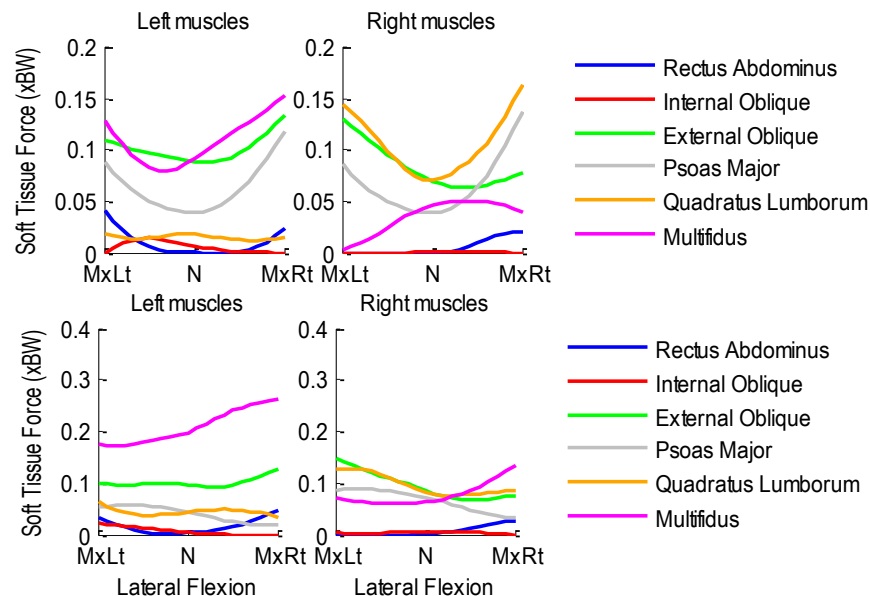


Figure A.488 Patient 1HDS pre- (top row) and post-operative (bottom row) bilateral muscle forces normalized with respect to body weight during left-to-right lateral flexion.

A.41.3 Axial Rotation Activity

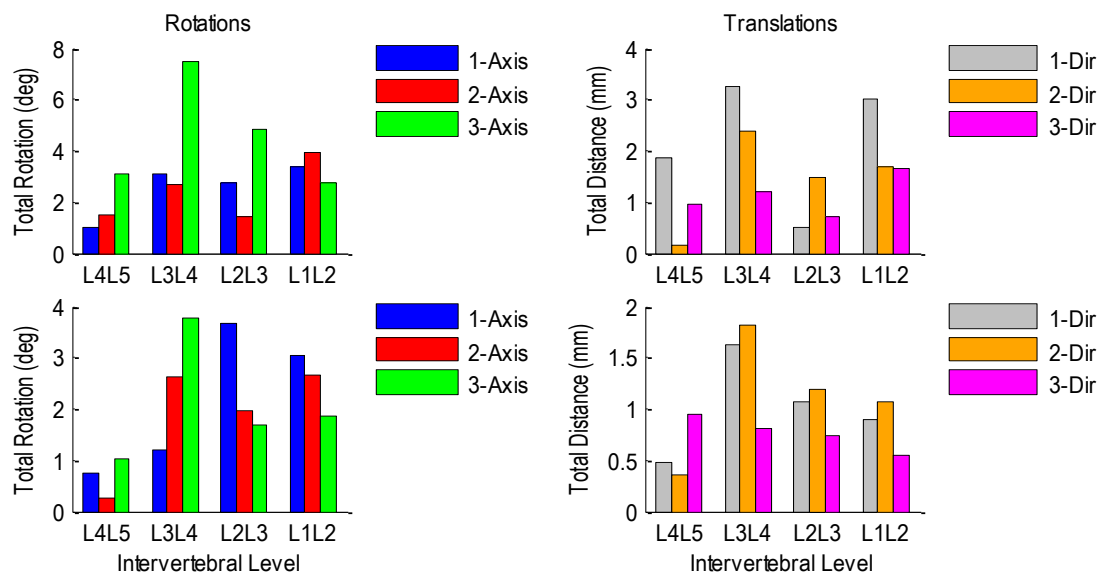


Figure A.489 Patient 1HDS pre-operative (top row) and post-operative (bottom row) relative rotations (left) and translations (right) at each vertebral level during left-to-right axial rotation.

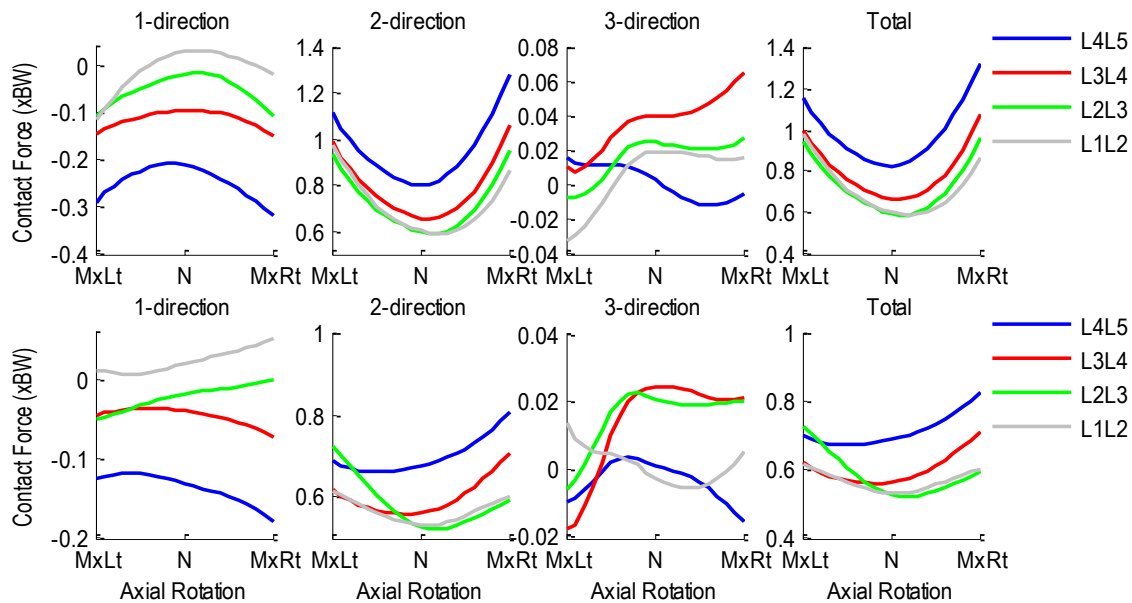


Figure A.490 Patient 1HDS pre- (top row) and post-operative (bottom row) intervertebral contact forces normalized with respect to body weight during left-to-right axial rotation. 1-dir= Ant(+)/Post(-), 2-dir=Sup(+)/Inf(-), 3-dir=Rt(+)/Lt(-).

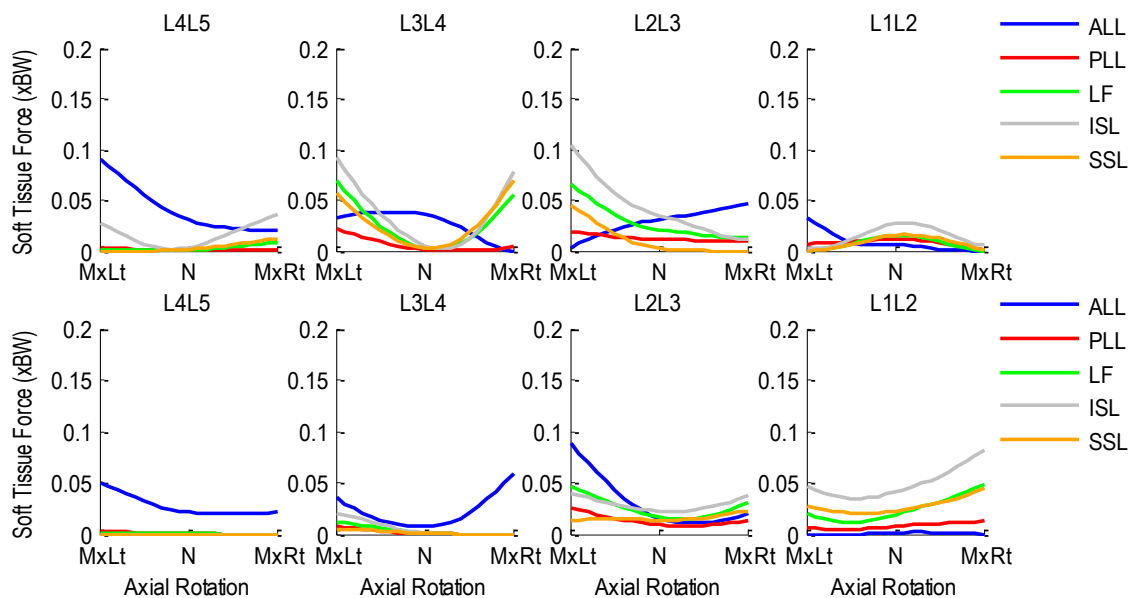


Figure A.491 Patient 1HDS pre- (top row) and post-operative (bottom row) segmental ligament forces normalized with respect to body weight during left-to-right axial rotation.

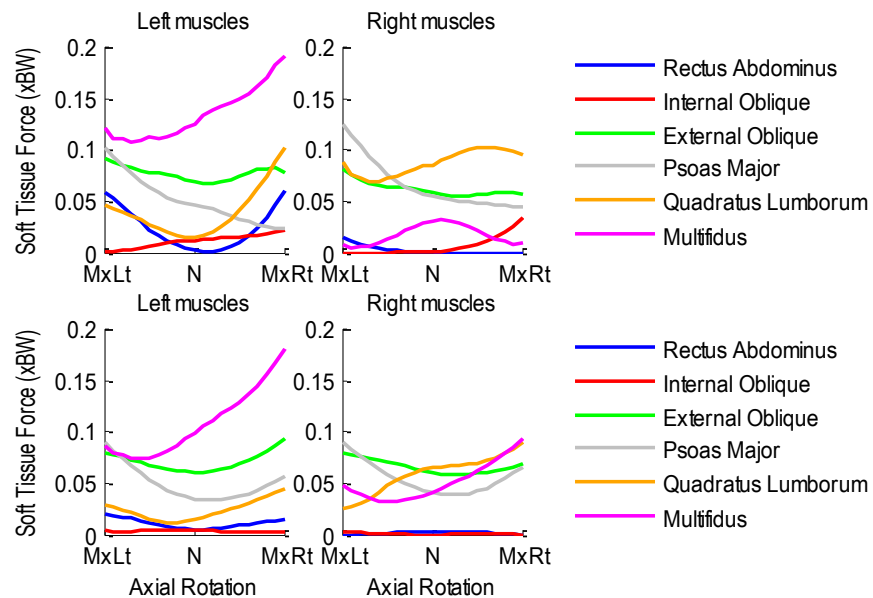


Figure A.492 Patient 1HDS pre- (top row) and post-operative (bottom row) bilateral muscle forces normalized to body weight during left-to-right axial rotation.

A.42 Patient 2HDS

Age: 34 years

Gender: Male

Height: 1.73 m

Mass: 82 kg

Condition: Posterior lumbar interbody fusion at L5S1 with dynamic stabilization at L4L5

A.42.1 Flexion-Extension Activity

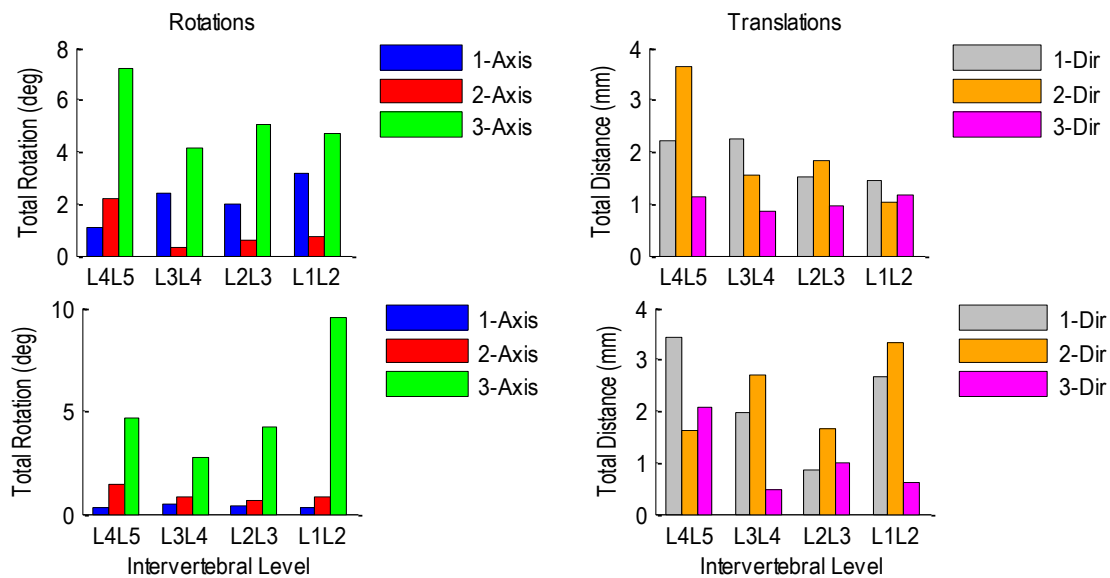


Figure A.493 Patient 2HDS pre-operative (top row) and post-operative (bottom row) relative rotations (left) and translations (right) at each vertebral level during flexion-extension.

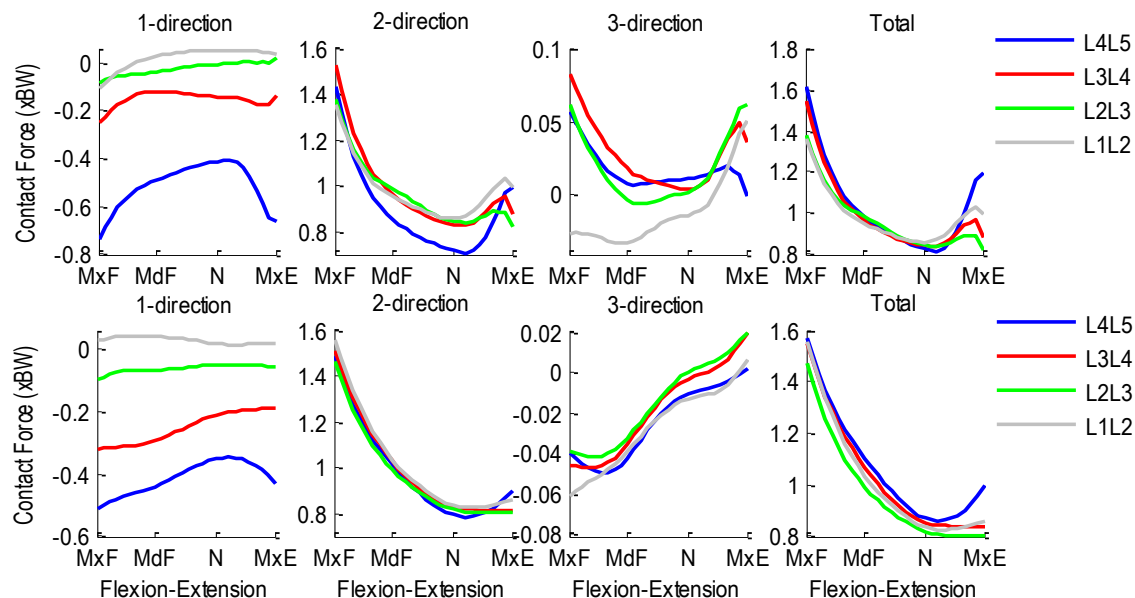


Figure A.494 Patient 2HDS pre- (top row) and post-operative (bottom row) intervertebral contact forces normalized with respect to body weight during flexion-extension. 1-dir=Ant (+)/Post(-), 2-dir=Sup(+)/Inf(-), 3-dir=Rt (+)/Lt(-).

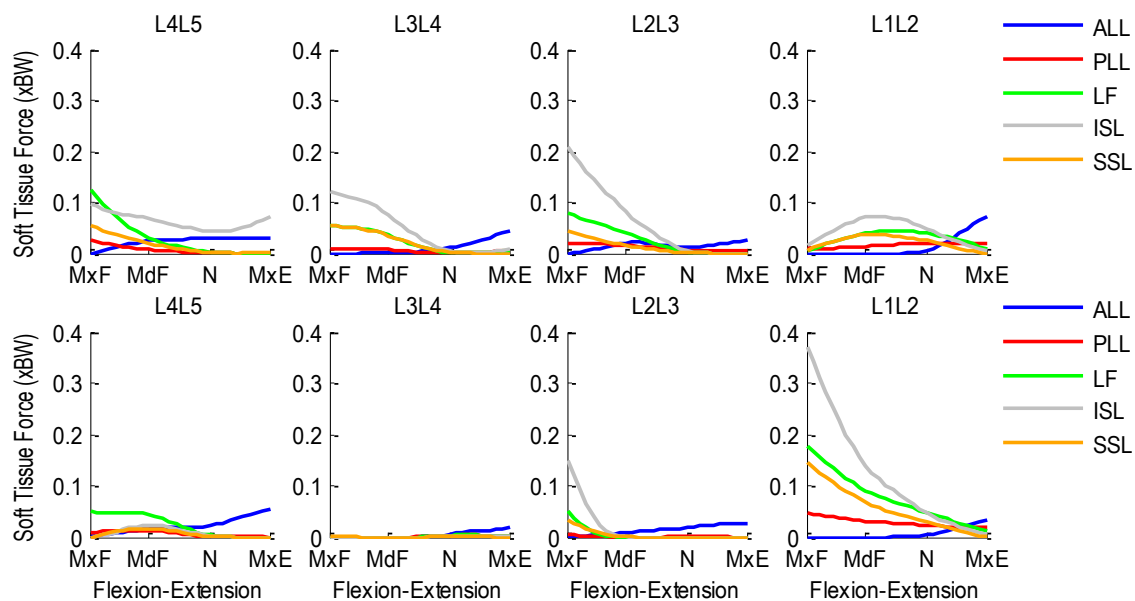


Figure A.495 Patient 2HDS pre- (top row) and post-operative (bottom row) segmental ligament forces normalized with respect to body weight during flexion-extension.

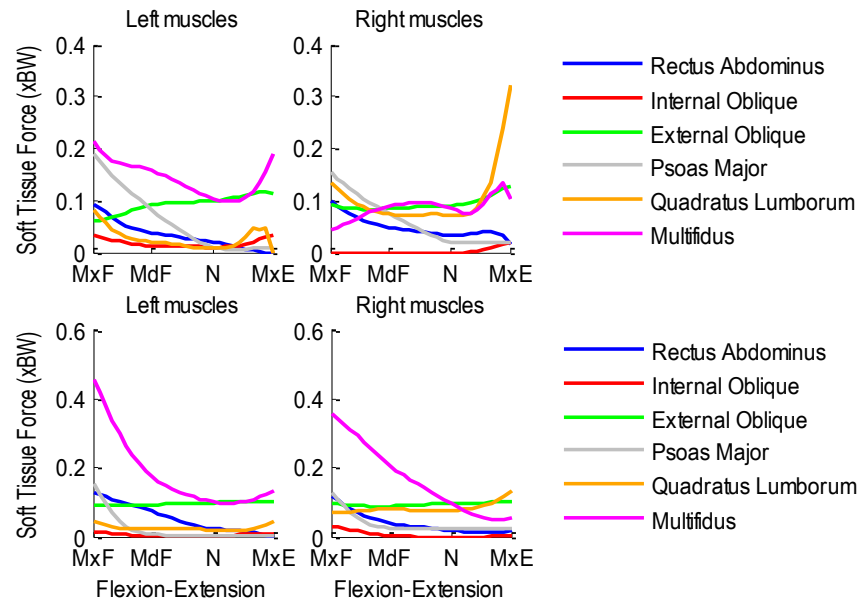


Figure A.496. Patient 2HDS pre- (top row) and post-operative (bottom row) bilateral muscle forces normalized with respect to body weight during flexion-extension.

A.42.2 Lateral Flexion Activity

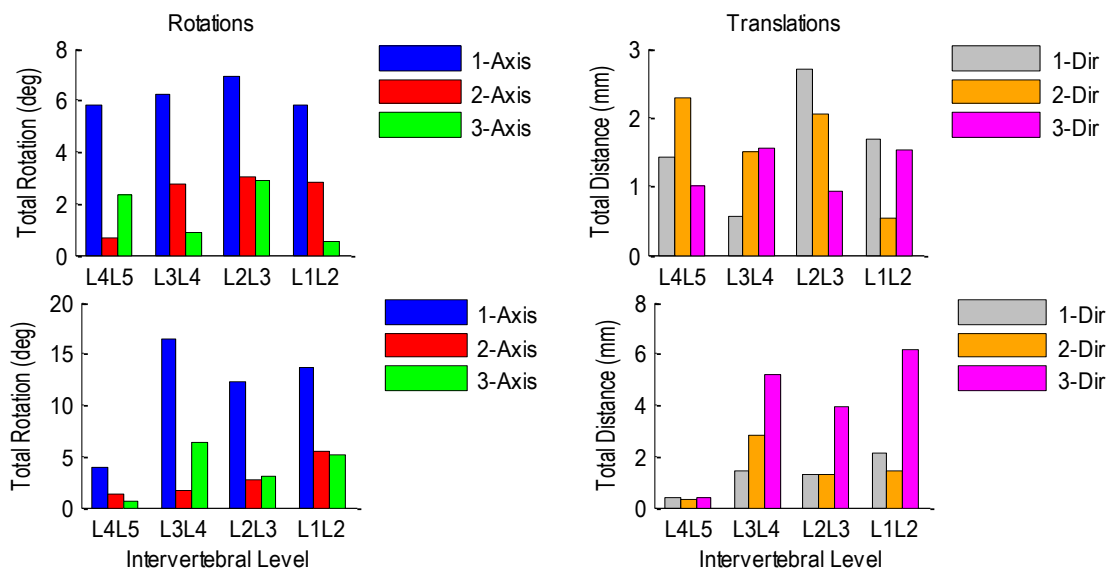


Figure A.497 Patient 2HDS pre-operative (top row) and post-operative (bottom row) relative rotations (left) and translations (right) at each vertebral level during left-to-right lateral flexion.

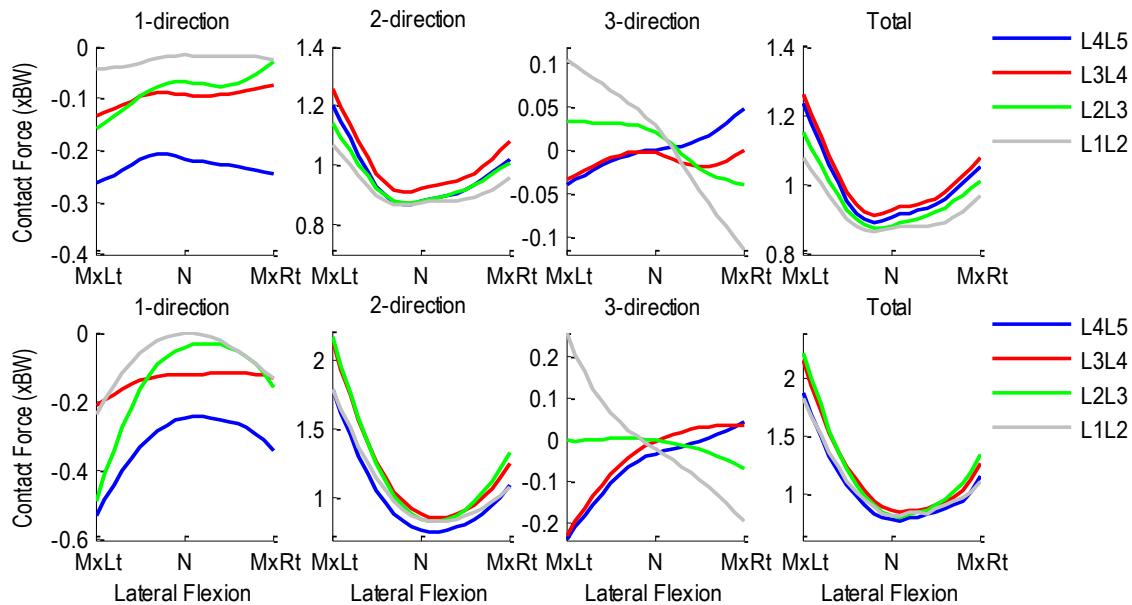


Figure A.498 Patient 2HDS pre- (top row) and post-operative (bottom row) intervertebral contact forces normalized with respect to body weight during right-to-left lateral flexion. 1-dir= Ant (+)/Post (-), 2-dir=Sup (+)/Inf(-), 3-dir=Rt(+)/Lt(-).

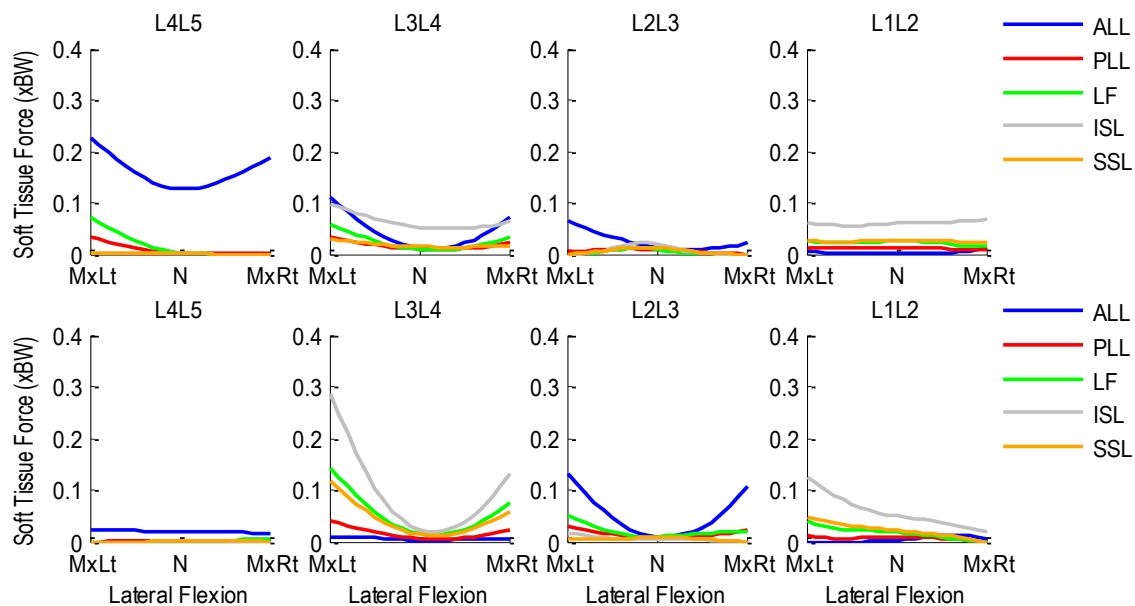


Figure A.499 Patient 2DS pre- (top row) and post-operative (bottom row) segmental ligament forces normalized with respect to body weight during left-to-right lateral flexion.

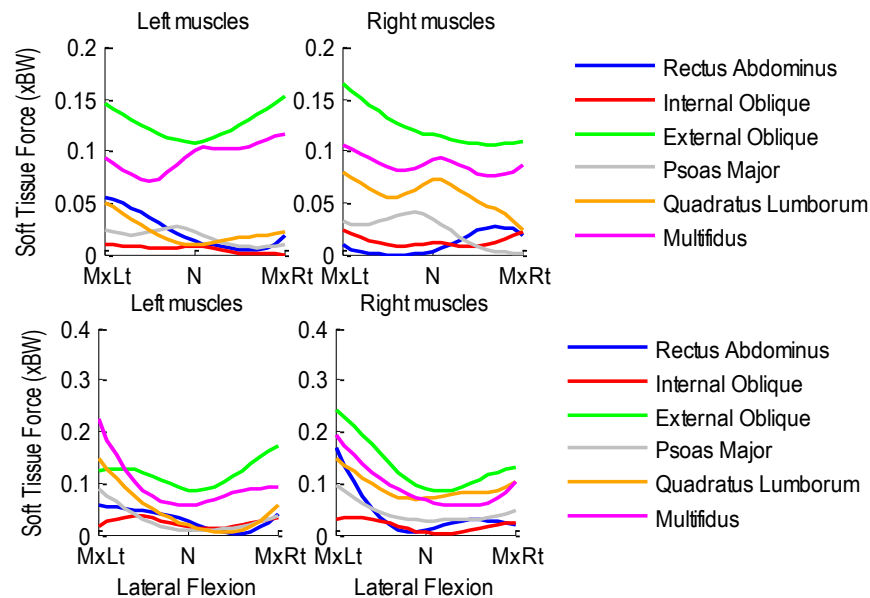


Figure A.500 Patient 2HDS pre- (top row) and post-operative (bottom row) bilateral muscle forces normalized with respect to body weight during left-to-right lateral flexion.

A.42.3 Axial Rotation Activity

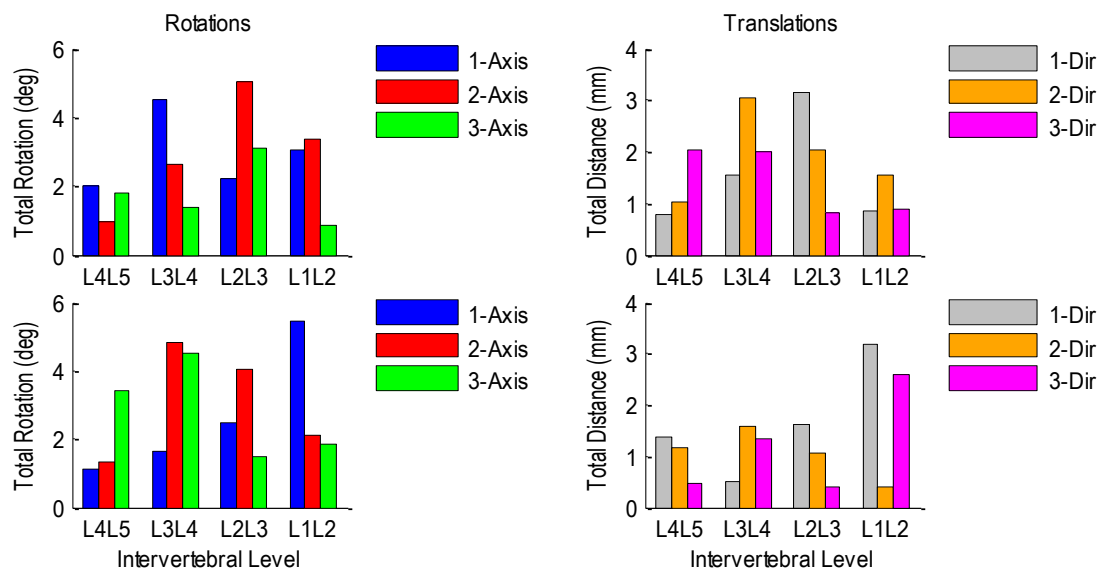


Figure A.501 Patient 2HDS pre-operative (top row) and post-operative (bottom row) relative rotations (left) and translations (right) at each vertebral level during left-to-right axial rotation.

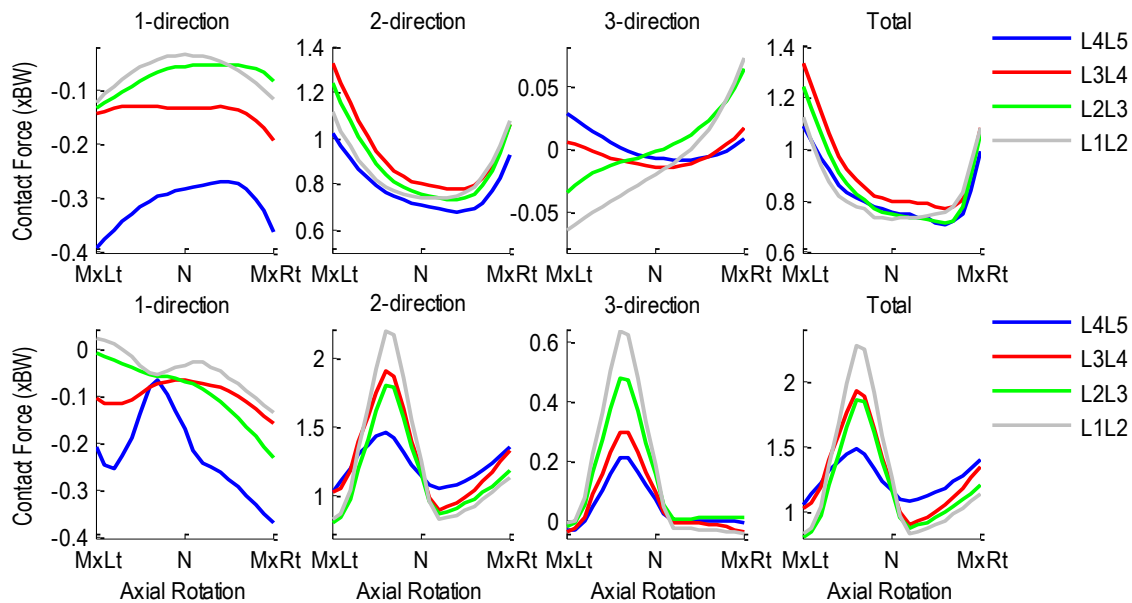


Figure A.502 Patient 2HDS pre- (top row) and post-operative (bottom row) intervertebral contact forces normalized with respect to body weight during left-to-right axial rotation. 1-dir= Ant(+)/Post(-), 2-dir=Sup(+)/Inf(-),3-dir=Rt(+)/Lt(-).

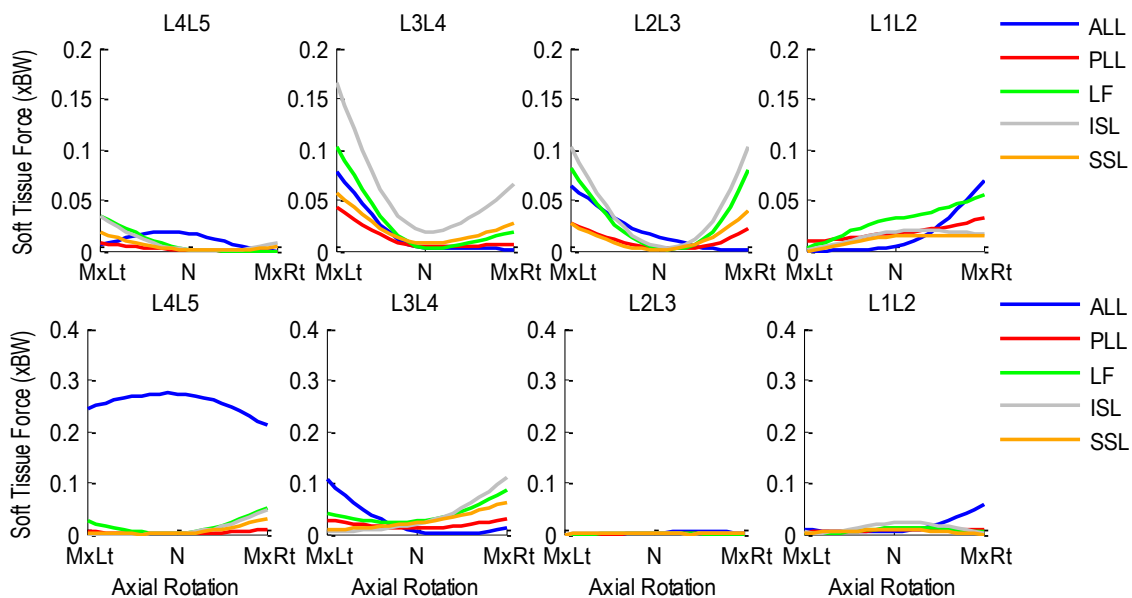


Figure A.503 Patient 2HDS pre- (top row) and post-operative (bottom row) segmental ligament forces normalized with respect body weight during left-to-right axial rotation.

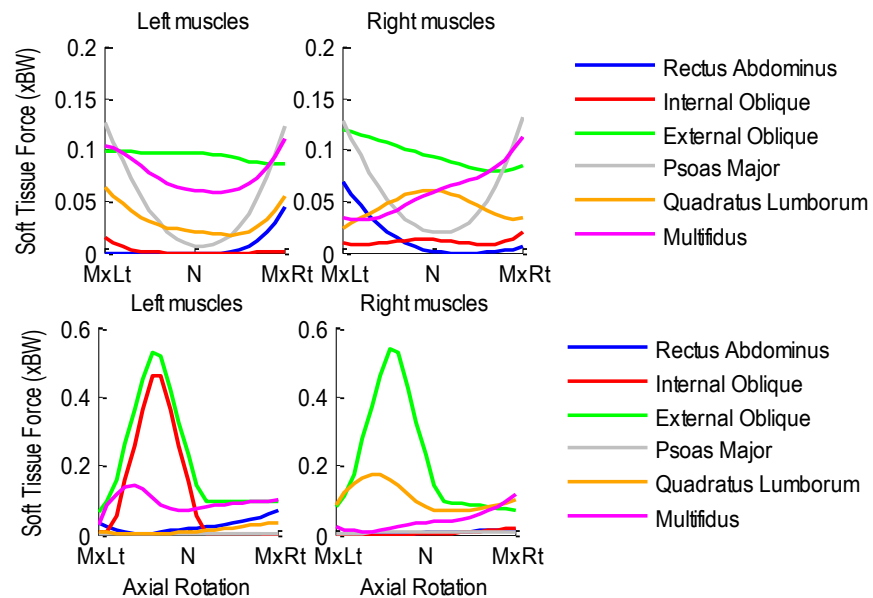


Figure A.504 Patient 2HDS pre- (top row) and post-operative (bottom row) bilateral muscle forces normalized to body weight during left-to-right axial rotation.

A.43 Patient 1LADR

Age: 56 years

Gender: Female

Height: 1.65 m

Mass: 68 kg

Condition: Lumbar artificial disc replacement at L5S1; Pt evaluated post-operatively only

A.43.1 Flexion-Extension Activity

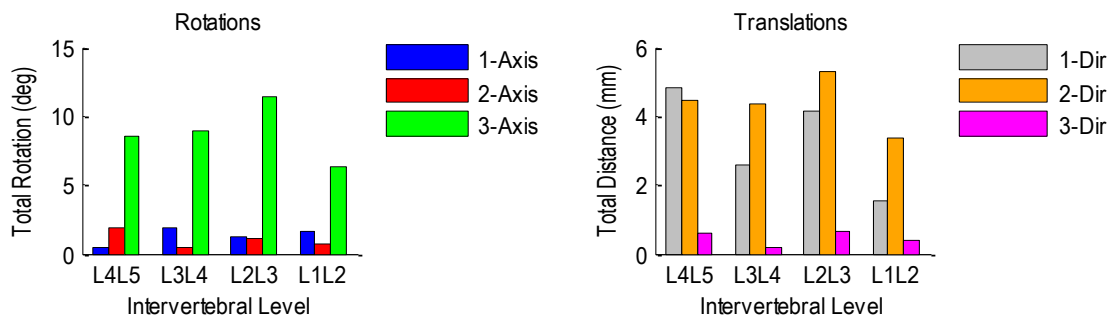


Figure A.505 Patient 1LADR post-operative relative rotations (left) and translations (right) at each vertebral level during flexion-extension.

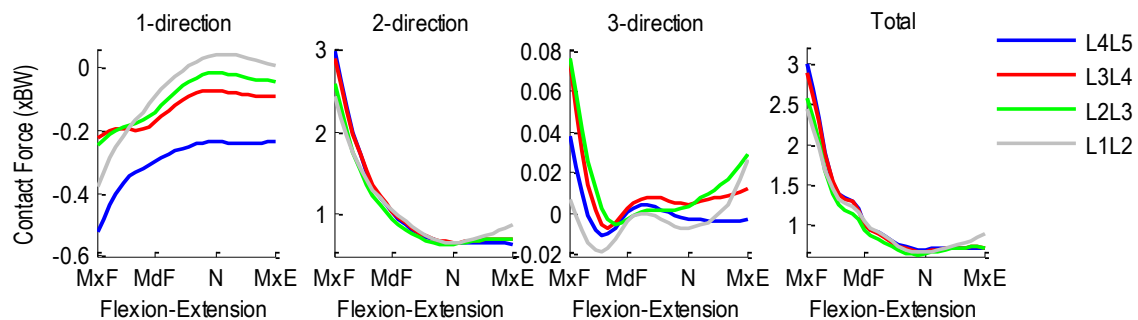


Figure A.506 Patient 1LADR post-operative intervertebral contact forces normalized with respect to body weight during flexion-extension. 1-dir=Ant (+)/Post(-), 2-dir=Sup(+)/Inf(-), 3-dir=Rt (+)/Lt(-).

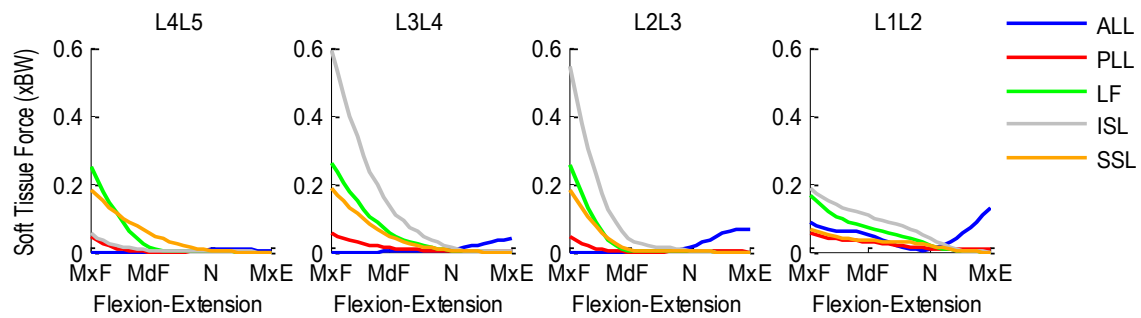


Figure A.507. Patient 1LADR post-operative segmental ligament forces normalized with respect to body weight during flexion-extension.

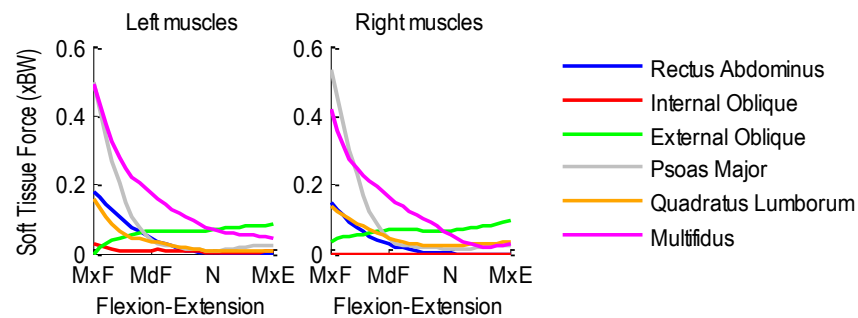


Figure A.508 Patient 1LADR post-operative bilateral muscle forces normalized with respect to body weight during flexion-extension.

A.43.2 Lateral Flexion Activity

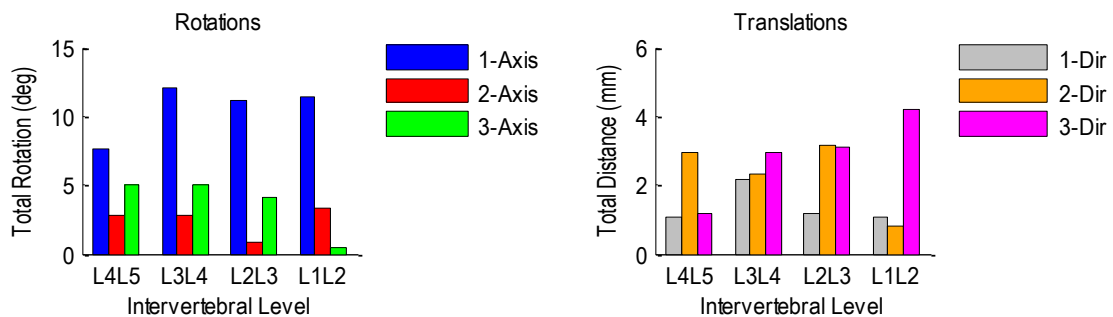


Figure A.509 Patient 1LADR post-operative relative rotations (left) and translations (right) at each vertebral level during left-to-right lateral flexion.

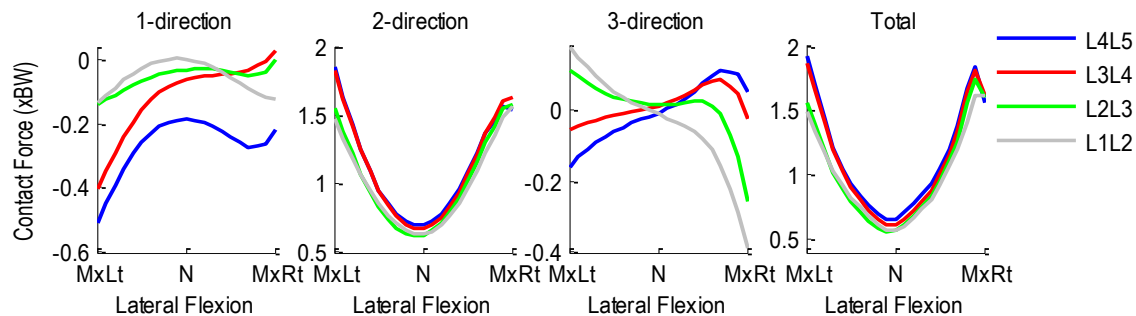


Figure A.510 Patient 1LADR post-operative intervertebral contact forces normalized with respect to body weight during right-to-left lateral flexion. 1-dir= Ant (+)/Post (-), 2-dir=Sup (+)/Inf(-), 3-dir=Rt(+)/Lt(-).

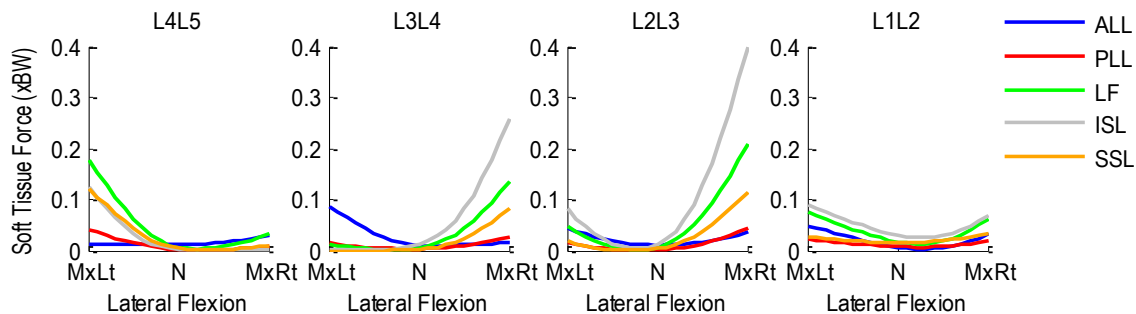


Figure A.511 Patient 1LADR post-operative segmental ligament forces normalized with respect to body weight during left-to-right lateral flexion.

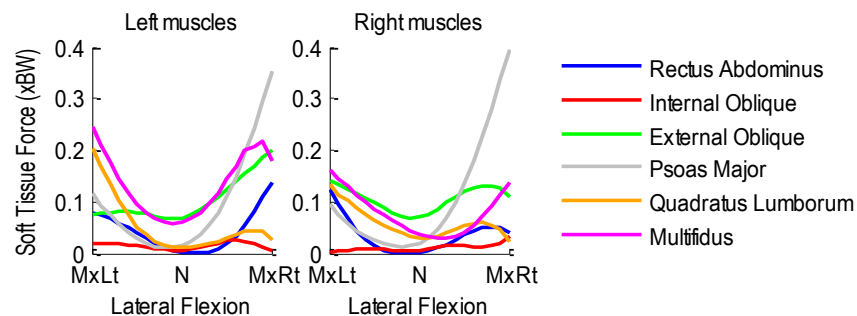


Figure A.512 Patient 1LADR post-operative bilateral muscle forces normalized with respect to body weight during left-to-right lateral flexion.

A.43.3 Axial Rotation Activity

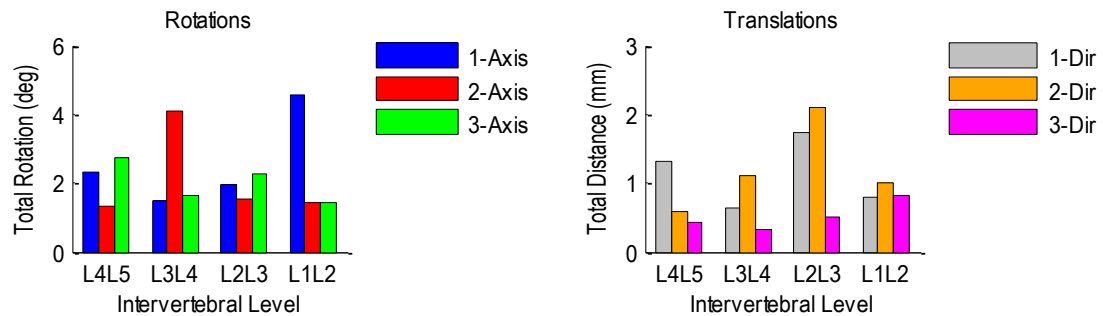


Figure A.513 Patient 1LADR post-operative relative rotations (left) and translations (right) at each vertebral level during left-to-right axial rotation.

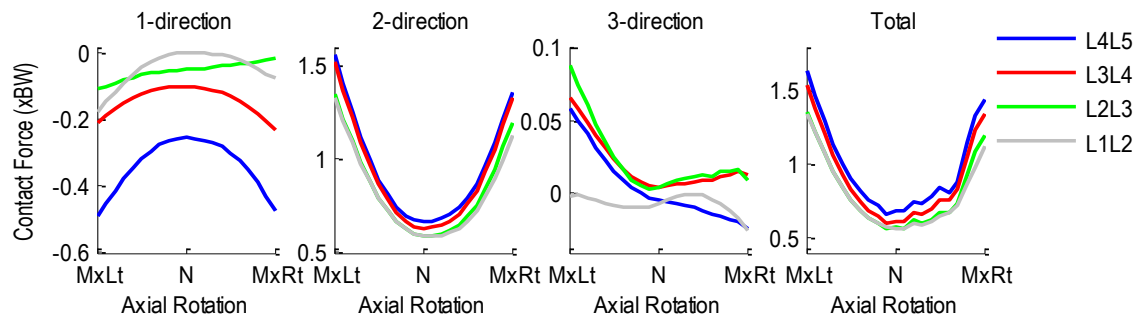


Figure A.514. Patient 1LADR post-operative intervertebral contact forces normalized with respect to body weight during left-to-right axial rotation. 1-dir= Ant(+)/Post(-), 2-dir=Sup(+)/Inf(-), 3-dir=Rt(+)/Lt(-).

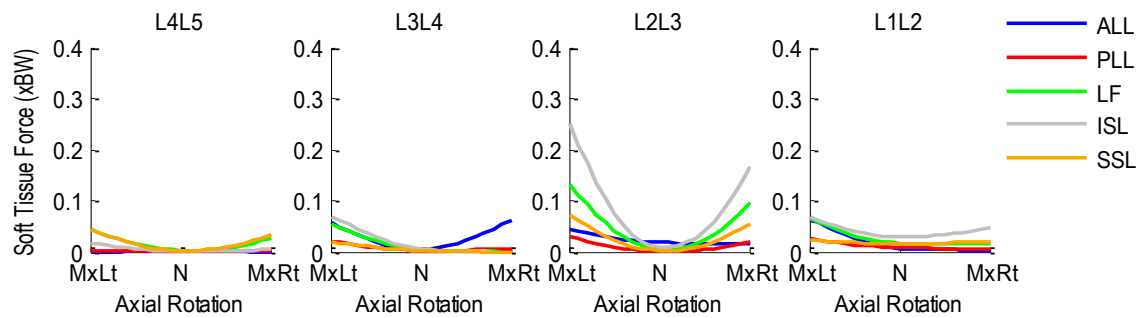


Figure A.515 Patient 1LADR post-operative segmental ligament forces normalized with respect to body weight during left-to-right axial rotation.

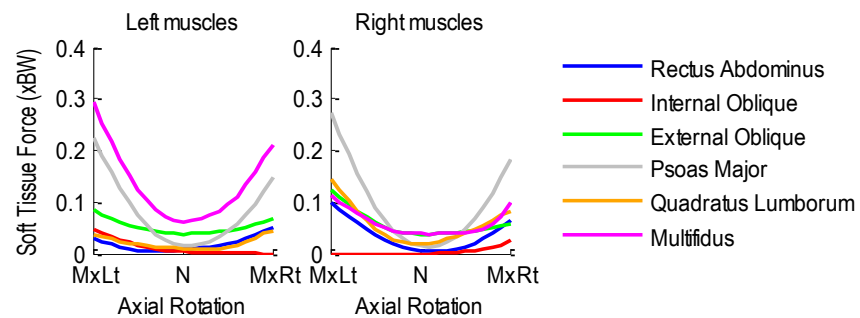


Figure A.516 Patient 1LADR post-operative bilateral muscle forces normalized to body weight during left-to-right axial rotation.

A.44 Patient 2LADR

Age: 56 years

Gender: Female

Height: 1.65 m

Mass: 68 kg

Condition: Lumbar artificial disc replacement at L5S1; Pt evaluated post-operatively only

A.44.1 Flexion-Extension Activity

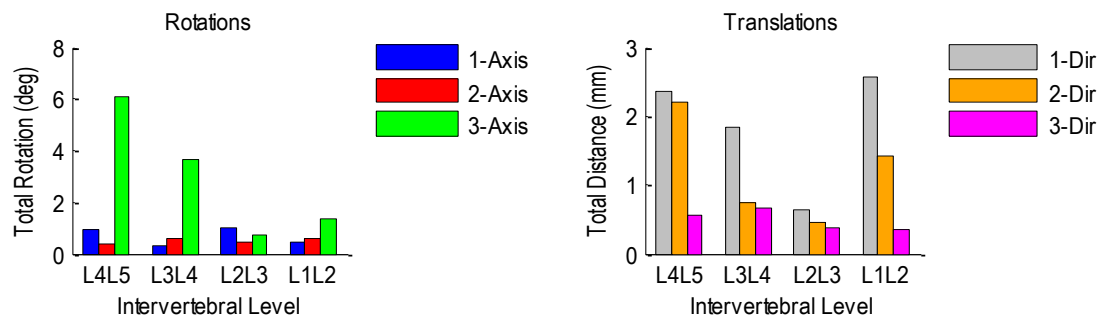


Figure A.517 Patient 2LADR post-operative relative rotations (left) and translations (right) at each vertebral level during flexion-extension.

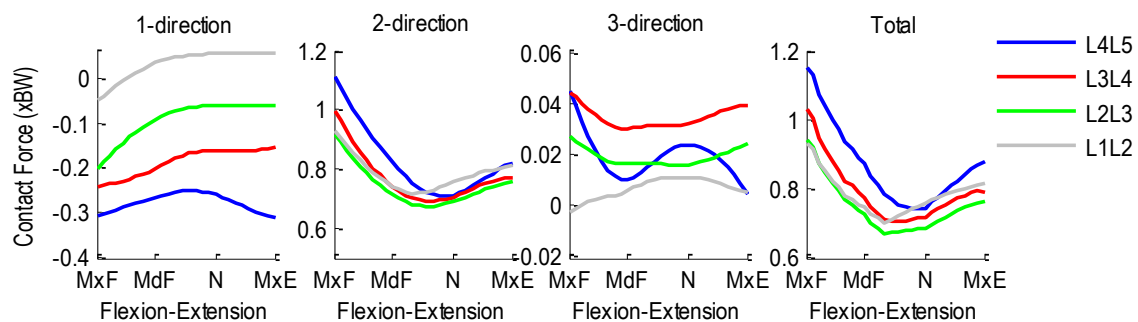


Figure A.518 Patient 2LADR post-operative intervertebral contact forces normalized with respect to body weight during flexion-extension. 1-dir=Ant (+)/Post(-), 2-dir=Sup(+)/Inf(-), 3-dir=Rt (+)/Lt(-).

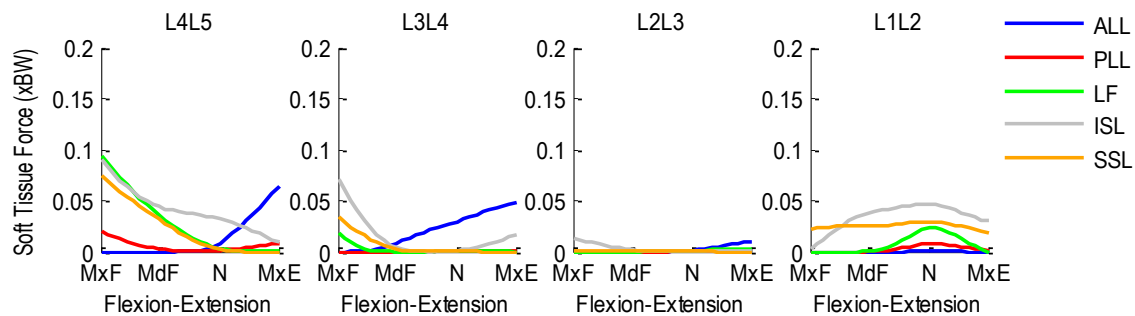


Figure A.519 Patient 2LADR post-operative segmental ligament forces normalized with respect to body weight during flexion-extension.

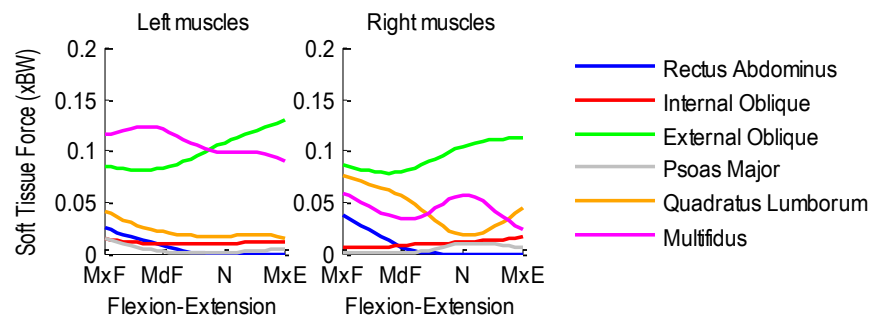


Figure A.520 Patient 2LADR post-operative bilateral muscle forces normalized with respect to body weight during flexion-extension.

A.44.2 Lateral Flexion Activity

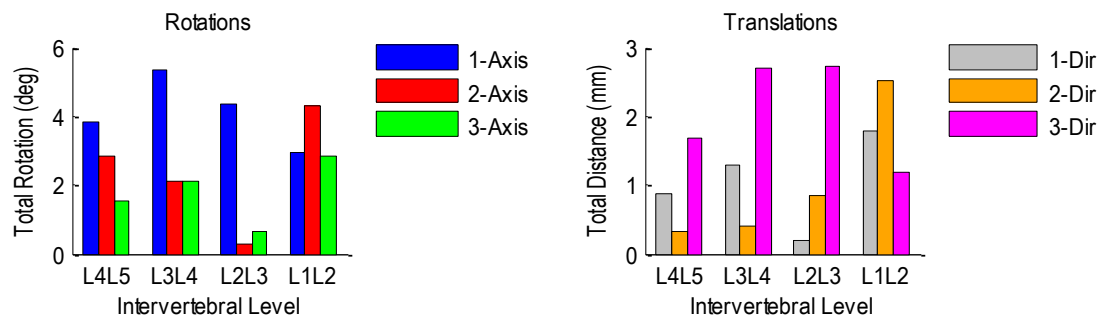


Figure A.521 Patient 2LADR post-operative relative rotations (left) and translations (right) at each vertebral level during left-to-right lateral flexion.

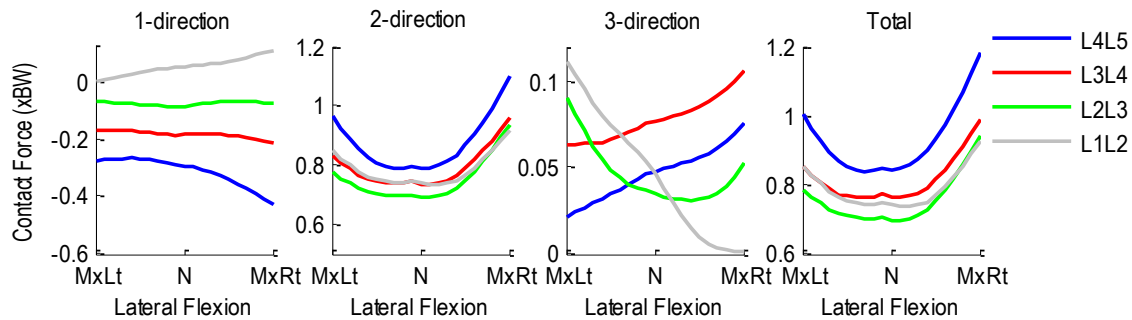


Figure A.522 Patient 2LADR post-operative intervertebral contact forces normalized with respect to body weight during right-to-left lateral flexion. 1-dir= Ant (+)/Post (-), 2-dir=Sup (+)/Inf(-), 3-dir=Rt(+)/Lt(-).

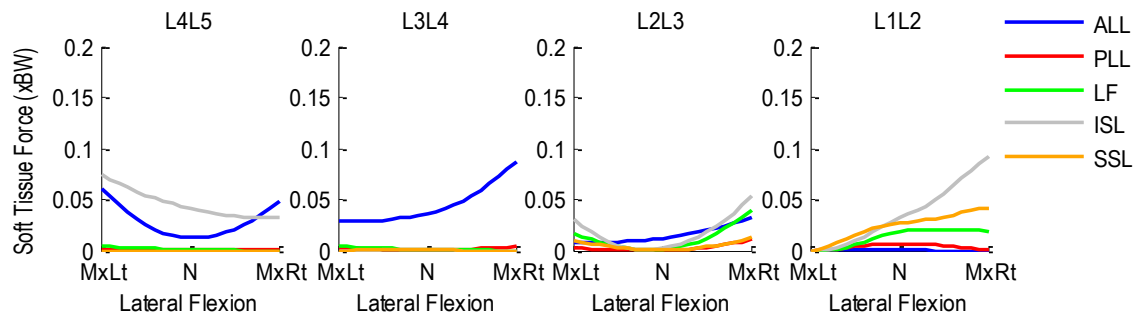


Figure A.523 Patient 2LADR post-operative segmental ligament forces normalized with respect to body weight during left-to-right lateral flexion.

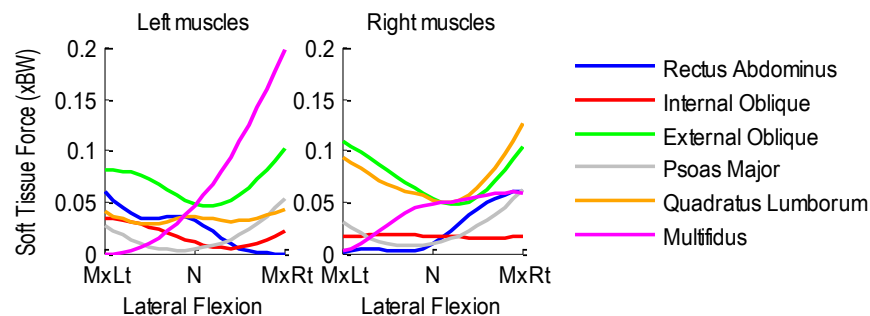


Figure A.524 Patient 2LADR post-operative bilateral muscle forces normalized with respect to body weight during left-to-right lateral flexion.

A.44.3 Axial Rotation Activity

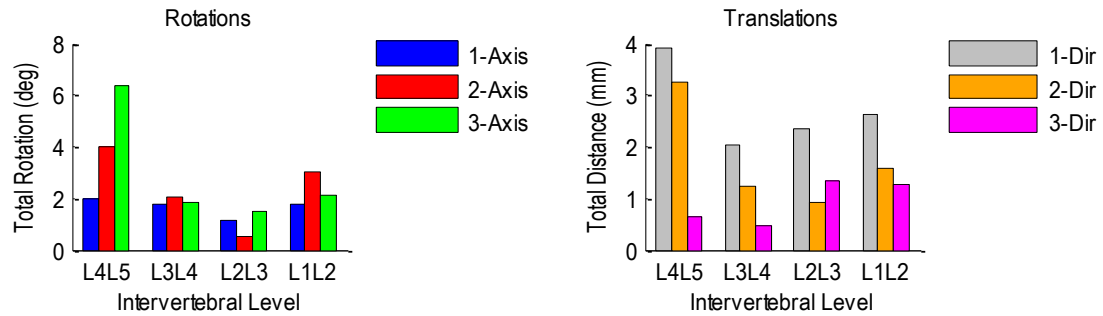


Figure A.525 Patient 2LADR post-operative relative rotations (left) and translations (right) at each vertebral level during left-to-right axial rotation.

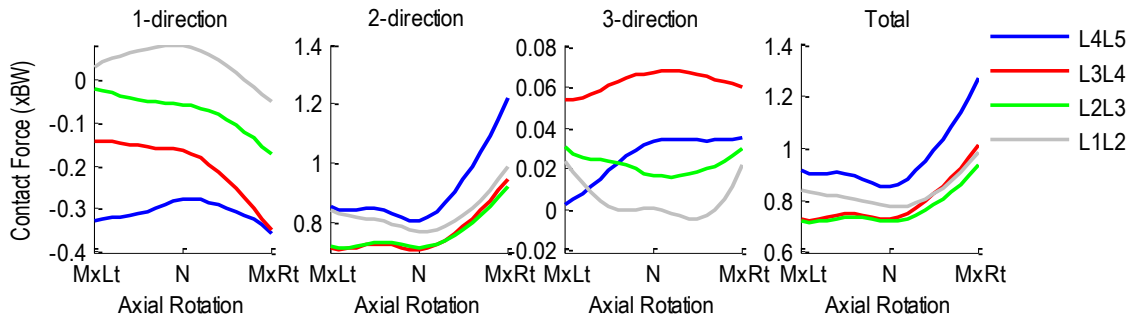


Figure A.526 Patient 2LADR post-operative intervertebral contact forces normalized with respect to body weight during left-to-right axial rotation. 1-dir= Ant(+)/Post(-), 2-dir=Sup(+)/Inf(-), 3-dir=Rt(+)/Lt(-).

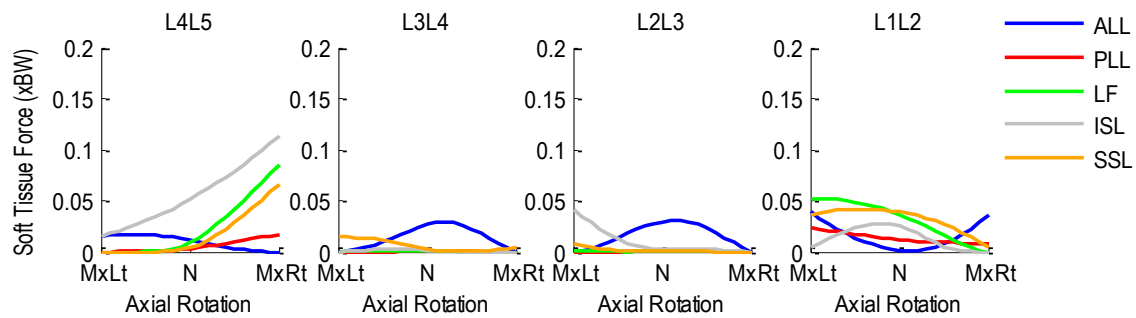


Figure A.527 Patient 2LADR post-operative segmental ligament forces normalized with respect to body weight during left-to-right axial rotation.

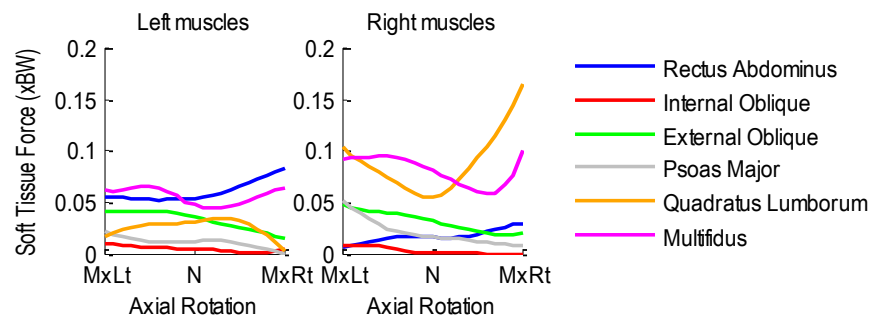


Figure A.528 Patient 2LADR post-operative bilateral muscle forces normalized to body weight during left-to-right axial rotation.

Vita

Christopher Brian Carr was born in Titusville, FL near Cape Canaveral on January 19, 1978. At two years of age, he moved to Jackson, TN and lived there for several years before later moving across the state to Kingsport. This would be where his family would remain, and in 1996, he graduated from Sullivan South High School. He moved on to the University of Tennessee, where he received a B.S. in Biochemistry and Molecular Biology with a minor in Business Administration in 2001. Initially, Chris had plans to enter medical school, but instead decided to work in the healthcare field for a time to confirm his aspiration of becoming a physician. Three years later, he had spent time in the ER and cardiac catheterization lab, while gaining a tremendous appreciation for the work healthcare professionals do to provide for people in need. Ultimately, he decided against medical school and instead chose to once again enroll at the University of Tennessee as a graduate student. In 2007, Chris was accepted into the Ph.D. program for Biomedical Engineering with a focus in biomechanics of human joints under the direction of Dr. Richard Komistek. As a graduate research assistantship at the Center for Musculoskeletal Research, he had the privilege to work on several projects investigating the knee, cervical and lumbar spines. His dissertation research offered many great opportunities to work with the National Institutes of Health and collaborate with a prominent neurosurgeon at Vanderbilt Medical Center while investigating the mechanics of the lumbar spine. He graduated with a doctoral degree in summer 2013 and hopes to continue his work in the orthopaedic field while contributing the well-being of others through his research.